frontiers | Research Topics

Advances in molecular plant pathology, plant abiotic and biotic stress

Edited by
Kun Zhang, Laura Medina-Puche, Xiaofeng Zhang and Zhenggang Li

Published in
Frontiers in Plant Science
Frontiers in Microbiology

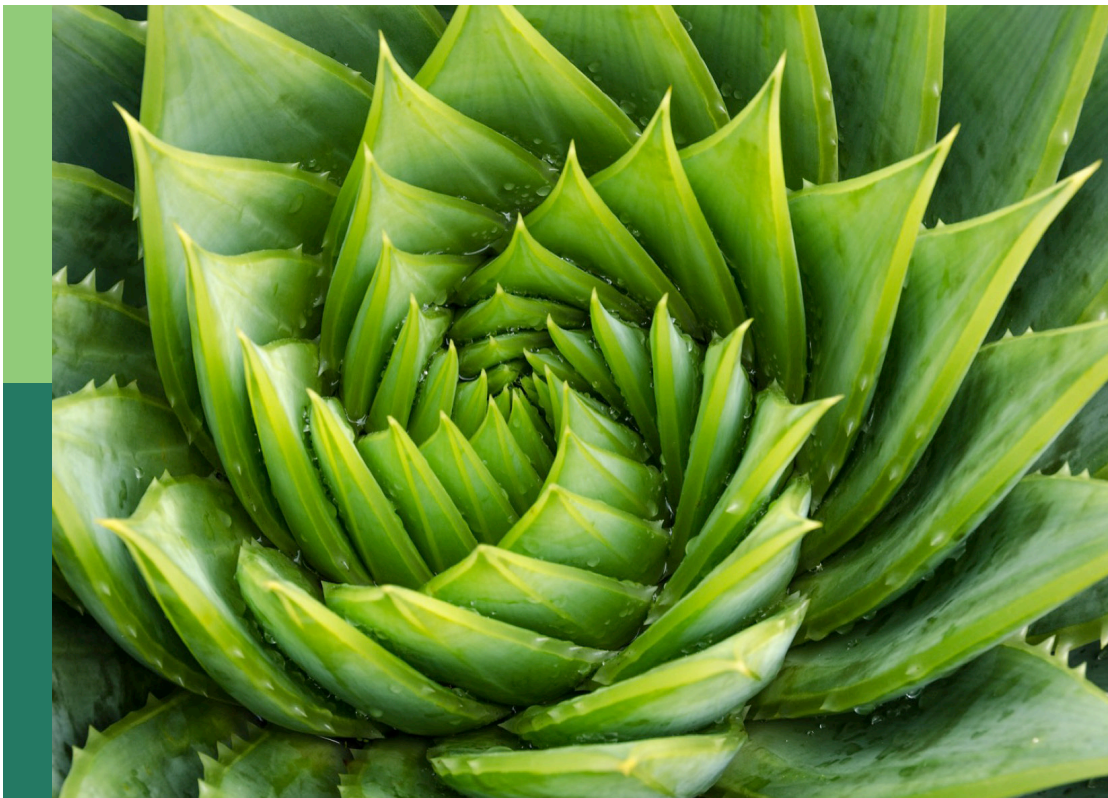

ISSN 1664-8714
ISBN 978-2-8325-4712-0
DOI 10.3389/978-2-8325-4712-0

About Frontiers

Frontiers is more than just an open access publisher of scholarly articles: it is a pioneering approach to the world of academia, radically improving the way scholarly research is managed. The grand vision of Frontiers is a world where all people have an equal opportunity to seek, share and generate knowledge. Frontiers provides immediate and permanent online open access to all its publications, but this alone is not enough to realize our grand goals.

Frontiers journal series

The Frontiers journal series is a multi-tier and interdisciplinary set of open-access, online journals, promising a paradigm shift from the current review, selection and dissemination processes in academic publishing. All Frontiers journals are driven by researchers for researchers; therefore, they constitute a service to the scholarly community. At the same time, the *Frontiers journal series* operates on a revolutionary invention, the tiered publishing system, initially addressing specific communities of scholars, and gradually climbing up to broader public understanding, thus serving the interests of the lay society, too.

Dedication to quality

Each Frontiers article is a landmark of the highest quality, thanks to genuinely collaborative interactions between authors and review editors, who include some of the world's best academicians. Research must be certified by peers before entering a stream of knowledge that may eventually reach the public - and shape society; therefore, Frontiers only applies the most rigorous and unbiased reviews. Frontiers revolutionizes research publishing by freely delivering the most outstanding research, evaluated with no bias from both the academic and social point of view. By applying the most advanced information technologies, Frontiers is catapulting scholarly publishing into a new generation.

What are Frontiers Research Topics?

Frontiers Research Topics are very popular trademarks of the *Frontiers journals series*: they are collections of at least ten articles, all centered on a particular subject. With their unique mix of varied contributions from Original Research to Review Articles, Frontiers Research Topics unify the most influential researchers, the latest key findings and historical advances in a hot research area.

Find out more on how to host your own Frontiers Research Topic or contribute to one as an author by contacting the Frontiers editorial office: frontiersin.org/about/contact

Advances in molecular plant pathology, plant abiotic and biotic stress

Topic editors

Kun Zhang — Yangzhou University, China

Laura Medina-Puche — University of Tübingen, Germany

Xiaofeng Zhang — Fujian Agriculture and Forestry University, China

Zhenggang Li — Plant Protection Research Institute, Guangdong Academy of Agricultural Sciences, China

Citation

Zhang, K., Medina-Puche, L., Zhang, X., Li, Z., eds. (2024). *Advances in molecular plant pathology, plant abiotic and biotic stress*. Lausanne: Frontiers Media SA. doi: 10.3389/978-2-8325-4712-0

Table of contents

frontiers | Frontiers in Plant Science

TYPE Editorial
PUBLISHED 22 March 2024
DOI 10.3389/fpls.2024.1398469

OPEN ACCESS

EDITED AND REVIEWED BY
Choong-Min Ryu,
Korea Research Institute of Bioscience and Biotechnology (KRIBB), Republic of Korea

*CORRESPONDENCE
Laura Medina-Puche
laura.medina-puche@zmbp.uni-tuebingen.de

RECEIVED 10 March 2024
ACCEPTED 15 March 2024
PUBLISHED 22 March 2024

CITATION
Medina-Puche L (2024) Editorial: Advances in molecular plant pathology, plant abiotic and biotic stress.
Front. Plant Sci. 15:1398469.
doi: 10.3389/fpls.2024.1398469

Editorial: Advances in molecular plant pathology, plant abiotic and biotic stress

Laura Medina-Puche*

Department of Plant Biochemistry, Center for Plant Molecular Biology (ZMBP), Eberhard Karls University, Tübingen, Germany

KEYWORDS

plant-pathogen interactions, plant viruses, abiotic stress responses, plant pathogenic bacteria, plant immunity, soil-pathogen interactions, disease management strategies, herbicide resistance mechanisms

Editorial on the Research Topic
Advances in molecular plant pathology, plant abiotic and biotic stress

Frontiers in Plant Science is delighted to present a diverse and comprehensive collection of research articles in the esteemed Research Topic titled "*Advances in Molecular Plant Pathology, Plant Abiotic and Biotic Stress*". Among the 18 articles featured within this Research Topic, several investigations offer significant contributions to our understanding of molecular plant pathology and plant responses to abiotic and biotic stresses. This compilation serves as a testament to the relentless efforts of researchers worldwide in unraveling the complexities of plant responses to various stressors, thereby advancing our understanding of plant biology, and bolstering agricultural sustainability.

Abiotic stress responses

Contributions focusing on plant responses to abiotic stresses offer valuable insights into stress perception, signal transduction, and tolerance mechanisms. Tu et al. present a comprehensive review discussing the current advances in understanding the molecular regulation of abiotic stress tolerance in sorghum. This review synthesizes recent progress in physiological, transcriptomic, proteomic, and metabolomic studies, highlighting the molecular mechanisms underlying sorghum's remarkable tolerance to diverse stressors. Furthermore, it emphasizes the importance of studying combined abiotic stresses, offering valuable insights for enhancing stress tolerance in crops crucial for global food security.

In the work carried out by Guo et al. explore the influence of temperature on glyphosate efficacy on glyphosate-resistant and -susceptible goosegrass (*Eleusine indica*). This study reveals the intricate interplay between temperature and herbicide efficacy, demonstrating that temperature fluctuations significantly affect glyphosate performance on different biotypes of *E. indica*. By elucidating the mechanisms underlying temperature-mediated variations in herbicide efficacy, this research provides valuable insights for glyphosate application and resistance management in weed control practices.

Qiu et al. delve into the adaptation mechanisms of $NaHCO_3$-tolerant chlorella and uncover the critical role of cellulose in conferring resistance to carbonate stress. By investigating cell wall polysaccharide composition and gene expression patterns, the researchers unveil the molecular basis of NaHCO3 tolerance in chlorella, highlighting the significance of cell wall-related genes, particularly *JbKOBITO1*, in mediating cellulose accumulation and stress resistance. These findings offer valuable insights into the genetic resources for crop breeding and the genetic modification of microalgae for sustainable biofuel production.

Advances in plant-pathogen interactions: insights from systems genomics to molecular mechanisms

Several articles within this Research Topic deepen into the molecular mechanisms underlying plant-pathogen interactions, shedding light on strategies employed by both plants and pathogens during infection.

Deciphering resistance mechanisms across multiple pathosystems

Notable among these is the work by Million et al., which employs a systems genomics approach to elucidate the molecular mechanisms underpinning quantitative resistance to *Phytophthora sojae* in *Glycine max*. Furthermore, Tun et al. elucidate the role of sucrose in promoting defense responses to blast fungus in rice through the preferential expression of defense-related genes.

In the study by Xu et al., the authors investigate the molecular mechanisms underlying iron (Fe)-mediated tobacco resistance to potato virus Y (PVY) infection. This study provides novel insights into the regulatory network of Fe-mediated resistance to PVY infection in plants. By elucidating the transcriptomic responses and identifying key candidate genes involved in PVY resistance, this research offers important theoretical bases for improving host resistance against PVY infection, thus contributing to the development of effective disease management strategies. Another contribution in the realm of plant-pathogen interactions is the study elaborated by Chang et al. which sheds light on the intricate dynamics of virus-virus interactions and their impact on mechanical transmissibility and host range alterations of begomoviruses. Their findings reveal how mixed infections can influence the transmission efficiency and host specificity of these pathogens, providing valuable insights for disease management strategies.

Zhao et al. investigate the responses of sugarcane to two strains of *Xanthomonas albilineans* differing in pathogenicity. By employing molecular analyses, they elucidate the differential modulation of salicylic acid and reactive oxygen species in the sugarcane defense response to pathogen attack. This study provides novel insights into the pathogenic diversity of *X. albilineans* and the molecular mechanisms underlying sugarcane defense strategies. Similarly, Gao et al. conduct a comparative transcriptome profiling of susceptible and tolerant citrus species infected with "*Candidatus liberibacter* asiaticus," offering novel perspectives on citrus Huanglongbing disease management. Chen et al. characterize gene expression patterns in response to orthotospovirus infection between two diploid peanut species and their hybrid, shedding light on the genetic basis of virus resistance in peanut. In the publication led by Zhao et al., the authors explore genetic and morphological variants of *Acidovorax avenae* subsp. *avenae* causing red stripe disease of sugarcane in China, offering insights into the genetic diversity and virulence mechanisms of this pathogen.

Understanding plant immunity and stress responses

The Research Topic also encompasses studies addressing a range of other pathogens and stress factors. In the study by Lipps et al., the authors delve into the inhibition of ethylene and its role in resistance to Northern corn leaf blight (NCLB) in maize. By employing a multifaceted approach combining genome-wide association studies, metabolic pathway analyses, and ethylene inhibition experiments, the researchers elucidate the complex interplay between genetic factors, metabolic pathways, and hormonal signaling in maize resistance to NCLB. This study not only identifies novel markers associated with NCLB resistance but also underscores the importance of ethylene in plant defense against fungal pathogens, paving the way for future investigations into the genetic basis of disease resistance. In addition, Yang et al. shed light on the pivotal role of microRNAs (miRNAs) in tobacco defense against *Phytophthora nicotianae*, the causal agent of tobacco black shank. Through meticulous experimentation and genetic manipulation, the researchers demonstrate that overexpression of Nta-miR6155 enhances tobacco resistance to *P. nicotianae* infection by modulating reactive oxygen species (ROS) levels, salicylic acid signaling, and the expression of key defense-related genes. Moreover, the study elucidates the regulatory role of Nta-miR6155 in tobacco growth and development, underscoring the multifaceted functions of species-specific miRNAs in plant stress responses.

The contribution to this Research Topic coming from Shang et al. explore the dynamic interplay between light intensity and soybean mosaic virus (SMV) infection in soybean. Through RNA-seq analysis and gene expression profiling, the researchers uncover the pivotal role of light in modulating soybean defense responses to viral infection. This study enhances our understanding of the molecular mechanisms underlying plant-virus interactions and highlights the importance of environmental factors in shaping plant defense strategies.

An original approach is presented by Li et al.. The authors investigate the potential of exogenous melatonin application in enhancing radish defense against *Alternaria brassicae*, the causative agent of radish blight disease. Through a combination of

physiological assays and transcriptomic analyses, the researchers reveal the dose-dependent effects of melatonin on both host immunity and pathogen virulence. Their findings provide a mechanistic understanding of melatonin-mediated defense responses in radish, offering promising prospects for the development of melatonin-based strategies for disease control in vegetable crops.

Unraveling soil-pathogen interactions

Gauthier et al. contribute to our understanding of soil-borne wheat mosaic virus (SBWMV) and Soil-borne cereal mosaic virus (SBCMV) infection in wheat by investigating the influence of soil properties and plant nutrition on virus infection rates. Through meticulous analyses of soil structure parameters, nutrient contents, and infection rates, the researchers reveal the intricate relationship between soil characteristics, plant nutrition, and virus transmission. These findings not only offer insights into the environmental factors influencing virus infection but also provide potential avenues for developing microenvironment-adapted agricultural practices to mitigate virus spread.

Investigating alternative disease management strategies and exploring herbicide resistance mechanisms in weed species

Trouvelot et al. investigate the impact of sodium arsenite on grapevine physiology and its potential as an alternative treatment for grapevine trunk diseases (GTDs). By employing metabolomic and histological analyses, the researchers elucidate the effects of sodium arsenite on wood tissues and secondary metabolite production, shedding light on its mode of action against GTD pathogens. This study contributes valuable insights into the development of sustainable strategies for GTD management, addressing the urgent need for eco-friendly alternatives to conventional treatments.

Cao et al. provide a comprehensive analysis of metamifop resistance in *Digitaria ciliaris* var. *chrysoblephara*, a problematic grass weed in China. Through genome sequencing, gene expression profiling, and whole-plant bioassays, the researchers unravel the molecular mechanisms underlying metamifop resistance, identifying a target-site mutation in the ACCase gene associated with resistance. Additionally, the study elucidates cross-resistance patterns to other herbicides, offering valuable insights into the management of herbicide-resistant weed populations.

Future directions and implications/ concluding remarks

As global climate change escalates, understanding plant stress responses becomes increasingly critical. By deciphering the molecular basis of these responses, researchers not only empower farmers with tools to mitigate crop losses but also contribute to the sustainable intensification of agriculture, promoting both environmental stewardship and economic viability.

Collectively, these articles underscore the interdisciplinary nature of research in plant science and highlight the interconnectedness of molecular mechanisms governing plant responses to diverse stressors. By elucidating these mechanisms, researchers pave the way for the development of resilient crops capable of withstanding environmental challenges, thereby ensuring global food security and sustainability.

Author contributions

LM-P: Conceptualization, Writing – original draft, Writing – review & editing.

Acknowledgments

My deepest and most sincere gratitude to the authors, reviewers, and co-editors (Kun Zhang, Xiaofeng Zhang, and Zhenggang Li) whose dedication and expertise have enriched this Research Topic. It is my hope that the findings presented herein will inspire further inquiry, innovation, and collaboration, fostering continued advancements in the dynamic field of plant science.

Conflict of interest

The author declares that the research was conducted in the absence of any commercial or financial relationships that could be construed as a potential conflict of interest.

Publisher's note

frontiers | Frontiers in Plant Science

TYPE Original Research
PUBLISHED 15 December 2022
DOI 10.3389/fpls.2022.1087525

OPEN ACCESS

EDITED BY
Kun Zhang,
Yangzhou University, China

REVIEWED BY
Zhen He,
Yangzhou University, China
Kunal Singh,
Institute of Himalayan Bioresource Technology (CSIR), India

*CORRESPONDENCE
Philippe C. Rott
philippe.rott@cirad.fr
San-Ji Gao
gaosanji@fafu.edu.cn

SPECIALTY SECTION
This article was submitted to Plant Pathogen Interactions, a section of the journal Frontiers in Plant Science

RECEIVED 02 November 2022
ACCEPTED 02 December 2022
PUBLISHED 15 December 2022

CITATION
Zhao J-Y, Chen J, Shi Y, Fu H-Y, Huang M-T, Rott PC and Gao S-J (2022) Sugarcane responses to two strains of *Xanthomonas albilineans* differing in pathogenicity through a differential modulation of salicylic acid and reactive oxygen species. *Front. Plant Sci.* 13:1087525. doi: 10.3389/fpls.2022.1087525

Sugarcane responses to two strains of *Xanthomonas albilineans* differing in pathogenicity through a differential modulation of salicylic acid and reactive oxygen species

Jian-Ying Zhao[1], Juan Chen[1], Yang Shi[1], Hua-Ying Fu[1], Mei-Ting Huang[1], Philippe C. Rott[2*] and San-Ji Gao[1*]

[1]National Engineering Research Center for Sugarcane, Fujian Agriculture and Forestry University, Fuzhou, Fujian, China, [2]CIRAD, UMR PHIM, Montpellier, France, and PHIM Plant Health Institute, Univ Montpellier, CIRAD, INRAE, Institut Agro, IRD, Montpellier, France

Leaf scald caused by *Xanthomonas albilineans* is one of the major bacterial diseases of sugarcane that threaten the sugar industry worldwide. Pathogenic divergence among strains of *X. albilineans* and interactions with the sugarcane host remain largely unexplored. In this study, 40 strains of *X. albilineans* from China were distributed into three distinct evolutionary groups based on multilocus sequence analysis and simple sequence repeats loci markers. In pathogenicity assays, the 40 strains of *X. albilineans* from China were divided into three pathogenicity groups (low, medium, and high). Twenty-four hours post inoculation (hpi) of leaf scald susceptible variety GT58, leaf populations of *X. albilineans* strain XaCN51 (high pathogenicity group) determined by qPCR were 3-fold higher than those of strain XaCN24 (low pathogenicity group). Inoculated sugarcane plants modulated the reactive oxygen species (ROS) homoeostasis by enhancing respiratory burst oxidase homolog (ScRBOH) expression and superoxide dismutase (SOD) activity and by decreasing catalase (CAT) activity, especially after infection by *X. albilineans* XaCN51. Furthermore, at 24 hpi, plants infected with XaCN51 maintained a lower content of endogenous salicylic acid (SA) and a lower expression level of SA-mediated genes (*ScNPR3*, *ScTGA4*, *ScPR1*, and *ScPR5*) as compared to plants infected with XaCN24. Altogether, these data revealed that the ROS production-scavenging system and activation of the SA pathway were involved in the sugarcane defense response to an attack by *X. albilineans*.

KEYWORDS

xanthomonas albilineans, genetic divergence, pathogenicity, Reactive oxygen species (ROS) homeostasis, Salicylic acid (SA) signaling pathway, defense response, sugarcane

1 Introduction

The genus *Xanthomonas* of the *Xanthomonadaceae* family is formed by plant pathogenic bacteria infecting numerous crop plants, thus having a significant economic and agricultural impact (Jacques et al., 2016; Te Molder et al., 2021). A distinct characteristic of *Xanthomonas* species (Gram-negative bacteria) is the production of the extracellular polysaccharide xanthan. This compound contributes to pathogenicity of xanthomonads and the taxonomic name of the genus derived from the yellow (xanthós in Greek) appearance on culture media (Ryan et al., 2011; da Silva et al., 2017). Wide genome and pathogenic divergences are often observed at *Xanthomonas* species or pathovar level (Te Molder et al., 2021; Tambong et al., 2022).

Xanthomonas albilineans causes leaf scald, a vascular disease of sugarcane that occurs in almost all sugarcane-growing countries (Rott & Davis, 2000; Ntambo et al., 2019b). White-yellow 'pencil' lines running along the main leaf veins are characteristic of leaf scald, and this symptom gave the name to the pathogen's species name. Other disease symptoms include leaf chlorosis and leaf necrosis that result in stalk or entire plant death in susceptible sugarcane varieties (Rott & Davis, 2000; Lin et al., 2018). Leaf scald can cause severe yield losses and reduction of juice quality, and even the loss of entire sugarcane fields (Ricaud & Ryan, 1989; Rott & Davis, 2000; Ntambo et al., 2019b).

High immunological and genetic diversity exists among *X. albilineans* strains. Twenty-eight isolates from 11 different countries were divided into three serovars and six lysovars (Rott et al., 1986). Occurrence of three serovars within *X. albilineans* was confirmed with an additional set of 215 strains of the pathogen from 28 different geographical locations (Rott et al., 1994b). Thirty-eight strains of *X. albilineans* from different countries were also distributed into three main groups and eight subgroups based on DNA fingerprinting and serological reactions with monoclonal antibodies (Alvarez et al., 1996). Using a worldwide collection of isolates, 54 genetic haplotypes and eight pulsed-field gel electrophoresis (PFGE) groups (A-H) were identified within the leaf scald pathogen by genome mapping (Davis et al., 1997). Later on, three additional PFGE groups (I and J) were identified, and this genomic variation was confirmed by multilocus sequence analysis (MLSA) and genomics (Pieretti et al., 2012; Ntambo et al., 2019b; Zhang et al., 2020). Congruent genetic divergence within *X. albilineans* populations was also reported using fingerprinting methods such as random amplified fragment polymorphism (RAPD), rep-PCR, amplified fragment length polymorphism (AFLP), and simple sequence repeats (SSR) (Permaul et al., 1996; Lopes et al., 2001; Shaik et al., 2009; Tardiani et al., 2014).

Besides immunological and genetic divergences, variation in pathogenicity was also reported for the sugarcane leaf scald pathogen. For example, strains of *X. albilineans* belonging to different serovars varied in pathogenicity based on multiplication of the pathogen in sugarcane varieties (Mohamed et al., 1996). High variation in disease severity (DS) among strains of *X. albilineans* was found in Australia, Brazil, Guadeloupe, Mexico, and in the Guangxi province of China (Persley, 1973; Champoiseau et al., 2006b; Huerta-Lara et al., 2009; Tardiani et al., 2014; Wu et al., 2022). Notably, significant strain effects and variety × strain interactions were observed for strains originating from different countries (Mohamed et al., 1996). In contrast, no correlation was found between genetic variants or haplotypes and variation in pathogenicity of the leaf scald pathogen (Champoiseau et al., 2006b; Tardiani et al., 2014).

Pathogenicity factors of *X. albilineans* are involved in sugarcane colonization and disease progress including epiphytic survival, sensitivity to oxidative stress, plant cell adhesion, plant cell degradation by extracellular enzymes, bacterial motility, and biofilm development (Rott et al., 2013; Mensi et al., 2016; Mielnichuk et al., 2021). Albicidins produced by *X. albilineans* are a family of potent antibiotics and phytotoxins that inhibit DNA replication in bacteria and plastids (Birch and Patil, 1987b; Birch, 2001). *In planta*, albicidin production is closely associated with appearance of leaf pencil lines and chlorosis (Birch and Patil, 1987a). Mutagenesis of locus XALc_0557, coding for an OmpA protein of the *X. albilineans* cell membrane, strongly affects sugarcane stalk colonization by the pathogen (Rott et al., 2011a; Fleites et al., 2013). Other putative pathogenicity genes of *X. albilineans* include ABC transporter genes, a methyl-accepting chemotaxis protein gene, a gene conferring resistance to novobiocin, and an oxidoreductase gene (Rott et al., 2011b; Pieretti et al., 2012).

Plants are continuously challenged by diverse pathogens and have evolved a two-tiered immunity system, namely pattern-triggered immunity (PTI) and effector-triggered immunity (ETI) (Tabassum and Blilou, 2022; Ngou et al., 2022). At PTI stage, the pathogen recognized by the plant activates a complex network of signaling pathways such as reactive oxygen species (ROS), mitogen-activated protein kinase (MAPK), Ca^{2+} pathways, and hormone signaling that constitute the plant's basal defense response (Tabassum and Blilou, 2022). Salicylic acid (SA) biosynthesis and SA-mediated signaling pathway play a key role in plants for establishment of resistance to many pathogens (Ding and Ding, 2020). Genes involved in metabolic pathways, biosynthesis of secondary metabolites, MAPK signaling, hormone signal transduction, and plant-defense related pathways contribute to the response of sugarcane after an attack by *X. albilineans* (Meng et al., 2020; Ali et al., 2021; Javed et al., 2022; Ntambo et al., 2019a). The molecular mechanisms triggered in sugarcane after infection by strains of *X. albilineans* differing in pathogenicity have, however, not been explored so far.

This first objective of this study was to perform molecular genotyping of 40 strains of *X. albilineans* from China using MLSA and SSR methods. The second objective was to

characterize the pathogenicity of these strains by inoculation under greenhouse conditions of a sugarcane variety susceptible to leaf scald. The third objective was to investigate the molecular mechanisms triggered by one strain of *X. albilineans* with low pathogenicity and another strain of the pathogen with high pathogenicity. Explored mechanisms included ROS production and scavenging, as well as SA content and SA-mediated signaling pathway regulation.

2 Materials and methods

2.1 *X. albilineans* strains and DNA extraction

Thirty-nine strains of *X. albilineans* were isolated from 38 sugarcane leaf or stalk samples and one leaf sample of *Pennisetum purpureum* (Table S1). All samples were taken from plants exhibiting leaf scald symptoms and were collected during 2018-2019. The diseased sugarcane plants originated in six provinces (Fujian, Guangdong, Guangxi, Guizhou, Hainan, and Zhejiang) and the diseased pennisetum was collected in Fujian province. Isolation of *X. albilineans* was performed as described by Lin et al. (2018). Reference strain Xa-FJ1 from China was added to this collection of *X. albilineans* (Zhang et al., 2020). Total genomic DNA was extracted from the 40 strains using the Bacterial Genomic DNA extraction kit and following the manufacturers' protocol (Tiangen Biotechnology Co. Ltd, Beijing, China). All DNA samples were adjusted to a concentration of 100 ng/μL with sterile water, and then stored at 80 °C until further use.

2.2 Amplification and sequencing of bacterial housekeeping genes

Four housekeeping genes were amplified from extracted total DNA and sequenced as described by (Ntambo et al. 2019b). These four genes included *rpoD* (encoding the β subunit of the bacterial RNA polymerase), *glnA* (encoding a citrate synthase), *gyrB* (encoding the β subunit of the DNA gyrase), and *atpD* (encoding the β subunit of ATP synthase) (Table S2). The 156 gene sequences (4 genes x 39 strains) of *X. albilineans* obtained in this study were deposited at the NCBI GenBank database under accession numbers MT776038-MT776077 (*gyrB*), MT776128-MT776139 and ON112140-ON112166 (*rpoD*), MT776144-MT776155 and ON112168-ON112194 (*atpD*), and MT776160-MT776171 and ON112107-ON112138 (*glnA*).

2.3 Multilocus sequence analysis

For each of the 39 *X. albilineans* strains, the sequences of the four housekeeping genes were concatenated, thus yielding sequences of 4,165 nucleotides (nt) in length. The corresponding sequences of strain Xa-FJ1 from China and 14 additional strains of *X. albilineans* from different countries were also downloaded from the GenBank database (Table S1). The 54 sequences were aligned with the ClustalW algorithm implemented in MEGA 11 and a phylogenetic tree was constructed using the neighbor-joining (NJ) method (Tamura et al., 2021). Bootstrap values were determined for 1,000 replications. Classification of PFGE groups of each clade was performed as reported by Pieretti et al. (2012).

2.4 SSR genotyping through sequencing

Fifteen SSR markers developed by Tardiani et al. (2014) were used to assess the diversity and population structure of the 40 *X. albilineans* strains from China. The PCR reaction was performed in a volume of 20 μL consisting of 1x HotStarTaq buffer, 2.0 mM Mg^{2+}, 0.2 mM dNTP, 0.2 U HotStarTaq polymerase (Qiagen Inc, Frankfurt, Germany), 1.0 μM each of the forward and reverse primers, and 10-30 ng/μl of genomic DNA. The reaction conditions included an initial denaturation step at 95 °C for 2 min, followed by 11 cycles of 94 °C for 20 s and 65 °C for 40 s for primer annealing, and an extension step at 72 °C for 2 min; and then 24 cycles of 94 °C for 20 s and 59 °C for 30 s for primer annealing, and an extension step at 72 °C for 2 min; the final step was an extension period at 72 °C for 10 min. The PCR products were diluted 10 times and 1 μL of the diluted product was denatured at 95 °C for 5 min and then mixed with 0.5 μL fluorescein standard (GeneScan 500 LIZ™, ABI) and 8.5 μL formamide (Hi-Di). Lastly, capillary electrophoresis of the PCR products was conducted on an ABI3730XL DNA sequencer (Applied Biosystems, Foster City, CA, USA) to generate GeneScan files according to the manufacturer's instructions.

The GeneScan files were analyzed using GeneMapper 4.1 software (Applied Biosystems, Foster City, CA, USA) to reveal capillary electrophoregrams of PCR amplified SSR-DNA fragments. Each specific peak (band) of SSR fingerprinting was marked as "1" or "A" when present and "0" or "C" when absent in each of the 40 strains of *X. albilineans*. The polymorphism information content (PIC) of loci was calculated according to the formula, where P_{ij} is the frequency of j_{th} allele for i_{th} locus and summation extends over n alleles. A distance tree was constructed using clustering with the Unweighted Pair Group Method with Arithmetic Mean (UPGMA) in the SHAN program of NTSYS-PC 2.10e software (University of Kansas, Lawrence, USA).

2.5 Plant growth and inoculation with *X. albilineans*

Sugarcane plants with 1–2 fully expanded leaves (8–10 cm tall) of variety GT58 susceptible to leaf scald were used for

inoculation with *X. albilineans*. To compare pathogenicity of the 40 *X. albilineans* strains, bacterial suspensions adjusted to 10^8 CFU/mL were used for inoculation by the decapitation method. Briefly, the sugarcane stalk was cut 3–4 cm below the top visible dewlap leaf with scissors previously dipped in the bacterial inoculum. A sterile cotton ball was twined on the cut section before addition of 200 µl of bacterial inoculum (Figure S1). One day post inoculation (dpi), the cotton ball was removed from the cut section.

The 40 strains of *X. albilineans* were each inoculated to 35 sugarcane stalks and 35 control stalks were inoculated with only XAL medium (XAS liquid medium; Davis et al., 1994). Inoculated plants were randomly distributed and grown in an intelligent climate incubator (PLT-RGS-15PFC, Ningbo, China) at 28 °C, 65% humidity, and with a 16/8 h light/dark period. Three independent experiments were performed, which resulted in 105 inoculated plants per strain of the pathogen.

Furthermore, strains XaCN51 (high pathogenicity) and XaCN24 (low pathogenicity) of *X. albilineans* were used to investigate differential responses in sugarcane after inoculation with the leaf cutting method (Lin et al., 2018). The number of stalks inoculated per strain and the growing conditions of inoculated plants were identical to those described above. At each analysis time point [0, 12, and 24 hours post inoculation (hpi)], four leaf fragments were collected from each of 35 inoculated plants and these fragments were equally distributed into four pooled samples. These pooled samples with 35 leaf fragments each were used for the molecular and biochemical assays described below. The pooled sample for determination of bacterial population densities and the one for determination of gene expression were each divided in three biological subsamples. The pooled sample for measuring ROS and SA contents and the one for measuring oxidative enzyme activities were each divided in five biological subsamples.

2.6 Disease severity (DS) assessment

DS of leaf scald was assessed as reported by Rott et al. (1997) and Fu et al. (2021). Briefly, all inoculated stalks were rated individually at 7, 14, 21, 28 dpi, using a symptom severity scale ranging from 0 to 5 (Table 1). DS was calculated following the following formula: DS = [(0 × AP + 1 × FL + 2 × ML + 3 × CB + 4 × LN + 5 × PD)/5 × T] × 100, where AP, FL, ML, CB, LN, and PD are the number of stalks for each disease score and T is the total number of stalks. Mean DS at 28 dpi of each bacterial strain (three replications of 35 stalks) was used to perform a clustering analysis with Euclidean Distance implemented in SPSS software (version 18.0).

2.7 Determination of bacterial population densities

Total DNA was extracted from leaf tissues with the CTAB reagent and the qPCR assay (TaqMan probe, *abc* gene, Table S2) was performed as described by Shi et al. (2021). Population densities of *X. albilineans* were determined in three leaf subsamples collected for each strain at 0, 12, and 24 hpi. Three technical replications were performed for each subsample.

2.8 Physico-biochemical assays

The activity of ROS, endogenous SA, and four antioxidant enzymes was determined with commercial kits and according to the manufacturers' instructions (Beijing Solarbio Science & Technology Co., Ltd. China). The antioxidant enzymes were ascorbate peroxidase (APX, EC.1.11.1.11), superoxide dismutase (SOD, EC1.15.1.1), peroxidase (POD, EC1.11.1.7), and catalase (CAT, EC 1.11.1.6). Each leaf subsample (0.1 g each) was ground in 1 mL of 10 mM PBS buffer (pH = 7.4) using a freeze grinder (JXFSTPRP-CL, Shanghai, China). Ground leaf tissue was centrifuged at 2500 rpm for 20 min at 25 °C and the supernatant was used for subsequent determination of SA and ROS contents. Leaf fragments (0.1 g) of another subsample were ground in 1 mL extracting solution provided in the kit using the freeze grinder and, after homogenization, the tubes were centrifuged at 10,000 rpm for 10 min at 4 °C. The supernatant was used for determination of APX, SOD, POD, and CAT activities. ROS and SA contents were determined by sandwich ELISA and optical density was measured at 450 nm using a

TABLE 1 Rating of leaf scald symptoms on a sugarcane stalk.

Score	Code	Symptoms
0	AP	None (Asymptomatic plant)
1	FL	One or two white pencil lines on the foliage (Few lines)
2	ML	More than two white pencil lines on the foliage (Many lines)
3	CB	Leaf chlorosis, bleaching, or yellowing
4	LN	Leaf necrosis
5	PD	Stalk/Plant death

spectrophotometer, as per instructions of the corresponding kits (Beijing Solarbio Science & Technology Co., Ltd. China). ROS and SA concentrations were determined by comparison of OD values of each subsample with the standard curves. Following instructions of the extraction kits (Beijing Solarbio Science & Technology Co., Ltd. China), a spectrophotometric method was used to determine the activity of the four antioxidant enzymes at different visible wavelength, i.e., 240 nm (CAT), 290 nm (APX), 470 nm (POD), and 560 nm (SOD). The relative content or activity of each molecule was expressed as the ratio of values at 12 or 24 hpi versus values at 0 hpi. Five leaf subsamples were analyzed at each time point for each strain of the pathogen, and three technical replicates were performed per subsample.

2.9 Gene expression determined by qRT-PCR assay

Transcript expression of five genes was measured using a qRT-PCR assay with specific primer pairs (Table S2). These genes included the respiratory burst oxidase homolog gene (*ScRboh*) coding for the key enzyme in ROS production, and four SA signaling pathway related genes: *ScNPR3* (nonexpresser of pathogenesis-related gene 3), *ScTGA4* (encoding a TGA transcription factor), and *ScPR1* and *ScPR5* coding respectively for pathogenesis-related proteins PR1 and PR5. Total RNA was extracted from leaf subsamples and cDNA was synthesized by reverse transcription as previously described (Chu et al., 2020). The SYBR green dye method was used for qRT-PCR amplification with the QuantStudio 3 fluorescence quantitative PCR system (Applied Biosystems, USA). The qPCR mix contained 10.0 µL 2× ChamQ Universal SYBR qPCR Master Mix, 0.4 µL of each primer (10 µmol/µL), 1.0 µL cDNA (100 ng/µL), and 9.2 µL sterile high purity water. The amplification program was as follows: denaturation at 95 °C for 30 s, followed by 40 cycles at 95 °C for 10 s, and 60 °C for 30 s. The glyceraldehyde 3-phosphate dehydrogenase (*ScGAPDH*) gene was used as a reference gene, and the $2^{-\triangle\triangle CT}$ method was implemented to calculate relative gene expression. Three leaf subsamples were assayed at each time point for each strain of the pathogen, and three technical replicates were performed per subsample.

2.10 Statistical analysis

Data sets were compared by variance analysis (ANOVA) and Duncan's test was used to identify mean differences at $p < 0.05$. All analyses were conducted using SPSS version 18.0 software (IBM, China).

3 Results

3.1 Molecular genotyping of worldwide strains of *X. albilineans* by MLSA

In a phylogenetic tree constructed with the concatenated sequences of four housekeeping genes, 54 strains of *X. albilineans* (this study = 40, and NCBI library = 14) were distributed in three major phylogenetic clades (Figure 1). Clade I contained a first sub-clade formed by 27 strains (including Xa-FJ1) from different provinces in China, one strain from USA/Florida (XAFL07-1), MTQ032 from Martinique, and three strains from Guadeloupe (GPE PC86, GPE PC73, and GPE PC17). The five strains from the USA and the Caribbean islands all belonged to PFGE group B. A second sub-clade of clade I was formed by a single strain (REU174) of PFGE group D. The last sub-clade of clade I contained only strain LKA070 representing PFGE group G. Clade II included three strains representing PFGE groups C (HVO082), F (HVO005), and J (REU209), and these strains were located on two different branches supported by a 100% bootstrap value.

Clade III was formed by two sub-groups supported by a 100% bootstrap value (Figure 1). The first one included two strains from Florida (USA048 and Xa23R1) belonging to PFGE group A, one strain from Papua New Guinea (PNG130) representing PFGE group H, and one from Fiji (FIJ080) belonging to PFGE group E. The second sub-clade of clade II contained 13 strains that were all from the city of Ruian in the Zhejiang province of China. This group of strains was named the Xa-RA group as it was not associated with any strain representing a PFGE group of *X. albilineans*.

3.2 Genetic diversity analysis among strains of *X. albilineans* from China using SSR markers

Fifteen primer pairs of SSR markers each amplified 1-12 loci for a total of 81 amplified loci present in the genome of the 40 strains of *X. albilineans* from China (Table S3). Among the 15 markers, 10 were highly polymorphic as their PIC value was > 0.50. Four markers were moderately polymorphic ($0.25 \leq PIC \leq 0.50$) and one showed no polymorphism (PIC = 0). The 40 strains of *X. albilineans* were distributed in three clades of an UPGMA phylogenetic tree, namely SSR-CN1, SSR-CN2, and SSR-CN3 (Figure 2). Clade SSR-CN1 included 23 strains from six provinces (Fujian, Guangdong, Guangxi, Guizhou, Hainan, and Zhejiang). All these strains were associated to strains of *X. albilineans* from other countries belonging to PFGE group B (Figure 1 and section 3.1). Clade SSR-CN2 was formed by three

10.3389/fpls.2022.1087525

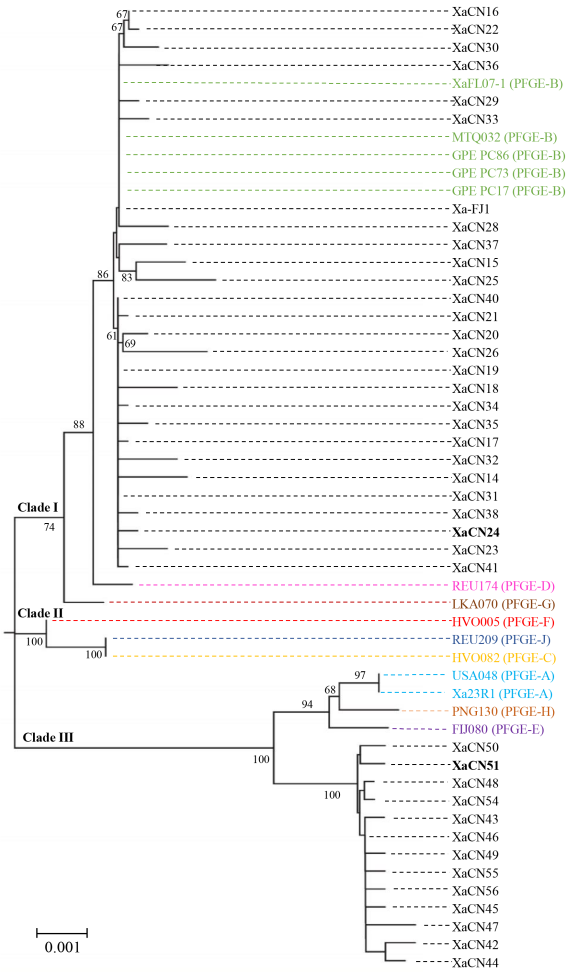

FIGURE 1
Neighbor-joining phylogenetic tree constructed with the concatenated sequence (4,165 nucleotides) of four housekeeping genes of 54 strains of *Xanthomonas albilineans* (40 from China and 14 from other geographical locations). Bootstrap values were determined for 1,000 replications and only bootstrap values >60% are shown at nodes. Strains XaCN24 and XaCN51 used for molecular investigations *in planta* are in bold. Strains from different pulsed-field gel electrophoresis (PFGE) groups (A-H, and -J) are written with different colors.

strains (XaCN32, XaCN33, and XaCN34) from Wenling city in the Zhejiang province. These strains were also associated with foreign strains of PFGE group B based on MLSA. Clade SSR-CN3 consisted of 14 strains from the Zhejiang province. One of these 14 strains (XaCN31 from Wenling city) was associated to foreign strains of PFGE group B whereas the remaining 13 strains (from Ruian city) belonged to the Xa-RA group previously identified by MLSA.

3.3 Pathogenicity variation among strains of *X. albilineans*

The 40 strains of *X. albilineans* from China were inoculated into sugarcane variety GT58 and DS regularly increased from 7-28 dpi (Figure S2). At 28 dpi, mean DS varied between 30.2% (strain XaCN24) and 78.0% (strain XaCN51), revealing significant differences in pathogenicity among the strains of *X. albilineans* from China. The 40 stains of the pathogen were also distributed into three pathogenicity groups after a clustering analysis based on DS at 28 dpi (Figure S3). DS of the strains in the low pathogenicity group varied from 30.2-49.6%, from 47.3-64.2% in the medium group, and from 55.0-78.0% in the high pathogenicity group (Table 2).

3.4 Bacterial population densities in sugarcane after inoculation with *X. albilineans*

Two strains of *X. albilineans* belonging to different evolutionary groups and differing in pathogenicity were used to investigate variation in population densities of the pathogen and sugarcane

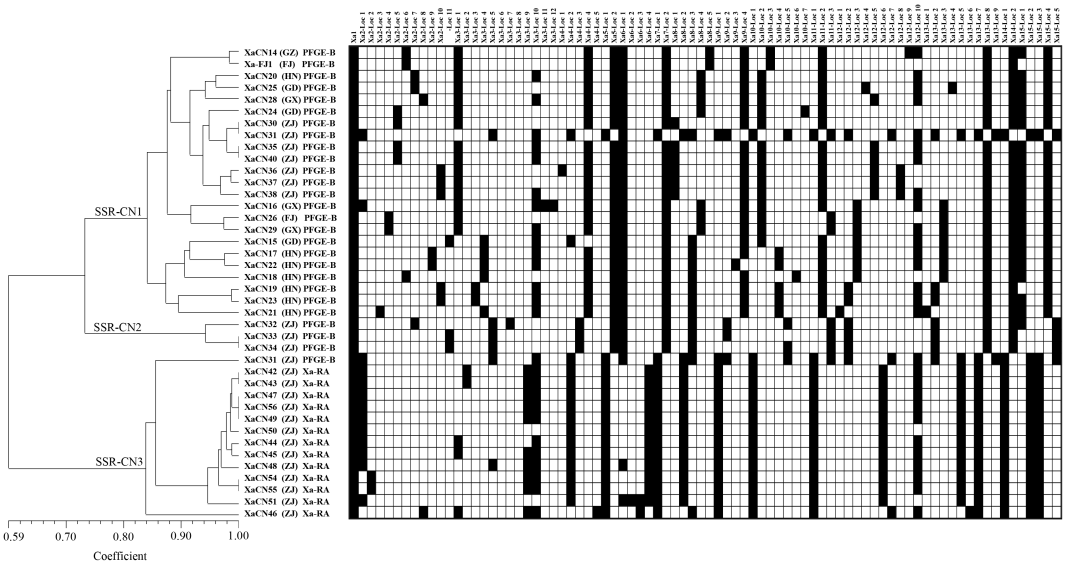

FIGURE 2
UPGMA phylogenetic tree of 40 strains of *Xanthomonas albilineans* from China based on 15 SSR marker loci (model = Maximum Composite Likelihood).

response mechanisms: strain XaCN24 (associated to group PFGE-B) with low pathogenicity and strain XaCN51 (Xa-RA group) with high pathogenicity. As determined by qPCR, mean bacterial population densities of the two strains were not significantly different in the leaves at 12 hpi (Figure 3). Leaf bacterial densities of XaCN51 increased from 1.45 x 10^4 genome copies (GC)/µL at 12 hpi to 2.59 x 10^4 GC/µL at 24 hpi. Population densities of XaCN24 were 9.12×10^3 and 8.63×10^3 GC/µL at 12 and 24 hpi, respectively.

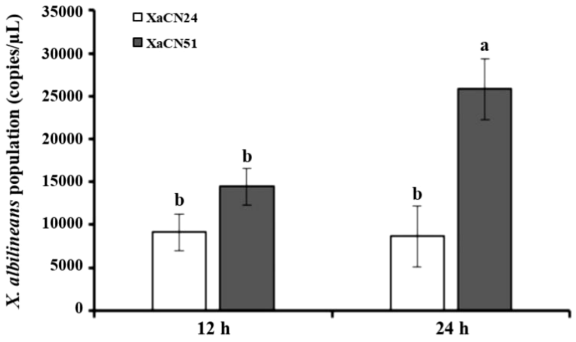

FIGURE 3
Population densities of two strains of *Xanthomonas albilineans* (XaCN24 and XaCN51) expressed as the number of genome copies determined by qPCR. Each vertical bar represents the mean ± standard deviation of three leaf subsamples collected 12 and 24 hours after inoculation and three technical replicates per subsample. Each leaf subsample is issued from a pooled sample of fragments collected from 35 inoculated leaves. Means with the same letter are not significantly different at $P = 0.05$ according to Duncan's test.

At 24 hpi, population densities of XaCN51 were significantly 3-fold higher than those of XaCN24.

3.5 Antioxidant capacity in sugarcane inoculated with *X. albilineans*

The dynamic changes of antioxidant capacity of enzymes APX, POD, SOD, and CAT were measured in sugarcane plants inoculated with strains XaCN24 and XaCN51. At 12 and 24h hpi, the relative activities of APX and POD were similar for both strains of the pathogen (Figure 4). For each enzyme and each bacterial strain, no significant increase or decrease of activity was observed from 12 to 24 hpi either. The relative activity of SOD in sugarcane inoculated with XaCN51 significantly increased 2.5 times from 12 to 24 hpi. In contrast, the relative activity of SOD in sugarcane inoculated with XaCN24 was not significantly different between 12 and 24 hpi (although a trend towards activity reduction was observed between the two time points). Relative activity of SOD was also higher as compared to APX and POD, regardless of inoculated strain and time point. The relative activity of CAT in sugarcane inoculated with each of the two strains was reduced from 12 to 24 hpi but was not significantly different between the two strains at each time point.

3.6 ROS content and *ScRboh* gene expression in sugarcane after inoculation with *X. albilineans*

The relative level of ROS production was 18% lower in sugarcane leaves from 12 to 24 hpi with strain XaCN24 of *X. albilineans*. This

TABLE 2 Distribution of 40 strains of *Xanthomonas albilineans* in different pathogenicity groups based on disease severity of sugarcane stalks 28 days post inoculation.

Pathogenicity group	Strain (Putative PFGE or other group)[a]	Number of strains	Disease severity (%)[b]	Mean ± SD[c]
Low	XaCN56 (Xa-RA), XaCN43 (Xa-RA), XaCN31 (PFGE-B), XaCN26 (PFGE-B), **XaCN24 (PFGE-B)**, XaCN20 (PFGE-B), XaCN16 (PFGE-B), XaCN14 (PFGE-B)	8	30.2–49.6	42.4 ± 5.8 a
Medium	Xa-FJ1 (PFGE-B), XaCN50 (Xa-RA), XaCN49 (Xa-RA), XaCN48 (PFGE-A), XaCN47 (PFGE-A), XaCN44 (Xa-RA), XaCN40 (PFGE-B), XaCN33 (PFGE-B), XaCN25 (PFGE-B), XaCN17 (PFGE-B), XaCN42 (Xa-RA), XaCN38 (PFGE-B)	12	47.3–64.2	55.0 ± 4.5 b
High	**XaCN51 (Xa-RA)**, XaCN30 (PFGE-B), XaCN23 (PFGE-B), XaCN22 (PFGE-B), XaCN15 (PFGE-B), XaCN36 (PFGE-B), XaCN54 (Xa-RA), XaCN46 (Xa-RA), XaCN55 (Xa-RA), XaCN19 (PFGE-B), XaCN45 (Xa-RA), XaCN35 (PFGE-B), XaCN32 (PFGE-B), XaCN21 (PFGE-B), XaCN34 (PFGE-B), XaCN37 (PFGE-B), XaCN18(PFGE-B), XaCN28 (PFGE-B), XaCN29 (PFGE-B), XaCN41 (PFGE-B)	20	55.0–78.0	66.3 ± 5.6 c

a Putative pulse-field gel electrophoresis (PFGE) group or other groups as determined in Figure 1. Strains in bold were used in this study for molecular investigations *in planta*.
b Minimum and maximum mean disease severity within a pathogenicity group.
c Mean and standard deviation (SD) were calculated with 105 plants inoculated per strain of *X. albilineans*. Means followed by the same letter are not significantly different at $P = 0.05$ according to Duncan's test.

level was not different between the two time points after inoculation with strain XaCN51 (Figure 5). The transcript level of gene *ScRboh*, which acts as a key enzyme in ROS production, was not significantly different between 12 and 24 hpi with strain XaCN24 of *X. albilineans* (Figure 5). After infection with XaCN51, the transcript level of *ScRboh* in sugarcane leaves increased by 60% from 12 to 24 hpi. At 24 hpi, expression level of *ScRboh* was also higher in leaves infected with XaCN51 than in leaves infected with XaCN24.

3.7 Endogenous SA level and SA-mediated gene expression in sugarcane infected by *X. albilineans*

The relative SA content in leaves inoculated with XaCN51 was not different at 12 and 24 hpi (Figure 6). In contrast, this content increased from 12 to 24 hpi by 26% in leaves inoculated with XaCN24. At 24 hpi, the relative SA content was also higher

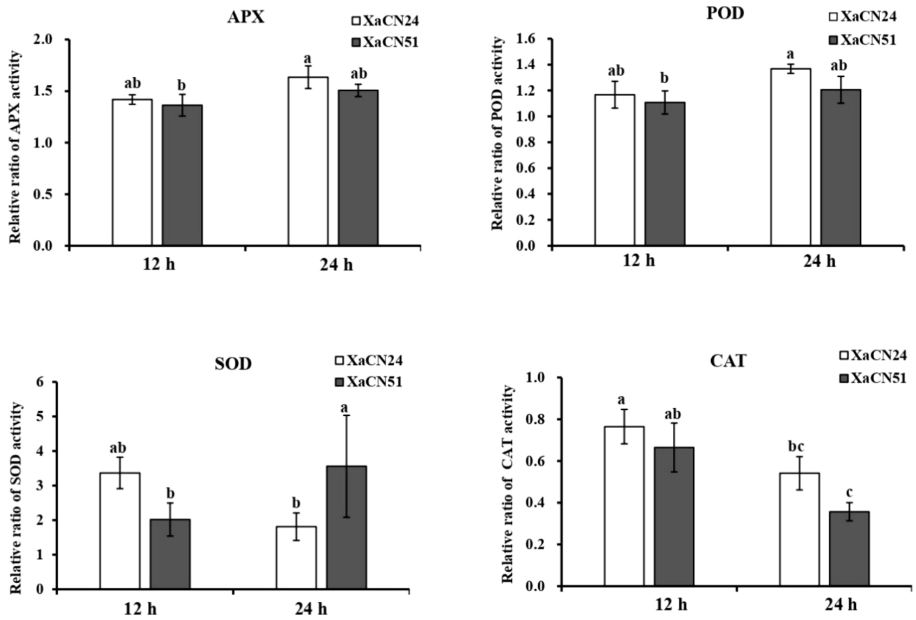

FIGURE 4
Changes of relative ratio of antioxidant enzyme activity in sugarcane leaves inoculated with two strains of *Xanthomonas albilineans* (XaCN24 and XaCN51). APX, ascorbate peroxidase; POD, peroxidase; SOD, peroxidase, and CAT, catalase. Each vertical bar represents the mean ± standard deviation of five leaf subsamples collected 12 and 24 hours after inoculation and three technical replicates per subsample. Each leaf subsample is issued from a pooled sample of fragments collected from 35 inoculated leaves. Means with the same letter are not significantly different at $P = 0.05$ according to Duncan's test.

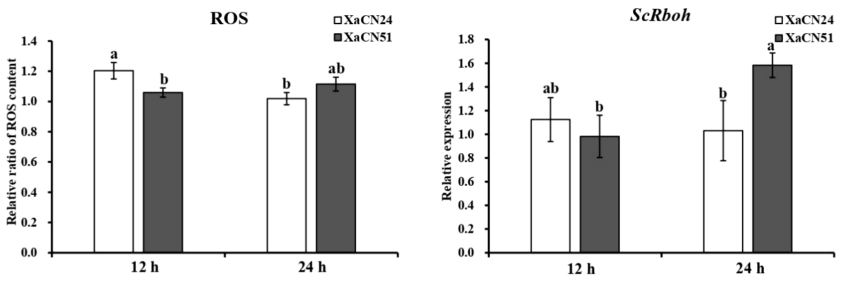

FIGURE 5
Changes of relative ratio of reactive oxygen species (ROS) content and relative expression of gene *ScRboh* gene in sugarcane leaves inoculated with two strains of *Xanthomonas albilineans* (XaCN24 and XaCN51). Each vertical bar represents the mean ± standard deviation of five (ROS) or three (*ScRboh*) leaf subsamples collected 12 and 24 hours after inoculation and three technical replicates per subsample. Each leaf subsample is issued from a pooled sample of fragments collected from 35 inoculated leaves. Means with the same letter are not significantly different at P = 0.05 according to Duncan's test.

in leaves infected with XaCN24 as compared to leaves infected with XaCN51.

In sugarcane leaves inoculated with *X. albilineans* XaCN24, the transcript level of SA-mediated genes *ScPR-1* and *ScPR-5* increased by 176 and 75% from 12 to 24 hpi, respectively (Figure 7). The transcript level of two additional SA-mediated genes (*ScNPR3* and *ScTGA4*) was not significantly different between the two time points, although a trend towards increase was observed.

After inoculation with *X. albilineans* XaCN51, the transcript level of genes *ScNPR-3*, *ScTGA4*, and *ScPR-5* decreased in sugarcane leaves by 50, 33, and 60% from 12 to 24 hpi, respectively (Figure 7). The transcript level of *ScPR1* was not significantly different between the two time points. At 24 hpi, the expression level of *ScNPR-3, ScPR-1*, and *ScPR5* was 280, 300, and 220% higher in leaves infected with XaCN24 than in leaves infected by XaCN51.

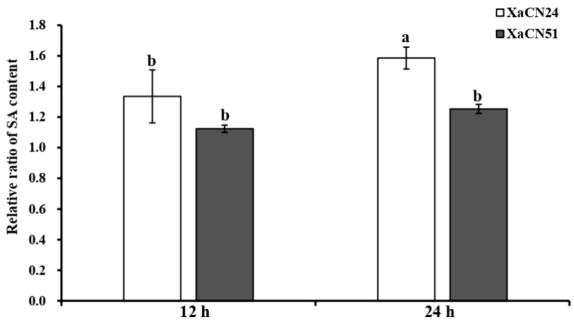

FIGURE 6
Changes of relative ratio of salicylic acid (SA) content in sugarcane leaves inoculated with two strains of *Xanthomonas albilineans* (XaCN24 and XaCN51). Each vertical bar represents the mean ± standard deviation of five leaf subsamples collected 12 and 24 hours after inoculation and three technical replicates per subsample. Each leaf subsample is issued from a pooled sample of fragments collected from 35 inoculated leaves. Means with the same letter are not significantly different at P = 0.05 according to Duncan's test.

4 Discussion

Leaf scald occurs in most sugarcane-producing countries including China, which poses a threat to the worldwide sugarcane industry (Ricaud & Ryan, 1989; Rott & Davis, 2000; Meng et al., 2019). The genetic diversity of *X. albilineans* has been investigated using strains from various geographical locations (Alvarez et al., 1996; Davis et al., 1997; Champoiseau et al., 2006a; Meng et al., 2019; Cervantes-Romero et al., 2021). In China, sugarcane is mainly grown in the south, the east, and the west-south parts of the country where the ecological environments and climates are differing, thus contributing to the diversity of plant pathogenic bacteria. Up to now, only *X. albilineans* strains clustering with foreign strains of PFGE group B were reported in China (Zhang et al., 2017; Ntambo et al., 2019b). Nevertheless, recent observations suggested that other phylogenetic groups of *X. albilineans* occur in China (Duan et al., 2021).

In this study, presence in China of previously unreported strains belonging to a putatively new phylogenetic group (Xa-RA) was identified using MLSA and SSR markers. This group of strains (XaCN42-XaCHN51 and XaCN54-56) was collected from a specific chewing cane (Taoshanguozhe) that is an ancient clone of *S. officinarum* planted in the city of Ruian (Zhejiang province). This specific association of Xa-RA strains to a single host may suggest specific evolutionary driving forces for this group of strains. Additional investigations are needed to determine if the Xa-RA group of strains is unique to China or if it is connected to other strains in the world. Our study included sequences of strains representing all PFGE groups with the exception of PFGE group I (Martinique) that is not available in GenBank.

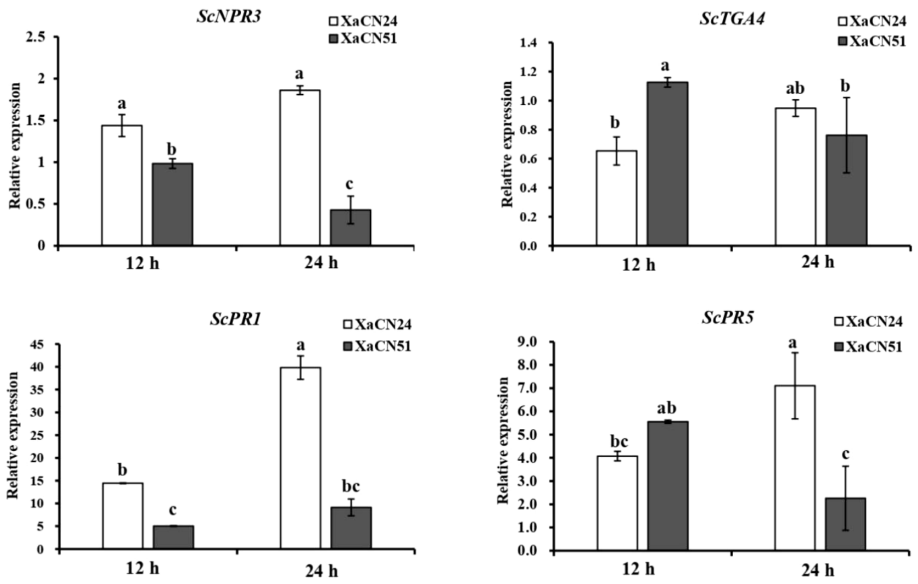

FIGURE 7
Expression pattern of salicylic acid (SA) signaling pathway related genes in sugarcane leaves inoculated with two strains of *Xanthomonas albilineans* (XaCN24 and XaCN51). Each vertical bar represents the mean ± standard deviation of three leaf subsamples collected 12 and 24 hours after inoculation and three technical replicates per subsample. Each leaf subsample is issued from a pooled sample of fragments collected from 35 inoculated leaves. Means with the same letter are not significantly different at $P = 0.05$ according to Duncan's test.

Besides genetic diversity, variation in pathogenicity also occurs among strains of *X. albilineans* from different countries or within the same geographical location (Mohamed et al., 1996; Champoiseau et al., 2006b; Tardiani et al., 2014; Wu et al., 2022). Resistance of sugarcane to leaf scald is closely associated with limited colonization of the host plant by the pathogen (Rott et al., 1994a; Rott et al., 1997; Garces et al., 2014). Consequently, disease severity and pathogen populations are lower in plants infected by low pathogenic strains of *X. albilineans* than in plants infected by high pathogenic strains (Mohamed et al., 1996). In our study, strains of *X. albilineans* varied from low to highly pathogenic and this variation was observed within and among sugarcane-producing provinces, and even within growing areas. No correlation was observed between the phylogenetic grouping and variation in pathogenicity of these strains, which confirms observations previously reported for *X. albilineans* (Champoiseau et al., 2006b; Tardiani et al., 2014) but also for other bacterial pathogens such as *X. citri* pv. *malvacearum* causing angular leaf spot and leaf blight of cotton (Kumar et al., 2018) and *Acidovorax avenae* subsp. *avenae* causing red stripe of sugarcane (Bertani et al., 2021).

Species of the genus *Xanthomonas* usually possess a Hypersensitive response and pathogenicity (Hrp) type III secretion system (Hrp-T3SS) that plays a critical role in inhibition of host defenses (Rossier et al., 1999; White et al., 2009). This secretion system allows Gram-negative plant pathogenic bacteria to inject bacterial effector proteins into the cytoplasm of the plant cell and thus participate in adaptation of a pathogen to its host (Büttner and Bonas, 2010; Timilsina et al., 2020). The sugarcane leaf scald pathogen, *X. albilineans*, does not possess this Hrp-T3SS and needs to rely on other secretion systems to interact with the proteins of the sugarcane host (Pieretti et al., 2009 and Pieretti et al., 2012; Zhang et al., 2020). These specific molecular interactions remain to be investigated, including among strains of the pathogen differing in pathogenicity.

The ROS, especially RBOH-dependent ROS, is a critical and effective component of plant disease resistance (Vidhyasekaran, 2014; Chen and Yang, 2020; Mittler et al., 2022). Overexpression of *GbRboh5/18* in *Gossypium barbadense* enhanced plant resistance to *Verticillium dahliae* by accumulation of ROS (Chang et al., 2020). Similarly, transcript levels of most *MeRboh* genes from cassava were increased following infection with *X. axonopodis* pv. *manihotis* (Huang et al., 2021). Genes *MeRbohB* and *MeRbohF* overexpressed in *Arabidopsis* also enhanced plant resistance to *Pseudomonas syringae* pv. tomato DC3000, most likely *via* the H_2O_2 signal transduction pathway and ROS generation (Huang et al., 2021). In our study, ROS production did not significantly change between 12 and 24 hpi but expression of Sc*Rboh* increased between these two time points in sugarcane leaves infected with the most pathogenic strain of *X. albilineans* (Xa-CN51). This suggested that ROS was also involved in response to *X. albilineans*. Additional time points after sugarcane inoculation need to be studied for better

characterization of this defense mechanism, especially in varieties resistant to leaf scald.

Various antioxidants (non-enzymatic metabolites) and ROS scavenging enzymes such as SOD, CAT, POD, and APX are involved in scavenging H_2O_2 in plant cells (Afzal et al., 2014; Li and Ma, 2021). In our study, no significant changes were observed for the relative activities of POD and APX while the SOD activity increased between 12 and 24 hpi in sugarcane leaves infected with *X. albilineans* Xa-CN51 (the high pathogenic strain) but not with CXaCN24 (the low pathogenic strain). CAT activity decreased in leaves infected with Xa-CN51 and XaCN24 between 12 and 24 hpi, thus suggesting that SOD and CAT enzymes play important roles in sugarcane defense to infection by *X. albilineans*. Antioxidants SOD and CAT are crucial factors to modulate ROS scavenging and increased antioxidant activity is usually considered as a marker of reduced production and accumulation of H_2O_2 (Hong et al., 2021).

SOD or superoxide dismutase is a primary enzyme in the defense system against oxidative stress. SOD catalyzes the dismutation of superoxide anion ($O_2^{\bullet-}$) to hydrogen peroxidase (H_2O_2) and molecular oxygen (O_2), while CAT catalyzes the dismutation of H_2O_2 into water (H_2O) and O_2 (Manna et al., 2019; Li and Ma, 2021). Antioxidant effects of SOD and CAT enzymes are directly linked during conversion of superoxide to H_2O_2 and H_2O_2 to H_2O and O_2 (Xu et al., 2013). Usually, increased production of SOD and CAT corresponds to augmented tolerance of plants against adverse oxidative stresses (Xu et al., 2013; Suman et al., 2021). Rice mutants of gene *osnramp1* (natural resistance-associated macrophage proteins) had an increased SOD activity and H_2O_2 content but a decreased activity of CAT after infection by *X. oryzae* pv. *oryzicola*, *Magnaporthe oryzae*, and *Ustilaginoidea virens* (Chu et al., 2022a). This contributed to enhanced broad-spectrum resistance of rice against bacterial and fungal pathogens.

A similar response was found herein for sugarcane in response to infection by *X. albilineans*, especially in sugarcane infected by highly pathogenic strain XaCN51. Sugarcane variety GT58 susceptible to leaf scald appeared to regulate ROS homoeostasis by upregulating *ScRboh* expression (contributing to ROS production) and enhancing H_2O_2 production (elevating SOD and decreasing CAT activities) during early host-pathogen interaction. Notably, excessive ROS production triggers an oxidative stress response, cellular damage, and cell death (Manna et al., 2019). Furthermore, excess of H_2O_2 causes chloroplast and peroxisome autophagy and programmed cell death (Smirnoff and Arnaud, 2019). Increased H_2O_2 altering ROS homoeostasis may result in increased susceptibility of sugarcane to *X. albilineans*. On the other hand, this pathogen (especially strain Xa-CN51) may be tolerant to high concentrations of H_2O_2. In barley, H_2O_2 levels were higher in inoculated leaves of a susceptible variety than in a more resistant one during later stages of Ramularia leaf spot. The causal agent of this disease, *Ramularia collo-cygni*, was also able to grow *in vitro* on media containing relatively high concentrations of H_2O_2 (McGrann and Brown, 2018).

Among phytohormones, SA is involved in the hypersensitive response (HR) and systemic acquired resistance (SAR) of plants. Consequently, SA plays a critical role in plant defense against biotrophic and semi-biotrophic pathogens (Yang et al., 2015; Peng et al., 2021). Accumulated SA activates SA-signaling pathways to induce the expression of defense-related genes such as PR1 and PR5 (Chu et al., 2022b). To achieve successful infection of a plant, pathogenic organisms have evolved three main strategies to disrupt SA-mediated defense genes: i/disruption of SA biosynthesis by targeting the isochorismate synthase I pathway, ii/reduction of SA accumulation by conversion of SA into its inactive derivatives, and iii/various mechanisms to interfere with SA downstream signaling (Qi et al., 2018). An effector produced by *Ralstonia solanacearum*, causing wilt of arabidopsis (*Arabidopsis thaliana*) and tomato (*Solanum lycopersicum*), disrupts SA signaling by inhibiting TGA activity to establish successful infections (Qi et al., 2022). In our study, the highly pathogenic strain of *X. albilineans* was associated with low levels of endogenous SA and reduced expression of genes involved in the SA pathway as compared to the low pathogenic strain. Similarly, expression of SA-mediated sugarcane defense genes *PR1* and *PR5* was reduced after infection with XaCN51 whereas expression of these two genes was upregulated in response to the low pathogenic strain of *X. albilineans*. This is evidence for involvement of these genes and SA in resistance of sugarcane to leaf scald.

The nonexpressor of pathogenesis-related gene 1 (NPR1) protein is an SA receptor of the plant that promotes SA-induced defense gene expression (Backer et al., 2019; Chen et al., 2021). However, when endogenous concentrations of SA are low, NPR3/4 (paralogs of NPR1) inhibit the expression of genes downstream of the SA signal transduction pathway (Ding and Ding, 2020; Peng et al., 2021). SA also regulates ROS homeostasis and the antioxidant defense system, both at physiological and molecular levels (Saleem et al., 2021). In *Nicotiana benthamiana*, both local and systemic resistances to tobacco mosaic virus were differentially modulated by SA and ROS under glutathione mediation (Zhu et al., 2021). Lower levels of SA in sugarcane infected by the highly pathogenic strain of *X. albilineans* may therefore also inhibit expression of sugarcane genes involved in resistance to leaf scald. Molecular cross talks between the SA and ROS signals during the sugarcane and *X. albilineans* interactions remain to be further investigated.

5 Conclusion

We demonstrated for the first time in this study that at least two phylogenetic groups of *X. albilineans* were present in

sugarcane-producing regions of China. Forty strains of *X. albilineans* were distributed into three pathogenicity groups (i.e. low, medium, and high) after inoculation of a sugarcane variety susceptible to leaf scald. Based on qPCR data, population densities of highly pathogenic strain XaCN51 were higher in infected leaves than population densities of low pathogenic strain XaCN24. ROS production and the antioxidant defense system, as well as SA generation and SA-mediated genes (*ScNPR3*, *ScTGA4*, *ScPR1*, and *ScPR5*), participated in the response of sugarcane to infection by *X. albilineans*. Preformation and gene expression of these stress-related signal molecules differed according to the two strains of the pathogen varying in pathogenicity. This foundation work should be useful for further research on the defense mechanisms of sugarcane in response to an attack of *X. albilineans* and possibly other pathogens.

Data availability statement

The original contributions presented in the study are publicly available. This data can be found in the text.

Author contributions

Conceptualization, J-YZ and S-JG. Writing—original draft preparation, J-YZ and YS. Writing—review and editing, PR and S-JG. Data curation, JC and YS. Experiments preformation, JC, YS, H-YF, and M-TH. Supervision, funding acquisition, and project administration, S-JG. All authors contributed to the article and approved the submitted version.

Funding

This work was supported by the earmarked fund for China Agriculture Research System (grant no. CARS-170302).

Acknowledgments

We sincerely thank Ms. Chun-Yu Hu and Rui-Min Si for their technical help.

Conflict of interest

The authors declare that the research was conducted in the absence of any commercial or financial relationships that could be construed as a potential conflict of interest.

Publisher's note

Supplementary material

The Supplementary Material for this article can be found online at: https://www.frontiersin.org/articles/10.3389/fpls.2022.1087525/full#supplementary-material

References

Afzal, F., Khurshid, R., Ashraf, M., and Kazi, A. G. (2014). "Eactive oxygen species and antioxidants in response to pathogens and wounding," in *Oxidative damage to plants*. Ed. P. Ahmad (London: Academic Press), 397–424. doi: 10.1016/B978-0-12-799963-0.00013-7

Ali, A., Chu, N., Ma, P., Javed, T., Zaheer, U., Huang, M. T., et al. (2021). Genome-wide analysis of mitogen-activated protein (MAP) kinase gene family expression in response to biotic and abiotic stresses in sugarcane. *Physiol. Plant* 171, 86–107. doi: 10.1111/ppl.13208

Alvarez, A., Schenck, S., and Benedict, A. (1996). Differentiation of *Xanthomonas albilineans* strains with monoclonal antibody reaction patterns and DNA fingerprints. *Plant Pathol.* 45 (2), 358–366. doi: 10.1046/j.1365-3059.1996.d01-118.x

Backer, R., Naidoo, S., and Van den Berg, N. (2019). The nonexpressor of pathogenesis-related genes 1 (NPR1) and related family: mechanistic insights in plant disease resistance. *Front. Plant Sci.* 10. doi: 10.3389/fpls.2019.00102

Bertani, R. P., Perera, M. F., Joya, C. M., Henriquez, D. D., Funes, C., Chaves, S., et al. (2021). Genetic diversity and population structure of *Acidovorax avenae* subsp. *avenae* isolated from sugarcane in Argentina. *Plant Pathol.* 70, 1719–1732. doi: 10.1111/ppa.13413

Birch, R. G. (2001). *Xanthomonas albilineans* and the antipathogenesis approach to disease control. *Mol. Plant Pathol.* 2 (1), 1–11. doi: 10.1046/j.1364-3703.2001.00046.x

Birch, R. G., and Patil, S. S. (1987a). Correlation between albicidin production and chlorosis induction by *Xanthomonas albilineans*, the sugarcane leaf scald pathogen. *Physiol. Mol. Plant Pathol.* 30 (2), 199–206. doi: 10.1016/0885-5765(87)90033-6

Birch, R. G., and Patil, S. S. (1987b). Evidence that an albicidin-like phytotoxin induces chlorosis in sugarcane leaf scald disease by blocking plastid DNA replication. *Physiol. Mol. Plant Pathol.* 30, 207–214. doi: 10.1016/0885-5765(87)90034-8

Büttner, D., and Bonas, U. (2010). Regulation and secretion of *Xanthomonas* virulence factors. *FEMS Microbiol. Rev.* 34 (2), 107–133. doi: 10.1111/j.1574-6976.2009.00192.x

Cervantes-Romero, B., Pérez-Rodríguez, P., Rott, P., Valdez-Balero, A., and Silva-Rojas, H. V. (2021). Distribution, phylogeny, and pathogenicity of *Xanthomonas albilineans* causing sugarcane leaf scald in Mexico. *Crop Prot.* 150, 105799. doi: 10.1016/j.cropro.2021.105799

Champoiseau, P., Daugrois, J. H., Girard, J. C., Royer, M., and Rott, P. C. (2006a). Variation in albicidin biosynthesis genes and in pathogenicity of *Xanthomonas albilineans*, the sugarcane leaf scald pathogen. *Phytopathology* 96, 33–45. doi: 10.1094/PHYTO-96-0033

Champoiseau, P., Daugrois, J. H., Pieretti, I., Cociancich, S., Royer, M., and Rott, P. (2006b). High variation in pathogenicity of genetically closely related strains of

Xanthomonas albilineans, the sugarcane leaf scald pathogen, in Guadeloupe. *Phytopathology* 96, 1081–1091. doi: 10.1094/PHYTO-96-1081

Chang, Y., Li, B., Shi, Q., Geng, R., Geng, S., Liu, J., et al. (2020). Comprehensive analysis of respiratory burst oxidase homologs (Rboh) gene family and function of GbRboh5/18 on verticillium wilt resistance in *Gossypium barbadense*. front. *Genet.* 11. doi: 10.3389/fgene.2020.00788

Chen, Q., and Yang, G. (2020). Signal function studies of ROS, especially RBOH-dependent ROS, in plant growth, development and environmental stress. *J. Plant Growth Regul.* 39 (1), 157–171. doi: 10.1007/s00344-019-09971-4

Chen, J., Zhang, J., Kong, M., Freeman, A., Chen, H., and Liu, F. (2021). More stories to tell: nonexpressor of pathogenesis-related genes1, a salicylic acid receptor. *Plant Cell Environ.* 44 (6), 1716–1727. doi: 10.1111/pce.14003

Chu, C., Huang, R., Liu, L., Tang, G., Xiao, J., Yoo, H., et al. (2022a). The rice heavy-metal transporter OsNRAMP1 regulates disease resistance by modulating ROS homoeostasis. *Plant Cell Environ.* 45 (4), 1109–1126. doi: 10.1111/pce.14263

Chu, N., Sun, H. D., Zhou, J. R., Fu, H. Y., Li, X. Y., and Gao, S. J. (2020). Research advances of sugarcane red stripe disease and its pathogeny biology. *Sugar Crops China* 42 (1), 66–70. doi: 10.13570/j.cnki.scc.01.012

Chu, N., Zhou, J. R., Rott, P., Li, J., Fu, H. Y., and Huang, M. T. (2022b). ScPR1 plays a positive role in the regulation of resistance to diverse stresses in sugarcane (Saccharum spp.) and arabidopsis thaliana. *Ind. Crops Prod.* 180, 114736. doi: 10.1016/j.indcrop.2022.114736

da Silva, L. C. C., Targino, B. N., Furtado, M. M., Pinto, M. A. O., and Rodarte, M. P. (2017). "Xanthan: Biotechnological production and applications," in *Microbial production of food ingredients and additives*. Eds. A. M. Holban and A. M. Grumezescu (London: Academic Press), 385–422. doi: 10.1016/B978-0-12-811520-6.00013-1

Davis, M. J., Rott, P., Baudin, P., and Dean, J. L. (1994). Evaluation of selective media and immunoassays for detection of *Xanthomonas albilineans*, causal agent of sugarcane leaf scald disease. *Plant Dis.* 78 (1), 78–82. doi: 10.1094/PD-78-0078

Davis, M. J., Rott, P., Warmuth, C., Warmuth, C. J., Chatenet, M., and Baudin, P. (1997). Intraspecific genomic variation within *Xanthomonas albilineans*, the sugarcane leaf scald pathogen. *Phytopathology* 87 (3), 316–324. doi: 10.1094/PHYTO.1997.87.3.316

Ding, P., and Ding, Y. (2020). Stories of salicylic acid: A plant defense hormone. *Trends Plant Sci.* 25 (6), 549–565. doi: 10.1016/j.tplants.2020.01.004

Duan, Y. Y., Zhang, Y. Q., Xu, Z., Lin, Y., and Mao, L. R. (2021). First report of *Xanthomonas albilineans* causing leaf scald on two chewing cane clones in zhejiang province, China. *Plant Dis.* 105 (2), 485–485. doi: 10.1094/PDIS-06-20-1312-PDN

Fleites, L. A., Mensi, I., Gargani, D., Zhang, S., Rott, P., and Gabriel, D. ,. W. (2013). *Xanthomonas albilineans* OmpA1 appears to be functionally modular and both the OMC and c-like domains are necessary for leaf scald disease of sugarcane. *Mol. Plant Microbe In.* 26 (10), 1200–1210. doi: 10.1094/MPMI-01-13-0002-R

Fu, H. Y., Zhang, T., Peng, W. J., Duan, Y. Y., Xu, Z. X., and Lin, Y. H. (2021). Identification of resistance to leaf scald in newly released sugarcane varieties at seedling stage by artificial inoculation. *Crop J.* 47 (8), 9–21. doi: 10.3724/SP.J.1006.2021.04203

Garces, F. F., Gutierrez, A., and Hoy, J. W. (2014). Detection and quantification of *Xanthomonas albilineans* by qPCR and potential characterization of sugarcane resistance to leaf scald. *Plant Dis.* 98, 121–126. doi: 10.1094/PDIS-04-13-0431-RE

Hong, D. K., Talha, J., Yao, Y., Zou, Z. Y., Fu, H. Y., and Gao, S. J. (2021). Silicon enhancement for endorsement of *Xanthomonas albilineans* infection in sugarcane. *Ecotoxicol. Environ. Saf.* 220, 112380. doi: 10.1016/j.ecoenv.2021.112380

Huang, S., Tang, Z., Zhao, R., Hong, Y., Zhu, S., Fan, R., et al. (2021). Genome-wide identification of cassava MeRboh genes and functional analysis in *Arabidopsis*. *Plant Physiol. Biochem.* 167, 296–308. doi: 10.1016/j.plaphy.2021.07.039

Huerta-Lara, M., Rojas-Martinez, R. I., Bautista-Calles, J., Reyes-Lopez, D., and Becerril-Herrera, M. (2009). Genetic and pathogenic diversity of *Xanthomonas albilineans* (Ashby) dowson, in Mexico. *Res. J. Biol. Sci.* 4 (3), 312–319. doi: rjbsci.2009.312.319

Jacques, M. A., Arlat, M., Boulanger, A., Boureau, T., Carrère, S., and Cesbron, S. (2016). Using ecology, physiology, and genomics to understand host specificity in *Xanthomonas*. *Annu. Rev. Phytopathol.* 54 (1), 163–187. doi: 10.1146/annurev-phyto-080615-100147

Javed, T., Zhou, J. R., Li, J., Hu, Z. T., Wang, Q. N., and Gao, S. J. (2022). Identification and expression profiling of WRKY family genes in sugarcane in response to bacterial pathogen infection and nitrogen implantation dosage. *Front. Plant Sci.* 13. doi: 10.3389/fpls.2022.917953

Kumar, A. S., Aiyanathan, K. E. A., Nakkeeran, S., and Manickam, S. (2018). Documentation of virulence and races of *Xanthomonas citri* pv. *Malvacearum* in India and its correlation with genetic diversity revealed by repetitive elements (REP, ERIC, and BOX) and ISSR markers. *3 Biotech.* 8 (11), 479. doi: 10.1007/s13205-018-1503-9

Li, Y., and Ma, Z. (2021). "Antioxidants and reactive oxygen species (ROS) scavenging enzymes," in *Research methods of environmental physiology in aquatic sciences*. Eds. K. Gao, D. A. Hutchins and J. Beardall (Singapore: Springer), 85–91. doi: 10.1007/978-981-15-5354-7_10

Lin, L. H., Ntambo, M. S., Rott, P. C., Wang, Q. N., Lin, Y. H., Fu, H. Y., et al. (2018). Molecular detection and prevalence of *Xanthomonas albilineans*, the causal agent of sugarcane leaf scald, in China. *Crop Prot.* 109, 17–23. doi: 10.1016/J.CROPRO.2018.02.027

Lopes, S. A., Damann, K. E., and Grelen, L. B. (2001). *Xanthomonas albilineans* diversity and identification based on rep-PCR fingerprints. *Curr. Microbiol.* 42 (3), 155–159. doi: 10.1007/s002840010196

Manna, M., Achary, V. M. M., and Reddy, M. K. (2019). "ROS signaling and its role in plants," in *Sensory biology of plants*. Ed. S. Sopory (Singapore: Springer). doi: 10.1007/978-981-13-8922-1_14

McGrann, G. R. D., and Brown, J. K. M. (2018). The role of reactive oxygen in the development of ramularia leaf spot disease in barley seedlings. *Ann. Bot.* 121 (3), 415–430. doi: 10.1093/aob/mcx170

Meng, J. Y., Ntambo, M. S., Rott, P. C., Fu, H. Y., Huang, M. T., and Zhang, H. L. (2020). Identification of differentially expressed proteins in sugarcane in response to infection by *Xanthomonas albilineans* using ITRAQ quantitative proteomics. *Microorganisms* 8 (1), 76. doi: 10.3390/microorganisms8010076

Meng, J. Y., Zhang, H. L., Lin, L. H., Huang, H. Y., and Gao, S. J. (2019). Research advances in sugarcane leaf scald disease and its causal agent *Xanthomonas albilineans*. *J. Plant Prot.* 46, 257–265. doi: 10.13802/j.cnki.zwbhxb.2019.2018092

Mensi, I., Daugrois, J. H., Pieretti, I., Gargani, D., Fleites, L. A., Noell, J., et al. (2016). Surface polysaccharides and quorum sensing are involved in the attachment and survival of *Xanthomonas albilineans* on sugarcane leaves. *Mol. Plant Pathol.* 17 (2), 236–246. doi: 10.1111/mpp.12276

Mielnichuk, N., Bianco, M. I., Yaryura, P. M., Bertani, R. P., Toum, L., Daglio, Y., et al. (2021). Virulence factors analysis of native isolates of *Xanthomonas albilineans* and *Xanthomonas sacchari* from tucumán, Argentina, reveals differences in pathogenic strategies. *Plant Pathol.* 70, 1072–1084. doi: 10.1111/ppa.13367

Mittler, R., Zandalinas, S. I., Fichman, Y., and Breusegem, F. (2022). Reactive oxygen species signalling in plant stress responses. *Nat. Rev. Mol. Cell Biol.* 23 (10), 663–679. doi: 10.1038/s41580-022-00499-2

Mohamed, I. S., Rott, P. C., Davis, M. J., and Chatenet, M. (1996). Differentiation of *Xanthomonas albilineans* strains based on multiplication of the pathogen in sugarcane varieties. *Proc. Int. Soc. Sugar Cane Technol.* 22, 486–492. doi: 10.1046/j.1365-3059.1996.d01-118.x

Ngou, B. P. M., Ding, P., and Jones, J. D. G. (2022). Thirty years of resistance: Zig-zag through the plant immune system. *Plant Cell.* 34 (5), 1447–1478. doi: 10.1093/plcell/koac041

Ntambo, M. S., Meng, J. Y., Rott, P. C., Henry, R. J., Zhang, H. L., and Gao, S. J. (2019a). Comparative transcriptome profiling of resistant and susceptible sugarcane cultivars in response to infection by *Xanthomonas albilineans*. *Intern. J. Mol. Sci.* 20 (24), 6138. doi: 10.3390/ijms20246138

Ntambo, M. S., Meng, J. Y., Rott, P. C., Royer, M., Lin, L. H., Zhang, H. L., et al. (2019b). Identification and characterization of *Xanthomonas albilineans* causing sugarcane leaf scald in China using multilocus sequence analysis. *Plant Pathol.* 68, 269–277. doi: 10.1111/ppa.12951

Peng, Y., Yang, J., Li, X., and Zhang, Y. (2021). Salicylic acid: Biosynthesis and signaling. *Annu. Rev. Plant Biol.* 72, 761–791. doi: 10.1146/annurev-arplant-081320-092855

Permaul, K., Pillay, D., and Pillay, B. (1996). Random-amplified polymorphic DNA (RAPD) analysis shows intraspecies differences among *Xanthomonas albilineans* strains. *Lett. Appl. Microbiol.* 23 (5), 307–311. doi: 10.1111/j.1472-765x.1996.tb00196.x

Persley, G. J. (1973). Pathogenic variation in *Xanthomonas albilineans* (Ashby) dowson, the causal agent of leaf-scald disease of sugar cane. *Aust. J. Biol. Sci.* 26, 781–786. doi: 10.1071/BI9730781

Pieretti, I., Royer, M., Barbe, V., Carrere, S., Koebnik, R., Couloux, A., et al. (2012). Genomic insights into strategies used by *Xanthomonas albilineans* with its reduced artillery to spread within sugarcane xylem vessels. *BMC Genomics* 13 (1), 1–23. doi: 10.1186/1471-2164-13-658

Pieretti, I., Royer, M., Barbe, V., Koebnik, R., Couloux, A., Cociancich, S., et al. (2009). The complete genome sequence of *Xanthomonas albilineans* provides new insights into the reductive genome evolution of the xylem-limited *Xanthomonadaceae*. *BMC Genomics* 10 (1), 1–15. doi: 10.1186/1471-2164-10-616

Qi, G., Chen, J., Chang, M., Chen, H., Hall, K., Korin, J., et al. (2018). Pandemonium breaks out: Disruption of salicylic acid-mediated defense by plant pathogens. *Mol. Plant* 11 (12), 1427–1439. doi: 10.1016/j.molp.2018.10.002

Qi, P., Huang, M., Hu, X., Zhang, Y., Wang, Y., Li, P., et al. (2022). A *Ralstonia solanacearum* effector targets TGA transcription factors to subvert salicylic acid signaling. *Plant Cell.* 34 (5), 1666–1683. doi: 10.1093/plcell/koac015

Ricaud, C., and Ryan, C. C. (1989). "Leaf scald," in *Diseases of sugarcane/Major diseases, diseases of sugarcane major diseases*. Eds. C. Ricaud, B. T. Egan, A. G.

Gillaspie Jr. and C. G. Hughes (Amsterdam: Elsevier Science Publisher), 39–58. doi: 10.1016/B978-0-444-42797-7.50006-5

Rossier, O., Wengelnik, K., Hahn, K., and ULLA, B. (1999). The *Xanthomonas* hrp type III system secretes proteins from plant and mammalian bacterial pathogens. *Proc. Nat. Acad. Sci. U.S.A.* 96 (16), 9368–9373. doi: 10.1073/pnas.96.16.9368

Rott, P., Abel, M., and Soupa, D. (1994a). Population dynamics of *Xanthomonas albilineans* in sugarcane plants as determined with an antibiotic-resistant mutant. *Plant Dis.* 78 (3), 241–247. doi: 10.1094/PD-78-0241

Rott, P., Arnaud, M., and Baudin, P. (1986). Serological and lysotypical variability of *Xanthomonas albilineans* (Ashby) dowson, causal agent of sugarcane leaf scald disease. *J. Phytopathol.* 116 (3), 201–211. doi: 10.1111/j.1439-0434.1986.tb00912.x

Rott, P., and Davis, M. J. (2000). "Leaf scald," in *A guide to sugarcane diseases*. Eds. P. Rott, R. A. Bailey, J. C. Comstock, B. J. Croft and A. S. Saumtally (Montpellier, France: CIRAD/ISSCT, La Librairie du Cirad), 38–44.

Rott, P., Davis, M. J., and Baudin, P. (1994b). Serological variability in *Xanthomonas albilineans*, causal agent of leaf scald disease of sugarcane. *Plant Pathol.* 43, 344–349. doi: 10.1111/j.1365-3059.1994.tb02694.x

Rott, P., Fleites, L., Marlow, G., Royer, M., and Gabriel, D. W. (2011a). Identification of new candidate pathogenicity factors in the xylem-invading pathogen *Xanthomonas albilineans* by transposon mutagenesis. *Mol. Plant Microbe In.* 24 (5), 594–605. doi: 10.1094/MPMI-07-10-0156

Rott, P., Fleites, L., Mensi, I., Sheppard, L., Daugrois, J.-H., Dow, J. M., et al. (2013). The RpfCG two-component system negatively regulates the colonization of sugarcane stalks by *Xanthomonas albilineans*. *Microbiol. SGM* 159, 1149–1159. doi: 10.1099/mic.0.065748-0

Rott, P., Marguerettaz, M., Fleites, L., Cociancich, S., Girard, J. C., and Pieretti, I. (2011b). Unravelling pathogenicity of *Xanthomonas albilineans*, the causal agent of sugarcane leaf scald. *Int. Sugar J.* 113 (1351), 490–496. doi: 10.1094/PHYTO.1997.87.12.1202

Rott, P., Mohamed, I., and Klett, P. (1997). Resistance to leaf scald disease is associated with limited colonization of sugarcane and wild relatives by *Xanthomonas albilineans*. *Phytopathology* 87 (12), 1202–1213. doi: 10.1094/PHYTO.1997.87.12.1202

Ryan, R. P., Vorhölter, F. J., Potnis, N., Jones, J. B., Van Sluys, M. A., Bogdanove, A. J., et al. (2011). Pathogenomics of *Xanthomonas*: understanding bacterium-plant interactions. *Nat. Rev. Microbiol.* 9 (5), 344–355. doi: 10.1038/nrmicro2558

Saleem, M., Fariduddin, Q., and Castroverde, C. D. M. (2021). Salicylic acid: A key regulator of redox signalling and plant immunity. *Plant Physiol. Biochem.* 168, 381–397. doi: 10.1016/j.plaphy.2021.10.011

Shaik, R., Pillay, D., and Pillay, B. (2009). Amplified fragment length polymorphisms reveal genetic differentiation among strains of *Xanthomonas albilineans*. *J. Microbiol. Meth.* 76 (1), 43–51. doi: 10.1016/j.mimet.2008.09.008

Shi, Y., Zhao, J.-Y., Zhou, J.-R., Ntambo, M. S., Xu, P. Y., Rott, P. C., et al. (2021). Molecular detection and quantification of *Xanthomonas albilineans* in juice from symptomless sugarcane stalks using a real-time quantitative PCR assay. *Plant Dis.* 105 (11), 3451–3458. doi: 10.1094/PDIS-03-21-0468-RE

Smirnoff, N., and Arnaud, D. (2019). Hydrogen peroxide metabolism and functions in plants. *New Phytol.* 221, 1197–1214. doi: 10.1111/nph.15488

Suman, S., Bagal, D., Jain, D., Singh, R., Singh, I. K., and Singh, A. (2021). "Biotic stresses on plants: reactive oxygen species generation and antioxidant mechanism," in *Frontiers in plant-soil interaction*. Eds. T. Aftab and R. K. Hakeem (London: Academic Press), 381–411. doi: 10.1016/B978-0-323-90943-3.00014-6

Tabassum, N., and Blilou, I. (2022). Cell-to-cell communication during plant-pathogen interaction. *Mol. Plant Microbe Interact.* 35 (2), 98–108. doi: 10.1094/MPMI-09-21-0221-CR

Tambong, J. T., Xu, R., Cuppels, D., Chapados, J., Gerdis, S., and Eyres, J. (2022). Whole-genome resources and species-level taxonomic validation of 89 plant-pathogenic *Xanthomonas* strains isolated from various host plants. *Plant Dis.* 106 (6), 1558–1565. doi: 10.1094/PDIS-11-21-2498-SC

Tamura, K., Stecher, G., and Kumar, S. (2021). MEGA11: Molecular evolutionary genetics analysis version 11. *Mol. Biol. Evol.* 38, 7. doi: 10.1093/molbev/msab120

Tardiani, A. C., Perecin, D., Peixoto Junior, R. F., Sanguino, A., and Creste, S. (2014). Molecular and pathogenic diversity among Brazilian isolates of *Xanthomonas albilineans* assessed with SSR marker loci. *Plant Dis.* 98 (4), 540–546. doi: 10.1094/PDIS-07-13-0762-RE

Te Molder, D., Poncheewin, W., Schaap, P. J., and Koehorst, J. J. (2021). Machine learning approaches to predict the plant-associated phenotype of *Xanthomonas* strains. *BMC Genomics* 22 (1), 848. doi: 10.1186/s12864-021-08093-0

Timilsina, S., Potnis, N., Newberry, E. A., Liyanapathiranage, P., Iruegas-Bocardo, F., White, F. F, et al. (2020). *Xanthomonas* diversity, virulence and plant–pathogen interactions. *Nat. Rev. Microbiol.* 18 (8), 415–427. doi: 10.1038/s41579-020-0361-8

Vidhyasekaran, P. (2014). "Reactive oxygen species and cognate redox signaling system in plant innate immunity," in *PAMP signals in plant innate immunity. signaling and communication in plants* (Dordrecht: Springer), 283–306. doi: 10.1007/978-94-007-7426-1_5

White, F. F., Potnis, N., Jones, J. B., and Koebnik, R. (2009). The type III effectors of *Xanthomonas*. *Mol. Plant Pathol.* 10 (6), 749–766. doi: 10.1111/j.1364-3703.2009.00590.x

Wu, G. Y., Li, Y. S., Li, M. L., and Zhang, G. Y. (2022). Identification and pathogenicity analysis of *Xanthomonas albilineans* causing sugarcane leaf scald in guangxi. *Acta Phytopathol. Sin.* 52 (1), 9–16. doi: 10.1111/ppa.12951

Xu, J., Duan, X., Yang, J., Beeching, J. R., and Zhang, P. (2013). Enhanced reactive oxygen species scavenging by overproduction of superoxide dismutase and catalase delays postharvest physiological deterioration of cassava storage root. *Plant Physiol.* 161, 1517–1528. doi: 10.1104/pp.112.212803

Yang, L., Li, B., Zheng, X. Y., Li, J., Yang, M., Dong, X., et al. (2015). Salicylic acid biosynthesis is enhanced and contributes to increased biotrophic pathogen resistance in arabidopsis hybrids. *Nat. Commun.* 6, 7309. doi: 10.1038/ncomms8309

Zhang, H. L., Ntambo, M. S., Rott, P. C., Chen, G., Chen, L. L., Huang, M. T., et al. (2020). Complete genome sequence reveals evolutionary and comparative genomic features of *Xanthomonas albilineans* causing sugarcane leaf scald. *Microorganisms* 8 (2), 182. doi: 10.3390/microorganisms8020182

Zhang, R. Y., Shan, H. L., Li, W. F., Cang, X. Y., Wang, X. Y., and Yin, J. (2017). First report of sugarcane leaf scald caused by *Xanthomonas albilineans* (Ashby) dowson in the province of guangxi, China. *Plant Dis.* 101 (8), 1541. doi: 10.1094/PDIS-12-16-1774-PDN

Zhu, F., Zhang, Q. P., Che, Y. P., Zhu, P. X., Zhang, Q. Q., and Ji, Z. L. (2021). Glutathione contributes to resistance responses to TMV through a differential modulation of salicylic acid and reactive oxygen species. *Mol. Plant Pathol.* 22 (12), 1668–1687. doi: 10.1111/mpp.13138

frontiers | Frontiers in Plant Science

TYPE Original Research
PUBLISHED 27 January 2023
DOI 10.3389/fpls.2023.1117023

OPEN ACCESS

EDITED BY
Xiaofeng Zhang,
Fujian Agriculture and Forestry University, China

REVIEWED BY
Yifeng Wang,
China National Rice Research Institute (CAAS), China
Mazahar Moin,
University of Hyderabad, India

*CORRESPONDENCE
Gynheung An
genean@khu.ac.kr
Jong-Seong Jeon
jjeon@khu.ac.kr

SPECIALTY SECTION
This article was submitted to Plant Pathogen Interactions, a section of the journal Frontiers in Plant Science

RECEIVED 06 December 2022
ACCEPTED 13 January 2023
PUBLISHED 27 January 2023

CITATION
Tun W, Yoon J, Vo KTX, Cho L-H, Hoang TV, Peng X, Kim E-J, Win KTYS, Lee S-W, Jung K-H, Jeon J-S and An G (2023) Sucrose preferentially promotes expression of *OsWRKY7* and *OsPR10a* to enhance defense response to blast fungus in rice.
Front. Plant Sci. 14:1117023.
doi: 10.3389/fpls.2023.1117023

Sucrose preferentially promotes expression of *OsWRKY7* and *OsPR10a* to enhance defense response to blast fungus in rice

Win Tun[1], Jinmi Yoon[2], Kieu Thi Xuan Vo[1], Lae-Hyeon Cho[2], Trung Viet Hoang[1], Xin Peng[3], Eui-Jung Kim[1], Kay Tha Ye Soe Win[1], Sang-Won Lee[1], Ki-Hong Jung[1], Jong-Seong Jeon[1]* and Gynheung An[1]*

[1]Graduate School of Green-Bio Science, Kyung Hee University, Yongin, Republic of Korea, [2]Department of Plant Bioscience, Pusan National University, Miryang, Republic of Korea, [3]Rice Research Institute, Guangdong Academy of Agricultural Sciences, Guangzhou, China

Sucrose controls various developmental and metabolic processes in plants. It also functions as a signaling molecule in the synthesis of carbohydrates, storage proteins, and anthocyanins, as well as in floral induction and defense response. We found that sucrose preferentially induced *OsWRKY7*, whereas other sugars (such as mannitol, glucose, fructose, galactose, and maltose) did not have the same effect. A hexokinase inhibitor mannoheptulose did not block the effect of sucrose, which is consequently thought to function directly. MG132 inhibited sucrose induction, suggesting that a repressor upstream of *OsWRKY7* is degraded by the 26S proteasome pathway. The 3-kb promoter sequence of *OsWRKY7* was preferentially induced by sucrose in the luciferase system. Knockout mutants of *OsWRKY7* were more sensitive to the rice blast fungus *Magnaporthe oryzae*, whereas the overexpression of *OsWRKY7* enhanced the resistance, indicating that this gene is a positive regulator in the plant defense against this pathogen. The luciferase activity driven by the *OsPR10a* promoter was induced by OsWRKY7 and this transcription factor bound to the promoter region of *OsPR10a*, suggesting that OsWRKY7 directly controls the expression of *OsPR10a*. We conclude that sucrose promotes the transcript level of *OsWRKY7*, thereby increasing the expression of *OsPR10a* for the defense response in rice.

KEYWORDS

***Magnaporthe oryzae*, OsPR10a, OsWRKY7, rice, sucrose**

1 Introduction

Sugars derived from the photosynthetic process are the basic raw materials for cell vitality and function as intermediate substances to build macromolecules such as nucleic acids and the cell wall (Plaxton, 1996; Wang et al., 2007). Sugars also act as signal molecules in various cellular processes, such as seed germination, seedling growth, storage organ development,

flowering, and senescence (Li and Sheen, 2016; Sakr et al., 2018; Yoon et al., 2021). Among various sugars, glucose is widely accepted as a signaling molecule in plants, yeast, and mammals. However, studies on sucrose-specific signaling are scarce, because this sugar is readily metabolized to fructose and glucose in plants. It has been shown that a significant amount of glucose is converted to sucrose in detached tobacco leaves within 8 hours after glucose feeding (Morcuende et al., 1998). Similarly, nourishing detached spinach leaves with glucose rapidly increases their sucrose level (Krapp et al., 1991).

Nonetheless, several studies have also reported that the transcript levels of various genes are preferentially controlled by sucrose (Yoon et al., 2021). For example, the mRNA level of the sucrose transporter *BvSUT1* is reduced by a high concentration of sucrose in sweet beet leaves (Nieberl et al., 2017). Sucrose also preferentially induces various genes that encode starch biosynthesis enzymes, such as UDP-glucose pyrophosphorylase, ADP-glucose pyrophosphorylase (AGPase), and granule-bound starch synthase (Müller-Röber et al., 1992; Ciereszko et al., 2001; Wang et al., 2001; Li et al., 2002).

Sucrose functions as a specific signaling molecule to control plant development stages (Yoon et al., 2021). *Arabidopsis* plants that overexpress the homeodomain–leucine zipper gene, *ATH13*, show the narrow leaf phenotype when they are grown on sucrose-containing medium (Hanson et al., 2001). Sucrose concentration in the phloem sap increases dramatically upon floral induction in various plant species, such as *Sinapis alba, Xanthium strumarium, Lolium temulentum*, and *Arabidopsis thaliana* (Bodson and Outlaw, 1985; Houssa et al., 1991; Corbesier et al., 1998). Exogenous application of sucrose promotes flowering in *Brassica campestris, S. alba*, and chrysanthemum (Friend et al., 1984; Sun et al., 2017).

Sucrose also functions as a signaling molecule to protect plants from pathogen invasion by modulating the production of peroxidase and pathogen-related proteins (Thibaud et al., 2004; Morkunas et al., 2005). The expression of the maize fungal-inducible *PRms* gene in transgenic tobacco and rice plants causes the accumulation of a high level of sucrose that provides protection against various pathogens, which suggests that this sugar may promote plant defense (Murillo et al., 2003; Gómez-Ariza et al., 2007). In line with this hypothesis, the exogenous application of sucrose was shown to induce the expression of several PR genes in tobacco and rice (Murillo et al., 2003; Gómez-Ariza et al., 2007). Similarly, sucrose was reported to induce the expression of genes *PR-1*, *PR-2*, and *PR-5* in *Arabidopsis* (Thibaud et al., 2004). Although glucose also increases the *PR-2* transcript level, the induction is weak and non-metabolizable glucose analogs (i.e., 3-*O*-methylglucose and 2-deoxyglucose) do not promote gene expression, suggesting that the induction is not hexokinase dependent.

Several WRKY transcription factors play a role in the defense response in various plant species, including *Arabidopsis*, rice, wheat, grape, pepper, and cotton (Jiang et al., 2016; Jimmy and Babu, 2019). In rice, several WRKY genes are rapidly induced or repressed upon infection with bacterial and fungal pathogens, such as *Xanthomonas oryzae* pv. *oryzae* (*Xoo*) and *Magnaporthe oryzae*, respectively (Ryu et al., 2006; Jimmy and Babu, 2015). Among these genes, more than 10 were shown to induce resistance against fungal blast (Chen and Wang, 2014). For example, *OsWRKY22* appears to be involved in defense responses because the *oswrky22* mutant lines are highly susceptible to *M. oryzae* and *Blumeria graminis* (Abbruscato et al., 2012). Another WRKY gene, *OsWRKY30*, which is inducible by salicylic acid (SA) and jasmonic acid (JA), also enhances resistance to *M. oryzae*, *Rhizoctonia solani*, and *Xoo* when it is overexpressed in transgenic rice plants (Peng et al., 2012). Tao et al. (2009) identified a pair of *OsWRKY45* alleles that function as a positive factor during *M. oryzae* infections but play an opposite role in the defense against bacterial pathogens. Whereas *OsWRKY45-1* knockout plants are resistant to *Xoo* and *X. oryzae* pv. *oryzicola*, *OsWRKY45-2*-suppressing plants show increased susceptibility to these pathogens. OsWRKY45 forms a heterodimer with OsWRKY62 that acts as a strong activator, while the OsWRKY62 homodimer acts as a repressor (Fukushima et al., 2016). A number of WRKY factors function negatively in defending the plants against *M. oryzae*. The transcriptional repressor OsWRKY13 binds to the promoter regions of both the *OsWRKY45-1* and *OsWRKY45-2* genes, thereby repressing the target gene expression (Xiao et al., 2013). Similarly, OsWRKY42, which functions downstream of WRKY45-2, negatively affects rice resistance by suppressing JA-dependent signaling (Cheng et al., 2015).

Sucrose induces several WRKY genes. For example, it was shown to increase the mRNA level of *AtWRKY20*, which activates the *AGPase* gene in *Arabidopsis* (Nagata et al., 2012). Similarly, sucrose addition to *Arabidopsis* leaves induces the ectopic expression of an endosperm-specific WRKY transcription factor, *SUSIBA2* (Sun et al., 2003). However, the effects of other sugars have not been examined in either of the two above-mentioned studies. In the present study, we investigated the signal roles of sucrose in plant defense.

2 Materials and methods

2.1 Plant materials and growth conditions

The Oc suspension cell line that was established from seedling roots of *Oryza sativa* L. indica type accession C5928 (Baba et al., 1986) was cultured in 50 mL of R2S liquid medium (Ohira et al., 1973) in a 120-rpm shaking incubator at 28°C, as previously reported (Cho et al., 2016; Yoon et al., 2021). After 2 weeks of culture, 20 mL of the upper liquid layer was decanted, and 10 mL of the remaining cell suspension was transferred to a fresh flask containing 40 mL of R2S culture medium.

The *OsWRKY7* mutant (line number 5A-00022) was identified from T-DNA tagging lines generated in *Oryza sativa* var. *japonica*, cultivar 'Dongjin' (Jeon et al., 2000; Jeong et al., 2002; An et al., 2005a; An et al., 2005b; Jeong et al., 2006). Homozygous mutant plants from the T2 progeny were identified by PCR using genomic DNA isolated from the blade of the second leaf of each plant. The genotyping primers were GTGTCGGGTGCGTATTTAAAAAC (F), GGGAAT TGGCGCTAAATCTGC (R), and atccagactgaatgcccacag (NGUS2) (Supplementary Table 1). Null mutations of *OsWRKY7* were obtained using the CRISPR/Cas9 method in 'Donjin' background. Homozygous mutants at T1 generation were detected through the subcloning and multiple sequencing of the mutated region using the genomic DNA extracted from the leaf blades of individual plants.

For overexpression of *OsWRKY7*, a full length of the gene was cloned by PCR using the specific primers (Supplementary Table 1) with *Hind*III and *Sac*I restriction enzyme sites. The gene was subcloned between the maize ubiquitin (*ZmUbi*) promoter and HA

tag in the binary vector pGA3428 (Kim et al., 2009). The resulting vector was used to generate transgenic rice plants overexpressing OsWRKY7-HA. Produced plants were verified by western blot analysis using protein extracts from the leaf blades after 24 hours of *M. oryzae* infection. All plants were grown in the paddy field or in a controlled growth room under a long day conditions (i.e., 14 hours of light at 28°C/10 hours of darkness at 23°C, humidity of approximately 50%).

2.2 RNA-sequencing and data analysis

Oc cells were grown for 10 days in R2S solution complemented with 3% glucose as a carbon source. They were divided into two equal parts; one was added with sucrose and the other with glucose, obtaining a final sugar concentration of 3% in two replications. Samples were collected immediately before the transfer to new media (0 h) and 4 hours after sugar addition (4 h). Total RNA was extracted using the QIAGEN RNA purification kit (Hilden, Germany), and the purity and concentration of RNA were estimated using a NanoDrop 2000 spectrophotometer (Thermo scientific). RNA-seq analysis was performed based on protocols previously reported in Peng et al. (2021). The gene ontology (GO) terms of the differentially expressed genes were analyzed using the Rice Oligo Array Database (ricephylogenomics-khu.org). All the mapped genes were downloaded and filtered based on the following criteria: hyper *p*-value < 0.05 and query numbers > 10. Additional significance of the GO terms was denoted by a fold enrichment value > 1.5, which was obtained by dividing the query number by the query expectation value (Hong et al., 2020; Kim et al., 2021). The biotic stress category was obtained *via* the MapMan analysis toolkit 3.5.1 R2 (Thimm et al., 2004).

2.3 RNA isolation and the expression analysis

Total RNA was extracted from the leaves, roots, and Oc cells using RNAiso Plus (Takara, Japan). After combining 3 μg of RNA with 10 ng of oligo (dT), the first-strand cDNA was synthesized using 100 units of Moloney murine leukemia virus (M-MLV) reverse transcriptase (Promega, Madison, WI, USA), 100 units of RNasin (Promega), and 2.5 mM deoxyribonucleotide triphosphates. The gene expression levels were analyzed by quantitative RT-PCR using SYBR Green I, Prime Q-Matermix (2x) (GENET Bio, Daejeon, Korea) in a Rotor-Gene Q system (Qiagen, Hilden, Germany). Rice *Actin1* (*OsActin1*) was used as an endogenous control to normalize the expression level of the respective genes. All experiments were repeated at least three times, and the relative transcript levels were calculated using the ΔΔCt method (Schmittgen and Livak, 2008; Yoon et al., 2022). The primers used in this study are listed in Supplementary Table 1.

2.4 Generation of CRISPR/Cas9 mutants

After selecting a potential target sequence with the CRISPR web tool, the RNA scaffold structure was analyzed using the RNAfold web server (univie.ac.at), and off-target sites were checked with the web tools (http://crispr.dbcls.jp; Naito et al., 2015 and CRISPOR (tefor.net); Concordet and Haeussler, 2018). A potential target sequence (5'-ATGTCATCGTACTTCTCCCA-3') within the first exon of *OsWRKY7* was cloned into the CRISPR vector pRGEB32 through the *Bsa*I restriction site. The construct was transformed into the *Agrobacterium tumefaciens* strain LBA4404 using the freeze–thaw method (An, 1987). Transgenic rice plants were obtained *via* the *Agrobacterium*-mediated co-cultivation method (Lee et al., 1999).

2.5 Plasmid construction for the reporter assay

The 3.081-kb promoter region (−3098 to −18 bp from the ATG start codon) of *OsWRKY7* from cultivar 'Nipponbare' was cloned into the *Hind*III-digested pGA3452 vector (Kim et al., 2009) upstream of the luciferase (*LUC*) coding region using the 5X In-Fusion HD enzyme Premix (Takara, Japan), which generated the p*OsWRKY7-LUC* reporter vector. The 2.856-kb promoter portion (−2856 to −1 bp from the start ATG codon) of *OsPR10a* was inserted into pGA3452, which resulted in p*OsPR10a-LUC*. The *ZmUbi-GUS* (Cho et al., 2009) construct was used as the internal control. For effector constructs, the coding regions of *OsWRKY7, OsWRKY28*, and *OsWRKY10* were amplified by PCR and were inserted between the *ZmUbi* promoter and 6X Myc of pGA3697 (Kim et al., 2009).

2.6 Transient assay

Protoplasts were prepared from Oc cells based on methods described in Cho et al. (2016) and He et al. (2016). In brief, Oc cells were incubated in an enzyme solution (2% cellulose RS, 1% macerozyme, 0.1% $CaCl_2$, 0.4 M mannitol, 0.1% MES, pH 5.7) for 4 hours at 28°C in the dark. After incubation, they were added with an equal volume of KMC solution (117 mM potassium chloride, 82 mM magnesium chloride, and 85 mM calcium chloride). The number of protoplasts was quantified with a hemocytometer to ensure that a cell density of 2×10^6 cells mL^{-1} was reached. The isolated protoplasts were transformed with 10 μg of each plasmid DNA using the PEG method (Yoo et al., 2007; Cho et al., 2022). *ZmUbi : GUS* construct (2 μg) was co-transfected as an internal control (Cho et al., 2009). The GUS activity was used to normalize the LUC activity.

2.7 Chromatin immunoprecipitation assay

The chromatin immunoprecipitation (ChIP) assay was performed using the protocols described in Haring et al. (2007) and Yoon et al. (2022) with some modifications. Firstly, the fresh leaves from the *OsWRKY7-HA* transgenic plants were collected and the proteins and chromatin were cross-linked using 3% formaldehyde. After the isolation of nuclei, DNA was broken into fragments of approximately 200–800 bp in length by sonication. Agarose beads of G and A proteins (Milipore; http://www.emdmilipore.com) were used to preclear the sheared chromatin for 1 hour at 4°C. Anti-HA monoclonal antibody (C29F4, https://www.cellsignal.com) was used for immunoprecipitation together with the precleared agarose beads for 4 hours at 4°C. The washing and reverse cross-linking steps

described in Haring et al. (2007) were followed. The enriched chromatin was analyzed by qRT-PCR using the primers listed in Supplementary Table 1. The obtained data were normalized using the fold enrichment method (Haring et al., 2007; Yoon et al., 2022).

2.8 Electrophoresis mobility shift assay (EMSA)

The oligonucleotide (-808 to -831 from the start ATG of *OsPR10a*) was end labeled with biotin (Microgen, Korea). To produce MBP-tagged OsWRKY7 protein, the coding sequence of *OsWRKY7* was amplified by PCR and cloned into the pMAL-c2X vector (Addgene plasmid # 75286; http://n2t.net/addgene:75286; RRID : Addgene_75286; walker et al., 2010) through the *EcoR*1 and *Sal*1 enzyme sites. The MBP-OsWRKY7 protein were extracted using amylose resin (E8021S, New England, Biolabs Inc.) The MBP-OsWRKY7 protein (1 μg) and biotin labeled ds-DNA fragment (750 fmol) were incubated in the reagent (KIT 0020148, Thermo scientific) containing 1× binding buffer, 10% glycerol, 5 mM $MgCl_2$, 0.5 μg poly (dI-dC), and 0.05% NP-40 in a final volume of 20 μL for 30 min at 25°C. After electrophoresis in 6% polyacrylamide gel, the DNA-protein complexes were transferred to membrane. The procedure for detection of immobilized nucleic acids was according to the protocol provided by the manufacture.

2.9 Pathogen infection

The *Magnaporthe oryzae* PO6-6 strain was cultured on an agar medium containing 8% V8 juice (Cambell's Soup Company, USA) for 2 weeks under fluorescent light. The resulting spores were collected and diluted in distilled water to obtain the concentration of 5×10^6 mL^{-1} for spot inoculation. A solution containing 2×10^5 spores per mL was sprayed onto the fully expanded healthy leaves of 6-week-old plants. Leaf samples were harvested and photographed to calculate the size of the lesions developed in the susceptible plants (Vo et al., 2019).

3 Results

3.1 Identification of sucrose-induced genes

To identify genes that preferentially responded to exogenously provided sucrose, RNA-seq analysis was performed using Oc cell lines that had been maintained in suspension culture for a long period (Baba et al., 1986). Because the cells were grown in a culture medium containing sucrose, the carbon source was replaced with glucose to deplete sucrose when the cells were sub-cultured. Ten days after subculture, sucrose was added to a culture flask to obtain a final concentration of 3%. As a control, glucose was added to another culture flask to reach the same final concentration. Four hours after adding the sugars, cells were harvested and mRNAs were isolated to construct cDNA libraries. RNA-seq analyses of the libraries showed that the transcript levels of 1,336 genes were at least doubled by the sucrose addition during the 4-h culture period (Supplementary Figure 1A). Among these genes, 871 were also induced by glucose, leaving 465 that were sucrose preferential. The analyses also revealed that 1,148 genes were preferentially suppressed by sucrose (Supplementary Figure 1B). To validate the RNA-seq data, 12 upregulated and 12 downregulated genes were selected for qRT-PCR analysis, which confirmed that eight and 10 genes belonging to the two groups, respectively, were sucrose responsive (Supplementary Table 2). GO analysis of the 465 genes preferentially induced by sucrose showed that the biological terms dominated by sucrose were protein amino acid phosphorylation, defense response, and transport (Supplementary Figure 1C).

3.2 Sucrose preferentially induces the transcription initiation of *OsWRKY7*

Mapman analysis of all the sucrose up-regulated genes from the RNA-seq analysis showed that three groups of transcription factors were enriched in biotic stress (Supplementary Figure 2). Because WRKY transcription factors are involved in defense response against pathogens, we selected all three WRKY genes (*OsWRKY7*, *OsWRKY26*, and *OsWRKY108*) that were sucrose inducible. qRT-PCR analysis showed that the transcript level of *OsWRKY7* was increased by sucrose, reaching the maximum level at 2 hours after sucrose addition, and then rapidly declining to the basal level at 6 hours (Figure 1A). Glucose also induced the transcript level, but not significantly. Mannitol did not increase gene expression during the 8-h incubation time, which indicated that the expression of *OsWRKY7* was preferentially induced by sucrose. The level of *OsWRKY26* transcript started to increase at 2 hours after sucrose addition, reached the maximum at 4 hours, and then declined (Figure 1B). The transcript level was also increased by glucose addition. However, the gene was not induced at 2 hours after glucose addition, but its transcript was increased to approximately half of the sucrose-induced level at 4 hours and continuously increased at 6 and 8 h. The transcript level was not changed by mannitol. The above observations suggest that *OsWRKY26* responded to both sucrose and glucose, but the gene was more rapidly induced by sucrose. Another WRKY gene, *OsWRKY108*, was also induced by sucrose. Compared to the other two genes discussed above, *OsWRKY108* responded more rapidly to sucrose, reaching the maximum level at 0.5 hours after sucrose addition, and declining to the basal level at 2 hours (Figure 1C). This gene was weakly induced by glucose and did not respond to mannitol. The pathogen marker gene *OsPR10a* was also preferentially induced by sucrose, but not by glucose or mannitol (Figure 1D).

Because *OsWRKY7* was specifically and transiently induced by sucrose, further tests were conducted to determine whether this gene was induced by other sugars. In addition to glucose, other monosaccharides such as galactose and fructose, as well as glucose and fructose added at the same time, did not induce gene expression above the control level during the 2-h incubation period (Figure 2A). Also, gene expression was not stimulated by maltose, a disaccharide that consists of two glucose molecules. The results suggest that *OsWRKY7* is specifically induced by sucrose. Lowering sucrose concentration to 2%, 1%, and 0.5% did not influence the rate and level of *OsWRKY7* induction (Figure 2B), however, further reductions

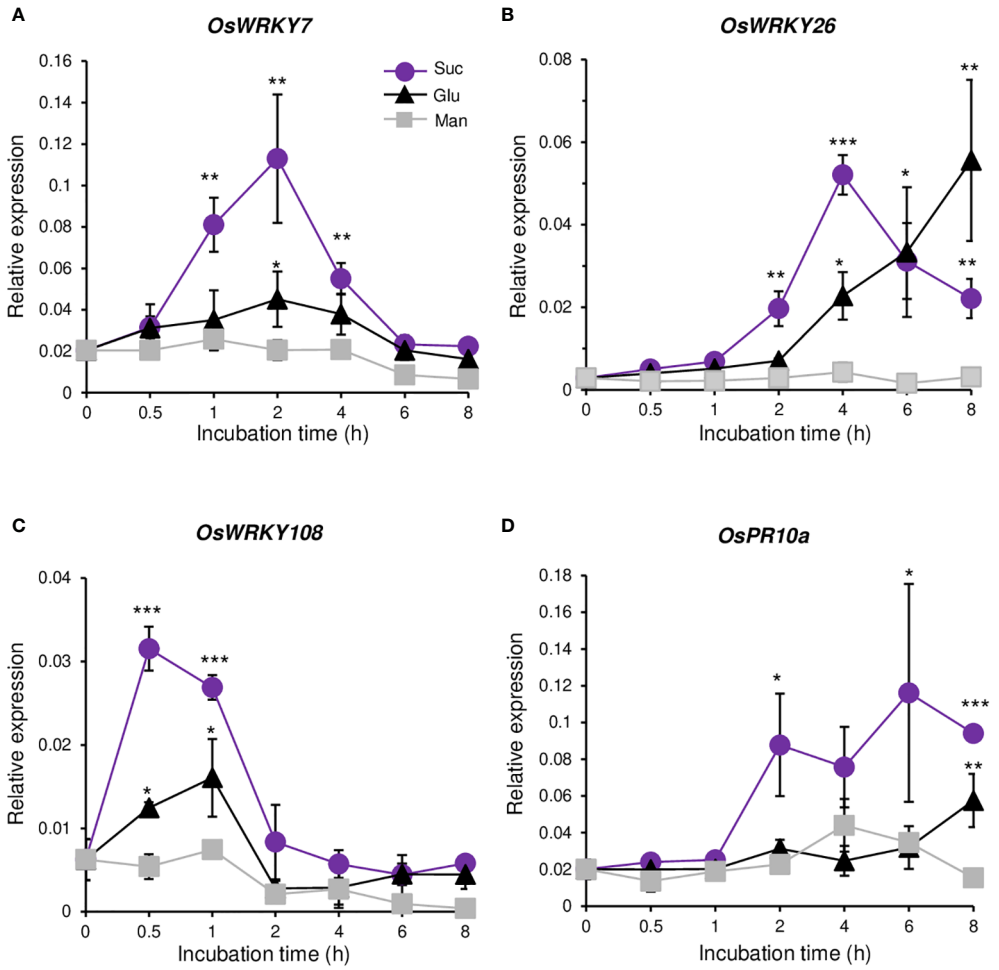

FIGURE 1
Response to sugars. Quantitative RT-PCR analyses of *OsWRKY7* **(A)**, *OsWRKY26* **(B)**, *OsWRKY108* **(C)**, and *OsPR10a* **(D)** in Oc cells after addition of 3% sucrose (Suc), 3% glucose (Glu) or 3% mannitol (Man). The gene expression levels are relative to those of *OsActin1*. Error bars indicate standard deviations; n = 3 or more. Statistical significance is indicated by *($P < 0.05$) **($P < 0.01$) and ***($P < 0.001$).

to concentrations of 0.25% and 0.1% slightly reduced the sucrose inducibility.

To investigate whether gene expression was induced by sucrose in plants, 14-day-old rice seedlings grown hydroponically in Yoshida solution were left in the dark for 48 hours to reduce their endogenous sugar level. After this period, sucrose was added to the culture medium at the final concentration of 3%. Analysis of the *OsWRKY7* transcript level in the roots showed that it increased significantly at 8 hours after sucrose addition (Figure 2C). Glucose also induced gene expression in the roots, but the induced levels were only slightly higher than those achieved by mannitol in the control.

The effect of mannoheptulose, which blocks hexose-mediated signaling (Chiou and Bush, 1998), was also tested. The results showed that the addition of 5 μM mannoheptulose to the sucrose solution did not interfere with the sucrose-induced expression of *OsWRKY7* (Figure 2D). This observation suggests that hexoses produced from sucrose metabolism are probably not involved in the induction of the gene and that sucrose may function directly to promote *OsWRKY7* expression.

To elucidate whether protein stability was involved in the sucrose response, MG132, which is an inhibitor of the 26S proteasomal protease (Genschik et al., 1998), was added to the sucrose solution. Analysis of the *OsWRKY7* transcript level showed that the sucrose-induced expression of the gene was suppressed by 100 μM MG132 (Figure 2E). As a control, the sucrose-induced *OsWRKY108* gene was also tested and it was shown that the expression of this gene was not affected by MG132 (Supplementary Figure 3). This result suggests that a regulatory protein that represses *OsWRKY7* expression is degraded by an E3 ligase during the sucrose treatment.

To examine whether the induction of *OsWRKY7* by sucrose occurred at the transcriptional level, the 3.081-kb promoter sequence of *OsWRKY7* was placed upstream of the *LUC* coding region and the construct was introduced into protoplasts prepared from Oc cells. As an internal control, the *GUS* coding region driven by the *ZmUbi* promoter was co-transfected. After dividing the treated cells into three portions, sucrose, glucose, and mannitol at the final concentration of 3% were added to each aliquot. After 15 hours of incubation, the samples were analyzed and it was shown that the LUC activity in the sucrose-added cells was considerably higher than that in the mannitol-added cells (Figure 2F). On the contrary, the induction of the reporter gene expression by glucose was only slightly above that achieved by mannitol. This experiment

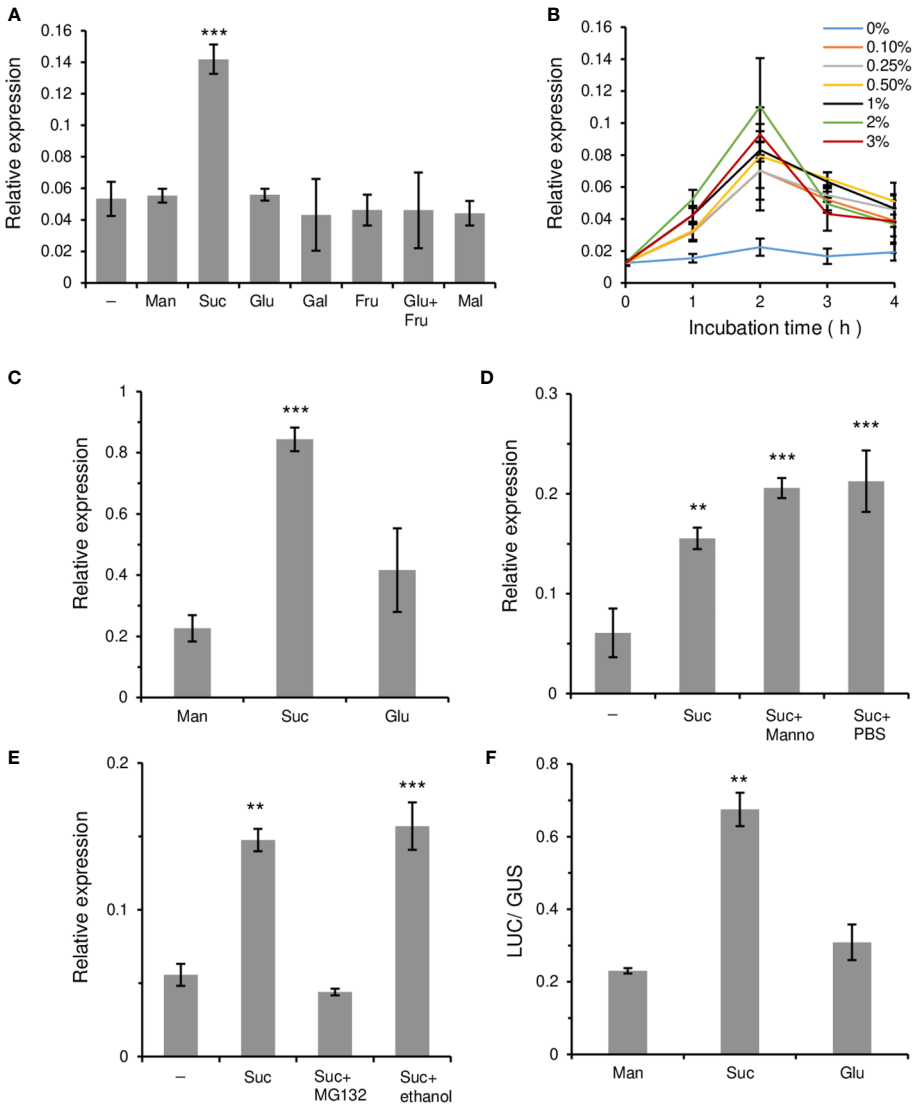

FIGURE 2
Relative transcripts level of *OsWRKY7* affected by various sugars and inhibitors. **(A-D)** Effects of various sugars and chemicals. **(A)** Effect of sugars at 3% concentration in Oc cells. Samples were collected at 2 hours after sugar addition. **(B)** Effect of different sucrose concentrations. **(C)** Effect of 3% sugars in roots of 14-d-old seedlings. **(D)** Effects of 5 μM mannoheptulose (Manno). Effect of PBS was tested because mannoheptulose was dissolved in PBS before adding to the sucrose-containing medium. **(E)** Influence of MG132. Samples were collected at 1 hours after addition of 3% sucrose, 3% sucrose plus 100 μM MG132, or 3% sucrose plus 0.5% ethanol. We tested the effect of ethanol because MG132 was dissolved in ethanol. **(F)** Luciferase activity driven by the *OsWRKY7* promoter and LUC coding region. *ZmUbi::GUS* construct was used as an internal control. Man, mannitol; Suc, sucrose; Glu, glucose; Gal; galactose; Fru, fructose; Mal, maltose. Minus sign (-) means basal media. Gene expression levels are relative to those of *OsActin1*. The error bars indicate standard deviations; n = 3 or more. Statistical significance is indicated by **(P < 0.01) and ***(P < 0.001).

demonstrated that sucrose preferentially induced *OsWRKY7* at the transcription initiation level.

3.3 Mutations of *OsWRKY7* reduce the defense response against *M. oryzae*

Expression of *OsWRKY7* was induced by *M. oryzae* 48 hours after infection (Supplementary Figure 4A). To study the functional roles of *OsWRKY7*, we identified T-DNA tagging line 5A-00022, in which T-DNA was inserted at 375 bp upstream of the start ATG codon of *OsWRKY7* (Supplementary Figure 4B). Homozygous progeny of the *oswrky7-1* mutant was used for characterization of the gene function. In the mutant line, the expression level of *OsWRKY7* was decreased to approximately a half of the wild type (WT) level, which indicated that the inserted T-DNA reduced gene expression (Supplementary Figure 4C). When the plants were infected with *M. oryzae*, the lesions were longer and broader than those observed in the segregated WT plants (Supplementary Figures 4D, E), suggesting that *OsWRKY7* is involved in the defense response against this pathogen.

To confirm this observation, knockout mutations were generated in the first exon of *OsWRKY7 via* the CRISPR/Cas9 system (Figure 3A). Among 28 independent transgenic plants, five were selected to determine the flanking regions of the target site. Two mutant lines were chosen: *oswrky7-2* carrying a single-bp deletion and *oswrky7-3*

10.3389/fpls.2023.1117023

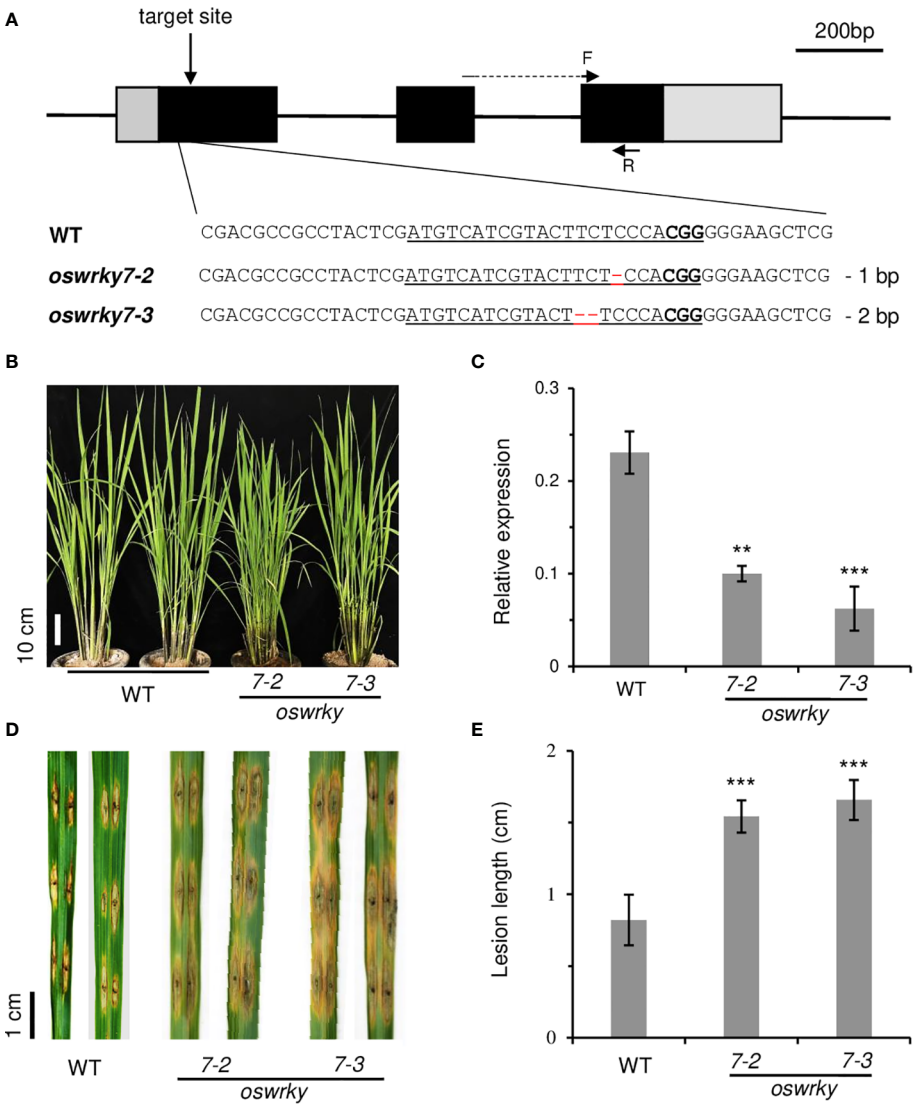

FIGURE 3
Characterization of *oswrky7* mutants generated by the CRISPR/Cas9 method. **(A)** Schematic diagram of *OsWRKY7* gene structure and sequence comparison of sgRNA target regions between WT and mutants. The target sequence and PAM site are underlined. Deleted sequences are indicated with red dashes. In the schematic gene structure, black boxes are exons; gray boxes are 5′- UTR and 3′-UTR regions; lines between the boxes are introns. F and R are primers used for measuring the transcript level of *OsWRKY7*. Scale bar = 200 bp. **(B)** Phenotypes of the WT and the knockout mutant plants grown under the paddy field at T1 generation. Scale bar = 10 cm. **(C)** Transcript level of *OsWRKY7* in the WT and knockout mutant plants. Samples were collected at 42 DAG **(D)** Comparison of the lesions between the WT and mutants. Phenotype was observed at 9 days after *M. oryzae* infection. Scale bar = 1 cm. **(E)** The length of the lesion developed by the pathogen. The error bars show standard deviations; n = 10. Statistical significance is indicated by **(P < 0.01) and ***(P < 0.001).

carrying a two-bp deletion (Figure 3A, Supplementary Figures 5A, B). The deletions generated frameshift mutations, causing early termination during translation of the *OsWRKY7* transcript. The mutant plants grew normally without any significant phenotypic alteration in the plant height, grain numbers per panicle, panicle length, and 100-grain weight (Figure 3B, Supplementary Figure 6). Interestingly, the *OsWRKY7* transcript levels in the frameshift mutants were reduced compared to those in the WT plants, suggesting that the deletion mutations affected either the transcription rate or the stability of the transcript (Figure 3C). When the plants were inoculated with *M. oryzae*, the mutants displayed a phenotype that was more susceptible to the fungus compared with the WT controls (Figures 3D, E). These experiments confirmed that *OsWRKY7* is involved in the defense response against *M. oryzae*.

3.4 Overexpression of *OsWRKY7* increases the defense response against *M. oryzae*

To obtain transgenic rice plants that constitutively expressed *OsWRKY7*, the gene was placed after the *ZmUbi* promoter and the construct was introduced to rice embryonic calli. However, it was quite difficult to obtain transgenic plants, which suggested that the overexpression of *OsWRKY7* was harmful to the plants. To overcome the difficulty, the HA tag was added at the end of the *OsWRKY7* coding region, and the fusion molecule was placed after the *ZmUbi* promoter. In this way, several transgenic plants expressing *OsWRKY7-HA* were obtained, which indicated that attaching the tag reduced the harmful effect of the gene (Figure 4A). Plants #5 and #7, which expressed the fusion transcript and the HA-tagged protein

10.3389/fpls.2023.1117023

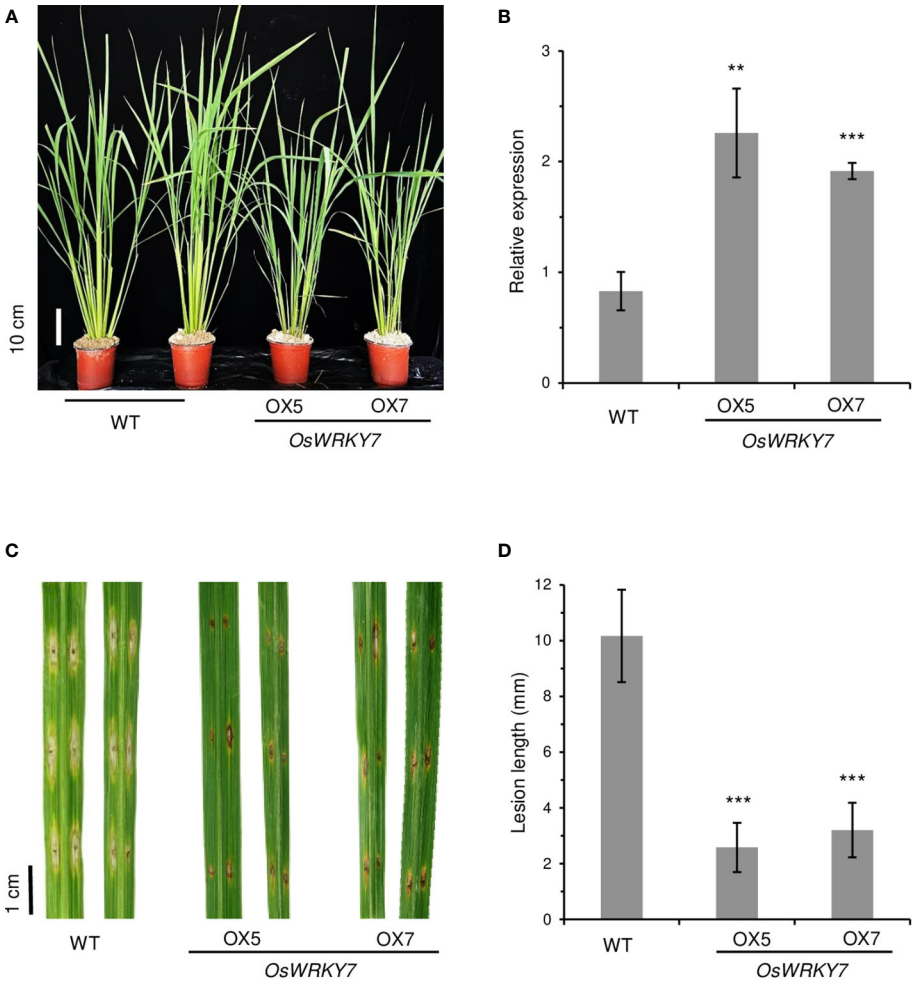

FIGURE 4
Phenotypes of *OsWRKY7* overexpression plants. **(A)** Phenotype of the WT and transgenic plants overexpressing *OsWRKY7*. Scale bar = 10 cm. **(B)** The relative transcript level of *OsWRKY7* in the WT and transgenic plants OX5 and OX7 overexpressing *OsWRKY7*. The gene expression levels are relative to those of *OsActin1*. Errors bars indicate standard deviation; n = 3. **(C)** Phenotypes of the lesions at 9 days after infection with *M. oryzae*. Bar = 1 cm. **(D)** The length of the lesion developed by the pathogen. Errors bars indicate standard deviation; n = 10. Statistical significance is indicated by **(P < 0.01) and ***(P < 0.001).

at high levels, were selected (Figure 4B and Supplementary Figure 7). After inoculating the mature leaves of the transgenic plants with *M. oryzae*, it was observed that the lesion lengths and widths at the infection sites were significantly smaller in the transgenic plants than in the WT control plants (Figures 4C, D). This observation confirmed that *OsWRKY7* is a positive regulatory element in the defense response to *M. oryzae*.

The expression level of the genes that were induced in response to pathogen infection were then analyzed. The levels of the pathogen-responsive marker genes *OsPR1a*, *OsPR1b*, and *OsPR10a*, were significantly reduced in *oswrky7* mutant plants (Figures 5A-C). On the contrary, expression levels of the pathogen responsive marker genes were markedly increased in the plants of expressing *OsWRKY7-HA* (Figures 5D-F). This result indicates that the markers function downstream of *OsWRKY7*. It was then tested whether SA or JA were involved in the induction of the marker genes by *OsWRKY7*. The mutations of this gene did not affect the expression of *phenylalanine ammonia-lyase* (*OsPAL*) or *isochorismate synthase 1* (*OsICS1*), which are involved in SA biosynthesis (Supplementary Figures 8A, B). In addition, a key regulator of systemic acquired resistance, *NPR1 homolog 1* (*OsNH1*), was also not affected in mutant (Supplementary Figure 8C). Likewise, the mutations did not influence the expression of genes encoding enzymes associated with JA biosynthesis, namely *allene oxide synthase* (*OsAOS2*), *allene oxide cyclase 1* (*OsAOC1*), and *oxophytodienoate reductase 3* (*OsOPR3*) (Supplementary Figures 8D-F). These results suggest that the signaling pathway of SA or JA did not mediate the induction of the pathogen-responsive marker genes by *OsWRKY7*.

To evaluate whether the *OsWRKY7*-induced PR genes were sucrose-inducible, hydroponically grown seedlings were treated with 3% sucrose at 14 days after germination (DAG). After 8 hours of incubation in the solution, the expression levels of the PR genes in the roots were measured. The assay showed that the transcript level of *OsPR10a* was considerably higher in the sucrose-treated seedlings than in the control seedlings treated with 3% mannitol (Figure 6A). Glucose treatment did not induce gene expression above the level observed in the control. This result is consistent with the data observed in Oc cells (Figure 2D). On the contrary, the expression of *OsPR1a* was induced by both sucrose and glucose (Figure 6B). The *OsPR1b* transcript levels in sugar solutions were similar to those

10.3389/fpls.2023.1117023

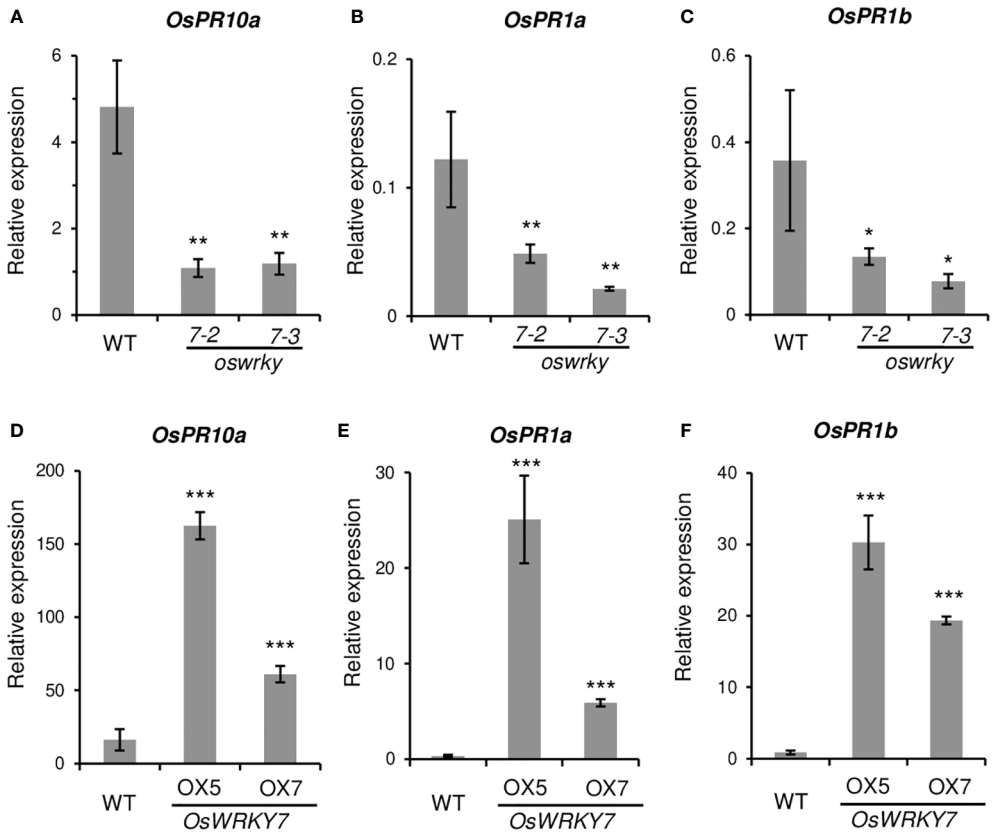

FIGURE 5
Expression levels of pathogen related genes in the WT and transgenic plants. **(A-C)** Relative transcript levels of *OsPR10a* **(A)**, *OsPR1a* **(B)** and *OsPR1b* **(C)** in the leaves of the WT and *oswrky7* mutants. **(D-F)** Relative transcript levels of *OsPR10a* **(D)**, *OsPR1a* **(E)** and *OsPR1b* **(F)** in the leaves of the WT and *OsWRKY7* overexpression plants. Samples were collected from the leaf blades at 42 DAG. The gene expression levels are relative to those of *OsActin1*. Error bars indicate standard deviation; n = 3 or more. Statistical significance is indicated by *(P < 0.05), **(P < 0.01) and ***(P < 0.001).

observed in mannitol solution (Figure 6C). These experiments indicate that, among the three PR genes tested, only *OsPR10a* was preferentially induced by sucrose.

We tested whether *OsPR10a* expression in *oswrky7* mutant was recovered by the sucrose treatment. The WT and *oswrky7* plants that were grown hydroponically in Yoshida solution for 14 days were treated with mannitol or sucrose at the final concentration of 3%. After 9 hours treatment in the solutions, the root were sampled and the expression level of *OsPR10a* was measured. The experiment showed that sucrose significantly increased *OsPR10a* expression in the WT as observed in the previous experiments. Similarly, the transcript level of the gene in the mutant was also induced by sucrose, although the induced level was lower compared with WT (Supplementary Figure 9). This observation suggests that there are other sucrose-inducible transcription factors that induce *OsPR10a* expression.

3.5 Expression of *OsPR10a* is stimulated by *OsWRKY7*

Because the expression of *PR10a* was significantly reduced in *OsWRKY7* mutants, *PR10a* may be directly controlled by the transcription factor. To prove this hypothesis, a construct containing the 2.856-kb promoter region of *OsPR10a* was placed in front of the *LUC* gene. We also constructed another molecule in which the coding region of *OsWRKY7* was placed under the *ZmUbi* promoter. Both molecules, p*OsPR10a-LUC* and p*Ubi-WRKY7*, were co-transfected into the Oc cell protoplasts and incubated for 15 hours to express the introduced genes. The results showed that the *LUC* expression level in the protoplasts co-transferred with both molecules were significantly higher than that in the protoplasts transferred with p*OsPR10a-LUC* alone (Figure 6D). As controls, *OsWRKY10* and *OsWRKY28* were inserted downstream of the *ZmUbi* promoter. It has been previously reported that *OsWRKY10* functions as a positive regulatory element for the expression of *PR10a*, whereas *OsWRKY28* does not influence the PR gene (Ersong et al., 2021). In this study, when p*Ubi-WRKY28* was co-introduced with p*OsPR10a-LUC*, the luciferase activity was not increased above the background level that was observed from p*OsPR10a-LUC* alone (Figure 6D). On the contrary, co-transfection of p*OsPR10a-LUC* and p*Ubi-OsWRKY10* significantly induced the reporter gene expression (Figure 6D). The above observations showed that the transient assay resembled the previous results and suggested that OsWRKY7 directly promoted the expression of p*OsPR10a-LUC*.

To test whether the *OsPR10a* promoter region responded directly to sucrose, the p*OsPR10a-LUC* vector was introduced into the protoplasts and was incubated in the culture solution containing three different sugars. Although the *LUC* expression level in the protoplasts cultured in sucrose-containing medium was slightly

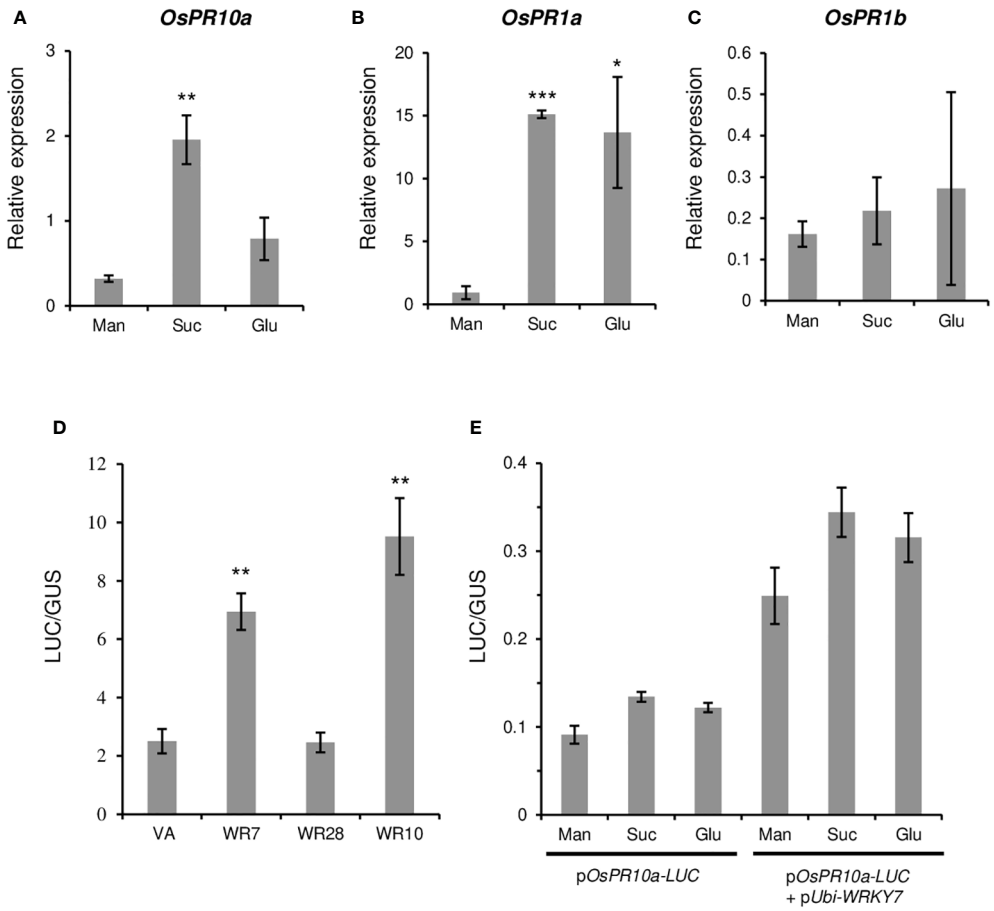

FIGURE 6
Effect of sugars and WRKY genes on the PR gene expression. **(A-C)** Effect of sugars on PR gene expression. Fourteen-day-old seedlings were grown in a hydroponic culture medium under constant light and they were transferred to the dark condition for two additional days before sucrose treatment. Mannitol, sucrose, or glucose were added at 3% final concentration. After the treatment for 8 hours, expression levels of *OsPR10a* **(A)**, *OsPR1a* **(B)**, and *OsPR1b* **(C)** in roots were measured. Gene expression levels are relative to those of *OsActin1*. Error bars indicate standard deviations; n = 3 or more. **(D)** Luciferase activity driven by the *OsPR10a* promoter. The p*OsPR10a-LUC* construct was transfected to Oc cell protoplasts alone (VA) or with p*Ubi-OsWRKY7* (WR7), p*Ubi-OsWRKY10* (WR10), or p*Ubi-OsWRKY28* (WR28). The LUC activity was assayed 15 hours after transfection of the molecules. *ZmUbi-GUS* construct was used as an internal control in each combination. **(E)** Effect of sugars on the *OsPR10a* promoter activity. p*OsPR10a-LUC* alone or together with p*Ubi-WRKY7* were transferred to Oc protoplasts and incubated in a culture medium containing mannitol (Man), sucrose (Suc) or glucose (Glu) at 3% final concentration. Luciferase activity was measured 15 hours after transfection. *ZmUbi-GUS* construct was used as an internal control in each experiment. Error bars indicate standard deviations; n = 3. Statistical significance is indicated by *($P < 0.05$), **($P < 0.01$) and ***($P < 0.001$).

higher than that in the mannitol control, a similar expression level was achieved for the protoplasts grown in the glucose-containing medium (Figure 6E). This suggests that sucrose did not induce the gene directly. It was also tested whether the increased expression of the *OsPR10a* promoter by the OsWRKY7 protein was sucrose dependent. To answer this question, both p*OsPR10a-LUC* and p*Ubi-WRKY7* were introduced into the protoplasts and the effects of sucrose were examined. The experiment showed that sucrose did not significantly increase the p*OsPR10a* promoter activity above the levels obtained from mannitol or glucose (Figure 6E). This suggests that the sucrose induction of *PR10a* was not due to the stability of the OsWRKY7 mRNA or protein during sucrose treatments.

To confirm that OsWRKY7 directly controlled the *OsPR10a* promoter, chromatin immunoprecipitation (ChIP) experiments were performed with transgenic plants expressing the OsWRKY7-HA protein. Primers were designed to target W-box elements, W-box like elements 1 (WLE1), and ASF1MOTIF, which all belong to the WRKY protein-binding TGAC core elements (Maleck et al., 2001; Hwang et al., 2008) (Figure 7A). In the ChIP *in vivo* assay, the P2 and P3 DNA fragments containing the WLE1 element were enriched (Figure 7B).

To further confirm the interaction between OsWRKY7 and the OsPR10a promoter, the oligonucleotide (-808 to - 831 from the start ATG) containing the WLE1 element within the P2 fragment were used for EMSA experiment using MBP tagged OsWRKY7 protein (Figure 7C). The experiment showed that OsWRKY7 protein bind to the sequence and the binding was reduced when the unlabeled probe was used as a competitor. Both ChIP and EMSA assays support the hypothesis that OsWRKY7 directly binds to the promoter region of *OsPR10a*.

4 Discussion

A hypothesized model for high sugar resistance suggested that a yet unknown sugar receptor senses the elevation of the levels of extracellular sugars and triggers defense through a signaling cascade

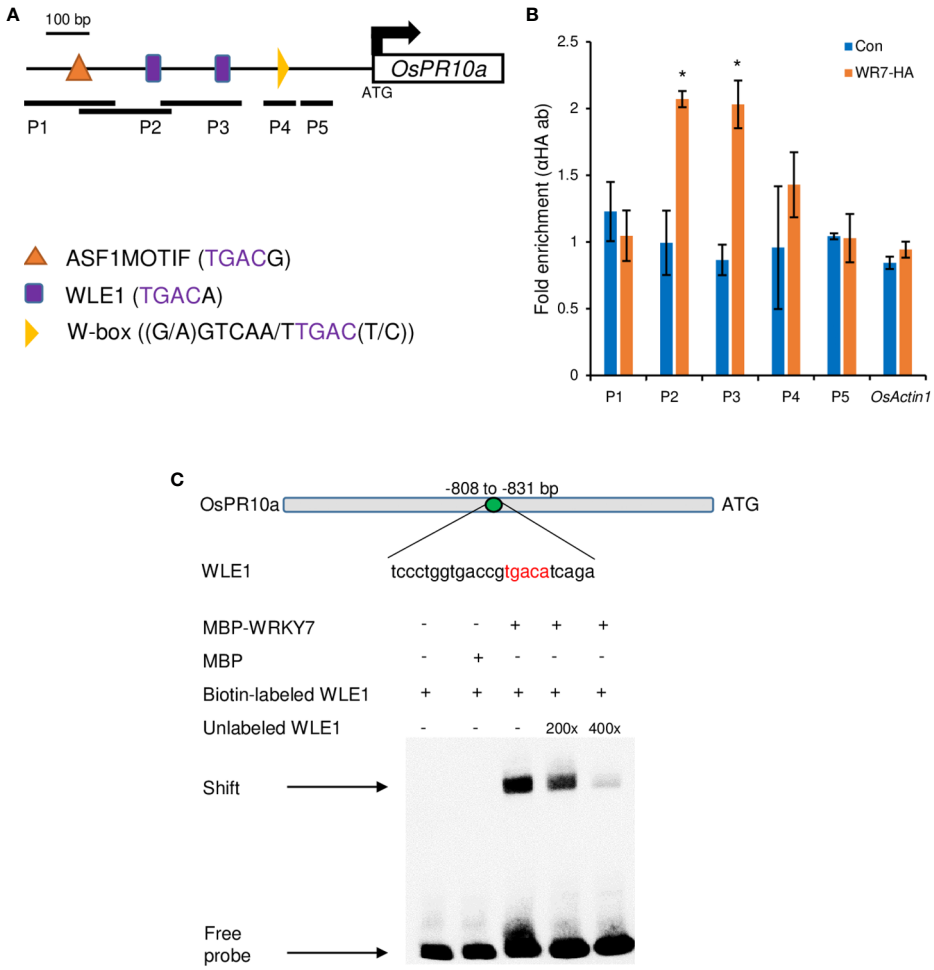

FIGURE 7
ChIP assay on the OsPR10a chromatin region and EMSA experiment. **(A)** Promoter region of *OsPR10a*. The black lines under the promoter region indicate the DNA fragment amplified by RT-PCR. Five pairs of primer set were used in ChIP assay; P1, 849-967 bp from the ATG start codon; P2, 795-946 bp from the ATG start codon; P3, 647-801 bp from the ATG start codon; P4, 207-289 bp from the ATG start codon; P5, 102-205 bp from the ATG start codon. Scale bar = 100 bp. **(B)** Chromatin enrichment of the *OsPR10a* promoter region. Transgenic plants expressing *OsWRKY7-HA* were used for the ChIP assay. Error bars indicate standard deviations; n = 2. Statistical significance is indicated by *(P < 0.05). **(C)** EMSA experiment using the sequence that contains WLE1 element on the promoter of *OsPR10a*. Biotin-labeled probe WLE1 without MBP-OsWRKY7 protein and biotin-labeled WLE1 with MBP protein were used as negative control. Excess unlabeled WLE1 was used as competitors.

(Bezrutczyk et al., 2018). Notably, it was shown that rice plants treated with sucrose through the root system exhibited an accumulation of transcripts associated with defense genes in leaves and increased resistance to *M. oryzae* (Gómez-Ariza et al., 2007). This is consistent with previous results indicating that transgenic tobacco and rice plants expressing *PRms* accumulated sucrose in leaf tissues and enhanced their defense response (Murillo et al., 2003; Gómez-Ariza et al., 2007). As PRms is localized in plasmodesmata in infected maize radicles (Murillo et al., 1997), the accumulation of sucrose is possibly due to an alteration of sugar distribution. These observations clearly suggest the implication of plants' sucrose dependent responses in the defense against invading pathogens. However, it remains to be determined how high levels of sucrose can regulate defense genes in plants.

In the present study, to investigate the functions of sucrose in the defense response, we examined *OsWRKY7*, which is inducible by exogenously applied sucrose. The transcript level of this gene was rapidly increased by the addition of sucrose in both cultured cells and seedlings, suggesting that this sugar functions as a signal molecule to induce gene expression.

Although sucrose controls various processes, such as starch metabolism, storage proteins, and anthocyanin biosynthesis, studies on sucrose responsive transcription factors that may be involved in sucrose signaling are scarce (Yoon et al., 2021). In *Arabidopsis*, sucrose-induced anthocyanin biosynthesis is mediated by *Myb75* (Teng et al., 2005); however, other sugars, such as glucose and fructose, also stimulate anthocyanin accumulation. In addition, mannoheptulose, which is a competitive inhibitor of hexokinase1, inhibits sucrose induction (Neta-Sharir et al., 2000). Therefore, *Myb75* may not be a mediator of sucrose-specific signaling. Another transcription factor that is induced by sucrose is *AtWRKY20* (Nagata et al., 2012). This regulatory gene controls the expression of *ApL3*, which encodes AGPase in *Arabidopsis*. Similarly, the barley starch synthesis gene *isoamylase1* is regulated by the sucrose-inducible WRKY gene *SUSIBA2* (Sun et al., 2003). However, it has not been tested whether these WRKY genes are

specifically induced by sucrose. In this study, we demonstrated that sucrose preferentially controlled the expression of *OsWRKY7* because hexoses and mannose were unable to induce this gene. Mannoheptulose did not reduce the sucrose induction of the gene, suggesting that glucose or other hexoses metabolized from sucrose were not responsible for this process.

Sucrose regulates gene expression at the transcriptional or post-transcriptional level. It increases the transcript levels of the WRKY and *Myb75* genes, but controls the translation of the *bZIP11* transcript post-transcriptionally (Wiese et al., 2004). In the present study, the expression of the *LUC* reporter gene driven by the 3-kb *OsWRKY7* promoter sequence was shown to be increased by sucrose, which indicated that sucrose regulates *OsWRKY7* at the transcriptional level.

Because several WRKY genes are involved in plant defense mechanisms, we tested whether *OsWRKY7* functions in disease tolerance against *M. oryzae* using a knockdown mutant generated by T-DNA tagging and knockout mutants created by CRISPR/Cas9. These mutants were more susceptible to the rice blast fungus, however, transgenic plants overexpressing the gene showed reduced disease symptoms. These results suggest that the transcription factor functions positively in the defense against *M. oryzae.* The transcript levels of the pathogen-related genes *OsPR1a*, *OsPR1b*, and *OsPR10a* were significantly reduced in the mutants and increased in the plants exhibiting overexpression, supporting the hypothesis that *OsWRKY7* plays a role in plant defense. However, genes involved in SA synthesis or SA-mediated resistance were not affected by the mutations, and this was the case also for JA biosynthesis genes, suggesting that *OsWRKY7* functions independently from the hormones.

Interestingly, the transcript level of *OsWRKY7* was significantly reduced when MG132 was added during sucrose induction, which indicates that an upstream repressor protein of *OsWRKY7* may be degraded through the proteasome pathway and that sucrose promotes this pathway. AtWRKY50, an ortholog of OsWRKY7, interacts with *Botrytis*-induced kinase 1 (BIK1), a receptor-like cytoplasmic kinase VII member that is localized in the nucleus and degraded by the proteasome (Lal et al., 2018). This suggests that OsWRKY7 may interact with a kinase. Further study will be needed to investigate how the protein is degraded by a proteasome.

Among the three PR genes that were influenced by *OsWRKY7*, only *OsPR10a* was preferentially induced by sucrose. *OsPR1a* was also induced by glucose, which indicates that other regulatory elements besides OsWRKY7 also control its expression. In contrast, *OsPR1b* was not induced by either sucrose or glucose. Because *OsPR1b* also functions downstream of the sucrose-inducible *OsWRKY7* gene, the induction of this PR gene by sucrose was expected. It will be interesting to investigate how the sucrose signaling was diminished in the PR gene. To study whether the induction of *PR10a* expression by sucrose occurred directly or was mediated by OsWRKY7 protein, the promoter of *PR10a* was tested using the *LUC* reporter system. It was shown that sucrose did not induce the promoter activity of *OsPR10a*. Ru et al. (2015) reported that GFP fused OsWRKY7 protein is localized in the nucleus and OsWRKY7 protein has transcriptional activity in yeast hybrid assay, which indicated that the sucrose induction of the *PR10a* promoter was mediated by OsWRKY7. Direct control of this PR gene by OsWRKY7 was also confirmed by the ChIP and EMSA assays. All the results presented in this study provide a definitive proof that sucrose has a role in defense response in rice by activating the transcription factor OsWRKY7, which triggers the expression of *PR10a*. Further experiment is needed to investigate what is the upstream element that mediates sucrose signaling and whether OsWRKY7 interacts with a partner to control the downstream gene expression.

Data availability statement

The datasets presented in this study can be found in online repositories. The names of the repository/repositories and accession number(s) can be found in the article/Supplementary Material.

Author contributions

GA, S-WL, K-HJ, J-SJ designed the project. WT, JY, KV, L-HC, TH, XP, E-JK, and KW performed experiments and analyzed data. WT, JY, J-SJ, and GA wrote the paper. All authors contributed to the article and approved the submitted version.

Funding

This work was supported, in part, by grants from the National Research Foundation of Korea (NRF-2020R1A2C2006826 to GA; NRF-2021R1C1C2007906 to JY) and the Rural Development Administration, Korea (PJ01690101 to JSJ).

Acknowledgments

We are thankful to Kyungsook An for maintaining the transgenic T-DNA tagging lines and providing the seed stock.

Conflict of interest

The authors declare that the research was conducted in the absence of any commercial or financial relationships that could be construed as a potential conflict of interest.

Publisher's note

Supplementary material

The Supplementary Material for this article can be found online at: https://www.frontiersin.org/articles/10.3389/fpls.2023.1117023/full#supplementary-material

References

Abbruscato, P., Nepusz, T., Mizzi, L., Corvo, M., Morandini, P., Fumasoni, I., et al. (2012). *OsWRKY22*, a monocot WRKY gene, plays a role in the resistance response to blast. *Mol. Plant Pathol.* 13, 828–841. doi: 10.1111/j.1364-3703.2012.00795.x

An, G. (1987). Binary Ti vectors for plant transformation and promoter analysis. *In. Methods Enzymol.* 153, 292–305. doi: 10.1016/0076-6879(87)53060-9

An, G., Jeong, D.-H., Jung, K.-H., and Lee, S. (2005a). Reverse genetic approaches for functional genomics of rice. *Plant Mol. Biol.* 59, 111–123. doi: 10.1007/s11103-004-4037-y

An, G., Lee, S., Kim, S.-H., and Kim, S.-R. (2005b). Molecular genetics using T-DNA in rice. *Plant Cell Physiol.* 46, 14–22. doi: 10.1093/pcp/pci502

Baba, A., Hasezawa, S., and Syōno, K. (1986). Cultivation of rice protoplasts and their transformation mediated by *Agrobacterium spheroplasts*. *Plant Cell Physiol.* 27, 463–471. doi: 10.1093/oxfordjournals.pcp.a077122

Bezrutczyk, M., Yang, J., Eom, J.-S., Prior, M., Sosso, D., Hartwig, T., et al. (2018). Sugar flux and signaling in plant–microbe interactions. *Plant J.* 93, 675–685. doi: 10.1111/tpj.13775

Bodson, M., and Outlaw, W. H. (1985). Elevation in the sucrose content of the shoot apical meristem of *Sinapis alba* at floral evocation 1. *Plant Physiol.* 79, 420–424. doi: 10.1104/pp.79.2.420

Cheng, H., and Wang, S. (2014). The important player of rice-pathogen interactions: WRKY-type transcription factors. *Sci Sin Vitae* 44, 784–793.

Cheng, H., Liu, H., Deng, Y., Xiao, J., Li, X., and Wang, S. (2015). The *WRKY45-2, WRKY13 WRKY42* transcriptional regulatory cascade is required for rice resistance to fungal pathogen. *Plant Physiol.* 167, 1087–1099. doi: 10.1104/pp.114.256016

Chiou, T. J., and Bush, D. R. (1998). Sucrose is a signal molecule in assimilate partitioning. *Proc. Natl. Acad. Sci. U.S.A.* 95, 4784–4788. doi: 10.1073/pnas.95.8.4784

Cho, J.-I., Ryoo, N., Eom, J.-S., Lee, D.-W., Kim, H.-B., Jeong, S.-W., et al. (2009). Role of rice hexokinases *OsHXK5* and *OsHXK6* as glucose sensors. *Plant Physiol.* 149, 745–759. doi: 10.1104/pp.108.131227

Cho, L.-H., Yoon, J., Pasriga, R., and An, G. (2016). Homodimerization of Ehd1 is required to induce flowering in rice. *Plant Physiol.* 170, 2159–2171. doi: 10.1104/pp.15.01723

Cho, L.-H., Yoon, J., Tun, W., Baek, G., Peng, X., Hong, W.-J., et al. (2022). Cytokinin increases vegetative growth period by suppressing florigen expression in rice and maize. *Plant J.* 10 (6), 1619–1635 doi: 10.1111/tpj.15760

Ciereszko, I., Johansson, H., and Kleczkowski, L. A. (2001). Sucrose and light regulation of a cold-inducible UDP-glucose pyrophosphorylase gene *via* a hexokinase-independent and abscisic acid-insensitive pathway in arabidopsis. *Biochem. J.* 354, 67–72. doi: 10.1042/bj3540067

Concordet, J.-P., and Haeussler, M. (2018). CRISPOR: Intuitive guide selection for CRISPR/Cas9 genome editing experiments and screens. *Nucleic Acids Res.* 46, W242–W245. doi: 10.1093/nar/gky354

Corbesier, L., Lejeune, P., and Bernier, G. (1998). The role of carbohydrates in the induction of flowering in *Arabidopsis thaliana*: Comparison between the wild type and a starchless mutant. *Planta* 206, 131–137. doi: 10.1007/s004250050383

Ersong, Z., Xuming, W., Rumeng, X., Feibo, Y., Chao, Z., Yong, Y., et al. (2021). Regulation of *OsPR10a* promoter activity by phytohormone and pathogen stimulation in rice. *Rice Sci.* 28, 442–456. doi: 10.1016/j.rsci.2021.07.005

Friend, D. J., Bodson, M., and Bernier, G. (1984). Promotion of flowering in *Brassica campestris* l. cv Ceres by sucrose. *Plant Physiol.* 75, 1085–1089. doi: 10.1104/pp.75.4.1085

Fukushima, S., Mori, M., Sugano, S., and Takatsuji, H. (2016). Transcription factor *WRKY62* plays a role in pathogen defense and hypoxia-responsive gene expression in rice. *Plant Cell Physiol.* 57, 2541–2551. doi: 10.1093/pcp/pcw185

Genschik, P., Criqui, M. C., Parmentier, Y., Derevier, A., and Fleck, J. (1998). Cell cycle–dependent proteolysis in plants: Identification of the destruction box pathway and metaphase arrest produced by the proteasome inhibitor MG132. *Plant Cell.* 10, 2063–2075. doi: 10.1105/tpc.10.12.2063

Gómez-Ariza, J., Campo, S., Rufat, M., Estopà, M., Messeguer, J., Segundo, B. S., et al. (2007). Sucrose-mediated priming of plant defense responses and broad-spectrum disease resistance by overexpression of the maize pathogenesis-related PRms protein in rice plants. *Mol. Plant-Microbe Interactions.* 20, 832–842. doi: 10.1094/MPMI-20-7-0832

Hanson, J., Johannesson, H., and Engström, P. (2001). Sugar-dependent alterations in cotyledon and leaf development in transgenic plants expressing the *HDZhdip* gene *ATHB13*. *Plant Mol. Biol.* 45, 247–262. doi: 10.1023/A:1006464907710

Haring, M., Offermann, S., Danker, T., Horst, I., Peterhansel, C., and Stam, M. (2007). Chromatin immunoprecipitation: Optimization, quantitative analysis and data normalization. *Plant Methods* 3, 11. doi: 10.1186/1746-4811-3-11

He, F., Chen, S., Ning, Y., and Wang, G.-L. (2016). Rice (*Oryza sativa*) protoplast isolation and its application for transient expression analysis. *Curr. Protoc. Plant Biol.* 1, 373–383. doi: 10.1002/cppb.20026

Hong, W.-J., Jiang, X., Ahn, H. R., Choi, J., Kim, S.-R., and Jung, K.-H. (2020). Systematic analysis of cold stress response and diurnal rhythm using transcriptome data in rice reveals the molecular networks related to various biological processes. *Int. J. Mol. Sci.* 21, 6872. doi: 10.3390/ijms21186872

Houssa, P., Bernier, G., and Kinet, J. M. (1991). Qualitative and quantitative analysis of carbohydrates in leaf exudate of the short-day plant, *Xanthium strumarium* l. during floral transition. *J. Plant Physiol.* 138, 24–28. doi: 10.1016/S0176-1617(11)80724-8

Hwang, S.-H., Lee, I. A., Yie, S. W., and Hwang, D.-J. (2008). Identification of an *OsPR10a* promoter region responsive to salicylic acid. *Planta* 227, 1141–1150. doi: 10.1007/s00425-007-0687-8

Jeong, D.-H., An, S., Kang, H.-G., Moon, S., Han, J.-J., Park, S., et al. (2002). T-DNA Insertional mutagenesis for activation tagging in rice. *Plant Physiol.* 130, 1636–1644. doi: 10.1104/pp.014357

Jeong, D.-H., An, S., Park, S., Kang, H.-G., Park, G.-G., Kim, S.-Y., et al. (2006). Generation of a flanking sequence-tag database for activation-tagging lines in japonica rice. *Plant J.* 45, 123–132. doi: 10.1111/j.1365-313X.2005.02610.x

Jeon, J.-S., Lee, S., Jung, K.-H., Jun, S.-H., Jeong, D.-H., Lee, J., et al. (2000). T-DNA Insertional mutagenesis for functional genomics in rice. *Plant J.* 22, 561–570. doi: 10.1046/j.1365-313x.2000.00767.x

Jiang, Y., Guo, L., Liu, R., Jiao, B., Zhao, X., Ling, Z., et al. (2016). Overexpression of poplar *PtrWRKY89* in transgenic *Arabidopsis* leads to a reduction of disease resistance by regulating defense-related genes in salicylate- and jasmonate-dependent signaling. *PloS One* 11, e0149137. doi: 10.1371/journal.pone.0149137

Jimmy, J. L., and Babu, S. (2015). Role of OsWRKY transcription factors in rice disease resistance. *Trop. Plant Pathol.* 1, 355–361. doi: 10.1007/s40858-015-0058-0

Jimmy, J. L., and Babu, S. (2019). Variations in the structure and evolution of rice *WRKY* genes in indica and japonica genotypes and their co-expression network in mediating disease resistance. *Evol. Bioinf.* 15, 1–12. doi: 10.1177/1176934319857720

Kim, E.-J., Hong, W.-J., Kim, Y.-J., and Jung, K.-H. (2021). Analysis of triple mutant for *OsMADS62*, *OsMADS63*, and *OsMADS68* reveals the downstream regulatory mechanism for pollen germination in rice (*Oryza sativa*). *Int. J. Mol. Sci.* 23, 239. doi: 10.3390/ijms23010239

Kim, S.-R., Lee, D.-Y., Yang, J.-I., Moon, S., and An, G. (2009). Cloning vectors for rice. *J. Plant Biol.* 52, 73. doi: 10.1007/s12374-008-9008-4

Krapp, A., Quick, W. P., and Stitt, M. (1991). Ribulose-1,5-bisphosphate carboxylase-oxygenase, other calvin-cycle enzymes, and chlorophyll decrease when glucose is supplied to mature spinach leaves *via* the transpiration stream. *Planta* 186, 58–69. doi: 10.1007/BF00201498

Lal, N. K., Nagalakshmi, U., Hurlburt, N. K., Flores, R., Bak, A., Sone, P., et al. (2018). The receptor-like cytoplasmic kinase *BIK1* localizes to the nucleus and regulates defense hormone expression during plant innate immunity. *Cell Host Microbe* 23, 485–497.e5. doi: 10.1016/j.chom.2018.03.010

Lee, S., Jeon, J.-S., Jung, K.-H., and An, G. (1999). Binary vectors for efficient transformation of rice. *J. Plant Biol.* 42, 310–316. doi: 10.1007/BF03030346

Li, L., and Sheen, J. (2016). Dynamic and diverse sugar signaling. *Curr. Opin. Plant Biol.* 33, 116–125. doi: 10.1016/j.pbi.2016.06.018

Li, X., Xing, J., Gianfagna, T. J., and Janes, H. W. (2002). Sucrose regulation of ADP-glucose pyrophosphorylase subunit genes transcript levels in leaves and fruits. *Plant Sci.* 162, 239–244. doi: 10.1016/S0168-9452(01)00565-9

Maleck, K., Levine, A., Eulgem, T., Morgan, A., Schmid, J., Lawton, K., et al. (2001). The transcriptome of *Arabidopsis thaliana* during systemic acquired resistance. *Nat. Genet.* 26, 403–410. doi: 10.1038/82521

Morcuende, R., Krapp, A., Hurry, V., and Stitt, M. (1998). Sucrose-feeding leads to increased rates of nitrate assimilation, increased rates of α-oxoglutarate synthesis, and increased synthesis of a wide spectrum of amino acids in tobacco leaves. *Planta* 206, 394–409. doi: 10.1007/s004250050415

Morkunas, I., Marczak, Ł., Stachowiak, J., and Stobiecki, M. (2005). Sucrose-induced lupine defense against *Fusarium oxysporum*: Sucrose-stimulated accumulation of isoflavonoids as a defense response of lupine to *Fusarium oxysporum*. *Plant Physiol. Biochem.* 43, 363–373. doi: 10.1016/j.plaphy.2005.02.011

Müller-Röber, B., Sonnewald, U., and Willmitzer, L. (1992). Inhibition of the ADP-glucose pyrophosphorylase in transgenic potatoes leads to sugar-storing tubers and influences tuber formation and expression of tuber storage protein genes. *EMBO J.* 11, 1229–1238. doi: 10.1002/j.1460-2075.1992.tb05167.x

Murillo, I., Cavallarin, L., and San Segundo, B. (1997). The maize pathogenesis-related PRms protein localizes to plasmodesmata in maize radicles. *Plant Cell.* 9, 145–156. doi: 10.1105/tpc.9.2.145

Murillo, I., Roca, R., Bortolotti, C., and San Segundo, B. (2003). Engineering photoassimilate partitioning in tobacco plants improves growth and productivity and provides pathogen resistance. *Plant J.: For. Cell Mol. Biol.* 36, 330–341. doi: 10.1046/j.1365-313X.2003.01880.x

Nagata, T., Hara, H., Saitou, K., Kobashi, A., Kojima, K., Yuasa, T., et al. (2012). Activation of ADP-glucose pyrophosphorylase gene promoters by a WRKY transcription factor, *AtWRKY20*, in *Arabidopsis thaliana* l. and sweet potato (*Ipomoea batatas* lam.). *Plant Prod. Sci.* 15, 10–18. doi: 10.1626/pps.15.10

Naito, Y., Hino, K., Bono, H., and Ui-Tei, K. (2015). CRISPRdirect: Software for designing CRISPR/Cas guide RNA with reduced off-target sites. *Bioinformatics* 31, 1120–1123. doi: 10.1093/bioinformatics/btu743

Neta-Sharir, I., Shoseyoy, O., and Weiss, D. (2000). Sugars enhance the expression of gibberellin-induced genes in developing petunia flowers. *Physiol. Plant.* 109, 196–202. doi: 10.1034/j.1399-3054.2000.100212.x

Nieberl, P., Ehrl, C., Pommerrenig, B., Graus, D., Marten, I., Jung, B., et al. (2017). Functional characterisation and cell specificity of *BvSUT1*, the transporter that loads sucrose into the phloem of sugar beet (*Beta vulgaris* l.) source leaves. *Plant Biol.* 19, 315–326. doi: 10.1111/plb.12546

Ohira, K., Ojima, K., and Fujiwara, A. (1973). Studies on the nutrition of rice cell culture i. a simple, defined medium for rapid growth in suspension culture. *Plant Cell Physiol.* 14, 1113–1121. doi: 10.1093/oxfordjournals.pcp.a074950

Peng, X., Hu, Y., Tang, X., Zhou, P., Deng, X., Wang, H., et al. (2012). Constitutive expression of rice *WRKY30* gene increases the endogenous jasmonic acid accumulation, PR gene expression and resistance to fungal pathogens in rice. *Planta* 236, 1485–1498. doi: 10.1007/s00425-012-1698-7

Peng, X., Tun, W., Dai, S., Li, J., Zhang, Q., Yin, G., et al. (2021). Genome-wide analysis of CCT transcript factors to identify genes contributing to photoperiodic flowering in *Oryza rufipogon*. *Front. Plant Sci.* 12, 736419. doi: 10.3389/fpls.2021.736419

Plaxton, W. C. (1996). The organization and regulation of plant glycolysis. *Annu. Rev. Plant Physiol. Plant Mol. Biol.* 47, 185–214. doi: 10.1146/annurev.arplant.47.1.185

Ru, L., Jie, Z., Doung-yue, L., Xu-ming, W., Young, Y., Chu-lang, Y., et al. (2015). Expression of *OsWRKY7* in rice. *Chi. J. Rice Sci.*, 29 (6), 559–570. doi: 10.3969/j.issn.1001-7216.2015.06.001

Ryu, H.-S., Han, M., Lee, S.-K., Cho, J.-I., Ryoo, N., Heu, S., et al. (2006). A comprehensive expression analysis of the *WRKY* gene superfamily in rice plants during defense response. *Plant Cell Rep.* 25, 836–847. doi: 10.1007/s00299-006-0138-1

Sakr, S., Wang, M., Dédaldéchamp, F., Perez-Garcia, M.-D., Ogé, L., Hamama, L., et al. (2018). The sugar-signaling hub: Overview of regulators and interaction with the hormonal and metabolic network. *Int. J. Mol. Sci.* 19, 2506. doi: 10.3390/ijms19092506

Schmittgen, T. D., and Livak, K. J. (2008). Analyzing real-time PCR data by the comparative CT method. *Nat. Protoc.* 3, 1101–1108. doi: 10.1038/nprot.2008.73

Sun, C., Palmqvist, S., Olsson, H., Borén, M., Ahlandsberg, S., and Jansson, C. (2003). A novel *WRKY* transcription factor, *SUSIBA2*, participates in sugar signaling in barley by binding to the sugar-responsive elements of the *iso1* promoter. *Plant Cell.* 15, 2076–2092. doi: 10.1105/tpc.014597

Sun, J., Wang, H., Ren, L., Chen, S., Chen, F., and Jiang, J. (2017). *CmFTL2* is involved in the photoperiod- and sucrose-mediated control of flowering time in chrysanthemum. *Hortic. Res.* 4, 17001. doi: 10.1038/hortres.2017.1

Tao, Z., Liu, H., Qiu, D., Zhou, Y., Li, X., Xu, C., et al. (2009). A pair of allelic *WRKY* genes play opposite roles in rice- bacteria interactions. *Plant Physiol.* 151, 936–948. doi: 10.1104/pp.109.145623

Teng, S., Keurentjes, J., Bentsink, L., Koornneef, M., and Smeekens, S. (2005). Sucrose-specific induction of anthocyanin biosynthesis in *Arabidopsis* requires the *MYB75/PAP1* gene. *Plant Physiol.* 139, 1840–1852. doi: 10.1104/pp.105.066688

Thibaud, M.-C., Gineste, S., Nussaume, L., and Robaglia, C. (2004). Sucrose increases pathogenesis-related *PR-2* gene expression in *Arabidopsis thaliana* through an SA-dependent but NPR1-independent signaling pathway. *Plant Physiol. Biochem.* 42, 81–88. doi: 10.1016/j.plaphy.2003.10.012

Thimm, O., Bläsing, O., Gibon, Y., Nagel, A., Meyer, S., Krüger, P., et al. (2004). Mapman: A user-driven tool to display genomics data sets onto diagrams of metabolic pathways and other biological processes. *Plant J.* 37, 914–939. doi: 10.1111/j.1365-313X.2004.02016.x

Vo, K. T. X., Lee, S.-K., Halane, M. K., Song, M.-Y., Hoang, T. V., Kim, C.-Y., et al. (2019). *Pi5* and *Pii* paired NLRs are functionally exchangeable and confer similar disease resistance specificity. *Mol. Cells* 42, 637–645. doi: 10.14348/molcells.2019.0070

Walker, I. H., Hsieh, P. C., and Riggs, P. D. (2010). Mutations in maltose-binding protein that alter affinity and solubility properties. *Appl. Microbiol. Biotechnol.*, 88 (1), 187–197. doi: 10.1007/s00253-010-2696-y

Wang, H.-J., Wan, A.-R., Hsu, C.-M., Lee, K.-W., Yu, S.-M., and Jauh, G.-Y. (2007). Transcriptomic adaptations in rice suspension cells under sucrose starvation. *Plant Mol. Biol.* 63, 441–463. doi: 10.1007/s11103-006-9100-4

Wang, S.-J., Yeh, K.-W., and Tsai, C.-Y. (2001). Regulation of starch granule-bound starch synthase I gene expression by circadian clock and sucrose in the source tissue of sweet potato. *Plant Sci.* 161, 635–644. doi: 10.1016/S0168-9452(01)00449-6

Wiese, A., Elzinga, N., Wobbes, B., and Smeekens, S. (2004). A conserved upstream open reading frame mediates sucrose-induced repression of translation. *Plant Cell.* 16, 1717–1729. doi: 10.1105/tpc.019349

Xiao, J., Cheng, H., Li, X., Xiao, J., Xu, C., and Wang, S. (2013). Rice *WRKY13* regulates cross talk between abiotic and biotic stress signaling pathways by selective binding to different cis-elements. *Plant Physiol.* 163, 1868–1882. doi: 10.1104/pp.113.226019

Yoo, S.-D., Cho, Y.-H., and Sheen, J. (2007). Arabidopsis mesophyll protoplasts: A versatile cell system for transient gene expression analysis. *Nat. Protoc.* 2, 1565–1572. doi: 10.1038/nprot.2007.199

Yoon, J., Cho, L.-H., Tun, W., Jeon, J.-S., and An, G. (2021). Sucrose signaling in higher plants. *Plant Sci.* 302, 110703. doi: 10.1016/j.plantsci.2020.110703

Yoon, J., Jeong, H.-J., Baek, G., Yang, J., Peng, X., Tun, W., et al. (2022). A VIN3-like protein OsVIL1 is involved in grain yield and biomass in rice. *Plants* 11, 83. doi: 10.3390/plants11010083

frontiers | Frontiers in Plant Science

TYPE Original Research
PUBLISHED 06 February 2023
DOI 10.3389/fpls.2023.1127928

OPEN ACCESS

EDITED BY
Zhenggang Li,
Guangdong Academy of Agricultural Sciences, China

REVIEWED BY
Rasappa Viswanathan,
Indian Council of Agricultural Research (ICAR), India
Malkhan Singh Gurjar,
Indian Agricultural Research Institute (ICAR), India

*CORRESPONDENCE
Philippe C. Rott
philippe.rott@cirad.fr
San-Ji Gao
gaosanji@fafu.edu.cn

†These authors have contributed equally to this work

SPECIALTY SECTION
This article was submitted to Plant Pathogen Interactions, a section of the journal Frontiers in Plant Science

RECEIVED 20 December 2022
ACCEPTED 13 January 2023
PUBLISHED 06 February 2023

CITATION
Zhao J-Y, Chen J, Hu Z-T, Li J, Fu H-Y, Rott PC and Gao S-J (2023) Genetic and morphological variants of *Acidovorax avenae* subsp. *avenae* cause red stripe of sugarcane in China. *Front. Plant Sci.* 14:1127928. doi: 10.3389/fpls.2023.1127928

Genetic and morphological variants of *Acidovorax avenae* subsp. *avenae* cause red stripe of sugarcane in China

Jian-Ying Zhao[1†], Juan Chen[1†], Zhong-Ting Hu[1], Juan Li[1], Hua-Ying Fu[1], Philippe C. Rott[2,3*] and San-Ji Gao[1*]

[1]National Engineering Research Center for Sugarcane, Fujian Agriculture and Forestry University, Fuzhou, Fujian, China, [2]CIRAD, UMR PHIM, Montpellier, France, [3]PHIM Plant Health Institute, Univ Montpellier, CIRAD, INRAE, Institut Agro, IRD, Montpellier, France

Sugarcane (*Saccharum* spp.) is an important cash crop for production of sugar and bioethanol. Red stripe caused by *Acidovorax avenae* subsp. *avenae* (*Aaa*) is a disease that occurs in numerous sugarcane-growing regions worldwide. In this study, 17 strains of *Aaa* were isolated from 13 symptomatic leaf samples in China. Nine of these strains produced white-cream colonies on nutrient agar medium while the other eight produced yellow colonies. In pairwise sequence comparisons of the 16S-23S rRNA internally transcribed spacer (ITS), the 17 strains had 98.4-100% nucleotide identity among each other and 98.2-99.5% identity with the reference strain of *Aaa* (ATCC 19860). Three RFLP patterns based on this ITS sequence were also found among the strains of *Aaa* obtained in this study. Multilocus sequence typing (MLST) based on five housekeeping genes (*ugp*B, *pil*T, *lep*A, *trp*B, and *glt*A) revealed that the strains of *Aaa* from sugarcane in China and a strain of *Aaa* (30179) isolated from sorghum in Brazil formed a unique evolutionary subclade. Twenty-four additional strains of *Aaa* from sugarcane in Argentina and from other crops worldwide were distributed in two other and separate subclades, suggesting that strains of *A. avenae* from sugarcane are clonal populations with local specificities. Two strains of *Aaa* from China (CNGX08 forming white-cream colored colonies and CNGD05 forming yellow colonies) induced severe symptoms of red stripe in sugarcane varieties LC07-150 and ZZ8 but differed based on disease incidence in two separate inoculation experiments. Infected plants also exhibited increased salicylic acid (SA) content and transcript expression of gene *PR-1*, indicating that the SA-mediated signal pathway is involved in the response to infection by *Aaa*. Consequently, red stripe of sugarcane in China is caused by genetically different strains of *Aaa* and at least two morphological variants. The impact of these independent variations on epidemics of red stripe remains to be investigated.

KEYWORDS

***Acidovorax avenae* subsp. *avenae*, genetic diversity, multilocus sequence typing, pathogenicity, red stripe, *Saccharum* spp., salicylic acid**

1 Introduction

Bacterial species of *Acidovorax* (family *Comamonadaceae*) are gram-negative beta-proteobacteria that can be separated in two major groups. One group is formed by four non-plant species (*A. delafieldii*, *A. defluvii*, *A. facilis*, and *A. temperans*) isolated from environmental and clinical sources, while the other group includes three plant pathogenic species (*A. avenae*, *A. cattleyae*, and *A. citrulli*) (Willems and Gillis, 2015). Additional species of *Acidovorax* are commensal bacteria or plant growth-promoting bacteria (Siani et al., 2021); for example, *A. radicis* (strain N35) isolated from wheat roots increases the growth of barley cultivars and reduces aphid density (Zytynska et al., 2020). A list of 15 *Acidovorax* species, including three subspecies, was recently established (De Vos et al., 2018). In the 2015 Bergey's Manual of Systematic Bacteriology, *A. avenae* includes three subspecies that cause economically important diseases in a wide range of plants (Willems and Gillis, 2015). Each of these subspecies has a different host range. *A. avenae* subsp. *citrulli* (*Aac*) infects plants of the *Cucurbitaceae*, while *A. avenae* subsp. *cattleyae* (*Aaca*) infects only orchid species of the genera *Cattleya* and *Phalaenopsis*. The third subspecies, *A. avenae* subsp. *avenae* (*Aaa*), causes bacterial blight or red/brown stripe diseases in a variety of plants of the *Gramineae* (including barley, creeping bentgrass, maize, millet, oat, rice, rye, sorghum, sugarcane, and vasey grass), the *Theaceae* (tea), and the *Strelitziaceae* (white bird of paradise) (Willems and Gillis, 2015; Li et al., 2018; Fontana et al., 2019).

Sugarcane (*Saccharum* spp.) is the most important sugar crop, accounting for 80% and 90% of the sugar production in the world and in China, respectively (Liu et al., 2022). Red stripe caused by *Aaa* has been reported in more than 60 countries and is one of three main bacterial diseases of sugarcane distributed worldwide (Rott and Davis, 2000). Leaf stripes and stalk top rot are two types of symptoms of sugarcane red stripe. These symptoms can appear separately or simultaneously in the field (Martin et al., 1989; Rott and Davis, 2000; Fu et al., 2017). The disease, and especially the top rot form, can result in significant yield losses. In Argentina, red stripe recently affected 30% of the millable stems, thus causing economic losses (Fontana et al., 2019). Disease incidences greater than 50% were observed in variety CoJ 85 in India and in variety COLMEX 9408 in Mexico (Bipen et al., 2014; Hernández-Juárez et al., 2021). During the last decade, red stripe outbreaks occurred in two main sugarcane-growing provinces in China. In the Guangxi province, disease incidences in the field reached 23% in variety FN38 (Fu et al., 2017), 39% in BT15-173 (Li et al., 2021), 50% in GT58, and 22% in LC05-136 (Li et al., 2022). In the Yunnan province, 80% of plants of variety YZ03-194 were symptomatic (Shan et al., 2017).

Efficient pathogen diagnostic and genotyping methods are needed for epidemiological surveillance and disease management (Bertani et al., 2021; Strachan et al., 2022). Besides microbiological methods, molecular typing methods have contributed to accurate identification and characterization of *Aaa* worldwide. In Mexico, molecular identification of *Aaa* was performed using 16S rDNA sequences of strains of the pathogen from three sugarcane-producing agroecological regions (Hernández-Juárez et al., 2021). The pathogen was identified in Argentina using PCR and primers Oaf1/Oar1 targeting the 16S–23S rDNA ITS (internally transcribed spacer) region (Fontana et al., 2013). Presence of at least four different genotypes and ten phylogenetic groups of *Aaa* was reported in this country using random amplified polymorphic DNA (RAPD) markers and repetitive element polymorphism-based polymerase chain reaction (rep-PCR), respectively (Bertani et al., 2021). Furthermore, multilocus sequence typing (MLST) of *Aaa* strains from different hosts revealed that a novel clonal group of strains was causing red stripe of sugarcane in Argentina (Fontana et al., 2019). Five major groups of *Aaa* strains were found in China by restriction fragment length polymorphism (RFLP) analysis (Li et al., 2018).

Multiple genes and proteins and their related metabolites and signal pathways are involved in sugarcane response to *Aaa* infection, as revealed by transcriptomic (Santa et al., 2016; Thiebaut et al., 2017; Chu et al., 2020), proteomic (Zhou et al., 2021), and genome-wide analyses (Zhou et al., 2021; Chu et al., 2022). Several genes related to signal transduction by salicylic acid (SA) are involved in sugarcane resistance to *Aaa*, but their specific role remains to be investigated (Chu et al., 2020; Chu et al., 2022). The first objective of this study was to characterize isolates of *Aaa* from China using conventional microbiological and pathogenicity assays, as well as MLST. The second objective was to investigate the importance of SA-medicated resistance gene *PR-1* (coding for pathogenesis-related protein 1) in response of sugarcane to infection by two morphologically different strains of *Aaa*.

2 Materials and methods

2.1 Leaf sample collection

From May to July 2021, 13 sugarcane leaves with red stripe symptoms were collected in sugarcane fields of the provinces of Guangdong and Guangxi in China (Table S1). The symptoms of the diseased samples were photographed on site and taken to the laboratory for isolation and identification of the causal agent(s) (Figure S1).

2.2 Isolation and molecular diagnosis of pathogenic bacteria

The isolation and purification of bacteria was performed using the agar-streak method. Briefly, symptomatic leaves were first disinfected for 1 min with 75% alcohol and then rinsed three times with sterile water. At the junction of the diseased and healthy leaf tissue, two or three fragments (2-3 mm × 4-5 cm) were cut into small pieces that were introduced in a 2 mL-microtube. This microtube contained one 4 mm-steel ball, two 2 mm-steel balls, and 100 µL of sterile water. Leaf tissue was homogenized for 60 s with a MM400 beater (Verder Shanghai Instruments and Equipment Co., Ltd, Shanghai, China). Subsequently, 400 µL of sterile water were added to each tube. After a 30 min incubation, the supernatant of each tube was spread on nutrient agar (NA) medium using the quadrant streak method. Agar plates were then incubated at 30°C for 12-16 h. Bacterial colonies with a yellow or a white color were isolated, purified, and tested by PCR using *Aaa*-specific primers RS-ITS-F1 and RS-ITS-R1,

as described by Li et al. (2018). The PCR program was 3 min at 94°C for initial denaturation; 35 cycles of 45 s at 94°C for denaturation, 30 s at 58°C for annealing, and 45 s at 72°C for extension; and 10 min at 72°C for final extension. All PCR-positive colonies were stored on NA plates at 4°C and in 20% glycerol at -80°C until further investigations. Five colonies of 24 hour-old bacteria growing on NA medium were randomly selected for each strain to measure their colony size.

2.3 Morphological observation of bacterial colonies

Freshly isolated and 24-hour-old single colonies of *Aaa* CNGX08 (white) and CNGD05 (yellow) were suspended in 50 µL sterile H_2O. A loop of bacterial suspension was placed on a copper mesh for 1 min and excess of liquid was removed with a filter paper. Bacteria were stained with a solution of 2.5% phosphor-tungstic acid (pH 7.0) for 3 s. Morphology of bacterial cells was observed with a HT-7700 transmission electron microscope (Hitachi High-Tech, Shanghai, China) and digital images were acquired with an AMT CCD camera (Hitachi High-Tech).

2.4 Bacterial genomic DNA extraction

Bacterial genomic DNA was extracted using the Bacterial Genome DNA Extraction Kit (Tiangen, Beijing, China). DNA quality and quantity tests were performed using 1% agar gel electrophoresis and the SynergyTM H1 multifunctional microplate reader (BioTek, Vermont, USA). The DNA samples were stored at -80°C until further use.

2.5 PCR amplification of housekeeping genes

Five housekeeping genes (*ugp*B, *pil*T, *lep*A, *trp*B, and *glt*A) were amplified by PCR using primer pairs reported by Feng et al. (2009). The 50 µL reaction mix included 1.0 µL bacterial genomic DNA (100 ng/µL), 20 µL Green Taq Mix (Vazyme Biotech, Nanjing, China), 1.0 µL each of forward and reverse primers (10 µmol/L), and 27 µL sterile water. The PCR program was 5 min at 95°C for initial denaturation; 35 cycles of 30 s at 95°C for denaturation, 30 s at 60°C for annealing, and 30 s at 72°C for extension; and 5 min at 72°C for final extension. The expected amplification product had a size of 444, 398, 489, 434, and 481 bp for *ugp*B, *pil*T, *lep*A, *trp*B, and *glt*A, respectively. Bacterial genomic DNA of *Aaa* strain ATCC 19860 (Institute of Microbiology, Chinese Academy of Sciences) was used as the positive control. Sterile distilled water was used as the blank control. All primer information is given in Table S2.

2.6 Cloning of PCR products

All the PCR products (sections 2.2 and 2.5) were purified and then cloned into the pMD19-T vector. Three positive clones per PCR product were randomly selected for sequencing by Sangon Biotech (Shanghai, China). Sequences were deposited at the NCBI GenBank database under accession numbers OP738811-OP738827 for the 16S-23S rDNA ITS region, and under accession numbers ON707276-ON707358 and OP747511-OP747512 for the five house-keeping genes.

2.7 RFLP, MLST and nucleotide identity analysis

A restriction fragment length polymorphism (RFLP) analysis of the *Aaa* sequences obtained with primers RS-ITS-F1/RS-ITS-R1 was performed *in silico* using restriction enzymes *Hin*dIII and *Eco*RI with DNAMAN software (Lynnon Biosoft, San Ramon, USA). The restriction patterns were identified and labelled as described by Li et al. (2018).

A concatenated sequence of the five housekeeping genes mentioned in section 2.5 was produced for 54 bacterial strains: 42 *Aaa* strains (17 obtained in this study and 25 retrieved from the NCBI library), 10 *Aac* strains, one *Aaca* strain, and one *A. facilis* strain (used as outgroup strain). The 54 concatenated sequences were aligned using the ClustalW algorithm in the software MEGA 11 (Tamura et al., 2021). A phylogenetic tree was constructed using the neighbor-joining (NJ) method with 1000 bootstrap replicates. Sequence identity analysis was performed with BioEdit V7.0.9.0 (Borland, Scotts Valley, USA). A heat map was produced with SDTv1.2 (The University of Cape Town, South Africa). The characteristics of all tested strains of *Acidovorax* are given in Table S1.

2.8 Pathogenicity assay of two bacterial strains

Stalk cuttings with a single bud each were prepared from healthy sugarcane varieties LC07-150 (source of *Aaa* strain CNGX08) and ZZ8 (source of *Aaa* strain CNGD05). Cuttings were planted in pots (5.5 x 4 x 6 cm) filled with nutrient soil (Pindstrup Mosebrug A/S, PINDSTRUP, Denmark) and grown in a climate chamber at 30°C with 16 h light/8 h night and 65% humidity. When plants had 1-2 fully expanded leaves, they were inoculated using the leaf puncture method. Briefly, the upper side of the leaf was punctured but not pierced with a disposable syringe and the wounded area was wrapped with sterile cotton. One mL of bacterial suspension (10^8 CFU/mL) was placed on the cotton for inoculation with a single strain of the pathogen whereas 0.5 mL of each strain was used for mixed inoculations. Only sterile water was used for the control plants. Inoculated plants were grown using the same conditions as described above but humidity was increased to 85%. These plants were also covered with a transparent plastic bag for the first three days post inoculation (dpi).

The pathogenicity assay included eight different treatments, namely two sugarcane varieties (LC07-150 and ZZ8) each inoculated with four different inocula: two single strains of *Aaa* (CNGX08 and CNGD05), a mix (1:1) of these two strains, and sterile water (negative control). Thirty plants were inoculated for each treatment and the pathogenicity assay was conducted independently two times. Disease incidence (%) was calculated as

follows: (Number of plants with red stripes/Total number of inoculated plants) x 100. Area under disease progress curve (AUDPC) was calculated as follows for each treatment of each of the two inoculation experiments (Shaner, 1977):

$$\text{AUDPC} = \sum_{i=1}^{n}\left[\frac{1}{2}(X_{i+1}+X_i)(T_{i+1}-T_i)\right]$$

X_i and X_{i+1} represent the disease incidence at time points T_i and T_{i+1}, respectively; n is the total number of time points (0, 3, 6, 9, 12, and 15 dpi). At 15 dpi, three inoculated leaves with red stripe symptoms were used for bacterial isolation and characterization. Bacterial colonies isolated from symptomatic leaves were identified by PCR with *Aaa*-specific primers RS-ITS-F1 and RS-ITS-R1 (Li et al., 2018).

2.9 Determination of SA content

Six leaf samples (three from each inoculation experiment) of varieties LC07-150 and ZZ8 inoculated with *Aaa* strains CNGX08 and CNGD05 were collected at 0, 12, 24, 48, and 72 hours post inoculation (hpi). Endogenous SA content of the leaf tissue was determined following the instructions of a plant SA ELISA kit (Beijing Solarbio Science & Technology Co., Ltd. China). Each leaf subsample (0.1 g each representing the six collected samples) was homogenized in 1 mL of 10 mM PBS buffer (pH = 7.4) using a freeze grinder (JXFSTPRP-CL, Shanghai, China). Homogenized leaf tissue was centrifuged at 2500 rpm and 25°C for 20 min and the supernatant was used for determination of SA content by sandwich ELISA and a 450 nm optical density. Three leaf subsamples were analyzed at each time point for each treatment, and three technical replicates were performed per subsample.

2.10 Transcript expression analysis of gene *PR-1*

The six leaf samples collected for determination of SA content (section 2.9) were also used to determine relative expression of gene *PR-1*. The transcript expression of gene *PR-1* involved in the SA signaling pathway was determined by RT-qPCR assay using the QuantStudio 3 qPCR System (Applied Biosystems, USA). Total RNA was extracted from the leaf tissue using the TRIzol reagent kit (Invitrogen, USA). The cDNA was synthesized using HiScript II Q RT SuperMix with a qPCR (+gDNA wiper) reverse transcription kit (Vazyme Biotech). The qPCR mix was composed of 10.0 µL of 2× ChamQ Universal SYBR qPCR Master Mix (Vazyme Biotech), 0.4 µL of forward and reverse primers (10 µM), 1.0 µL of cDNA, and sterile high-purity water to obtain a final volume of 20 µL. The qPCR program included denaturation at 95°C for 30 s followed by 40 cycles at 95°C for 10 s, and 60°C for 30 s. The glyceraldehyde 3-phosphate dehydrogenase (GAPDH) gene was used as a reference gene (Zheng et al., 2017). The relative expression of gene *PR-1* was calculated with the $2^{-\triangle\triangle CT}$ method. Characteristics of the primers is given in Table S2. Three leaf subsamples were analyzed at each time point and for each treatment, and three technical replicates were performed per subsample.

2.11 Statistical analyses

An analysis of variance (one-way ANOVA) was conducted with AUDPC data obtained for the two sugarcane varieties inoculated with the two strains of *Aaa* (single and mixed inocula). The same type of analysis was performed with each data set of the SA content and of the transcript level of gene *PR*-1 in plants at each time point (0, 12, 24, 48, and 72 h). Duncan's test was used to identify mean differences at $p \leq 0.05$ between the treatments. All analyses were conducted with the software SAS version 8.01 (SAS Institute Inc., North Carolina, USA).

3 Results

3.1 Isolation of bacteria from leaves showing red stripe symptoms

Seventeen bacterial strains were isolated on NA medium from the 13 sugarcane leaves (A-M) with typical red stripe symptoms collected from the provinces of Guangxi and Guangdong (Figure S1). The color of the colonies varied among these strains (Figure 1A). Five leaf samples yielded only white-cream, circular, and translucent colonies whereas another four leaf samples yielded only yellow, circular, and translucent colonies. Colonies of both morphological types were obtained from the remaining four leaf samples. The white-cream colonies grew slower than the yellow colonies as mean size of white-cream colonies was 1.14 mm (± 0.06) vs. 0.91 mm (± 0.06) for yellow colonies after 24 h of growth on NA medium (Figures 1B, C). A colony of strain CNGX08 (white-cream) and a colony of CNGD05 (yellow) were taken for observation of bacterial cell morphology by electron microscopy. No bacterial spores were observed in the microscopic preparations and cells of both strains were straight rods with a single polar flagellum (Figures 1D, E).

3.2 PCR detection and sequence identification of *Aaa* strains

A 454 bp fragment was amplified by PCR from total genomic DNA of the 17 bacterial strains from China using the *Aaa*-specific primers (RS-ITS-F1/RS-ITS-R1) (Table S1). Based on the nucleotide sequence of this amplicon, the strains originating from two geographical regions (Guangxi *vs.* Guangdong) or with different morphological types (white-cream *vs.* yellow) were 98.4-100% identical (Figure S2). These strains had also 98.2-99.5%, 97.7-98.8%, and 96.2-97.3% sequence identity with *Aaa* strain ATCC 19860 *Aac* strain W6, and *Aaca* strain 30134, respectively. The specific PCR amplification and sequence data suggested that the 17 bacterial strains from sugarcane in China belong to the subspecies *Aaa*.

10.3389/fpls.2023.1127928

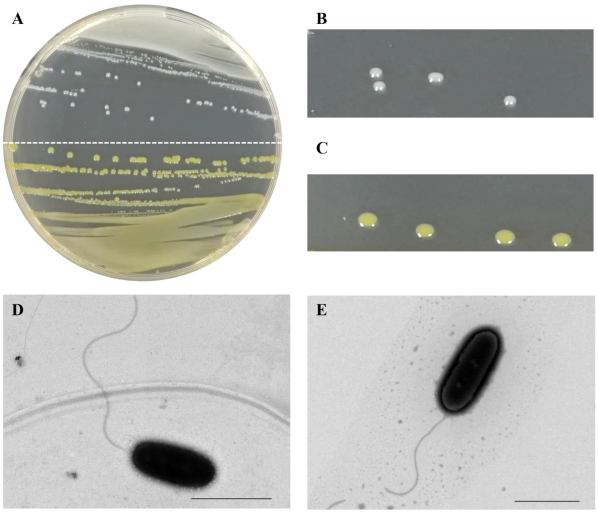

FIGURE 1
Colony and cell morphology of two strains of *Acidovorax avenae* subsp. *avenae* isolated from sugarcane in China. **(A)** Colonies of strain CNGX08 (white-cream; upper half plate) and strain CNGD05 (yellow; lower half plate) growing on a nutrient agar (NA) medium plate. **(B, C)** Close up view of the colonies of strains CNGX08 and CNGD05, respectively. **(D, E)** Cell morphology of strains CNGX08 and CNGD05 observed by transmission electron microscopy (x10,000), respectively. The scale bar corresponds to 2.0 μm.

3.3 RFLP analysis of *Aaa* strains based on the 16S-23S rDNA ITS region

The 17 *Aaa* strains from sugarcane in China were divided into three groups based on their *in silico* restriction patterns (I, II, and IIIb) of the 16S-23S rDNA ITS region (454 bp) cut with enzymes *Hin*dIII and *Eco*RI (Table 1). Pattern RFLP I consisted of two bands (330 and 124 bp) whereas pattern II had three bands (330, 68, and 56 bp). Two bands, one of 386 bp and the other of 68 bp, formed pattern RFLP IIIb. The RFLP pattern I group included seven *Aaa* strains from the Guangxi province (four with white-cream colonies and three with yellow colonies). RFLP pattern II group contained nine strains from the provinces of Guangxi and Guangdong (four with white-cream colonies and five with yellow colonies). Only strain CNGD01 with white-cream colonies from the province of Guangdong showed RFLP pattern IIIb (Table 1).

3.4 Sequence identity analysis of five housekeeping genes

To further investigate the genetic variability among the 17 strains of *Aaa* from sugarcane in China, pairwise sequence comparisons were carried out with the single sequence of five housekeeping genes (*ugp*B, *pil*T, *lep*A, *trp*B, and *glt*A) and with the concatenated sequence (2,246 nucleotides) of these five genes. When the housekeeping genes were

TABLE 1 *In silico* analysis of RFLP patterns of 17 strains of *Acidovorax avenae* subsp. *avenae* from sugarcane in China based on the internal transcribed spacer (ITS) region of 16S-23S rDNA.

Strain name	Colony color	Size of sequence (bp)	Restriction fragments (bp) obtained after digestion with			Restriction pattern [a]
			*Hin*dIII	*Eco*RI	*Hin*dIII + *Eco*RI	
CNGX01	white	454	330, 124	454	330, 124	I
CNGX02	yellow	454	330, 124	454	330, 124	I
CNGX03	yellow	454	330, 124	386, 68	330, 68, 56	II
CNGX04	white	454	330, 124	386, 68	330, 68, 56	II
CNGX05	yellow	454	330, 124	454	330, 124	I
CNGX06	white	454	330, 124	454	330, 124	I
CNGX07	yellow	454	330, 124	454	330, 124	I
CNGX08	white	454	330, 124	454	330, 124	I
CNGX09	yellow	454	330, 124	454	330, 124	I
CNGX10	white	454	330, 124	386, 68	330, 68, 56	II
CNGX11	yellow	454	330, 124	386, 68	330, 68, 56	II
CNGD01	white	454	454	386, 68	386, 68	IIIb
CNGD02	white	454	330, 124	386, 68	330, 68, 56	II
CNGD03	white	454	330, 124	386, 68	330, 68, 56	II
CNGD04	yellow	454	330, 124	386, 68	330, 68, 56	II
CNGD05	yellow	454	330, 124	386, 68	330, 68, 56	II
CNGD06	white	454	330, 124	386, 68	330, 68, 56	II

[a]Classification of restriction patterns as described by Li et al. (2018).

analyzed separately, the lowest sequence identities were found for gene *lep*A (95.0-100%), followed by *ugp*B (95.7-100%) and *glt*A (96.8-100%). Highest sequence identities were observed for genes *trp*B (99.5-100%) and *pil*T (97.9-100%) (Table S3). The 17 strains of *Aaa* had 97.8-100% sequence identity among each other and 96.7-97.5% with seven strains of *Aaa* from Argentina when comparisons were based on the concatenated sequence of all five genes. This latter identity was 97.0-97.7%, 94.6-95.4%, and 95.7-96.3% with strain ATCC 19860 of *Aaa*, strain AacW6 of *Aac*, and strain 30134 of *Aaca*, respectively (Table S3).

3.5 Genotyping of *Aaa* strains by MLST

To further investigate the evolutionary clustering of *Aaa*, the 17 strains of this subspecies obtained in this study from sugarcane in China were compared to 25 additional strains of *Aaa* (from bentgrass, maize, millet, rice, sorghum, sugarcane, and Vasey grass), 10 strains of *Aac* (from melon and watermelon), and one strain of *Aaca* (from orchid) retrieved from the NCBI library (Table S1). MLST conducted with the concatenated sequence of five housekeeping genes (section 3.4) revealed that all *A. avenae* strains were divided at subspecies level into three major evolutionary clades (Figure 2). The 10 strains of *Aac* (from China, Israel, and the USA) and strain 30134 of *Aaca* (from the USA) were distributed in two separate evolutionary clades. The 42 strains of *Aaa* forming the third clade were further distributed into three subclades. The 17 strains of *Aaa* from sugarcane obtained in this study and *Aaa* strain 30179 from sorghum in Brazil formed subclade Aaa-I, while seven strains from sugarcane in Argentina and 11 additional strains from bentgrass, maize, rice, and Vasey grass from Japan and the USA grouped in subclade Aaa-II. Six strains of *Aaa* from Creeping bentgrass originating from the USA formed subclade Aaa-III (Figure 2). In subclade Aaa-I, the 17 strains of *Aaa* from sugarcane obtained in this study were distributed in three different phylogenetic subgroups.

3.6 Pathogenicity of two strains of *Aaa* in sugarcane plants

Red stripe symptoms developed in sugarcane varieties LC07-150 and ZZ8 after single and mixed inoculation with strains CNGX08 and CNGD05 of *Aaa* from China. At 3 dpi, water-green stripes appeared in the middle of the leaf blade and these lesions rapidly turned into

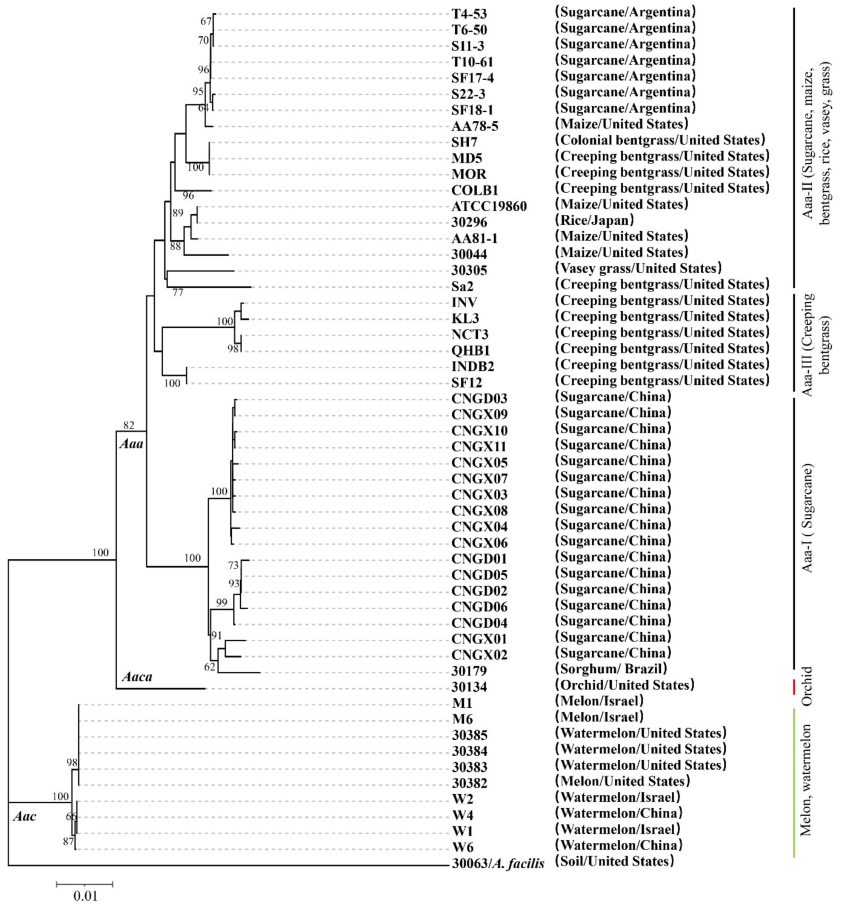

FIGURE 2
Neighbor-joining phylogenetic tree constructed with the concatenated sequence (2,246 nucleotides) of five housekeeping genes from 42 strains of *Acidovorax avenae* subsp. *avenae* (17 obtained in this study and 25 retrieved from the NCBI library), 10 strains of *A. avenae* subsp. *citrulli* and one strain of *A. avenae* subsp. *cattleyae* retrieved from the NCBI library. Strain 30063 of *A. facilis* was used as an outgroup. The characteristics of all strains are given in Table S1. Bootstrap values were determined for 1,000 replications and only bootstrap values >60% are shown at nodes.

10.3389/fpls.2023.1127928

TABLE 2 Analysis of variance of area under disease progress curve (AUDPC*) of two sugarcane varieties inoculated with two strains of *Acidovorax avenae* subsp. *avenae* (*Aaa*).

Treatment	AUDPC**
Sugarcane variety LC07-150 inoculated with *Aaa* strain CNGX08	9.726 a
Sugarcane variety LC07-150 inoculated with *Aaa* strain CNGD05	7.000 c
Sugarcane variety LC07-150 inoculated with *Aaa* strains CNGX08 + CNGD05	8.301 b
Sugarcane variety ZZ8 inoculated with *Aaa* strain CNGX08	7.450 b
Sugarcane variety ZZ8 inoculated with *Aaa* strain CNGD05	8.725 a
Sugarcane variety ZZ8 inoculated with *Aaa* strains CNGX08 + CNGD05	7.425 b

(*AUDPC) values were calculated with disease incidence (percent diseased plants) determined for two separate experiments at 3, 6, 9, 12, and 15 days post inoculation.
(**AUDPC) followed by the same letter are not different at P = 0.05 according to Duncan's test.

red-brown stripes. The sugarcane plants of varieties LC07-150 and ZZ8 inoculated with sterile water remained symptomless (Figures 3A, B). The disease incidence of all inoculation treatments with *Aaa* was greater than 20 and 65% at 3 and 12 dpi, respectively (Figure 3C). At 15 dpi, lowest incidence (73.3%) was observed for variety LC07-150 inoculated with strain CNGD05 and highest incidence (88.3%) was found for the same variety inoculated with strain CNGX08. After isolation from symptomatic plants, the strains of *Aaa* shared 100% sequence identities of ITS of 16S-23S rDNA and same colony color with inoculated strain.

A significant bacterial strain effect (P = 0.0007) but a not significant sugarcane variety effect (P = 0.0680) was found based on AUDPC analysis of all inoculation treatments of combined experiments. The variety x strain interaction effect was also not significant (P = 0.0591). Strain CNGX08 of *Aaa* was more pathogenic than strain CNGD05 in sugarcane variety LC07-150, while strain CNGD05 was more pathogenic than strain CNGX08 in sugarcane variety ZZ8 (Table 2). Strain CNGX08 was also more pathogenic in LC07-150 when inoculated alone than in mixed inoculation with strain CNGD05. The same result was observed for strain CNGD05 in variety ZZ8.

3.7 Changes of SA content in sugarcane after infection by *Aaa*

To investigate whether the SA signal transduction pathway was involved in sugarcane affected by red stripe, the SA content and the expression of the SA-mediated resistance gene (*PR-1*) were determined in sugarcane varieties LC07-150 and ZZ8 after single or mixed inoculation with strains CNGX08 and CNGD05 of *Aaa*. Similar changes in SA content were observed in the two sugarcane varieties 0-72 hpi, regardless of the bacterial inoculum (Figure 4). When compared to the control plants inoculated with water, the SA

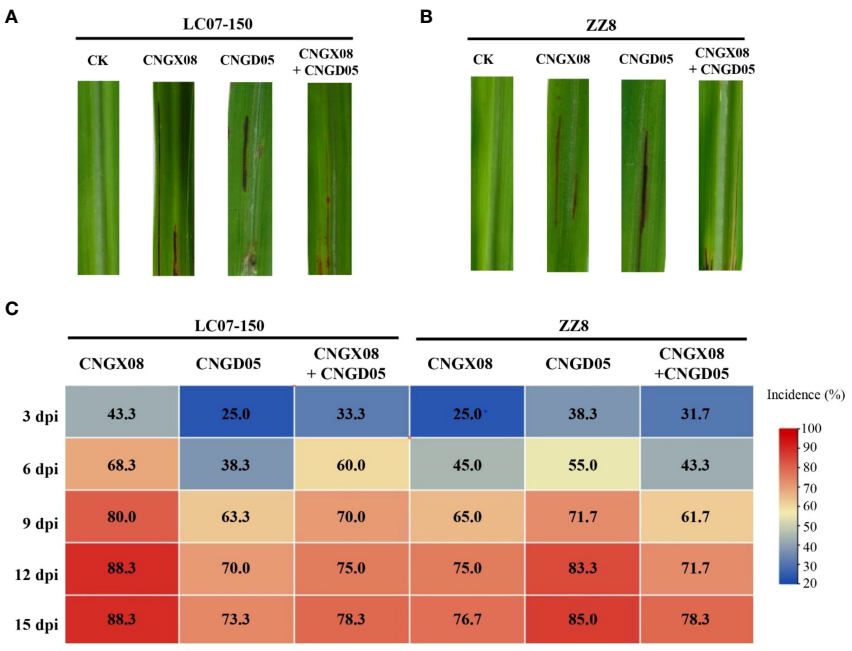

FIGURE 3
Symptoms and disease incidence of red stripe in two sugarcane varieties (LC07-150 and ZZ8) inoculated with strains CNGX08 and CNGD05 of *Acidovorax* avenae subsp. avenae. **(A)** Red stripe symptoms observed 15 days post inoculation (dpi) in variety LC07-150, CK = water control. **(B)** Red stripe symptoms observed 15 dpi in variety ZZ8, CK = water control. **(C)** Heatmap of disease incidence of inoculated plants from 3-15 dpi.

10.3389/fpls.2023.1127928

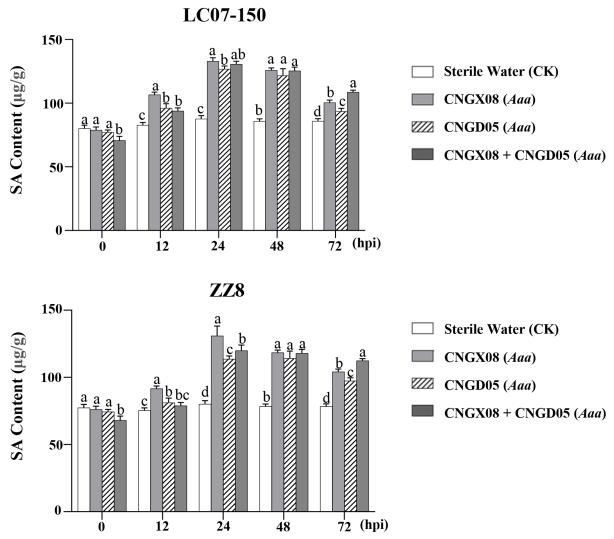

FIGURE 4
Salicylic acid (SA) content in two sugarcane varieties (LC07-150 and ZZ8) inoculated with strains CNGX08 and CNGD05 of *Acidovorax avenae* subsp. *avenae* (*Aaa*). Inoculated leaf samples were collected 0, 12, 24, 48, and 72 hours post inoculation (hpi). Each vertical bar represents the mean ± standard deviation of three biological and three technical replicates per subsample. At each time point, means with the same letter are not significantly different at $P = 0.05$ according to Duncan's test.

content increased in varieties LC07-150 and ZZ8 after all *Aaa* treatments. Highest SA increases (40-65%) were observed in these varieties at 24-48 hpi. Significant differences between *Aaa* treatments were observed at some time points but they were not always consistent throughout the 12-72 hpi. Nevertheless, SA content was greater in varieties LC07-150 and ZZ8 inoculated with strain CNGX08 of *Aaa* than with strain CNGD05 at 12, 24, and 72 hpi (Figure 4).

3.8 Expression of gene *PR-1* in sugarcane infected by *Aaa*

Expression of gene *PR-1* involved in the SA signal transduction pathway was significantly upregulated in varieties LC07-150 and ZZ8 inoculated with the two strains of *Aaa* (CNGX08 and CNGD05), as compared to control plants inoculated with water only (Figure 5). Significant increases of *PR-1* expression were observed for single and mixed inocula as soon as 12 hpi, but greatest expression was found at 72 hpi. At his time point, *PR-1* transcript levels had increased 16-23 times in variety LC07-150 after single or mixed inoculation with strains CNGX08 and CNGD05 of *Aaa*. A 21-30-time increase was observed for the same strains in variety ZZ8. In each infected sugarcane variety, relative expression of gene *PR-1* differed among strains at one time point or another but no consistent pattern was observed, except at 24 and 48 hpi. At these two time points, relative expression of gene *PR-1* was higher in plants of the two varieties inoculated simultaneously with strains CNGX08 and CNGD05 than in plants inoculated with the single strains of the pathogen.

4 Discussion

Variation in color of *Aaa* colonies has been reported, especially when this bacterial subspecies was grown on different agar media. For example, colonies of *Aaa* from sugarcane were off-white on potato dextrose agar (PDA) (Zia-ul-Hussnain et al., 2011), yellow or beige on yeast extract-dextrose-calcium carbonate (YDC) (Zia-ul-Hussnain et al., 2011; Fontana et al., 2013; Bertani et al., 2021), yellow-cream on yeast peptone glucose agar (YPGA) (Girard et al., 2014), white-cream on NA medium (Fontana et al., 2013; Li et al., 2018; Bertani et al., 2021), and grayish-white on Wilbrinks agar medium (Hernández-Juárez et al., 2021). However, only 35-50% of white-cream colonies isolated from sugarcane in Argentina on NA medium were positive by PCR with *Aaa*-specific primers Oaf1/Oar1 (Fontana et al., 2013; Bertani et al., 2021). PCR-negative colonies and other yellow-colored colonies grown on NA or YDC media belonged to other bacterial species of the *Erwinia* and *Pantoea* genera.

Colonies of *A. avenae* are usually white-cream and do not produce pigments on NA medium at optimal growth temperature of 30-35°C (Willems and Gillis, 2015). In our study based on microbiological, molecular, and pathogenicity assays, two types of colored colonies (yellow and white) growing on NA medium were identified as the causal agents of sugarcane red stripe in China. A bias of color caused by the medium composition was excluded because both colored colonies were observed on the same plates and under the same environmental conditions. Furthermore, only one color type of

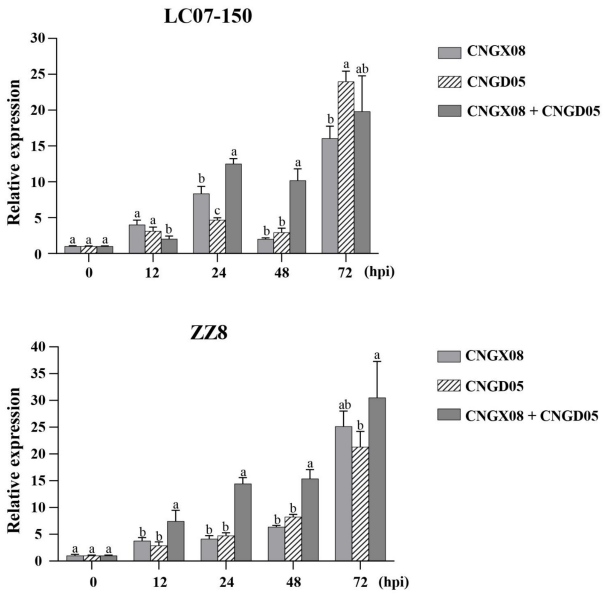

FIGURE 5
Relative expression of pathogenesis-related protein 1 (PR-1) gene in two sugarcane varieties (LC07-150 and ZZ8) inoculated with strains CNGX08 and CNGD05 of *Acidovorax avenae* subsp. *avenae* (*Aaa*). Inoculated leaf samples were collected 0, 12, 24, 48, and 72 hours post inoculation (hpi). Each vertical bar represents the mean ± standard deviation of three biological and three technical replicates per subsample. At each time point, means with the same letter are not significantly different at $P = 0.05$ according to Duncan's test.

colony was reisolated from plants inoculated with pure cultures of two strains, namely white-cream colored strain CNGX08 and yellow-colored CNGD05. No difference in cell morphology (shape of bacteria) was found between these two strains that differed from each other based on growth rate on NA medium (CNGX08 grew slower than CNGD05), RFLP profile (I for CNGX08 and II for CNGD05), and phylogenetic subgrouping in the Aaa-I clade. The genetic mechanism for color variation in *Aaa* remains to be investigated. Occurrence of two colored types of *Aaa* in some infected plants also revealed that red stripe can be caused by a mix of strains. Mixed plant infections with diverse strains of a microorganism (including pathogens) are common in crops, especially in sugarcane that is propagated vegetatively by stalk cuttings (He et al., 2022).

Genetic diversity of *Aaa* strains in sugarcane-growing countries was previously unraveled by various molecular typing methods such as RAPD (Fontana et al., 2013), PCR-based RFLP (Li et al., 2018), MLST (Fontana et al., 2019), rep-PCR and AFLP (Bertani et al., 2021). Among these methods, MLST is very powerful to analyze the taxonomic structure, evolutionary processes, and population speciation of bacteria, including *Aaa* (Rong and Huang, 2014; Fontana et al., 2019). In our study, the MLST analysis revealed that all *Aaa* strains hosted by various plant species worldwide formed a distinct and separate clade from strains of *Aac* (hosted by watermelon and melon) and *Aaca* (hosted by orchid) at the subspecies level. Additionally, the strains of *Aaa* isolated from sugarcane in Argentina and China were distributed in two different evolutionary subclades. The subclade of sugarcane strains from Argentina also contained strains from other *Poaceae* such as bentgrass, maize, rice, sorghum, and Vasey grass, whereas the subclade of sugarcane strains from China only included one strain from sorghum in Brazil. Similarly, several strains of *Aaa* from bentgrass in the USA were closer to strains of *Aaa* from maize or rice rather than to other strains collected from bentgrass in the same country (Zeng et al., 2017). These data suggested that *A. avenae* strains exhibit clonal behavior, geographical and host specificity to a certain extent, as previously reported (Yan et al., 2017; Fontana et al., 2019; Bertani et al., 2021). Among seven housekeeping genes used for a MLST study in Argentina, gene *lep*A exhibited greatest variability for strains of *Aaa* from sugarcane (Fontana et al., 2019).

Besides the 16S rDNA, the ITS region of 16S–23S rDNA is also very useful for bacterial and fungal species or strain classification because PCR amplification and sequencing of this region provides specific and accurate data using universal primers (Ji et al., 2017; Li et al., 2018). Consequently, this method has also been widely applied to identify and differentiate *A. avenae* at species, subspecies, and strain levels (Schaad et al., 2008; Song et al., 2003; Li et al., 2018). For example, Song et al. (2003) developed the species-specific primers Oafl/Oarl for rapid identification of *A. avenae* strains from all hosts, whereas the *citrulli*-specific primers Aacf2/Aacr2 are for specific identification of subsp. *citrulli*. Schaad et al. (2008) reported that sequence identities of the ITS of the 16S–23S rDNA were high (97.3-99.0%) among strains of *A. avenae* from various hosts, whereas the other three plant pathogenic species (*A. konjaci*, *A. anthurii*, and *A. valerianellae*) shared lower identities (81.8–87.8%) with *A. avenae* strains. Li et al. (2018) demonstrated that these nucleotide sequences had also different sizes (from 436 to 454 bp) and that their identities diverged from 89.2 to 100% among *Aaa* strains infecting sugarcane from China and *A. avenae* strains infecting other plants worldwide. Furthermore, seven RFLP profiles based on the ITS region of 16S-23S rDNA were reported for strains of *Aaa* from sugarcane in China, among which profiles I, II, IIIb, and IVa were reported in the provinces of Guangxi and Guangdong (Li et al., 2018). The most recent strains collected in our study from the same provinces belonged to RFLP profiles I, II, and IIIb, thus confirming previous results.

No relationship was found between the three RFLP profiles of the 17 strains of *Aaa* obtained herein and the geographical origin, host variety, and colony color. Similarly, no correlation was found between the geographical origin and the sampling year of strains of *Aaa* from Argentina using MLST (Fontana et al., 2019). Genetic diversity of *Aaa* identified by rep-PCR was not related either with sugarcane genotype, ratoon cycle, tissue type, field fertilization, or year of sampling (Bertani et al., 2021). It has been hypothesized that dispersal rates of *Aaa* are too high to maintain spatially structured populations within a limited geographic distance and in a single host (Zeng et al., 2017; Bertani et al., 2021). Nevertheless, specific genetic populations of *Aaa* were identified by MLST in China in this study and previously in Argentina. To confirm this, further studies need to be conducted with a more extensive collection of strains of the pathogen from additional locations affected by sugarcane red stripe.

After inoculation of two sugarcane varieties susceptible to red stripe, strains CNGX08 (white-cream colonies) and CNGD05 (yellow colonies) of *Aaa* induced development of disease symptoms and disease incidence was high (≥70%) 15 days after inoculation. Similarly, high disease incidence (53-70%) was reported seven days post inoculation of variety FN41 with *Aaa* strain SC-026 from China (Li et al., 2018). Creeping bentgrass inoculated with strain MSU4 of *Aaa* exhibited up to 68% of leaf necrosis two weeks after inoculation (Giordano et al., 2012). Variation in pathogenicity among strains of *Aaa* is currently poorly known, although different levels of aggressiveness in a resistant sugarcane variety were found among isolates of this pathogen in Argentina (Bertani et al., 2021).

Strain CNGX08 of *Aaa* from China was more pathogenic than strain CNGD05 in one sugarcane variety (LC07-150) whereas strain CNGD05 was more pathogenic than CNGX08 in the other variety (ZZ8). This is strong evidence for variation in pathogenicity and possible occurrence of races within *Aaa* as the variety x strain interaction effect was almost significant (P = 0.0591). The genetic basis for resistance of sugarcane to red stripe is currently unknown. Besides specific features of the pathogen involved in pathogenicity variation, the host cytoplasm may also play an important role in the sugarcane response to a specific strain of *Aaa* as strains CNGX08 and CNGD05 were more pathogenic in the sugarcane variety from which they were originally isolated. Use of additional inoculation experiments and different sugarcane varieties might be necessary to prove these hypotheses. In the host variety in which their incidence was highest, strains CNGX08 and CNGD05 of *Aaa* were also more pathogenic in single inoculations than in mixed inoculations, suggesting a negative interaction between the two strains. No significant difference in pathogenicity was found for *Cylindrocarpon destructans* when single and mixed inocula of this root pathogen of oak (*Quercus* spp.) were compared (Sánchez et al., 2002). In contrast, the nonpathogenic *hrcC* mutant of *Xanthomonas campestris* pv. *vesicatoria* 85-10::hrpA22

multiplied in pepper leaves when it was mixed with the pathogenic wild type strain, thus indicating a positive effect of this latter strain in mixed inoculation (Keshavarzi et al., 2004). When tested alone, lineage IV of *Cephalosporium maydis* from Egypt was the most virulent of four clonal lineages toward greenhouse-grown maize. However, this lineage was the least competitive in susceptible maize clones inoculated with mixtures of all four lineages of the pathogen (Zeller et al., 2002). Further investigations are needed to understand the interactions among strains of *Aaa*, especially in diseased plants infected by the two differently colored types of the pathogen.

SA and the SA-mediated signal transduction pathway are major players in plant immunity by mediating local and systemic immune responses against pathogen invasion (Seyfferth and Tsuda, 2014; Khan et al., 2022). SA levels are usually elevated in plants upon pathogen infections, thus promoting massive transcriptional reprogramming including increased expression of gene *PR-1* (Chu et al., 2020; Chu et al., 2022; Khan et al., 2022). SA and Jasmonic (JA) treatments induced tolerance to *Aaa* infection in creeping bentgrass (Liu et al., 2018). In our study, the two strains of *Aaa* induced significant increases of endogenous SA content and expression of gene *PR-1* in infected sugarcane, especially at 24-72 hpi. Increased content of SA and transcript expression of *PR-1* was observed in sugarcane after inoculation with two strains (XaCN51 and XaCN24) of *X. albilineans* differing in pathogenicity (Zhao et al., 2022). Moreover, plants infected with the high pathogenic strain of *X. albilineans* (XaCN51) maintained a lower content of SA and a lower expression level of SA-medicated gene *PR-1* as compared to plants infected with the low pathogenic strain of the pathogen (XaCN24). In contrast to the study on *X. albilineans*, the content of SA and the expression level of SA-mediated gene *PR-1* in *Aaa* infected sugarcane were not associated with disease level caused by the two strains of the pathogen (CNGX08 and CNGD05). One reason could be the high expression of disease symptoms for the two strains even if their disease incidences were significantly different. Another reason could be that the SA signaling pathway plays a minor role in the defense response against *Aaa* as compared to other signaling pathways. These hypotheses remain to be explored. Significant difference in disease incidence and in the SA plant response between the two strains of *Aaa* from China (single and mixed infections) suggested that colony color could be associated with pathogenicity of the red stripe pathogen of sugarcane. This hypothesis needs to be investigated by testing a larger number of strains of each color type and by functional genomics of genes involved in colony color.

5 Conclusion

In this study, we demonstrated that at least two strains of *Aaa* with different colony colors (i.e. white-cream and yellow) cause red stripe of sugarcane in China. Based on MLST and PCR-based RFLP data, plant species and geographical origin at country level appeared to contribute to genetic diversity of *Aaa* populations rather than host varieties in a given small geographical environment. SA and gene *PR-1* that are usually involved in resistance to biotic stresses are also produced/expressed in a susceptible interaction leading to disease. Additional studies are needed to elucidate the significance of color variation in *Aaa* and the impact of the genetic diversity of this pathogen in red stripe epidemics of sugarcane and other crops.

Data availability statement

The original contributions presented in the study are included in the article/Supplementary Material. Further inquiries can be directed to the corresponding authors.

Author contributions

Conceptualization, PR and S-JG. Writing—original draft preparation, J-YZ and JC. Writing—review and editing, PR and S-JG. Data curation, Z-TH and JL. Experiments preformation, J-YZ, JC, and H-YF. Supervision, funding acquisition, and project administration, S-JG. All authors contributed to the article and approved the submitted version.

Funding

This work was supported by the earmarked fund for China Agriculture Research System (grant no. CARS-170302).

Acknowledgments

We sincerely thank Miss Mei-Ting Huang for her technical help and Dr. Hui-Li Zhang and Jin-Da Wang for field sample collection.

Conflict of interest

The authors declare that the research was conducted in the absence of any commercial or financial relationships that could be construed as a potential conflict of interest.

Publisher's note

Supplementary material

The Supplementary Material for this article can be found online at: https://www.frontiersin.org/articles/10.3389/fpls.2023.1127928/full#supplementary-material

References

Bertani, R. P., Perera, M. F., Joya, C. M., Henriquez, D. D., Funes, C., Chaves, S., et al. (2021). Genetic diversity and population structure of *Acidovorax avenae* subsp. *avenae* isolated from sugarcane in Argentina. *Plant Pathol.* 70, 1719–1732. doi: 10.1111/ppa.13413

Bipen, K., Rakesh, Y., and Ratinderbir, K. (2014). Present status of bacterial top rot disease of sugarcane in Indian punjab. *Plant Dis. Res.* 29 (1), 68–70.

Chu, N., Zhou, J. R., Fu, H. Y., Huang, M. T., Zhang, H. L., and Gao, S. J. (2020). Global gene responses of resistant and susceptible sugarcane cultivars to *Acidovorax avenae* subsp. *avenae* identified using comparative transcriptome analysis. *Microorganisms.* 8 (1), 10. doi: 10.3390/microorganisms8010010

Chu, N., Zhou, J. R., Rott, P. C., Li, J., Fu, H. Y., Huang, M. T., et al. (2022). *ScPR1* plays a positive role in the regulation of resistance to diverse stresses in sugarcane (*Saccharum* spp.) and *Arabidopsis thaliana*. *Ind. Crop Prod.* 180, 114736. doi: 10.1016/j.indcrop.2022.114736

De, Vos., P., Willems, A., and Jones, J. B. (2018). "Taxonomy of the *Acidovorax* genus," in *Plant-pathogenic* Acidovorax *species*. Eds. S. Burdman and R. R. Walcott(Minnesota, USA), 5–37. doi: 10.1094/9780890546062.002

Feng, J., Schuenzel, E. L., Li, J., and Schaad, N. W. (2009). Multilocus sequence typing reveals two evolutionary lineages of *Acidovorax avenae* subsp. *citrulli*. *Phytopathology.* 99 (8), 913–920. doi: 10.1094/PHYTO-99-8-0913

Fontana, P. D., Rago, A. M., Fontana, C. A., Vignolo, G. M., Cocconcelli, P. S., and Mariotti, J. A. (2013). Isolation and genetic characterization of *Acidovorax avenae* from red stripe infected sugarcane in northwestern Argentina. *Eur. J. Plant Pathol.* 137, 525–534. doi: 10.1007/s10658-013-0263-y

Fontana, P. D., Tomasini, N., Fontana, C. A., Di, P. V., Cocconcelli, P. S., Vignolo, G. M., et al. (2019). MLST reveals a separate and novel clonal group for *Acidovorax avenae* strains causing red stripe in sugarcane from Argentina. *Phytopathology.* 109 (3), 358–365. doi: 10.1094/PHYTO-08-18-0303-R

Fu, H. Y., Ge, D. F., Li, X. Y., Wu, X. B., Chen, R. K., and Gao, S. J. (2017). Nested-PCR detection of *Acidovorax avenae* subsp. *avenae*, the pathogen of red stripe on sugarcane. *J. Plant Prot.* 44 (2), 276–282. doi: 10.13802/j.cnki.zwbhxb.2017.2015156

Giordano, P. R., Chaves, A. M., Mitkowski, N. A., and Vargas C.OMMAJr., J. M. (2012). Identification, characterization, and distribution of *Acidovorax avenae* subsp. *avenae* associated with creeping bentgrass etiolation and decline. *Plant Dis.* 96 (12), 1736–1742. doi: 10.1094/PDIS-04-12-0377-RE

Girard, J. C., Noëll, J., Larbre, F., Roumagnac, P., and Rott, P. (2014). First report of *Acidovorax avenae* subsp. *avenae* causing sugarcane red stripe in Gabon. *Plant Dis.* 98 (5), 684. doi: 10.1094/PDIS-09-13-0914-PDN

He, E.-Q., Bao, W.-Q., Sun, S.-R., Hu, C.-Y., Chen, J.-S., Bi, Z.-W., et al. (2022). Incidence and distribution of four viruses causing diverse mosaic diseases of sugarcane in China. *Agronomy.* 12, 302. doi: 10.3390/agronomy12020302

Hernández-Juárez, C., Silva-Rojas, H. V., De León García de Alba, C., Hernandez-Juárez, E., Osnaya-González, M., and Valdovinos-Ponce, G. (2021). Molecular identification, incidence, and distribution of *Acidovorax avenae* in the sugarcane-producing agroecological regions of Mexico. *Sugar Tech.* 23, 891–899. doi: 10.1007/s12355-021-00964-w

Ji, L., Liu, C., Zhang, L., Liu, A., and Yu, J. (2017). Variation of rDNA internal transcribed spacer sequences in *Rhizoctonia cerealis*. *Curr. Microbiol.* 74 (7), 877–884. doi: 10.1007/s00284-017-1258-2

Keshavarzi, M., Soylu, S., Brown, I., Bonas, U., Nicole, M., Rossiter, J., et al. (2004). Basal defenses induced in pepper by lipopolysaccharides are suppressed by *Xanthomonas campestris* pv. *vesicatoria*. *Mol. Plant Microbe Interact.* 17 (7), 805–815. doi: 10.1094/MPMI.2004.17.7.805

Khan, M., Islam, F., Chen, H., Chang, M., Wang, D., Liu, F., et al. (2022). Transcriptional coactivators: Driving force of plant immunity. *Front. Plant Sci.* 13, 823937. doi: 10.3389/fpls.2022.823937

Li, D., Luo, Y., Qin, Z., Huang, X., Tang, L., and Luo, S. (2021). Occurrence and evaluation of red stripe disease of sugarcane for sugarcane variety (lines) in guangxi in 2020. *Chin. J. Trop. Agric.* 41, 96–101. doi: 10.12008/j.issn.1009-2196.2021.03.016

Li, J., Shan, H. L., Wang, C. M., Cang, X. Y., Wang, X. Y., Zhang, R. Y., et al. (2022). Investigation and molecular detection of sugarcane red stripe caused by *Acidovorax avenae* subsp. *avenae* in Nanning, Guangxi. *Plant Prot.* 48 (1), 279–283. doi: 10.16688/j.zwbh.2020662

Li, X. Y., Sun, H. D., Rott, P. C., Wang, J. D., Huang, M. T., Zhang, Q. Q., et al. (2018). Molecular identification and prevalence of *Acidovorax avenae* subsp. *avenae* causing red stripe of sugarcane in China. *Plant Pathol.* 67, 929–937. doi: 10.1111/ppa.12811

Liu, S., Vargas, J., and Merewitz, E. (2018). Jasmonic and salicylic acid effects on bacterial etiolation and decline disease of creeping bentgrass. *Crop Prot.* 109, 9–16. doi: 10.1016/j.cropro.2018.02.023

Liu, X., Wu, Z., and Zhou, J. (2022). Domestic and foreign sugar markets in 2021/22 crushing season and their prospect for 2022/23 crushing season. *Sugarcane Canesugar.* 51 (4), 54–65.

Martin, J., Wismer, C., and Ryan, C. (1989). "Red stripe," in *Diseases of sugarcane*. Eds. C. Ricaud, B. T. Egan, A. G. Gillaspie and C. G. Hughes (Amsterdam, Netherlands: Elsevier Science Publishers BV), 81–95. doi: 10.1016/B978-0-444-42797-7.50009-0

Rong, X., and Huang, Y. (2014). "Multi-locus sequence analysis: Taking prokaryotic systematics to the next level," in *Methods in microbiology*. Eds. M. Sutcliffe and J. Chun (London, UK: Elsevier Ltd), 221–251. doi: 10.1016/bs.mim.2014.10.001

Rott, P., and Davis, M. J. (2000). "Red stripe (top rot)," in *A guide to sugarcane diseases*. Eds. P. Rott, R. A. Bailey, J. C. Comstock and B. J. Croft(Montpellier, France: La Librairie du Cirad), 58–62.

Sánchez, M. E., Lora, F., and Trapero, A. (2002). First report of *Cylindrocarpon destructans* as a root pathogen of mediterranean *quercus* species in Spain. *Plant Dis.* 86 (6), 693. doi: 10.1094/PDIS.2002.86.6.693C

Santa, B. A. B., Rojas, C. A., Grativol, C., Armas., E. M., Entenza, J. O., Thiebaut, F., et al. (2016). Sugarcane transcriptome analysis in response to infection caused by *Acidovorax avenae* subsp. *avenae*. *PloS One* 11 (12), e0166473. doi: 10.1371/journal.pone.0166473

Schaad, N. W., Postnikova, E., Sechler., A., Claflin., L. E., Vidaver, A. K., Jones, J. B., et al. (2008). Reclassification of subspecies of *Acidovorax avenae* as *A. avenae* (Manns 1905) emend., *A. cattleyae* (Pavarino 1911) comb. nov., *A. citrulli* schaad et al. 1978) comb. nov., and proposal of *A. oryzae* sp. nov. *Syst. Appl. Microbiol.* 31 (6-8), 434–446. doi: 10.1016/j.syapm.2008.09.003

Seyfferth, C., and Tsuda, K. (2014). Salicylic acid signal transduction: the initiation of biosynthesis, perception and transcriptional reprogramming. *Front. Plant Sci.* 5, 697. doi: 10.3389/fpls.2014.00697

Shaner, G. (1977). The effect of nitrogen fertilization on the expression of slow-mildewing resistance in Knox wheat. *Phytopathology.* 77 (8), 1051–1051. doi: 10.1094/phyto-67-1051

Shan, H. L., Li, W., Huang, Y., Wang, X., Zhang, R., Luo, Z., et al. (2017). First detection of sugarcane red stripe caused by *Acidovorax avenae* subsp. *avenae* in Yuanjiang, Yunnan, China. *Trop. Plant Pathol.* 42, 137–141. doi: 10.1007/s40858-017-0132-x

Siani, R., Stabl, G., Gutjahr, C., Schloter, M., and Radl, V. (2021). *Acidovorax* pan-genome reveals specific functional traits for plant beneficial and pathogenic plant-associations. *Microb. Genom.* 7 (12), 666. doi: 10.1099/mgen.0.000666

Song, W. Y., Sechler, A. J., Hatziloukas, E., Kim, H. M., and Schaad, N. W. (2003). "Use of PCR for rapid identification of *Acidovorax* avenae and *A. avenae* subsp. citrulli," in *Pseudomonas syringae and related pathogens*. Eds. N. S. Iacobellis, A. Collmer, S. W. Hutcheson, J. W. Mansfield, C. E. , Morris, J. Murillo, N. W. Schaad, D. E. Stead, G. Surico and M. S. Ullrich. (Dordrecht, Netherlands: Springer), 531–544. doi: 10.1007/978-94-017-0133-4_59

Strachan, S., Bhuiyan, S. A., Thompson, N., Nguyen, N. T., Ford, R., and Shiddiky, M. J.A.. (2022). Latent potential of current plant diagnostics for detection of sugarcane diseases. *Curr. Opin. Biotech.* 4, 475–492. doi: 10.1016/j.crbiot.2022.10.002

Tamura, K., Stecher, G., and Kumar, S. (2021). MEGA11: Molecular evolutionary genetics analysis version 11. *Mol. Biol. Evol.* 38, 7. doi: 10.1093/molbev/msab120

Thiebaut, F., Rojas, C. A., Grativol, C., Calixto, E. P., d., R., Motta, M. R., et al. (2017). Roles of non-coding RNA in sugarcane-microbe interaction. *Non-coding RNA* 3 (4), 25. doi: 10.3390/ncrna3040025

Willems, A., and Gillis, M. (2015). "Acidovorax," in *Bergey's manual of systematics of archaea and bacteria*. Ed. W. John (University of Georgia, USA: John Wiley & Sons, Inc.), 1–16. doi: 10.1002/9781118960608.gbm00943

Yan, L., Hu, B., Chen, G., Zhao, M., and Walcott, R. (2017). Further evidence of cucurbit host specificity among *Acidovorax citrulli* groups based on a detached melon fruit pathogenicity assay. *Phytopathology* 107 (11), 1305–1311. doi: 10.1094/PHYTO-11-16-0416-R

Zeller, K. A., Ismael, A. M., El-Assiuty, E. M., Fahmy, Z. M., Bekheet, F. M., and Leslie, J. F. (2002). Relative competitiveness and virulence of four clonal lineages of *Cephalosporium maydis* from Egypt toward greenhouse-grown maize. *Plant Dis.* 86 (4), 373–378. doi: 10.1094/PDIS.2002.86.4.373

Zeng, Q., Wang, J., Bertels, F., Giordano, P. R., Chilvers, M. I., Huntley, R. B., et al. (2017). Recombination of virulence genes in divergent *Acidovorax avenae* strains that infect a common host. *Mol. Plant Microbe Interact.* 30, 813–828. doi: 10.1094/MPMI-06-17-0151-R

Zhao, J. Y., Chen, J., Shi, Y., Fu, H. Y., Huang, M. T., Rott, P. C., et al. (2022). Sugarcane responses to two strains of *Xanthomonas albilineans* differing in pathogenicity through a differential modulation of salicylic acid and reactive oxygen species. *Front. Plant Sci.* 13, 1087525. doi: 10.3389/fpls.2022.1087525

Zheng, L., Lin, J., and Huang, X. (2017). Screening of reference genes of quantitative real-time PCR (qRT-PCR) in *Arabidopsis pumila*. *Genom. Appl. Biol.* 36, 774–783. doi: 10.13417/j.gab.036.000774

Zhou, J. R., Sun, H. D., Ali, A., Rott, P. C., Javed, T., Fu, H. Y., et al. (2021). Quantitative proteomic analysis of the sugarcane defense responses incited by *Acidovorax avenae* subsp. *avenae* causing red stripe. *Ind. Crop Prod.* 162, 113275. doi: 10.1016/j.indcrop.2021.113275

Zia-ul-Hussnain, S., Haque, M. I., Mughal, S. M., Shah, K. N., Irfan, A., Afghan, S., et al. (2011). Isolation and biochemical characterizations of the bacteria (*Acidovorax avenae* subsp. *avenae*) associated with red stripe disease of sugarcane. *Afr J. Biotechnol.* 10 (37), 7191–7197. doi: 10.5897/AJB11.953

Zytynska, S. E., Eicher, M., Rothballer, M., and Weisser, W. W. (2020). Microbial-mediated plant growth promotion and pest suppression varies under climate change. *Front. Plant Sci.* 11, 573578. doi: 10.3389/fpls.2020.573578

frontiers | Frontiers in Plant Science

TYPE Original Research
PUBLISHED 21 February 2023
DOI 10.3389/fpls.2023.1133798

OPEN ACCESS

EDITED BY
Zhenggang Li,
Guangdong Academy of Agricultural Sciences, China

REVIEWED BY
Chun Zhang,
Guangdong Academy of Agricultural Sciences, China
Weitang Liu,
Shandong Agricultural University, China

*CORRESPONDENCE
Hongchun Wang
Hongchun023@126.com

SPECIALTY SECTION
This article was submitted to Plant Pathogen Interactions, a section of the journal Frontiers in Plant Science

RECEIVED 29 December 2022
ACCEPTED 30 January 2023
PUBLISHED 21 February 2023

CITATION
Cao J, Tao Y, Zhang Z, Gu T, Li G, Lou Y and Wang H (2023) Mechanism of metamifop resistance in *Digitaria ciliaris* var. *chrysoblephara* from Jiangsu, China. *Front. Plant Sci.* 14:1133798. doi: 10.3389/fpls.2023.1133798

Mechanism of metamifop resistance in *Digitaria ciliaris* var. *chrysoblephara* from Jiangsu, China

Jingjing Cao, Yuan Tao, Zichang Zhang, Tao Gu, Gui Li, Yuanlai Lou and Hongchun Wang*

Institute of Plant Protection, Jiangsu Academy of Agricultural Sciences, Nanjing, Jiangsu, China

Digitaria ciliaris var. *chrysoblephara* is one of the most competitive and problematic grass weeds in China. Metamifop is an aryloxyphenoxypropionate (APP) herbicide that inhibits the activity of acetyl-CoA carboxylase (ACCase) of sensitive weeds. Following the introduction of metamifop to China in 2010, it has been continuously used in rice paddy fields, thereby substantially increasing selective pressure for resistant *D. ciliaris* var. *chrysoblephara* variants. Here, populations of *D. ciliaris* var. *chrysoblephara* (JYX-8, JTX-98, and JTX-99) were observed to be highly resistant to metamifop, with resistance index (RI) values of 30.64, 14.38, and 23.19, respectively. Comparison of resistant and sensitive population ACCase gene sequences revealed that a single nucleotide substitution from TGG to TGC resulted in an amino acid substitution from tryptophan to cysteine at position 2,027 in the JYX-8 population. No corresponding substitution was observed for JTX-98 and JTX-99 populations. The ACCase cDNA of *D. ciliaris* var. *chrysoblephara* was successfully obtained by PCR and RACE methods, representing the first amplification of full length ACCase cDNA from *Digitaria* spp. Investigation of the relative expressions of ACCase gene revealed the lack of significant differences between sensitive and resistant populations before and after herbicide treatments. ACCase activities in resistant populations were less inhibited than in sensitive populations and recovered to the same or even higher levels compared to untreated plants. Whole-plant bioassays were also conducted to assess resistance to other ACCase inhibitors, acetolactate synthase (ALS) inhibitors, auxin mimic herbicide, and protoporphyrinogen oxidase (PPO) inhibitor. Cross-resistance and some multi-resistance were observed in the metamifop-resistant populations. This study is the first to focus on the herbicide resistance of *D. ciliaris* var. *chrysoblephara*. These results provide evidence for a target-site resistance mechanism in metamifop-resistant *D. ciliaris* var. *chrysoblephara*, while providing a better understanding of cross- and multi-resistance characteristics of resistant populations that will help in the management of herbicide-resistant *D. ciliaris* var. *chrysoblephara*.

KEYWORDS

***Digitaria ciliaris* var. *chrysoblephara*, metamifop, weed resistance, target-site resistance, cross- and multi-resistance**

1 Introduction

Digitaria spp. are annual gramineae weeds that infest turfgrass, roadsides, wastelands, and crop systems like *Zea mays*, *Glycine max*, and *Saccharum officinarum*, among others (Basak et al., 2019). They are globally widely distributed in tropical, subtropical, and temperate regions, including in the eastern, northern, northwestern, and northeastern areas of China. Labor shortages and agricultural mechanization have led to the popularization of dry direct-seeding rice cultivation due to its high potentials for resource conservation and economic returns (Matloob et al., 2015; Rao et al., 2017). Dry direct-seeding rice cultivation accounts for over 35% of rice cultivation in China and has become one of the primary methods of rice cultivation in the Jiangsu Province. Dry-wet changes of soils in dry direct-seeding rice fields benefit weeds growth. Various weeds are present in fields that have larger occurrence and longer symbiotic times, thereby seriously threatening the yields and quality of rice. *Digitaria* spp. weeds have consequently become the dominant weeds in dry direct-seeding rice fields of the Jiangsu Province due to their adaptation to changes in local cropping systems and ecological environments (Wang et al., 2019).

Acetyl-CoA carboxylase (ACCase) inhibitors are one of the most widely used and important classes of herbicides used to control grass in rice fields. ACCase inhibitors can be divided into three types based on differences in their active components, including aryloxyphenoxypropionate (APP), cyclohexenone (CHD), and phenylpyrazole (PPZ) types (Fang et al., 2020). Plant ACCase catalyzes the carboxylation of acetyl-CoA to malonyl-CoA, thereby providing substrates for the synthesis of fatty acids and numerous secondary metabolites (Adina-Zada et al., 2012). Two forms of ACCase are typically present in plants, including heteromeric and homomeric forms (Takano et al., 2020). Poaceae plants possess homomeric ACCase, while dicotyledonous plants have homomeric form in the cytoplasm and heteromeric form in the plastids. Consequently, ACCase-inhibiting herbicides exhibit specific activities against gramineae plants that can selectively inhibit homomeric plastidic ACCase only found in monocots, but do not inhibit heteromeric plastic nor homomeric cytosolic forms, allowing dicots to become tolerant to them (Kukorelli et al., 2013; Takano et al., 2020).

Previous studies have shown that the application of ACCase inhibitors leads to the gradual development of resistance after continuous use over 6 to 10 years (Huang et al., 2003), suggesting a relatively high risk of herbicide resistance. Mechanisms of weed resistance can be divided into target-site resistance (TSR) and non-target-site resistance (NTSR). TSR to ACCase inhibitors is primarily associated with changes in amino acids caused by mutations of ACCase gene, leading to changes in proteins that bind to herbicides, and ultimately leading to the resistance of weeds to herbicides. Sixteen amino acid substitutions at seven sites have been identified in the carboxyl-transferase (CT) domain of plastidic ACCase, including: Ile-1781-Leu, Ile-1781-Val, Ile-1781-Thr, Trp-1999-Cys, Trp-1999-Leu, Trp-1999-Ser, Trp-2027-Cys, Trp-2027-Ser, Ile-2041-Asn, Ile-2041-Val, Ile-2041-Thr, Asp-2078-Gly, Asp-2078-Glu, Cys-2088-Arg, and Gly-2096-Ala, and Gly-2096-Ser (Collavo et al., 2011; Kaundun et al., 2013a; Kaundun et al., 2013b; Papapanagiotou et al., 2015; Guo et al., 2017; Li et al., 2017; Wang et al., 2021). The overexpression of ACCase gene was also identified as a TSR mechanism that effectively increases the amount of target protein to mitigate the toxic effects of herbicide on weeds, as has been primarily shown for glyphosate resistance (Kupper et al., 2017; Zhang et al., 2018). However, few studies have evaluated ACCase gene expression involved in herbicide resistance. Notably, Laforest et al. observed that the overexpression of ACCase gene led to the resistance of *Digitaria sanguinalis* to ACCase inhibitors (Laforest et al., 2017). NTSR mechanisms are more complicated and include reduced penetration and translocation, sequestration, and enhanced herbicide metabolism (Delye et al., 2011a). These mechanisms can confer complex cross-resistance to herbicides *via* different modes of action (Yu and Powles, 2014). Further, various enzymes are involved in conferring non-target-site resistance to herbicides, including cytochrome P450 monooxygenases and gluthathione-S-transferases (Brazier et al., 2002).

Metamifop is a type of APP herbicide that has been used continuously following its introduction to China. The herbicide features advantages of low toxicity, high efficiency, environmental safety, and excellent miscibility, among other characteristics. It is a common agent used to control most annual gramineae weeds and exhibits good control of *Digitaria* spp. weeds. Continuous and extensive use of metamifop has led to increased selection pressures on weeds, eventually leading to a serious risk of herbicide resistance. Analogously, *Echinochloa* spp. and *Leptochloa chinensis* have developed resistance to metamifop in China and elsewhere (Won et al., 2014). Mutations of ACCase gene corresponding to Ile-1781-Leu, Trp-1999-Ser, and Trp-2027-Cys are the most common TSR mechanisms identified in metamifop-resistant *Echinochloa* spp. in China. Furthermore, NTSR mechanisms of *Echinochloa crus-galli* to metamifop have also been identified (Xia et al., 2016). Moreover, it has been reported that *Leptochloa chinensis* developed resistance to metamifop due to the ACCase gene mutation Trp-2027-Ser (Yuan et al., 2021). Few studies have evaluated metamifop resistance in *D. ciliaris*. Yu et al. observed that *D. ciliaris* can be resistant to sethoxydim and cross-resistant to fenoxaprop and fluazifop (Yu et al., 2017). Further, Basak et al. observed that the Ile-1781-Leu mutation of the ACCase gene led to pinoxaden resistance (Basak et al., 2019). However, herbicide-resistant *D. ciliaris* var. *chrysoblephara* populations have not yet been observed in China.

In this study, three *D. ciliaris* var. *chrysoblephara* populations that are resistant to metamifop were collected from dry direct seeding rice fields in Jiangsu Province, China. The aims of the present study were consequently to: (1) determine the level of resistance to metamifop in putatively resistant *D. ciliaris* var. *chrysoblephara* populations; (2) identify the mechanisms responsible for metamifop resistance in *D. ciliaris* var. *chrysoblephara* based on ACCase gene sequencing, gene expression, and enzyme activity; and (3) characterize cross- and multi-resistance of the resistant populations to various herbicides with different modes of action.

2 Materials and methods

2.1 Plant materials

Seeds of *D. ciliaris* var. *chrysoblephara* suspected of being resistant to metamifop were collected from dry direct-sown rice fields in October 2020 (Table 1). Seeds of plants from each field were pooled to represent a population. JYX-8, JTX-98, and JTX-99 were presumed

to be resistant populations and JSS-19 was presumed to be a sensitive population based on single dose assay pre-experiments. *D. ciliaris* var. *chrysoblephara* seeds were germinated on filter paper in Petri dishes in June 2021 over a 12 h photoperiod with 2,500 xL lighting and incubation at 30/25°C for several days. Fifteen seedlings were then transplanted to a plastic pot (9.5 cm diameter and 16 cm height) containing loam soil and grown in an incubator under the above-mentioned conditions.

2.2 Dose response to metamifop

Dose response experiments were performed when the seedlings reached the four-leaf stage. Presumed resistant and sensitive populations were sprayed using a 3WPSH-500D type bioassay spray tower (Nanjing Institute of Agricultural Mechanization, Ministry of Agriculture and Rural Affairs) using a disc diameter of 50 cm, a nozzle diameter of 0.3 mm, a spray pressure of 0.3 MPa, a droplet diameter of 100 μm, and a sprinkler flow of 90 mL·min^{-1}. Metamifop doses of 0-, 0.03125-, 0.0625-, 0.125-, 0.25-, 0.5-, 1-, and 2-fold the recommended dose (120 g a.i ha^{-1}) were applied to the sensitive population, while 0-, 0.25-, 0.5-, 1-, 2-, 4-, 8-, and 16-fold the recommended dose were applied to the resistant populations. Each pot with 15 seedlings was set up as a replicate. Each treatment comprised four replicates and the experiment was conducted twice.

The above-ground fresh weights of plants were measured 21 days after treatment. Data were pooled since no significant differences between the two repeated experiments were identified based on *t*-test ($p< 0.05$) by ANOVA (SPSS v.16.0). The SigmaPlot 12.0 software was used to calculate the GR_{50} values (herbicide dose causing 50% growth reduction) for different populations of *D. ciliaris* var. *chrysoblephara*. A log-logistic model was used to analyze the test data, with the fitting equation as follows:

$$y = c + (d - c)/[1 + (x/GR_{50})^b]$$

In the equation, y is the fresh weight percentage of the control, c is the lower limit, d is the upper limit, b is the slope, and x is the herbicide dose (Seefeldt et al., 1995). The resistance index (RI) was obtained based on the GR_{50} values of the resistant population/GR_{50} of the sensitive population.

2.3 ACCase CT domain and cDNA sequencing

Young leaves from individual plants at the four-leaf stage were subjected to total DNA extraction using a plant genomic DNA extraction kit (Tiangen, China), according to the manufacturer's instructions. The conserved CT domain of ACCase gene was then amplified using two pairs of the previously designed universal primers ACcp1/ACcp1R and ACcp4/ACcp2R (Delye et al., 2011b). PCR reaction volumes were 50 μL and included 2 μL of DNA, 2 μL of forward and reverse primers (10 μM), 25 μL of 2×PCR long Taq Mix (Vazyme, China), and ddH_2O up to 50 μL. Reactions included a pre-denaturation step of 5 min at 95°C, followed by 30 cycles at 94°C for 30 s, 58°C for 30 s, and 72°C for 30 s. The PCR products were subject to electrophoresis in a 0.75% agarose gel in 1×TAE buffer, and PCR fragments were cloned into the PMD-18T vector (Takara, China) for sequencing. Amplicons from individual plants in each population were sequenced and at least 10 clones from each plant were subjected to sequencing to construct ACCase consensus sequences. Each segment was sequenced in the forward and reverse directions at Invitgen Biotechnology, Ltd. (Shanghai, China) to reduce sequencing errors. The BioEdit sequence alignment editor software was used to align and compare sequence data.

Total RNA was extracted using the RNApre Pure Plant Kit, followed by first strand cDNA generation with the FastQuant RT Kit (Tiangen, China). ACCase cDNA gene sequences of gramineae plants with high homology to *D. ciliaris* var. *chrysoblephara* were downloaded from NCBI, including those from *Beckmannia syzigachne* (GenBank accession number: KF501575), *Alopecurus myosuroides* (GenBank accession number: AJ310767) and *Lolium rigidum* (GenBank accession number: AY995232). The sequences were compared with the DNAMAN software. Eight pairs of primers were designed based on homologous sequence comparison of conserved regions (Table 2). In addition, 5' cDNA terminal rapid amplification (RACE) gene specific primers (Table 2) were designed, and the ACCase cDNA ends were amplified using the HiScript-TS 5'/3' RACE Kit (Vazyme, China). PCR fragments amplified from resistant populations were cloned into the PMD-18T vector (Takara, China) and amplicons from ten plants of each population were sequenced. For each biological replicate, at least ten clones were sequenced and used to construct ACCase consensus sequences. The BioEdit sequence alignment editor and DNAMAN software were then used to analyze and compare the sequence data.

TABLE 1 *D. ciliaris* var. *chrysoblephara* seed collection information.

Populations	Collection Site	Collection Time
JSS-19	Sucheng, Suqian, Jiangsu	2020.9
JYX-8	Xiangshui, Yancheng, Jiangsu	2020.9
JTX-98	Xinghua, Taizhou, Jiangsu	2020.9
JTX-99	Xinghua, Taizhou, Jiangsu	2020.9

2.4 ACCase gene expression assay

After growing to the four-leaf stage, plant seedlings from four *D. ciliaris* var. *chrysoblephara* populations were sprayed with the recommended dose of metamifop (120 g a.i.ha^{-1}). Seedlings from each population were collected at 0, 12, and 24 h after treatment. Tissues were subjected to RNA extraction and cDNA synthesis, as described above. Primers were designed with the Primer premier 5.0 software package (AC-F: CTGTTGTGGGCAAGGAGGATG; AC-R: TACCAAGCCGAGCAAGATAAG) to amplify 153 bp fragments of target ACCase gene. Actin was used as the internal reference gene and amplified using primers designed using the large crabgrass actin gene (GenBank: KY967696) (Actin-F1: CGGAGAATAGCATGAGGAAGTG; Actin-R1: AGTGGTCGAACAACTGGTATTG). Real-time PCR was conducted with an ABI QuantStudio™ 7 Flex Real-Time PCR System (Thermofisher, USA) using a 2×TSINGKE Master qPCR Mix (SYBR Green I) kit (Tsingke, China). Thermal cycling

TABLE 2 PCR primers used to amplify ACCase cDNA of *D. ciliaris* var. *chrysoblephara*.

Primer	Sequence (5′ to 3′)	Annealing temperature (°C)	Gene location
5GSP	TCTCCTCAGGTATCGAGTCC	For nested PCR	For nested PCR
5GNP	AGGCCATCCAAGAATCAAAG		
A.C-F2	TTCAGCTCTCATTGCTCAAG	59.3	777–1,971
A.C-R2	TAGAGCTCCTCCAACCACTG		
A.C-F3	ATTCAAATTCGTGGAGAAAT	55.8	1,801–3,153
A.C-R3	AGCTTTGTTCCTCACACCCT		
A.C-F4	TTTTCAGTGATGGCATTCAG	57.6	3,038–4,052
A.C-R4	CGTGATGGAGTATACTTCAT		
A.C-F5	AGATCAGATTCTCCGGCATG	56.4	3,951–5,031
A.C-R5	TGGGCCAAATGATCCAGCTC		
A.C-F6	TTACTAGTCACACCTGTACAG	57.6	4,544–5,683
A.C-R6	TAGGAAGAGGTCCACCAATG		
A.C-F7	GACTGTTTCAGATGACCTTG	55.9	5,598–6,631
A.C-R7	AAGGATATCTGAAGATGTTC		
A.C-F8	TGTTATGCTGAGAGGACTG	56.0	6,259–6,966
A.C-R8	CAGCCGCCTTGTATCCATCT		

conditions were used according to the manufacturer's instructions. Three biological replicates and four technical replicates were used for each sample. The relative expression of ACCase gene were calculated using the $2^{-\Delta\Delta CT}$ method, while expression from the untreated sensitive population was used as the negative control.

2.5 ACCase activity assay

After growing to the four-leaf stage, seedlings of four *D. ciliaris* var. *chrysoblephara* populations were sprayed with the recommended dose of metamifop (120 g a.i.ha^{-1}). Seedlings were collected from each population at 0, 2, 12, 24, 48, and 72 h after treatment, respectively. ACCase catalyzes the transformation of Acetyl-CoA, $NaHCO_3$, and ATP to generate Malonyl-CoA, ADP, and inorganic phosphorus. The interaction of molybdenum blue and phosphate can generate products with characteristic absorption peaks at 660 nm. Thus, ACCase activity was determined based on inorganic phosphorus levels using the ammonium molybdate method. Specifically, ACCase activity was quantified using an ACCase activity assay kit (Biobox, China) and a microplate spectrophotometer (Agilent BioTek Epoch2, USA). Crude enzyme was prepared by adding 1 mL of extracting solution to 0.1 g of leaf tissue. The enzymatic reactions and phosphate quantification were then conducted based on the manufacturer's instructions. Absorbance values at 660 nm were determined for experimental reactions, in addition to those for negative controls, blank controls, and to establish a standard curve. Three biological replicates and three technical replicates were used for each sample.

The unit of ACCase activity was calculated based on sample mass, as defined by the amount of 1 μmol of inorganic phosphorus generated for 1 g tissue over 1 h. Specifically, ACCase activity was calculated with the following equation:

$$\begin{aligned} &ACCase\ activity(U/g\ mass) \\ &\quad = x*_V total/[(V_{sample}*W)/V_{total\ sample})]/T \\ &\quad = 20x/W \end{aligned}$$

In the formula, V_{total} is the total volume of the enzymatic reaction (0.1 mL), V_{sample} is the volume of added sample (0.01 mL), $V_{total\ sample}$ is the volume of extracting solution (1 mL), T is the time of enzymatic reaction (0.5 h), and W is the fresh weight of sample (0.1 g).

2.6 Cross- and multi-resistance to other herbicides

Dose-response experiments were performed to determine whether the *D. ciliaris* var. *chrysoblephara* populations exhibited cross- or multi-resistance to other herbicides. Experiments were described as in section 2.2, and the other evaluated herbicides are listed in Table 3.

3 Results

3.1 Dose response to metamifop exposure

Dose response experiments revealed that the JYX-8, JTX-98, and JTX-99 populations were resistant to metamifop (Figure 1; Table 4). Specifically, the GR_{50} values of these populations were much higher than the recommended dosage of metamifop (120 g a.i.ha^{-1}). Moreover, their RI values were 30.64, 14.38, and 23.19, respectively.

TABLE 3 Information for herbicides evaluated in this study.

Herbicide	Mode of Action	Company	Doses evaluated (g a.i ha^{-1})	
			Sensitive population	Resistant population
Fenoxaprop-P-ethyl	ACCase Inhibitor	Jiangsu Agrochem Laboratory Co., Ltd.	8, 16, 32, 64, 128	32, 64, 128, 256, 512
Cyhalofop-butyl	ACCase Inhibitor	Jiangsu Fengshan Group Co., Ltd.	11.25, 22.5, 45, 90, 180	45, 90, 180, 360, 720
Penoxsulam	ALS Inhibitor	Jiangsu Institute of Ecomones Co., Ltd.	2.8, 5.6, 11.25, 22.5, 45	2.8, 5.6, 11.25, 22.5, 45
Bispyribac-sodium	ALS Inhibitor	Jiangsu Institute of Ecomones Co., Ltd.	7.5, 15, 30, 60, 120	7.5, 15, 30, 60, 120
Pyraclonil	PPO Inhibitor	Hubei Xianghe Machinery Manufacturing Co., Ltd.	7.5, 15, 30, 60, 120	7.5, 15, 30, 60, 120
Quinclorac	Synthetic Auxin	Jiangsu Institute of Ecomones Co., Ltd.	47, 94, 188, 376, 752	47, 94, 188, 376, 752

ACCase, acetyl-CoA carboxylase; ALS, acetolactate synthase; PPO, protoporphyrinogen oxidase.

3.2 ACCase gene sequencing

The ACCase CT domain gene fragment amplified by the ACcp1/ACcp1R primers was 551 bp in length and contained a previously reported variable Ile/Leu codon at site 1,781. The gene fragment amplified by the primers ACcp4/ACcp2R was 406 bp in length and contained four previously known variable codons (Trp/Cys, Ile/Asn, Asp/Gly, and Gly/Ala) located at sites 2,027, 2,041, 2,078, and 2,096, respectively. After sequence alignment of gene fragments from the resistant and sensitive populations (Table 5), a single nucleotide substitution was observed from TGG to TGC that resulted in an amino acid substitution at position 2,027 from tryptophan in the susceptible population to cysteine in the resistant population JYX-8. No corresponding substitutions were observed for JTX-98 and JTX-99 ACCase gene.

Using the extracted total RNA as template, eight primer pairs were designed using homologous sequence comparison to amplify ACCase cDNA sequences *via* PCR and RACE. The sizes of the target fragments amplified by the eight primer pairs were 1,265 bp, 1,304 bp, 1,448 bp, 1,136 bp, 1,144 bp, 1,232 bp, 1,130 bp, and 1,124 bp

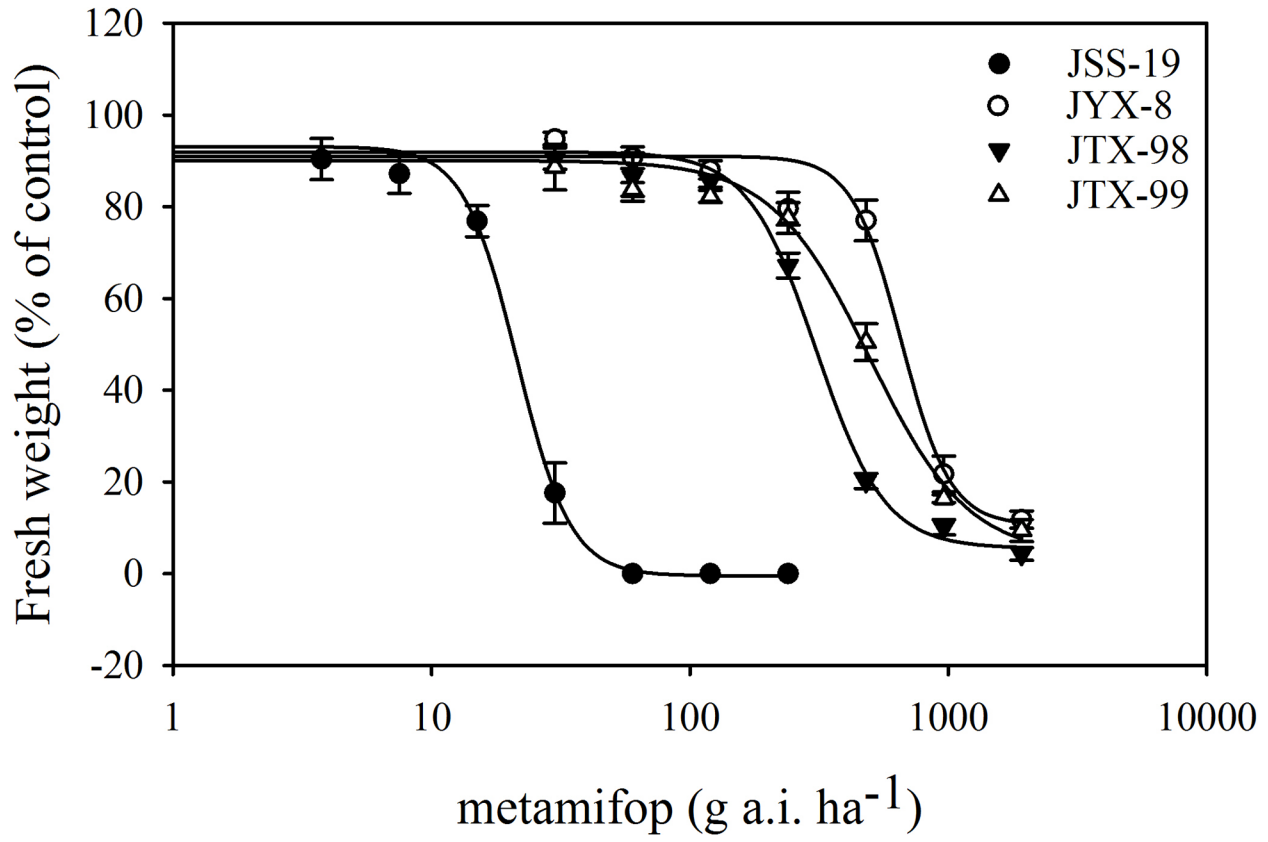

FIGURE 1
Dose response curves for four populations of *D. ciliaris* var. *chrysoblephara* to metamifop generated from dose response experiments. A log-logistic model was used to analyze the test data (the fresh weight percentage of the control). The GR_{50} values of resistant populations (JYX-8, JTX-98, and JTX-99) were significantly higher than in the sensitive population JSS-19. Vertical bars indicate standard errors.

TABLE 4 GR_{50} and RI values for four populations of *D. ciliaris* var. *chrysoblephara* exposed to metamifop in this study.

Population	GR_{50}+SE (g a.i ha^{-1})	Susceptibility	RI
JSS-19	21.45 ± 0.79	S	–
JYX-8	657.22 ± 43.86	R	30.64
JTX-98	308.36 ± 14.14	R	14.38
JTX-99	497.38 ± 43.54	R	23.19

GR_{50}, herbicide dose causing 50% growth reduction; SE, standard error; RI, GR_{50} value of resistant population divided by that of susceptible population; S, sensitive population; R, resistant population.

(Figure 2). The complete ACCase cDNA fragment was 7,277 bp in length and the ORF length was 6,966 bp. BLASTx analysis of the complete sequence against the NCBI database (Table 6) indicated the presence of amino acid sequence homology of 95.17%, 95.04%, 95%, and 94.10% between the ACCase encoded by the gramineae weeds *Panicum hallii*, *Setaria viridis*, *Setaria italica*, and *Echinochloa crus-galli*, respectively, suggesting that the amplified sequence was indeed an ACCase gene.

3.3 Expression of ACCase gene

The expression levels of ACCase gene in resistant and sensitive populations were quantified by RT-qPCR. Relative ACCase gene expression levels for each population are indicated as fold-level values compared to control assays in the sensitive JSS-19 population in the absence of metamifop (Figure 3). Expression levels were not significantly different between control and metamifop treatments, both in the sensitive and resistant populations. Thus, the resistance of the JYX-8, JTX-98, and JTX-99 populations to metamifop was not related to ACCase gene expression.

3.4 ACCase activity

The influence of metamifop to ACCase activity within four *D. ciliaris* var. *chrysoblephara* populations was determined using the ammonium molybdate spectrophotometric method. ACCase activities were not clearly different between 0 and 2 h, and then significantly decreased at 12 and 24 h, followed by a final gradual

TABLE 5 The mutation sites of ACCase gene in different *D. ciliaris* var. *chrysoblephara* populations.

Population	Ile1781	Trp2027	Ile2041	Gly2078	Gly2096
JSS-19	ATA	TGG	ATT	GAT	GGC
JYX-8	ATA	TGC	ATT	GAT	GGC
JTX-98	ATA	TGG	ATT	GAT	GGC
JTX-99	ATA	TGG	ATT	GAT	GGC

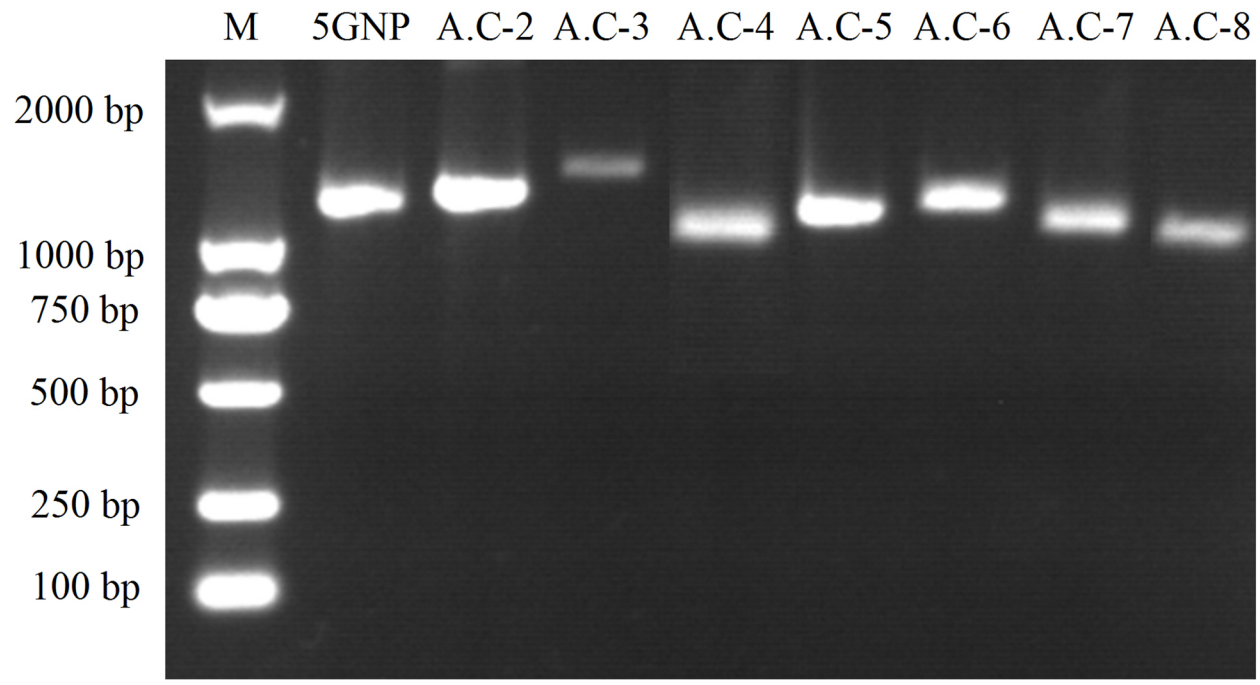

FIGURE 2
PCR amplification results for ACCase cDNA sequences. Eight primer pairs were designed based on homologous sequence comparison to amplify ACCase cDNA sequences *via* PCR and RACE. The sizes of the target fragments were 1,265, 1,304, 1,448, 1,136, 1,144, 1,232, 1,130, and 1,124 bp. The abbreviations above the image represent corresponding primers and the numbers on the left-hand side of the image indicate the size of DNA markers.

TABLE 6 BLAST results for *D. ciliaris* var. *chrysoblephara* ACCase proteins against the NCBI database.

Accession ID	Accession species	Maximum amino acid similarity
XP_025823701	*Panicum hallii*	95.17%
XP_034603265	*Setaria viridis*	95.05%
AAO62903.1	*Setaria italica*	95.00%
ADR32358.1	*Echinochloa crus-galli*	94.10%

recovery at 48 and 72 h (Figure 4). The ACCase activity trends were similar between sensitive and resistant populations, although statistically significant differences remained. After treatment for 2 h, their activities were inhibited to 85.85%, 108.43%, 94.69%, and 89.93% of the control levels for the JSS-19, JYX-8, JTX-98, and JTX-99 populations, respectively. The lowest activities were observed at 24 h, with activities inhibited to 64.39%, 77.35%, 80.54%, and 71.84% levels of the controls, respectively. ACCase activity in the sensitive population JSS-19 was most inhibited across the above period. After treatment for 72 h, their activities were recovered to 80.04%, 98.87%, 115.24%, and 97.32% of control levels, respectively. ACCase activities returned to the same or even higher levels than in the control for the resistant populations, but only recovered to 80.04% of that of the control in the sensitive population. These results suggest that ACCase activities in resistant populations were less inhibited than in sensitive populations and recovered to the same or even higher levels compared to untreated plants.

3.5 Cross- and multi-resistance to other herbicides

Three metamifop-resistant populations of *D. ciliaris* var. *chrysoblephara* were cross-resistant to other ACCase-inhibiting herbicides (Table 7). Specifically, the JYX-8, JTX-98, and JTX-99 populations exhibited high resistance to cyhalofop-butyl, with GR_{50} values of 233.46, 157.8, and 185.06 g a.i.ha^{-1} and RI values of 21.83, 14.76, and 17.31, respectively. The populations also exhibited resistance to fenoxaprop-P-ethyl, with GR_{50} values of 174.47, 139.57, and 151.46 g a.i.ha^{-1} and RI values of 14.36, 11.79, and 12.47, respectively. Thus, the three resistant populations exhibited similar cross-resistance patterns to ACCase inhibitors.

The multi-resistance characteristics of metamifop-resistant *D. ciliaris* var. *chrysoblephara* plants were also evaluated by whole-plant bioassays. The GR_{50} values of the four populations to the ALS inhibitor penoxsulam (101.64-185.43 g a.i.ha^{-1}) were significantly higher than the recommended field dosage (30 g a.i.ha^{-1}), suggesting the existence of

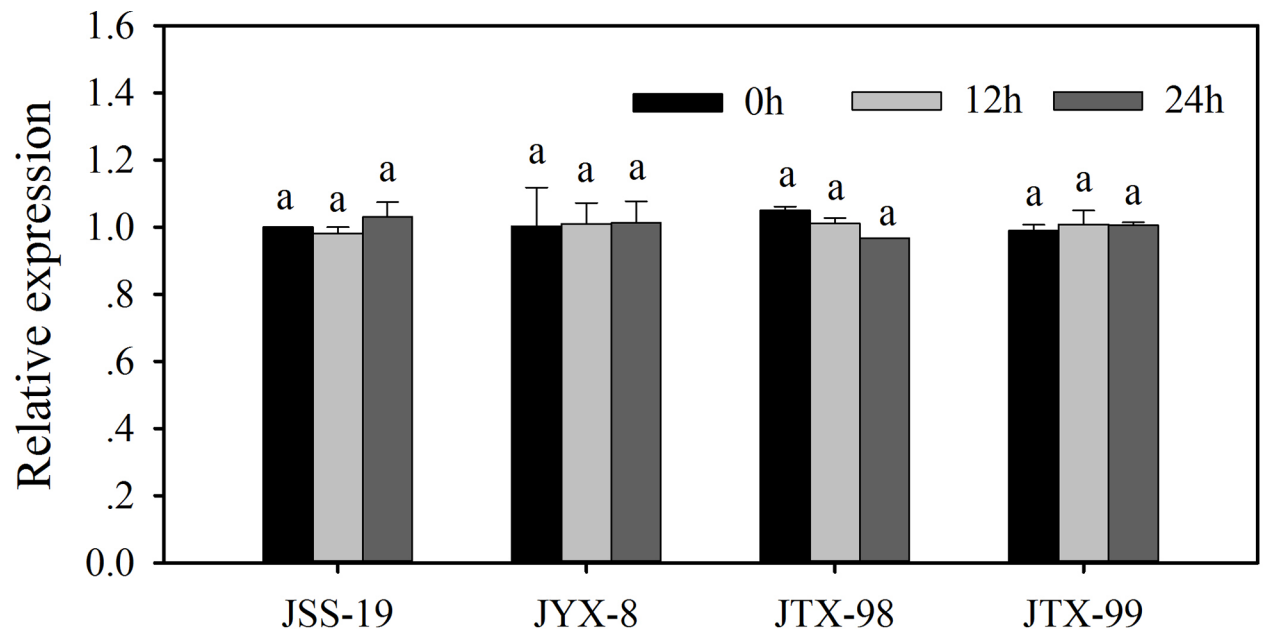

FIGURE 3
ACCase gene expression in four populations of *D. ciliaris* var. *chrysoblephara* after metamifop treatment. Gene expression levels were quantified by RT-qPCR and were not significantly different between control and metamifop treatments, both in the sensitive and resistant populations. Vertical bars indicate standard errors. The same lowercase letters indicate the lack of statistically significant differences based on Tukey's tests.

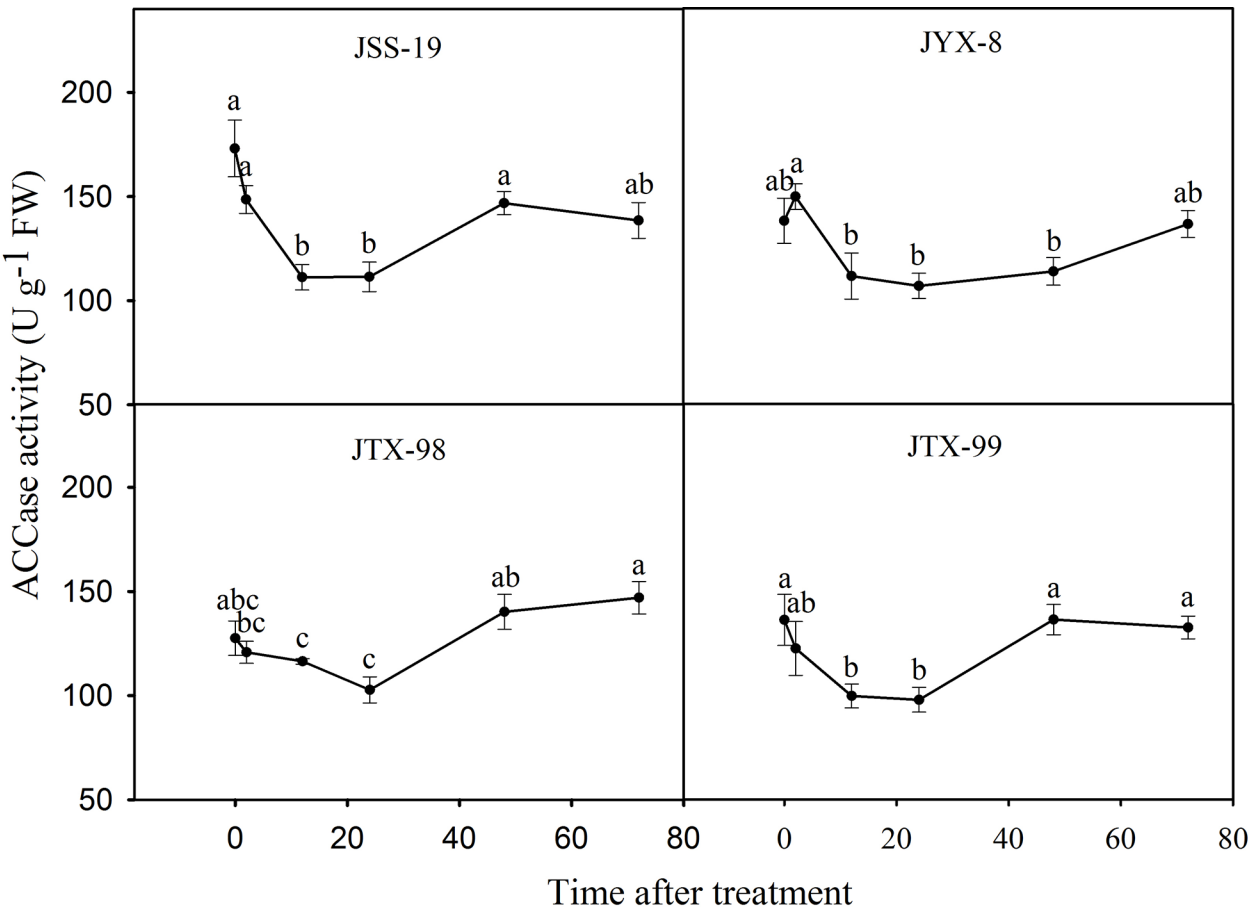

FIGURE 4
ACCase activities in four populations of *D. ciliaris* var. *chrysoblephara* after metamifop treatment. ACCase activities were determined using the ammonium molybdate spectrophotometric method. ACCase activities in resistant populations were less inhibited than in sensitive populations and also recovered to the same or even higher levels compared to untreated plants. Vertical bars indicate standard errors. Different lowercase letters indicate statistically significant differences ($P < 0.05$) based on Tukey's tests.

multi-resistance to penoxsulam. The GR_{50} values of the resistant populations to the ALS-inhibiting herbicide bispyribac-sodium, the auxin mimic herbicide quinclorac, and the PPO-inhibiting herbicide pyraclonil were significantly lower than their recommended field dosages. In addition, the RI values were all< 2, suggesting the absence of multi-resistance to these herbicides.

4 Discussion

Jiangsu is one of the most important rice production areas of China. Metamifop has been used to control gramineae weeds in Jiangsu paddy fields for over 10 years. Consequently, metamifop use carries a high risk for herbicide resistance development. Consistently, we observed that continuous high-intensity use of metamifop did not mitigate the rapid spread of *D. ciliaris* var. *chrysoblephara* in paddy fields. We hypothesized that this lack of effect may be due to resistance of *D. ciliaris* var. *chrysoblephara* to metamifop. A high level of resistance to ACCase-inhibiting herbicides has been previously reported in various weed species including in wild oat (*Avena fatua* L.), Japanese foxtail (*Alopecurus japonicus*), and Amazon sprangletop [*Leptochloa panicoides* (J. Presl) Hitchc.] (Seefeldt et al., 1996; Xu et al., 2013; Tehranchian et al., 2016). *D. ciliaris* has only been previously observed to be resistant to ACCase herbicides *via* collection of plants from sod production fields in Georgia (Yu et al., 2017; Basak et al., 2019). In this study, *D. ciliaris* var. *chrysoblephara* populations collected from dry direct-seeding rice fields in the Jiangsu province were shown to exhibit high resistance to metamifop. ACCase inhibitors remain the primary herbicides used to control *D. ciliaris* var. *chrysoblephara*. However, the continued use of the same herbicides will inevitably lead to increased selection pressure, leading to rapid development of resistant populations and inestimable harm to rice production efforts.

The change of target enzyme activity caused by mutation or overexpression of target gene is the direct cause of weed resistance to herbicide. Herbicide efficacy is determined by the affinity of herbicides to enzymes. Physicochemical interactions are main factors that determine the affinity. For ACCase-inhibiting herbicides, their affinity and efficacy are determined by the interactions between the herbicides and the amino acids at specific positions of the polypeptide chain on ACCase CT domain. Thus, a single nucleotide mutation in the ACCase gene can result in amino acid substitutions imparting resistance to herbicides (Takano et al., 2020). Several amino acid substitutions of ACCase CT

10.3389/fpls.2023.1133798

TABLE 7 Sensitivity of *D. ciliaris* var. *chrysoblephara* to other herbicides.

Herbicide	Recommended dose (g a.i.ha^{-1})	Population	GR_{50}+SE (g a.i.ha^{-1})	Susceptibility	RI
Cyhalofop-butyl	62.1	JSS-19	10.69 ± 0.15	S	–
		JYX-8	233.46 ± 5.51	R	21.83
		JTX-98	157.8 ± 18.27	R	14.76
		JTX-99	185.0 6 ± 7.5	R	17.31
Fenoxaprop-P-ethyl	105	JSS-19	12.15 ± 1.27	S	–
		JYX-8	174.47 ± 6.87	R	14.36
		JTX-98	139.57 ± 6.33	R	11.79
		JTX-99	151.46 ± 8.59	R	12.47
Penoxsulam	30	JSS-19	101.64 ± 4.20	R	/
		JYX-8	185.43 ± 14.95	R	/
		JTX-98	118.71 ± 4.56	R	/
		JTX-99	156.55 ± 11.73	R	/
Bispyribac-sodium	45	JSS-19	12.90 ± 1.82	S	–
		JYX-8	12.87 ± 1.74	S	1
		JTX-98	12.07 ± 0.77	S	0.79
		JTX-99	12.33 ± 0.87	S	0.85
Pyraclonil	210	JSS-19	69.90 ± 7.22	S	–
		JYX-8	112.10 ± 18.37	S	1.6
		JTX-98	89.22 ± 4.89	S	1.28
		JTX-99	80.61 ± 7.39	S	1.15
Quinclorac	375	JSS-19	93.67 ± 0.44	S	–
		JYX-8	86.83 ± 0.65	S	0.93
		JTX-98	93.70 ± 0.31	S	1
		JTX-99	96.65 ± 0.11	S	1.03

GR_{50}, herbicide dose causing 50% growth reduction; SE, standard error; RI, GR_{50} value of resistant population divided by that of susceptible population; S, sensitive population; R, resistant population.

domain of grassy weeds have been reported to be involved in resistance to ACCase-inhibiting herbicides, including the Trp-2027-Cys substitution (Deng et al., 2020). Following the first report of the Trp-2027-Cys substitution in *Alopecurus myosuroides*, it has been observed in many weeds resistant to ACCase-inhibiting herbicides like *Avena sterilis*, *Lolium rigidum*, *Beckmannia syzigachne*, and *A. japonicus* (Delye et al., 2005; Liu et al., 2007; Yu et al., 2007; Xu et al., 2013; Pan et al., 2015). In this study, the Trp-2027-Cys substitution, resulting from a TGG to TGC nucleotide change, was observed in JYX-8 ACCase. Thus, the interaction between herbicide and target enzyme was influenced by target site mutation of ACCase gene and lead to the resistance of JYX-8 to metamifop. However, similar mutations were not observed for JTX-98 and JTX-99 populations. Overexpression of ACCase gene can confer resistance in large crabgrass to ACCase-inhibiting herbicides (Laforest et al., 2017). In this study, ACCase gene expression levels were not significantly different between control and metamifop treatments, both in the sensitive and resistant populations. ACCase activities were less inhibited in the resistant populations than in the sensitive population. Thus, ACCase from the resistant populations was much less sensitive to metamifop than the sensitive population (Xu et al., 2013). ACCase gene sequencing, gene expression, and enzyme activity investigations suggested that target-site resistance was the most likely mechanism conferring resistance in JYX-8, although the existence of NTSR mechanisms cannot be ruled out. A NTSR mechanism to metamifop, such as enhanced metabolism, may be present in JTX-98 and JTX-99, rather than a directed TSR. The unknown resistance mechanisms require further exploration.

The Trp-2027-Cys substitution can lead to cross-resistance to APP herbicides (Li et al., 2014), consistent with the results of this study. The JYX-8 population carrying the Trp-2027-Cys substitution was resistant to the APP herbicides cyhalofop-butyl and fenoxaprop-P-ethyl, with RI values of 21.83 and 14.36, respectively. In addition, no target site mutations were observed for the JTX-98 and JTX-99 populations, but they also exhibited cross-resistance to the APP herbicides cyhalofop-butyl and fenoxaprop-P-ethyl (RI values > 11.79) *via* unknown resistance mechanisms. The multi-resistance of the JYX-8, JTX-98, and JTX-99

populations to the ALS inhibitor penoxsulam was observed, but to the ALS inhibitor bispyribac-sodium, the auxin mimic quinclorac, and the PPO inhibitor pyraclonil was not observed. Bispyribac-sodium, quinclorac, and pyraclonil exerted good control on these populations. Thus, these herbicides with different modes of action could still be used to control metamifop-resistant *D. ciliaris* var. *chrysoblephara*.

Nevertheless, many studies have shown that different resistance mechanisms (i.e., TSR and/or NTSR mechanisms) may be present in a single weed population that is resistant to a variety of herbicides (Beckie et al., 2012). Multiple target-site resistance to ACCase and ALS inhibitors has been observed in black-grass (Bailly et al., 2012). Further, glyphosate-resistant rigid ryegrass exhibited multiple resistance to ACCase- and ALS- inhibiting herbicides. Specifically, ALS resistance in the population was due to an insensitive target enzyme, while ACCase resistance was due to a non-target-site mechanism (Neve et al., 2004). Consequently, control methods should be carefully evaluated for weed populations with different resistance mechanisms. No evidence of non-target-site resistance has been shown for *Digitaria* spp. weeds. However, the resistant populations JTX-98 and JTX-99 investigated in this study likely exhibit NTSR mechanisms, warranting additional attention to control methods.

In conclusion, three populations of *D. ciliaris* var. *chrysoblephara* collected from dry direct-sown rice fields of the Jiangsu province have evolved resistance to metamifop, and the target-site mutation Trp-2027-Cys is responsible for resistance in the JYX-8 population. To our knowledge, this study represents the first evidence for a molecular mechanism of *D. ciliaris* var. *chrysoblephara* resistance to metamifop. In addition, cross- and multi-resistance patterns to other herbicides were also investigated in this study. Non-target-site resistance mechanisms cannot be presently ruled out for the resistance of *D. ciliaris* var. *chrysoblephara* to metamifop. Consequently, additional studies are needed to comprehensively understand the mechanism underlying the resistance traits evaluated here.

Data availability statement

The original contributions presented in the study are included in the article/supplementary material. Further inquiries can be directed to the corresponding author.

Author contributions

HW and YL conceived and designed the experiments; JC and YT performed the lab work, data acquisition, and data analysis; JC and YT wrote the manuscript; TG assisted in performing the experiment; ZZ and GL contributed to the discussion and reviewed the manuscript. All authors contributed to the article and approved the submitted version.

Funding

This work was supported by the National Natural Science Foundation of China (31801773 and 31801755) and the Jiangsu Agricultural Science and Technology Innovation Fund [CX(22)3021].

Acknowledgments

We thank LetPub (www.letpub.com) for linguistic assistance and pre-submission expert review.

Conflict of interest

The authors declare that the research was conducted in the absence of any commercial or financial relationships that could be construed as a potential conflict of interest.

Publisher's note

References

Adina-Zada, A., Zeczycki, T. N., and Attwood, P. V. (2012). Regulation of the structure and activity of pyruvate carboxylase by acetyl CoA. *Arch. Biochem. Biophysics* 519, 118–130. doi: 10.1016/j.abb.2011.11.015

Bailly, G., Dale, R., Archer, S., Wright, D., and Kaundun, S. (2012). Role of residual herbicides for the management of multiple herbicide resistance to ACCase and ALS inhibitors in a black-grass population. *Crop Prot.* 34, 96–103. doi: 10.1016/j.cropro.2011.11.017

Basak, S., Mcelroy, J. S., Brown, A. M., Gon Alves, C. G., Patel, J. D., and Mccullough, P. E. (2019). Plastidic ACCase ile-1781-Leu is present in pinoxaden-resistant southern crabgrass (*Digitaria ciliaris*). *Weed Sci.* 68, 41–50. doi: 10.1017/wsc.2019.56

Beckie, H. J., Warwick, S. I., and Sauder, C. A. (2012). Basis for herbicide resistance in Canadian populations of wild oat (*Avena fatua*). *Weed Sci.* 60, 10–18. doi: 10.1614/WS-D-11-00110.1

Brazier, M., Cole, D. J., and Edwards, R. (2002). O-Glucosyltransferase activities toward phenolic natural products and xenobiotics in wheat and herbicide-resistant and herbicide-susceptible black-grass (*Alopecurus myosuroides*). *Phytochemistry* 59, 149–156. doi: 10.1016/S0031-9422(01)00458-7

Collavo, A., Panozzo, S., Lucchesi, G., Scarabel, L., and Sattin, M. (2011). Characterisation and management of phalaris paradoxa resistant to ACCase-inhibitors. *Crop Prot.* 30, 293–299. doi: 10.1016/j.cropro.2010.11.011

Delye, C., Gardin, J., Boucansaud, K., Chauvel, B., and Petit, C. (2011a). Non-target-site-based resistance should be the centre of attention for herbicide resistance research: Alopecurus myosuroides as an illustration. *Weed Res.* 51, 433–437. doi: 10.1111/j.1365-3180.2011.00864.x

Delye, C., Pernin, F., and Michel, S. (2011b). 'Universal' PCR assays detecting mutations in acetyl-coenzyme a carboxylase or acetolactate synthase that endow herbicide resistance in grass weeds. *Weed Res.* 51, 353–362. doi: 10.1111/j.1365-3180.2011.00852.x

Delye, C., Zhang, X. Q., Michel, S., MatJicek, A., and Powles, S. B. (2005). Molecular bases for sensitivity to acetyl-coenzyme a carboxylase inhibitors in black-grass. *Plant Physiol.* 137, 794–806. doi: 10.1104/pp.104.046144

Deng, W., Yang, Q., Chen, Y., Yang, M., Xia, Z., Zhu, J., et al. (2020). Cyhalofop-butyl and glyphosate multiple-herbicide resistance evolved in an eleusine indica population collected in Chinese direct-seeding rice. *J. Agric. Food Chem.* 68, 2623–2630. doi: 10.1021/acs.jafc.9b07342

Fang, J., He, Z., Liu, T., Li, J., and Dong, L. (2020). A novel mutation asp-2078-Glu in ACCase confers resistance to ACCase herbicides in barnyardgrass (*Echinochloa crus-galli*). *Pesticide Biochem. Physiol.* 168, 104634. doi: 10.1016/j.pestbp.2020.104634

Guo, W., Zhang, L., Wang, H., Li, Q., Liu, W., and Wang, J. (2017). A rare ile-2041-Thr mutation in the ACCase gene confers resistance to ACCase-inhibiting herbicides in shortawn foxtail (*Alopecurus aequalis*). *Weed Sci.* 65, 239–246. doi: 10.1017/wsc.2016.32

Huang, S., Wang, Q., Dong, L., and Lou, Y. (2003). Acetyl-CoA carboxylase-inhibiting herbicides and resistance of weeds. *Weed Sci.*, 2–6. doi: 10.19588/j.issn.1003-935x.2003.02.001

Kaundun, S. S., Bailly, G. C., Dale, R. P., Hutchings, S.-J., and Mcindoe, E. (2013a). A novel W1999S mutation and non-target site resistance impact on acetyl-CoA carboxylase inhibiting herbicides to varying degrees in a UK lolium multiflorum population. *PLoS One* 8, e58012. doi: 10.1371/journal.pone.0058012

Kaundun, S. S., Hutchings, S.-J., Dale, R. P., and Mcindoe, E. (2013b). Role of a novel I1781T mutation and other mechanisms in conferring resistance to acetyl-CoA carboxylase inhibiting herbicides in a black-grass population. *PLoS One* 8, e69568. doi: 10.1371/journal.pone.0069568

Kukorelli, G., Reisinger, P., and Pinke, G. (2013). ACCase inhibitor herbicides – selectivity, weed resistance and fitness cost: a review. *Int. J. Pest Manage.* 59, 165–173. doi: 10.1080/09670874.2013.821212

Kupper, A., Borgato, E. A., Patterson, E. L., Netto, A. G., Nicolai, M., De Carvalho, S. J., et al. (2017). Multiple resistance to glyphosate and acetolactate synthase inhibitors in palmer amaranth (*Amaranthus palmeri*) identified in Brazil. *Weed Sci.* 65, 317–326. doi: 10.1017/wsc.2017.1

Laforest, M., Soufiane, B., Simard, M. J., Obeid, K., Page, E., and Nurse, R. E. (2017). Acetyl-CoA carboxylase overexpression in herbicide-resistant large crabgrass (*Digitaria sanguinalis*). *Pest Manage. Sci.* 73, 2227–2235. doi: 10.1002/ps.4675

Li, L., Du, L., Liu, W., Yuan, G., and Wang, J. (2014). Target-site mechanism of ACCase-inhibitors resistance in American sloughgrass (*Beckmannia syzigachne* steud.) from China. *Pesticide Biochem. Physiol.* 110, 57–62. doi: 10.1016/j.pestbp.2014.03.001

Li, L., Luo, X., and Wang, J. (2017). Resistance level and target-site mechanism to fenoxaprop-p-ethyl in *Beckmannia syzigachne* (Steud.) fernald populations from China. *Chilean J. Agric. Res.* 77, 150–154. doi: 10.4067/S0718-58392017000200150

Liu, W., Harrison, D. K., Chalupska, D., Gornicki, P., O'donnell, C. C., Adkins, S. W., et al. (2007). Single-site mutations in the carboxyltransferase domain of plastid acetyl-CoA carboxylase confer resistance to grass-specific herbicides. *Proc. Natl. Acad. Sci.* 104, 3627–3632. doi: 10.1073/pnas.0611572104

Matloob, A., Khaliq, A., and Chauhan, B. S. (2015). Weeds of direct-seeded rice in Asia: Problems and opportunities. *Adv. Agron.* 130, 291–336. doi: 10.1016/bs.agron.2014.10.003

Neve, P., Sadler, J., and Powles, S. B. (2004). Multiple herbicide resistance in a glyphosate-resistant rigid ryegrass (*Lolium rigidum*) population. *Weed Sci.* 52, 920–928. doi: 10.1614/WS-04-007R1

Pan, L., Li, J., Xia, W., Zhang, D., and Dong, L. (2015). An effective method, composed of LAMP and dCAPS, to detect different mutations in fenoxaprop-p-ethyl-resistant American sloughgrass (*Beckmannia syzigachne* steud.) populations. *Pesticide Biochem. Physiol.* 117, 1–8. doi: 10.1016/j.pestbp.2014.10.008

Papapanagiotou, A. P., Paresidou, M. I., Kaloumenos, N. S., and Eleftherohorinos, I. G. (2015). ACCase mutations in avena sterilis populations and their impact on plant fitness. *Pesticide Biochem. Physiol.* 123, 40–48. doi: 10.1016/j.pestbp.2015.01.017

Rao, A. N., Brainard, D. C., Kumar, V., Ladha, J. K., and Johnson, D. E. (2017). Preventive weed management in direct-seeded rice: targeting the weed seedbank. *Adv. Agron.* 144, 45–142. doi: 10.1016/bs.agron.2017.02.002

Seefeldt, S. S., Fuerst, E. P., Gealy, D. R., Shukla, A., Irzyk, G. P., and Devine, M. D. (1996). Mechanisms of resistance to diclofop of two wild oat (*Avena fatua*) biotypes from the Willamette valley of Oregon. *Weed Sci.* 44, 776–781. doi: 10.1017/S0043174500094704

Seefeldt, S. S., Jensen, J. E., and Fuerst, E. P. (1995). Log-logistic analysis of herbicide dose-response relationships. *Weed Technol.* 9, 218–227. doi: 10.1017/S0890037X00023253

Takano, H. K., Ovejero, R. F. L., Belchior, G. G., Maymone, G. P. L., and Dayan, F. E. (2020). ACCase-inhibiting herbicides: mechanism of action, resistance evolution and stewardship. *Scientia Agricola* 78. doi: 10.1590/1678-992x-2019-0102

Tehranchian, P., Norsworthy, J. K., Korres, N. E., Mcelroy, S., Chen, S., and Scott, R. C. (2016). Resistance to aryloxyphenoxypropionate herbicides in Amazon sprangletop: Confirmation, control, and molecular basis of resistance. *Pesticide Biochem. Physiol.* 133, 79–84. doi: 10.1016/j.pestbp.2016.02.010

Wang, J., Peng, Y., Chen, W., Yu, Q., Bai, L., and Pan, L. (2021). The ile-2041-Val mutation in the ACCase gene confers resistance to clodinafop-propargyl in American sloughgrass (*Beckmannia syzigachne* steud). *Pest Manage. Sci.* 77, 2425–2432. doi: 10.1002/ps.6271

Wang, H., Xu, P., Sun, Y., Lou, Y., and Xu, S. (2019). Status of damage and control strategy for paddy field weeds in jiangsu province. *J. Weed Sci.* 37, 1–5. doi: 0.19588/j.issn.1003-935X.2019.04.001

Won, O. J., Lee, J. J., Eom, M. Y., Suh, S. J., Park, S. H., Hwang, K. S., et al. (2014). Identification of herbicide-resistant barnyardgrass (*Echinochloa crus-galli* var. *crus-galli*) biotypes in Korea. *Weed Turfgrass Sci.* 3, 110–113. doi: 10.5660/WTS.2014.3.2.110

Xia, X., Tang, W., He, S., Kang, J., Ma, H., and Li, J. (2016). Mechanism of metamifop inhibition of the carboxyltransferase domain of acetyl-coenzyme a carboxylase in *Echinochloa crus-galli*. *Sci. Rep.* 6, 1–10. doi: 10.1038/srep34066

Xu, H., Zhu, X., Wang, H., Li, J., and Dong, L. (2013). Mechanism of resistance to fenoxaprop in Japanese foxtail (*Alopecurus japonicus*) from China. *Pesticide Biochem. Physiol.* 107, 25–31. doi: 10.1016/j.pestbp.2013.04.008

Yu, Q., Collavo, A., Zheng, M.-Q., Owen, M., Sattin, M., and Powles, S. B. (2007). Diversity of acetyl-coenzyme a carboxylase mutations in resistant lolium populations: evaluation using clethodim. *Plant Physiol.* 145, 547–558. doi: 10.1104/pp.107.105262

Yu, J., Mccullough, P. E., and Czarnota, M. A. (2017). First report of acetyl-CoA carboxylase–resistant southern crabgrass (*Digitaria ciliaris*) in the united states. *Weed Technol.* 31, 252–259. doi: 10.1017/wet.2016.34

Yu, Q., and Powles, S. (2014). Metabolism-based herbicide resistance and cross-resistance in crop weeds: a threat to herbicide sustainability and global crop production. *Plant Physiol.* 166, 1106–1118. doi: 10.1104/pp.114.242750

Yuan, G., Tian, Z., Li, T., Qian, Z., Guo, W., and Shen, G. (2021). Cross-resistance pattern to ACCase-inhibiting herbicides in a rare trp-2027-Ser mutation Chinese sprangletop (*Leptochloa chinensis*) population. *Chilean J. Agric. Res.* 81, 62–69. doi: 10.4067/S0718-58392021000100062

Zhang, C., Feng, L., and Tian, X. S. (2018). Alterations in the 5' untranslated region of the 5-enolpyruvylshikimate-3-phosphate synthase (EPSPS) gene influence EPSPS overexpression in glyphosate-resistant eleusine indica. *Pest Manage. Sci.* 74, 2561–2568. doi: 10.1002/ps.5042

frontiers | Frontiers in Plant Science

TYPE Original Research
PUBLISHED 27 February 2023
DOI 10.3389/fpls.2023.1126669

OPEN ACCESS

EDITED BY
Kun Zhang,
Yangzhou University, China

REVIEWED BY
Qian Sun,
Shenyang Agricultural University, China
Zhengnan Li,
Inner Mongolia Agricultural University, China

*CORRESPONDENCE
Wanping Zhang
drwpzhang@163.com

SPECIALTY SECTION
This article was submitted to Plant Pathogen Interactions, a section of the journal Frontiers in Plant Science

RECEIVED 18 December 2022
ACCEPTED 14 February 2023
PUBLISHED 27 February 2023

CITATION
Li J, Huang T, Xia M, Lu J, Xu X, Liu H and Zhang W (2023) Exogenous melatonin mediates radish (*Raphanus sativus*) and *Alternaria brassicae* interaction in a dose-dependent manner.
Front. Plant Sci. 14:1126669.
doi: 10.3389/fpls.2023.1126669

Exogenous melatonin mediates radish (*Raphanus sativus*) and *Alternaria brassicae* interaction in a dose-dependent manner

Jingwei Li[1,2], Tingmin Huang[1,2], Ming Xia[1,2,3], Jinbiao Lu[1,2], Xiuhong Xu[1,2], Haiyi Liu[1,2] and Wanping Zhang[1,2]*

[1]Institute of Vegetable Industry Technology Research, Guizhou University, Guiyang, China, [2]College of Agriculture, Guizhou University, Guiyang, China, [3]School of Computing, Chongqing College of Humanities, Science and Technology, Hechuan, China

Radish (*Raphanus sativus* L.) is an economically important vegetable worldwide, but its sustainable production and breeding are highly threatened by blight disease caused by *Alternaria brassicae*. Melatonin is an important growth regulator that can influence physiological activities in both plants and microbes and stimulate biotic stress resistance in plants. In this study, 0-1500 μM melatonin was exogenously applied to healthy radish seedlings, *in vitro* incubated *A. brassicae*, and diseased radish seedlings to determine the effects of melatonin on host, pathogen, and host-pathogen interaction. At sufficient concentrations (0-500 μM), melatonin enhanced growth and immunity of healthy radish seedlings by improving the function of organelles and promoting the biosynthesis of antioxidant enzymes, chitin, organic acid, and defense proteins. Interestingly, melatonin also improved colony growth, development, and virulence of *A. brassicae*. A strong dosage-dependent effect of melatonin was observed: 50-500 μM promoted host and pathogen vitality and resistance (500 μM was optimal) and 1500 μM inhibited these processes. Significantly less blight was observed on diseased seedlings treated with 500 μM melatonin, indicating that melatonin more strongly enhanced the growth and immunity of radish than it promoted the development and virulence of *A. brassicae* at this treatment concentration. These effects of MT were mediated by transcriptional changes of key genes as identified by RNA-seq, Dual RNA-seq, and qRT-PCR. The results from this work provide a theoretical basis for the application of melatonin to protect vegetable crops against pathogens.

KEYWORDS

radish, *Alternaria brassicae*, melatonin, interaction, dose-dependent manner

1 Introduction

Radish (*Raphanus sativus* L.) is an economically important vegetable worldwide, but its sustainable production and breeding are highly threatened by blight disease caused by *Alternaria brassicae* (Rashid et al., 2011; Dixit et al., 2020). Approximately 300 species of genus *Alternaria* can infect nearly 400 plant species (Lee et al., 2015; Meena et al., 2017). Control of *A. brassicae* is very difficult because of its multiple transmission channels and variation in the level of disease (Rashid et al., 2011).

Melatonin (N-acetyl-5-methoxytryptamine, MT) was first identified by Lerner et al. (Lerner et al., 1958) and is a natural growth regulator with many biological functions including circadian rhythm regulation (Grima et al., 2016), anti-oxidation (Nazarian and Ghanati, 2020), plant-yield boosting, and plant stress resistance inducement (Mandal et al., 2018; Sharma and Zheng, 2019; Moustafa-Farag et al., 2020; Sadak et al., 2020). Various biological processes participate in MT-induced plant biotic stress resistance. For example, MT stimulates salicylic acid (SA) and jasmonic acid (JA) biosynthesis to activate pathogensis-related protein (PR) synthesis and enhance *Xanthomonasoryzae* resistance of *Oryza sativa* (Chen et al., 2021). MT promotes JA synthesis by activating *PbOPR3* transcription (Liu et al., 2019) and it improves the resistance of pear (*Pyrus bretschneideri* Rehd.) to ring rot disease at least partly through the induction of ethylene (ETH) to activate PR and defense-related genes (Lee et al., 2015). Effects of MT on plants can include thickened cell wall and elevated defense to pathogen infection (Qian et al., 2015; Zhao et al., 2015). Exogenous MT induces cotton (*Gossypium hirsutum*) immunity by increasing lignin and gossypol synthesis to stimulate the expression of genes in the phenylpropanoid, mevalonate and gossypol pathways after *Verticillium dahlia* (Li et al., 2019).

MT is found in animals, plants, and microbes (Arendt, 2005; Pandi-Perumal et al., 2006; Rodriguez-Naranjo et al., 2012; Tan et al., 2012; Reiter et al., 2014). Many studies have described the effects of MT on growth, immunity, and defense improvement of plants (Lee and Back, 2016; Liu et al., 2019; Sadak et al., 2020), and on growth inhibition of pathogens (Arnao and Hernández-Ruiz, 2015; Zhang et al., 2017). However, some microorganisms synthesize MT, so the effects of MT on microorganisms may be complex, with both negative and positive effects (Hardel, 2016; Chen et al., 2018; Ma et al., 2018). For instance, exogenous MT inhibits mycelial growth, cell ultrastructure development, and stress tolerance of *Phytophthora infestans* (Zhang et al., 2017), while it promotes the growth and development of *Rhizophagus intraradices* under stress (Yang et al., 2020). Diseased leaves load pathogens, so spraying of MT on diseased plants could affect both host and pathogen. However, limited studies have the investigating ability of MT to mediate plant-pathogen interactions.

In this work, we investigated the direct effects of MT on growth and immunity of radish seedlings, on development and virulence of *in vitro* incubated *A. brassicae*, and how MT mediates the radish-*A. brassicae* interaction. The results provide insight into the mechanism of MT activity on radish and *A. brassicae* and the physiological and transcriptional effects of MT to alter the defense of radish to *A. brassicae*.

2 Materials and methods

2.1 Materials and chemicals

The *A. brassicae* susceptable radish variety "Jiangnan Yuanbai" ("JNYB") was selected for this study. After sprouting, seedlings were incubated in a climate chamber at 28°C with 16-hour light of 120-150 μmol quanta m^2/s irradiance/8 h dark cycles with humidity at 65%, seedlings with two euphylla were collected at 20 days. Standard horticultural practices were utilized. A monospore culture of *A. brassicae* (Berk.) Sacc was previously isolated from *Alternaria* blight-diseased radish leaves and kept on synthetic low nutrient agar (SNA) medium at 25°C in the dark. A single colony of *A. brassicae* was incubated for 7 days to allow mycelial growth, and another 7 days of incubation with exposure to ultraviolet light was used to stimulate conidia formation. Unless otherwise stated, all chemicals used in this study were purchased from Sigma-Aldrich (Sigma-Aldrich, St Louis, MO, USA).

2.2 Measuring the effects of exogenous MT on radish "JYNB" growth and immunity

2.2.1 Treatments

"JNYB" seedlings of uniform size were evenly sprayed with 2 mL of 50, 100, 500, 1000, and 1500 μM of MT once every 2 days to determine the effects of MT on growth and immunity. Ethanol solvent (V: V=0.6%; 0 μM MT) was used as a negative control. The culture conditions were as described above. The solvent was previously shown to have no effect on seedlings. Fifteen days post-treatment, the seedlings were harvested and analyzed.

2.2.2 Growth and immunity assessment

The leaf length and width, shoot height, and stem diameter were measured for plants subjected to each MT treatment. Measurements were made using an electronic vernier caliper (500-196-30, Mitutoyo, Japan) and the number of leaves were counted manually. *A. brassicae* conidia were collected and adjusted to a concentration of 10^6/mL by ddH_2O. The apex (1 cm in length) of the second expanded leaves from control and each treatment were cut and the wounded leaves were immersed into conidia suspension for 2 min. Seedlings carrying conidia were then incubated for 14 days. The numbers of symptomatic plants were determined and the disease incidence and the disease index (DI) were calculated (Method S1). Three replicates of 20 plants were used for each treatment.

2.2.3 Microscopy

The second fully expanded healthy leaves were randomly selected from each treatment for transmission electron microscope (TEM) examination. The leaf samples were fixed, sectioned according to the method described by Basma et al. (Basma et al., 2011), and then examined using a H-7500 TEM (Hitachi, Tokyo, Japan). Five replicates of control, 500 μM, and 1500 μM MT treatments were collected to analysis the effects of MT on subcellular structure.

2.2.4 Physiological index assessment

Chlorophyll content was measured using a portable chlorophyll meter (HED-YB, Horde, China) according to the manufacturer's instructions. Oxidation levels and activities of oxidoreduction-related enzymes were assessed by spectrophotometry or by enzyme-linked immunosorbent assay (ELISA) according to kit instructions (kit listed in Table S1). Phytohormones including JA, SA, aminocyclopropanecarboxylic acid (ACC, an ETH precursor) and abscisic acid (ABA) were detected by multi reaction monitoring (MRM) technology using 100 mg radish leaf samples from 0, 500 or 1500 μM MT treatment. The detection protocols are described in Method S2. Each treatment group contained three replicates of 20 plants, thus 60 plants were measured for each MT content.

2.2.5 mRNA library construction, sequencing and analysis

Total RNA was isolated from 100 mg of radish leaf mix from 0, 500, or 1500 μM MT treatment and purified using TRIzol reagent (Invitrogen, Carlsbad, CA, USA) following the manufacturer's procedure. The concentration of the purified RNA samples was quantified by NanoDrop (ND-1000, Wilmington, DE, USA) and the integrity was assessed by Bioanalyzer (2100, Agilent, CA, USA) and confirmed by electrophoresis on denaturing agarose gel. The mRNA library construction, sequencing, and analysis were conducted by LC-Bio Technology Co., Ltd., Hangzhou, China. Detailed analysis protocols are listed in Method S3. Additional data analysis was completed on the analytic platform of Technology Co., Ltd. (https://www.omicstudio.cn/login). The obtained sequence data were mapped to the published radish genome (https://www.ncbi.nlm.nih.gov/genome/12929?genome_assembly_id=249276). The RNA-seq raw data have been deposited into the National Center for biotechnology Information's Sequence Read Archive (NCBI's SRA, https://submit.ncbi.nlm.nih.gov/subs/sra/), the file code is PRJNA 831633.

2.2.6 Real-time qRT-PCR

Total RNA extraction was conducted using the Universal Plant Total RNA Rapid Extraction Kit (PR3302, Bioteke, Wuxi, China) according to the manufacturer's instruction. RNA quality and integrity were checked by electrophoresis and using a Nano photometer spectrophotometer (Implen, WestlakeVillage, CA, USA). The first-strand cDNA was synthesized using reverse transcriptase (Toyobo, Osaka, Japan) and qRT-PCR was performed using SYBR Premix Ex Taq (Takara, Dalian, China) on a CFX1000 instrument (Bio-Rad, Shanghai, China). The amount of the amplified DNA was monitored by fluorescence at the end of each cycle and comparison to the levels of target and reference genes, using the primers listed in Table S2. Each sample was tested three times in independent runs for all reference and selected genes based on separate RNA extracts from at least three samples. Gene expression was evaluated by the $2^{-\triangle\triangle Ct}$ method.

2.3 Measuring the effects of exogenous MT on *A. brassicae* growth, development, and pathogenicity

2.3.1 Treatments

Sterilized filter paper disks (0.5 cm in diameter) carrying 0.5 mL of 10^6 CFU/mL *A. brassicae* conidia were prepared, and the disks was placed onto the center of 20 mL SNA medium (9 mm in diameter) containing 0, 50, 100, 500, 1000, or 1500 μM of MT. The medium plates were incubated at 25 ± 2°C in the dark for 7 days.

2.3.2 Colony growth and development assessment

Diameters of single colonies were measured using an electronic vernier caliper Conidia were harvested from each treatment with 3 mL of water, and conidia yield was counted with a blood count board. Development of mycelium and germination of conidia chain were observed by optical microscope (LeicaDM2000, Wetzlar, Germany). Three replicates of 5 colonies were measured.

2.3.3 Virulence assessment

A detached leaf assay was conducted to assess virulence. *A. brassicae* hyphae discs 0.5 cm in diameter were harvested randomly from each MT treatment and touched to the up-surface of the second expanded leaves of MT untreated "JNYB" seedlings. The seedlings were then incubated under 25 ± 2°C with 16 h of light for 7 days, and the petioles were moisturized by wet cotton. Lesion area was then measured. Ten leaves in 3 replications were included in each treatment. *A. brassicae* conidia suspensions (10^6 CFU/mL) were prepared for each MT treatment as well, and radish leaves were inoculated as described above. Fourteen days after symptom development, disease incidence, and index were calculated as described above. Each treatment contained at least 30 seedlings and experiments were repeated 3 times.

2.3.4 Enzyme activity assessment

Activities of Glutathione peroxidase (GSH-PX), catalase (CAT), glycosyl transferases (GT), and Fungus cell Wall degrading enzymes (PCWDES) of MT treated *A. brassicae* were assessed by spectrophotometry or by ELISA using kits according to the instructions (listed in Table S1).

2.3.5 RNA-seq and gene expression analyses

RNA was extracted from *A. brassicae* treated with 0, 500 and 1500 μM MT and purified by Spin Column Fungal Total RNA Purification Kit (B518659, Sangon Biotech, Shanghai, China) according to the kit instructions. Steps of mRNA library construction, sequencing, and analyses were performed according to Method S3. Data were mapped to the *A. alternate* genome: https://ftp.ncbi.nlm.nih.gov/genomes/refseq/fungi/Alternaria_alternata/latest_assemb-ly_versions. The transcriptome raw data (PRJNA 830515) have been deposited in NCBI's SRA. Gene expression analyses were conducted by qRT-PCR, as described above. Gene information and primer sequences are presented in Table S2.

2.4 Measuring the effects of exogenous MT on the interaction of *A. brassicae* and radish

2.4.1 Treatments and measurements of physiological parameters

A. brassicae was inoculated onto radish seedlings by leaf immersion as described above. Fourteen days after symptom development, diseased seedlings were evenly sprayed with 2 mL of 50, 100, 500, 1000, and 1500 μM of MT once 2 days, with solvent as control. Fifteen days post treatment, samples were harvested, and disease incidence and index were calculated as described above. At least 30 seedlings were tested, and the experiment was repeated three times. The innate phytohormones were also detected, as described in Method S2.

2.4.2 Dual RNA-seq and gene express analyses

Samples (100 mg) of the second expanded leaf mix from diseased radish seedlings treated with 0, 500, or 1500 μM MT were sampled. Total RNA isolation, mRNA library construction, sequencing, and analyses were performed as described above. Data were mapped to the *R. sativus* and *A. alternata* genomes. The transcriptome raw data have been deposited in NCBI's SRA (PRJNA 830523, PRJNA 830515 and PRJNA 831633). Gene expression levels were determined by qRT-PCR as described above. Gene information and primer sequences are listed in Table S2.

2.5 Statistical analysis

Data presented are expressed as mean ± SE. The statistical analysis was performed using Analysis of Variance (ANOVA) by SPSS 18.0, and $P < 0.05$ was considered a significant difference and indicated with different letters.

3 Results

3.1 Exogenous MT influences radish growth and immunity to *A. brassicae* in a dosage-dependent manner

3.1.1 MT influences seedling growth

Seedlings of *A. brassicae* susceptable radish cultivar "JNYB" were evenly sprayed with 2 mL of ethanol solvent, 50, 100, 500, 1000, and 1500 μM of MT once 2 days. Fifteen days post-treatment, growth and morphology were analyzed. A dosage-dependent response was observed: 500 μM MT spraying produced much wider leaves, higher shoots, and stouter stem than ones from other treatments and the control samples. Those parameters were similar in the groups treated with 50 and 100 μM of MT. The use of 1000 μM MT did not stimulate radish growth, and the leaf length, stem height and stem diameter were decreased to control level or even lower than that of the control. More serious inhibition was observed for the seedlings treated with 1500 μM MT, except for the No. of leaves, leaf length, stem height, and stem diameter were significantly lower than that of the control (Figures 1A, S1). The results indicate a dose-dependence of exogenous MT effects on radish growth, which increases first and then decreases. A concentration of 500 μM of MT exhibited the strongest ability to stimulate radish growth.

3.1.2 MT influences innate immunity

A spore suspension of *A. brassicae* was inoculated onto MT pretreated seedlings to test the effect of exogenous MT on radish immunity. MT positively regulated innate immunity of radish against *A. brassicae* at higher concentrations (50-1000 μM). *Alternaria* blight symptoms, including chlorosis and black spots on leaves, were much more severe in the control, the DI equaled to 23, samples sprayed with 1500 μM (DI=21.5) than in other treatments at 14th day post inoculation. No significant difference was found among 50 (DI = 14.7), 100 (DI = 12.8), and 1000 μM (DI = 16.1) MT treated individuals, with strongest immunity observed when 500 μM of MT was applied (DI = 8.6) (Figures 1B, C). Thus, the results indicate a dose-dependent effect on plant innate immunity.

3.1.3 MT influences subcellular structures

To determine the effects of MT on radish subcellular structures, TEM was conducted on samples of leaves from the top of seedlings treated with 0, 500 and 1500 μM MT. The cell wall thickness, the number of starch grain, mitochondria and chloroplast, and the volume of starch gain of 500 μM MT treated samples were significantly increased 1.2–2.5 fold. In particular, the volume of starch grains and the number of chloroplasts were sharply increased. No significant differences were observed for these parameters between the control and 1500 μM treatment group (Figures 1D, S2). The total chlorophyll content was detected in control and treated samples to confirm the TEM results. The highest value was found in plants treated with 100 and 500 μM MT, there were no significant differences between the control and 1500 μM MT treated plants, with both significantly lower than other treatments (Figure S3). The above results further support a dose-dependent effect of MT on radish subcellular structures.

3.1.4 MT influences redox reaction

To further investigate the underlying mechanisms of MT action, redox-related enzymatic activities were measured for the treated plants. The phenylalanine ammonialyase (PAL) and superoxide dismutase (SOD) activities were significantly higher for those in the MT-treated group compared to the control. PAL activity was highest in 100 μM MT treated samples (103 μM/g), followed by the 50 and 500 μM treated groups, then the 1000 μM MT treated samples, and finally the 1500 μM MT treated samples (Figure 1E). SOD activity increased sharply in the 500 μM MT treated group (462 μM/g), with no significant difference found between 100 and 1000 μM MT treated samples, which were significantly higher than the other two groups; the SOD activity of the 1500 μM MT sprayed samples was obviously higher than that

10.3389/fpls.2023.1126669

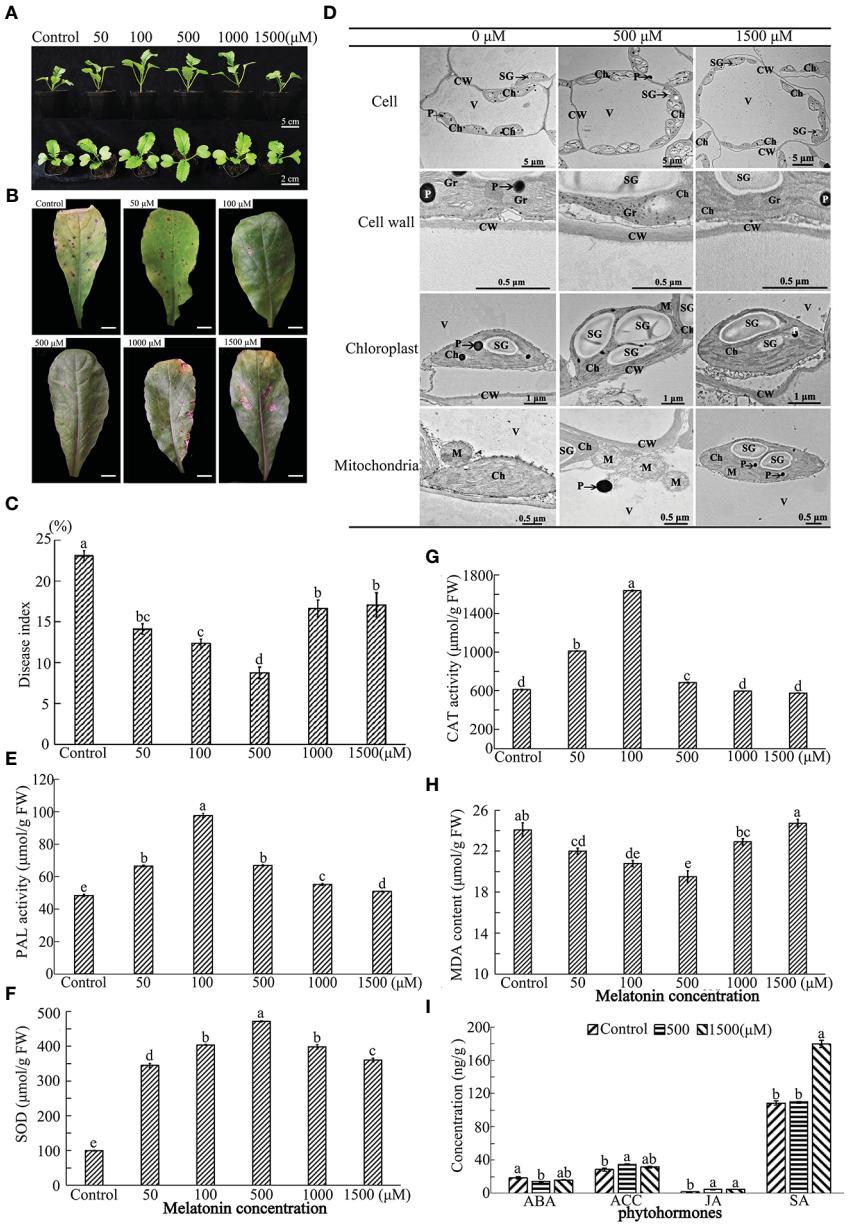

FIGURE 1
Effect of exogenous MT on growth and immunity of radish "JNYB" seedlings. Radish 20-day-old seedlings were pretreated with solvent (control) and 50-1500 μM of MT for 14 days. **(A)** growth and morphology of radish seedlings pretreated with MT; **(B, C)** *Alternaria* blight symptoms and disease index after inoculation of *A brassicae* on MT-pretreated leaves, bar in B indicates 1 cm; **(D)** TEM analysis of subcellular structure of leaf cells treated with MT. **(E–H)** Activity of redox reaction related enzymes for different treatments; **(I)** Phytohormone concentrations of samples pretreated with MT. CW, cell wall; Ch, chloroplast; Gr, grana; M, mitochondria; SG, starch grains; V, vacuole; P, plastoglobuli. At least three repeats of samples were analyzed; values are means ± standard error (SE); letters indicate significant difference; statistical analysis was performed by one-way ANOVA, $p < 0.05$.

of the 50 μM treated samples (Figure 1F). The 1000 and 1500 μM MT treated groups MT group had no significant changes in CAT activity compared with the control. This enzyme activity increased rapidly with application of 100 μM MT (1653 μM/g), followed by 50 and 500 μM treatments (Figure 1G). Exogenous application of 1500 μM MT did not affect malondialdehyde (MDA) content, but for other MT treatments, MDA levels were lower. The MDA level was lowest in 100 and 500 μM MT treatments (21.8 and 20.2 μM/g, respectively) (Figure 1H). Generally speaking, 50-500 μM MT stimulated reduction reactions, and 500-1500 μM MT shut off this effect.

3.1.5 MT influences phytohormone content

Fresh radish leaf mixtures were prepared from 0, 500 or 1500 μM MT treatments to determine ABA, JA, ACC, and SA content using MRM technology. Generally speaking, exogenous application of 500 μM of MT positively regulated innate immunity-related hormones, with significantly lower ABA content (14.7 ng/g)

and higher levels of ACC (18.9 ng/g) and JA (5.1 ng/g), but no stimulation of SA biosynthesis (77.1 ng/g). ABA first decreased at 500 μM of MT treatment and then increased at 1500 μM (16.5 ng/g), with no significant difference from that of the control (18.9 ng/g). ACC was slightly decreased at 1500 μM MT (32.1 ng/g), but no differences in JA content were observed between 500 and 1500 μM (5.3 ng/g) MT treatments. Application of 1500 μM MT increased SA biosynthesis sharply (180.0 ng/g), but SA levels in samples treated with 500 μM MT (109.0 ng/g) were similar to those in the control plants (110.2 ng/g FW) (Figure 1I).

3.1.6 MT influences the global transcription of healthy radish seedling

To investigate the changes in gene expression in radish leaves after MT treatment, RNA-seq and qRT-PCR were used. More than 35,900,000 mapped reads were obtained from each replicate of three treatments (data not shown). The differentially expressed mRNAs were selected with fold change > 2 or fold change < 0.5 and p value < 0.05. Analysis revealed 1458 genes and 928 genes that were up- and down-regulated, respectively, after 500 μM MT treatment, and 4850 and 3911 genes that were up- and down-regulated, respectively, after 1500 μM MT treatment. Comparison of 1500 μM MT treatment *vs.* 500 μM, 3798 and 4078 genes were up- and down-regulated, respectively (Figure 2A). Among thousands of differentially expressed genes (DEGs), only 470 genes were differentially expressed in 500 μM MT *vs.* control, 1500 μM MT *vs.* control and 1500 μM MT *vs.* 500 μM MT (Figure 2B). The most unigenes, 2118, were detected in 1500 μM MT treatment and only 638 were found in the 500 μM MT group. A total of 1226 (756 + 470) genes were differentially expressed in both the 500 and 1500 μM MT applied samples, however, 5887 (5417 + 470) DEGs were identified in both 1500 μM MT *VS* control and 1500 *VS* 500 μM MT comparisons (Figure 2B). The above results indicated totally different gene expression patterns between the 500 and 1500 μM MT treated groups. To further investigate the gene expression changes with MT treatment, all DEGs in 0 μM *VS* 500 μM *VS* 1500 μM MT treatment contract set were selected and subjected to Gene ontology (GO) classification and Kyoto Encyclopedia of Genes and Genomes (KEGG) pathway analysis, the top 30 classifications and pathways were shown in Figures 2C, D. GO analysis revealed enrichment of membrane-, chloroplast-, oxidation-reduction process-, stress response-, biological process-response and cell wall-related terms. KEGG pathway analysis revealed enrichment of DEGs in categories of plant hormone signal transduction, mitogen-activated protein kinase (MAPK) signaling pathway, sugar metabolism, amino acid metabolism, carbon fixation, porphyrin and chlorophyll metabolism, peroxisome, ATP binding cassette (ABC) transporters and so forth. The top 10 up-regulated and down-regulated GO classifications and KEGG enrichments of DEGs for each contrast set are presented in Table S3.

To verify the RNA-seq data, qRT-PCR was used to analyze the expression patterns of 15 DEGs, involved in plant growth regulation, redox reaction, cell structure development, and defense response according to the GO or KEGG annotation and previous reports (description, full name of DEGs, and their primer sequences were listed in Table S2). The results showed that the expression patterns were generally consistent between qRT-PCR and RNA-seq data, with the fold changes of most genes greater in RNA-seq data than in the qRT-PCR data. Among the tested genes, *TTS*, *TTS-like2*, and *GLP1* exhibited the highest expression in the control samples, and expression was down-regulated by exogenous MT. *ERF3-like*, *LOX3*, *DEF1*, *USPA-like*, *BTP1-like*, *MYB51-like* and *UMP* were expressed at a significantly higher level in 500 μM MT treated samples compared with the other two groups; the expression of *MYC2*, *CPC1-like*, *ERF1B-like* and *FBA1* increased as the concentration of exogenously applied MT increased, and *COP1-X1* was most highly expressed in 1500 μM MT treated samples followed by the control samples (Figure 2E).

3.2 Exogenous MT affects *A. brassicae* growth, conidia formation, and virulence in a dosage-dependent manner

3.2.1 MT affects colony growth and development

Single clones of *A. brassicae* were incubated on SNA medium supplemented with 0-1500 μM of exogenous MT to assay mycelium growth and conidia development. Exogenous MT affected *A. brassicae* growth and conidia formation in a dose-dependent manner. Lower concentrations of exogenous MT (50, 100 and 500 μM) improved *A. brassicae* aerial hyphae growth significantly, with the best effect seen for 500 μM MT (6.5 cm in diameter). Significant growth inhibition compared with the control was observed for 1500 μM of MT (diameter = 4.3 cm) (Figures 3A, B). In terms of conidia development, *A. brassicae* treated with 500-1500 μM of MT produced conidia in long, dark brown conidial chains of 5-7 individuals with muriform septation. Treatment with 0-100 μM MT resulted in much shorter chains of 1-4 conidia (Figure 3A). A concentration of 500 μM of exogenous MT enhanced the filament development of conidia, with single conidia generating 1-5 mycelium and the control allowing germination of only 1-2 mycelium (Figure 3A). The conidia yield of 500, 1000, and 1500 μM MT treatments (33.4×10^5, 33.1×10^5, and 31.1×10^5 CFU/mL respectively) were significantly higher than for 50 and 100 μM MT applications, 25.4×10^5 and 28.6×10^5 CFU/mL, respectively (Figure 3B). Conidia morphology was unchanged as the concentration of MT increased.

3.2.2 MT affects virulence

The function of MT on conidia virulence was assessed through a detached leaf assay. Seven days after incubation, the symptoms, including wilt, chlorosis, and spots on leaves, were more severe on samples inoculated with hyphae harvested from 50-1000 μM MT colonies. Substantially larger infected areas were observed, and no significant differences were found between control and leaves infected by 1500 μM MT treated hyphae (Figure 3C). DI increased with the increase of MT concentration in the range of 50-500 μM, and 500 μM MT treatment resulted in the highest virulence of conidia (DI = 33.6). A concentration of 1000 μM MT eliminated the effects of 500 μM MT, and the virulence of conidia

10.3389/fpls.2023.1126669

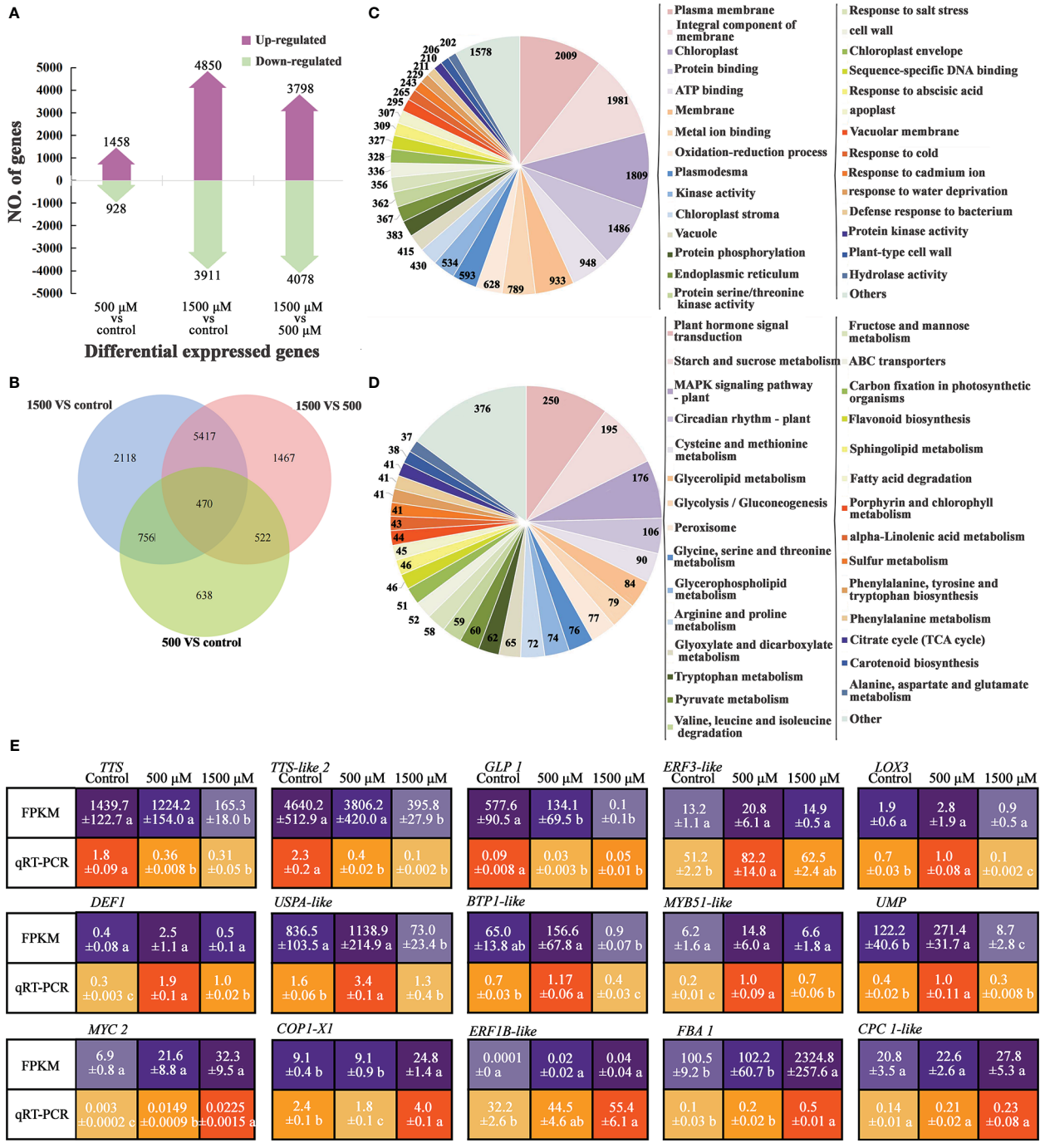

FIGURE 2
Analysis of DEGs by RNA-seq and qRT-PCR of MT treated radish "JNYB". **(A)** Numbers of genes up- and down-regulated of contrast sets of 500 μM MT treated group *VS* control, 1500 μM MT treated group *VS* control and 1500 μM *VS* 500 μM MT treated groups; **(B)** Numbers of DEGs of comparison sets. The Venn diagrams depict the number of DEGs for each comparison with the numbers in the overlapped area representing the number of genes shared for the comparison; **(C, D)** DEG functional annotation (top 30) by GO classification and KEGG pathway analysis; **(E)** Verification of selected DEGs using qRT-PCR; the relative expression level of a gene was determined using a $2^{-\triangle\triangle}$Ct method; values presented are means ± SE; significant difference at $P < 0.05$ relative to the control is indicated by lowercase letter.

germinated from 1500 μM MT treated group (DI = 27.3) was significantly lower than that of the control (DI = 29.4) (Figure 3D).

3.2.3 MT affects enzyme activities

Colonies from 0-1500 μM MT treatment were harvested and activities of virulence and oxide related enzymes were measured. Generally, compared with the control, exogenous MT in the range of 0-500 μM increased the activities of GT and PCWDES and decreased the activities of GSH-Px and CAT. An obvious dose-dependence of MT was seen for enzyme activities. Activities of GT and PCWDES substantially increased as the MT concentration increased to 500 μM (563.5 and 812.1 U/L) and abruptly

10.3389/fpls.2023.1126669

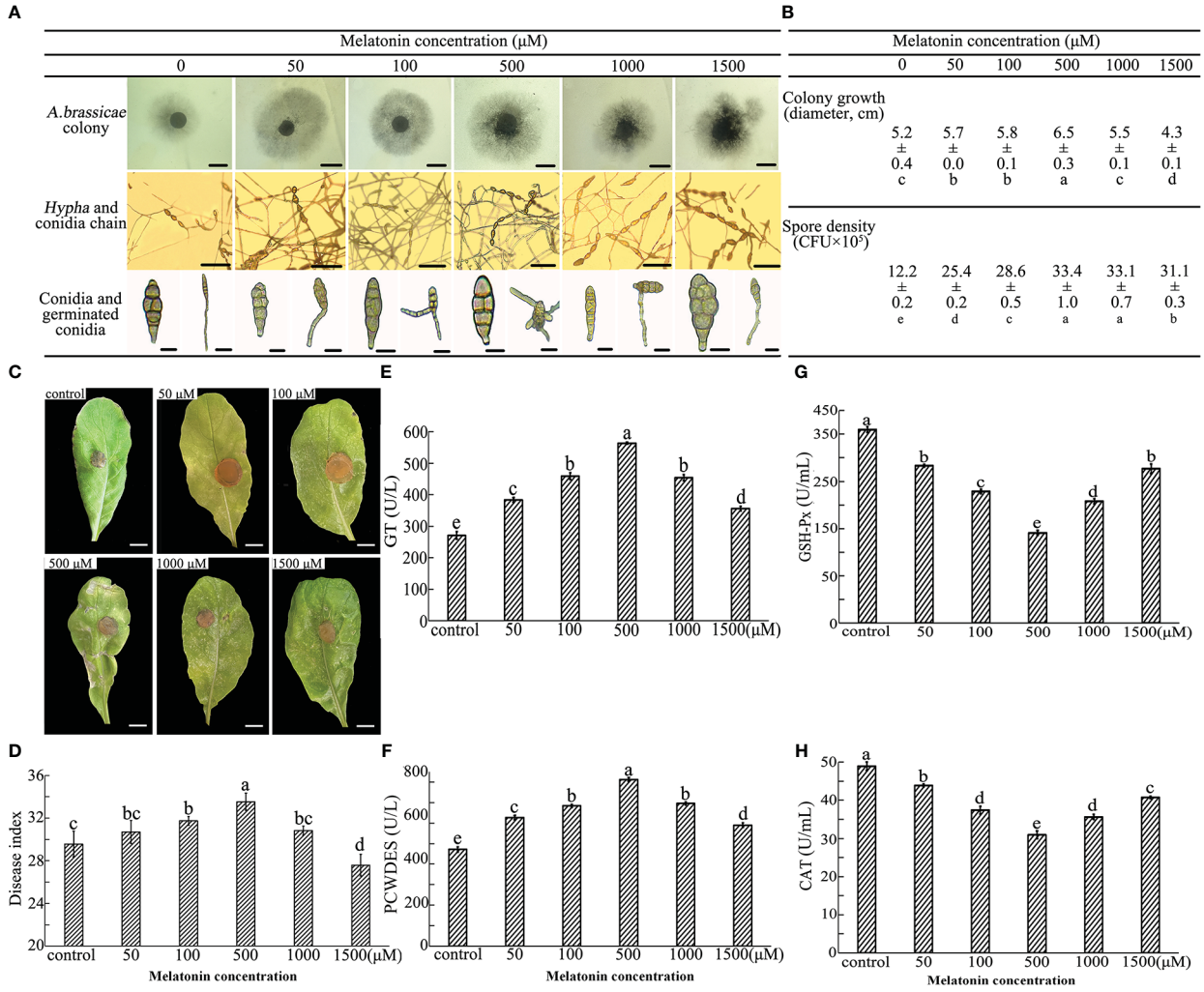

FIGURE 3
Effect of exogenous MT on *A brassicae* growth, development, virulence, and enzyme activities. *A brassicae* were applied to SNA medium supplemented with 0-1500 μM exogenous MT and incubated for 7 days for colony growth and additional 7 days under ultraviolet for conidia formation and germination. **(A, B)** Colony growth, conidia development and conidia germination of *A brassicae*, bars in 1st, 2nd and 3rd lines of image A indicate 0.5 cm, 100 μm, and 10 μm respectively. **(C, D)** Pathology of MT-treated *A brassicae*; **(E-H)** Activity of redox- and virulence-related enzymes. At least 3 repeats were performed; the values are means ± SE; letters indicate significant differences; statistical analysis was performed by one-way ANOVA, $p < 0.05$.

decreased at MT concentrations of 1000 and 1500 μM, though remained higher than that of the control (Figure 3D). The activities of GSH-Px and CAT decreased firstly and then increased as the concentration of exogenous MT increased, and samples treated with 500 μM MT had the lowest activity (190.9 and 30.4 U/mL).

3.2.4 Transcriptomic analysis of *A. brassicae* after MT treatment

To investigate potential changes in gene expression in *A. brassicae* after exogenous application of 0, 500, and 1500 μM MT, RNA-seq analysis and qRT-PCR were conducted. At least 4186158 mapped reads and 89.02% mapping ratio were obtained from each treatment (data not shown). Compared with the control (no MT added), 525 and 577 genes were up- or down-regulated, respectively, in the 500 μM MT treatment group and only 160 and 201 up- and down-regulated genes, respectively, were seen in the 1500 μM group. In the comparison of 1500 *VS* 500 μM MT, 577 and 700 genes were up- and down-regulated (Figure 4A). The DEGs were identified for each pairwise comparison and revealed 28 DEGs that were found for all comparisons. A larger number of unigenes (489) was detected in contrast of 500 *VS* 1500 μM MT treatment than in the 500 μM MT group *VS* control (418), and the fewest unigenes (103) were identified for the 1500 μM MT treatment. A total of 621 genes (593 + 28) were differently expressed in 500 μM MT treatment *VS* control and 500 μM *VS* 1500 μM comparisons, while only 91 same genes (63 + 28) were identified in 500 μM MT treatment *VS* control and 1500 μM *VS* control comparisons (Figure 4B), indicating very different gene expression patterns between the 500 and 1500 μM MT treated groups, but a relatively similar gene expression patten between the control and 1500 μM MT treated group. DEGs were selected from the control *VS* 500 μM *VS* 1500 μM MT treatments for GO classification and KEGG pathway analysis, the top 14 classifications and pathways are shown in Figures 4C, D.

10.3389/fpls.2023.1126669

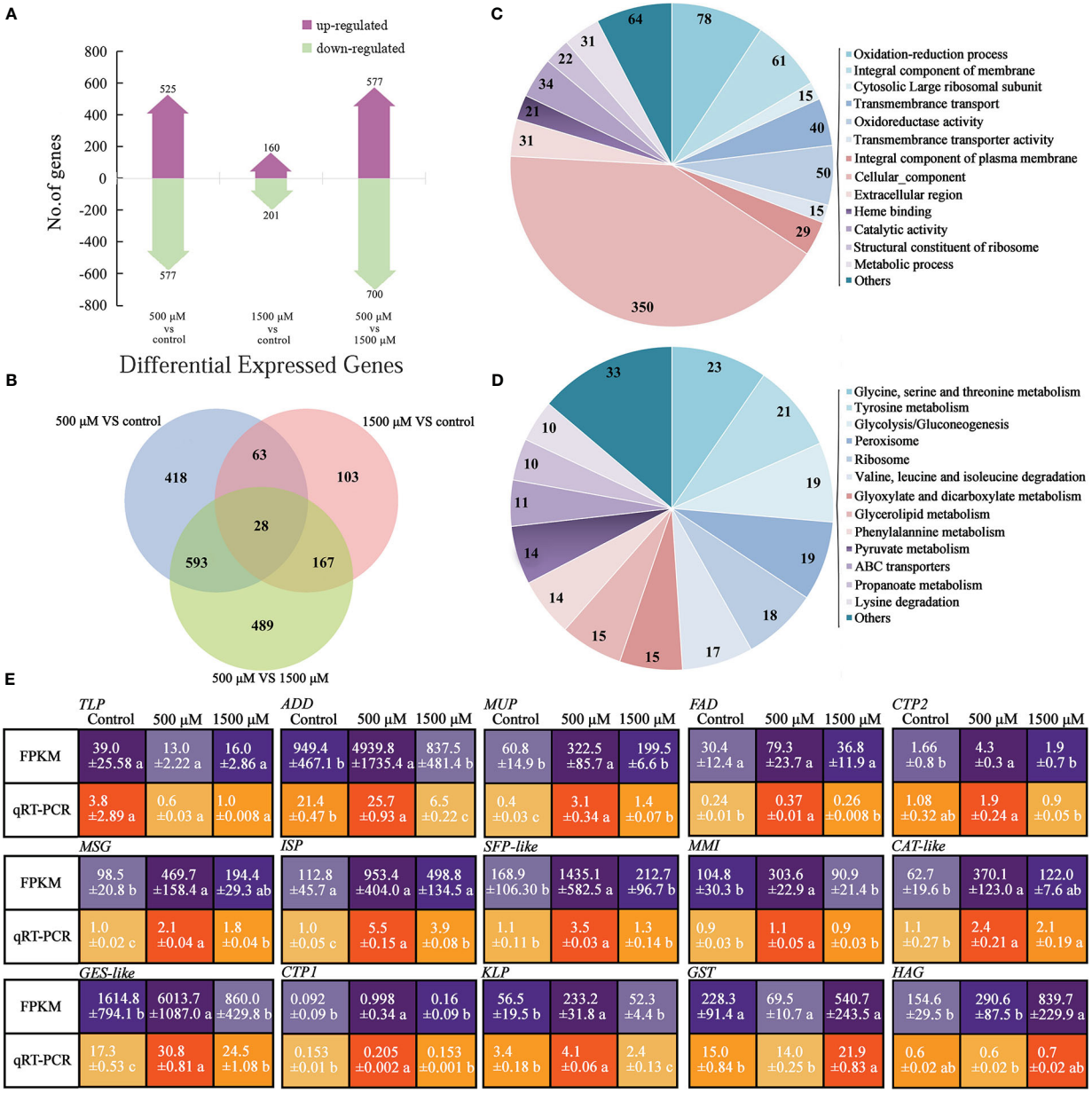

FIGURE 4
Analysis and functional categorization of DEGs and verification by qRT-PCR of 0, 500 and 1500 μM MT treated *A brassicae*. **(A)** Number of genes up- and down-regulated in contrast sets of 500 μM MT treated group *VS* control, 1500 μM MT treated group *VS* control, and 1500 μM *VS* 500 μM MT treated groups; **(B)** Comparison of the number of DEGs for different comparisons; **(C, D)** Main function of DEGs annotated by GO classification and KEGG pathway analysis; **(E)** Verification of selected DEGs from RNA-seq using qRT-PCR. The relative expression level of a gene in was determined using a $2^{-\triangle\triangle}$Ct method, and significant difference at $P < 0.05$ compared to the control is indicated by lowercase letter.

DEGs were enriched in categories of oxidation-reduction, and oxidoreductase activity, membrane and transmembrane transport, cytosolic large ribosomal subunit, cellular component, extracellular region, catalytic activity, ribosome, and metabolic process. KEGG pathway analysis of DEGs showed enrichment in categories of glycine, serine and threonine, tyrosine, glyoxylate and dicarboxylate, glycerolipid, phenylalanine, pyruvate and propanoate metabolism; glycolysis/gluconegenesis; peroxisome; ribosome; valine, leucine, and isoleucine degradation; and ABC transporters. The top 10 up-regulated and down-regulated GO and KEGG categories for all comparisons are presented in Table S4.

To verify the sequencing data, qRT-PCR was conducted to determine the expression patterns of 15 DEGs. The selected genes are involved in cell proliferation, development, and virulence according to the GO or KEGG annotation and previous reports (description, full name of DEGs, and their primer sequences were listed in Table S2). Generally, the expression patterns were consistent between RNA-seq data and qRT-PCR, with fold changes in expression greater in RNA-seq data than in qRT-PCR data (Figure 4E). Thioredoxin-like protein (TLP) was expressed most highly the control, decreased with exogenous MT, and increased again as the concentration elevated to 1500 μM. *ADD*,

MUP, *FAD*, *CTP2*, *MSG*, *ISP*, *SFP-like*, *MMI*, *CAT-like*, *GES-like*, *CTP1*, and *KLP* were expressed at significantly higher levels in 500 µM MT treated samples compared with the other two groups. *GST* and *HAG* showed highest expression in the 1500 µM MT treated samples (Figure 4E).

3.3 The effects of exogenous MT on the interaction of radish and A. brassicae

3.3.1 MT affects radish blight disease development and phytohormone biosynthesis

Exogenous MT application improved the resistance of "JNYB" radish seedlings to *A. brassicae* (Figures 5A, B). After incubation, diseased leaves without MT treatment turned chlorotic and their leaf spots coalesced; DI of 35.73. The addition of 50-500 µM MT noticeably offset the development of disease and alleviated the blotch damage to varying degrees. DI of MT treatments ranged from 32.24 (50 µM) ~ 24.74 (500 µM), and those in the 500 µM MT subgroup showed the greatest decline in disease. Higher concentration attenuated the suppression of disease, and no significant differences were found among 50 µM, 1000 µM (32.66), and 1500 µM (32.47) treatments (Figures 5A, B). Compared with the control, those in the 500 µM MT treated group had significantly lower ABA (14.6 ng/g FW) levels and significantly higher ACC (35.1 ng/g FW), JA (5.1 ng/g FW), and SA (81.3 ng/g FW) levels. The 1500 µM MT group exhibited no significant changes in ABA (16.5 ng/g FW) and ACC (32.1 ng/g FW) compared with the control and 500 µM MT treatment groups, the JA content was similar to that of the 500 µM group and higher than the control, and the content of SA (142.4 ng/g FW) was significantly higher than that of the control and the 500 µM MT treatment (Figure 5C).

3.3.1 MT affects radish and *A. brassicae* interaction at transcriptional level

Both RNA-seq and qRT-PCR were conducted to investigate changes in gene expression of host and pathogen on diseased leaves treated with 0, 500 and 1500 µM of MT. More than 126692247 reads were obtained with at least 88.2% mapped to the radish genome for each treatment, with at least 98.27% of these reads mapped to exons. For *A. brassicae*, only 49428-82141 reads were mapped from the 3 treatments, with only 0.02%-0.06% mapping to the genome, of these, at least 98.34% were mapped to exon regions (data not shown). In the host (radish), compared with the control, 588 genes were up-regulated and 898 genes were down regulated in 500 µM MT treatment, and 1185 up-regulated and 1325 down-regulated genes were detected in 1500 µM MT treatment. For 1500 µM MT treatment *VS* 500 µM, 606 and 526 genes were up- and down-regulated, respectively (Figure 6A). In the pathogen, few DEGs were detected, with 6 up- and 47 down-regulated genes seen in the 500 µM MT treatment compared with the control, and 6 up-regulated and 136 down-regulated genes detected for 1500 µM treatment. Comparison of 1500 µM treatment *VS* 500 µM revealed 0 and 4 genes that were up- and down-regulated, respectively (Figure 6B). In radish, 35 same DEGs were found in all contrast sets and 702 (667 + 35) DEGs had similar functions. The largest number of unigenes (1415) were detected in the 1500 µM MT treated group *vs*. control, followed by 509 unigenes in 500 µM MT *vs*. control, a total of 402 unigenes were identified in the 500 µM *VS* 1500 µM contrast set (Figure 6C). The above results indicate very different gene expression patterns between 500 and 1500 µM MT treated groups. Only few DEGs were identified in *A. brassicae* so overlapping gene analysis could not be performed for these data.

All DEGs of radish in 0 µM *VS* 500 µM *VS* 1500 µM MT treatment contrast set were selected for GO classification and KEGG pathways analysis, top enriched classification and pathways are shown in Figures 6D, G. GO analysis showed enrichment of genes in function terms such as plasma membrane, chloroplast, protein binding, cytosol, transcription, ion binding, defense response, response to stress, and cell wall. Thirteen categories were enriched by KEGG pathway analysis, including plant-pathogen interaction; hormone signal transduction; MAPK signaling pathway; glycerophospholipid metabolism; circadian

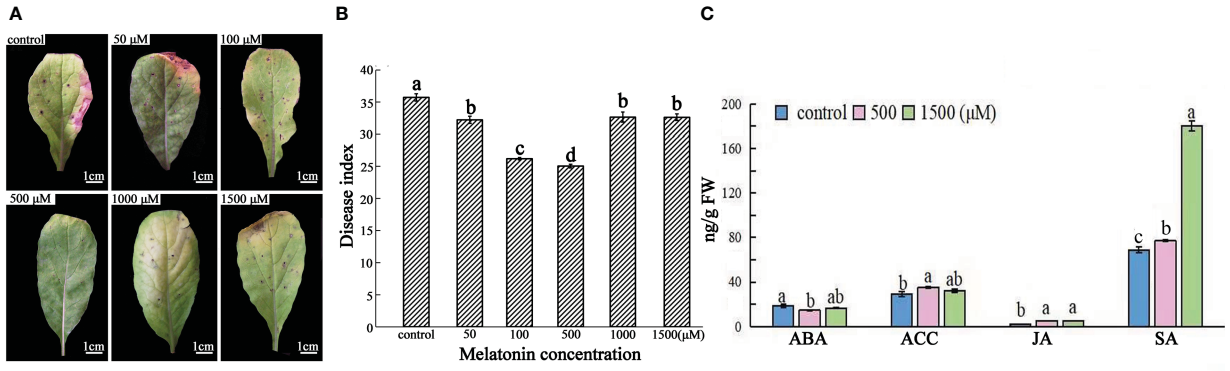

FIGURE 5
Effects of exogenous MT at different concentrations on radish "JNYB" defense to *A brassicae* and levels of innate phytohormones. Black spot-diseased radish seedlings were exogenously spayed with 0-1500 µM exogenous MT once two days for 15 days. **(A)** Representative 2nd expanded leaves of diseased seedlings of each treatment. **(B)** Average disease index (DI) for each treatment. **(C)** ABA, ACC, JA, and SA contents for the control, 500, and 1500 µM MT treatments. Effects of MT were significantly dose dependent. At least three repeats were performed for each sample, and the values presented are the means ± SE. Letters indicate significant difference and statistical analysis was performed by one-way ANOVA, $p < 0.05$.

10.3389/fpls.2023.1126669

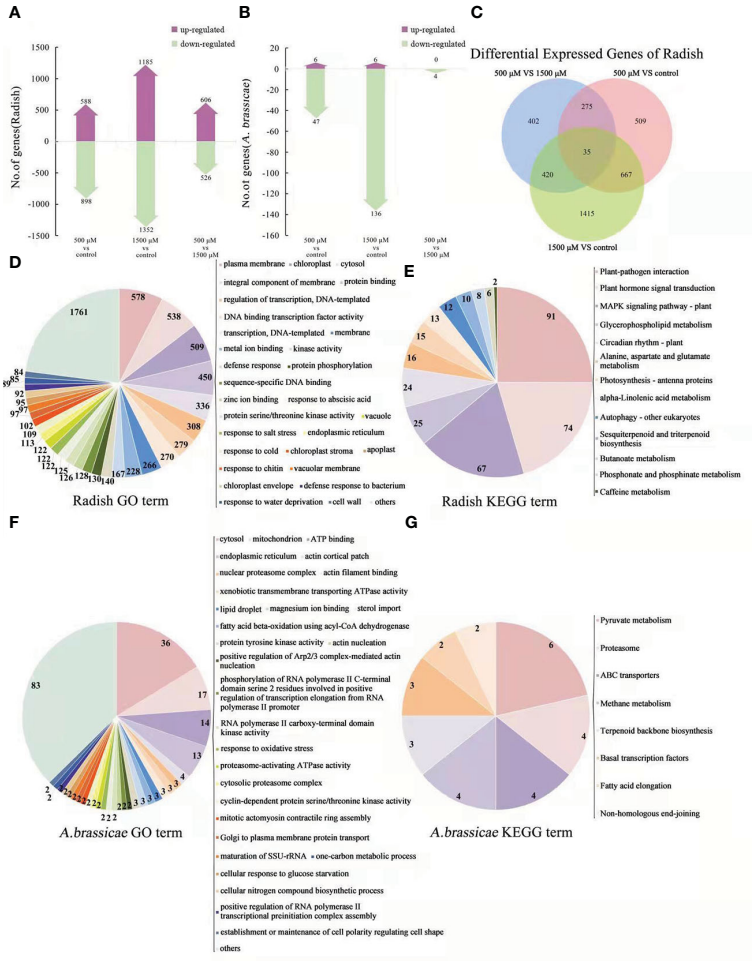

FIGURE 6
Analysis and functional categories of DEGs of radish "JNYB" and *A brassicae* from 0, 500, and 1500 μM MT treated diseased radish leaves. **(A)** and **(B)**: Number of genes up- and down-regulated of contrast sets of 500 μM MT treated group *VS* control, 1500 μM MT treated group *VS* control, and 1500 μM MT *VS* 500 μM MT treated group of radish and *A brassicae*. **(C)** Overlapping gene analysis of radish DEGs. **(D, E)**: Main functions of radish "JNYB" DEGs annotated by GO classification and KEGG pathway analysis. **(F, G)**: Main functions of DEGs of *A brassicae* annotated by GO classification and KEGG pathway analysis.

rhythm; alanine, aspartate, and glutamate metabolism; photosynthesis-antenna proteins, alpha-linolenic acid metabolism; autophagy; sesquiterpenoid and triterpenoid biosynthesis; butanoate metabolism; phosphonate and phosphinate metabolism; and caffeine metabolism. For *A. brassicae*, GO analysis classified the DEGs into categories of cytosol, mitochondria, ATP binding, endoplasmic reticulum, actin cortical patch and filament binding, nuclear proteasome, ATPase activity, kinase activity, sterol import, response to oxidative stress, cellular nitrogen compound biosynthetic process, and establishment or maintenance of cell polarity regulating cell shape (Figure 6F). Eight categories were classified by KEGG pathway analysis: pyruvate metabolism, proteasome, ABC transporter, methane metabolism, terpenoid backbone biosynthesis, basal transcription factors, fatty acid elongation, and non-homologous end-joining (Figure 6G). The top 10 differentially regulated GO classifications and KEGG enrichment categories of contrast sets of 500 μM MT treatment *VS* control, 1500 μM MT treatment *VS* control, 1500 μM *VS* 500 μM MT treatment, and 0 μM *VS* 500 μM *VS* 1500 μM MT treatment for radish or *A. brassicae* are presented in Table S5.

To confirm the results from the dual RNA-seq analysis, 19 DEGs from "JNYB" radish and 6 DEGs from *A. brassicae* were selected, and their expression levels were assessed by qRT-PCR analysis. The selected genes are involved in plant growth and biotic stress resistance regulation in plant or cell proliferation, development, and virulence in fungi according to gene description, GO term, and KEGG pathway data, the information and primer sequences of selected genes are listed in Table S2. The qRT-PCR results showed that the transcription levels of these genes were stimulated by exogenous melatonin treatment and were generally consistent with the RNA-seq results, although the fold changes of most genes were greater in RNA-seq data than in qRT-PCR data. In radish, *IGO1*, *DCP*, *EUP* and *IGO2* exhibited the highest expression in control, were down-regulated by MT, and increased again as the concentration elevated to 1500 μM. *PIR*, *ERT*, *DLP*, *PPL*, *TTS*, *PRL*, *KDA*, *RPS*, *PCC*, *CAB1*, and *CAB2* were

expressed significantly higher in 500 μM MT treated samples compared with other two groups. *ET1*, *SSC1*, *SSC2*, and *L3C* were expressed highest in 1500 μM MT treated samples. In *A. brassicae*, *MD2* and *CPX* were most highly expressed in untreated samples, but 500 μM MT increased the expression of *CDP*, *ICM*, *GGT*, and *TDC*. There were no DEGs identified for 500 μM *VS* 1500 μM MT, so we did not conduct qRT-PCR verification on up-regulated genes for 1500 μM MT treated samples (Figure 7).

4 Discussion

4.1 MT affects radish growth and immunity in a dose-dependent manner

Plants can be strongly affected by biotic stressors through the life cycle. To combat pathogens, plants adopt different physiological strategies including MT, which functions as a first-line defense against stresses (Tan et al., 2007), to enhance plant growth, immunity, and alter physiological functions (Ali et al., 2021; Guo et al., 2022). The effects of MT on living being growth, development, and immunity are dosage dependent (Jin et al., 2013), and MT concentration outside a certain range can be ineffective or inhibitory. For example, exogenous application of MT with 10-60 μM in rice (*Oryza sativa*) and maize (*Zea mays*) plants increased their tolerance to salt stress or semi-arid stress, whereas higher concentrations attenuated the promoting effect and even had inhibitory impacts (Liang et al., 2015; Ahmad et al., 2020). Similar situation of exogenous MT was observed on the elongation of *Arabidopsis thaliana* hypocotyl (Ren et al., 2019) and plant endogenous ATP biosynthesis (Acuna-Castroviejo et al., 2007). In our study, 50-500 μM of MT enhanced "JNYB" seedling growth and immunity to *A. brassicae*, but 1000-1500 μM of MT attenuated that promotion, generally, 500 μM was the optimal concentration (Figures 1A–C, S1, S2).

We observed that 500 μM MT resulted in thicker cell wall and more mitochondria (Figures 1D, S2). The cell wall serves as a primary, formidable, and dynamic barrier to protect plant cells form pathogens, it's integrity is tightly linked to innate immunity (Malinovsky et al., 2014). Once pathogens enter cells, mitochondria are critical to stimulate the innate immune signaling cascade, since they are the major resource of ROS (Chen et al., 2017), pathogens usually suppresses plant innate immunity by disrupting mitochondrial functions (Block et al., 2010). A number of studies have shown the protective and strengthening effects of appropriate concentration of MT on cell wall and plant mitochondria under unfavorable environments (Cao et al., 2018), which is consistent with the results of this study. Here, lower concentration (50-500 μM) of MT significantly elevated the activities of antioxidant enzymes and decreased peroxidation (Figure 1D). Additionally, MT in this concentration range promoted chlorophyll biosynthesis and chloroplast function and the accumulation of photosynthetic products (Figures 1F, S2, S3). Higher MT offset these effects. Photosynthetic efficiency and redox level are important indexes of plant stress resistance (Chen et al., 2014; Fan et al., 2015; Hu et al., 2016). These effects of MT to improve the activity of the photosynthetic system and chlorophyll fluorescence and to induce the activity of antioxidant enzymes comprehensively stimulate plant stress resistance (Arnao and Hernández-Ruiz, 2015; Nawaz et al., 2018). In addition, MT stimulated the biosynthesis of

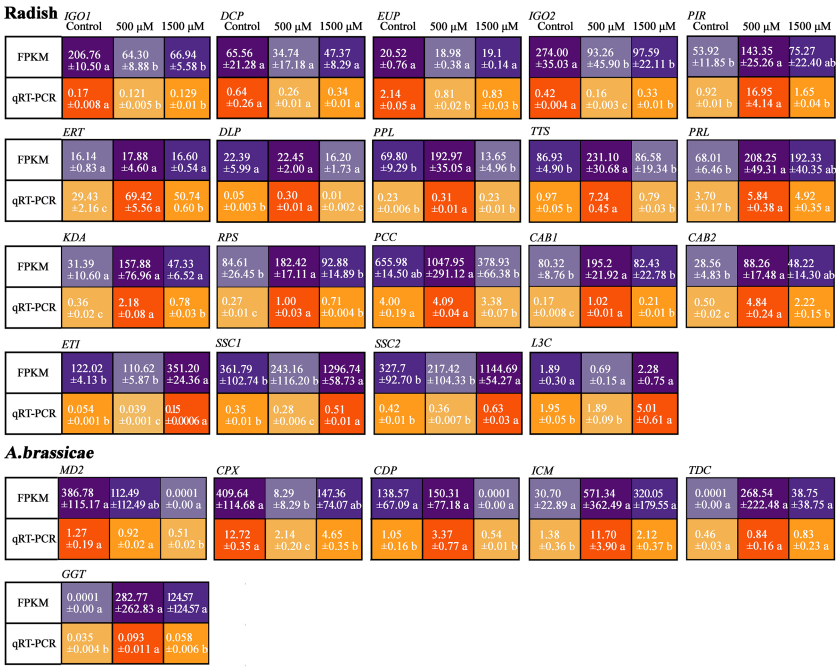

FIGURE 7
Verification of selected DEGs of "JNYB" radish and *A. brassicae* from dual RNA-seq using qRT-PCR. The relative expression level of a gene in was determined using a $2^{-\triangle\triangle}$Ct method, and significant difference at $P < 0.05$ compared with the control is indicated by lowercase letter.

phytohormones, such as ETH, SA, and JA, which play important roles in plant growth and innate immunity (Li et al., 2016), and decreased the ABA content, which negatively regulates plant anti-fading in this study (Figure 1E). By rapidly decreasing the ABA content, exogenous MT alleviated salinity stress resistance of cucumber (*Cucumis sativus*) and cotton seeds during the early stage of germination (Zhang et al., 2014; Li et al., 2019). Biosynthesis and maintenance of ETH, SA, and JA are significantly affected by MT, so MT can improve disease resistance of *Areca catechu* against pathogens (Yin et al., 2020). At the physiological level, 500 μM MT significantly strengthened the structure and function of organelles, biosynthesis of photosynthetic products, antioxidant enzymes and phytohormones, while 1500 μM MT set-off those effects (except for phytohormones). The dose-dependent manner of MT were consistent for effects on radish seedling growth and for effects on immunity promotion (Figures 1, S1–S3).

MT broadly altered gene expression and a significant dose-effect of MT on the transcriptional pattern of radish genome was identified. Greater number of DEGs were identified in the 1500 μM MT treated radish than in the 500 μM MT treated group (Figure 2A). Uniquely expressed DEGs were mostly detected in 1500 μM MT group compared to the 500 μM MT treated counterpart (Figure 2B). Interestingly, the effects of 1500 μM MT on radish morphology and physiology were weaker than that of 500 μM MT (Figure 1), suggesting constraints on gene expression changes for the 1500 μM MT treated samples, the mechanism is under reveal. The dose-dependence effect of MT have rarely been reported for plant global transcription.

Regardless of MT concentration, DEGs were enriched in cell components, crucial molecular functions, stress response, and growth regulation by GO term analysis (Figure 2C). The identified DEGs and related processes are consistent with our observations of physiological changes as well as reports of MT-mediated senescence delay and salt stress tolerance of rice (Liang et al., 2015) and MT-enhanced disease resistance in grapefruit (*Vitis vinifera*) (Gao et al., 2020). According to KEGG analysis, many DEGs were enriched in categories of metabolism, biosynthesis, and degradation of secondary substances. Transcription of many genes related to plant hormone signal transduction changed in response to MT (Figure 2D), which is consistent with the observed effect of exogenous MT to stimulate phytohormone content (Figure 1I). Our results are supported by previous studies on grapefruit (Ma et al., 2021), gardenia (*Gardenia jasminoides*) (Zhao et al., 2017), and cotton (Chen et al., 2021). MT has been reported to stimulate plant growth itself by regulating biosynthesis of various growth regulator. For example, the MAPK pathway responds to various biotic and abiotic stresses as an integral component of cellular signaling (Atkins et al., 1998), and significant MT regulation of this signaling pathway was observed here. Circadian rhythm adjustment in animals and plants is the most important function of exogenous MT, allowing regulation of immune responses and inflammation in animals (Caniato et al., 2003; Pham et al., 2021). Transcriptome analysis revealed that circadian rhythms are linked to plant phytoplasma defense (Fan et al., 2015), but there have been limited studies investigating the mechanisms through which MT regulates plant immunity and stress tolerance through circadian rhythm regulation. Plant peroxisomes are involved in diverse functions, including primary and secondary metabolism, development, abiotic stress response, and pathogen defense, the peroxisome proliferator-activated receptor (PPAR) is involved in MT regulation of animal diseases (Qi and Wang, 2020), but there have been few studies on plants. MT promotes mitochondrial biogenesis in animal cells *via* PPAR (Kato et al., 2015; Qi and Wang, 2020), and a similar effect was seen for the 500 μM MT treated samples, suggesting an involvement of the peroxisome pathway. ABC transporters in plants are involved in detoxification, organ growth, nutrition metabolism, plant development, response to abiotic stress, and plant interactions with the environment (Kang et al., 2010), and our result indicates that ABC transporters may also play an important role in exogenous MT-mediated immunity improvement of radish. Transcriptional changes were detected in genes enriched in pathways of carbon fixation in photosynthetic organisms, and a function of plant growth regulation and biomass accumulation of exogenous MT was previously reported as describe above (Figures 2C, D).

We confirmed the FPKM data of some key DEGs by qRT-PCR (Figure 2E). Thiamine thiazole synthase is responsible for thiamine biosynthesis, which is only synthesized in plants but is required for growth and development of all living beings (Li et al., 2016; Feng et al., 2019). Interesting, exogenous MT decreased the expression of genes related to thiamine biosynthesis (*TTS* and *TTS-like 2*) regardless of dose, suggesting that this pathway may not be required for MT-mediated process. This was also observed for *GLP 1*, which mediates stress resistance by hyper-accumulation of H_2O_2 (Banerjee et al., 2010), while MT reacts as an antioxidant (Nazarian and Ghanati, 2020), and may also suppress the expression of *GLP1*. The transcription analysis revealed MT dose-dependent effects on the expression of genes, which were *ERF3-like*, *LOX3*, *DEF1*, *BTP-like*, *MYB51-Like* and *UMP*, involved in JA and ETH-dependent systemic resistance, linoleic acid metabolism, response to auxin, response to salicylic acid, transcription regulation, response to ABA, fungus defense response, and response to stress (Figure 2E and Table S2). These changes are consistent with broad effects on radish gene expression to improve radish resistance to *A. brassicae*. *MYC2*, *COP1- X1*, *ERF1B-like*, *FBA 1*, and *CPC 1-like* synthesis were gradually enhanced as the concentration of MT increased. These genes are closely related to pathways of plant hormone signal transduction, carbohydrate metabolism, and plant circadian rhythm, so the lower expression of these genes may promote radish growth and immunity and excessive expression may lead to negative effects (Figure 2E and Table S2).

4.2 MT affects *A. brassicae* growth, reproduction, and virulence in a dose-dependent manner

MT's protective function against pathogen infection has been reported for many plants (Lee and Back, 2016; Mandal et al., 2018;

Liu et al., 2019). MT is amphiphilic and can penetrate the cell membrane and reach organelles of various living organisms (Asghari et al., 2017), so the effects of MT on pathogen physiology may be complex. Several studies have verified the function of MT as a pathogen inhibitor (Zhang et al., 2017; Ali et al., 2021), but it showed no effect on *Verticillium dahliae* (Li et al., 2019) and promoted growth of *Rhizophagus intraradices* (Yang et al., 2020). Our results demonstrated that MT influences *A. brassicae* colony growth, mycelium prolongation, conidia germination and pathogenesis *in vitro* in a dose-dependent manner (Figure 3). MT at 50-500 μM increased mycelium growth, conidia germination and virulence of colonies compared with that of control, where 500 μM MT showed the best effect, with lesser promotion or inbition seen for 1000-1500 μM MT (Figures 3A–D). Interestingly, dose-dependent effect of MT was not found on conidia formation, condensed MT solution promoted the germination of conidia chains, there were no significant differences found among 500-1500 μM treated colonies (Figures 3A, B). The dose-dependent effect MT was also observed for activities of GT and PCWDEs, key enzymes in survival and virulence regulating of pathogens (Koiv, 2001; Kim et al., 2002; Nath and Ghosh, 2005; Sjöblom et al., 2006). The enhancement of GT and PCWDEs activities may explain the strong virulence of 500 μM MT treated colonies (Figures 3E, F). Lower concentration of MT inhibited activities of GSH-Px and CAT, important antioxidant enzymes that protect cells from ROS, and 1500 μM MT offset this inhibition (Figures 3G, H). Previous studies verified that MT applied at the proper dose promoted the activities of antioxidant enzymes in animals and plants under various stresses (Chabra et al., 2014; Ali et al., 2021), however functions of MT may vary by conditions. With maternal undernutrition, MT induced CAT activity and alleviated oxidative stress, but these effects were not observed under hypoxic conditions (Richter et al., 2008). In another example, the oxidative stress alleviation function of MT was dependent on gender (Lamtai et al., 2021). In this study, colonies of *A. brassicae* were incubated in an environment without stress, and we speculate that the 50-1000 μM MT treatment may have acted as a direct antioxidant agent against ROS without inducing antioxidant enzymes as it can penetrate the cell membrane and reach organelles (Asghari et al., 2017). A higher dose may result in oxidative stress, which could trigger biosynthesis of CAT and GSH-Px. The effects of MT on *A. brassicae* growth, development and physiology indicate complex biological relationships.

In the 500 μM MT treated *A. brassicae* colonies, there were 525 up-regulated and 577 down-regulated genes. This was more than the numbers for the 1500 μM MT treatment. There were more up- and down-regulated DEGs of 1500 μM *VS* 500 μM contrast group compared to the 500 μM *VS* control and/or 1500 μM *VS* control (Figure 4A). Analysis of the 500 μM and 1500 μM MT treatments resulted in only 28 DEGs with similar functions, with more unigenes in the 500 μM MT treated samples (Figure 4B). This result indicates a significant dose-effect of MT on the transcriptional pattern of *A. brassicae*.

Functional patterns of MT included redox reactions, cell composition, and key molecular functions as identified by GO term analysis (Figure 4C). The importance of oxidation-reduction and membrane integrity protection has been previously described (Reiter et al., 2014). In addition to metabolism, biosynthesis, and degradation of secondary substances, *A. brassicae* genes related to peroxisome and ABC transporters were significantly affected by exogenous MT as identified by KEGG pathway analysis (Figure 4D). These results are consistent with the results for MT-treated radish seedlings, indicating an important relationship between MT, peroxisome and ABC transporters in growth and development regulation among different living beings. The transcriptional level of genes enriched in ribosome pathways was highly influenced by MT *in vitro*. Exogenous MT promoted mycelium growth and development, suggesting that protein biosynthesis may play a key role in *A. brassicae* proliferation mediated by exogenous MT.

The FPKM data of some key DEGs was confirmed by qRT-PCR (Figure 4E). The role of thioredoxin in microbes are complicate, it's positive response to oxidative stress, abiotic stress, and virulence response in *Alternaria* is well studied (Ma et al., 2018), while for *Escherichia coli*, chaperone and ATPase activities of the GroESL chaperonin complex are inhibited by thioredoxin-like protein YbbN, which caused negative effects on *E. coli* vitality (Lin and Wilson, 2011). In this study, 500 μM MT suppressed *TLP* expression and increased *A. brassicae* vitality (Figure 4E). The complex relationships among *TLP*, MT, and *A. brassicae* physiology remain unclear and require further investigation. RNA-Seq and qRT-PCR revealed dose-dependent expression of genes related to oxidoreductase activity, ribosome, translation, plasma membrane organization, pathogenesis, oxidoreductase activity, tryptophan metabolism, carbohydrate metabolism, and tyrosine metabolism (Figure 4E and Table S2). These genes (*ADD*, *MUP*, *FAD*, *CTP2*, *MSG*, *ISP*, *SFP-like*, *MMI*, *CAT-like*, *GES-like*, *CTP1* and *KLP*) were consistent with the phenotype of MT-treated colonies determined previously, indicating the positive roles of these genes in 500 μM MT mediated enhancement of *A. brassicae* proliferation and virulence. *HAG* was expressed at higher levels as exogenous MT condensed, while *GST* was expressed lowest in the 500 μM MT treated sample, and higher in the control and 1500 μM groups (Figure 4E). *HAG* may positively regulate carbohydrate accumulation and increase *A. brassicae* proliferation according to its function annotation (Table S2), but excessive expression may have a negative effect, while *GST* may function as a negative regulator according to our results, further studies are needed.

4.3 MT affects *A. brassicae* resistance of radish "JNYB" in a dose-dependent manner

Our results demonstrated that application of exogenous MT exhibited a protective function against *A. brassicae* infection in radish plants at all concentrations. While plants in the 500 μM MT subgroup showed the greatest decline in disease, higher concentrations attenuated this effect, but protection from *A. brassicae* was still observed. The lesioned areas and disease index were reduced

(Figures 5A, B). Additionally, 500 μM MT treatment promoted the biosynthesis of ETH, JA, and SA, and decreased the level of ABA compared to healthy seedlings (Figure 5C). MT exhibits dose-dependent effects on pathogen defense in both animals and plants (Zhao et al., 2019; Ali et al., 2021). In plants, the melatonin biosynthetic enzyme N-acetylserotonin O-methyltransferase 2 physically interacts with anti-bacterial pathogenesis related (PR) protein to promote defense activity (Guo et al., 2022). Previous reports conformed that 100 μM MT induced *Nicotiana glutinosa* resistance to tobacco mosaic virus (TMV) infections by accumulation of SA and nitric oxide (NO) and increased expression of defense-related genes *PR1* and *PR5* (Zhao et al., 2019), and induced *Capsicum annuum* resistance to *Colletotrichum gloeosporioides* by increasing the efficiency of *CaChiIII2* and *PR1* and *PO1* (Ali et al., 2021), with weaker effects for higher concentrations of MT.

Dual-RNA Seq was conducted to analyze host and pathogen interaction at the transcriptional level. Treatment with 500 μM MT significantly increased the vitality and resistance or virulence of both host and pathogen, but this effect was seriously weakened at 1500 μM MT. Given the individual effects of MT on both the host and the pathogen, we investigated if the same dose-dependent mode would be observed for MT-mediated resistance to black spot disease on radish. In diseased seedlings, 1500 μM MT resulted in 2537 DEGs compared to 1468 DEGs for the 500 μM treatment (Figure 6A). The effects of 1500 μM MT on radish defense were weaker than that of 500 μM MT (Figures 5A, B). The effect of MT on expression pattern of diseased radish genes was normalized to that of healthy radish (Figure 2A), however, fewer DEGs were detected in the contrast of 1500 μM *VS* 500 μM relative to the other two pairwise comparisons (Figure 6A). Various concentrations of MT resulted in differential gene expression modes, only 35 same DEGs were found in all comparisons, fewer unigenes (509 DEGs) were detected in 500 μM and 1500 μM MT treated samples with more uniquely expressed genes (1415 DEGs) (Figure 6C). GO analysis of diseased radish samples at all MT concentrations revealed changes in genes related to cell component, crucial molecular functions, and response to stress (Figure 6D). According to KEGG pathway analysis of diseased radish samples, MT treatment caused changes in genes involved in plant hormone signal transduction, MAPK signaling pathway, metabolism and biosynthesis of secondary substances, and photosynthesis. In addition to these genes, MT regulated genes involved in plant-pathogen interaction and autophagy in diseased seedlings.

The application of MT suppressed the expression of *IGO1*, *DCP*, *EUP* and *IGO2*. GO term and KEGG pathway analysis of these genes suggested MT may restrain methylation and RNA degradation and adjust light perception in radish (Figure 7A and Table S2). Transcriptional analysis revealed positive response to 500 μM MT for key genes (*PIR*, *ERT*, *DLP*, *PPL*, *TTS*, *PRL*, *KDA*, *RPS*, *PCC*, *CAB1* and *CAB2*) related to DNA methylation, ethylene mediated (positive or negative) defense response, MAPK signal-related defense response, cell wall function, thiamine metabolism, ribosome biogenesis, lipid metabolism, plasma membrane function, oxidation-reduction process, chloroplast function, and photosynthesis (Table S2); these genes exhibited a dose-dependent pattern, 0 and 1500 μM MT down regulated their express (Figure 7A). Condensed MT did not inhibit the expression of plant senescence, lipid oxidation, and host programmed cell death-related genes (*ETI*, *SSC1*, *SSC2* and *L3C)* (Figure 7A and Table S2), in this study, we further verified that excessive MT hinders living being development and stress resistance (Liang et al., 2019; Pliss et al., 2019).

Different patterns of MT effects on *A. brassicae* transcription were observed *in vitro* and *in vivo*. In radish-loading *A. brassicae*, many genes were down-regulated by MT application, and there were only 4 DEGs identified in the 1500 μM *VS* 500 μM contrast, indicating very weak dose-dependence (Figure 6B). There were significantly fewer DEGs enriched to diverse GO terms, and very limited DEGs were identified by KEGG pathway analysis compared with what was identified using *in vitro* tests (Figures 6E, G). This result emphasized the small biomass of *A. brassicae* on diseased leaves. Since the relative contact area and relative perceiving quantity of *A. brassicae* on leaves to exogenous MT was significantly decreased compared to that of *in vitro* incubated colonies, which may explain the varied effect of MT on *A. brassicae*.

The expression of two genes, *MD2* and *CPX*, which regulates oxidation and peroxidation reaction (Tabuchi et al., 1981), were inhibited by MT at all concentrations, demonstrating its reductive effect on microorganisms. *CDP*, *ICM*, *TDC* and *GGT*, which regulate transmembrane transport, calcium-dependent phospholipid binding, glucose/galactose transport, transcription regulation, and glutathione metabolism (Table S2) were enhanced in response to 500 μM MT in *in vivo* experiments. Among 6 MT induced up-regulated genes of *A. brassicae*, two of them shared opposite results of FPKM value and qRT-PCR data, thus their function in the present study cannot be concluded.

In this study, techniques of plant physiology and transcriptomic studies were applied to healthy radish plants, *in vitro* incubated *A. brassicae*, and radish plants infected with black spot disease respectively to reveal how MT participates in the interaction between radish and *A. brassicae*. Transcriptomics revealed many important biological pathways and genes related to plant immunity, pathogen toxicity and host resistance, as well as their expression changes under different conditions. These results have important value in the breeding of disease-resistant *Cruciferous* crops, improving crop quality and reducing the cost of disease control on crop production. However, the expression of these genes was simply verified by RT-qPCR, which is obviously insufficient for revealing the functions of important pathways and genes and molecular assisted breeding. In the future research, more complex verification methods will be used to study the function and action pathway of those important genes.

4.4 Conclusion

Our results provide insight into the mechanism underlying the effects of MT on radish and *A. brassicae*, expanding our understanding of the relationships among MT, host, and pathogen. An appropriate concentration of MT (500 μM)

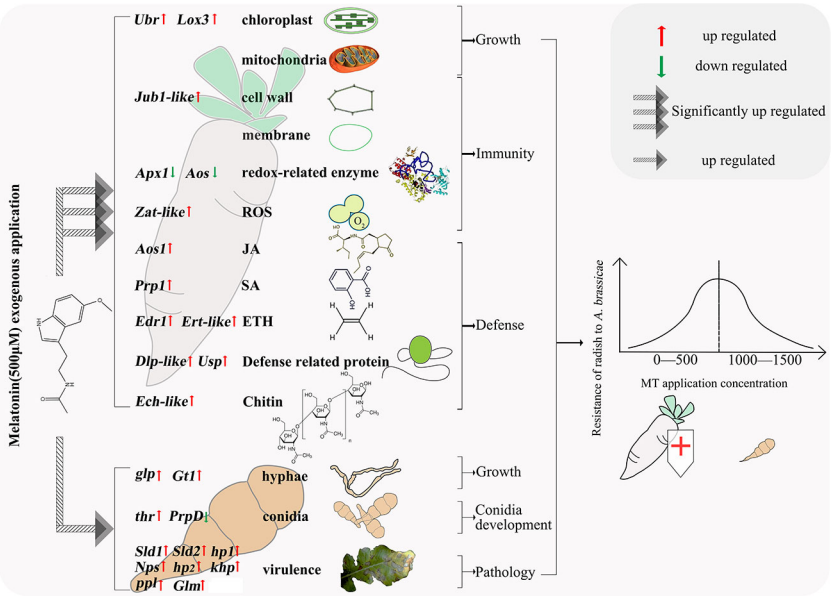

FIGURE 8
Molecular mechanisms of radish resistance to *A. brassicae* affected by exogenous MT.

significantly enhanced radish growth, immunity, and biotic stress defense by reinforcing carbon fixation of chloroplasts, energy metabolism of mitochondria, cell wall and membrane strength, activities of redox-related enzymes, biosynthesis of phytohormones, defense-related proteins and chitin, and decreasing ROS. MT also strengthened mycelium growth, conidia development, and pathology of *A. brassicae in vitro*. We speculate that, with a greater impact of MT on radish than on *A. brassicae*, the resistance of radish to *A. brassicae* therefore increased. Exogenous MT application exhibited a dose-dependent effect, where lower concentration (50-500 μM) improves radish defense and higher concentration (1500 μM) inhibits defense (Figure 8). The findings of this study will facilitate exploration of MT-based approaches to *Alternaria* blight disease control in radish and other *Brassicaceae* plants.

Data availability statement

The datasets presented in this study can be found in online repositories. The names of the repository/repositories and accession number(s) can be found in the article/Supplementary Material.

Author contributions

JWL designed the experiments and edited manuscript, TMH, JBL, MX and HYL performed experiments and analyzed data. WPZ and XHX edited manuscript. All authors contributed to the article and approved the submitted version.

Funding

This study was financially supported by the Guizhou Science and Technology Planning Project (Qiankehe basic-ZK [2021] Normal 153), the Introduction of Talents and Scientific Research Project of Guizhou University (Guidarenjihezi (2019) No. 69), The Cultivation Project of Guizhou University (Guidapeiyu (2019) No. 41).

Conflict of interest

The authors declare that the research was conducted in the absence of any commercial or financial relationships that could be construed as a potential conflict of interest.

Publisher's note

Supplementary material

The Supplementary Material for this article can be found online at: https://www.frontiersin.org/articles/10.3389/fpls.2023.1126669/full#supplementary-material

References

Acuna-Castroviejo, D., Escames, G., Rodriguez, M. I., and Lopez, L. C. (2007). Melatonin role in the mitochondrial function. *Front. Biosci-Landmrk.* 12, 947–963. doi: 10.2741/2116

Ahmad, S., Su, W., Kamran, M., Ahmad, I., Meng, X., Wu, X., et al. (2020). Foliar application of melatonin delay leaf senescence in maize by improving the antioxidant defense system and enhancing photosynthetic capacity under semi-arid regions. *Protoplasma* 257, 1079–1092. doi: 10.1007/s00709-020-01491-3

Ali, M., Kamran, M., Abbasi, G. H., Saleem, M. H., Ahmad, S., Parveen, A., et al. (2021). Melatonin-induced salinity tolerance by ameliorating osmotic and oxidative stress in the seedlings of two tomato (*Solanum lycopersicum* l.) cultivars. *J. Plant Growth Regul.* 40, 2236–2248. doi: 10.1007/s00344-020-10273-3

Arendt, J. (2005). Melatonin: characteristics, concerns, and prospects. *J. Biol. Rhythms.* 20, 291–303. doi: 10.1177/0748730405277492

Arnao, M. B., and Hernández-Ruiz, J. (2015). Functions of melatonin in plants: A review. *J. Pineal Res.* 59, 133–150. doi: 10.1111/jpi.12253

Asghari, M. H., Abdollahi, M., de Oliveira, M. R., and Nabavi, S. M. (2017). A review of the protective role of melatonin during phosphine-induced cardiotoxicity: focus on mitochondrial dysfunction, oxidative stress and apoptosis. *J. Pharm. Pharmaco.* 69, 236–243. doi: 10.1111/jphp.12682

Atkins, C. M., Selcher, J. C., Petraitis, J. J., Trzaskos, J. M., and Sweatt, J. D. (1998). The MAPK cascade is required for mammalian associative learning. *Nat. Neurosci.* 1, 602–609. doi: 10.1038/2836

Banerjee, J., Das, N., Dey, P., and Maiti, M. K. (2010). Transgenically expressed rice germin-like protein1 in tobacco causes hyper-accumulation of H_2O_2 and reinforcement of the cell wall components. *Biochem. Biophys. Res. Commun.* 402, 637–643. doi: 10.1016/j.bbrc.2010.10.073

Basma, A. A., Zuraini, Z., and Sasidharan, S. (2011). A transmission electron microscopy study of the diversity of *Candida albicans* cells induced by *Euphorbia hirta l.* leaf extract *in vitro*. *Asian Pac J. Trop. Biomed.* 1, 20–22. doi: 10.1016/S2221-1691(11)60062-2

Block, A., Guo, M., Li, G., Elowsky, C., Clemente, T. E., and Alfano, J. R. (2010). The *Pseudomonas syringae* type III effector HopG1 targets mitochondria, alters plant development and suppresses plant innate immunity. *Cell Microbiol.* 12, 318–330. doi: 10.1111/j.1462-5822.2009.01396.x

Caniato, R., Filippini, R., Piovan, A., Puricelli, L., Borsarini, A., and Cappelletti, E. M. (2003). Melatonin in plants. *Developments Tryptophan Serotonin Metab.* 527, 593–597. doi: 10.1007/978-1-4615-0135-0_68

Cao, S., Bian, K., Shi, L., Chung, H. H., and Yang, Z. (2018). Role of melatonin in cell-wall disassembly and chilling tolerance in cold-stored peach fruit. *J. Agri Food Chem.* 66, 5663–5670. doi: 10.1021/acs.jafc.8b02055

Chabra, A., Shokrzadeh, M., Naghshvar, F., Salehi, F., and Ahmadi, A. (2014). Melatonin ameliorates oxidative stress and reproductive toxicity induced by cyclophosphamide in male mice. *Hum. Exp. Toxicol.* 33, 185–195. doi: 10.1177/0960327113489052

Chen, X., Cao, Z., Zhang, Y., Jinnong, L., Wang, S., Du, J., et al. (2017). Fuzheng qingjie granules inhibit growth of hepatoma cells *via* inducing mitochondria-mediated apoptosis and enhancing immune function. *Integr. Cancer Ther.* 16, 329–338. doi: 10.1177/1534735416654761

Chen, L., Lu, B., Liu, L., Duan, W., Jiang, D., Li, J., et al. (2021). Melatonin promotes seed germination under salt stress by regulating ABA and GA3 in cotton (*Gossypium hirsutum* l.). *Plant Physiol. Biochem.* 162, 506–516. doi: 10.1016/J.PLAPHY.2021.03.029

Chen, L. J., Xiang, H. Z., Miao, Y., Zhang, L., Guo, Z. F., Zhao, X. H., et al. (2014). An overview of cold resistance in plants. *J. Agron. Crop Sci.* 200, 237–245. doi: 10.1111/jac.12082

Chen, Y., Zhao, Q., Sun, Y., Jin, Y., Zhang, J., and Wu, J. (2018). Melatonin induces anti-inflammatory effects *via* endoplasmic reticulum stress in RAW264. 7 macrophage. *Mol. Med. Rep.* 17, 6122–6129. doi: 10.3892/mmr.2018.8613

Dixit, S., Jangid, V. K., and Grover, A. (2020). Evaluation of physiological and molecular effect of variable virulence of *Alternaria brassicae* isolates in *Brassica juncea, sinapis alba* and *Camelina sativa*. *Plant Physiol. Biochem.* 155, 626–636. doi: 10.1016/j.plaphy.2020.08.025

Fan, G., Cao, X., Zhao, Z., and Deng, M. (2015). Transcriptome analysis of the genes related to the morphological changes of *Paulownia tomentosa* plantlets infected with phytoplasma. *Acta Physiol. Plant* 37, 1–12. doi: 10.1007/s11738-015-1948-y

Feng, X., Yang, S., Tang, K., Zhang, Y., Leng, J., Ma, J., et al. (2019). GmPGL1, a thiamine thiazole synthase, is required for the biosynthesis of thiamine in soybean. *Front. Plant Sci.* 10. doi: 10.3389/fpls.2019.01546

Gao, S., Ma, W., Lyu, X., Cao, X., and Yao, Y. (2020). Melatonin may increase disease resistance and flavonoid biosynthesis through effects on DNA methylation and gene expression in grape berries. *BMC Plant Biol.* 20, 1–15. doi: 10.1186/s12870-020-02445-w

Grima, N. A., Ponsford, J. L., St., Hilaire, M. A., Mansfield, D., and Rajaratnam, S. M. (2016). Circadian melatonin rhytham following traumatic brain injury. *Neurorehabil. Neural Repair* 30, 972–977. doi: 10.1177/1545968316650279

Guo, J., Bai, Y., Wei, Y., Dong, Y., Zeng, H., Reiter, R. J., et al. (2022). Fine-tuning of pathogenesis-related protein 1 (PR1) activity by the melatonin biosynthetic enzyme ASMT2 in defense response to cassava bacterial blight. *J. Pineal Res.* 72, e12784. doi: 10.1111/jpi.12784

Hardel, R. (2016). Melatonin: Another phytohormone. *Res. Rev J. Bot. Sci.* 2, 5. doi: 10.1111/j.1438-8677.1996.tb00560.x/abstract

Hu, H., He, X., Tu, L., Zhu, L., Zhu, S., Ge, Z., et al. (20162016). GhJAZ2 negatively regulates cotton fiber initiation by interacting with the R2R3-MYB transcription factor GhMYB25-like. *Plant J.* 88, 921–935. doi: 10.1111/tpj.1327

Jin, Y., Lin, C. J., Dong, L. M., Chen, M. J., Zhou, Q., and Wu, J. S. (2013). Clinical significance of melatonin concentrations in predicting the severity of acute pancreatitis. *World J. Gastroenterol.* 19, 4066. doi: 10.3748/wjg.v19.i25.4066

Kang, J., Hwang, J. U., Lee, M., Kim, Y. Y., Assmann, S. M., Martinoia, E., et al. (2010). PDR-type ABC transporter mediates cellular uptake of the phytohormone abscisic acid. *Proc. Natl. Acad. Sci.* 107, 2355–2360. doi: 10.1073/pnas.0909222107

Kato, H., Tanaka, G., Masuda, S., Ogasawara, J., Sakurai, T., Kizaki, T., et al. (2015). Melatonin promotes adipogenesis and mitochondrial biogenesis in 3T3-L1 preadipocytes. *J. Pineal Res.* 59, 267–275. doi: 10.1111/jpi.12259

Kim, Y. K., Wang, Y., Liu, Z. M., and Kolattukudy, P. E. (2002). Identification of a hard surface contact-induced gene in *Colletotrichum gloeosporioides* conidia as a sterol glycosyl transferase, a novel fungal virulence factor. *Plant J.* 30, 177–187. doi: 10.1046/j.1365-313X.2002.01284.x

Koiv, V. (2001). Quorum sensing controls the synthesis of virulence factors by modulating rsmA gene expression in erwinia *carotovora* subsp. *carotovora*. *Mol. Genet. Genom.* 265, 287–292. doi: 10.1007/s004380000413

Lamtai, M., Azirar, S., Zghari, O., Ouakki, S., El Hessni, A., Mesfioui, A., et al. (2021). Melatonin ameliorates cadmium-induced affective and cognitive impairments and hippocampal oxidative stress in rat. *Biol. Trace Elem Res.* 199, 1445–1455. doi: 10.1007/s12011-020-02247-z

Lee, H. Y., and Back, K. (2016). Mitogen-activated protein kinase pathways are required for melatonin-mediated defense responses in plants. *J. Pineal Res.* 60, 327–335. doi: 10.1111/jpi.12314

Lee, H. B., Patriarca, A., and Magan, N. (2015). *Alternaria* in food: Ecophysiology, mycotoxin production and toxicology. *Mycobiology* 43, 93–106. doi: 10.5941/myco.2015.43.2.93

Lerner, A. B., Case, J. D., Takahashi, Y., Lee, T. H., and Mori, W. (1958). Isolation of melatonin, the pineal gland factor that lightens melanocyteS1. *J. Am. Chem. Soc* 80, 2587–2587. doi: 10.1021/ja01543a060

Li, H., He, J., Yang, X., Li, X., Luo, D., Wei, C., et al. (2016). Glutathione-dependent induction of local and systemic defense against oxidative stress by exogenous melatonin in cucumber (*Cucumis sativus l.*). *J. Pineal Res.* 60, 206–216. doi: 10.1111/jpi.12304

Li, C., He, Q., Zhang, F., Yu, J., Li, C., Zhao, T., et al. (2019). Melatonin enhances cotton immunity to *Verticillium* wilt *via* manipulating lignin and gossypol biosynthesis. *Plant J.* 100, 784–800. doi: 10.1111/tpj.14477

Liang, D., Ni, Z., Xia, H., Xie, Y., Lv, X. L., Wang, J., et al. (2019). Exogenous melatonin promotes biomass accumulation and photosynthesis of kiwifruit seedlings under drought stress. *Sci. Hortic.* 246, 34–43. doi: 10.1016/j.scienta.2018.10.058

Liang, C., Zheng, G., Li, W., Wang, Y., Hu, B., Wang, H., et al. (2015). Melatonin delays leaf senescence and enhances salt stress tolerance in rice. *J. Pineal Res.* 59, 91–101. doi: 10.1111/jpi.12243

Lin, J., and Wilson, M. A. (2011). Escherichia coli thioredoxin-like protein YbbN contains an atypical tetratricopeptide repeat motif and is a negative regulator of GroEL. *J. Biol. Chem.* 286, 19459–19469. doi: 10.1074/jbc.m111.238741

Liu, J., Yang, J., Zhang, H., Cong, L., Zhai, R., Yang, C., et al. (2019). Melatonin inhibits ethylene synthesis *via* nitric oxide regulation to delay postharvest senescence in pears. *J. Agric. Food Chem.* 67, 2279–2288. doi: 10.1021/acs.jafc.8b06580

Ma, H., Wang, M., Gai, Y., Fu, H., Zhang, B., Ruan, R., et al. (2018). Thioredoxin and glutaredoxin systems required for oxidative stress resistance, fungicide sensitivity, and virulence of *Alternaria alternata*. *Appl. Environ. Microbiol.* 84, e00086–e00018. doi: 10.1128/AEM.00086-18

Ma, W., Xu, L., Gao, S., Lyu, X., Cao, X., and Yao, Y. (2021). Melatonin alters the secondary metabolite profile of grape berry skin by promoting VvMYB14-mediated ethylene biosynthesis. *Hort Res.* 8, 43. doi: 10.1038/S41438-021-00478-2

Malinovsky, F. G., Fangel, J. U., and Willats, W. G. T. (2014). The role of the cell wall in plant immunity. *Front. Plant Sci.* 5. doi: 10.3389/fpls.2014.00178

Mandal, M. K., Suren, H., Ward, B., Boroujerdi, A., and Kousik, C. (2018). Differential roles of melatonin in plant-host resistance and pathogen suppression in cucurbits. *J. Pineal Res.* 65, e12505. doi: 10.1111/jpi.12505

Meena, M., Gupta, S. K., Swapnil, P., Zehra, A., Dubey, M. K., and Upadhyay, R. S. (2017). *Alternaria* toxins: potential virulence factors and genes related to pathogenesis. *Front. Microbiol.* 8. doi: 10.3389/fmicb.2017.01451

Moustafa-Farag, M., Elkelish, A., Dafea, M., Khan, M., Arnao, M. B., Abdelhamid, M. T., et al. (2020). Role of melatonin in plant tolerance to soil stressors: salinity, pH and heavy metals. *Molecules* 25, 5359. doi: 10.3390/molecules25225359

Nath, P., and Ghosh, J. (2005). Seasonal effects of melatonin on ovary and plasma gonadotropin and vitellogenin levels in intact and pinealectomized catfish, *Clarias batrachus (Linn)*. *Indian J. Exp. Biol.* 43, 224–232.

Nawaz, M. A., Jiao, Y., Chen, C., Shireen, F., Zheng, Z., Imtiaz, M., et al. (2018). Melatonin pretreatment improves vanadium stress tolerance of watermelon seedlings by reducing vanadium concentration in the leaves and regulating melatonin biosynthesis and antioxidant-related gene expression. *J. Plant Physiol.* 220, 115–127. doi: 10.1016/j.jplph.2017.11.003

Nazarian, M., and Ghanati, F. (2020). The role of melatonin in reinforcement of antioxidant system of rice plant (*Oryza sativa* l.) under arsenite toxicity? *Plant Physiol. Rep.* 25, 395–404. doi: 10.1007/s40502-020-00523-7

Pandi-Perumal, S. R., Srinivasan, V., Maestroni, G. J. M., Cardinali, D. P., Poeggeler, B., and Hardeland, R. (2006). Melatonin: Nature's most versatile biological signal? *FEBS J.* 273, 2813–2838. doi: 10.1111/ejb.2006.273.issue-13

Pham, L., Baiocchi, L., Kennedy, L., Sato, K., Meadows, V., Meng, F., et al. (2021). The interplay between mast cells, pineal gland, and circadian rhythm: Links between histamine, melatonin, and inflammatory mediators. *J. Pineal Res.* 70, e12699. doi: 10.1111/jpi.12699

Pliss, M. G., Kuzmenko, N. V., Rubanova, N. S., and Tsyrlin, V. A. (2019). Dose-dependent mechanisms of melatonin on the functioning of the cardiovascular system and on the behavior of normotensive rats of different ages. *Adv. Gerontol.* 9, 327–335. doi: 10.1134/S2079057019030111

Qi, X., and Wang, J. (2020). Melatonin improves mitochondrials biogenesis through the AMPK/PGC1α pathway to attenuate ischemia/reperfusion-induced myocardial damage. *Aging (Albany NY).* 12, 7299. doi: 10.18632/aging.103078

Qian, Y., Tan, D. X., Reiter, R. J., and Shi, H. (2015). Comparative metabolomic analysis highlights the involvement of sugars and glycerol in melatonin-mediated innate immunity against bacterial pathogen in *Arabidopsis*. *Sci. Rep.* 5, 1–11. doi: 10.1038/srep15815

Rashid, M. M., Hossain, I., and Khalequzzaman, K. M. (2011). Effect of weather factors on inoculum density and leaf spot development in radish seed crop infected with *Alternaria brassicae*. *Bull. Institute Trop. Agriculture Kyushu Univ.* 34, 43–47. doi: 10.11189/bita.34.43

Reiter, R. J., Tan, D. X., and Galano, A. (2014). Melatonin reduces lipid peroxidation and membrane viscosity. *Front. Physiol.* 5. doi: 10.3389/fphys.2014.00377

Ren, S., Rutto, L., and Katuuramu, D. (2019). Melatonin acts synergistically with auxin to promote lateral root development through fine tuning auxin transport in *Arabidopsis thaliana*. *PLoS One* 14, e0221687. doi: 10.1371/journal.pone.0221687

Richter, H. G., Raut, S., Hansell, J. A., and Giussani, D. A. (2008). Melatonin up-regulates placental expression of catalase and manganese superoxide dismutase under maternal undernutrition but not hypoxic conditions. *Placental Perinatal Physiol.* 11, C28. University of Cambridge Proc Physiol Soc.

Rodriguez-Naranjo, M. I., Torija, M. J., Mas, A., Cantos-Villar, E., and Garcia-Parrilla, M. D. C. (2012). Production of melatonin by *Saccharomyces* strains under growth and fermentation conditions. *J. Pineal Res.* 53, 219–224. doi: 10.1111/j.1600-079X.2012.00990.x

Sadak, M. S., Abdalla, A. M., Abd Elhamid, E. M., and Ezzo, M. I. (2020). Role of melatonin in improving growth, yield quantity and quality of *Moringa oleifera* l. plant under drought stress. *Bull. Natl. Res. Cent.* 44, 1–13. doi: 10.1186/s42269-020-0275-7

Sharma, A., and Zheng, B. (2019). Melatonin mediated regulation of drought stress: Physiological and molecular aspects. *Plants* 8, 190. doi: 10.3390/plants8070190

Sjöblom, S., Brader, G., Koch, G., and Palva, E. T. (2006). Cooperation of two distinct ExpR regulators controls quorum sensing specificity and virulence in the plant pathogen erwinia *carotovora*. *J. Mol. Microbiol. Biotechnol.* 60, 1474–1489. doi: 10.1111/j.1365-2958.2006.05210.x

Tabuchi, T., Aoki, H., Uchiyama, H., and Nakahara, T. (1981). 2-methylcitrate dehydratase, a new enzyme functioning at the methylcitric acid cycle of propionate metabolism. *Agric. Biol. Chem.* 45, 2823–2829. doi: 10.1080/00021369.1981.10864960

Tan, D. X., Hardeland, R., Manchester, L. C., Korkmaz, A., Ma, S., Rosales-Corral, S., et al. (2012). Functional roles of melatonin in plants, and perspectives in nutritional and agricultural science. *J. Exp. Bot.* 63, 577–597. doi: 10.1093/jxb/err256

Tan, D. X., Manchester, L. C., Terron, M. P., Flores, L. J., and Reiter, R. J. (2007). One molecule, many derivatives: a never-ending interaction of melatonin with reactive oxygen and nitrogen species? *J. Pineal Res.* 42, 28–42. doi: 10.1111/j.1600-079X.2006.00407.x

Yang, Y., Cao, Y., Li, Z., Zhukova, A., Yang, S., Wang, J., et al. (2020). Interactive effects of exogenous melatonin and *Rhizophagus intraradices* on saline-alkaline stress tolerance in *Leymus chinensis*. *Mycorrhiza* 30, 357–371. doi: 10.1007/s00572-020-00942-2

Yin, X., Wei, Y., Song, W., Zhang, H., Liu, G., Chen, Y., et al. (2020). Melatonin as an inducer of arecoline and their coordinated roles in anti-oxidative activity and immune responses. *Food Funct.* 11, 8788–8799. doi: 10.1039/D0FO01841D

Zhang, H. J., Zhang, N. A., Yang, R. C., Wang, L., Sun, Q. Q., Li, D. B., et al. (2014). Melatonin promotes seed germination under high salinity by regulating antioxidant systems, ABA and GA 4 interaction in cucumber (*Cucumis sativus l.*). *J. Pineal Res.* 57, 269–279. doi: 10.1111/jpi.12167

Zhang, S., Zheng, X., Reiter, R. J., Feng, S., Wang, Y., Liu, S., et al. (2017). Melatonin attenuates potato late blight by disrupting cell growth, stress tolerance, fungicide susceptibility and homeostasis of gene expression in *Phytophthora infestans*. *Front. Plant Sci.* 8 1993. doi: 10.3389/fpls.2017.01993

Zhao, D., Wang, R., Meng, J., Li, Z., Wu, Y., and Tao, J. (2017). Ameliorative effects of melatonin on dark-induced leaf senescence in gardenia (*Gardenia jasminoides ellis*): leaf morphology, anatomy, physiology and transcriptome. *Nat. Neurosci.* 7, 1–19. doi: 10.1038/s41598-017-10799-9

Zhao, H., Xu, L., Su, T., Jiang, Y., Hu, L., and Ma, F. (2015). Melatonin regulates carbohydrate metabolism and defenses against *Pseudomonas syringae* pv. *tomato DC 3000* infection in *Arabidopsis thaliana*. *J. Pineal Res.* 59, 109–119. doi: 10.1111/jpi.12245

Zhao, D., Yu, Y., Shen, Y., Liu, Q., Zhao, Z., Sharma, R., et al. (2019). Melatonin synthesis and function, evolutionary history in animals and plants. *Front. Endocrinol.* 10. doi: 10.3389/fendo.2019.00249

frontiers | Frontiers in Plant Science

TYPE Original Research
PUBLISHED 22 March 2023
DOI 10.3389/fpls.2023.1169726

OPEN ACCESS

EDITED BY
Kun Zhang,
Yangzhou University, China

REVIEWED BY
Wei Deng,
Yangzhou University, China
Zhiwei Fan,
Chinese Academy of Tropical Agricultural Sciences, China
Hongju Ma,
Huazhong Agricultural University, China

*CORRESPONDENCE
Xingshan Tian
1070470768@qq.com

SPECIALTY SECTION
This article was submitted to Plant Pathogen Interactions, a section of the journal Frontiers in Plant Science

RECEIVED 20 February 2023
ACCEPTED 09 March 2023
PUBLISHED 22 March 2023

CITATION
Guo W, Zhang C, Wang S, Zhang T and Tian X (2023) Temperature influences glyphosate efficacy on glyphosate-resistant and -susceptible goosegrass (*Eleusine indica*). *Front. Plant Sci.* 14:1169726. doi: 10.3389/fpls.2023.1169726

Temperature influences glyphosate efficacy on glyphosate-resistant and -susceptible goosegrass (*Eleusine indica*)

Wenlei Guo[1,2], Chun Zhang[1,2], Siwei Wang[1,2], Taijie Zhang[1,2] and Xingshan Tian[1,2]*

[1]Guangdong Provincial Key Laboratory of High Technology for Plant Protection, Institute of Plant Protection, Guangdong Academy of Agricultural Sciences, Guangzhou, China, [2]Key Laboratory of Green Prevention and Control on Fruits and Vegetables in South China Ministry of Agriculture and Rural Affairs, Guangzhou, China

Glyphosate has been widely used to control *Eleusine indica* and other weeds in South China for many years. Among the most troublesome weeds in South China, *E. indica* can remain alive all year round. However, the influence of temperature on glyphosate efficacy on *E. indica*, especially under days with fluctuating temperature, is unknown. This study evaluated the influence of two temperature regimes on glyphosate efficacy on glyphosate-resistant (R) and -susceptible (S) *E. indica* biotypes. Plants of the R and S biotypes were cultivated under two temperature regimes (high: 30°C/20°C day/night; low: 20°C/15°C day/night). Dose-response experiments showed improved efficacy of glyphosate at the low temperature compared with that at the high temperature for both biotypes. Based on the LD_{50} values, the R biotype was 8.9 times more resistant to glyphosate than the S biotype at the high temperature; however, the resistance index (R/S) decreased to 3.1 at the low temperature. At 4 days after glyphosate application, shikimic acid accumulation was greater at the low temperature than at the high temperature in plants of both biotypes, and the increase was higher in plants of the R biotype than in the S biotype. At a sublethal glyphosate dose (R: 400 g ai ha^{-1}; S: 200 g ai ha^{-1}), plants grown at the low temperature showed a strong decrease in leaf chlorophyll content and Fv/Fm value compared with those of plants grown at the high temperature and the untreated control. At 3 days after treatment, glyphosate absorption was similar between biotypes at the high temperature, but absorption decreased to 64.9% and 53.1% at the low temperature for the R and S biotypes, respectively. For both biotypes, glyphosate translocation from the leaf to the remainder of the plant was reduced at the low temperature compared with that at the high temperature. No differences in glyphosate translocation were observed between biotypes within each temperature regime. This is the first report on the effect of temperature on glyphosate efficacy on *E. indica*, and provides important insights for glyphosate application and resistance management.

KEYWORDS

low temperature, glyphosate, control efficacy, shikimate, absorption, translocation

1 Introduction

Since its commercialization in 1974, glyphosate has been widely used as a broad-spectrum, nonselective, post-emergence herbicide. It has been regarded as among the most important and successful herbicides (Duke and Powles, 2008). Glyphosate kills weeds by inhibiting the activity of 5-enolpyruvylshikimate-3-phosphate synthase (EPSPS) (Steinrucken and Amrhein, 1980), a key enzyme in the shikimate pathway in plants. If EPSPS is inhibited by glyphosate, one physiological response is rapid accumulation of shikimic acid (Holländer-Czytko and Amrhein, 1983), which is a biomarker for assessment of glyphosate efficacy in plants (Mueller et al., 2003; Zelaya et al., 2011). Elevated contents of shikimic acid in a treated plant indicates sensitivity to glyphosate, whereas a lack of or limited accumulation of shikimic acid indicates tolerance to glyphosate (Singh and Shaner, 1998; Burgos et al., 2013). Environmental factors may influence glyphosate efficacy and the level of glyphosate resistance in plants (Cerdeira et al., 2007). Among various environmental factors, temperature has received greater attention given that the absorption and translocation of glyphosate often varies considerably with temperature (Singh et al., 2020).

South China is located in the subtropical monsoon climate zone. Winter in South China is much warmer than in northern China. Taking Guangzhou as an example, from 1991 to 2020, the average maximum and average minimum temperatures were 20.7°C and 11.9°C in December, and 18.7°C and 10.6°C in January (http://www.tqyb.com.cn/gz/climaticprediction/static/). As a result, the life history of many weed species in South China differs from those in northern China. Goosegrass (*Eleusine indica*) is a troublesome grass weed that is widely distributed in most regions of China and other tropical or subtropical areas in the world (Chauhan and Johnson, 2008; Zhu et al., 2020). It often infests corn, vegetable, and fruit crops, and significantly reduces crop yield and quality (Zhang, 2003). In northern China, *E. indica* usually germinates from April to May and dies from October to November. However, because of the warm winter, *E. indica* can remain alive all year round and seeds can germinate in different months in South China. *E. indica* has shown 35%–60% germination at 15°C constant temperature or 15–20°C fluctuating temperature (Ismail et al., 2002; Chauhan and Johnson, 2008).

South China is one of the first areas in China to control weeds with glyphosate (Yang et al., 2012). Similar to other countries, the long-term application of glyphosate has resulted in development of glyphosate resistance in some weed species in China (Song et al., 2011; Chen et al., 2015; Zhang et al., 2015a; Deng et al., 2020; Li et al., 2022), especially in *E. indica*. Considering that paraquat use has been banned and the extent of glyphosate-resistant crops may increase significantly in the near future, it is likely that glyphosate will continue to play an important role in the nonselective herbicide market in China for the foreseeable future (Liu et al., 2021; Zhang et al., 2022). *E. indica* grows vigorously and shows strong competitive ability with crops in summer, so farmers in South China willingly spray glyphosate repeatedly in this period (Yang et al., 2012). Conversely, farmers usually do not apply glyphosate to control *E. indica* in low-temperature seasons because most *E. indica* plants are shorter and less competitive than other weeds or crops. Greater attention should be given to the vulnerable period of a weed's lifecycle for effective weed control.

E. indica emerges at different times of the year in South China and the growth rate is relatively slow during the cold season, which may provide an excellent opportunity to control the plants by applying herbicide in winter or early spring. The plant biomass increases rapidly with the rise in temperature in spring and profuse seed production eventuates in the absence of control measures. To the best of our knowledge, the influence of temperature on the glyphosate efficacy or degree of glyphosate resistance in *E. indica* remains unknown. Therefore, the objectives of this study were to (1) determine the whole-plant dose-response of glyphosate-resistant and -susceptible biotypes of *E. indica* under high- and low-temperature regimes, (2) assess the changes in physiological indicators after glyphosate treatment under the different temperature regimes, including shikimic acid accumulation, chlorophyll content and chlorophyll fluorescence, and (3) compare absorption and translocation of glyphosate in the resistant and susceptible biotypes under the different temperature regimes.

2 Materials and methods

2.1 Plant material and temperature regimes

Two biotypes of *E. indica* were used in all experiments of this study. The glyphosate-resistant (R) biotype was purified from the R5 population described by Zhang et al. (2021). The R5 population was collected from a corn field in Baiyun district, Guangdong province (23°23′ N, 113°26′ E), where glyphosate had been applied consistently for at least 10 years. In the R5 population, plants surviving glyphosate treatment (1080 g ai ha^{-1}) harbored different target-site mechanisms. The mother plants of the R biotype were related to *EPSPS* gene amplification, without *EPSPS* gene mutation (Zhang et al., 2021). Seeds of the susceptible (S) biotype were harvested from a nearby uncultivated area with the same geographic background as the R biotype (23°29′ N, 113°21′ E). The results of qPCR confirmed that the *EPSPS* gene copy number (relative to the acetolactate synthase gene) of the R biotype was 24 times higher than that of the S biotype (data not shown). The seeds were air-dried and stored in a cabinet at the ambient room temperature and 10%–14% relative humidity until use.

The seeds were rubbed with sandpapers to remove the thin pericarp, and then sown in plastic trays containing moistened nutrient soil. The trays were placed in a greenhouse with day/night temperature of 25°C/20°C, relative humidity of 70 ± 5%, and illuminated by natural sunlight. Seedlings of the R and S biotypes were transplanted individually into 200-mL pots containing nutrient soil. When most plants had attained the five-leaf stage, healthy plants of uniform size of each biotype were divided into two groups. The two groups were cultivated in different growth chambers under the same growing conditions, except that the day/night temperature regime was either 30°C/25°C (high

temperature) or 20°C/15°C (low temperature). The plants were grown under a photoperiod of 12 h/12 h (day/night) with light intensity in the chambers of 200 µmol m^{-2} s^{-1} photon flux. The relative humidity in the growth chambers was maintained at 75 ± 5% throughout the experiment and the plants were watered every second day.

The plants were incubated in the respective growth chambers for 3 days to allow acclimation to the temperature regime before being treated with glyphosate.

2.2 Whole-plant dose-response experiment

After temperature acclimation for 3 days, the *E. indica* plants were treated with glyphosate (Roundup®, 41% isopropylamine salt of glyphosate; Bayer Crop Science, St. Louis, MO, USA) using a moving Teejet 9503EVS flat-fan nozzle cabinet sprayer (Beijing Research Center for Information Technology in Agriculture, Beijing, China) with a spray volume of 450 L ha^{-1} at 0.28 MPa. Glyphosate was applied at the rate of 0, 50, 100, 200, 400, 800, 1600, 3200, or 6400 g ai ha^{-1} for R biotype and 0, 12.5, 25, 50, 100, 200, 400, 800, or 1600 g ai ha^{-1} for the S biotype. Each treatment consisted three replications and each replication comprised five plants. At approximately 20 min after treatment, the plants were returned to the corresponding chambers. At 14 days after treatment (DAT), the number of surviving plant was recorded. Plants were classified as dead if they showed symptoms such as chlorosis and desiccation, and as alive if they were actively growing and tillering (Vila-Aiub et al., 2021). Two independent experiments were performed.

2.3 Shikimic acid accumulation

Glyphosate was applied to *E. indica* plants (grown under different temperature regimes) as described above at the rate of 0, 100, 200, 400, 800, 1600, 3200 g ai ha^{-1} for R biotype and 0, 25, 50, 100, 200, 400, 800 g ai ha^{-1} for S biotype.

The shikimate assay was conducted as described in Chen et al. (2015) with some modifications. Shikimic acid was extracted at 4 DAT. Tissue from fully expanded mature leaves (200 mg) was placed in a 2-mL centrifuge tube and then flash-cooled in liquid nitrogen before crushed using an automatic sample fast grinding machine (Shanghai Jingxin Industrial Development Co. Ltd, Shanghai, China). Immediately after crushing, 1 mL HCl (0.25 mol L^{-1}) was added to the centrifuge tube. The tubes were vortexed for 10 s to ensure that the crushed tissue was fully dissolved in HCl. After centrifugation at 25,000 g for 20 min at 4 °C, 0.16 mL supernatant was transferred to a 5-mL centrifuge tube. Next, 1.6 mL periodic acid (1%, w/v) was added with sufficient mixing and the tube was incubated at room temperature. After incubation for 3 h, 1.6 mL NaOH (1 mol L^{-1}) was added to the reaction mixture, followed by the addition of 0.96 mL glycine (0.1 mol L^{-1}). The absorbance at 380 nm was measured using a Multiskan SkyHigh Microplate Spectrophotometer (Thermo Fisher Scientific (China) Co., Ltd, Shanghai, China). A standard curve was constructed after replacing the supernatant with a known concentration (6.25–800 µg mL^{-1}) of shikimic acid solution.

2.4 Determination of chlorophyll content

As described in section 2.1, *E. indica* plants were grown under the high- and low- temperature regimes for 3 days before treatment with glyphosate. Commercial glyphosate at a sublethal dose was applied to plants of the R (400 g ai ha^{-1}) and S (200 g ai ha^{-1}) biotypes. Plants treated with deionized water were used as the untreated control. At 10 DAT, chlorophyll was extracted from 0.1 g leaf samples with 10 mL of a mixed solution of acetone and ethanol (1:1, v/v). The light absorbance at 647 nm and 663 nm was measured using a spectrophotometer as described in section 2.3. The chlorophyll content determinations were based on the methods and equations of Lichtenthaler (1987):

$$chlorophyll\ a\ (mg\ g^{-1}) = [(11.25 \times A_{663} - 2.79 \times A_{647}) \times x]/(1000 \times y)$$

$$chlorophyll\ b\ (mg\ g^{-1}) = [(21.5 \times A_{647} - 5.1 \times A_{663}) \times x]/(1000 \times y)$$

$$chlorophyll\ (a+b)\ (mg\ g^{-1}) = [(18.71 \times A_{647} - 6.15 \times A_{663}) \times x]/(1000 \times y)$$

where A is absorbance, x (mL) is the volume of the extraction solution, and y (g) is the fresh weight of the leaf sample.

2.5 Measurement of chlorophyll fluorescence

The glyphosate doses and treatments were identical to those of the chlorophyll content analysis. At 0, 2, 4, 6, and 8 DAT, the chlorophyll fluorescence was measured using a Dual-PAM-100 fluorescence measuring system (Heinz Walz GmbH, Effeltrich, Germany). At each time point, measurements were conducted at 09:00 to 12:00 after dark adaptation for 30 min. The investigation was performed with four replications corresponding to four individual plants. Data used for analysis were the leaf maximal quantum yields (Fv/Fm) of *E. indica* plants as described by Zhang et al. (2015b).

2.6 Absorption and translocation of glyphosate

Seeds of the R and S biotypes were germinated on 0.6% (w/v) agar-solidified Hoagland's nutrient solution. Seedlings at two-leaf stage were transplanted into quadrate plastic containers (30 cm × 30 cm × 5 cm) containing Hoagland's nutrient solution. Each seedling

was clamped by a sponge and separated into a planting basket with a hole at the bottom. A daily supplement of the nutrient solution was guaranteed. The environmental conditions in this phase were identical to those described for the greenhouse.

When the plants attained the five-leaf stage, they were transferred to the growth chambers maintained at the aforementioned high- and low- temperature regimes. After 3 days, a commercial glyphosate solution was applied using a topical application method. Commercial glyphosate was diluted to 5000 mg L^{-1} (ai), then 8 µL of glyphosate solution was applied to the center of the fourth leaf of each plant using a micropipettor. The plants were returned to the growth chambers once the droplet had dried. Plants were harvested at 3 DAT. Each treatment comprised three replications each consisting of 25 plants. The treated leaf was excised with scissors. The treated leaves from one replication were rinsed in a glass test tube with 10 mL of wash solution (a mixture [1:1 v/v] of methanol and deionized water with 0.45% Tween-20) for 2 min to remove the unabsorbed glyphosate from the surface of the treated leaves (Ganie et al., 2017). The samples to be analyzed for each treatment were separated into treated leaves, other tissues (including shoots, roots and other leaves), and the wash solution.

For sample preparation, 0.5 mL of the wash solution was transferred to a fresh centrifuge tube, mixed with 0.5 mL methanol by vortexing for 1 min, and the mixed solution was filtered through a 0.22-µm 165 hydrophilic PTFE needle filter for subsequent liquid chromatography–tandem mass spectrometry (LC-MS/MS) analysis. The treated leaf and other parts of the plants were cut into pieces and weighed, then transferred to a 50-mL centrifuge tube, and 10 mL methanol was added. The mixture was homogenized for 3 min and centrifuged at 3200 g for 5 min. The supernatant was filtered through a 0.22-µm filter as described above and then subjected to LC-MS/MS analysis. The LC-MS/MS analysis of glyphosate and aminomethyl phosphonic acid (AMPA) was performed in accordance with the Chinese national standard SN/T 4655-2016 (General Administration of Quality Supervision, Inspection and Quarantine of the People's Republic of China; https://www.sdtdata.com/)

2.7 Statistical analysis

Data for plant survival were transformed into a percentage of the untreated control before use to estimate the glyphosate dose required to cause 50% mortality (LD_{50}) of the plants. The transformed data were then subjected to a four-parameter log-logistic regression model implemented in SigmaPlot 12.5 software: $y = c + (d - c)/[1 + (x/LD_{50})^b]$, where y is the plant survival rate, c is the lower limit around indefinitely high doses, d is the upper limit at indefinitely low doses, b is the slope around the LD_{50}, and x is the glyphosate dose. The resistance index (RI) was calculated by dividing the LD_{50} value of the R biotype by that of the S biotype.

The means for shikimic acid accumulation, chlorophyll content, glyphosate absorption and translocation were compared, and the effects of temperature (or glyphosate dose) were analyzed by an unpaired Student's test or one-way ANOVA (followed by a Fisher's protected LSD test) using SPSS 21.0 software.

3 Results

3.1 Whole-plant dose-response experiment

The efficacy of glyphosate on *E. indica* was distinctly influenced by temperature. Within a certain dose range, glyphosate killed more plants under the low-temperature regime than at the high-temperature regime (Figure 1). The LD_{50} values of the R biotype decreased from 3133.5 g ai ha^{-1} to 677.4 g ai ha^{-1} under the high- and low-temperature regimes, respectively (Table 1). The S biotype had LD_{50} values of 352.8 g ai ha^{-1} under the high-temperature regime and 219.2 g ai ha^{-1} under the low-temperature regime (Table 1). Therefore, the resistance index (R/S) dropped from 8.9 (high temperature) to 3.1 (low temperature) (Table 1).

3.2 Shikimic acid accumulation

At the same glyphosate dose, shikimic acid accumulation was greater under the low-temperature regime than under the high-temperature regime for both biotypes (Figure 2). At the high temperature, the amount of shikimic aicd in the R biotype showed muted increment from 18.0 to 44.1 µg g^{-1} at the glyphosate doses of 0–1600 g ai ha^{-1} and increased to 130 µg g^{-1} at 3200 g ai ha^{-1} (Figure 2), indicating high tolerance to glyphosate under this temperature regime. At the low temperature, the shikimic acid content gradually increased from 49.3 to 275.3 µg g^{-1} in the R biotype in response to glyphosate application (Figure 2). At glyphosate doses of 0–800 g ai ha^{-1}, plants of the S biotype grown at the low temperature accumulated greater quantities of shikimic acid than those grown at high temperature (52.4–397.2 and 21.7–248.2 µg shikimic acid g^{-1} fresh weight, respectively) (Figure 2).

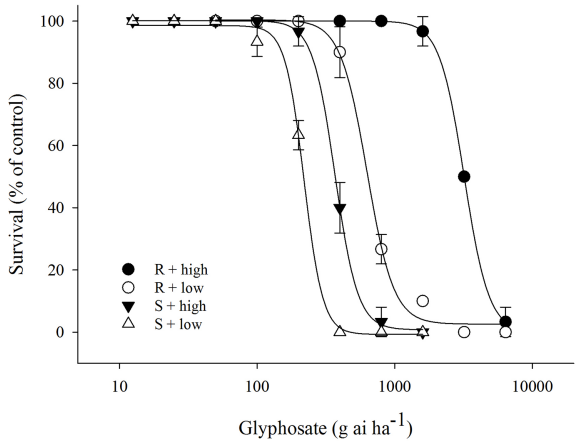

FIGURE 1
Plant survival response to glyphosate treatment in glyphosate-resistant (R) and -susceptible (S) *Eleusine indica* biotypes grown under high temperature (30°C/25°C day/night) and low temperature (20°C/15°C day/night) regimes. The experiment was repeated with similar results. Each data point is the mean ± standard error of three replicates from one experiment.

TABLE 1 Estimated LD_{50} values in glyphosate-resistant (R) and -susceptible (S) *Eleusine indica* plants grown under high temperature (30°C/25°C day/night) and low temperature (20°C/15°C day/night) regimes.

Temperature regime	Biotype	LD_{50} (g ai ha^{-1})[a]	RI[b]
High	R	3133.5 ± 70.5	8.9
	S	352.8 ± 16.3	
Low	R	677.4 ± 20.6	3.1
	S	219.2 ± 2.8	

[a]LD_{50} is the glyphosate dose required to cause 50% mortality of the plants. Each value represents the mean ± standard error of two repeated experiments.
[b]RI (resistance index)=LD_{50} (R)/LD_{50} (S).

Irrespective of the temperature regime, the S biotype always accumulated greater shikimic acid contents than plants of the R biotype, although the difference between the two biotypes was narrower at the low temperature. For example, S plants accumulated 151.9 μg shikimic acid g^{-1} fresh weight at the high temperature under the glyphosate dose of 400 g ai ha^{-1} (Figure 2), which was 4.1 times higher than that for the R plants; however, although S plants accumulated substantially more shikimic acid (258.6 μg g^{-1}) at the low temperature under the same glyphosate treatment (Figure 2), the amount was only 1.3 times higher than that accumulated by the R plants.

3.3 Chlorophyll content

In the 0 g ai ha^{-1} glyphosate treatment, temperature regime did not influence the leaf chlorophyll contents of *E. indica* plants of either the R or S biotype (Table 2). In addition, the chlorophyll a and chlorophyll b contents increased in response to a sublethal dose of glyphosate (R: 400 g ai ha^{-1}; S: 200 g ai ha^{-1}) under the high-temperature regime compared with the untreated control (Table 2). However, the leaf chlorophyll contents of the R and S biotypes under the low-temperature regime decreased dramatically under the same glyphosate treatment (Table 2).

3.4 Chlorophyll fluorescence

In the control, only slight changes in Fv/Fm of the R and S biotypes were detected under the two temperature regimes (Figure 3). A sublethal dose of glyphosate (R: 400 g ai ha^{-1}; S: 200 g ai ha^{-1}) did not cause a distinct decline in Fv/Fm in the R and S biotypes grown at the high temperature (Figure 3). However, different responses were observed under the low-temperature regime; the Fv/Fm values of the R and S biotypes dramatically decreased to 0.72 and 0.53 at 8 DAT with the sublethal dose of glyphosate (Figure 3), which were 93% and 69% of the initial values, respectively.

3.5 Absorption and translocation of glyphosate

At 3 DAT, the mean absorption of glyphosate was 74.9% and 77.5% under the high-temperature regime, and decreased to 64.9% and 53.1% under the low-temperature regime, in the R and S biotypes, respectively (Figure 4). As a result, absorption was significantly higher under the high-temperature regime than under the low-temperature regime for both biotypes (Figure 4).

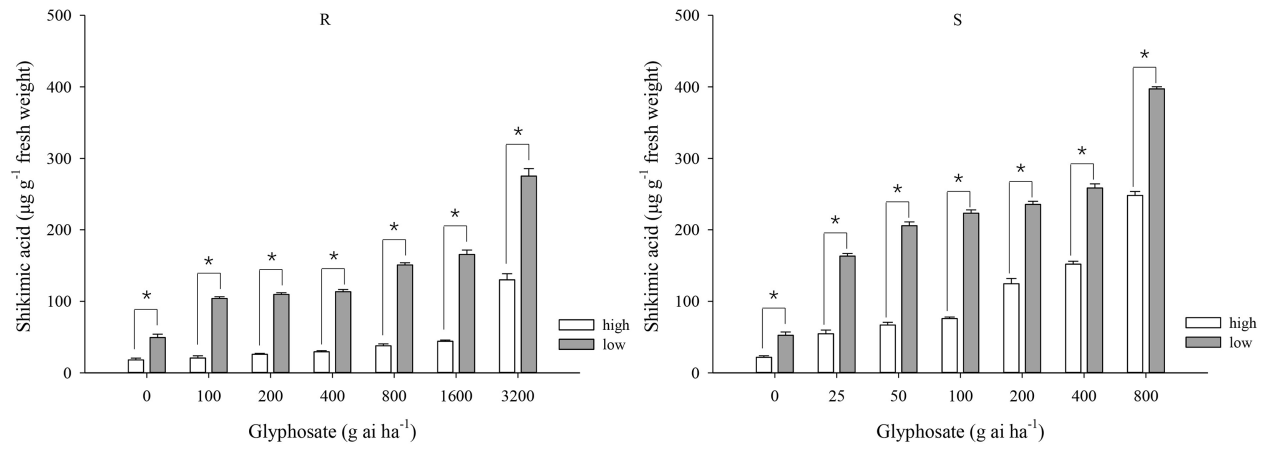

FIGURE 2
Shikimic acid accumulation in leaf tissue of glyphosate-resistant (R) and -susceptible (S) *Eleusine indica* biotypes at 4 days after glyphosate treatment under high temperature (30°C/25°C day/night) and low temperature (20°C/15°C day/night) regimes. Each data point is the mean ± standard error of three biological replications. An asterisk indicates a significant difference in shikimic acid content within the same glyphosate treatment between temperature regimes (Student's *t*-test, $\alpha = 0.05$).

10.3389/fpls.2023.1169726

TABLE 2 Influence of glyphosate on leaf chlorophyll content of glyphosate-resistant (R) and -susceptible (S) *Eleusine indica* plants grown under high temperature (30°C/25°C day/night) and low temperature (20°C/15°C day/night) regimes.

Biotype	Glyphosate dose (g ai ha^{-1})	Temperature regime	Chlorophyll a (mg g^{-1})[a]	Chlorophyll b (mg g^{-1})[a]	Chlorophyll a+b (mg g^{-1})[a]
R	0	High	1.00 ± 0.03b	0.32 ± 0.02ab	1.32 ± 0.05b
		Low	0.96 ± 0.02b	0.29 ± 0.02b	1.26 ± 0.05b
	400	High	1.08 ± 0.01a	0.35 ± 0.01a	1.43 ± 0.02a
		Low	0.79 ± 0.02c	0.25 ± 0.02c	1.04 ± 0.04c
S	0	High	0.93 ± 0.02b	0.29 ± 0.02b	1.22 ± 0.03b
		Low	0.90 ± 0.01b	0.26 ± 0.03b	1.16 ± 0.04b
	200	High	1.02 ± 0.03a	0.38 ± 0.02a	1.40 ± 0.05a
		Low	0.48 ± 0.05c	0.16 ± 0.01c	0.65 ± 0.07c

[a]Chlorophyll extraction was conducted at 10 days after glyphosate treatment. Within the same biotype, values in the same column followed by different lowercase letter are statistically different (Fisher's protected LSD, $\alpha = 0.05$). Each value represents the mean ± standard error.

Significant differences in glyphosate translocation were detected between the temperature regimes, but not between the biotypes within the same temperature regime. Both biotypes translocated a smaller proportion of the absorbed glyphosate from the treated leaf to the rest of the plant under the low-temperature regime. At 3 DAT, 65.7% (R) and 67.5% (S) of the absorbed glyphosate were retained in the treated leaf under the high-temperature regime compared with 83.3% (R) and 82.3% (S) under the low-temperature regime (Figure 4). The amount of glyphosate detected in the rest of the plant was 34.3% (R) and 32.5% (S) under the high-temperature regime compared with 16.7% (R) and 17.7% (S) at the low temperature (Figure 4)

In the experiment, AMPA was not detected in the treated leaf or in the remainder of the plant, and only a small amount of AMPA were detected in the wash solution (data not shown).

4 Discussion

The efficacy of glyphosate at different temperatures varies depending on the weed species and/or populations. The present study demonstrated that both the R and S biotypes of *E. indica* were more sensitive to glyphosate when grown at a low temperature. Compared with the S biotype, the sensitivity to glyphosate of the R biotype was more strongly elevated at the low temperature, resulting in reduced resistance level to glyphosate. Populations of *Echinochloa colona*, a graminaceous weed with a growing season similar to that of *E. indica*, displayed different trends in glyphosate tolerance at 20°C and 30°C. The efficacy of glyphosate on the sensitive *E. colona* population was not affected by temperature, but increased efficacies were observed at low temperature on six glyphosate-resistant *E. colona* populations (Nguyen et al., 2016).

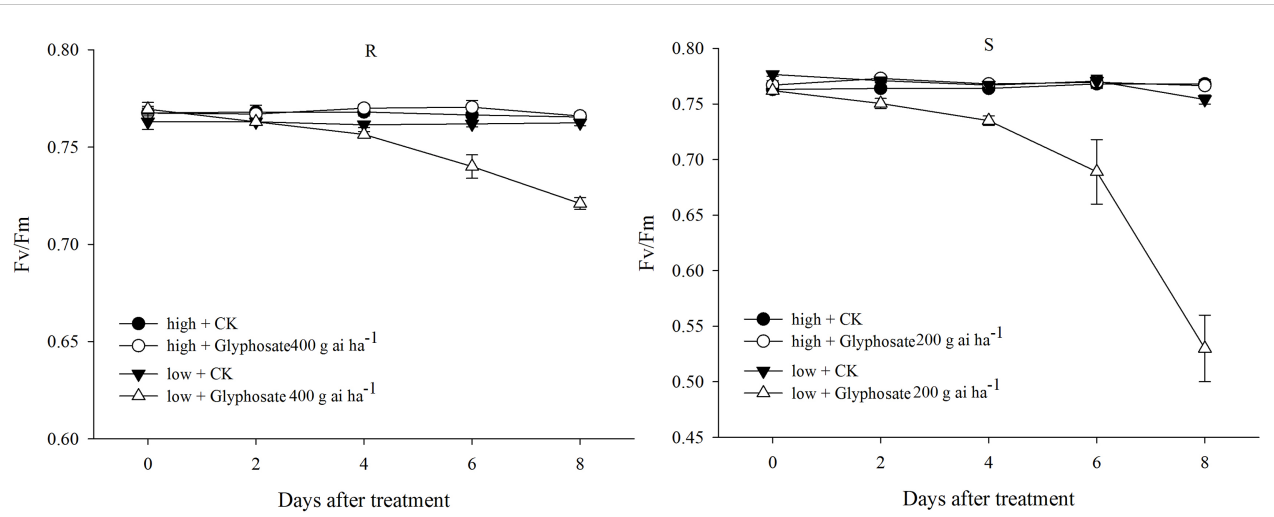

FIGURE 3
Fv/Fm value of glyphosate-resistant (R) and -susceptible (S) *Eleusine indica* biotypes after glyphosate treatment under high temperature (30°C/25°C day/night) and low temperature (20°C/15°C day/night) regimes. Each data point is the mean ± standard error of four biological replications.

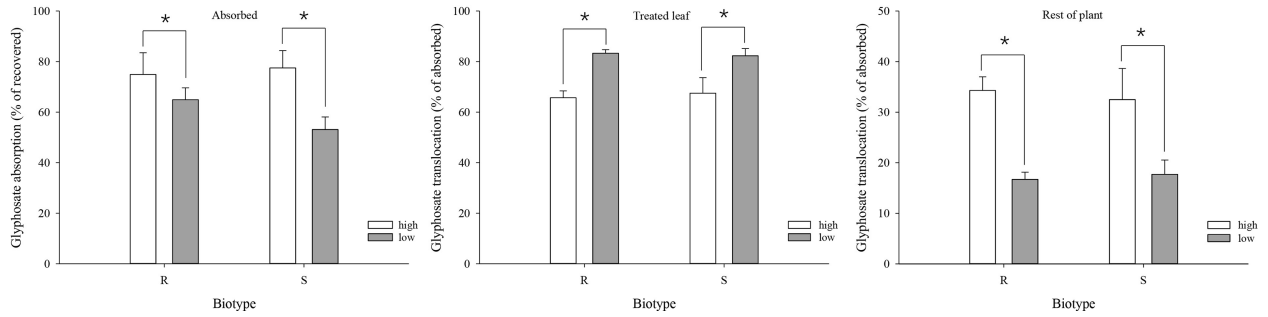

FIGURE 4
Glyphosate absorption and translocation in glyphosate-resistant (R) and -susceptible (S) *Eleusine indica* biotypes at 3 days after glypphosate treatment under high temperature (30°C/25°C day/night) and low temperature (20°C/15°C day/night) regimes. Each data point is the mean ± standard error of three biological replications. An asterisk indicates a significant difference between temperature regimes (Student's *t*-test, $\alpha = 0.05$).

Tanpipat et al. (1997) demonstrated that increase in temperature reduces the control effect of glyphosate on *E. colona* under field conditions. An additional grass weed, *Lolium rigidum*, is less tolerant to glyphosate at a low temperature (Powles et al., 1998; Vila-Aiub et al., 2013). In addition, three glyphosate-resistant *Conyza* species (*C. sumatrensis*, *C. bonariensis*, and *C. canadensis*) show a reduction in glyphosate resistance at a low temperature (Ge et al., 2011; Okumu et al., 2019; Palma-Bautista et al., 2019). It is interesting that the efficacy of glyphosate on a sensitive biotype of *C. sumatrensis* decreases, but that on a resistant biotype increases, at a low temperature (Palma-Bautista et al., 2019). However, giant ragweed (*Ambrosia artemisiifolia*) and common ragweed (*Ambrosia trifida*) show higher mortality and biomass reduction at a high temperature regardless of the degree of susceptibility or resistance to glyphosate (Ganie et al., 2017).

The background shikimic acid amounts of the R and S biotypes of *E. indica* were similar in untreated plants under the same temperature regime, which increased from 18.0–21.7 μg g^{-1} at the high temperature to 49.3–52.4 μg g^{-1} at the low temperature. According to Mueller et al. (2008, 2011), shikimic acid concentrations are less than 80 μg g^{-1} in untreated plants of *E. indica*, and are usually less than 100 μg g^{-1} in nine other weedy species. Hence, it is reasonable to assume that the low-temperature treatment enhanced the background amount of shikimic acid in untreated *E. indica* plants, which was nonfatal to the plants. With exposure to glyphosate, shikimic acid may accumulate rapidly in the plant if EPSPS activity is partially or entirely inhibited by the herbicide. In most studies that have performed shikimate assays, glyphosate was applied at the field rate and the shikimic acid amount was measured during the period of 0–8 DAT. Generally, the shikimic acid amount is probably close to the maximum at 4–6 DAT for most species, including *E. indica* (Mueller et al., 2008; Mueller et al., 2011). In the present study, *E. indica* plants were incubated for 4 days at the different temperatures to evaluate the effect of temperature on shikimic acid accumulation after glyphosate treatment. The data for shikimic acid accumulation were in accordance with the results of the whole-plant experiment, in that a lower dose of glyphosate at a low temperature could achieve a comparable effect to that with a higher dose at a high temperature. In addition, the increasing difference in shikimic acid accumulation between the high- and low-temperature regimes was higher in the R biotype than in the S biotype of *E. indica*. The resistant biotype of *C. bonariensis* accumulated approximately five times more shikimic acid at 15 °C than at 27 °C, whereas the susceptible biotype only doubled the amount of shikimic acid (Okumu et al., 2019). In *C. sumatrensis*, the differences in shikimic acid accumulation between resistant and susceptible biotype were more divergent when plants were grown at a high temperature (Palma-Bautista et al., 2019). In *E. colona*, however, less shikimic acid was accumulated at a low temperature (20 °C) than at a high temperature (30 °C) (Nguyen et al., 2016).

The influences of glyphosate on chlorophyll content reflects the doses applied. Previous studies confirm that a lethal dose of glyphosate sharply reduces the chlorophyll content of plants (Chen et al., 2015). In contrast, plants treated with sublethal doses of glyphosate may have a higher chlorophyll content than the untreated control. For example, the chlorophyll content of *Chenopodium album* plants treated with a glyphosate dose of 90 and 180 g ai ha^{-1} was significantly higher than that of the untreated control (Ketel, 1996). Similar results were observed in *Amaranthus retroflexus* (Meseldžija et al., 2020). It is noteworthy that the stimulatory effect of glyphosate may differ with environmental factors (Belz and Duke, 2014). In the present study, when grown under the high temperature regime, the *E. indica* plants exposed to a sublethal dose of glyphosate had a higher leaf chlorophyll content than that of the untreated plants, but the stimulatory effect was not observed for plants grown under the low temperature regime, indicating that certain physiological processes may be impaired. The Fv/Fm value can be used as an indicator of tolerance to a herbicide and other environmental stress. A previous study of our team showed that a sublethal dose of glyphosate does not result in an obvious reduction in Fv/Fm in *E. indica* plants (Zhang et al., 2015b), which is consistent with the results obtained under the high-temperature regime in the present study. However, a sublethal dose caused a significant decrease in Fv/Fm in plants grown under the low temperature regime, especially for the S biotype, indicating

that the functioning of photosystem II may be severely damaged. The observation that *E. indica* plants treated with sublethal doses of glyphosate showed reductions in chlorophyll content and Fv/Fm at a low temperature may be further evidence for the influence of temperature on glyphosate efficacy.

In many plant species, temperature has been reported to influence the absorption and/or translocation of glyphosate. In *E. colona*, glyphosate absorption was reduced with increase in temperature, whereas translocation from the treated leaf was not affected by temperature (Nguyen et al., 2016). The indication that glyphosate absorption and translocation are enhanced at a low temperature has been observed in many other plant species, such as *C. sumatrensis* (Palma-Bautista et al., 2019), Glycine max (McWhorter et al., 1980), and *Kochia scoparia* (Ou et al., 2018). In contrast, McWhorter et al. (1980) reported that *Sorghum halepense* absorbed two times the amount of glyphosate at 30 °C compared with at 24°C, and the degree of glyphosate translocation was also increased. Similarly, in *Brunnichia ovata*, Reddy (2000) noted that a greater amount of glyphosate was absorbed and translocated under a higher temperature. In the present study, it is interesting that increase in the glyphosate efficacy on *E. indica* was accompanied by reduced glyphosate absorption and translocation at a low temperature. A reduction in glyphosate absorption and translocation has been reported to confer glyphosate resistance in some weed species (Sammons and Gaines, 2014; Gaines et al., 2020). Hence, the increase in glyphosate efficacy on *E. indica* at a low temperature was likely caused by other mechanisms. A low temperature is not optimal for growth of *E. indica*; therefore, we hypothesize that an extended low-temperature treatment may disrupt certain physiological processes, resulting in reduced glyphosate tolerance. For example, if *EPSPS* gene expression of *E. indica* is suppressed under a low temperature, the amount of EPSPS enzyme would be reduced in cells and a lower glyphosate concentration would be required to inhibit its activity.

The present findings revealed that temperature impacted on the efficacy of glyphosate for control of the troublesome weed *E. indica* in South China. Therefore, temperature should be considered before glyphosate application, especially for applications in winter or early spring in South China, where strong fluctuations in the spring temperature usually occur. For control of *E. indica*, the temperature forecast in the days subsequent to glyphosate application should be colder for improved efficacy. The present research was conducted under artificial controlled conditions with precise temperatures and relative humidity; thus, the results may vary under field conditions owing to the complex variability of environmental factors, including temperature, relative humidity, wind, and light (Ramsey et al., 2005; Varanasi et al., 2016). In addition, considering that a premix formulation or tank mixture of glyphosate and other herbicides (such as glufosinate, dicamba, oxyfluorfen and flumioxazin) is increasingly popular (Beckie, 2011; Liu et al., 2021), the effect of temperature on the efficacy of other herbicides should also be considered. Further studies are needed to evaluate the combined effect of temperature and other environmental factors on weed control efficacy under field conditions. Moreover, molecular studies, such as analysis of gene expression for target enzymes or metabolic enzymes under different environmental conditions, may provide additional evidence to explain the variable response to herbicide application under different environmental conditions.

Data availability statement

The raw data supporting the conclusions of this article will be made available by the authors, without undue reservation.

Author contributions

WG and XT conceived and designed the study. WG, SW, and TZ performed experiments, acquired data and completed formal analysis. WG prepared the original draft. CZ and XT reviewed the manuscript, supervised and acquired the funding. All authors contributed to the article and approved the submitted version.

Funding

This research was supported by the National Natural Science Foundation of China (31901900), the Guangzhou Science and Technology Planning Project (202201010517), and the Department of Science and Technology of Guangdong Province, China (2019B121201003).

Conflict of interest

The authors declare that the research was conducted in the absence of any commercial or financial relationships that could be construed as a potential conflict of interest.

Publisher's note

References

Beckie, H. J. (2011). Herbicide-resistant weed management: Focus on glyphosate. *Pest Manage. Sci.* 67 (9), 1037–1048. doi: 10.1002/ps.2195

Belz, R. G., and Duke, S. O. (2014). Herbicides and plant hormesis. *Pest Manage. Sci.* 70, 698–707. doi: 10.1002/ps.3726

Burgos, N. R., Tranel, P. J., Streibig, J. C., Davis, V. M., Shaner, D., Norsworthy, J. K., et al. (2013). Confirmation of resistance to herbicides and evaluation of resistance levels. *Weed Sci.* 61 (1), 4–20. doi: 10.1614/WS-D-12-00032.1

Cerdeira, A. L., Gazziero, D. L. P., Duke, S. O., Matallo, M. B., and Spadotto, C. A. (2007). Review of potential environmental impacts of transgenic glyphosate-resistant soybean in Brazil. *J. Environ. Sci. Hlth. B.* 42 (5), 539–549. doi: 10.1080/03601230701391542

Chauhan, B. S., and Johnson, D. E. (2008). Germination ecology of goosegrass (*Eleusine indica*): An important grass weed of rainfed rice. *Weed Sci.* 56 (5), 699–706. doi: 10.1614/WS-08-048.1

Chen, J. C., Huang, H. J., Wei, S. H., Zhang, C. X., and Huang, Z. F. (2015). Characterization of glyphosate-resistant goosegrass (*Eleusine indica*) populations in China. *J. Integr. Agr.* 14 (5), 919–925. doi: 10.1016/S2095-3119(14)60910-2

Deng, W., Yang, Q., Chen, Y. R., Yang, M. T., Xia, Z. M., Zhu, J., et al. (2020). Cyhalofop-butyl and glyphosate multiple-herbicide resistance evolved in an *Eleusine indica* population collected in Chinese direct-seeding rice. *J. Agric. Food Chem.* 68 (9), 2623–2630. doi: 10.1021/acs.jafc.9b07342

Duke, S. O., and Powles, S. B. (2008). Glyphosate: A once-in-a-century herbicide. *Pest Manage. Sci.* 64, 319–325. doi: 10.1002/ps.1518

Gaines, T. A., Duke, S. O., Morran, S., Rigon, C. A. G., Tranel, P. J., Küpper, A., et al. (2020). Mechanisms of evolved herbicide resistance. *J. Biol. Chem.* 295 (30), 10307–10330. doi: 10.1074/jbc.REV120.013572

Ganie, Z. A., Jugulam, M., and Jhala, A. J. (2017). Temperature influences efficacy, absorption, and translocation of 2,4-d or glyphosate in glyphosate-resistant and glyphosate-susceptible common ragweed (*Ambrosia artemisiifolia*) and giant ragweed (*Ambrosia trifida*). *Weed Sci.* 65, 588–602. doi: 10.1017/wsc.2017.32

Ge, X., d'Avignon, D. A., Ackerman, J. J. H., Duncan, B., Spaur, M. B., and Sammons, R. D. (2011). Glyphosate-resistant horseweed made sensitive to glyphosate: Low-temperature suppression of glyphosate vacuolar sequestration revealed by 31P NMR. *Pest Manage. Sci.* 67, 1215–1221. doi: 10.1002/ps.2169

Holländer-Czytko, H., and Amrhein, N. (1983). Subcellular compartment of shikimic acid and phenylalanine in buckwheat cell suspension cultures grown in the presence of shikimate pathway inhibitors. *Plant Sci. Lett.* 29, 89–96. doi: 10.1016/0304-4211(83)90027-5

Ismail, B. S., Chuah, T. S., Salmijah, S., Teng, Y. T., and Schumacher, R. W. (2002). Germination and seedling emergence of glyphosate-resistant and susceptible biotypes of goosegrass (*Eleusine indica* [L.] gaertn.). *Weed Biol. Manage.* 2, 177–185. doi: 10.1046/j.1445-6664.2002.00066.x

Ketel, D. H. (1996). Effect of low doses of metamitron and glyphosate on growth and chlorophyll content of common lambsquarters (*Chenopodium album*). *Weed Sci.* 44 (1), 1–6. doi: 10.1017/S0043174500093462

Li, J. Y., Mei, Y., Zhang, L. L., Hao, L. B., and Zheng, M. Q. (2022). The resistance levels and target-site based resistance mechanisms to glyphosate in *Eleusine indica* from China. *Agronomy.* 12 (11), 2780. doi: 10.3390/agronomy12112780

Lichtenthaler, H. K. (1987). Chlorophylls and carotenoids: pigments of photosynthetic biomembranes. *Methods Enzymol.* 148, 350–385. doi: 10.1016/0076-6879(87)48036-1

Liu, X. Y., Merchant, A., Xiang, S. H., Zong, T., Zhou, X. G., and Bai, L. Y. (2021). Managing herbicide resistance in China. *Weed Sci.* 69 (1), 4–17. doi: 10.1017/wsc.2020.68

McWhorter, C. G., Jordan, T. N., and Wills, G. D. (1980). Translocation of 14C-glyphosate in soybeans (*Glycine max*) and johnsongrass (*Sorghum halepense*). *Weed Sci.* 28 (1), 113–118. doi: 10.1017/S0043174500027892

Meseldžija, M., Lazić, S., Dudić, M., Šunjka, D., Rajković, M., Marković, T., et al. (2020). Is there a possibility to involve the hormesis effect on the soybean with glyphosate sub-lethal amounts used to control weed species *Amaranthus retroflexus* l? *Agronomy* 10, 850. doi: 10.3390/agronomy10060850

Mueller, T. C., Ellis, A. T., Beeler, J. E., Sharma, S. D., and Singh, M. (2008). Shikimate accumulation in nine weedy species following glyphosate application. *Weed Res.* 48, 455–460. doi: 10.1111/j.1365-3180.2008.00648.x

Mueller, T. C., Massey, J. H., Barnett, K. A., Brosnan, J. T., and Steckel, L. E. (2011). Glyphosate resistant goosegrass (*Eleusine indica*) confirmed in Tennessee. *Weed Sci.* 59 (4), 562–566. doi: 10.1614/WS-D-11-00063.1

Mueller, T. C., Massey, J. H., Hayes, R. M., Main, C. L., and Stewart, C. N. (2003). Shikimate accumulates in both glyphosate-sensitive and glyphosate-resistant horseweed (*Conyza canadensis* l. cronq.). *J. Agric. Food Chem.* 51 (3), 680–684. doi: 10.1021/jf026006k

Nguyen, T. H., Malone, J. M., Boutsalis, P., Shirley, N., and Preston, C. (2016). Temperature influences the level of glyphosate resistance in barnyardgrass (*Echinochloa colona*). *Pest Manage. Sci.* 72, 1031–1039. doi: 10.1002/ps.4085

Okumu, M. N., Vorster, B. J., and Reinhardt, C. F. (2019). Growth-stage and temperature influence glyphosate resistance in *Conyza bonariensis* (L.) cronquist. *South Afr. J. Bot.* 121, 248–256. doi: 10.1016/j.sajb.2018.10.034

Ou, J., Stahlman, P. W., and Jugulam, M. (2018). Reduced absorption of glyphosate and decreased translocation of dicamba contribute to poor control of kochia (*Kochia scoparia*) at high temperature. *Pest Manage. Sci.* 74, 1134–1142. doi: 10.1002/ps.4463

Palma-Bautista, C., Alcántara-de la Cruz, R., Rojano-Delgado, A. M., Dellaferrera, I., Domínguez-Martínez, P. A., and De Prado, R. (2019). Low temperatures enhance the absorption and translocation of 14C-glyphosate in glyphosate-resistant *Conyza sumatrensis*. *J. Plant Physiol.* 240, 153009. doi: 10.1016/j.jplph.2019.153009

Powles, S. B., Lorraine-Colwill, D. F., Dellow, J. J., and Preston, C. (1998). Evolved resistance to glyphosate in rigid ryegrass (*Lolium rigidum*) in Australia. *Weed Sci.* 46 (5), 604–607. doi: 10.1017/S0043174500091165

Ramsey, R. J. L., Stephenson, G. R., and Hall, J. C. (2005). A review of the effects of humidity, humectants, and surfactant composition on the absorption and efficacy of highly water-soluble herbicides. *Pestic. Biochem. Physiol.* 82 (2), 162–175. doi: 10.1016/j.pestbp.2005.02.005

Reddy, K. N. (2000). Factors affecting toxicity, absorption, and translocation of glyphosate in redvine (*Brunnichia ovata*). *Weed Technol.* 14 (3), 457–462. doi: 10.1614/0890-037X(2000)014[0457:FATAAT]2.0.CO;2

Sammons, D. R., and Gaines, T. A. (2014). Glyphosate resistance: State of knowledge. *Pest Manage. Sci.* 70, 1367–1377. doi: 10.1002/ps.3743

Singh, S., Kumar, V., Datta, S., Wani, A. B., Dhanjal, D. S., Romero, R., et al. (2020). Glyphosate uptake, translocation, resistance emergence in crops, analytical monitoring, toxicity and degradation: A review. *Environ. Chem. Lett.* 18, 663–702. doi: 10.1007/s10311-020-00969-z

Singh, B. K., and Shaner, D. L. (1998). Rapid determination of glyphosate injury to plants and identification of glyphosate-resistant plants. *Weed Technol.* 13, 527–530. doi: 10.1017/S0890037X00044250

Song, X. L., Wu, J. J., Zhang, H. J., and Qiang, S. (2011). Occurrence of glyphosate-resistant horseweed (*Conyza canadensis*) population in China. *Agr. Sci. China* 10 (7), 1049–1055. doi: 10.1016/S1671-2927(11)60093-X

Steinrucken, H. C., and Amrhein, N. (1980). The herbicide glyphosate is a potent inhibitor of 5-enolpyruvyl shikimate acid-3-phosphate synthase. *Biochim. Biophys. Res. Commun.* 94 (4), 1207–1212. doi: 10.1016/0006-291X(80)90547-1

Tanpipat, S., Adkins, S. W., Swarbrick, J. T., and Boersma, M. (1997). Influence of selected environmental factors on glyphosate efficacy when applied to awnless barnyard grass (*Echinochloa colona* (L.) link). *Aust. J. Agric. Res.* 48, 695–702. doi: 10.1071/A96141

Varanasi, A., Prasad, P. V., and Jugulam, M. (2016). Impact of climate change factors on weeds and herbicide efficacy. *Adv. Agron.* 135, 107–146. doi: 10.1016/bs.agron.2015.09.002

Vila-Aiub, M. M., Gundel, P. E., Yu, Q., and Powles, S. B. (2013). Glyphosate resistance in *Sorghum halepense* and *Lolium rigidum* is reduced at suboptimal growing temperatures. *Pest Manage. Sci.* 69 (2), 228–232. doi: 10.1002/ps.3464

Vila-Aiub, M. M., Han, H. P., Yu, Q., García, F., and Powles, S. B. (2021). Contrasting plant ecological benefits endowed by naturally occurring EPSPS resistance mutations under glyphosate selection. *Evol. Appl.* 14 (6), 1635–1645. doi: 10.1111/eva.13230

Yang, C. H., Tian, X. S., Feng, L., and Yue, M. F. (2012). Resistance of *Eleusine indica* gaertn to glyphosate. *Scientia Agricultura Sinica.* 45 (10), 2093–2098. doi: 10.3864/j.issn.0578-1752.2012.10.023

Zelaya, I. A., Anderson, J. A. H., Owen, M. D. K., and Landes, R. D. (2011). Evaluation of spectrophotometric and HPLC methods for shikimic acid determination in plants: models in glyphosate-resistant and-susceptible crops. *J. Agric. Food Chem.* 59 (6), 2202–2212. doi: 10.1021/jf1043426

Zhang, Z. P. (2003). Development of chemical weed control and integrated weed management in China. *Weed Biol. Manage.* 3, 197–203. doi: 10.1046/j.1444-6162.2003.00105.x

Zhang, C., Feng, L., He, T. T., Yang, C. H., Chen, G. Q., and Tian, X. S. (2015a). Investigating the mechanisms of glyphosate resistance in goosegrass (*Eleusine indica*) population from south China. *J. Integr. Agr.* 14 (5), 909–918. doi: 10.1016/S2095-3119(14)60890-X

Zhang, T. J., Feng, L., Tian, X. S., and Gao, J. D. (2015b). Use of chlorophyll fluorescence and P700 absorbance to rapidly detect glyphosate resistance in goosegrass (*Eleusine indica*). *J. Integr. Agr.* 14 (4), 714–723. doi: 10.1016/S2095-3119(14)60869-8

Zhang, C., Yu, C. J., Yu, Q., Guo, W. L., Zhang, T. J., and Tian, X. S. (2021). Evolution of multiple target-site resistance mechanisms in individual plants of glyphosate-resistant *Eleusine indica* from China. *Pest Manage. Sci.* 77, 4810–4817. doi: 10.1002/ps.6527

Zhang, Y. H., Zhu, L. X., Hu, J., Zhu, Y. J., Zhang, X. J., and Cao, Y. Z. (2022). Opportunities and challenges of glyphosate in the application of biotechnology breeding in China. *Biotechnol. Bull.* 38 (11), 1–9. doi: 10.13560/j.cnki.biotech.bull.1985.2022-0924

Zhu, J. W., Wang, J., DiTommasoc, A., Zhang, C. X., Zheng, G. P., Liang, W., et al. (2020). Weed research status, challenges, and opportunities in China. *Crop Prot.* 134, 104449. doi: 10.1016/j.cropro.2018.02.001

frontiers | Frontiers in Plant Science

TYPE Original Research
PUBLISHED 30 March 2023
DOI 10.3389/fpls.2023.1163679

OPEN ACCESS

EDITED BY
Zhenggang Li,
Guangdong Academy of Agricultural Sciences, China

REVIEWED BY
Chao Zhang
Henan Agricultural University, China
Zhengnan Li,
Inner Mongolia Agricultural University, China

*CORRESPONDENCE
Zihao Xia
zihao8337@syau.edu.cn
Yuanhua Wu
wuyh09@syau.edu.cn

†These authors have contributed equally to this work

SPECIALTY SECTION
This article was submitted to Plant Pathogen Interactions, a section of the journal Frontiers in Plant Science

RECEIVED 11 February 2023
ACCEPTED 15 March 2023
PUBLISHED 30 March 2023

CITATION
Xu C, Guo H, Li R, Lan X, Zhang Y, Xie Q, Zhu D, Mu Q, Wang Z, An M, Xia Z and Wu Y (2023) Transcriptomic and functional analyses reveal the molecular mechanisms underlying Fe-mediated tobacco resistance to potato virus Y infection. *Front. Plant Sci.* 14:1163679. doi: 10.3389/fpls.2023.1163679

Transcriptomic and functional analyses reveal the molecular mechanisms underlying Fe-mediated tobacco resistance to potato virus Y infection

Chuantao Xu[1,2†], Huiyan Guo[1†], Rui Li[1], Xinyu Lan[1], Yonghui Zhang[2], Qiang Xie[2], Di Zhu[3], Qing Mu[3], Zhiping Wang[1], Mengnan An[1], Zihao Xia[1*] and Yuanhua Wu[1*]

[1]Liaoning Key Laboratory of Plant Pathology, College of Plant Protection, Shenyang Agricultural University, Shenyang, China, [2]Luzhou City Company of Sichuan Province Tobacco Company, Luzhou, China, [3]Guizhou Qianxinan Prefectural Tobacco Company, Xingyi, China

Potato virus Y (PVY) mainly infects Solanaceous crops, resulting in considerable losses in the yield and quality. Iron (Fe) is involved in various biological processes in plants, but its roles in resistance to PVY infection has not been reported. In this study, foliar application of Fe could effectively inhibit early infection of PVY, and a full-length transcriptome and Illumina RNA sequencing was performed to investigate its modes of action in PVY-infected *Nicotiana tabacum*. The results showed that 18,074 alternative splicing variants, 3,654 fusion transcripts, 3,086 long non-coding RNAs and 14,403 differentially expressed genes (DEGs) were identified. Specifically, Fe application down-regulated the expression levels of the DEGs related to phospholipid hydrolysis, phospholipid signal, cell wall biosynthesis, transcription factors (TFs) and photosystem I composition, while those involved with photosynthetic electron transport chain (PETC) were up-regulated at 1 day post inoculation (dpi). At 3 dpi, these DEGs related to photosystem II composition, PETC, molecular chaperones, protein degradation and some TFs were up-regulated, while those associated with light-harvesting, phospholipid hydrolysis, cell wall biosynthesis were down-regulated. At 9 dpi, Fe application had little effects on resistance to PVY infection and transcript profiles. Functional analysis of these potentially critical DEGs was thereafter performed using virus-induced gene silencing approaches and the results showed that *NbCat-6A* positively regulates PVY infection, while the reduced expressions of *NbWRKY26*, *NbnsLTP*, *NbFAD3* and *NbHSP90* significantly promote PVY infection in *N. benthamiana*. Our results elucidated the regulatory network of Fe-mediated resistance to PVY infection in plants, and the functional candidate genes also provide important theoretical bases to further improve host resistance against PVY infection.

KEYWORDS

PVY, Fe, full-length transcriptome, Illumina RNA sequencing, virus-induced gene silencing

1 Introduction

Potato virus Y (PVY) is the typical member of the genus *Potyvirus* in the family *Potyviridae* (Rybicki, 2015). PVY infects a wide host range mainly within the Solanaceous crops, such as potato, tomato, pepper and tobacco, and causes considerably economic losses worldwide (Gibbs et al., 2020; Yang et al., 2021). As known, viruses often rely on a complex network of interactions with host proteins to promote infection in plants (Garcia-Ruiz, 2019). In the arms race between hosts and pathogens, plants have evolved a series of strategies to resist viral infections (Lebaron et al., 2016). Virus infections also alter the expression levels of a large number of host genes (Garcia-Ruiz, 2019). A study has shown that the expression levels of differentially expressed genes (DEGs) related to plant-pathogen interactions, including heat shock proteins, are down-regulated, while those of terpene synthase and protein kinase encoding genes are up-regulated in the susceptible potato varieties after PVY infection (Ross et al., 2022). In PVY-infected tobacco plants, DEGs related to DNA/RNA binding, catalytic activity and signaling molecules are significantly enriched, and PVY-derived siRNAs are shown to target translationally controlled tumor protein (*NtTCTP*) mRNA that is associated with host resistance to viral infection (Guo et al., 2017).

Microelements, such as boron (B), chlorine (Cl), copper (Cu), iron (Fe), manganese (Mn) and zinc (Zn), play essential roles during plant growth (Merchant, 2010). Among them, Fe is known as the third most limiting microelements for plants due to its low solubility in alkaline and calcareous soils (Gyana and Rout, 2015). Fe is required for a variety of biological processes, such as DNA synthesis, photosynthesis, respiration, nitrogen reduction, biosynthesis and repair of nucleotide, amino acids, proteins, cofactors, and vitamins (Chhabra et al., 2020; Hendrix et al., 2022). Fe deficiency causes up-regulation of *bHLH38*, *bHLH100* and *bHLH101*, and inhibits flowering in *Arabidopsis* (Chen et al., 2021). The expression levels of the basic helix-loop-helix transcription factor *FER*, the ferric-chelate reductase *LeFRO1* and the Fe (II) transporter *LeIRT1* genes are up-regulated in the iron-deficient conditions, which promotes the production of nitric oxide (NO) in tomato plants (Graziano and Lamattina, 2007). In *Arabidopsis*, high iron concentrations promote NO production and induce *AtFer1* and *AtFer4* expression, thus allowing excess iron to be preserved in a bioavailable and non-toxic form (Arnaud et al., 2006). In addition, the regulatory roles of Fe in plant resistance during pathogen infection have been well investigated. Foliar spraying of Fe_3O_4 nanoparticles can activate the oxidative stress response, induce the synthesis of salicylic acid (SA), and up-regulate the expression of pathogenesis-related (PR) proteins, thus enhancing the resistance of plants to the infection of tobacco mosaic virus (TMV) (Cai et al., 2020). It was also indicated that iron treatment can induce reactive oxygen species (ROS) burst to regulate the resistance to *Curvularia lunata* in maize (Fu et al., 2022).

Next-generation sequencing (NGS) technology based on Illumina platform is a powerful method to provide insights into mechanisms underlying processes of global gene expression and secondary metabolism (Unamba et al., 2015). The single molecule real-time (SMRT) sequencing based on Pacific BioSciences (PacBio) platform allows the direct reading of cDNA and the maximum reading length to 70 kb, and accurately reconstructs full-length splice variants (Korlach et al., 2017). Overall, combining analysis of NGS and SMRT sequencing can provide high-quality, accurate, and complete isoforms in transcriptome studies, which is thereby conducive to discovering more alternative splicing (AS) isoforms, long non-coding RNAs (lncRNAs) and fusion genes. A reference transcriptome of impatiens infected with downy mildew has been constructed by full-length transcriptome sequencing and RNA sequencing (RNA-Seq), which provided a comprehensive data source to screen resistance genes (Peng et al., 2021).

Investigations on the roles of trace elements in plant antiviral responses are still limited. Our previous studies have shown that boron can inhibit cucumber green mottle mosaic virus (CGMMV) infection in watermelon by regulating the expression levels of genes related to carbohydrate metabolism, hormone biosynthesis, cell wall catabolism and ROS burst (Bi et al., 2022a; Bi et al., 2022b; Guo et al., 2022). In this study, we demonstrated that foliar spraying of Fe inhibited PVY infection in *N. tabacum*, and analyzed the expression patterns of tobacco genes under four different treatments with or without PVY infection after spraying Fe or H_2O at 1, 3, 9 days post inoculation (dpi) by full-length transcriptome and RNA-Seq analyses. The results revealed that PVY infection mainly affected the expression levels of host genes related to photosynthesis and biosynthesis, while Fe treatment regulated genes associated with lipid metabolism, photosynthesis, endoplasmic reticulum protein processing and cell wall biogenesis. Moreover, the roles of several genes were characterized by down-regulated their expressions through virus-induced gene silencing (VIGS) assays in the PVY-infected *N. benthamiana* plants. These results provide a new method for prevention of PVY infection and lay a theoretical foundation for disease resistant breeding in Solanaceous crops.

2 Materials and methods

2.1 Plant growth and virus inoculation

N. tabacum L. cv. K326 and *N. benthamiana* plants were cultivated in the artificial climate chamber with a day/night temperature of 25°C, 65 ± 5% relative humidity, and 16 h/8 h light/dark cycle environmental conditions. Potato virus Y (PVY-LN, GenBank ID: JQ971975) was isolated and purified by our laboratory and propagated on tobacco. *N. tabacum* leaves were sprayed twice every 2 days with H_2O or Fe^{2+} (EDTA-Fe) or $MgSO_4$ or $CuSO_4$ with concentration of 3.36 mg·L^{-1} or 240 mg·L^{-1} or 0.8 mg·L^{-1} at 4-5 leaf stage and then inoculated with phosphate-buffered saline (PBS solution) or PVY after one day, respectively (PBS solution + H_2O, P + H; PBS solution + Fe, P + Fe; PBS solution + Mg, P + Mg; PBS solution + Cu, P + Cu; PVY + H_2O, PVY + H; PVY + Fe; PVY + Mg; PVY + Cu). The samples were harvested from inoculated leaves at 1 dpi, and systematic leaves at 3

dpi and 9 dpi, and three independent experiments were performed in this study.

2.2 Library preparation and SMRT sequencing

We mixed all samples of different treatments (P + H, P + Fe, P + Mg, P + Cu, PVY + H, PVY + Fe, PVY + Mg, PVY + Cu) at 3 time points into one sample for full-length transcriptome analysis based on SMRT sequencing. Total RNA was extracted using a Trizol reagent (Invitrogen, CA, USA). The RNA quantity and purity were analyzed by Bioanalyzer 2100 and RNA 1000 Nano LabChip Kit (Agilent, CA, USA) with RIN number > 7.0. Full-length cDNA was synthesized using a SMAR Ter™ PCR cDNA Synthesis Kit (Clontech, CA, USA). The generated cDNA was then re-amplified using PCR. After end repair, the SMRT adaptor with a hairpin loop structure was ligated to the cDNA. The cDNA library was then constructed *via* exonuclease digesting. After quality measurement of the cDNA library, SMRT sequencing was performed using the Pacific Bioscience Sequel platform (Biomarker Technologies Co. Ltd., Beijing, China). The reference genome of tobacco K326 (https://solgenomics.net/organism/Nicotiana_tabacum/genome) was used. The sequencing data were deposited in the SRA database at NCBI with the accession number PRJNA903693.

2.3 Illumina RNA-seq library construction and sequencing

The mRNA extracted from samples in four different treatments (P + H, P + Fe, PVY + H, PVY + Fe) was purified using oligo (dT)-attached magnetic beads. Fragmentation was conducted in the NEBNext First Strand Synthesis Reaction Buffer. First-strand cDNA was obtained based on the random hexamers, and then the second-strand cDNA was synthesized with dNTPs, RNase H, and PrimeStar GXL DNA polymerase. The synthesized cDNA was purified with AMPure XP beads. After end repairing, adding poly-A and adaptor ligation, AMPure XP beads were used for size selection. The generated cDNA was then amplified for construction of cDNA libraries. The qualified libraries were pair-end sequenced on the Illumina HiSeq TM2500 (Biomarker Technologies Co. Ltd., Beijing, China). The sequencing data were deposited in the SRA database at NCBI with the accession number PRJNA903693. The relative gene expression levels were normalized as fragments per kilobase of transcript per million mapped reads (FPKM). The genes with threshold of false discovery rate (FDR) < 0.05 and |log2 fold change| ≥ 1 were defined as DEGs.

2.4 Functional annotation of transcripts

Gene Ontology (GO) enrichment of DEGs were analyzed by a GOseq R packages based Wallenius non-central hyper-geometric distribution (Young et al., 2010). A KOBAS software was used to perform KEGG enrichment analyses of DEGs (Mao et al., 2005).

2.5 WGCNA analyses

Weighted gene co-expression network analysis (WGCNA) was used to construct gene co-expression networks. Highly co-expressed gene modules were obtained using the WGCNA v3.1.1 package in R language (Langfelder et al., 2009). A gene expression adjacency matrix was constructed to analyze the network topology with minModuleSize of 30, and minimum height for merging modules of 0.1262.

2.6 Virus-induced gene silencing assays

The homologs of five DEGs were selected for functional verification using a tobacco rattle virus (TRV)-based VIGS vector in *N. benthamiana*, respectively. These fragments were amplified using specific primers (Supplementary Table 1) and PrimeSTAR® Max DNA Polymerase (TaKaRa, Dalian, China) through PCR. The details of construction of TRV-based VIGS vectors and infiltration of *Agrobacterium tumefaciens* referred to our previous study (Guo et al., 2022). After 10 days post infiltration, the upper non-infiltrated leaves were mechanically inoculated with PVY crude extracts. After 10 dpi, we monitored *N. benthamiana* plants symptoms and collected the upper two leaves to measure gene silencing efficiency and PVY accumulation.

2.7 Western blot analyses

Total proteins from tobacco K326 inoculated leaves at 1 dpi and systematic leaves at 3, 5, 7, 9 dpi, as well as the upper two leaves of *N. benthamiana* plants were extracted using a Plant Protein Extraction Kit (Solarbio, Shanghai, China) and quantified using the BCA protein quantification kit (Beyotime, Shanghai, China), respectively. After the completion of electrophoresis, the proteins separated by 12% SDS-PAGE were transferred to 0.20 μm polyvinylidene fluoride (PVDF) membranes (Millipore, Billerica, USA), which were then incubated in blocking solution for one hour (Solarbio, Shanghai, China). PVY CP monoclonal antibody was used at dilution of 1: 1000 (Youlong, Shanghai, China). Beta-actin antibody was used at dilution of 1: 5000 (Proteintech, Chicago, USA). After incubation with primary and secondary antibodies (ABclonal, Wuhan, China), membranes were washed twice for 10 min with 1×TTBS, and then transferred into ECL solution (Millipore, Billerica, USA) to detect signals by Tanon Chemiluminescence Gel Imager (Tanon, Shanghai, China).

2.8 Reverse transcription-quantitative real-time PCR (RT-qPCR)

The RNA of the inoculated leaves at 1 dpi and systematic leaves at 3, 5, 7, 9 dpi from *N. tabacum* K326, as well as the upper two leaves of *N. benthamiana* plants was extracted by TRIzol reagent (Tiangen, Beijing, China) and was reverse transcribed to yield

cDNA with a HiScript II Q Select RT SuperMix for qPCR (gDNA eraser) kit (Vazyme, Nanjing, China). The primer sets for partial sequence amplification were designed within the CDS region of nucleotide sequences (Supplementary Table 1). RT-qPCR analyses were performed using ChamQ Universal SYBR qPCR Master Mix (Vazyme, Nanjing, China) on a StepOne Plus real-time PCR system (ThermoFisher, Waltham, USA). The relative expression levels of genes were assessed by the $2^{-\Delta\Delta CT}$ method with the normalization using *Ntubc2* (AB026056.1) in *N. tabacum* and *NbActin* (AY179605.1) in *N. benthamiana* as reference genes by three biological replicates, respectively.

2.9 Statistical analyses

The data were presented as mean values ± standard error of three biological replicates and analyzed using SPSS Version 25.0 (IBM Inc., Armonk, USA). The differences among groups were analyzed through two-tailed *t* test and one-way analysis of variance (Duncan).

3 Results

3.1 Foliar application of exogenous Fe could alleviate PVY infection in tobacco plants

By observing the symptoms of tobacco plants infected with PVY in four different treatments (P + H, P + Fe, PVY + H, PVY + Fe) at five time points, the results revealed that the tobacco stems began to show brown necrosis at 7 dpi after PVY + H treatment, while did not show obvious disease symptoms treated by PVY + Fe (Figure 1A). At 9 dpi, we found that tobacco plants were dwarfed with necrotic veins and yellow leaves, while in PVY + Fe, the stems and veins of the tobacco showed mild brown necrosis (Figure 1B). RT-qPCR results showed that the accumulation of PVY RNAs in PVY + Fe treated plants was reduced by 28% at 7 dpi and 68% at 5 dpi, compared with that in PVY + H treated plants (Figure 1C). The results of western blot validated that the accumulation of PVY CP in plants after each treatment was generally consistent with the results of RT-qPCR (Figure 1D). These results generally proved that Fe had an inhibitory effect on PVY infection in tobacco.

3.2 PacBio SMRT sequencing analysis

To accurately obtain full-length transcripts and splice variants, the PacBio SMRT sequencing was performed using the pooled sample from all treatments at 1, 3 and 9 dpi. A total of 27.63Gb clean data was obtained with 353,258 circular consensuses (CCS) reads, 316,181 full-lengths non-chimeric (FLNC) sequences and 113,580 high-quality consensus sequences (Figures 2A–C). Totally 85,991 isoforms of known genes, 41,415 novel isoforms of known genes and 7,938 isoforms of novel genes were obtained by aligning the transcripts to the *N. tabacum* genome database (Figure 2D). The novel transcript sequences obtained were searched for NR, Swissprot, GO, COG, KOG, Pfam, and KEGG databases, and the functional annotations of 39,301 novel transcripts were listed (Supplementary Table 2).

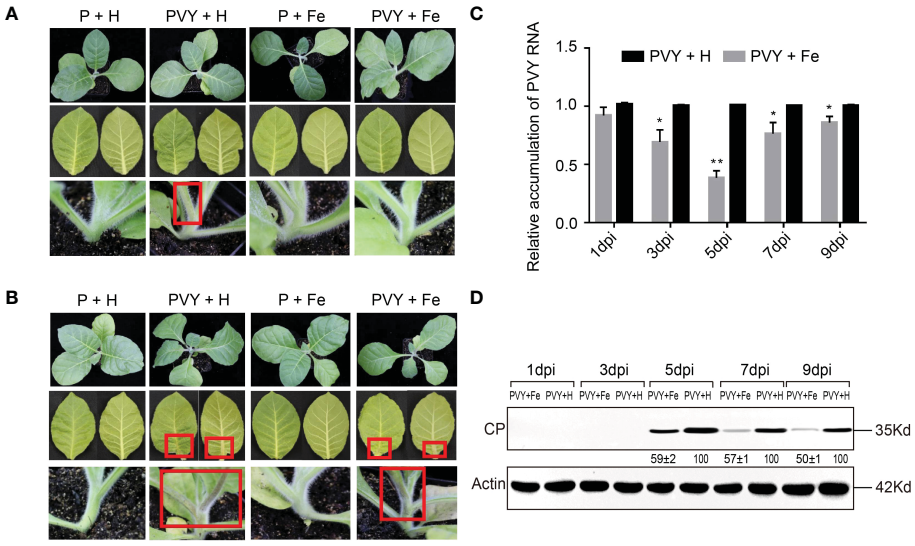

FIGURE 1
Foliar application of exogenous Fe alleviated PVY infection in tobacco plants. **(A)** Symptoms of the whole plant, leaves and stems at 7 dpi in four treatments. **(B)** Symptoms of the whole plant, leaves and stems at 9 dpi in four treatments. **(C)** The accumulation of PVY genomic RNA in tobacco leaves of PVY + H and PVY + Fe groups determined by RT-qPCR at 1, 3, 5, 7, and 9 dpi. Asterisks indicate statistically significant differences compared to control (Student's *t*-test): **P* < 0.05, ***P* < 0.01. **(D)** The accumulation of PVY CP protein in tobacco leaves of PVY + H and PVY + Fe groups determined by western blot assays at 1, 3, 5, 7, and 9 dpi.

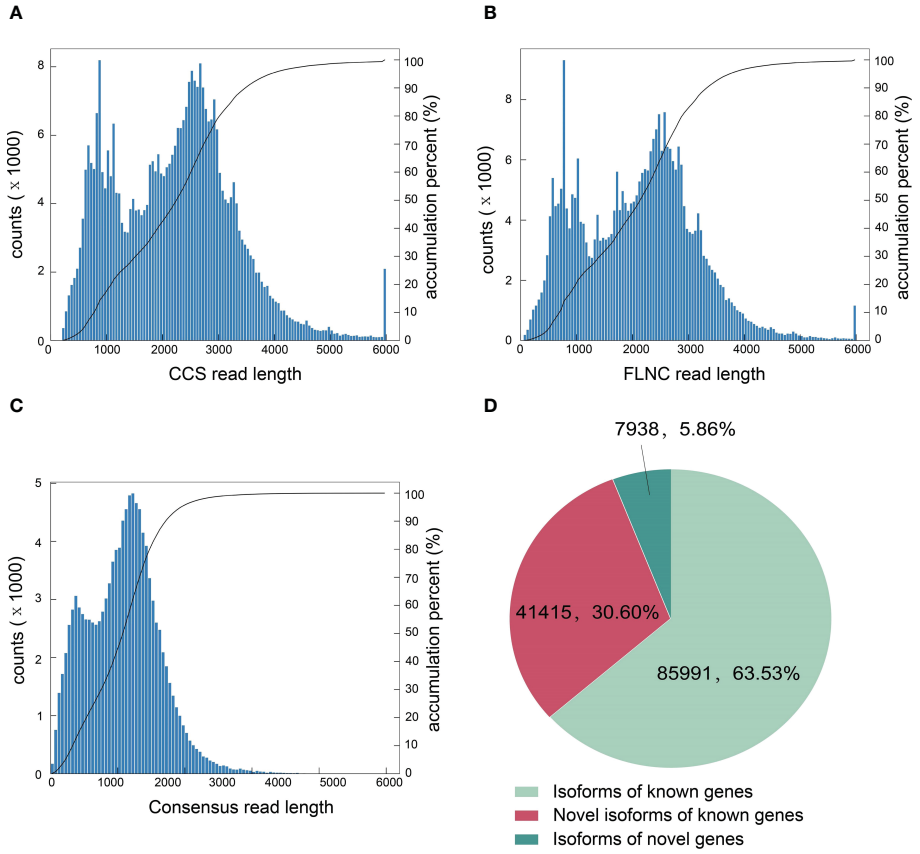

FIGURE 2
Characterization of tobacco full-length transcripts by PacBio SMRT sequencing. **(A)** The number of CCS reads in different lengths. **(B)** The number of FLNC reads in different lengths. **(C)** The number of consensus reads in different lengths. **(D)** Number and categories of isoforms based on the PacBio platform.

3.3 Analyses of alternative splicing, alternative polyadenylation and long non-coding RNA

Alternative splicing (AS) events were subsequently analyzed through an AStalavista tool (Foissac and Sammeth, 2007). A total of 18,074 AS events were indicated in transcripts, including 167 mutually exclusive exon, 10,333 intron retention, 2,086 exon skipping, 1,944 alternative 5' splice site, and 3,544 alternative 3' splice site (Figure 3A). Moreover, we further analyzed FLNC through TAPIS pipeline to identify alternative polyadenylation (APA) (Abdel-Ghany et al., 2016). We found that 6,284 genes with one APA site, 2,596 genes with two APA sites, 1,228 genes with three APA sites, 569 genes with four APA sites, 280 genes with five APA sites and 286 genes with more than five APA sites (Figure 3B). Moreover, a total of 3,086 lncRNAs were identified by coding potential calculator (CPC), coding-non-coding index (CNCI), coding potential assessment tool (CPAT) and Pfam protein domain analyses (Figure 3C) (Kong et al., 2007; Sun et al., 2013; Wang et al., 2013). According to the positions of lncRNAs on the reference genome, 1,836 intergenic lncRNAs (lincRNAs), 74 antisense lncRNAs, 77 intronic lncRNAs and 1,008 sense lncRNAs were obtained (Figure 3D). The target genes of all lncRNAs were predicted and the results were shown in Supplementary Table 3.

3.4 Illumina RNA sequencing analysis

To analyze the molecular mechanism of Fe-mediated *N. tabacum* resistance to PVY infection, RNA-Seq was performed on the leaves under four different treatments at three time points. A total of 1307.93 Gb of clean reads were obtained from 36 libraries, and each of these libraries contained ≥ 19.32 Gb of data with Q30 quality scores ≥ 91.67% (Supplementary Table 4). These reads were mapped uniquely with the ratios from 76.73% to 93.61% for each library (Supplementary Table 5).

3.5 Analyses of DEGs in different groups

To identify the genes in response to Fe application under PVY infection, five different pairwise comparisons were conducted (PVY + Fe vs. PVY + H, PVY + Fe vs. P + Fe, PVY + Fe vs. P + H, PVY + H vs. P + H, and P + Fe vs. P + H) at 1, 3, and 9 dpi. Through these comparisons, a total of 2,745 DEGs at 1 dpi, 1,277 DEGs at 3 dpi, and 12,255 DEGs at 9 dpi were obtained (Figure 4A). In PVY + H vs. P + H, we found more DEGs at 9 dpi than that at 1 dpi and 3 dpi (Figures 4A, B). In PVY + Fe vs. PVY + H, more DEGs were obtained at 1 dpi and 3 dpi than that at 9 dpi (Figures 4A, B).

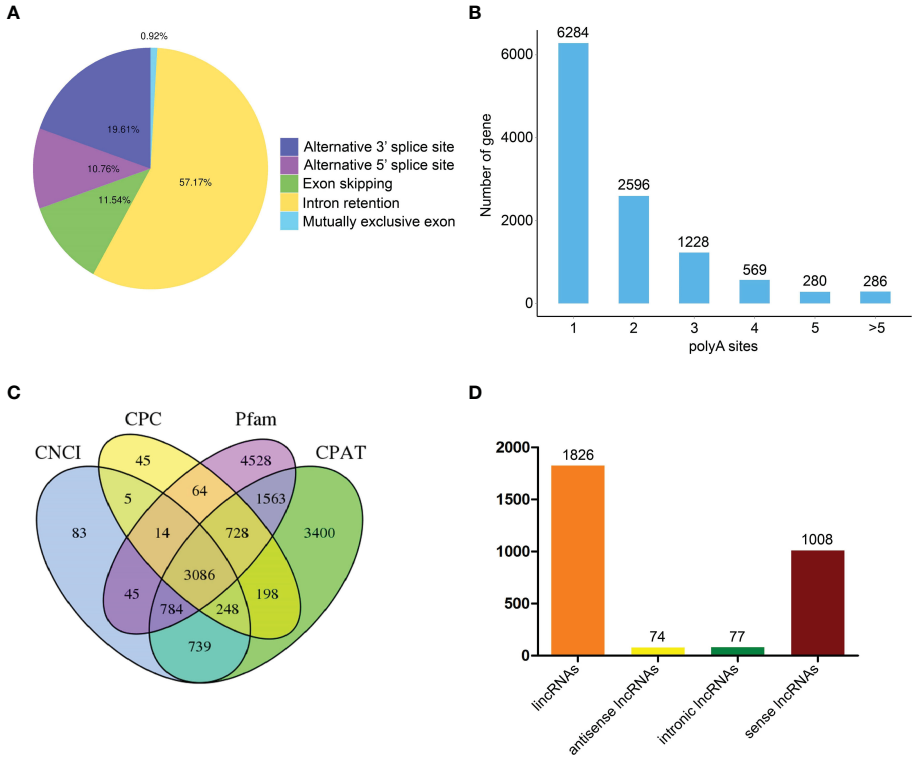

FIGURE 3
Identification of alternative splicing (AS) events, alternative polyadenylation (APA) and long non-coding RNAs (lncRNAs) based on full-length transcriptome analyses. **(A)** Number and categories of AS events. **(B)** Number of genes with different APA sites. **(C)** Number of lncRNAs based on four analysis methods. **(D)** Number of various lncRNAs.

These results indicated that the changes in *N. tabacum* gene expression were increased with the progress of PVY infection, and Fe-regulated host resistance to PVY infection mainly functioned at early stage.

3.6 GO and KEGG enrichment analyses of DEGs

To further explore the effects of PVY infection on tobacco biological processes, we analyzed the DEGs in PVY + H vs. P + H at 3 and 9 dpi using GO terms and KEGG pathway enrichment. Through GO analysis, these DEGs were mainly enriched in biological process (BP) terms 'cellular process', 'metabolic process', 'response to stimulus' and 'single-organism process', in cellular component (CC) terms 'cell', 'cell part', 'organelle' and 'membrane' and in molecular function (MF) terms 'binding', 'catalytic activity', 'transporter activity' and 'molecular transducer activity' at 3 dpi (Figure 5A and Supplementary Table 6). At 9 dpi, the enriched GO terms in BP and CC were the same as those at 3 dpi, while that in MF mainly were 'binding', 'catalytic activity', 'transporter activity' and 'nucleic acid binding transcription factor activity' (Figure 5A and Supplementary Table 6). The results of KEGG enrichment analyses showed that the DEGs were mainly enriched in 'protein processing in endoplasmic reticulum', 'glycosaminoglycan degradation', 'zeatin biosynthesis' at 3 dpi, while in 'photosynthesis-antenna proteins', 'photosynthesis' and 'porphyrin and chlorophyII metabolism' at 9 dpi (Figure 5B). To further investigate the responses in tobacco to Fe application during PVY infection, the DEGs obtained in PVY + Fe vs. PVY + H at 1 dpi and 3 dpi were analyzed through GO and KEGG enrichment. The results showed that the DEGs were mainly enriched in the GO terms under the 'cellular process', 'metabolic process', 'single-organism process' and 'response to stimulus' of BP, 'cell part', 'cell', 'organelle' and 'organelle part' of CC, 'binding', 'catalytic activity', 'transporter activity' and 'structural molecule activity' of MF at 1 dpi (Figure 5C and Supplementary Table 6). At 3 dpi, these DEGs were mainly enriched in BP terms 'cellular process', 'metabolic process', 'single-organism process' and 'response to stimulus', CC terms 'cell part', 'cell', 'organelle' and 'membrane', and MF terms 'binding', 'catalytic activity', 'transporter activity' and 'nucleic acid binding transcription factor activity' (Figure 5B and Supplementary Table 6). The KEGG enrichment analysis results indicated that the DEGs were mainly in the 'nitrogen metabolism', 'RNA degradation', 'aminoacyl-tRNA biosynthesis' and 'inositol phosphate metabolism' at 1 dpi, while in 'photosynthesis', 'protein processing in endoplasmic reticulum', 'thiamine metabolism' and 'photosynthesis-antenna proteins' at 3 dpi (Figure 5D). These results indicated that PVY infection mainly affected the protein processing, secondary metabolism and biosynthesis of tobacco at 3 dpi, and the photosynthesis of tobacco at 9 dpi. Meanwhile, we found that Fe application

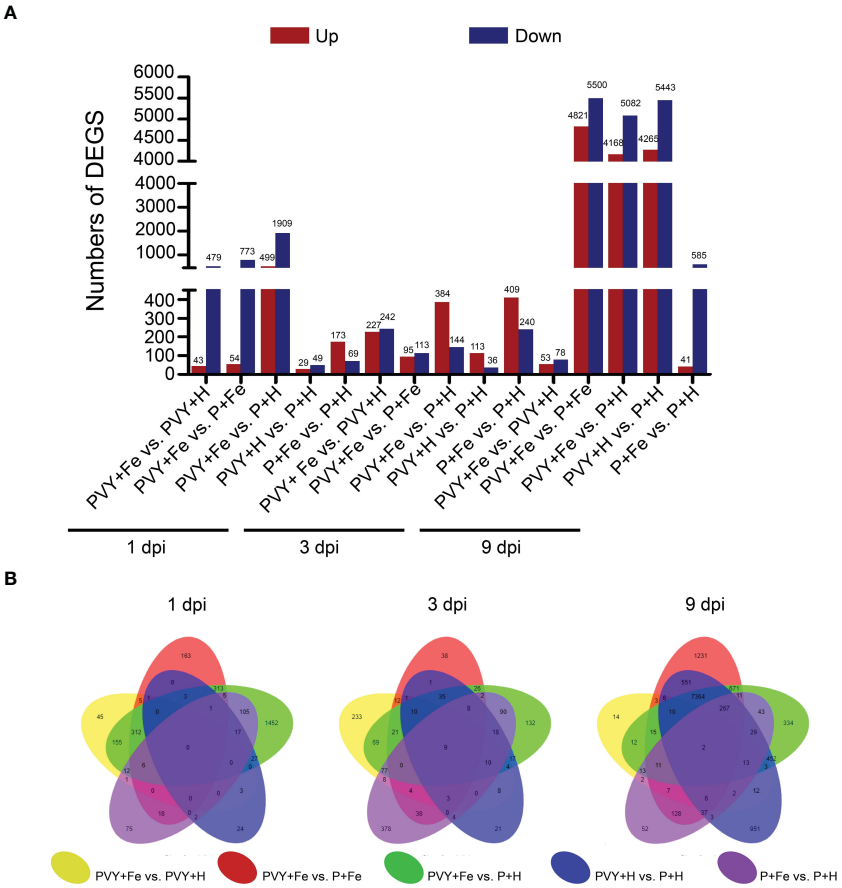

FIGURE 4
Comparative analyses of DEGs in different treatments at 1, 3, and 9 dpi. **(A)** The number of DEGs in five pairwise comparisons at 1, 3, and 9 dpi. **(B)** The overlapping DEGs in five pairwise comparisons at 1, 3, and 9 dpi showed by Venn diagram.

exhibited major regulatory effects on protein processing, photosynthesis, oxidative phosphorylation of tobacco at 3 dpi.

3.7 Coexpression network analyses of DEGs

In order to further clarify the roles of Fe application in regulating tobacco anti-PVY infection, WGCNA analysis was performed using all DEGs under different treatments, and eight gene regulatory network modules were obtained, including black module (32 DEGs), blue module (94 DEGs), pink module (33 DEGs), green module (40 DEGs), turquoise module (3,585 DEGs), red module (36 DEGs), brown module (51 DEGs) and yellow module (71 DEGs) (Figure 6A and Supplementary Table 7). The correlations of modules and modules, modules and different treatments were also analyzed (Figures 6B, C). The results showed that there was a strong correlation between turquoise module and brown module. At 9 dpi, these two modules included DEGs that were highly expressed in PVY + H and PVY + Fe (Figure 6C). Top GO and KEGG pathway analyses showed that these DEGs were mainly enriched in fatty acid metabolism, fatty acid biosynthesis, plant-pathogen interaction, protein processing in endoplasmic reticulum and photosynthesis (Supplementary Tables 8, 9). These two modules mainly included DEGs related to TFs (*NtbHLH*, *NtMYB*, *NtNAC*, *NtWRKY*), chlorophyll a-b binding protein (*NtCabs*), lipid metabolism (*NtnsLTP*, *NtFAD*, *NtPNPLA*), and molecular chaperones (*NtHSP*, *NtDnaJ*) (Supplementary Table 8, 9). At 3 dpi, the blue and pink modules were highly correlated with PVY + Fe (Figure 6C). These DEGs were mainly enriched in plant-pathogen interaction, fatty acid elongation, protein processing in endoplasmic reticulum, glutathione metabolism and plant hormone signal transduction (Supplementary Table 8, 9). These two modules mainly included DEGs related to ethylene signal transduction (*NtERFs*), TFs (*NtWRKYs*), ROS scavenging (*NtGST*, *NtSOD*), protein degradation (*NtE3*), and molecular chaperones (*NtHSP*, *NtDnaJ*) (Supplementary Tables 8, 9).

3.8 Analyses of DEGs in different pathways

Transcription factors (TFs) play important roles in the regulation of plant life activities (Dubos et al., 2010). In this study, 222 DEGs related to TFs were identified (Figure 7A and Supplementary Table 10). At 9 dpi, 103 DEGs were up-regulated, including 52 *NtWRKYs* (*NtWRKY15*, *NtWRKY2*, *NtWRKY23*,

10.3389/fpls.2023.1163679

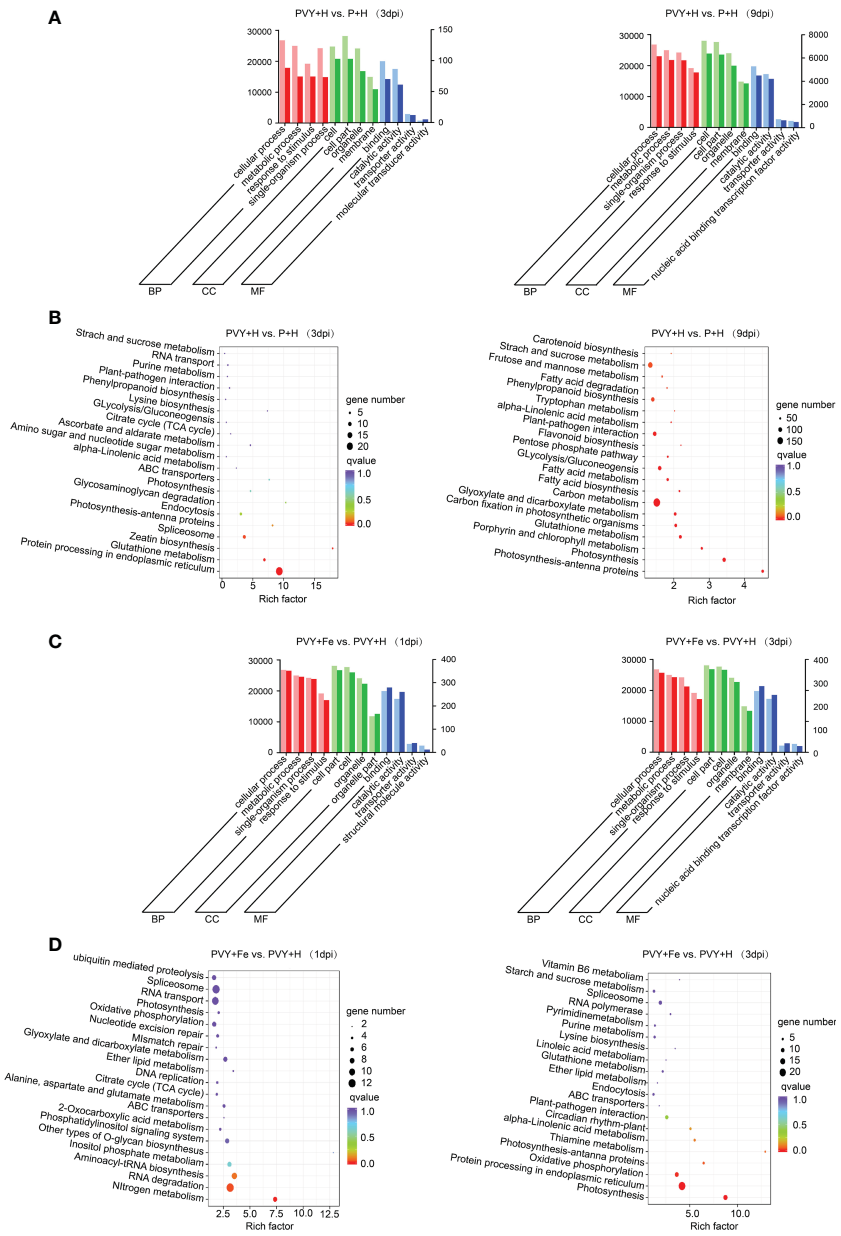

FIGURE 5
GO and KEGG enrichment analyses of DEGs. **(A)** GO analyses of DEGs in PVY + H vs. P + H at 3 and 9 dpi. **(B)** KEGG enrichment analyses of DEGs in PVY + H vs. P + H at 3 and 9 dpi. **(C)** GO analyses of DEGs in PVY + Fe vs. PVY + H at 1 and 3 dpi. **(D)** KEGG enrichment analyses of DEGs in PVY + Fe vs. PVY + H at 1 and 3 dpi.

NtWRKY26, *NtWRKY31*, *NtWRKY38*, *NtWRKY40*, *NtWRKY41*, *NtWRKY42*, *NtWRKY43*, *NtWRKY48*, *NtWRKY50*, *NtWRKY51*, *NtWRKY53*, *NtWRKY57*, *NtWRKY65*, *NtWRKY68*, *NtWRKY70*, *NtWRKY71*, *NtWRKY75*, *NtWRKY11*, *NtWRKY6*), eight *NtbHLHs* (*NtbHLH128*, *NtbHLH55*, *NtbHLH66*, *NtbHLH96*), 16 *NtNACs* (*NtNAC2*, *NtNAC72*, *NtNAC8*, *NtNAC29*), 19 *NtMYBs* (*NtMYB315*, *NtMYB330*, *NtMYB4*, *NtMYB108*, *NtMYB144*, *NtMYB1R1*, *NtMYB24*, *NtMYB3*, *NtMYB48*, *NtMYB57*), five *NtGATAs* (*NtGATA24*, *NtGATA26*) and two *NtTCP4*, while 64 DEGs were down-regulated, including 19 *NtMYBs* (*NtMYBAPL*, *NtMYB1R1*, *NtMYB306*, *NtMYB3R-1*, *NtMYB4*, *NtMYB32*, *NtMYB3*, *NtMYB86*), six *NtWRKYs* (*NtWRKY13*, *NtWRKY49*, *NtWRKY22*, *NtWRKY44*), 21 *NtbHLHs* (*NtbHLH122*, *NtbHLH35*, *NtbHLH48*, *NtbHLH49*, *NtbHLH52*, *NtbHLH63*, *NtbHLH71*, *NtbHLH74*, *NtbHLH78*, *NtbHLH79*, *NtbHLH93*, *NtbHLH96*), 12 *NtGATAs* (*NtGATA11*, *NtGATA12*, *NtGATA18*, *NtGATA4*, *NtGATA5*, *NtGATA8*), 6 *NtTCPs* (*NtTCP12*, *NtTCP14*, *NtTCP4*, *NtTCP7*) in PVY + H vs. P + H. In PVY + Fe vs. PVY + H, we found that two *NtNAC2*, one *NtMYB44* and one *NtWRKY22* were up-regulated at 3 dpi, while at 1 dpi, only one *NtbHLH30* was down-regulated. These results suggested that PVY infection seriously impacted the expression levels of many TFs at 9 dpi, while only several TFs might function in the Fe-mediated anti-PVY responses at 3 dpi.

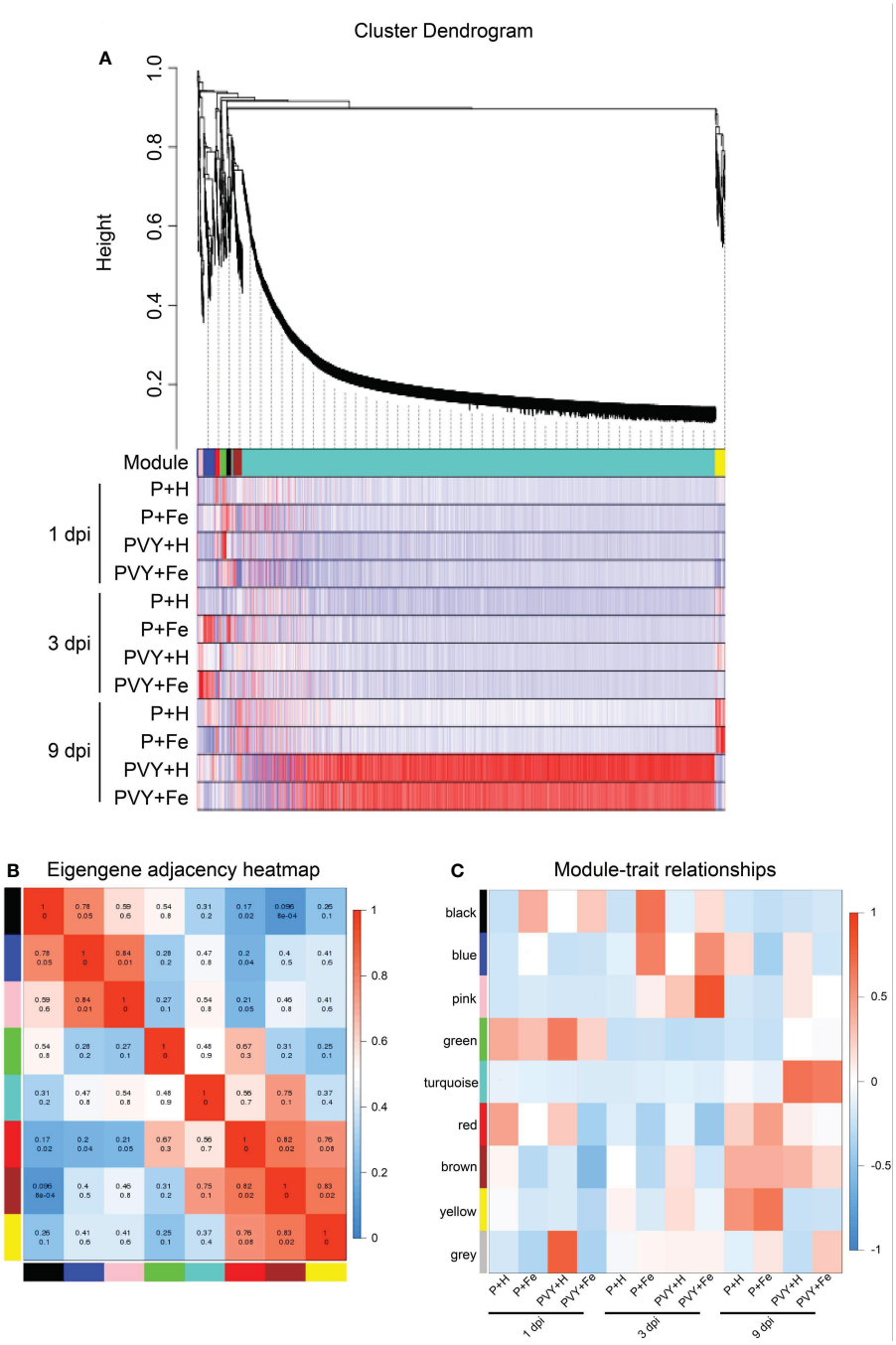

FIGURE 6
Weighted correlation network analysis (WGCNA) of DEGs. **(A)** Hierarchical cluster tree and heatmap of all DEGs. The hierarchical cluster tree shows co-expression modules identified through WGCNA. Each leaf in the tree represents one DEG. The major tree branches constitute eight modules labeled with different colors. The heatmap shows the relative expressions of the whole DEGs in different modules. **(B)** Eigengene adjacency heatmap of the eight modules shows the correlations among different modules. The darker red represents a higher correlation. The numbers in individual cells represent the correlations. **(C)** Associations between modules and traits. The colors of the modules are the same as that shown in **(A, B)**.

Virus infection often destroys chloroplasts and affects photosynthesis in plants (Zhao et al., 2016). In this study, we identified 154 photosynthesis-associated DEGs (Figure 7B and Supplementary Table 10). At 3 dpi, six DEGs were up-regulated in PVY + H vs. P + H, while at 9 dpi, a number of DEGs were down-regulated, including 61 chlorophyll a-b binding protein (*NtCab13*, *NtCab16*, *NtCab21*, *NtCab36*, *NtCab37*, *NtCab4*, *NtCab40*, *NtCab50*, *NtCab6A*, *NtCab7*, *NtCab8*, *NtCab10A*, *NtCabP4*), four PsbP-like protein (*NtPPL*), 12 oxygen-evolving enhancer protein (*NtOEE1*), two cytochrome b6 (*NtCyt-b6*), two plastocyanin (*NtPc*), five ferredoxin (*NtFd*) and 44 DEGs that involved in photosystem I (PSI) and II (PSII) assembly. In PVY + Fe vs. PVY + H, we found that *NtPSI-A2*, *NtPsaG*, *NtPc* and *NtCyt-b6* were up-regulated at 1 dpi. At 3 dpi, *NtCabs* (*NtCab16*, *NtCab40*, *NtCab50*) and *NtPsaG*

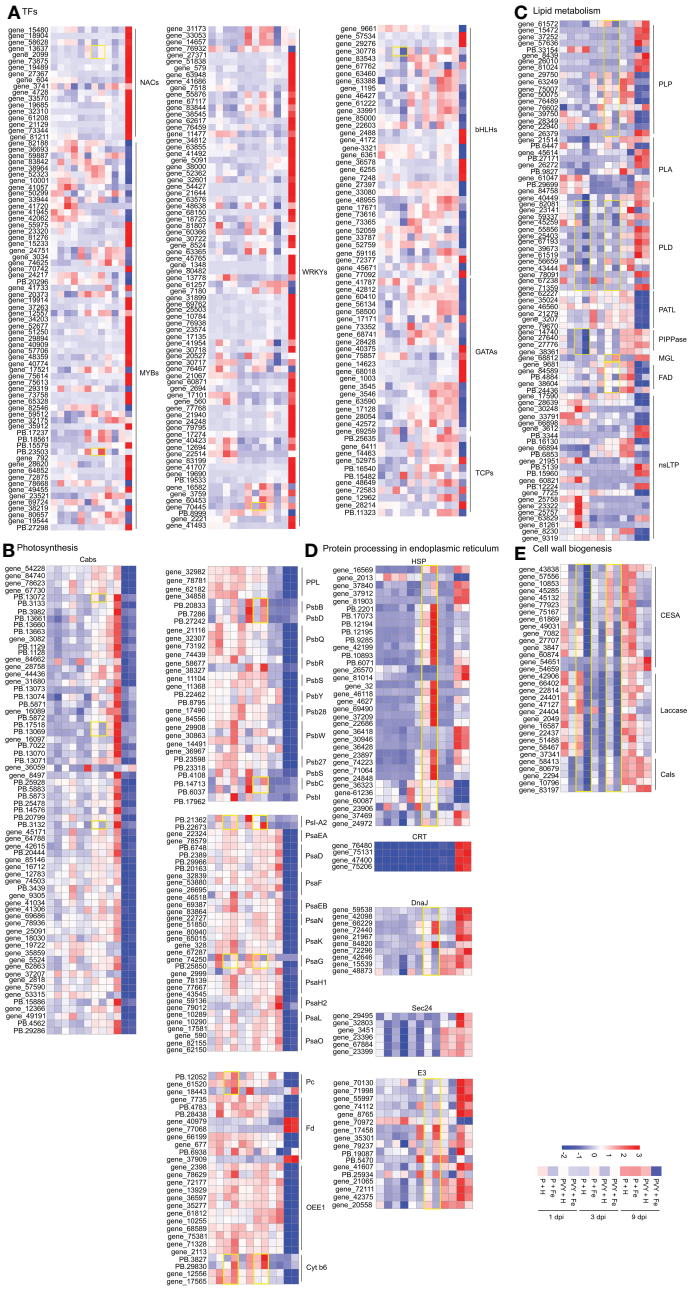

FIGURE 7
Heat map of the expression levels of DEGs involved in different pathways in tobacco. **(A)** DEGs in transcription factors. **(B)** DEGs in photosynthesis. **(C)** DEGs in lipid metabolism. **(D)** DEGs in protein processing in endoplasmic reticulum. **(E)** DEGs in cell wall biogenesis.

were down-regulated, while *NtPsbB*, *NtPsbD*, *NtPSI-A2*, *NtPsbC* and *NtCyt-b6* were up-regulated. These results indicated that PVY infection strongly suppressed photosynthesis at 9 dpi, and Fe might induce tobacco resistance to PVY infection by regulating cytochrome, chlorophyll, photosystem I and II assembly.

Besides participating in biofilm composition, lipids also play an important role in regulating plant metabolism in response to stress (Lim et al., 2017). Eighty-one DEGs identified at 1, 3 and 9 dpi were found to associate with lipid metabolism and transport (Figure 7C and Supplementary Table 10). In phospholipid metabolic pathway, we found that five patatin-like protein genes (*NtPLPs*), three phospholipase A genes (*NtPLAs*), five phospholipase D genes (*NtPLDs*) were up-regulated in PVY + H vs. P + H at 9 dpi, while seven *NtPLPs*, two *NtPLAs*, one *NtPLD* and six patellin genes (*NtPATLs*) were down-regulated. In PVY + Fe vs. PVY + H, three *NtPLDs* and four phosphoinositide phosphatase genes (*NtPIPPases*) were down-regulated at 1 dpi, only one *NtPLD* and one *NtPLP* were down-regulated at 3 dpi. In PVY + H vs. P + H at 9 dpi, monoglyceride lipase-like (*NtMGLs*) related to fatty acid synthesis were all up-regulated, and fatty-acid desaturase (*NtFADs*) related to unsaturated fatty acid synthesis were all down-regulated. Interestingly, similar changes in expression levels of *NtMGLs* and

NtFADs occurred in PVY + Fe vs. PVY + H at 3 dpi. Twenty-three non-specific lipid-transfer protein (*NtnsLTPs*) associated with lipid transport were identified. The expression levels of most of these genes were changed in PVY + H vs. P + H at 9 dpi. However, their expression was not affected by Fe application under PVY infection.

Protein processing in endoplasmic reticulum is closely related to protein folding, transport and degradation, which is essential for the normal function of proteins (Ito and Takeda, 2012). In PVY + H vs. P + H, 15 small heat shock protein (*NtHSP20s*) and two heat shock protein (*NtHSP90s*) genes were up-regulated at 3 dpi, while the expression levels of other genes involved in protein processing in endoplasmic reticulum remained unchanged. At 9 dpi, the expression levels of calreticulin (*NtCRTs*), DnaJ protein (*NtDnaJs*), most of E3 ubiquitin-protein ligase (*NtE3s*), 17 *NtHSP20s* and six *NtHSP90s* were up-regulated, while two *NtHSP20s* and three *NtHSP90* were down-regulated (Supplementary Table 10). In PVY + Fe vs. PVY + H, two *NtHSP70s*, two *NtDnaJs*, three *NtSec24s* and five *NtE3s* were down-regulated at 1 dpi. At 3 dpi, 13 *NtHSP20s*, two *NtHSP90s*, three *NtDnaJs* and six *NtE3s* were up-regulated, and two *NtDnaJs* and three *NtE3s* were down-regulated (Figure 7D and Supplementary Table 10).

Cell wall is the first defense line in plant against pathogen infection (Bacete et al., 2018). In this study, five cellulose synthase genes (*NtCESAs*) were down-regulated at 9 dpi, while the expression levels of other genes associated with cell walls biogenesis remained unchanged in PVY + H vs. P + H. In PVY + Fe vs. PVY + H, the gene expression of almost all the *NtCESAs*, *NtLaccases* and callose synthase genes (*NtCalSs*) were down-regulated at 1 dpi and 3 dpi (Figure 7E and Supplementary Table 10).

3.9 Validation of RNA-Seq data

To validate the results of RNA-Seq, four genes were randomly selected to determine their expression levels under different treatments by RT-qPCR (Figure 8). The results showed that the expression level of *NtRBCS* (gene_44833) remained unchanged at 1 dpi under four different treatments. At 3 dpi, the results showed that the expression levels of uncharacterized protein *LOC102603354* (PB.15726) and hypothetical protein *MTR_5g051050* (PB.27254) were up-regulated in P + Fe vs. P + H and PVY + Fe vs. PVY + H, while the expression levels of *NtSam3* (gene_42181) were down-regulated in PVY + Fe vs. PVY + H. These results were consistent with those of RNA-Seq.

3.10 Functional analyses of tobacco homologous genes in resistance to PVY infection in *Nicotiana benthamiana*

Transcriptome sequencing analysis showed that *NtCab-6a* was down-regulated at 3 dpi, *NtWRKY26* was up-regulated at 3 and 9 dpi, *NtHSP90* and *NtFAD3* were down-regulated at 9 dpi, and *NtnsLTP* was down-regulated in PVY + Fe vs. PVY + H (Figure 7). To further explore the genes in response to Fe application and PVY infection in tobacco, we selected homologs of these five tobacco genes for functional verification through TRV-based VIGS

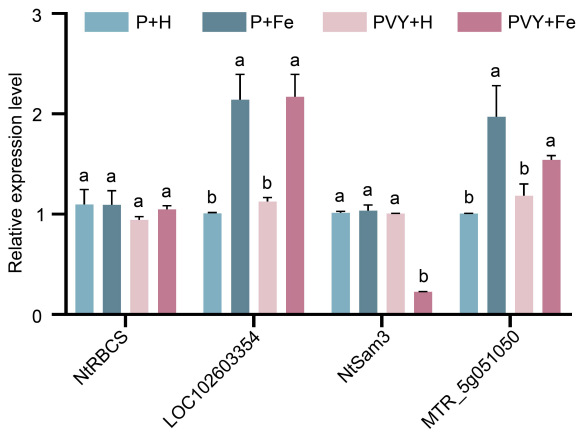

FIGURE 8
The expression levels of four genes determined by RT-qPCR under different treatments. Different lowercase letters indicate statistical difference between treatments. The statistical significances were determined using one-way analysis of variance followed by Duncan's multiple comparison test (*P* value < 0.05).

approaches in *N. benthamiana* plants. The results indicated that the leaves of *NbHSP90*-silenced plants showed severe yellowing and mottling compared with controls at 7 days post infiltration, while other gene-silenced plants showed no difference in symptoms. At 10 days post PVY inoculation, the *NbWRKY26*-, *NbHSP90*-, *NbnsLTP*- and *NbFAD3*-silenced plant leaves showed more severe curls and chlorosis than that in the control groups, while the *NbCab-6a*-silenced plant leaves were only slightly curled (Figures 9A, B). The accumulations of PVY RNAs and coat proteins were determined respectively by RT-qPCR and western blot, and the results were consistent with the symptomatic observations (Figures 9C, D). The gene silencing efficiencies were determined by RT-qPCR, and ranged from 66% to 84% (Figure 9E).

4 Discussion

Understanding the process of host plants in response to PVY infection can provide a theoretical basis for breeding of new antiviral plant using gene editing. Similarly, the study on nutrient element-induced resistance to PVY infection in host plants is also conducive to improving crop yield from the perspective of PVY control. Our laboratory has reported that leaf spraying with boron or growing in boron nutrient solution can relieve the symptoms of blood flesh disease caused by CGMMV infection in watermelon (Bi et al., 2022a). CGMMV infection affects the metabolism of carbohydrates in watermelon, and exogenous boron induces *ClNIP5;1* and *ClSWEET4* expression, restores and maintains their homeostasis (Bi et al., 2022a). In addition, boron can also induce watermelon resistance to CGMMV infection by regulating ROS-related genes, such as *ClCat*, *ClPrx* and *ClGST* (Guo et al., 2022). It has been reported that zinc treatment on tobacco leaves can improve the host resistance to TMV infection by regulating the expression of *ERF5*, which is involved in the inositol phosphate metabolism (Wang et al., 2022). Copper regulates the protein level

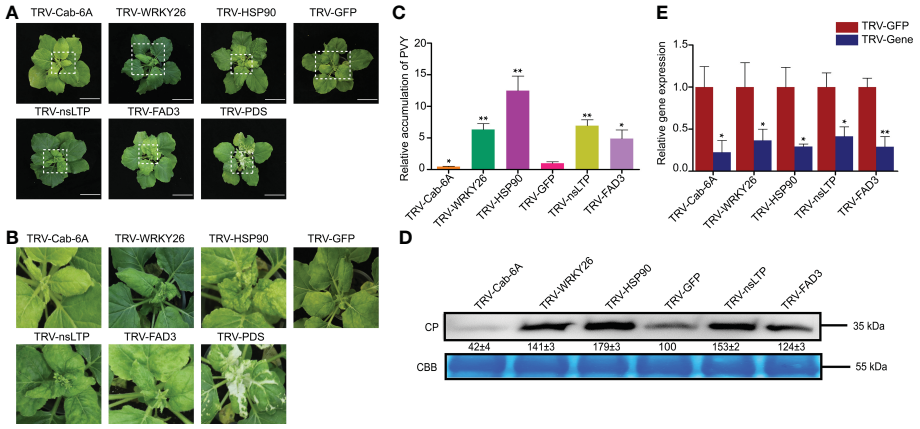

FIGURE 9
Functional analyses of five homologous genes in resistance to PVY infection through TRV-based VIGS assays in *N. benthamiana*. **(A)** Disease symptoms on different gene-silenced *N. benthamiana* plants after PVY infection. **(B)** Close-up views of upper leaves indicated by white dash boxes in **(A)**. **(C)** The accumulations of PVY genomic RNAs determined by RT-qPCR in different gene-silenced *N. benthamiana*. Asterisks indicate statistical difference between treatments, determined by the two-tailed *t* test (*, $P < 0.05$; **, $P < 0.01$). **(D)** The expression levels of PVY CP proteins in upper leaves of *N. benthamiana*. CP, coat protein; CBB, Coomassie brilliant blue. **(E)** Silencing efficiencies of target genes determined through RT-qPCR. Asterisks indicate statistical difference between treatments, determined by the two-tailed *t* test (*, $P < 0.05$; **, $P < 0.01$).

of SQUAMOSA promoter-binding-like protein 9 (SPL9) to inhibit transcriptional activation of *MIR528*, resulting in broad-spectrum resistance in *Oryza sativa* (Yao et al., 2022). In this study, the effect of PVY infection in *N. tabacum* gene expression and the molecular basis of Fe application against PVY infection were better understand through PacBio SMRT and Illumina RNA sequencing at 1, 3 and 9 dpi. Through transcriptome analyses, we found that PVY infection mainly affected the expression levels of genes related to photosynthesis and most biological processes, such as lipid metabolism and protein processing (Figure 5). The results suggested that Fe application can improve the resistance of tobacco to PVY infection mainly by regulating the expression levels of genes associated with photosynthesis, lipid metabolism, protein processing, cell wall biogenesis and TFs related to disease resistance at early stage of infection.

TFs can regulate the expression of plant genes and play important roles in response to stresses (Amorim et al., 2017). In this study, a total of 227 differentially expressed TFs from six families (NAC, WRKY, MYB, bHLH, GATA and TCP) were identified by RNA-Seq (Figure 7), which have been reported to play pivotal roles in plant immunity (Lopez et al., 2015, Behringer and Schwechheimer, 2015). At 1 dpi, we found that *NtbHLH30* and *NtGATA8* were down-regulated, while *NtNAC2*, *NtMYB4* and *NtWRKY22* were up-regulated at 3 dpi in PVY + Fe vs. PVY + H (Figure 7). Previously, it has been demonstrated that overexpression of *NbMYB4L* in *N. benthamiana* induced significant resistance to TMV (Zhu et al., 2022). It was demonstrated that *PlWRKY65* in *Paeonia lactiflora* leaves enhanced resistance to *A. tenuissima* by inducing pathogenesis-related (PR) gene expression and increasing jasmonic acid (JA) content (Wang et al., 2020). The CP protein of turnip crinkle virus (TCV) can interact with TIP, a NAC transcription factor, in *Arabidopsis* to inhibit the salicylic acid pathway and promote virus infection (Donze et al., 2014). Therefore, we hypothesized that Fe application could induce the expression of disease-resistant genes by regulating the expression of these above TFs, thereby enhancing tobacco resistance to PVY infection. In addition, silencing of *NbWRKY26* (the homologous gene of *NtWRKY22*) enhanced the accumulation of PVY in *N. benthamiana*, indicating the potential roles of *NbWRKY26* in resistance to PVY infection.

Photosynthesis is the basis of plant life activities and provides energy for all life processes (Zhao et al., 2016). Proteomic analysis of potatoes infected with PVY showed that the viral infection significantly affects the expression of chlorophyll a-b binding protein, as well as plant photosynthesis (Stare et al., 2017). In this study, we found that the expression levels of a large variety of photosynthesis related genes were down-regulated after PVY infection at 9 dpi (Figure 7). At 1 dpi, we found that *NtCyt b6*, *NtPSI-A2*, *NtPsaG* and *NtPc* were increased in PVY + Fe vs. PVY + H, while *NtCabs* were down-regulated at 3 dpi. Moreover, the roles of *NbCab-6A* in resistance to PVY infection were verified by TRV-based VIGS, and the results showed that the *NbCab-6A*-silenced plants showed higher PVY resistance. It has been reported that strawberry vein banding virus (SVBV)-encoded P1 can interact with chlorophyll a/b-binding protein of light-harvesting complex II type 1 like (LHC II-1L) and overexpression of *LHC II-1L* can accelerate SVBV infection (Xu et al., 2022). Therefore, *NbCab-6A* promoted PVY infection possibly by directly or indirectly interacting with PVY-encoded proteins, which needs to be further investigated.

There are many kinds of lipids in plants, which are mainly related to membrane structure composition (Lim et al., 2017). Multiple intermediates (i. e. PLD, PI-PLC) in lipid metabolism have been reported to participate in various stress responses by regulating JA and SA signal and inducing host PAMP-triggered immunity (PTI) responses (Lim et al., 2017). In this study, the accumulations of *NtPLD*, *NtPIPPase* and *NtnsLTP* at 1 dpi and *NtPLA*, *NtPLD* and *NtFAD* at 3 dpi were down-regulated in PVY + Fe vs. PVY + H (Figure 7). Studies have shown that overexpression of *StLTP6* in potato inhibit the expression of genes involved in RNA

silencing pathway and promote the infection of PVY and potato virus S (PVS) (Shang et al., 2022). *StLTP10*-overexpressing improve the expression of disease-resistant genes, and reduce oxidative stress to enhance the resistance to *Phytophthora infestans* (Wang et al., 2021). Fatty acid desaturation (FAD) catalyzes the formation of unsaturated fatty acids (UFA), which is a precursor for the biosynthesis of various hormones, such as JA, SA and terpenes (Xiao et al., 2022). The *fad3fad7fad8* triple mutant of *Arabidopsis* impaired SA synthesis, resulting in an enhanced sensitivity to oomycetes (Browse, 2009). In this study, we found that silencing of *NbnsLTP* or *NbFAD3* in *N. benthamiana* enhanced susceptibility to PVY infection (Figure 9). These results indicated that *NbFAD* and *NbnsLTP* play important roles in resistance to PVY infection, which may be related to their regulation on hormone signal transduction and oxidative stress response.

Protein folding and modification in plants occur mainly in the endoplasmic reticulum (Braakman and Hebert, 2013). Molecular chaperones, such as HSP and DnaJ, assist in protein folding in the plant endoplasmic reticulum, (Voellmy and Boellmann, 2007). Calreticulin (CRT) is a soluble protein of the endoplasmic reticulum lumen that recruits other molecular chaperones to facilitate glycosylated protein folding (Caramelo and Parodi, 2008). E3 ubiquitin ligase mainly degrades misfolded proteins (Al-Saharin et al., 2022). In this research, our results indicated that *NtHSP90*, *NtHSP20*, *NtDnaJ* and *NtCRT* were up-regulated at 9 dpi in PVY + H vs. P + H. Interestingly, *NtHSP90*, *NtHSP20* and *NtE3* were also up-regulated at 3 dpi in PVY + Fe vs. PVY + H (Figure 7). Through VIGS assays, we found that the accumulation of PVY RNAs and CP proteins were higher in the *NbHSP90*-silenced plants compared with that in the control plants. Previously, many studies have demonstrated that silencing of *NbHSP90* in *N. benthamiana* will lead to the reduction of *PR* gene expression level and promote the infection of potato virus X (PVX), *P. syringae* and TMV (Sangster and Queitsch, 2005). In contrast, a recent study indicated that silencing the homologous gene of potato *StHSP90.5* in *N. benthamiana* reduced PVY accumulation and induced defense-related gene expression (Li et al., 2022). Silencing *NbHSP90* gene in *N. benthamiana* could inhibit *Ralstonia solanacearum* infection by inducing *PR* gene expression (Ito et al., 2015). We hypothesized that different *NbHSP90s* of *N. benthamiana* might have diverse functions, and their roles in antiviral activity against PVY need to be further investigated.

The lignification and callose deposition of plant cell walls prevent pathogen infection and induce resistance responses by transmitting signaling molecules (Bacete et al., 2018). In this study, we found that *NtCESAs*, *NtLaccases* and *NtCaISs* involved in lignification and callose deposition were down-regulated at 9 dpi in PVY + H vs. P + H. The expression level of all *NtCESAs*, *NtLaccases* and *NtCaISs* were down-regulated at 1 and 3 dpi in PVY + Fe vs. PVY + H (Figure 7). Cellulose synthase is involved in cellulose synthesis during cell wall development in plants (Bashline et al., 2014). When *Botrytis cinerea* infected *Arabidopsis*, the expression level of cellulose synthase gene was down-regulated to enhanced its disease resistance, which may activate the immune response through signal transduction (Ramírez et al., 2011). Plant laccase regulates cell wall synthesis by participating in lignin synthesis (Wang et al., 2019). Inhibition of *GhLac1* gene expression in cotton can lead to accumulation of JA and secondary metabolites, and improve the resistance to *Verticillium dahlia* (Hu et al., 2018). Callose deposition is a part of the innate immune response of plants and callose is synthesized by callose synthase (Ostergaard et al., 2002). Silencing *CalS1* gene in citrus promoted the infection of *Xanthomonas citri* subsp. *citri* (Enrique et al., 2011). Callose deposition is closely related to abscisic acid content, which is inhibited by low abscisic acid content in *Arabidopsis* (Flors et al., 2008). In conclusion, we speculated that Fe enhanced host resistance to PVY infection possibly by inhibiting the expression of *NtCESA* and *NtLaccase* genes, thus promoting intracellular flow of cell wall signals, activating immune signal transduction, and inducing accumulation of secondary metabolites associated with resistance to disease.

Data availability statement

The datasets presented in this study can be found in online repositories. The names of the repository/repositories and accession number(s) can be found below: https://www.ncbi.nlm.nih.gov/, PRJNA903693.

Author contributions

ZX and YW conceived the research project; RL and XL completed element spray tests. CX, ZW, and MA completed transcriptome sequencing tests; CX, HG, YZ, QX, DZ, and QM performed transcriptome data analysis and gene function validation; CX and HG wrote the original draft; MA and ZW revised the manuscript; ZX and YW edited the final manuscript. All authors contributed to the article and approved the submitted version.

Funding

This research was funded by the Planning and Management Project of Sichuan Company for controlling plant vector-borne viruses, grant number SCYC202214, and the Science and Technology Project of Guizhou Qianxinan Prefectural Company for controlling plant vector-borne viruses, grant number 2022-01.

Acknowledgments

We thank Prof. Yule Liu (School of Life Sciences, Tsinghua University, Beijing, China) for providing the pTRV1 and pTRV2 vectors.

Conflict of interest

Authors CX, YZ and QX were employed by company Luzhou City Company of Sichuan Province Tobacco Company. Authors

DZ and QM were employed by company Guizhou Qianxinan Prefectural Tobacco Company.

The remaining authors declare that the research was conducted in the absence of any commercial or financial relationships that could be construed as a potential conflict of interest.

Publisher's note

All claims expressed in this article are solely those of the authors and do not necessarily represent those of their affiliated organizations, or those of the publisher, the editors and the reviewers. Any product that may be evaluated in this article, or claim that may be made by its manufacturer, is not guaranteed or endorsed by the publisher.

Supplementary material

The Supplementary Material for this article can be found online at: https://www.frontiersin.org/articles/10.3389/fpls.2023.1163679/full#supplementary-material

References

Abdel-Ghany, S. E., Hamilton, M., Jacobi, J. L., Ngam, P., Devitt, N., Schilkey, F., et al. (2016). A survey of the sorghum transcriptome using single-molecule long reads. *Nat. Commun.* 7, 11706. doi: 10.1038/ncomms11706

Al-Saharin, R., Hellmann, H., and Mooney, S. (2022). Plant E3 ligases and their role in abiotic stress response. *Cells.* 11, 890. doi: 10.3390/cells11050890

Amorim, L. L. B., da Fonseca Dos Santos, R., Neto, J. P. B., Guida-Santos, M., Crovella, S., and Benko-Iseppon, A. M. (2017). Transcription factors involved in plant resistance to pathogens. *Curr. Protein Pept. Sci.* 18, 335–351. doi: 10.2174/1389203717666160619185308

Arnaud, N., Murgia, I., Boucherez, J., Briat, J. F., Cellier, F., and Gaymard, F. (2006). An iron-induced nitric oxide burst precedes ubiquitin-dependent protein degradation for *Arabidopsis AtFer1* ferritin gene expression. *J. Biol. Chem.* 281, 23579–23588. doi: 10.1074/jbc.M602135200

Bacete, L., Melida, H., Miedes, E., and Molina, A. (2018). Plant cell wall-mediated immunity: Cell wall changes trigger disease resistance responses. *Plant J.* 93, 614–636. doi: 10.1111/tpj.13807

Bashline, L., Li, S., and Gu, Y. (2014). The trafficking of the cellulose synthase complex in higher plants. *Ann. Bot.* 114, 1059–1067. doi: 10.1093/aob/mcu040

Behringer, C., and Schwechheimer, C. (2015). B-GATA transcription factors - insights into their structure, regulation, and role in plant development. *Front. Plant Sci.* 6. doi: 10.3389/fpls.2015.00090

Bi, X., Guo, H., Li, X., Jiang, D., Dong, H., Zhang, Y., et al. (2022a). Suppression of cucumber green mottle mosaic virus infection by boron application: From the perspective of nutrient elements and carbohydrates. *J. Agric. Food Chem.* 70, 12270–12286. doi: 10.1021/acs.jafc.2c03069

Bi, X., Guo, H., Li, X., Zheng, L., An, M., Xia, Z., et al. (2022b). A novel strategy for improving watermelon resistance to cucumber green mottle mosaic virus by exogenous boron application. *Mol. Plant Pathol.* 23, 1361–1380. doi: 10.1111/mpp.13234

Braakman, I., and Hebert, D. N. (2013). Protein folding in the endoplasmic reticulum. *Cold Spring Harbor Perspect. Biol.* 5, a013201. doi: 10.1101/cshperspect

Browse, J. (2009). The power of mutants for investigating jasmonate biosynthesis and signaling. *Phytochemistry.* 70, 1539–1546. doi: 10.1016/j.phytochem

Cai, L., Cai, L., Jia, H., Liu, C., Wang, D., and Sun, X. (2020). Foliar exposure of Fe_3O_4 nanoparticles on *Nicotiana benthamiana*: Evidence for nanoparticles uptake, plant growth promoter and defense response elicitor against plant virus. *J. Hazard Mater.* 393, 122415. doi: 10.1016/j.jhazmat

Caramelo, J. J., and Parodi, A. J. (2008). Getting in and out from calnexin/calreticulin cycles. *J. Biol. Chem.* 283, 10221–10225. doi: 10.1074/jbc

Chen, W., Zhao, L., Liu, L., Li, X., Li, Y., Liang, G., et al. (2021). Iron deficiency-induced transcription factors bHLH38/100/101 negatively modulate flowering time in *Arabidopsis thaliana*. *Plant Sci.* 308, 110929. doi: 10.1016/j.plantsci.2021.110929

Chhabra, R., Saha, A., Chamani, A., Schneider, N., Shah, R., and Nanjundan, M. (2020). Iron pathways and iron chelation approaches in viral, microbial, and fungal infections. *Pharmaceuticals.* 13, 275. doi: 10.3390/ph13100275

Donze, T., Qu, F., Twigg, P., and Morris, T. J. (2014). Turnip crinkle virus coat protein inhibits the basal immune response to virus invasion in *Arabidopsis* by binding to the NAC transcription factor TIP. *Virology.* 20, 207–214. doi: 10.1016/j.virol.2013.11.018

Dubos, C., Stracke, R., Grotewold, E., Weissharr, B., Martin, C., and Lepiniec, L. (2010). MYB transcription factors in *Arabidopsis*. *Trends Plant Sci.* 15, 573–581. doi: 10.1016/j.tplants.2010.06.005

Enrique, R., Siciliano, F., Favaro, M. A., Gerhardt, N., Roeschlin, R., Rigano, L., et al. (2011). Novel demonstration of RNAi in citrus reveals importance of citrus callose synthase in defence against *Xanthomonas citri* subsp. citri. *Plant Biotechnol. J.* 9, 394–407. doi: 10.1111/j.1467-7652.2010.00555.x

Flors, V., Ton, J., van Doorn, R., Jakab, G., García-Agustín, P., and Mauch-Mani, B. (2008). Interplay between JA, SA and ABA signalling during basal and induced resistance against pseudomonas syringae and *Alternaria brassicicola*. *Plant J.* 54, 81–92. doi: 10.1111/j.1365-313X.2007.03397.x

Foissac, S., and Sammeth, M. (2007). ASTALAVISTA: Dynamic and flexible analysis of alternative splicing events in custom gene datasets. *Nucleic Acids Res.* 35, W297–W299. doi: 10.1093/nar/gkm311

Fu, D., Li, J., Yang, X., Li, W., Zhou, Z., Xiao, S., et al. (2022). Iron redistribution induces oxidative burst and resistance in maize against *Curvularia lunata*. *Planta.* 256, 46. doi: 10.1007/s00425-022-03963-7

Garcia-Ruiz, H. (2019). Host factors against plant viruses. *Mol. Plant Pathol.* 20, 1588–1601. doi: 10.1111/mpp.12851

Gibbs, A. J., Hajizadeh, M., Ohshima, K., and Jones, R. A. C. (2020). The potyviruses: An evolutionary synthesis is emerging. *Viruses.* 12, 132. doi: 10.3390/v12020132

Graziano, M., and Lamattina, L. (2007). Nitric oxide accumulation is required for molecular and physiological responses to iron deficiency in tomato roots. *Plant J.* 52, 949–960. doi: 10.1111/j.1365-313X.2007.03283.x

Guo, H., Bi, X., Wang, Z., Jiang, D., Cai, M., An, M., et al. (2022). Reactive oxygen species-related genes participate in resistance to cucumber green mottle mosaic virus infection regulated by boron in *Nicotiana benthamiana* and watermelon. *Front. Plant Sci.* 13. doi: 10.3389/fpls.2022.1027404

Guo, Y., Jia, M. A., Yang, Y., Zhan, L., Cheng, X., Cai, J., et al. (2017). Integrated analysis of tobacco miRNA and mRNA expression profiles under PVY infection provides insight into tobacco-PVY interactions. *Sci. Rep.* 7, 4895. doi: 10.1038/s41598-017-05155-w

Gyana, R., and Rout, S. (2015). Role of iron in plant growth and metabolism. *Rev. Agric. Sci.* 3, 1–24. doi: 10.7831/ras.3.1

Hendrix, S., Verbruggen, N., Cuypers, A., and Meyer, A. J. (2022). Essential trace metals in plant responses to heat stress. *J. Exp. Bot.* 73, 1775–1788. doi: 10.1093/JXB/ERAB507

Hu, Q., Min, L., Yang, X., Jin, S., Zhang, L., Li, Y., et al. (2018). Laccase *GhLac1* modulates broad-spectrum biotic stress tolerance *via* manipulating phenylpropanoid pathway and jasmonic acid synthesis. *Plant Physiol.* 176, 1808–1823. doi: 10.1104/pp.17.01628

Ito, M., Ohnishi, K., Hikichi, Y., and Kiba, A. (2015). Molecular chaperons and co-chaperons, Hsp90, RAR1, and SGT1 negatively regulate bacterial wilt disease caused by *Ralstonia solanacearum* in *Nicotiana benthamiana*. *Plant Signal. Behav.* 10, e970410. doi: 10.4161/15592316.2014.970410

Ito, Y., and Takeda, Y. (2012). Analysis of glycoprotein processing in the endoplasmic reticulum using synthetic oligosaccharides. *Proc. Japan Academy.* 88, 31–40. doi: 10.2183/pjab.88.31

Kong, L., Zhang, Y., Ye, Z. Q., Liu, X. Q., Zhao, S. Q., Wei, L., et al. (2007). CPC: Assess the protein-coding potential of transcripts using sequence features and support vector machine. *Nucleic Acids Res.* 35, W345–W349. doi: 10.1093/nar/gkm391

Korlach, J., Gedman, G., Kingan, S. B., Chin, C. S., Howard, J. T., Audet, J. N., et al. (2017). *De novo* PacBio long-read and phased avian genome assemblies correct and add to reference genes generated with intermediate and short reads. *GigaSci.* 6, 1–16. doi: 10.1093/gigascience/gix085

Langfelder, P., Horvath, S., Langfelder, P., and Horvath, S. (2009). WGCNA: An r package for weighted correlation network analysis. *BMC Bioinf.* 9, 559. doi: 10.1186/1471-2105-9-559

Lebaron, C., Rosado, A., Sauvage, C., Gauffier, C., German-Retana, S., Moury, B., et al. (2016). A new *eIF4E1* allele characterized by RNAseq data mining is associated with resistance to potato virus y in tomato albeit with a low durability. *J. Gen. Virol.* 97, 3063–3072. doi: 10.1099/jgv.0.000609

Li, K., Chen, R., Tu, Z., Nie, X., Song, B., He, C., et al. (2022). Global screening and functional identification of major HSPs involved in PVY infection in potato. *Genes.* 13, 566. doi: 10.3390/genes13040566

Lim, G. H., Singhal, R., Kachroo, A., and Kachroo, P. (2017). Fatty acid- and lipid-mediated signaling in plant defense. *Annu. Rev. PhytoPathol.* 55, 505–536. doi: 10.1146/annurev-phyto-080516-035406

Lopez, J. A., Sun, Y., Blair, P. B., and Mukhtar, M. S. (2015). TCP Three-way handshake: Linking developmental processes with plant immunity. *Trends Plant Sci.* 20, 238–245. doi: 10.1016/j.tplants.2015.01.005

Mao, X., Cai, T., Olyarchuk, J., and Wei, L. (2005). Automated genome annotation and pathway identification using the KEGG orthology (KO) as a controlled vocabulary. *Bioinformatics.* 21, 3787–3793. doi: 10.1093/bioinformatics/bti430

Merchant, S. S. (2010). The elements of plant micronutrients. *Plant Physiol.* 154, 512–515. doi: 10.1104/pp.110.161810

Ostergaard, L., Petersen, M., Mattsson, O., and Mundy, J. (2002). An *Arabidopsis* callose synthase. *Plant Mol. Biol.* 49, 559–566. doi: 10.1023/a:1015558231400

Peng, Z., He, Y., Parajuli, S., You, Q., Wang, W., Bhattarai, K., et al. (2021). Integration of early disease-resistance phenotyping, histological characterization, and transcriptome sequencing reveals insights into downy mildew resistance in impatiens. *Hortic. Res.* 8, 108. doi: 10.1038/s41438-021-00543-w

Ramírez, V., García-Andrade, J., and Vera, P. (2011). Enhanced disease resistance to *Botrytis cinerea* in *myb46* arabidopsis plants is associated to an early down-regulation of *CesA* genes. *Plant Signal. Behav.* 6, 911–913. doi: 10.4161/psb.6.6.15354

Ross, B. T., Zidack, N., McDonald, R., and Flenniken, M. L. (2022). Transcriptome and small RNA profiling of potato virus y infected potato cultivars, including systemically infected russet Burbank. *Viruses.* 14, 523. doi: 10.3390/v14030523

Rybicki, E. P. (2015). A top ten list for economically important plant viruses. *Arch. Virology.* 160, 17–20. doi: 10.1007/s00705-014-2295-9

Sangster, T. A., and Queitsch, C. (2005). The HSP90 chaperone complex, an emerging force in plant development and phenotypic plasticity. *Curr. Opin. Plant Biol.* 8, 86–92. doi: 10.1016/j.pbi

Shang, K., Xu, Y., Cao, W., Xie, X., Zhang, Y., Zhang, J., et al. (2022). Potato (*Solanum tuberosum* l.) non-specific lipid transfer protein StLTP6 promotes viral infection by inhibiting virus-induced RNA silencing. *Planta.* 256, 54. doi: 10.1007/s00425-022-03948-6

Stare, T., Stare, K., Weckwerth, W., Wienkoop, S., and Gruden, K. (2017). Comparison between proteome and transcriptome response in potato (*Solanum tuberosum* l.) leaves following potato virus y (PVY) infection. *Proteomes.* 5, 14. doi: 10.3390/proteomes5030014

Sun, L., Luo, H., Bu, D., Zhao, G., Yu, K., Zhang, C., et al. (2013). Utilizing sequence intrinsic composition to classify protein-coding and long non-coding transcripts. *Nucleic Acids Res.* 41, e166. doi: 10.1093/nar/gkt646

Unamba, C. I., Nag, A., and Sharma, R. K. (2015). Next generation sequencing technologies: The doorway to the unexplored genomics of non-model plants. *Front. Plant Sci.* 16, 1074. doi: 10.3389/fpls.2015.01074

Voellmy, R., and Boellmann, F. (2007). Chaperone regulation of the heat shock protein response. *Adv. Exp. Med. Biol.* 594, 89–99. doi: 10.1007/978-0-387-39975-1_9

Wang, C., Gao, H., Chu, Z., Ji, C., Xu, Y., Cao, W., et al. (2021). A nonspecific lipid transfer protein, StLTP10, mediates resistance to *Phytophthora infestans* in potato. *Mol. Plant Pathol.* 22, 48–63. doi: 10.1111/mpp.13007

Wang, X., Li, J., Guo, J., Qiao, Q., Guo, X., and Ma, Y. (2020). The WRKY transcription factor *PlWRKY65* enhances the resistance of *Paeonia lactiflora* (herbaceous peony) to *Alternaria tenuissima*. *Hortic. Res.* 7, 57. doi: 10.1038/s41438-020-0267-7

Wang, Q., Li, G., Zheng, K., Zhu, X., Ma, J., Wang, D., et al. (2019). The soybean laccase gene family: Evolution and possible roles in plant defense and stem strength selection. *Genes.* 10, 701. doi: 10.3390/genes10090701

Wang, L., Park, H. J., Dasari, S., Wang, S., Kocher, J. P., and Li, W. (2013). CPAT: Coding-potential assessment tool using an alignment-free logistic regression model. *Nucleic Acids Res.* 41, e74. doi: 10.1093/nar/gkt006

Wang, J., Zou, A., Xiang, S., Liu, C., Peng, H., Wen, Y., et al. (2022). Transcriptome analysis reveals the mechanism of zinc ion-mediated plant resistance to TMV in *Nicotiana benthamiana*. *Pesticide. Biochem. Physiol.* 184, 105100. doi: 10.1016/j.pestbp.2022.105100

Xiao, R., Zou, Y., Guo, X., Li, H., and Lu, H. (2022). Fatty acid desaturases (FADs) modulate multiple lipid metabolism pathways to improve plant resistance. *Mol. Biol. Rep.* 49, 9997–10011. doi: 10.1007/s11033-022-07568-x

Xu, S., Zhang, X., Xu, K., Wang, Z., Zhou, X., Jiang, L., et al. (2022). Strawberry vein banding virus movement protein P1 interacts with light-harvesting complex II type 1 like of *Fragaria vesca* to promote viral infection. *Front. Microbiol.* 13. doi: 10.3389/fmicb.2022.884044

Yang, X., Li, Y., and Wang, A. (2021). Research advances in *Potyviruses*: From the laboratory bench to the field. *Annu. Rev. PhytoPathol.* 25, 1–29. doi: 10.1146/annurev-phyto-020620-114550

Yao, S., Kang, J., Guo, G., Yang, Z., Huang, Y., Lan, Y., et al. (2022). The key micronutrient copper orchestrates broad-spectrum virus resistance in rice. *Sci. Adv.* 8, eabm0660. doi: 10.1126/sciadv.abm0660

Young, M., Wakefield, M., Smyth, G., and Oshlack, A. (2010). Gene ontology analysis for RNA-seq: Accounting for selection bias. *Genome Biol.* 11, R14. doi: 10.1186/gb-2010-11-2-r14

Zhao, J., Zhang, X., Hong, Y., and Liu, Y. (2016). Chloroplast in plant-virus interaction. *Front. Microbiol.* 7. doi: 10.3389/fmicb.2016.01565

Zhu, T., Zhou, X., Zhang, J. L., Zhang, W. H., Zhang, L. P., You, C. X., et al. (2022). Ethylene-induced *NbMYB4L* is involved in resistance against tobacco mosaic virus in *Nicotiana benthamiana*. *Mol. Plant Pathol.* 23, 16–31. doi: 10.1111/mpp.13139

frontiers | Frontiers in Plant Science

TYPE Original Research
PUBLISHED 11 April 2023
DOI 10.3389/fpls.2023.1141700

OPEN ACCESS

EDITED BY
Laura Medina-Puche,
University of Tübingen, Germany

REVIEWED BY
Walter Chitarra,
Council for Agricultural and Economics Research (CREA), Italy
Ales Eichmeier,
Mendel University in Brno, Czechia

*CORRESPONDENCE
Florence Fontaine
florence.fontaine@univ-reims.fr

†These authors share first authorship

‡These authors share last authorship

SPECIALTY SECTION
This article was submitted to Plant Pathogen Interactions, a section of the journal Frontiers in Plant Science

RECEIVED 10 January 2023
ACCEPTED 15 March 2023
PUBLISHED 11 April 2023

CITATION
Trouvelot S, Lemaitre-Guillier C, Vallet J, Jacquens L, Douillet A, Harir M, Larignon P, Roullier-Gall C, Schmitt-Kopplin P, Adrian M and Fontaine F (2023) Sodium arsenite-induced changes in the wood of esca-diseased grapevine at cytological and metabolomic levels.
Front. Plant Sci. 14:1141700.
doi: 10.3389/fpls.2023.1141700

Sodium arsenite-induced changes in the wood of esca-diseased grapevine at cytological and metabolomic levels

Sophie Trouvelot[1†], Christelle Lemaitre-Guillier[1†], Julie Vallet[2], Lucile Jacquens[1], Antonin Douillet[1], Mourad Harir[3,4], Philippe Larignon[5], Chloé Roullier-Gall[4], Philippe Schmitt-Kopplin[4], Marielle Adrian[1‡] and Florence Fontaine[2*‡]

[1]Agroécologie, Centre National de la Recherche Scientifique (CNRS), Institut National de Recherche pour l'agriculture, l'alimentation et l'environnement (INRAE), Institut Agro Dijon, Univ. Bourgogne, Univ. Bourgogne Franche-Comté, Dijon, France, [2]Université de Reims Champagne-Ardenne, Unité de recherche Résistance Induite et Bioprotection des Plantes (RIBP) USC Institut National de Recherche pour l'agriculture, l'alimentation et l'environnement (INRAE) 1488, Reims, France, [3]Research Unit Analytical BioGeoChemistry, Helmholtz Munich, Neuherberg, Germany, [4]Chair Analyt Food Chem, Technical University Munich, Freising, Germany, [5]Institut Français de la Vigne et du Vin (IFV) Pôle Rhône-Méditerranée, Rodilhan, France

In the past, most grapevine trunk diseases (GTDs) have been controlled by treatments with sodium arsenite. For obvious reasons, sodium arsenite was banned in vineyards, and consequently, the management of GTDs is difficult due to the lack of methods with similar effectiveness. Sodium arsenite is known to have a fungicide effect and to affect the leaf physiology, but its effect on the woody tissues where the GTD pathogens are present is still poorly understood. This study thus focuses on the effect of sodium arsenite in woody tissues, particularly in the interaction area between asymptomatic wood and necrotic wood resulting from the GTD pathogens' activities. Metabolomics was used to obtain a metabolite fingerprint of sodium arsenite treatment and microscopy to visualize its effects at the histo-cytological level. The main results are that sodium arsenite impacts both metabolome and structural barriers in plant wood. We reported a stimulator effect on plant secondary metabolites in the wood, which add to its fungicide effect. Moreover, the pattern of some phytotoxins is affected, suggesting the possible effect of sodium arsenite in the pathogen metabolism and/or plant detoxification process. This study brings new elements to understanding the mode of action of sodium arsenite, which is useful in developing sustainable and eco-friendly strategies to better manage GTDs.

KEYWORDS

Chardonnay, trunk diseases, metabolites, toxins, histology, autofluorescence, vineyard, plant defenses

Introduction

Viticulture is of great economic importance worldwide with an estimated area of 7.3 million hectares and a market of nearly 30 billion euros (OIV, April 2020, https://oiv.int/). However, it faces major problems including climate change and protection against diseases that affect yield, wine quality, and the safeguarding of vineyards. Most cryptogamic diseases are controlled by fungicides, some of which are known for their health and environmental risks as recently reported by Dumitriu Gabur et al. (2022). Related to these risks, some fungicides are prohibited, leaving ineffective solutions available for some diseases, especially grapevine trunk diseases (GTDs). These diseases were controlled by a pesticide based on sodium arsenite, banned in 2001 in France and 2003 in other European countries (Spinosi et al., 2009). This pesticide was strongly effective against esca disease, one of the three main GTDs with *Botryosphaeria* dieback and *Eutypa* dieback (Larignon et al., 2008; Larignon, 2016). These GTDs are considered to be the most destructive grapevine diseases in the world, leading to an alteration of vineyard heritage and serious economic losses in the wine industry (De la Fuente et al., 2016). The estimate of their incidence over 6 years reaches more than 10% of the 329 French studied vineyards for both esca disease and *Botryosphaeria* dieback and 25% for *Eutypa* dieback (Bruez et al., 2013). Considering a replacement of only 1% of plants per year, the overall annual global financial cost was estimated in 2012 at 1.132 billion euros, for example (Hofstetter et al., 2012).

Esca disease is a complex of diseases caused by several fungi, such as *Phaeoacremonium minimum*, *Phaeomoniella chlamydospora*, and *Fomitiporia mediterranea* (Surico et al., 2008; Surico, 2009). These pathogens are localized in the woody tissues of perennial organs and, to a lesser extent, in lignified 1-year-old canes but absent in the leaves where symptoms are expressed (Larignon and Dubos, 1997; Graniti et al., 2000; Fourié and Halleen, 2002; Retief et al., 2006; Bortolami et al., 2021). Leaf external symptoms consist of a chronic form characterized by the appearance of typical tiger-like necrosis and chlorosis. Apoplectic form turns to sudden wilting of leaves followed by rapid death of one or more canes or even the entire plant (Mugnai et al., 1999; Mondello et al., 2018a). The most common wood symptoms include degradation, namely, white rot and multiple discoloration patterns, such as i) black streaks in the wood involving one or more xylem vessels and ii) areas of brown and dark necrosis circumscribing the pith, which is most frequently observed (Larignon and Dubos, 2001; Lecomte et al., 2012; Mondello et al., 2018a).

Until 2003 in European countries, GTDs, especially esca disease, were limited in vineyards by the use of sodium arsenite (Spinosi et al., 2009). Since the banning of this fungicide, due to its high toxicity to human health (Saha et al., 1999; Spinosi et al., 2009), no effective treatment is now available to control them. Other chemical compounds such as triazoles (Dula et al., 2007; Gramaje et al., 2009) or Fosetyl-Al® (Di Marco et al., 2011; Díaz and Latorre, 2013) have been tested, but their effectiveness depends in particular on the application mode, location (nursery or vineyard), and the targeted pathogen (for review, see Gramaje et al., 2018; Mondello et al., 2018a). Recently, a copper-based product combined with a carrier, hydroxyapatite, and plant extracts have been evaluated (Battiston et al., 2021; Mondello et al., 2021; Reis et al., 2021; Mondello et al., 2022; Reis et al., 2022) as well as aqueous ozone (Romeo-Oliván et al., 2021). Meanwhile, preventive practices such as delayed pruning and application of pruning-wound protectants (Weber et al., 2007; Rolshausen et al., 2010), and "curative" practices such as trunk surgery by removing necrotic wood (Cholet et al., 2021; Pacetti et al., 2021) and regrafting are being developed (for review Mondello et al., 2018b). Finally, biocontrol strategies including the use of species of *Trichoderma* (Di Marco et al., 2021; Leal et al., 2021), *Pythium oligandrum* (Gerbore et al., 2013; Yacoub et al., 2016; Yacoub et al., 2020), and *Bacillus subtilis* or other bacteria (Halleen et al., 2010; Haidar et al., 2016; Pinto et al., 2018; Leal et al., 2021) are also being investigated and are still in progress. However, to date, all these strategies remain insufficient to control GTDs, especially esca disease, compared to sodium arsenite. Therefore, a better understanding of the sodium arsenite actions is needed to provide alternative eco-friendly solutions to prevent or limit GTD development and incidence.

Previous studies on the mode of action of sodium arsenite are rather limited and mainly focused on its impact on GTD pathogens (Da Costa, 1971; Carbonell-Barrachina et al., 1997; Larignon et al., 2008) and dynamics *in planta* after application (Carbonell-Barrachina et al., 1997; Larignon et al., 2008). Between 2013 and 2016, a global project dedicated to the characterization of the action of sodium arsenite was carried out in order to propose a mimic strategy against GTDs, of similar effectiveness but with lower environmental risks. This project particularly focused on the impact of sodium arsenite on i) the wood microbiota including GTD pathogens and ii) plant physiology at cytological, transcriptomic, and metabolomic levels. Regarding wood microbiota, Bruez et al. (2020) reported a stronger effect of sodium arsenite treatment on the fungal community compared to the bacterial one and highlighted its effectiveness, especially against *F. mediterranea*—an esca pathogen responsible for the necrotic white-rot tissues (Mugnai et al., 1999). On grapevine physiology, Songy et al. (2019) observed first a decrease and then stimulation of photosynthesis with simultaneous activation of some grapevine defense responses. The objective of this paper focuses on the effect of sodium arsenite in woody tissues, particularly in the interaction area between healthy wood and necrotic wood resulting from the GTD pathogens' activities. A combination of

Abbreviations: Asn, Vines treated with sodium arsenite and without Esca foliar symptoms (Asn = Arsenite); CH, Vines not treated with sodium arsenite and without Esca foliar symptom (CH = Control Healthy); CCh, Vines not treated with sodium arsenite, expressing chronic Esca foliar symptoms (CCh = Control Chronic); CA, Vines not treated with sodium arsenite, expressing apoplectic foliar symptoms (CA = Control Apoplectic); WH, Healthy wood, without necrosis; WS, Streaking wood, showing very localized (punctual) brown-black necrosis points; WI, Wood from the interaction area between unaltered and altered wood; GTD, Grapevine Trunk Disease; cv, cultivar; BBCH, Biologische Bundesanstalt, Bundessortenamt und CHemische Industrie; FT-ICR MS, Fourier Transform - Ion Cyclotron Resonance Mass Spectrometry; LSSIM, Leaf Stripe Symptoms-Inducing Molecules.

global and targeted approaches was used: metabolomics to obtain a metabolite fingerprint of sodium arsenite treatment and microscopy to visualize its effects at the histo-cytological level. Overall, these studies will provide useful insights into the process of protection by sodium arsenite against GTDs.

Materials and methods

Plant material

In 2013, spotting was performed in a 27-year-old vineyard of cv. Chardonnay grafted on SO4 rootstock planted at 7,575 plants/ha. Plants were vertically trained and pruned according to the Chablis method. The vineyard is located in the province of Epernay (Avize, France, GPS coordinates: 48°58′29″N, 04°00′46″E) and is owned by the professional school "Lycée VitiCampus". It is characterized by an average annual temperature of 10.8°C and 480 mm of annual precipitation, and the soil is clay and sandy loam. No treatment with sodium arsenite has been performed in this experimental plot in the past. Fifteen plants were selected and labeled: five were apparently healthy, without foliar esca disease symptoms, and 10 were diseased, with esca disease chronic foliar symptoms as described by Mugnai et al. (1999) and Mondello et al. (2018a). Among the latter, five were treated the next winter year (2014) with sodium arsenite. For both conditions, treated and not treated by sodium arsenite, a classical conventional phytosanitary itinerary was applied against downy mildew and powdery mildew. For the general diffusion of esca, the annual incidence was very low and close to 2% as globally observed in the Champagne vineyard (Mondello et al., 2022).

Treatment and sampling

The following year (2014), five plants that were chronically diseased in 2013 were selected and treated with sodium arsenite (Pyralesca RS) at 1,250 g/hL until streaming, at the end of winter after pruning (10 March 2014), and before bud bursting, BBCH 00 (Meier, 2001).

In the middle of September 2014, the labeled vines were divided into four groups (Figure 1; Supplementary Material): i) "Asn" for diseased vines in 2013 treated with sodium arsenite (Asn) and without external symptom expression in September 2014; ii) "CCh" for diseased vines in 2013 not treated with sodium arsenite (as control, C) and with chronic (Ch) form of esca expression in 2014; iii) "CA" for diseased vines in 2013 not treated with sodium arsenite (as control, C) and with apoplectic (A) form of esca expression in 2014; and iv) "CH" for apparently healthy vines not treated with sodium arsenite (as control, C) and visually healthy (H) in both 2013 and 2014 (Figure 1). In addition, the leaves of CH and Asn samples were asymptomatic of esca, whereas CCh and CA leaves were symptomatic. All vines were uprooted 1 week before harvest, and, for each vine, the wood of the trunk was collected and divided into three sample types: visually healthy area (WH), streaked area (WS), and interaction area (WI) covering unaltered and altered wood tissues (Figure 1). As much as possible, the samples of the different modalities were taken from equivalent wood strata, the most peripheral possible (i.e., where functional healthy wood could be found).

For metabolomics, WH, WS, and WI wood samples were immediately frozen with liquid nitrogen after being cut at the laboratory and subsequently stored at −80°C. For each modality, two and three independent vines (for CA and Asn, and CH and CCh, respectively) were sampled.

For microscopy, WH and WI samples were either i) stored at −20°C before being observed under a stereomicroscope or a scanning electron microscope or ii) sliced in pieces of strips 0.1 to 0.3 cm wide before being immediately fixed overnight at 4°C (see below). For this study, we chose not to sample the apoplectic modality (CA) for fear of reading artefactual repercussions associated with cell death of aerial parts. In this context, for each studied modality (CH, CCh, and Asn), three independent vines were sampled. For each one, a minimum of seven wood fragments were collected in each area (WS and WI).

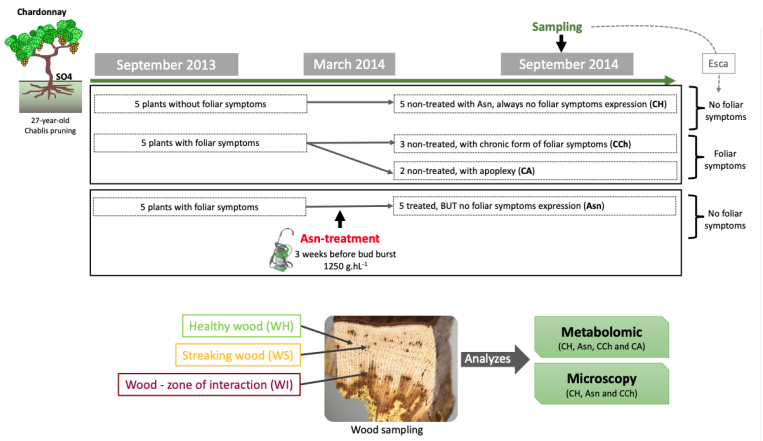

FIGURE 1
Experimental design of the study carried out in 2013–2014, including the description of the sodium arsenite treatment and the samples collected for both approaches, metabolomic and microscopy.

FTICR-MS analysis

In total, 26 wood samples (n = 10 WH, n = 7 WS, and n = 9 WI) were analyzed by Fourier-transform ion cyclotron resonance mass spectrometry (FTICR-MS). They were all prepared with the same protocol. Samples were ground to a fine powder in liquid nitrogen with a Mixer Mill MM 400 (Retsch, Haan, Germany) before analysis, and 15 mg of each was added with 1 ml of methanol (Liquid chromatography-mass spectrometry (LC-MS) grade, Fluka Analytical; Sigma-Aldrich, St. Louis, MO, USA). After sonication for 30 min and centrifugation (25,000 *g*, 10 min, room temperature), the supernatant was collected and re-diluted in methanol (1/50 v/v). Ultra-high-resolution mass spectra were acquired using an FTICR-MS (solariX, BrukerDaltonics GmbH, Bremen, Germany) equipped with a 12-Tesla superconducting magnet (Magnex Scientific Inc., Yarnton, UK) and an APOLO II ESI source (Bruker Daltonics GmbH, Bremen, Germany) operated in the negative ionization mode. Samples were introduced into the micro-electrospray source at a flow rate of 120 µl/h. Spectra were acquired with a time domain of 4 mega words over a mass range of 100 to 1,000, and 300 scans were accumulated per sample.

Spectra were externally calibrated on arginine clusters (10 mg/L in methanol). Further internal calibration was performed for each sample by using a list of ubiquitous fatty acids and recurrent wine compounds, allowing mass accuracies of 0.1 ppm (Gougeon et al., 2009). Exact masses were then run through the Netcalc algorithm, an in-house software tool to obtain unambiguous chemical formulas (Tziotis et al., 2011) and were validated next by setting van Krevelen chemical constraints (O/C ratio ≤ 1; double bond equivalent (DBE): 0 < DBE/C < 5 H/C ratio ≤ 2n + 2 and aromaticity index (IA): −20 < IA < 0.7; element counts: C ≤ 100, H ≤ 200, O ≤ 80, N ≤ 3, S ≤ 3 and P ≤ 1) applied to exclude rare or impossible formulas. It also enabled the classification of formulas according to their atomic compositions (i.e., CHO, CHOS, CHON, CHONS, CHOP, and CHONP CHONSP). Mass annotations were obtained by KEGG, HMDB, and LipidMaps databases queries against *Vitis vinifera* organism (0.1 ppm tolerance error value) by Masstrix software facility (https://metabolomics.helmholtz-muenchen.de/masstrix3/). The raw formula of the *m/z* was used for functional categorization of the annotated compounds (lipids, peptides, amino sugars, carbohydrates, nucleotides, phytochemicals (i.e., secondary metabolites), and NM when not matching) using the multidimensional stoichiometric constraint classification (MSCC) described by Rivas-Ubach et al. (2018), based on the C/H/O/N/P stoichiometric ratios. Perseus software version 1.6.8.0 (https://maxquant.net/perseus/) was used to determine significant compounds (ANOVA multivariate statistical analysis (p < 0.05)) to perform additional t-test comparisons (false discovery rate (FDR) < 0.05) between two sample groups and to draw heatmaps. The 20 most regulated annotated compounds between the two sample groups were sorted in the Top20 lists. Principal component analyses (PCAs) were performed, and illustrations were built with RStudio software (ade4 and vegan packages). Targeted fungal toxins and plant secondary metabolites were searched in the peak lists based on their theoretical *m/z* but should be considered putative (Supplementary Table S1).

Cytological approaches

For stereomicroscopy observations

The slices of the wood fragments (1 cm side cubes) were first refreshed using a razor blade before being directly observed under a stereo microscope (SMZ25 Nikon). Those fresh samples were thus observed in a bright field and under epifluorescence (UV excitation at 330–380 nm and/or blue at 420–495 nm). In bright fields, this method made it possible to visualize the state of plant cells (healthy areas, areas obstructed by tyloses or gums, or tinder areas). Under epifluorescence, it was possible to reveal the autofluorescence of defense compounds and in particular phenolic compounds, which are excitable at the wavelengths used.

Scanning electron microscopy observations

The slices of the wood fragments (1 cm side and 0.5 cm thick) were first refreshed using a razor blade before being directly observed under a scanning electron microscope (Philips XL-30 ESEM LaB6). This method allowed us to characterize the wood surfaces.

In addition, in order to detect some traces of Asn in the tissues observed, the samples were analyzed using a scanning microscope (JEOL JSM 7600F) coupled with an X-ray detector (EDX 80 mm X-Max, Oxford Instruments, Abingdon, UK). X-ray microanalysis allows elemental analysis by detecting the characteristic X-rays of the elements present. It allows in particular specific analyses with a spatial resolution of the order of 1 μm^3 and is qualitative as well as quantitative. In this sense, it is able to detect Asn of approximately 50 ppm.

All these observations were made at the DImaCell platform of the UMR Agroecology (INRAE, Université Bourgogne Franche-Comté, Dijon, France).

Light microscopy observations of semi-thin sections

Wood samples were first fixed overnight at 4°C in 0.1% glutaraldehyde/4% paraformaldehyde prepared in 0.1 M of phosphate buffer with pH 7.2 and supplemented with 1% sucrose and 0.1% Tween 20. Then, samples were dehydrated by successive baths in ethanol (30%, 30 min at 4°C; 50%, 1 h at −20°C; 70%, 1 h at −20°C; 95%, 30 min at −20°C; and 100%, 30 min at −20°C). The samples were then embedded in LR White resin (London Resin Company, London, UK) and underwent polymerization in Beem® capsules (Hemi-hyperbole beem capsule, Agar Scientific Limited, Stansted, UK) under UV at −20°C, as described in Trouvelot et al. (2008). Semi-thin transverse sections (500 nm thick) were then made using an UltraCut E ultra-microtome (Reichert-Jung) equipped with a "histo" diamond (6 mm, 45°). The semi-thin sections were placed on glass slides (76 × 26 mm, Knittel Glass; approximately 20 sections per slide) before being either i) stained

with toluidine blue (1% in aqueous solution) or ii) observed directly by epifluorescence. For each treatment, seven to nine distinct samples (i.e., woody fragments embedded in resin blocks) were studied, and at least two distant areas were observed per block.

Results and discussion

According to the first observations, the plants treated with sodium arsenite (Asn) did not express esca foliar symptoms, the five apparently healthy (CH) plants in 2013 retained the same status in 2014, and the five plants expressing esca symptoms (CCh) in 2013 re-expressed them in 2014, with three in chronic form and two apoplectic. The non-expression of esca foliar symptoms of diseased plants after sodium arsenite treatment confirms the healing and efficacy of this treatment against esca (Larignon et al., 2008; Songy et al., 2019; Del Frari et al., 2022).

Wood samples discriminate between sodium arsenite-treated and untreated grapevines

Principal component analyses of all wood samples (4,825 *m/z*) of asymptomatic (Asn and CH) and symptomatic vines (CCh and CA) were performed and compared (Figure 2). It showed a clear separation of healthy wood (WH) from streaked wood (WS) samples and even further from the interaction area (WI) for the three comparisons (Figure 2A). Focus was therefore placed on the wood of the interaction zone (WI), and the hierarchical clustering analysis confirmed that this subgroup allowed clear discrimination between Asn-treated grapevines and the other two, CCh and CH, by 1,132 and 1,162 *m/z*, respectively (Figure 2B).

The treatment by sodium arsenite therefore strongly and locally modified the metabolome of the interaction zone, which is the intermediate area between the healthy wood (WH), not yet infected by GTD pathogens, and the infected necrotic central wood. The interaction area by its location may have a role in limiting the colonization of GTD pathogens and perhaps in controlling the expression of GTD symptoms. A thorough characterization of the response in this particular area was performed.

Sodium arsenite induced significant changes in the metabolome of the interaction zone

Statistical analysis was performed on WI samples to compare Asn, CCh, and CH groups. Analyses were first applied to all *m/z* data sets; characterizations (formula and functional categorizations) and annotations were then carried out if significant ($p < 0.05$) *m/z* (Supplementary Table S2). Throughout the analysis process, the output lists were up to 98% identical.

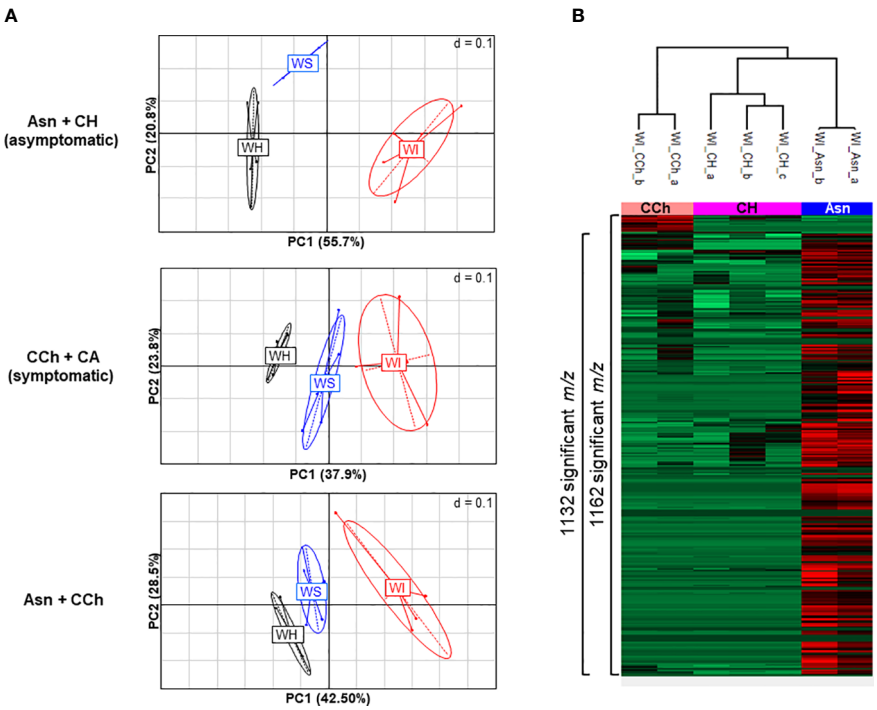

FIGURE 2
(A) PCA illustrations of cross-comparisons of wood samples: asymptomatic Asn+CH (top), symptomatic CCh+CA (middle), and Asn+CCh (bottom). Two to four replicates per wood area (healthy area, WH; streaked area, WS; and interaction zone, WI) per sample group (sodium arsenite-treated, Asn; healthy, CH; symptomatic expressing chronic disease, CCh; and apoplectic, CA). **(B)** Metabolite variations in wood interaction zone (WI) of significant 1,173 *m/z* ($p < 0.05$) between healthy (CH), chronic disease form (CCh), and sodium arsenite-treated grapevines (Asn). Numbers of significant t-test *m/z* (FDR < 0.05) that discriminate pair-to-pair groups are indicated on the side of the graph. PCA, principal component analysis; FDR, false discovery rate.

Although vines treated with sodium arsenite did not express leaf symptoms, the metabolome in the wood interaction area (WI-Asn) was quite different from that of the WI-CH group. The comparison between WI-Asn and WI-CH samples highlighted 1,132 *m/z* accumulated significantly differently (Supplementary Table S2). These *m/z* values led to the creation of a list of 1,071 raw formulas, of which 1,057 were chemically classified into compounds CHO (73%), CHON (14%), and CHONS (5%) (Figure 3A). The overall analysis ended with 1,037 unique raw formulas—when removing isotopic forms and adduct ions (Supplementary Table S2)—among which 1,033 were more accumulated in WI-Asn compared to WI-CH and four were less accumulated in WI-Asn than in WI-CH (Figure 3A). They were mainly phytochemicals (42%) and lipid-like (26%). From the 1,037 obtained raw formulas, 546 compounds could be identified in databanks. Among them, the Top20 most accumulated annotated compounds in WI-Asn samples were predicted to be phytochemicals (60%), lipids (20%), and carbohydrates (20%) (Supplementary Table S3A).

The metabolome of WI-Asn was also different from that of WI-CCh (Figure 2B). The comparison between these two sample sets highlighted 1,162 *m/z* significantly regulated, of which 1,121 were common to the comparison Asn *versus* CH (Supplementary Table S2). Of these, 1,087 *m/z* (distributed as 43 more accumulated in WI-CCh than in WI-Asn and 1,044 more accumulated in WI-Asn than in WI-CCh) were classified according to their raw formula. Those accumulated in WI-Asn (compared to WI-CCh) were mainly composed of CHO (71%), CHON (15%), and CHONS (6%), whereas those accumulated in WI-CCh (compared to WI-Asn) were mainly CHON (35%), CHO (23%), and CHONS (21%) (Figure 3B). Overall, it led to 1,068 unique formulas (Supplementary Table S2), with 39 more accumulated in WI-CCh and 1,029 more accumulated in WI-Asn (Figure 3B). The compounds accumulated in WI-Asn were predicted to be mainly phytochemicals (42%) and lipids (27%), while those accumulated in WI-CCh were rather phytochemicals (38%), peptides (28%), and amino sugars (21%, Figure 3B). Among them, the Top20 annotated compounds lesser accumulated in WI-Asn, compared to WI-CCh, were phytochemicals (60%), lipids (20%), and carbohydrates (20%). One was annotated as piceatannol, a resveratrol derivative (Supplementary Table S3B). Among the Top20 annotated compounds more abundant in WI-Asn, 60% were phytochemicals, 20% were lipids, and 20% were carbohydrates (Supplementary Table S3B). Altogether, treatment with sodium arsenite has effects on the metabolome of the wood interaction zone and mainly results in the accumulation of phytochemicals and lipids. These two categories were previously shown as a discriminant of the brown stripe of the wood of vines infected by *Botryosphaeria* dieback and the adjacent asymptomatic white wood (Lemaître-Guillier et al., 2020).

Putative toxins are detected in all wood samples, including those of asymptomatic vines

As the GTD pathogens produce phytotoxins (Andolfi et al., 2011; Abou-Mansour et al., 2015; Cimmino et al., 2017; Masi et al., 2018; Reveglia et al., 2019; Trotel-Aziz et al., 2019), a focus on the *m/z* corresponding to putative ones (Supplementary Table S1) was

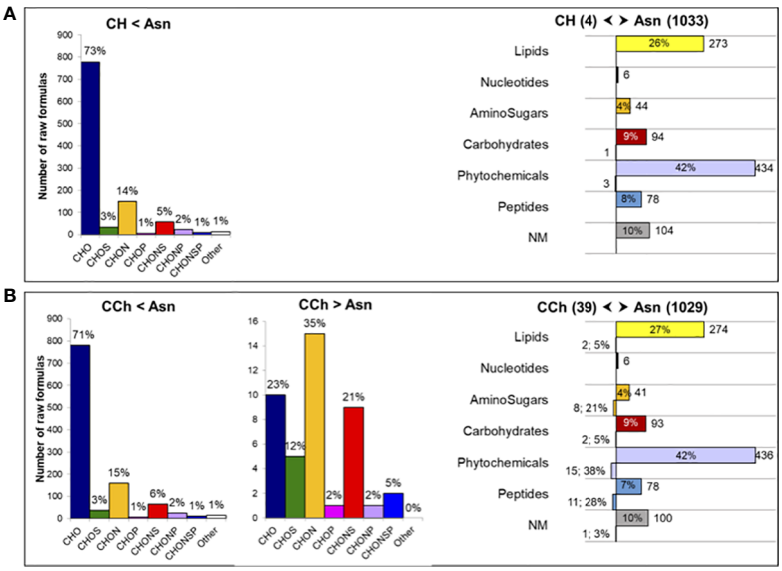

FIGURE 3
Comparison of the metabolome of the wood interaction area of vines treated or not by sodium arsenite. Comparison of the significantly regulated *m/z* of **(A)** healthy (CH) and Asn-treated (Asn) vines and **(B)** diseased (CCh) and Asn-treated (Asn) vines. Chemical classes of the corresponding raw formulas containing C, H, O, N, S, and P atoms (determined from 1,057 and 1,087 *m/z*), with the indication of the percentage of distribution in each class (left panels). Functional categorization (right panels) of the annotated compounds differently regulated in samples (1,037 and 1,068 compounds), with the indication of the number and percentage of distribution in each biochemical category. Functional categories were predicted from raw formulas according to Rivas-Ubach et al. (2018). NM, non-matched.

carried out on the wood samples WH, WS, and WI of CH, CCh, CA, and Asn-treated grapevines (Table 1).

Putative toxins were detected with different abundances, ranging from 10^5 for OH-tyrosol to 10^8 for OH-tyrosol 1-*O*-glucoside, in the different wood sample groups (Table 1). Indeed, some of them were detected preferentially in the wood of asymptomatic CH and Asn vines, compared to those of symptomatic vines, such as scopoletin, 6-methoxymellein, and OH-mellein. Six other toxins were rather more detected in the wood of apoplectic vines such as OH-tyrosol 1-*O*-glucoside, *cis*-4-hydroxy-scytalone, dimethylallyl-scopoletin, terremutin, tyrosol-4-sulfate, and mellein. Mellein and terremutin are especially produced by Botryosphaeriaceae species such as *Neofusicoccum parvum*, *Diplodia seriata*, or *Lasiodiplodia* (Andolfi et al., 2011; Abou-Mansour et al., 2015; Cimmino et al., 2017; Reveglia et al., 2019; Reveglia et al., 2021; Trotel-Aziz et al., 2022), and their detection in woody tissues was first reported by Abou-Mansour et al. (2015) in the brown-striped wood of *Botryosphaeria* dieback-diseased vines. Our results, therefore, are consistent with those of Bruez et al. (2021), who reported that these esca-expressing vines were colonized by Botryosphaeriaceae species.

Putative toxins could be found in the healthy (CH) and esca-diseased vines developing the chronic form (CCh). As discussed by Del Frari et al. (2022), the role of toxins in explaining the occurrence and yearly fluctuations of leaf stripe symptoms is not always obvious: wood degradation by-products and microbe-induced metabolites probably also play a key role (Mugnai et al., 1999; Bruez et al., 2020; Schilling et al., 2021; Del Frari et al., 2022). Our results also further suggest that in the apoplexy process, which is a more pronounced expression than the chronic form, there is a higher amount of toxins produced by GTD fungi. Similar observations were described by Magnin-Robert et al. (2016), who reported significant production of (3*R*,4*R*)-hydroxymellein in the green stem, cordon, and trunk of esca-apoplectic vines compared to esca-chronic and asymptomatic grapevines. Toxins are one of the three possible factors triggering the leaf stripe symptoms (Mugnai et al., 1999).

The next biological question was as follows: how can we explain the accumulation of some phytotoxins in the wood of vines treated

TABLE 1 Peak intensities of putative phytotoxins detected into wood samples (WH, WS and WI) in asymptomatic: healthy (CH) and sodium arsenite-treated (Asn), and symptomatic: chronic form of disease (CCh) and apoplectic (CA) grapevines.

Fungal toxins	CH	Asn	CCh	CA
Scopoletin ($\times10^7$)	2.83	2.58	2.17	1.49
± Std	2.62	2.64	2.44	1.11
6-Methoxymellein ($\times10^7$)	1.55	2.02	1.78	1.43
± Std	0.73	1.46	0.77	0.47
OH-Mellein (scytalone) ($\times10^6$)	6.96	7.82	6.39	6.47
± Std	3.63	4.79	3.04	2.63
Resveratrol-sulfate ($\times10^7$)	1.08	0.72	1.15	1.09
± Std	0.98	0.76	1.27	0.71
OH-Tyrosol ($\times10^5$)	2.69	0.00	5.82	3.16
± Std	6.59	0.00	8.92	7.74
OH-Tyrosol 1-*O*-glucoside ($\times10^8$)	1.00	1.13	0.99	1.20
± Std	0.18	0.73	0.39	0.71
cis-4-Hydroxy-scytalone ($\times10^7$)	1.23	2.21	1.52	2.57
± Std	0.34	1.30	0.37	1.25
Dimethylallyl-scopoletin ($\times10^6$)	3.60	3.08	3.09	5.66
± Std	0.63	2.95	0.73	3.18
Terremutin ($\times10^6$)	0.81	1.11	0.57	2.54
± Std	0.89	1.02	0.87	2.46
Tyrosol 4-sulfate ($\times10^6$)	1.23	1.01	2.01	2.19
± Std	2.17	1.52	1.85	1.20
Mellein ($\times10^6$)	1.64	1.41	2.10	2.14
± Std	1.41	2.04	1.31	0.36

Colored gradient indicates intensities averaged levels (scale folds indicated in brackets). Std: standard deviation per wood sample group (CH: n=6, Asn: n=6; CCh: n=8 and CA: n=6).

with sodium arsenite and the no-emergence of foliar symptoms? Could this mean that sodium arsenite does not directly "kill" fungi? The hypothesis could be that sodium arsenite, as described by Songy et al. (2019), induced physiological changes in leaves and/or other organs, such as the green stem (Fontaine F., personal communication), that could counteract the negative effect of phytotoxins and finally avoid the foliar symptom expression. Moreover, Bruez et al. (2021) reported that sodium arsenite treatment strongly impacts the fungal microbiota and observed, among other things, a strong reduction in the abundance of *F. mediterranea* and an unexpected increase in the abundance of *P. chlamydospora* occurring at the borders of wood symptoms. They hypothesized that arsenite treatment contributes to making the host wood area colonizable again, providing newly available nutrients for the endophytic microbiota. Del Frari et al. (2022) also proposed the host vascular-based transport hypothesis of leaf stripe symptom-inducing molecules (LSSIMs) to explain the development of leaf stripe symptoms. They suggested that sodium arsenite could indirectly reduce LSSIMs and thus contribute to preventing symptom expression.

Some relevant secondary metabolites are in higher abundance in the wood of vines treated by sodium arsenite

Similarly, plant secondary metabolites (Supplementary Table S1) were searched in sample peak lists. We particularly focused on stilbene phytoalexins (resveratrol, the resveratrol-glucoside piceid, oxy-resveratrol, dihydro-resveratrol, epsilon-viniferin, delta-viniferin, and astringin), flavonoids (quercetin-*O*-glucuronide and daidzein), phytohormones (salicylic acid and methyl salicylic acid), and precursors of tanins (galloyl-glucose) and lignins (caffeic acid and caftaric acid). Most of the stilbene compounds (Table 2) and other compounds, namely, phenolic compounds, salicylic acid, and methyl salicylate (Table 3), were detected with more intensity in WI-Asn samples than in the others. Piceid and astringin were rather found in apoplectic CA wood samples. Stilbenes are well-known grapevine phytoalexins, and some of them have a high antimicrobial activity (Jeandet et al., 2002; Chong et al., 2009; Adrian et al., 2012; Lambert et al., 2012). They can be induced by microbial colonization or by toxins (Abou-Mansour et al., 2015; Rusjan et al., 2017; Stempien et al., 2017; Trotel-Aziz et al., 2019). Del Frari et al. (2022) suggested that sodium arsenite could improve the vines' tolerance to LSSIMs by controlling the vines' physiology and defense response. In this way, most of the putative toxins tend to be found in lower amounts in Asn vines, concomitant with a higher abundance of some stilbenes and other secondary metabolites, which ultimately leads to asymptomatic vines, contrary to what was observed in CA vines, leading to the emergence of the severe form of GTDs. Overall, these putative toxin results enhance the involvement of these toxic compounds in the GTD foliar symptom expression as summarized in the conceptual model proposed by Claverie et al. (2020).

Sodium arsenite did not modify the wood surface aspect in esca-diseased grapevine

In order to determine whether sodium arsenite could have repercussions on the structuring of woody tissues, we first analyzed the surface of woody samples taken from vines affected by esca and treated or not with sodium arsenite. In the WI, the wood surface appeared similar between the samples treated (Asn) and not treated (CH and CCh) with sodium arsenite (Figure 4). Overall, the observed results reflected the repercussions of fungal activities in woody cells, consistent with what had already been reported in other studies (Scheck et al., 1998; Pouzoulet et al., 2014). Indeed, in these WI (brown in color), the presence of tyloses and gums obstructing the vessels was observed. This probably reflected a defensive reaction of the xylem cells in response to their colonization by vascular fungi (Yadeta and Thomma, 2013, for review; Kassemeyer et al., 2022). These observations are consistent with the presence of stilbenes reported above. Consequently, the circulation of raw sap was significantly reduced. Moreover, whatever the treatment, the closer we were to symptomatic areas of white rot characterized by wood degradation, the more we observed the presence of fungal hyphae inside the vessels. It also suggested that these fungi were not directly affected by sodium arsenite, at least in their hyphal structure. At this resolution, it was then not possible to discriminate the wood esca-diseased samples treated with sodium arsenite from the untreated samples.

In order to determine whether, in the modalities treated with Asn, we could detect and quantify arsenic, we carried out observations by scanning microscopy coupled with X-ray microanalysis. Indeed, this technique makes it possible to simultaneously obtain morphological (surface images by scanning) and chemical (elemental composition) information from a sample. In this context, we revealed that in the interaction area, no trace of arsenic was detected (Supplementary Figure S1). The same result was obtained in the healthy tissues of Asn-treated vines (data not shown). It, therefore, seemed i) that the treatment with sodium arsenite, carried out at the beginning of March in the vineyard, did not accumulate (nor certain products resulting from its metabolism) in the secondary wood of the treated and protected samples or ii) if it was present in these tissues, it was in a quantity of less than 50 ppm (detection threshold of the X-ray detector). However, this did not exclude that an accumulation of arsenic could have taken place in other non-targeted tissue areas (tinder in particular) or even in other plant organs, leaves, or roots in particular (Larignon and Fontaine, 2018).

Sodium arsenite induced an increase in woody tissue autofluorescence

In order to assess whether a sodium arsenite treatment could improve the defensive state of woody tissues by increasing the impregnation of cell walls with phenolic compounds, we then observed the autofluorescence (under UV and blue excitation) of the samples.

10.3389/fpls.2023.1141700

TABLE 2 Intensities of targeted stilbenes secondary metabolites in wood samples (WH, WS and WI) in asymptomatic: healthy (CH) and sodium arsenite-treated (Asn) and symptomatic: chronic form of disease (CCh) and apoplectic (CA) grapevines.

Stilbenes	CH	Asn	CCh	CA
Resveratrol ($\times10^{10}$)	3.38	3.16	1.60	0.74
± Std	3.76	4.15	2.73	0.67
Ellagic acid ($\times10^{8}$)	3.44	2.87	1.35	0.74
± Std	4.48	3.66	2.87	0.89
Methyl-resveratrol-glucoside ($\times10^{7}$)	1.47	1.16	0.90	1.32
± Std	1.97	0.95	0.27	0.85
epsilon-Viniferin ($\times10^{9}$)	3.69	7.18	2.60	4.82
± Std	4.30	9.02	2.36	3.91
Dihydro-resveratrol ($\times10^{8}$)	8.31	10.78	3.59	2.59
± Std	9.19	14.03	6.45	2.45
Oxy-resveratrol ($\times10^{8}$)	7.59	8.72	4.75	4.94
± Std	8.47	10.43	6.01	3.51
delta-Viniferin-glucoside ($\times10^{7}$)	1.99	3.84	1.36	2.46
± Std	2.31	4.71	1.47	1.86
Resveratrol-*O*-glucuronide ($\times10^{6}$)	5.47	9.11	4.64	5.41
± Std	4.46	10.43	4.06	3.82
Resveratrol-galloylglucoside ($\times10^{6}$)	6.16	6.71	3.36	1.47
± Std	6.41	3.26	5.07	3.59
epsilon-Viniferin-diglucoside ($\times10^{6}$)	0.00	1.82	0.41	1.30
± Std	0.00	1.72	1.22	2.05
Resveratrol-glucoside-sulfate ($\times10^{6}$)	0.70	1.48	1.67	1.54
± Std	1.08	1.41	1.31	1.75
Resveratrol-glucoside (Piceid) ($\times10^{9}$)	1.67	2.09	1.99	2.52
± Std	0.60	0.78	0.57	1.44
Astringin ($\times10^{8}$)	1.24	1.37	1.42	1.55
± Std	0.36	0.50	0.30	0.57

Colored gradient indicates intensities averaged levels (scale folds indicated in brackets). Std: standard deviation per wood sample group (CH: n=6, Asn: n=6; CCh: n=8 and CA: n=6).

Initially, the fresh samples were observed macroscopically under epifluorescence. Figure 5 shows next to each zone observed in bright-field optical microscopy, the combined image of the color spectra (bright field), UV excitation (excitation, 359–371; emission, 397 nm), and blue excitation (excitation, 455–495 nm; emission, 505–555 nm). At this resolution, no marked autofluorescence was detected in healthy tissues of asymptomatic (Figure 5A) and symptomatic vines (data not shown). In contrast, in the interaction zones (WI) of esca-diseased vines not treated with sodium arsenite (CCh, Figure 5B), an autofluorescence signal was detected under UV excitation (dark blue autofluorescence). However, we were able to observe that this signal appeared relatively weak and very punctual. Finally, in the interaction areas of esca-diseased vines treated with sodium arsenite (Asn, WI), the same autofluorescence signal (dark blue, in response to UV excitation) could be detected but with a much higher abundance and representativeness (Figure 5C). This is consistent with the accumulation of secondary metabolites, especially the phenolic compounds highlighted by FTICR-MS.

In order to study more precisely the cell types affected by these defensive processes, we then observed these same types of samples after fixation and inclusion in the LRWhite resin. The results are presented in Figures 6 and 7. In the case of healthy woody tissues (Figure 6), we observed that whatever the type of modality considered (CH, CCh, and Asn), very little autofluorescence was detected. However, it appeared that in the modality where esca-diseased grapevines were treated with Asn, the signal of autofluorescence was slightly higher (Figures 6J–L) than what could be detected for the other two modalities (CH and CCh vines, not treated with Asn).

10.3389/fpls.2023.1141700

TABLE 3 Amounts of targeted other secondary metabolites in wood samples (WH, WS, and WI) in asymptomatic (healthy (CH) and sodium arsenite-treated (Asn)) and symptomatic (chronic form of the disease (CCh) and apoplectic (CA)) grapevines.

Others	CH	Asn	CCh	CA
Linoleic acid ($\times10^9$)	4.75	3.06	2.21	1.64
± Std	5.00	3.38	4.23	1.85
Galloyl-glucose ($\times10^9$)	6.49	7.70	5.01	5.26
± Std	3.10	3.64	1.64	1.84
Caftaric acid ($\times10^8$)	0.40	1.71	0.29	0.88
± Std	0.18	2.19	0.10	0.52
Quercetin ($\times10^7$)	4.41	4.79	2.84	3.12
± Std	4.56	5.69	5.32	3.53
Quercetin-*O*-glucuronide ($\times10^7$)	0.97	1.31	0.93	1.20
± Std	0.53	0.54	0.42	0.33
Caffeic acid ($\times10^7$)	0.69	1.09	0.74	1.06
± Std	0.22	0.55	0.14	0.27
Daidzein ($\times10^6$)	3.20	4.13	2.07	2.76
± Std	2.29	5.66	1.68	1.63
Salicylic acid ($\times10^6$)	2.41	5.81	2.85	3.87
± Std	0.47	1.21	1.07	1.22
Methyl salicylate ($\times10^6$)	1.17	2.41	1.62	1.51
± Std	1.32	1.18	0.98	1.87

The colored gradient indicates intensity averaged levels (scale folds indicated in brackets).
Std, standard deviation per wood sample group (CH, n = 6; Asn, n = 5; CCh, n = 9; CA, n = 6).

In the case of woody tissues collected from the interaction area (Figure 7), the results were clearly discriminating. Indeed, while very little autofluorescence was detected in grapevines with esca-diseased symptoms (Figures 7J–L, N–P), this abundance increased considerably in the two modalities for which grapevines were asymptomatic (Figures 7B–D, F–H for CH modality; Figures 7R–T, V–X, Z–AB for Asn modality). Indeed, in the asymptomatic control vines (CH modality without leaf esca symptoms and untreated with sodium arsenite), an autofluorescence was detected in the cells of ligneous rays as well as in certain ligneous fibers. This resulted in the presence of intracellular precipitates and autofluorescence under blue (Figure 7F) and green (Figure 7G) excitations, which were more or less dispersed. Cell walls appeared also autofluorescent, suggesting the impregnation of the latter by some phenolic compounds. Concerning the modality treated with sodium arsenite (Asn), a generalized parietal autofluorescence was observed in the woody tissues (Figures 7R–T). It was also observed regardless of the excitation of wavelength tested, suggesting that different types of phenolic compounds might be involved in this response. As in the asymptomatic control vines (CH), an intracellular autofluorescence was also found, in particular for the cells of ligneous rays (Figures 7V, W). Finally and contrary to what was observed on untreated vines with esca leaf symptoms (CCh), the wall of the tyloses also appears fluorescent (Figures 7Z–AB), suggesting the establishment of a defensive barrier at this level.

As it is well known that defensive phenolic molecules, such as stilbene compounds, could be autofluorescent under UV light, our cytological and metabolomic results tended to suggest that in response to sodium arsenite, certain plant defense reactions were restored in esca-diseased vines and remained effective during the vegetative year of application. However, the biosynthesis of phenolic compounds is influenced by environmental factors and rootstock variety (Chitarra et al., 2017, Costa et al., 2020). As an example, rootstock variety impacts the scion's defensive capacity (i.e., sap phenolic levels) and its resistance against microbial pathogens (Wallis et al., 2013). Chitarra et al. (2017) reported the influence of the rootstock genotype on defense gene upregulation and stilbene accumulation in leaves of the scion. SO4, the rootstock planted in the experimental plot of our study, was among those inducing the highest stilbene inducers. In this context, it could be important to keep in mind that our results concerning Asn effects might be the result of the combination of Asn-treatment, the rootstock (SO4 in the present study) and scion (Chardonnay) varieties, and the pruning conditions (Chablis).

Conclusion

Grapevine dieback linked to GTDs remains a sanitary and economic problem, especially since the ban on the use of sodium

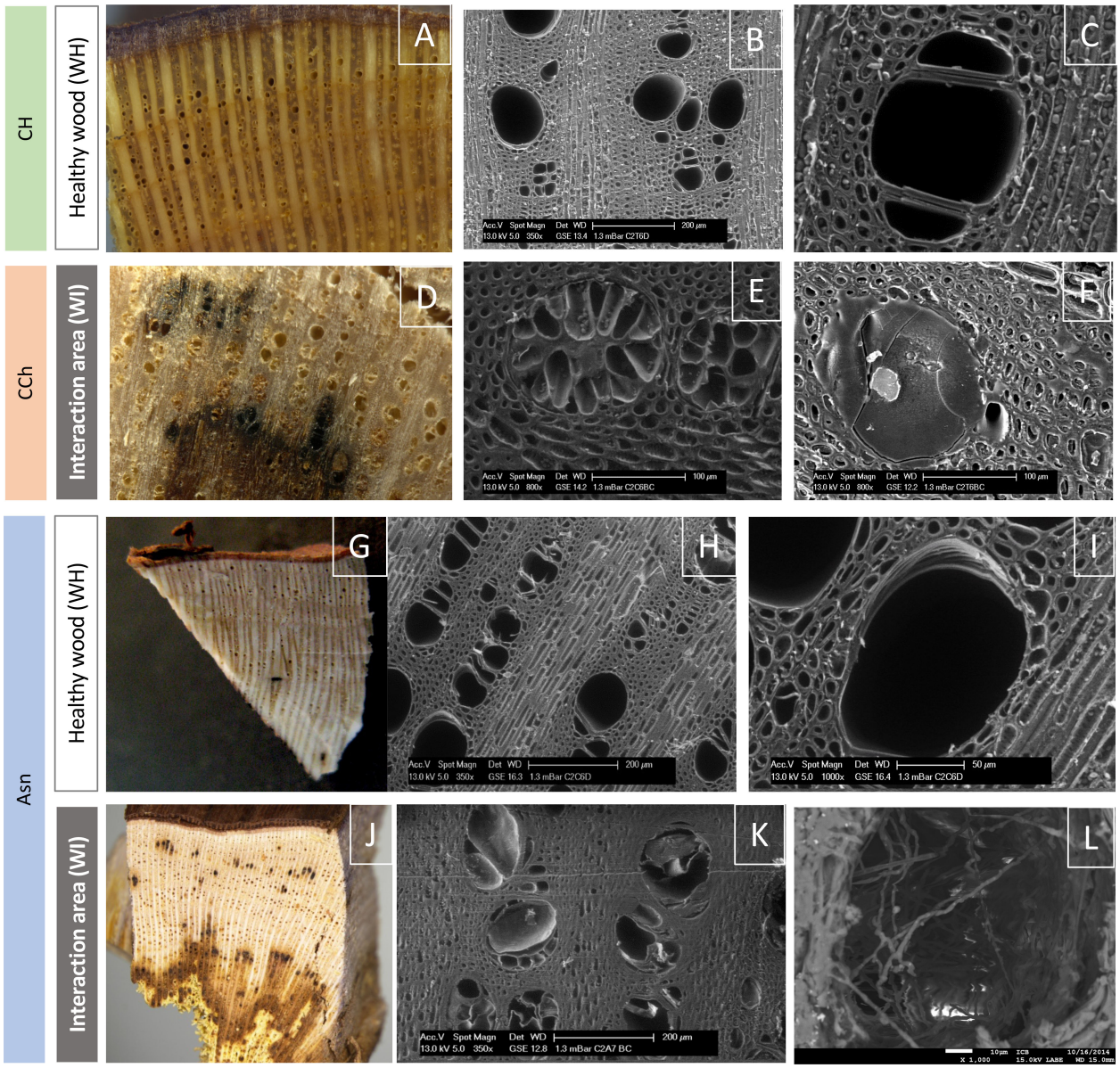

FIGURE 4
Observation of the surface of healthy woody tissues (WH) or of the interaction area (WI) by macroscopy (color photographs **A, D, G, J**) or by scanning electron microscopy (grayscale photographs **B, C, E, F, H, I, K, L**). Regardless of the modality observed (CH, CCh, and Asn), healthy woods have the same appearance **(A–C, G–I)**. In the same way, it is not possible to discriminate the modalities according to the appearance of the interaction area **(D–F, J–L)**. In this area, we observed, whatever the modality, vessels obstructed by tyloses **(E, K)** and/or gums **(F)**, as well as the presence of hyphae **(L)** approaching the zone of white-rot necrosis (amadou).

arsenite (Asn). In this study, we sought to better understand the impact of Asn on the physiology of vines in wood tissues at two scales: metabolomic and histological. We showed that Asn treatment carried out in March had repercussions in the wood of vines sampled until September of the same year. By comparing wood samples taken from vines symptomatic or asymptomatic of esca disease, treated or not with Asn, and in areas of healthy or interaction tissues, we revealed that Asn impacted both metabolome and structural barriers in the plant. This was all the more marked in the tissues of the interaction area. Thereby, this work highlighted for the first time that Asn enhanced the defensive pathway of the wood, especially in the interaction area where the confrontation with fungal pathogens occurred. Thus, in addition to its direct effect against certain pathogens or microbes, Asn also appeared to be able to act as a stimulator of plant secondary metabolites including defenses in the wood. The complex mode of action of Asn remains important to describe and understand with a view to developing new control techniques (phytosanitary treatments) that mimic its effects but are eco-friendly. Taking this into consideration, our recent work on the LC2017 product based on a low copper

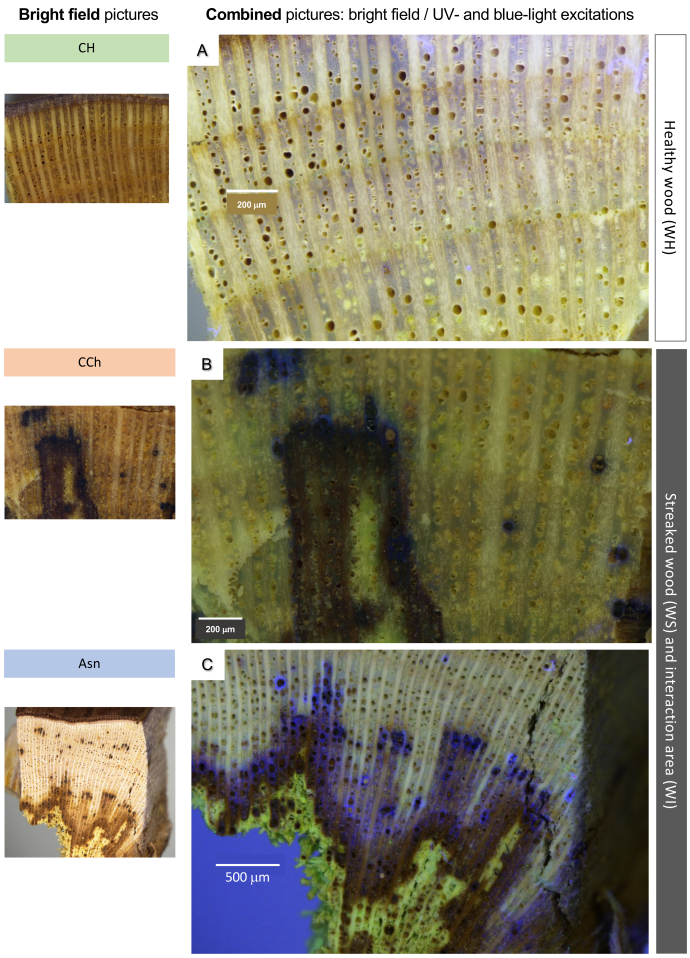

FIGURE 5
Observations, in bright-field (left pictures) and/or fluorescence microscopy **(A–C)**, of samples of woody tissues, collected on CH, CCh, or Asn vines, in healthy (WH) or interaction area (transition healthy/brown necrotic wood; WI). Bar: 200 µm **(A, B)** or 500 µm **(C)**.

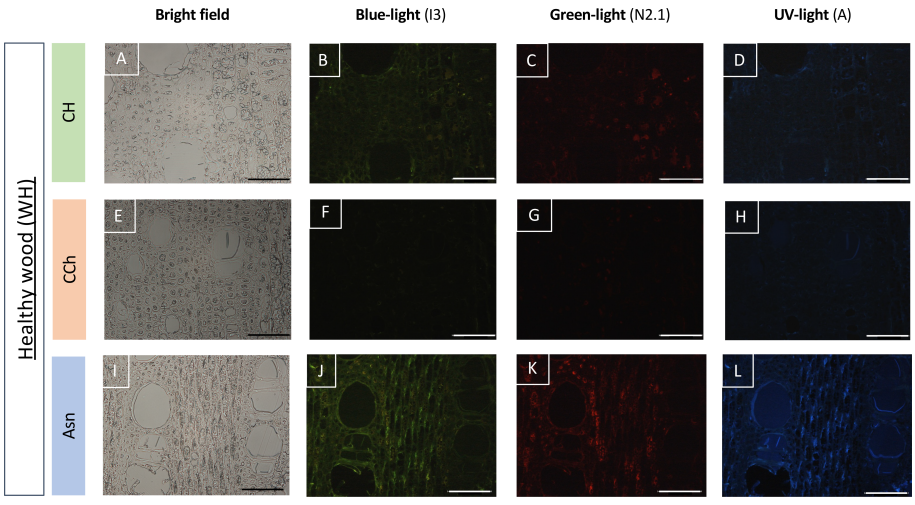

FIGURE 6
Observation of the autofluorescence of healthy woody tissues (WH) collected on CH **(A–D)**, CCh **(E–H)**, or Asn-treated vines **(I–L)** and compared according to different types of excitations (blue, green, or UV light) in epifluorescence microscopy **(B–D, F–H, J–L)**. For each modality, the observation of the same sample in bright field microscopy is given respectively in **A, E** and **I**. A slight increase in the autofluorescence signal is observed, whatever the excitation wavelength experienced, in the Asn modality **(J–L)**. Bar: 100 µm.

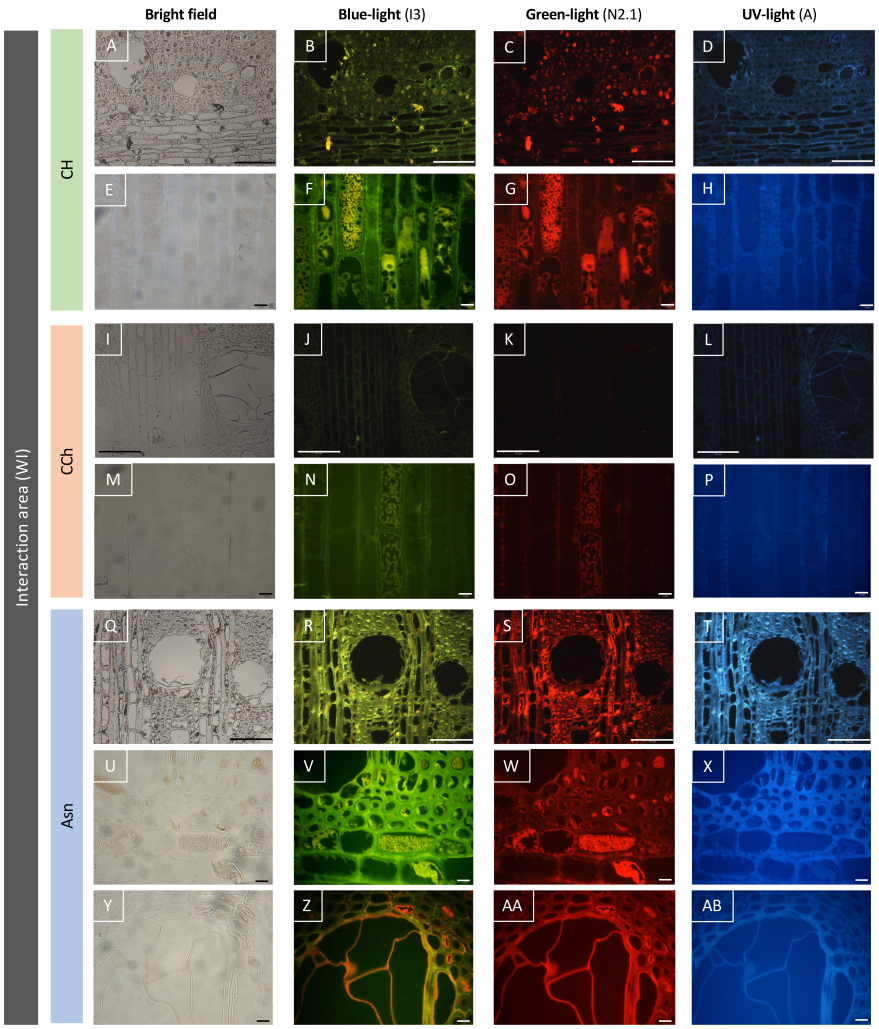

FIGURE 7
Observation of the autofluorescence of woody tissues sampled in the interaction area (WI), according to different types of excitations (blue, green, or UV light) revealed by epifluorescence microscopy. The Asn modality **(R–T, V–X, Z–AB)** reveals an intensity of autofluorescence higher than the asymptomatic control modality **(CH, B–D, F–H)**, and the wood of the CCh modality (with chronic symptoms, **J–L, N–P**) is the least autofluorescent. Bar: 100 µm **(A–D, I–L, Q–T)** or 10 µm **(E–H, M–P, U–AB)**.

concentration with other substances showed a similar combined effect of Asn, fungistatic activity, and plant defense elicitor (Mondello et al., 2021; Mondello et al., 2022). Similarly, the combination of biocontrol agents to achieve both effects is possible (Leal et al., 2022). Nevertheless, the level of protection is lower compared to that of Asn, and the development of the best combination should be followed.

Data availability statement

The original contributions presented in the study are included in the article/Supplementary Material, further inquiries can be directed to the corresponding author/s.

Author contributions

MA, FF, PL, and ST contributed to the experimental design. PL performed the Asn treatments in the vineyard. FF, PL, LJ, ST, and JV sampled the wood of vines for metabolomic analysis. LJ and ST also sampled the wood of vines for cytological approaches. ST managed the cytological approaches and the processing of corresponding data. ST and LJ performed the macroscopic analyses in collaboration with the DImaCell Imaging Center. ST performed the scanning electron microscopic (with or without an X-ray detector) analyses in collaboration with the DImaCell Imaging Center. ST and AD performed the epifluorescence microscopic analysis. MA, CL-G, and CR-G managed the metabolomic approach and the processing of corresponding data.

CL-G, CR-G, and MH performed the statistical analysis, and PS-K supervised the analysis. MA, FF, CL-G, and ST contributed to the draft of the manuscript. MA and FF managed the manuscript, and FF led the project. All authors contributed to the article and approved the submitted version.

Funding

The work included in the CASDAR V1301 project was funded by the French agriculture ministry and the interprofessional committee of the vine in France (CNIV).

Acknowledgments

We thank DImaCell Imaging Center (INRAE, Université Bourgogne Franche-Comté) and especially Christine Arnould for allowing us to carry out stereomicroscopic analyses, Aline Bonnotte for supporting us in conducting scanning electron microscopy experiments (with or without X-ray detector), the RCEN platform and especially Frederic Herbst for giving us access to the scanning electron microscope with an X-ray detector, and Alessandro Spagnolo and Jean-François Guise for their help in uprooting and cutting the plants. The authors thank also the Lycée VitiCampus for the availability of the experimental plot to carry out the treatment.

Conflict of interest

The authors declare that the research was conducted in the absence of any commercial or financial relationships that could be construed as a potential conflict of interest.

Publisher's note

Supplementary material

The Supplementary Material for this article can be found online at: https://www.frontiersin.org/articles/10.3389/fpls.2023.1141700/full#supplementary-material

SUPPLEMENTARY FIGURE 1
Observations of woody tissues sampled in the interaction area (WI) of Asn modality, by scanning microscopy coupled with X-ray microanalysis. By this method, we obtained simultaneously surface images (by scanning microscopy; **A, C, E, G**) and elemental composition information from a sample **(B, D, F, H)**. The elements detected in the analyzed spectra were expressed in atomic percentages **(B, D, F, H)**. This analysis revealed that no trace of Asn could be detected at this time and resolution.

References

Abou-Mansour, E., Débieux, J. L., and Ramirez-Suero, M. (2015). Phytotoxic metabolites from *Neofusicoccum parvum*, a pathogen of botryosphaeria dieback of grapevine. *Phytochemistry* 115, 207–215. doi: 10.1016/j.phytochem.2015.01.012

Adrian, M., De Rosso, M., Bavaresco, L., Poinssot, B., and Héloir, M.-C. (2012). "Resveratrol from vine to wine," in *Resveratrol sources, production and health benefits*. Ed. D. Delmas (New York: Nova Science Publishers Inc), 3–19.

Andolfi, A., Mugnai, L., Luque, J., Surico, G., Cimmino, A., and Evidente, A. (2011). Phytotoxins produced by fungi associated with grapevine trunk diseases. *Toxins (Basel)* 3, 12. doi: 10.3390/toxins3121569

Battiston, E., Compant, S., Antonelli, L., Mondello, V., Clément, C., Simoni, A., et al. (2021). *In planta* activity of novel copper(II) based formulations to inhibit the esca-associated fungus *Phaeoacremonium minimum* in grapevine propagation material. *Front. Plant Sci.* 12. doi: 10.3389/fpls.2021.649694

Bortolami, G., Gambetta, A. G., Cassan, C., Dayer, S., Farolfi, E., Ferrer, N., et al. (2021). Seasonal and long-term consequences of esca grapevine disease on stem xylem integrity. *J. Exp. Bot.* 72, 3914–3928. doi: 10.1073/pnas.2112825118

Bruez, E., Larignon, P., Bertsch, C., Robert-Siegwald, G., Lebrun, M., Rey, P., et al. (2021). Impacts of sodium arsenite on wood microbiota of esca-diseased grapevines. *J. Fungi* 7 (498), 1–18. doi: 10.3390/jof7070498

Bruez, E., Lecomte, P., Grosman, J., Doublet, B., Bertsch, C., Fontaine, F., et al. (2013). Overview of grapevine trunk diseases in France in the 2000s. *Phytopathol. Mediterr.* 52 (2), 262–275. doi: 10.14601/Phytopathol_Mediterr-11578

Bruez, E., Vallance, J., Gautier, A., Laval, V., Compant, S., Maurer, W., et al. (2020). Major changes in grapevine wood microbiota are associated with the onset of esca, a devastating trunk disease. *Environ. Microbiol.* 22, 5189–5206. doi: 10.1111/1462-2920.15180

Carbonell-Barrachina, A., Burl.-Carbonell, F., and Mataix- Beneyto, J. (1997). Effects of sodium arsenite on arsenic accumulation and distribution in leaves and fruit of *Vitis vinifera*. *J. Plant Nutr.* 20 (2–3), 379–387. doi: 10.1080/01904169709365258

Chitarra, W., Perrone, I., Avanzato, C. G., Minio, A., Boccacci, P., Santini, D., et al. (2017). Grapevine grafting: Scion transcript profiling and defense-related metabolites induced by rootstocks. *Front. Plant Sci.* 8. doi: 10.3389/fpls.2017.00654

Cholet, C., Bruez, E., Lecomte, P., Barsacq, A., Martignon, T., and Giudici, M. (2021). Plant resilience and physiological modifications induced by curettage of esca-diseased grapevines. *OenoOne* 1, 153–169. doi: 10.20870/oeno-one.2021.55.1.4478

Chong, J., Poutaraud, A., and Hugueney, P. (2009). Metabolism and roles of stilbenes in plants. *Plant Sci.* 177, 143–155. doi: 10.1016/j.plantsci.2009.05.012

Cimmino, A., Cinelli, T., Masi, M., Reveglia, P., da Silva, M. A., Mugnai, L., et al. (2017). Phytotoxic lipophilic metabolites produced by grapevine strains of lasiodiplodia species in Brazil. *J. Agric. Food Chem.* 65, 1102–1107. doi: 10.1021/acs.jafc.6b04906

Claverie, M., Notaro, M., Fontaine, F., and Wery, J. (2020). Current knowledge on grapevine trunk diseases with complex etiology: a systemic approach. *Phytopathol. Mediterr.* 59 (1), 29–53. doi: 10.36253/phyto-11150

Costa, R. R., Rodrigues, A., Vasconcelos, V., Costa, J., and Lima, M. (2020). Trellis systems, rootstocks and season influence on the phenolic composition of chenin blanc grape. *Scientia Agricola* 77 (3), e20180207. doi: 10.1590/1678-992X-2018-0207

Da Costa, E. W. B. (1971). Variation in the toxicity pf arsenic compounds to microorganisms and the suppression of the inhibitory effects by phosphate. *Appl. Microbiol.* 23 (1), 46–53. doi: 10.1128/am.23.1.46-53.1972

De la Fuente, M., Fontaine, F., Gramaje, D., Armengol, J., Smart, R., Nagy, Z. A., et al. (2016). *Grapevine trunk diseases. A review. 1st Edition* (Paris, France: OIV Publications), 4–7. Available at: www.oiv.int/public/medias/4650/trunk-diseases-oiv-2016.pdf.

Del Frari, G., Calzarano, F., and Boavida Ferreira, R. (2022). Understanding the control strategies effective against the esca leaf stripe symptom: the edge hypothesis. *Phytopathol. Mediterr.* 61 (1), 153–164. doi: 10.36253/phyto-13295

Díaz, G. A., and Latorre, B. A. (2013). Efficacy of paste and liquid fungicide formulations to protect pruning wounds against pathogens associated with grapevine trunk diseases in Chile. *Crop Prot.* 46, 106–112. doi: 10.1016/j.cropro.2013.01.001

Di Marco, S., Metruccio, E., Moretti, S., Nocentini, M., Carella, G., Pacetti, A., et al. (2021). Activity of *Trichoderma asperellum* strain ICC 012 and *Trichoderma gamsii* strain ICC 080 towards diseases of esca complex and associated pathogens. *Front. Microbiol.* 12. doi: 10.3389/fmicb.2021.813410

Di Marco, S., Osti, F., Calzarano, F., Roberti, R., Veronesi, A., and Amalfitano, C. (2011). Effects of grapevine applications of fosetyl-aluminium formulations for downy mildew control on "esca" and associated fungi. *Phytopathol. Mediterr.* 50 (SUPPL.), 285–299. doi: 10.2307/26458728

Dula, T., Kappes, E. M., Horvath, A., and Rabai, A. (2007). Preliminary trials on treatment of esca-infected grapevines with trunk injection of fungicides. *Phytopathol. Mediterr.* 46 (1), 91–95. doi: 10.1128/am.23.1.46-53.1972

Dumitriu Gabur, G. D., Gabur, I., Cucolea, E. I., Costache, T., Rambu, D., Cotea, V. V., et al. (2022). Investigating six common pesticides residues and dietary risk assessment of Romanian wine varieties. *Foods* 11 (15), 2225. doi: 10.3390/foods11152225

Fourié, P. H., and Halleen, F. (2002). Investigation on the occurrence of *Phaeomoniella chlamydospora* in canes rootstock mother vines. *Australas. Plant Pathol.* 31, 425–427. doi: 10.1071/AP02049

Gerbore, J., Benhamou, N., Vallance, J., Le Floch, G., Grizard, D., Regnault-Roger, C., et al. (2013). Biological control of plant pathogens: advantages and limitations seen through the case study of *Pythium oligandrum*. *Environ. Sci. Pollut. Res.* 21, 4847–4860. doi: 10.1007/s11356-013-1807-6

Gougeon, R. D., Lucio, M., De Boel, A., Frommberger, M., Hertkorn, N., Peyron, D., et al. (2009). Expressing forest origins in the chemical composition of cooperage oak woods and corresponding wines by using FTICR-MS. *Chemistry* 15, 600–611. doi: 10.1002/chem.200801181

Gramaje, D., Armengol, J., Mohammadi, H., Banihashemi, Z., and Mostert, L. (2009). Novel phaeoacremonium species associated with Petri disease and esca of grapevine in Iran and Spain. *Mycologia* 101, 920–929. doi: 10.3852/08-222

Gramaje, D., Urbez-Torres, J. R., and Sosnowski, M. R. (2018). Managing grapevine trunk diseases with respect to etiology and epidemiology: current strategies and future prospects. *Plant Dis.* 102 (1), 12–39. doi: 10.1094/PDIS-04-17-0512-FE

Graniti, A., Surico, G., and Mugnai, L. (2000). Esca of grapevine, a disease complex or a complex diseases? *Phytopathol. Mediterr.* 39, 16–20. doi: 10.14601/Phytopathol_Mediterr-1539

Haidar, R., Deschamps, A., Roudet, J., Calvo-Garrido, C., Bruez, E., Rey, P., et al. (2016). Multi-organ screening of efficient bacterial control agents against two major pathogens of grapevine. *Biol. Control* 9, 55–65. doi: 10.1016/j.biocontrol.2015.09.003

Halleen, F., Fourie, P. H., and Lombard, P. J. (2010). Protection of grapevine pruning wounds against *Eutypa lata* by biological and chemical methods. *South Afr. J. Enol. Vitic.* 31 (2), 125–132. doi: 10.21548/31-2-1409

Hofstetter, V., Buyck, B., Croll, D., Viret, O., Couloux, A., and Gindro, K. (2012). What if esca disease of grapevine were not a fungal disease? *Fungal Divers.* 54 (1), 51–67. doi: 10.1007/s13225-012-0171-z

Jeandet, P., Douillet-Breuil, A. C., Bessis, R., Debord, S., Sbaghi, M., and Adrian, M. (2002). Phytoalexins from the vitaceae: biosynthesis, phytoalexin gene expression in transgenic plants, antifungal activity, and metabolism. *J. Agric. Food Chem.* 50, 2731–2741. doi: 10.1021/jf011429s

Kassemeyer, H.-H., Kluge, F., Bieler, E., Ulrich, M., Grüner, J., Fink, S., et al. (2022). Trunk anatomy of asymptomatic and sympto- matic grapevines provides insights into degradation patterns of wood tissues caused by esca-associated pathogens. *Phytopathol. Mediterr.* 61 (3), 451–471. doi: 10.36253/phyto-13154

Lambert, C., Bisson, J., Waffo-Teguo, P., Papastamoulis, Y., Richard, T., Corio-Costet, M. F., et al. (2012). Phenolics and their antifungal role in grapevine wood decay, focus on the botryosphaeriaceae family. *J. Agric. Food Chem.* 60 (48), 11859–11868. doi: 10.1021/jf303290g

Larignon, P. (2016) *Maladies cryptogamiques du bois de la vigne : symptomatologie et agents pathogènes*. Available at: http://vignevin.com.

Larignon, P., Darne, G., Menard, E., Desache, F., and Dubos, B. (2008). Comment agissait l'arsénite de sodium sur l'Esca de la vigne? *Progrès Agricole Viticole* 125, 642–651.

Larignon, P., and Dubos, B. (1997). Fungi associated with esca disease in grapevine. *Eur. J. Plant Pathol.* 103, 147–157. doi: 10.1023/A:1008638409410

Larignon, P., and Dubos, B. (2001). The villainy of black dead arm. *Wines Vines* 82, 86–89.

Larignon, P., and Fontaine, F. (2018). *Comprendre le mode d'action de l'arsénite de sodium afin de proposer de nouveaux moyens de lutte* (France: Proceeding, Assise de Toulouse).

Leal, C., Richet, N., Guise, J. F., Gramaje, D., Armengol, J., Fontaine, F., et al. (2021). Cultivar contributes to the beneficial effects of *Bacillus subtilis* PTA-271 and *Trichoderma atroviride* SC1 to protect grapevine against *Neofusicoccum parvum*. *Front. Microbiol.* 12. doi: 10.3389/fmicb.2021.726132

Leal, C., Gramaje, D., Fontaine, F., Richet, N., Trotel-Aziz, P., Armengol, J., et al. (2022). Evaluation of Bacillus subtilis PTA-271 and Trichoderma atroviride SC1 to control Botryosphaeria dieback and black-foot pathogens in grapevine propagatopn material. *Pest Manag. Sci.*. doi: 10.1002/ps.7339

Lecomte, P., Darrieutort, G., Liminana, J. M., Comont, G., Muruamendiaraz, A., Legorburu, F. J., et al. (2012). New insights into esca of grapevine: the development of foliar symptoms and their association with xylem discoloration. *Plant Dis.* 96 (7), 924–934. doi: 10.1094/PDIS-09-11-0776-RE

Lemaître-Guillier, C., Fontaine, F., Roullier-Gall, C., Harir, M., Magnin-Robert, M., Clément, C., et al. (2020). Cultivar-and wood area-dependent metabolomic fingerprints of grapevine infected by botryosphaeria dieback. *Phytopathology* 110 (11), 1821–1837. doi: 10.1094/PHYTO-02-20-0055-R

Magnin-Robert, M., Spagnolo, A., Boulanger, A., Joyeux, C., Clément, C., Abou-Mansour, E., et al. (2016). Changes in plant metabolism and accumulation of fungal metabolites in response to esca proper and apoplexy expression in the whole grapevine. *Phytopathology* 109, 6. doi: 10.1094/PHYTO-09-15-0207-R

Masi, M., Cimmino, A., Reveglia, P., Mugnai, L., Surico, G., and Evidente, E. (2018). Advances on fungal phytotoxins and their role in grapevine trunk diseases. *J. Agric. Food Chem.* 66, 5948–5958. doi: 10.1021/acs.jafc.8b00773

Meier, U. (2001). "Growth stages of mono-and dicotyledonous plants," in *BBCH monograph, 2nd ed* (Federal Biological Research Centre for Agriculture and Forestry).

Mondello, V., Battiston, E., Pinto, C., Coppin, C., Trotel-Aziz, P., Clément, C., et al. (2018a). Grapevine trunk diseases: A review of fifteen years of trials for their control with chemicals and biocontrol agents. *Plant Dis.* 102, 1189–1217. doi: 10.1094/PDIS-08-17-1181-FE

Mondello, V., Fernandez, O., Guise, J.-F., Trotel-Aziz, P., and Fontaine, F. (2021). *In planta* activity of the novel copper product HA + Cu(II) based on a biocompatible drug delivery system on vine physiology and trials for the control of botryosphaeria dieback. *Front. Plant Sci.* 12. doi: 10.3389/fpls.2021.693995

Mondello, V., Larignon, P., Armengol, J., Kortekamp, A., Vaczy, K., Prezman, F., et al. (2018b). Management of grapevine trunk diseases: knowledge transfer, current strategies and innovative attempts adopted in Europe. *Phytopathol. Mediterr.* 57 (3), 369–383. doi: 10.14601/Phytopathol_Mediterr-23942

Mondello, V., Lemaître-Guillier, C., Trotel-Aziz, P., Gougeon, R., Acedo, A., Schmitt-Kopplin, P., et al. (2022). Assessment of a new copper-based formulation to control esca disease in field and study on its impact on the vine microbiome, vine physiology and enological parameters of the juice. *J. Fungi* 8, 151. doi: 10.3390/jof8020151

Mugnai, L., Graniti, A., and Surico, G. (1999). Esca (black measles) and brown wood-streaking: two old and elusive diseases of grapevines. *Plant Dis.* 83 (5), 404–418. doi: 10.1094/PDIS.1999.83.5.404

Pacetti, A., Moretti, S., Pinto, C., Farine, S., Bertsch, C., and Mugnai, L. (2021). Trunk surgery as a tool to reduce foliar symptoms in diseases of the esca complex and its influence on vine wood microbiota. *J. Fungi* 7 (521), 1–25. doi: 10.3390/jof7070521

Pinto, C., Custodio, V., Nunes, M., Songy, A., Rabenolelina, F., Courteaux, B., et al. (2018). Understand the potential role of *Aureobasidium pullulans*, a resident microorganism from grapevine, to prevent the infection caused by *Diplodia seriata*. *Front. Microbiol* 9, 3047. doi: 10.3389/fmicb.2018.03047

Pouzoulet, J., Pivovaroff, A. L., Santiago, L. S., and Rolshausen, P. (2014). Can vessel dimension explain tolerance toward fungal vascular wilt diseases in woody plant? lesson from Dutch elm disease and esca disease in grapevine. *Front. Plant Sci.* 5, 253. doi: 10.3389/fpls.2014.00253

Reis, P., Gaspar, A., Alves, A., Fontaine, F., and Rego, C. (2021).). combining an HA + Cu (II) site-targeted copper-based product with a pruning wound protection program to prevent infection with *Lasiodiplodia* spp. in grapevine. *Plants* 10, 2376. doi: 10.3390/plants10112376

Reis, P., Mondello, V., Diniz, I., Alves, A., Rego, C., and Fontaine, F. (2022). Effect of the combined treatments with LC2017 and *Trichoderma atrovide* strain I-1237 on disease development and defense responses in vines infected by *Lasiodiplodia theobromae*. *MDPI Agron.* 12, 996. doi: 10.3390/agronmy12050996

Retief, E., McLeod, A., and Fourié, P. H. (2006). Potential inoculum sources of *Phaeomoniella chlamydospora* in south African grapevine nurseries. *Eur. J. Plant Pathol.* 115, 331–339. doi: 10.1007/s10658-006-9025-4

Reveglia, P., Billones-Baaijens, R., Millera Niem, J., Masi, M., Cimmino, A., Evidente, A., et al. (2021). Production of phytotoxic metabolites by botryosphaeriaceae in naturally infected and artificially inoculated grapevines. *Plants* 10, 802. doi: 10.3390/plants10040802

Reveglia, P., Savocchia, S., Billones-Baaijens, R., Masi, M., Cimmino, A., and Evidente, A. (2019). Phytotoxic metabolites by nine species of botryosphaeriaceae involved in grapevine dieback in Australia and identification of those produced by *Diplodia mutila*, *Diplodia seriata*, *Neofusicoccum australe* and *Neofusicoccum luteum*. *Nat. Prod. Res.* 33, 2223–2229. doi: 10.1080/14786419.2018.1497631

Rivas-Ubach, A., Liu, Y., Bianchi, T. S., Tolić, N., Jansson, C., and Paša-Tolić, L. (2018). Moving beyond the van krevelen diagram: A new stoichiometric approach for compound classification in organisms. *Anal. Chem.* 90 (10), 6152–6160. doi: 10.1021/acs.analchem.8b00529

Rolshausen, P. E., Úrbez-Torres, J. R., Rooney-Latham, S., Eskalen, A., Smith, R. J., and Gubler, W. D. (2010). Evaluation of pruning wound susceptibility and protection against fungi associated with grapevine trunk diseases. *Am. J. Enol. Vitic.* 61 (1), 113–119. doi: 10.5344/ajev.2010.61.1.113

Romeo-Oliván, A., Pagès, M., Breton, C., Lagarde, F., Cros, H., Yobrégat, O., et al. (2021). Ozone dissolved in water: an innovative tool for the production of young plants in grapevine nurseries? *Ozone Sci. Eng.* 44 (6), 521–535. doi: 10.1080/01919512.2021.1984203

Rusjan, D., Persic, M., Likar, M., Biniari, K., and Mikulic-Petkovsek, M. (2017). Phenolic responses to esca-associated fungi in differently decayed grapevine woods from different trunk parts of "Cabernet sauvignon". *J. Agric. Food Chem.* 65, 6615–6624. doi: 10.1021/acs.jafc.7b02188

Saha, C., Dikshit, A. K., Bandyopadhyay, M., and Saha, K. C. (1999). A review of arsenic poisoning and its effects on human health. *Crit. Rev. Environ. Sci. Technol.* 29 (3), 281–313. doi: 10.1080/10643389991259227

Scheck, H., Vasquez, S., Fogle, D., and Gubler, W. D. (1998). Grape growers report losses to black foot and grapevine decline. *Calif. Agric.* 52 (4), 19–23. doi: 10.3733/ca.v052n04p19

Schilling, M., Farine, S., Peros, J.-P., Bertsch, C., and Gelhaye, E. (2021). Wood degradation in grapevine diseases. *Adv. Bot. Res.* 99, 175–207. doi: 10.1016/bs.abr.2021.05.007

Songy, A., Vallet, J., Gantet, M., Boos, A., Ronot, P., Tarnus, C., et al. (2019). Sodium arsenite effect in *Vitis vinifera* l. physiology. *J. Plant Phys* 238, 72-79. doi: 10.1007/s00425-019-03111-8

Spinosi, J., Fevotte, J., and Vial, G. (2009). *Élèments techniques sur l'exposition professionnelle aux pesticides arsenicaux. matrice cultures - expositions aux pesticides arsenicaux* (Santé Travail), 1–22.

Stempien, E., Goddard, M. L., Wilhelm, K., Tarnus, C., Bertsch, C., and Chong, J. (2017). Grapevine botryosphaeria dieback fungi have specific aggressiveness factor repertory involved in wood decay and stilbene metabolization. *PloS One* 12 (12), 1–22. doi: 10.1371/journal.pone.0188766

Surico, G. (2009). Towards a redefinition of the diseases within the esca complex of grapevine. *Phytopathol. Mediterr.* 48 (1), 5–10. doi: 10.14601/Phytopathol_Mediterr-287

Surico, G., Mugnai, L., and Marchi, G. (2008). "The esca disease complex," in *Integrated management of diseases caused by fungi, phytoplama and bacteria*. Eds. A. Ciancio and K. Mukerji (Dordrecht: Springer), 119–136.

Trotel-Aziz, P., Abou-Mansour, E., Courteaux, B., Rabenoelina, F., Clément, C., Fontaine, F, et al. (2019). Bacillus subtillis PTA-271 couteracts botryosphaeria dieback in grapevine, triggering immune responses and detoxification of fungal phytotoxins. *Font. Plant Sci.* 10, 25. doi: 10.3389/fpls.2019.00025

Trotel-Aziz, P., Robert-Siegwald, G., Fernandez, O., Leal, C., Villaume, S., Guise, J. F., et al. (2022). Diversity of *Neofusicoccum parvum* for the production of the phytotoxic metabolites (-)-terremutin and (R)–mellein. *J. Fungi* 8 (3), 319. doi: 10.3390/jof8030319

Trouvelot, S., Varnier, A. L., Mercier, L., Allègre, M., Baillieul, F., Arnould, C., et al. (2008). A beta-1,3 glucan sulfate induces resistance in grapevine against *Plasmopara viticola* through priming of defense responses, including HR-like cell death. *Mol. Plant Microbe Interact.* 21 (2), 232–243. doi: 10.1094/MPMI-21-2-0232

Tziotis, D., Hertkorn, N., and Schmitt-Kopplin, P. (2011). Kendrick-analogous network visualisation of ion cyclotron resonance Fourier transform mass spectra: improved options for the assignment of elemental compositions and the classification of organic molecular complexity. *Eur. J. Mass Spectrom.* 17, 415–421. doi: 10.1255/ejms.1135

Wallis, C. M., Wallingford, A., and Chen, J. (2013). Grapevine rootstock effects on scion sap phenolic levels, resistance to xylella fastidiosa infection, and progression of pierce's disease. *Front. Plant Sci.* 4, 502. doi: 10.3389/fpls.2013.00502

Weber, E. A., Trouillas, F. P., and Gubler, W. D. (2007). Double pruning of grapevines: a cultural practice to reduce infections by *Eutypa lata*. *Am. J. Enol. Vitic.* 58, 61–66. doi: 10.5344/ajev.2007.58.1.61

Yacoub, A., Gerbore, J., Magnin, N., Chambon, P., Dufour, M. C., Corio-Costet, M. F., et al. (2016). Ability of *Pythium oligandrum* strains to protect *Vitis vinifera* l., by inducing plant resistance against *Phaeomoniella chlamydospora*, a pathogen involved in esca, a grapevine trunk disease. *Biol. Control* 9, 7–16. doi: 10.5897/AJB11.290

Yacoub, A., Haidar, R., Gerbore, J., Masson, C., Dufour, M. C., Guyoneadu, R., et al. (2020). *Pythium oligandrum* induces grapevine defence mechanisms against the trunk pathogen *Neofusicoccum parvum*. phytopathol. *Mediterr.* 59 (3), 565–580. doi: 10.14601/Phyto-11270

Yadeta, K. A., and Thomma, B. P. H. J. (2013). The xylem as battleground for plant hosts and vascular wilt pathogens. *Front. Plant Sci.* 4, 97. doi: 10.3389/fpls.2013.00097

frontiers | Frontiers in Plant Science

TYPE Original Research
PUBLISHED 19 April 2023
DOI 10.3389/fpls.2023.1150870

OPEN ACCESS

EDITED BY
Xiaofeng Zhang,
Fujian Agriculture and Forestry University, China

REVIEWED BY
Zhaoji Dai,
Hainan University, China
Yanjuan Jiang,
Yunnan University, China

*CORRESPONDENCE
Jing Shang
shangjing_edu@163.com

†These authors have contributed equally to this work

SPECIALTY SECTION
This article was submitted to Plant Pathogen Interactions, a section of the journal Frontiers in Plant Science

RECEIVED 25 January 2023
ACCEPTED 08 March 2023
PUBLISHED 19 April 2023

CITATION
Shang J, Zhao L-P, Yang X-M, Qi X-L, Yu J-F, Du J-B, Li K, He C-S, Wang W-M and Yang W-Y (2023) Soybean balanced the growth and defense in response to SMV infection under different light intensities. *Front. Plant Sci.* 14:1150870. doi: 10.3389/fpls.2023.1150870

Soybean balanced the growth and defense in response to SMV infection under different light intensities

Jing Shang[1*†], Lu-Ping Zhao[1†], Xin-Miao Yang[1], Xiao-Li Qi[1], Jin-Feng Yu[1], Jun-Bo Du[1], Kai Li[2], Cheng-Shan He[1], Wen-Ming Wang[3] and Wen-Yu Yang[1]

[1]Sichuan Engineering Research Center for Crop Strip Intercropping System and College of Agronomy, Sichuan Agricultural University, Chengdu, China, [2]National Center for Soybean Improvement, National Key Laboratory for Crop Genetics and Germplasm Enhancement, Key Laboratory of Biology and Genetic Improvement of Soybean, Ministry of Agriculture, Nanjing Agricultural University, Nanjing, China, [3]State Key Laboratory of Crop Gene Exploration and Utilization in Southwest, Sichuan Agricultural University, Chengdu, China

Light is essential for the growth and defense of soybean. It is not clear how soybeans adjust their defenses to different light environments with different cropping patterns. The mechanism of soybean response to *Soybean mosaic virus* (SMV) infection under different light intensities was analyzed by RNA-seq sequencing method. Enrichment analysis illustrated that most defense-related genes were down-regulated in the dark and the shade, and up-regulated under hard light and normal light. Soybean can resist SMV infection mainly by activating salicylic acid signaling pathway. Light is essential for activating salicylic acid defense signaling pathways. With the increase of light intensity, the oxidative damage of soybean leaves was aggravated, which promoted the infection of virus. When light was insufficient, the growth of soybean was weak, and the plant-pathogen interaction pathway, MAPK pathway and hormone defense pathway in infected soybean was inhibited. Under hard light, some defense genes in infected soybean were down-regulated to reduce the degree of oxidative damage. The expression of differentially expressed genes was verified by real-time fluorescence quantitative RT-PCR. In order to adapt to the change of light intensity, soybean balanced allocation of resources between growth and defense through a series regulation of gene expression. The results of this study will provide a theoretical basis for the research of SMV resistance in intercropping soybean.

KEYWORDS

***Soybean mosaic virus*, light intensity, growth, defense, soybean**

1 Introduction

Intercropping system maximizes the productivity as well as resource utilization per unit of land. As explained by the biodiversity theory, the maize-soybean intercropping system is an ecological strategy to control or relieve diseases (Zhang et al., 2019). In intercropping system, soybean undergoes complex changes in light environment (Li et al., 2021). During the symbiotic period of soybean and corn, soybean was in the shade. After the corn is harvested, soybeans get plenty of light. *Soybean mosaic virus* (SMV) was the most important soybean virus, which resulted in soybean yield reduction. How the soybean precisely allocates its limited resources between growth and defense under different light intensities is critical to its survival. Recent studies suggest that there may be complex regulatory mechanisms in plants, with interactions between hormone-based signaling networks causing transcriptional changes that balance the growth and defense (Du et al., 2018).

Our previous studies have shown that light can induce the eruption of reactive oxygen species (Shang et al., 2019) and activate the defense against pathogenic microorganisms (Shang et al., 2011). At the same time, light promoted the improvement of plant photosynthetic efficiency, which was conducive to the growth and development of plants. When light is insufficient, the growth of intercropping soybeans is inhibited, and the resources allocated to defense are correspondingly reduced (Zhang et al., 2019). Rewiring of jasmonate and phytochrome B signaling uncouples plant growth-defense tradeoffs (Campos et al., 2016). Light and darkness affect not only the host's defense reaction, but also the pathogenicity of the pathogen (Telli et al., 2020).

Many studies have shown that light regulates the plant defense against pathogenic agents mainly through salicylic acid and jasmonic acid pathways (Zhang et al., 2019). NPR1 gene is a key gene in the salicylic acid pathway (Cao et al., 1998). Overexpression of NPR1 gene increases plant sensitivity to light, thereby enhancing disease resistance of Arabidopsis, crops and tobacco (Shang et al., 2011). Salicylic acid regulates NPRs protein to regulate the plant immunity (Backer et al., 2015). The expression of PR1 gene regulated by NPR1 protein is also induced by light (Agrawal et al., 2000). The expression of PR1 gene was down-regulated in stress treatments such as hard light, drought and salt (Wu et al., 2020). The main mechanism of defense inhibition is the simultaneous down-regulation of jasmonic acid and salicylic acid signaling through a low proportion of red: far-red light. Jasmonic acid signaling is inhibited by altering the balance between DELLA and Jasmonate ZIM DOMAIN (JAZ) proteins. The discovery of the link between photoreceptors and defense signals reveals a new mechanism that controls the allocation decisions of key resources in plant canopies. The decreased expression of phyB gene reduces the accumulation of jasmonic acid and inhibits the synthesis of insect-resistant protein in plants (Pierik and Ballare, 2021). Plants that silenced phyB genes showed decreased resistance to fungi (Courbier et al., 2020). Silencing photosystem II-related genes can reduce tobacco resistance to *Carrot mosaic virus* (Manfre et al., 2011). PhyA and phyB genes regulate RPS2 and R/MIN1 genes to enhance resistance to Pseudomonas cloves (Griebel and Zeier, 2008; Genoud et al., 2010). PhyA, phyB and phyC jointly regulate rice blast resistance (Xie et al., 2011). R gene (HRT) plays a role in Arabidopsis thaliana resistance to turnip leaf virus (TCV) (Jeong et al., 2010). Our previous studies revealed that WRKY transcription factor family genes participated in the interaction of salicylic acid and jasmonic acid signaling pathways (Shang et al., 2011; Zhang et al., 2019). Previous studies have also shown that GbWRKY1 negatively regulates the resistance of cotton to Boea cinerea through JA signaling pathway. OsWRKY13 regulates the expression of JA and SA upstream and downstream genes, and is involved in rice disease resistance.

Under the condition of limited resources, intercropping soybean should not only grow rapidly to compete for more light, but also improve the defense response to resist the harm of pathogenic microorganisms. How soybeans balance the allocation of resources between growth and defense is unclear. In this paper, we explored the effects of different light intensity on the physiological and biochemical indexes of SMV-infected soybeans, and compared the changes of defense mechanism of SMV-infected soybeans under different light intensities by RNA-seq sequencing method. The results of this study will provide a basis for the study of SMV resistance in intercropping soybean.

2 Methodology

2.1 Plant material, virus inoculation, and light treatment

Soybean seeds (Nannong 1138-2, a SMV susceptible variety) were kindly provided by Dr. Kai Li from Nanjing Agricultural University in China. The SMV isolate (YA87) was collected from the field soybean plants in Sichuan Province, China. The bean Phaseolus vulgaris cv. Topcrop was used for local-lesion purification of SMV, and then the virus was propagated on the soybean cv. Nannong 1138-2 (Zhang et al., 2019). Soybean seeds were surface-sterilized and sown in a mixed matrix containing PINDSTRUP organic soil (Pindstrup Mosebrug A/S, Ryomgaard, Denmark) and vermiculite (v:v, 4:1) in an artificial climate chamber with 25 °C/22 °C day/night temperature, 60% relative humidity and 14 h/10 h of photoperiod.

Select soybean seedlings with the same growth and inoculate them with the virus (Shang et al., 2011). Leave it in the dark for 12 hours for light treatment. They were treated with hard light, normal light, the shade and the dark. For each light condition, three soybean strains were inoculated with virus and three soybean strains were inoculated with virus-free phosphoric acid buffers as controls (Table 1). Placed in a culture environment with a temperature of 25°C and a humidity of 60%.

2.2 Sample collection and sequencing

Previous studies have shown that larger changes in transcriptional levels occurred in soybeans infected SMV at 10 dpi (Zhang et al., 2019). Therefore, we collected the V2 leaves (the

TABLE 1 Four light intensities gradients.

Light intensity	Control	Virus vaccination
8.11μmol/m^2s	DC: Dark/control	DS: Dark/SMV
121.63μmol/m^2s	LC: Low light/control	LS: Low light/SMV
349.73μmol/m^2s	NC: Normal light/control	NS: Low light/SMV
522.97μmol/m^2s	HC: Hard light/control	HS: Hard light/SMV

second trifoliolate leaf, newly grown) of soybean plants after treatment for 10 dpi. Total RNA was extracted using phenol-chloroform-isoamyl alcohol and lithium chloride, washed by using 70% ethanol, and finally checked by Agilent 2100 Bioanalyzer to ensure RIN number > 7.0. After the samples were tested, cDNA libraries were constructed and paired-end sequencing was performed based on the Illumina HiSeq 2500 platform at Nuohezhiyuan BioInformation Technology Co., LTD. (Tianjin, China). Three biological replicates were set up for each treatment and a total of 24 independent samples were used for RNA-Seq.

2.3 Read alignment and expression analysis

The reads number, Q30, N (%), Q20 (%), and Q30 (%) of raw data was counted. After removing reads containing sequencing adapters and reads of low quality, the clean data were mapped to the reference genome of Glycine max (Glyma2.0) using Bowtie2 and Tophat2. The reads mapped to exon region were also counted. HTSeq (Version 0.11) was used to calculate the read count mapped to each gene as the expression level of the gene at the initial stage. Gene expression levels were normalized using the RPKM (reads per kb per million reads) method. Differential expression analysis between treatments was identified by DESeq2 with screening parameters of $\log_2$FC (fold change) > 1 and p-adj (adjusted p-value) < 0.05 (Zhang et al., 2019).

2.4 Functional enrichment analysis of DEGs

The latest genomic reference information of Glycine max was obtained from the Soybase (www.soybase.org), including Gene Ontology (GO) annotations for each gene. The Kyoto Encyclopedia of Genes and Genomes (KEGG) annotations was obtained from the KEGG database. A hypergeometric test was used to find out the GO terms and KEGG pathways that was significantly enriched by DEGs. The enrichment analyses of GO and KEGG were performed using the OmicShare online website (www.omicshare.com/tools).

2.5 Validation of gene expression by qRT-PCR

To verify the accuracy and reproducibility of the RNA-Seq data, RT-qPCR assays were conducted with gene specific primers. Total RNA from the samples was extracted. Reverse transcription was performed using 5× All-In-One RT Master Mix kit (AccuRT Genomic DNA Removal Kit, ABM, Vancouver, Canada). In addition, 2×RealStar Fast SYBR qPCR Mix (GenStar, Beijing, China) was used and Eppendorf Mastercycler ep realplex (Eppendorf, Hamburg, Germany) instrument was used for the RT-qPCR experiment. Each treatment contained three independent biological replicates and three technical replicates. The expression level of soybean β-actin gene was used as an internal reference. The fold change value of gene expression was calculated using the $2^{-\Delta\Delta Ct}$ method. The sequences of specific primers were listed in Table S1.

2.6 Statistical analysis

The one-way ANOVA model was used for analyses of the error in IBM SPSS Statistic 27, and the average value was taken. The significance was judged by the new complex range method (Duncan's method) at $p < 0.01$.

3 Results and discussion

3.1 Phenotype and virus content of infected soybean

After inoculation with SMV, soybean leaves under hard and normal light showed obvious mosaic symptoms. Dwarfing was observed in all SMV-inoculated soybeans compared to the controls (Figure 1A). Compared with the control group, the plant height of infected soybean was not decreased significantly under normal light and hard light, but the pitch spacing was shortened. In the dark and the shade, the plant height of infected soybean decreased significantly compared with the control group. In the shade and under normal light, the stem diameter of infected soybeans increased slightly compared to the control group due to the virus infection, which caused significant shrinkage. However, the stem diameter of hard light and dark light was smaller than that of control group (Figures 1B, C). Compared with groups in the dark, the shade and under hard light, the accumulation of virus increases under normal light (Figure 1D).

Viral infection often causes plant dwarfing (Shang et al., 2011). SMV inoculation resulted in dwarfing of soybean plants. SMV-infected soybeans were dwarfed compared to controls even when the main stem of the soybeans in the shade and the dark was

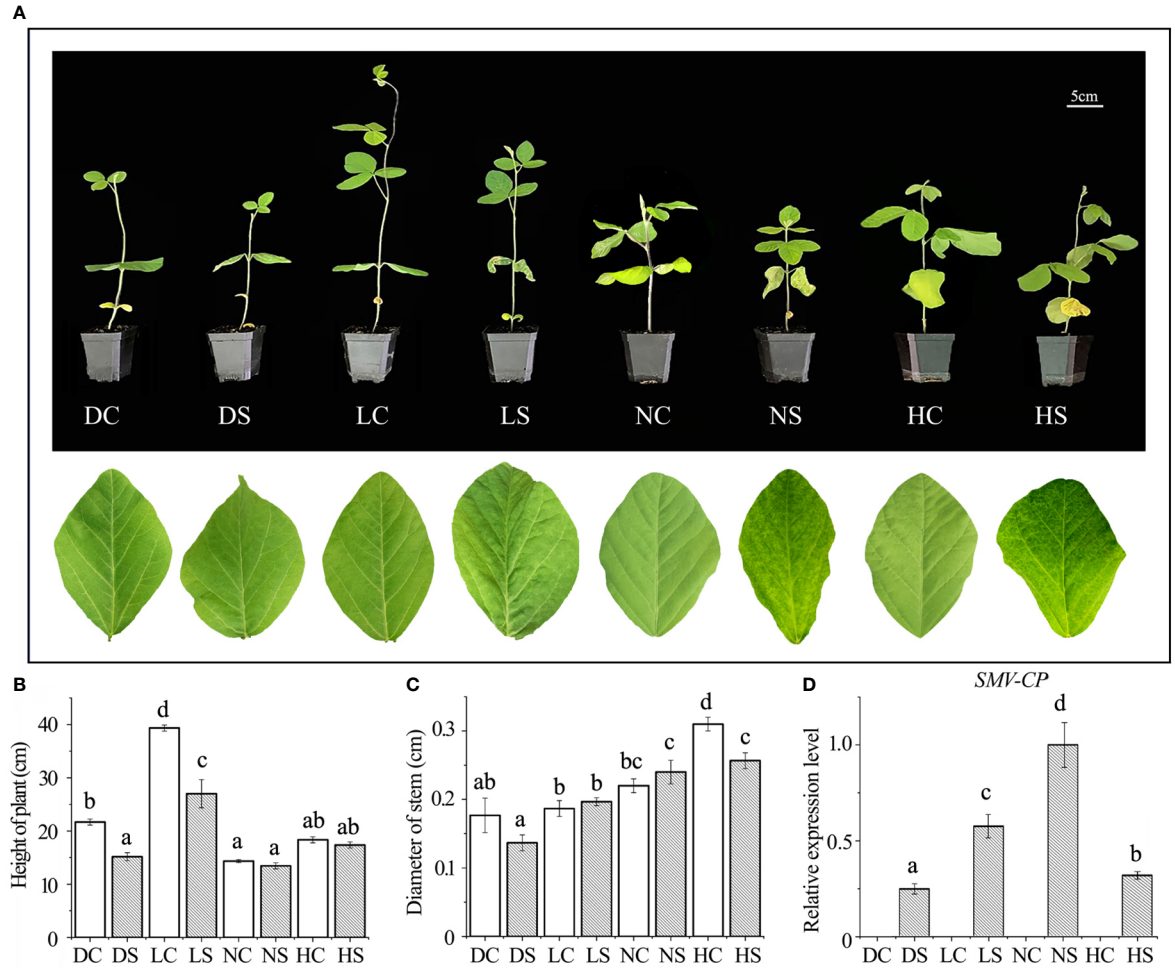

FIGURE 1
Phenotype and virus content of soybean infected with SMV under different light intensities. **(A)** Phenotype of SMV-infected soybean under different light intensities; **(B)** Plant height of soybean under different treatments; **(C)** Soybean stem diameter under different treatments; **(D)** Quantitative detection of SMV-CP content by qPCR. DC, dark+control; DS, dark+SMV; LC, low light+control; LS, low light+SMV; NC, normal light+control; NS, normal light+SMV; HC, hard light+control; HS, hard light+SMV; Data are expressed as mean ± standard deviation. Values with different letters in a column differ significantly ($p < 0.05$).

elongated. Our previous study found that shade resulted in decreased defense ability of soybean (Zhang et al., 2019). The down-regulation of defense ability reduced the inflammatory response of soybean, which was conducive to improving the tolerance to the pathogen. At the same time, more resources can be allocated to the growth of soybean. Our previous studies have shown that reactive oxygen species can promote viral infection (Shang et al., 2009; 2010; 2011; 2019; Tang et al., 2019). Compared with groups under normal and hard light, reactive oxygen species in soybean decreased in the shade and the dark (Figure 2A), leading to a decrease in virus content (Figure 1D).

Plant growth is regulated by auxin (IAA) and gibberellin (GA). The levels of gibberellin and auxin were detected in stems and leaves of soybean (Figure S1). The contents of gibberellin and auxin in soybean decreased after virus infection compared with the controls. Compared with control, auxin and gibberellin in stem and leaf of soybean decreased dramatically under normal light. Under normal light, soybeans have more resources allocated for defense. Compared with control, auxin and gibberellin in stem and leaf of soybean decreased slightly in the shade and the dark. This suggested that plants with limited resources are more likely to allocate resources to vegetative growth and moderate resistance to viruses. Compared with control, auxin and gibberellin in stems and leaves of soybean also decreased slightly under high light, which may be related to photo-inhibition.

3.2 Histochemical staining and membrane damage index determination

NBT and DAB staining showed the highest content of superoxide and hydrogen peroxide in soybean inoculated with SMV in the dark. With the increase of light, the content of superoxide and hydrogen peroxide increased gradually compared with the control group. Trypan blue staining showed more severe necrosis in SMV-inoculated soybeans than in healthy plants

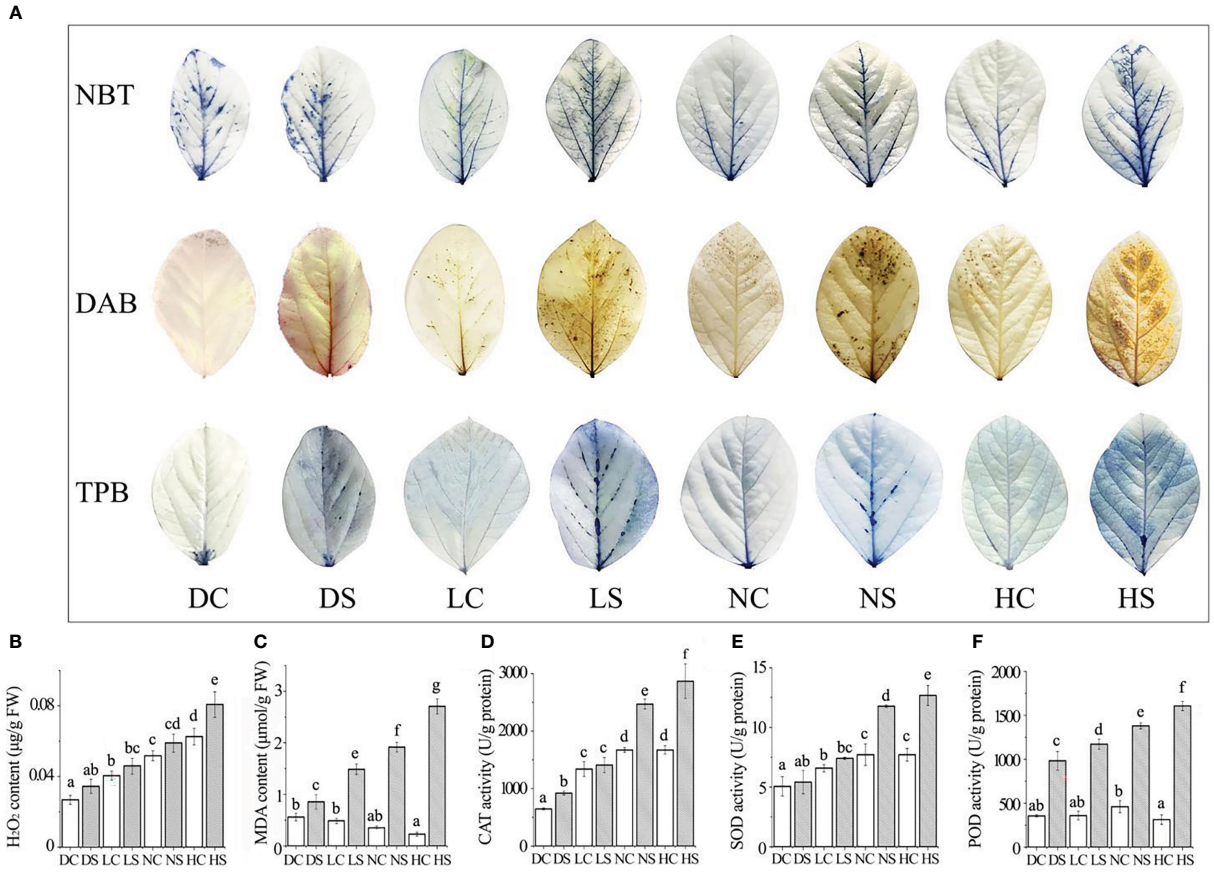

FIGURE 2
Staining results, membrane lipid peroxidation damage index and the enzyme activity were determined. **(A)** NBT, DAB and TPB staining results; **(B)** hydrogen peroxide; **(C)** malondialdehyde content; **(D)** CAT enzyme activity; **(E)** SOD enzyme activity; **(F)** POD enzyme activity. DC, dark+control; DS, dark+SMV; LC, low light+control; LS, low light+SMV; NC, normal light+control; NS, normal light+SMV; HC, hard light+control; HS, hard light+SMV; Data are expressed as mean ± standard deviation. Values with different letters in a column differ significantly ($p < 0.05$).

(Figure 2A). Compared with the healthy control, SMV infection induced the accumulation of hydrogen peroxide. As the light intensity increased, so did the hydrogen peroxide content (Figure 2B). But the accumulation of hydrogen peroxide in soybean plants under darkness was higher. Malondialdehyde (MDA) content increased with the increase of light exposure compared with the control group. SMV infection induced more MDA accumulation (Figure 2C).

Light increased the content of reactive oxygen species (ROS) (Vuleta and Manita, 2016). This was confirmed by soybean leaf staining results. ROS outbreaks activate defense signaling pathways to defend against pathogen attacks (Li et al., 2017). The accumulation of reactive oxygen species causes damage to cell membranes (Shang et al., 2011), thus increasing malondialdehyde levels. Hard light damages the photosynthetic system of leaves, and leaves suffer serious oxidative damage (Chang et al., 2013).

3.3 Determination of enzyme activity

The activity of antioxidant enzymes increased in SMV-infected soybeans compared to the control. The contents of catalase, superoxide dismutase and peroxidase showed the same trend (Figures 2D–F). The accumulation of reactive oxygen species activated the antioxidant enzyme system (Shang et al., 2019). Compared with the control group, soybean antioxidant enzyme activity increased significantly more under hard light and normal light than in the shade and the dark. This is because light stimulates cells to produce more reactive oxygen species (ROS) during disease resistance (Figure 2B), thus activating the activity of the antioxidant enzyme system.

3.4 Statistics of differential genes

Compared with the healthy control, 2590 genes were up-regulated and 1767 genes were down-regulated in the dark soybean infected with SMV. In the shade, 1467 genes in soybean were up-regulated and 970 genes were down-regulated. Under normal light, 2360 genes were up-regulated and 3156 genes were down-regulated. There were 3197 up-regulated genes and 1211 down-regulated genes in soybean under hard light. Soybean under normal light had the most differentially expressed genes and the most positive response to SMV (Figure 3A).

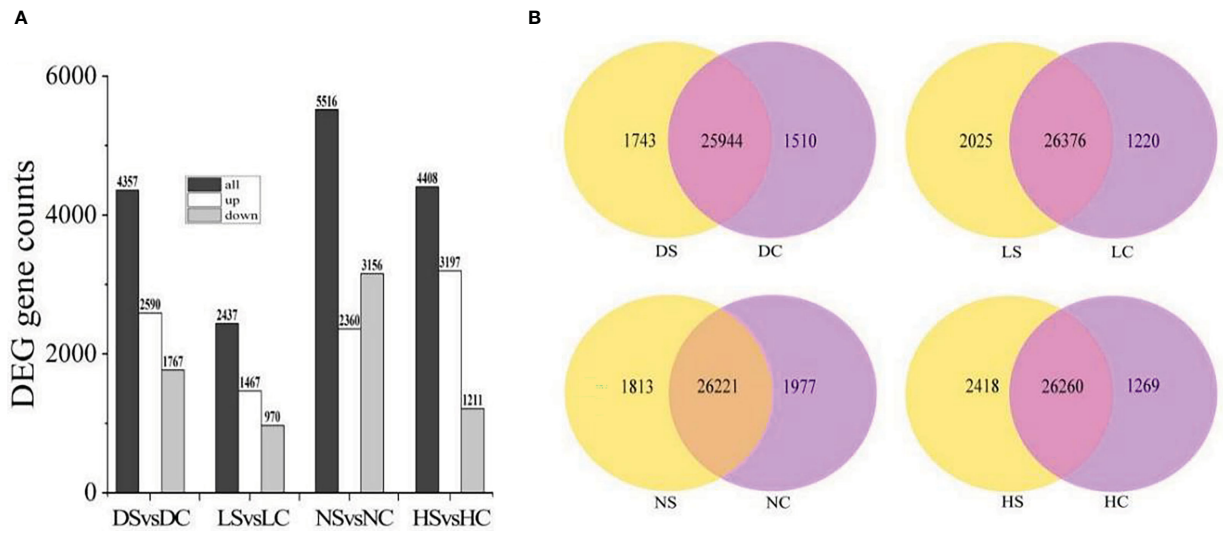

FIGURE 3
Differential gene statistics. **(A)** Statistics of differential genes between infected SMV and control under different light intensities; **(B)** Overlap analysis of differential genes in the dark, in the shade, under normal light, and under hard light. DC, dark+control; DS, dark+SMV; LC, low light+control; LS, low light+SMV; NC, normal light+control; NS, normal light+SMV; HC, hard light+control; HS, hard light+SMV.

There were 25,944 gene overlaps between SMV-inoculated soybean and healthy control in the dark, 26,376 gene overlaps between SMV-inoculated soybean and healthy control in the shade, 26,221 gene overlaps between SMV-inoculated soybean and healthy control under the normal light. There were 26260 gene overlaps between SMV-inoculated soybean and healthy control under the hard light (Figure 3B).

3.5 GO function enrichment analysis of DEGs

Gene Ontology (GO) enrichment analysis was used to determine the functional classification of DEGs between different treatments. Genes were divided into three categories: Biological process, molecular function, and cellular component. When looking at biological processes, the most genes are differentially expressed in cellular processes, metabolic processes and single-organism processes. Among cell components, the most differentially expressed genes were found in the synthesis of the cell wall and the macromolecule complex. In the molecular function (MF), binding and catalytic activity accounted for the highest proportion (Figure 4).

In the dark and the shade, differential genes were enriched in photosynthesis and growth and development regulation in infected soybeans (Figures 5A, B). In the dark, photosynthesis, cellular carbohydrate metabolic process, multicellular organism process, thylakoid in cellular components, the thylakoid part, photosystem II, photosystem II oxygen evolving complex, hydrolase activity, photosynthetic membrane, Thylakoid Part, Photosystem II oxygen evolving complex, the hydrolase activity, oxidoreductase activity, carbohydrate phosphatase activity and other pathways have the most differentially expressed genes. In the shade, sulfur compound transport, multicellular organism process, floral organ development, thylakoid, photosystem I, photosynthetic membrane, ADP binding, pattern binding, polysaccharide binding in molecular function, hydrolase activity pathway had the most genes.

Under sufficient light, differential genes enriched in cell wall components, cell recognition function and disease resistance in infected soybeans (Figures 6A, B). Under normal light, multi-organism process, cell recognition, extracellular region, the cell wall, the hydrolase activity, acting on glycosyl bonds, copper ion binding, hydrolase activity, cellulose synthase activity, acting on glycosyl bonds, copper ion binding, the hydrolase activity, cellulose synthase activity, transferase activity, oxidoreductase activity, cellular metabolic process, cellular glucan metabolic process, glucan metabolic process. Under hard light, cellular metabolic metabolic process, cellular glucan metabolic process, cellular

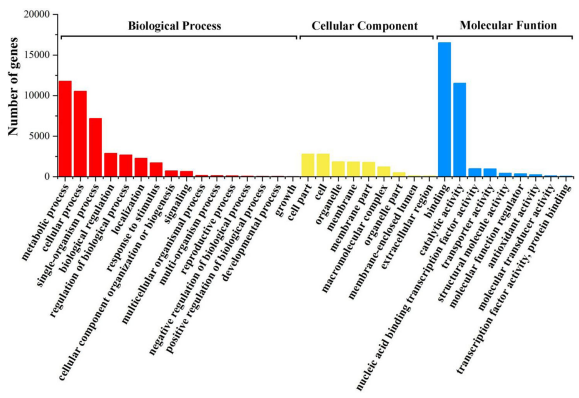

FIGURE 4
GO functional enrichment analysis of differential genes in total.

10.3389/fpls.2023.1150870

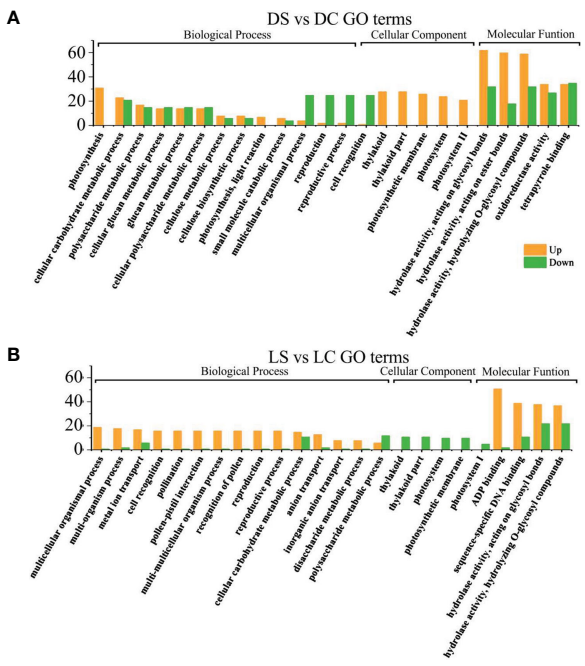

FIGURE 5
GO functional enrichment analysis of differential genes between infected SMV and control in the dark and the shade. **(A)** GO functional enrichment analysis of differential genes in the dark; **(B)** GO functional enrichment analysis of differential genes in the shade. DC, dark+control; DS, dark+SMV; LC, low light+control; LS, low light+SMV.

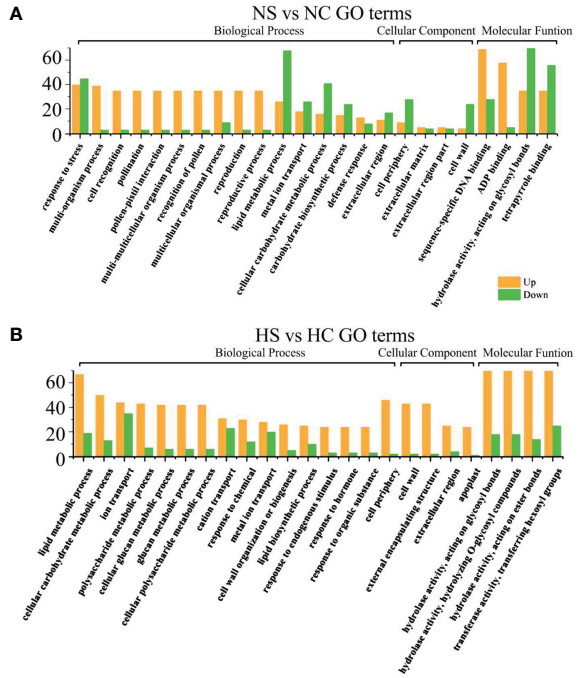

FIGURE 6
GO functional enrichment analysis of differential genes between infected SMV and control under normal light and hard light. **(A)** GO function enrichment analysis of differential genes under normal light; **(B)** GO function enrichment analysis of differential genes under hard light. NC, normal light+control; NS, normal light+SMV; HC, hard light+control; HS, hard light+SMV.

metabolic process, cell wall synthesis, cellulose metabolic process, cell periphery, cellular metabolic process, cell periphery, the cell wall, hydrolase activity, copper ion binding, glucosyltransferase activity, enzyme inhibitor activity, the hydrolase activity, heme binding, tetrapyrrole binding pathway had the most genes.

Under normal light and hard light, most of the DEGs in infected soybean were mainly expressed above regulation. Genes related to glucose metabolism, hydrolase activity, antioxidant enzyme activity, cellulose metabolism, cell wall synthesis and other pathways related to disease resistance were significantly up-regulated. When light is insufficient, plants allocate major resources to the regulation of photosynthetic system and growth and development. Previous studies have also shown that the disease resistance of plants decreased in the shade (Zhang et al., 2019). In the dark and the shade, the number of down-regulated genes increased in soybean infected with SMV compared with the controls. (Figures 5A, B). Our previous studies have shown that light is crucial for defense activation (Zhang et al., 2019). The results of this experiment further prove that light intensity has a positive regulatory effect on soybean defense response.

3.6 KEGG pathway enrichment analysis of DEGs

Metabolic pathways of the four light-intensity susceptible soybeans were analyzed, and the top 15 KEGG metabolic pathways with the most differentially expressed genes were shown in Figures 7 and 8. Differential genes enriched in carbon metabolism, glycolysis and photosynthesis pathways were most up-regulated in infected soybeans under darkness (Figure 7A). The most down-regulated genes were those enriched in plant-pathogen interaction pathway and MAPK signaling pathway (Figure 7B). In the shade, the most up-regulated genes in infected soybean were differentially expressed in plant-pathogen interaction pathway, the endocytosis pathway, starch and sucrose metabolic pathway (Figure 7C). The most down-regulated genes were MAPK signaling pathway, photosynthetic pathway and cysteine and methionine metabolic pathway (Figure 7D). Under normal light, the most up-regulated expression in infected soybeans was concentrated in plant-pathogen interaction pathway, MAPK signaling pathway, glutathione metabolic pathway, starch and sucrose metabolic pathway (Figure 8A). The most down-regulated genes were those that were enriched in phenylpropanoid biosynthesis, amino sugar and nucleotide sugar metabolism, ascorbic acid and alnus acid metabolism pathway, and flavonoid metabolism pathway (Figure 8B). Under hard light, the most up-regulated genes in infected soybeans were those that were enriched in amino sugar and nucleotide sugar metabolism, phenylpropanoid biosynthesis, pentose and glucuronic acid interconversion, and α-linolenic acid metabolism (Figure 8C). The most down-regulated genes were those enriched in MAPK signaling pathway and plant-pathogen interaction pathway (Figure 8D). These results suggest that when light intensity is low, plants allocate more resources to

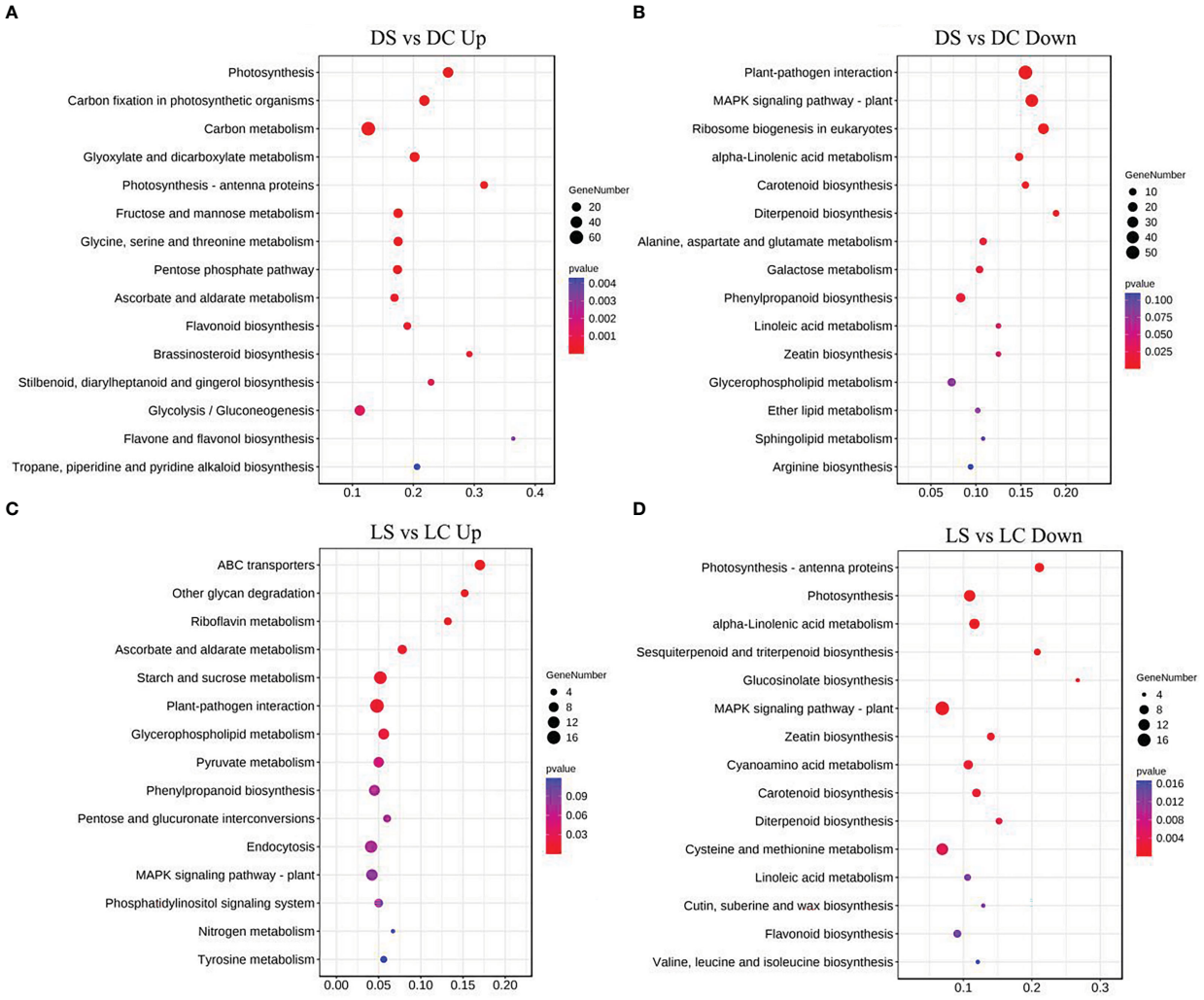

FIGURE 7
Differential gene KEGG pathway enrichment analysis in soybeans in the dark and the shade. **(A, B)** Up-regulated and down-regulated differential gene KEGG pathway enrichment analysis in the dark; **(C, D)** Up-regulated and down-regulated differential KEGG pathway enrichment analysis in the shade. DC: dark+control; DS, dark+SMV; LC, low light+control; LS, low light+SMV; NC, normal light+control; NS, normal light+SMV; HC, hard light +control; HS, hard light+SMV.

vegetative growth. Light intensity can positively regulate the defense regulation of plants, but too hard light intensity will reduce the defense.

3.7 DEGs involved in plant-pathogen interaction

Considering the expression levels of soybean related genes under four light intensities, 19 of the most differentially expressed genes were enriched into plant-pathogen interaction pathways. The genes involved in the plant immunity and the pathogen infection constitute the plant-pathogen interaction pathways (Dodds and Rathjen, 2010). Differentially expressed genes mainly included NBS-LRR family genes, WRKY transcription factors, MAPK genes, MYB transcription factors and hormone pathway-related defense genes (Tables 2, 3). WRKY and MYB are transcription factors involved in plant stress resistance under both biological and abiotic stresses (Zhang et al., 2019). WRKY transcription factors act on SA and JA downstream defense genes to play a positive and negative role in regulating disease resistance (Tang et al., 2013). The NBS-LRR class is the largest class of R genes and is mainly responsible for ATP hydrolysis as well as releasing signals. The NBS-LRR can help plants effectively fight against a variety of pathogens, including viruses, bacteria, fungi, nematodes, and insects. Most of these overlapping genes were induced under normal light. Some of those genes induced under hard light. In the dark and the shade, resistance-related genes were down-regulated. When light is insufficient, the defense of soybean is inhibited.

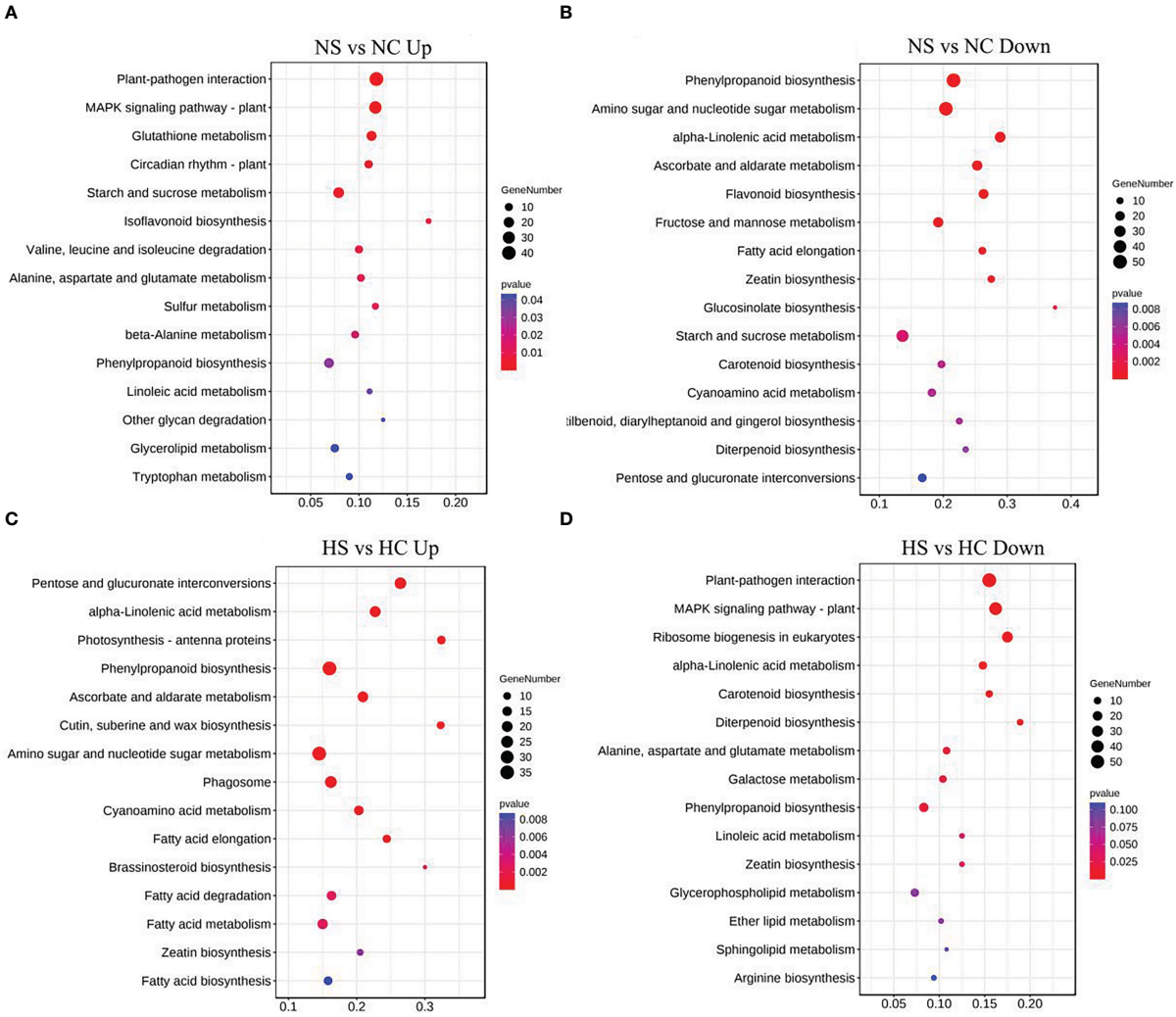

FIGURE 8
Differential gene KEGG pathway enrichment analysis in soybeans under normal light and hard light. **(A, B)** Up-regulated and down-regulated KEGG pathway enrichment analysis under normal light; **(C, D)** Enrichment analysis of up-regulated and down-regulated differential gene KEGG pathway under the hard light. DC, dark+control; DS, dark+SMV; LC, low light+control; LS, low light+SMV; NC, normal light+control; NS, normal light+SMV; HC, hard light+control; HS, hard light+SMV.

3.8 DEGs involved in plant hormone signal transduction

The differentially expressed genes involved in the three plant hormone signaling pathways of salicylic acid, jasmonic acid and ethylene are shown in Table 2. The virus is a live trophic pathogen (Shang et al., 2011). Soybean can resist the virus infection mainly by up-regulating salicylic acid signaling pathway genes. Normal light significantly activated salicylic acid pathway defense genes. In all treatments, defense genes of jasmonic acid pathway were down-regulated in infected soybeans. Under normal light and hard light, some defense genes of ethylene signaling pathway were significantly up-regulated and some were significantly down-regulated in infected soybeans.

3.9 Validation of RNA-Seq data by qRT-PCR

To further confirm the gene expression pattern obtained from RNA-Seq, 15 DEGs were selected for RT-qPCR, including NB-ARC (100820033, 100792603, 100793122), WRKY40 (100816991, 100810978), WRKY50 (100796836), WRKY70 (102670495), WRKY33 (100776837), NPR1 (100797074), PR1 (100807250), JAR1 (100792358), MYC2 (102663214), and the transcriptome sequencing results were fitted and analyzed (Figure 9).

Most of the gene expressions were sensitive to changes in light intensity and the virus invasion and were significantly induced under normal light. However, hard light down-regulated the expression of the above genes. The expression of these genes in

TABLE 2 Overlapped DEGs related to plant-pathogen interactions.

Gene ID	Gene Description	DSvsDC log_2FC	LSvsLC log_2FC	NSvsNC log_2FC	HSvsHC log_2FC
100820033	NB-ARC domain-containing protein	-1.781	7.878	12.378	-4.265
100803026	YODA MAPKK kinase	1.408	5.308	10.000	0.699
100792603	TMV resistance protein,NB-ARC	1.201	8.398	9.090	2.491
102659638	TMV resistance protein N, TIR domain	-0.233	7.815	7.261	—
100816991	probable WRKY transcription factor 40	—	6.685	7.261	-9.106
100793122	disease resistance protein, NB-ARC	-5.510	6.821	7.154	2.576
100796836	probable WRKY transcription factor 50	0.914	5.560	6.995	-1.522
100810978	probable WRKY transcription factor 40	0.236	3.577	5.889	-7.544
102670495	probable WRKY transcription factor 70	—	2.002	4.167	-7.131
100776837	probable WRKY transcription factor 33	-1.803	-1.171	2.140	-3.506
100792193	probable WRKY transcription factor 70	—	0.617	1.670	-8.377
100306201	Pathogenesis-related protein	—	2.461	1.311	-6.208
100791870	probable WRKY transcription factor 40	-1.612	2.457	0.695	-8.732
100781032	transcription factor MYB14	—	1.495	-1.084	-8.257
100783267	Pathogenesis-related protein	1.242	1.912	-1.992	9.144
100795186	Pathogenesis-related thaumatin protein	2.601	-1.290	-2.542	8.922
778179	MYB transcription factor MYB73	0.714	-3.010	-8.536	1.214
100819665	MAPK/ERK kinase 1	—	-2.429	-9.629	7.925
100775603	transcription factor MYB14	0.675	-2.639	-10.587	3.878

soybean was inhibited in the shade and the dark. It shows that suitable light is necessary to activation of the defense in soybean. When the growth of soybean was weak under low light, high resistance will be detrimental to the plant (Shang et al., 2011). Light induces excess heat energy in soybean during photosynthesis (Shang et al., 2019). In order to reduce soybean consumption under hard light, some resistance genes were down-regulated. In order to adapt to the change of light intensity, soybean balanced allocation of resources between growth and defense through a series regulation of gene expression. In general, gene expression patterns displayed by RT-qPCR and RNA Seq tend to be consistent.

3.10 Quantitative analysis of differentially expressed genes related to hormone pathways

Quantitative analysis of defense gene expression of salicylic acid pathway showed that NPR1 expression of infected soybean was up-regulated under normal light. Compared with the control, the expression of NPR1 gene in infected soybean was down-regulated under hard light, in the shade and the dark (Figure 10). At the same time, the expression level of NPR1 suppressor gene was opposite to that of NPR1 gene under different light intensities. The expression of NPR3 gene in infected soybean was down-regulated in the dark and under hard light compared with the control. The expression of NPR3 in infected soybean was up-regulated in the shade and under normal light compared with the control. Under normal light, PR1 and PR10 genes were significantly up-regulated in infected soybean compared with the control. In the dark and the shade, the above genes were slightly up-regulated. Previous studies have shown that PR family genes are induced by light, but suppressed under hard light (Agrawal et al., 2000; Wu et al., 2020). Under hard light, they significantly down-regulated expression. The expression of TGA1 gene in infected soybean was down-regulated in the shade and under normal light compared with the control. The expression of TGA3 gene in infected soybean was significantly down-regulated under hard light compared with the control. However, the expression of TGA3 in infected soybean was up-regulated in other treatments compared with the control. TGA gene may be a key regulatory gene for the antagonism between salicylic acid and jasmonic acid (Caarls et al., 2015). This indicates that light is one of the important conditions for activating salicylic acid defense reaction, which is consistent with previous studies (Backer et al., 2015). Hard light inhibited the expression of salicylic acid pathway defense genes in plants. The increase of light intensity will aggravate the mosaic symptoms of leaves. The severity of symptoms is proportional to the virus content (Figure 1). Hard light will cause light suppression and damage, and lack of light will make the plant grow weak. Therefore, down-regulating the expression of defense

10.3389/fpls.2023.1150870

TABLE 3 DEGs involved in plant defense hormone signaling.

Gene ID	Gene Description	DSvsD log_2FC	LSvsL log_2FC	NSvsN log_2FC	HSvsH log_2FC	Pathway
100527824	NPR1 interacting protein	0.251	1.559	4.449	-0.339	SA
100797074	NPR1 interacting	-2.459	1.970	3.417	-1.752	
100805261	Protein SUPPRESSOR OF NPR1-1	3.116	1.433	-1.217	1.478	
100814739	Regulatory protein NPR3	0.062	2.179	3.946	0.960	
100807250	pathogenesis-related protein 1	—	4.142	6.477	-2.628	
100805116	pathogenesis-related protein 1	-0.585	0.014	3.543	-1.573	
100527073	pathogenesis-related protein 10	-0.994	0.864	2.036	-1.822	
100808443	Transcription factor TGA1	2.088	1.090	1.905	0.080	
100794268	Transcription factor TGA3	0.212	1.208	1.393	-2.577	
100792358	Jasmonic acid-amido synthetase JAR1	0.244	-1.783	-3.467	2.225	JA
100813472	Jasmonic acid-amido synthetase JAR1	—	-0.426	-2.517	1.979	
100819069	Coronatine-insensitive protein 1	-0.322	0.511	1.311	-0.912	
100793081	Coronatine-insensitive protein 1	0.153	-0.137	1.201	-0.670	
102663214	transcription factor MYC1	-2.641	-0.806	2.284	-2.138	
100790854	transcription factor MYC2	-0.359	-2.319	-1.502	0.947	
100804965	transcription factor MYC2	-1.217	-2.593	-4.036	2.718	
100795733	transcription factor MYC2	0.020	-2.038	-4.168	3.759	
100819971	ethylene-responsive transcription ERF023	2.665	-0.355	-7.755	7.046	ET
100101914	ethylene-responsive transcription ERF034	-1.016	-1.123	-6.713	3.327	
100811328	ethylene-responsive transcription ERF054	-5.865	4.920	-5.856	7.152	
100778793	ethylene-responsive transcription ERF027	-6.274	-1.342	-5.028	1.974	
100785936	ethylene-responsive transcription factor 1B	-2.309	1.014	4.614	-4.511	
100804481	ethylene-responsive transcription factor 1B	-2.064	-1.140	2.791	-3.135	
100790598	ethylene-responsive transcription factor 1B	-2.368	-1.295	1.973	-1.994	
100801528	ethylene-responsive transcription ERF010	-0.672	-0.367	1.444	-2.449	
100786182	EIN3-binding F-box protein	-1.204	-0.460	1.240	-0.040	
100805418	EIN3-binding F-box protein	-1.356	-0.292	1.214	-0.293	

genes can reduce the inflammatory response, which is a self-protection mechanism to balance defense and growth of plants.

The determination of hormone content showed that the removal of salicylic acid played an important role in the antiviral process of soybean. Compared with the control, the salicylic acid content in infected soybeans increased significantly under normal light and hard light. Salicylic acid increased slightly in infected soybeans in the dark and the shade compared with the control (Figure S2). Levels of jasmonic acid and ethylene decreased in infected soybeans compared with the control, but increased under hard light. It indicated that soybean could resist the virus infection mainly by increasing salicylic acid content. But when salicylic acid concentration was too high, the contents of ethylene and jasmonic acid would increase and antagonize the salicylic acid pathway. In the shade, ethylene content in infected soybean increased significantly compared with control. This is more conducive to the downregulation of resistance and inflammatory response.

Quantitative analysis of defense gene expression of jasmonic acid pathway showed that JAR1 gene was down-regulated in infected soybean in the shade and under normal light. JAR1 gene was up-regulated in infected soybean under hard light. COI1 expression in soybean was up-regulated in the dark and the shade, and down-regulated under hard light. The expression of MYC2 gene was down-regulated in soybeans in the shade and under normal light, and up-regulated in soybeans under hard light. Our previous studies have shown that jasmonic acid pathway and salicylic acid pathway antagonizes each other against the virus infection (Shang et al., 2011).

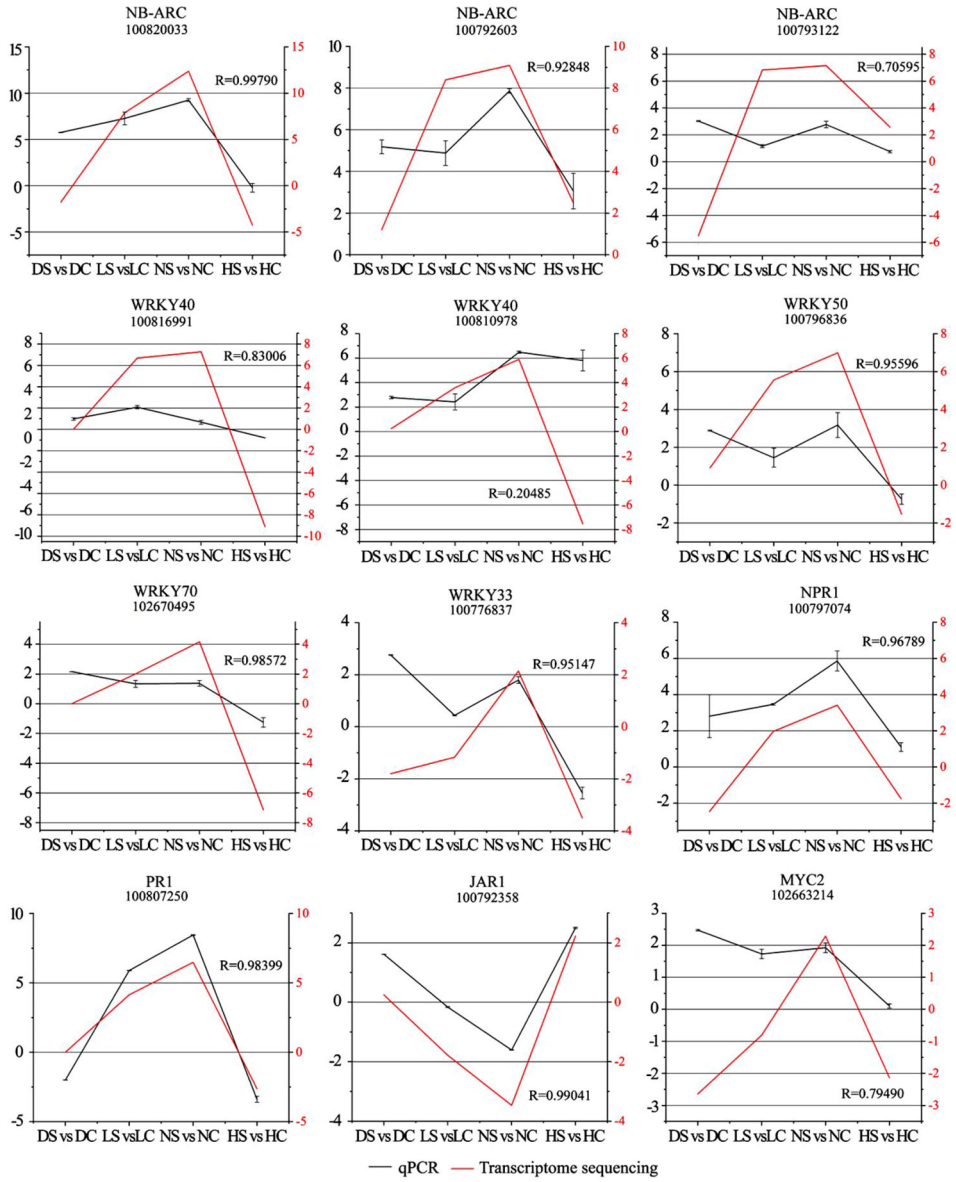

FIGURE 9
Comparison analysis of resistance-related highly differentially expressed genes by RT-qPCR and transcriptome sequencing. Note: Left vertical axis coordinate is relative expression level of RT-qPCR (black); right vertical axis coordinate is RPKM of RNA-Seq (red). Ordinate axis is the correlation coefficients between RT-qPCR and RNA-seq. DC, dark+control; DS, dark+SMV; LC, low light+control; LS, low light+SMV; NC, normal light+control; NS, normal light+SMV; HC, hard light+control; HS, hard light+SMV.

The expression of ethylene related ERF023, ERF034, ERF053 and ERF027 in infected soybean was significantly down-regulated in the shade and under normal light, and up-regulated under hard light. Under normal light, ERF1 gene expression in infected soybean was significantly up-regulated. ERF1 gene was down-regulated in infected soybean under hard light and in the shade. EIN3 gene was down-regulated in infected soybean in the dark and under normal light. Under hard light, EIN3 expression in infected soybean was significantly down-regulated. Hard light causes EIN3 to break down (Shi et al., 2016).

4 Conclusion

In this study, the mechanism of soybean response to *Soybean mosaic virus* infection under different light intensities was analyzed using RNA-seq sequencing technology. The induction of defense genes by light was significant. Soybean fights SMV infection mainly by activating the salicylic acid defense signaling pathway. Oxidative damage caused by increased light intensity promotes viral infection. In order to reduce oxidative damage, some defense genes of infected soybean were down-regulated under hard light.

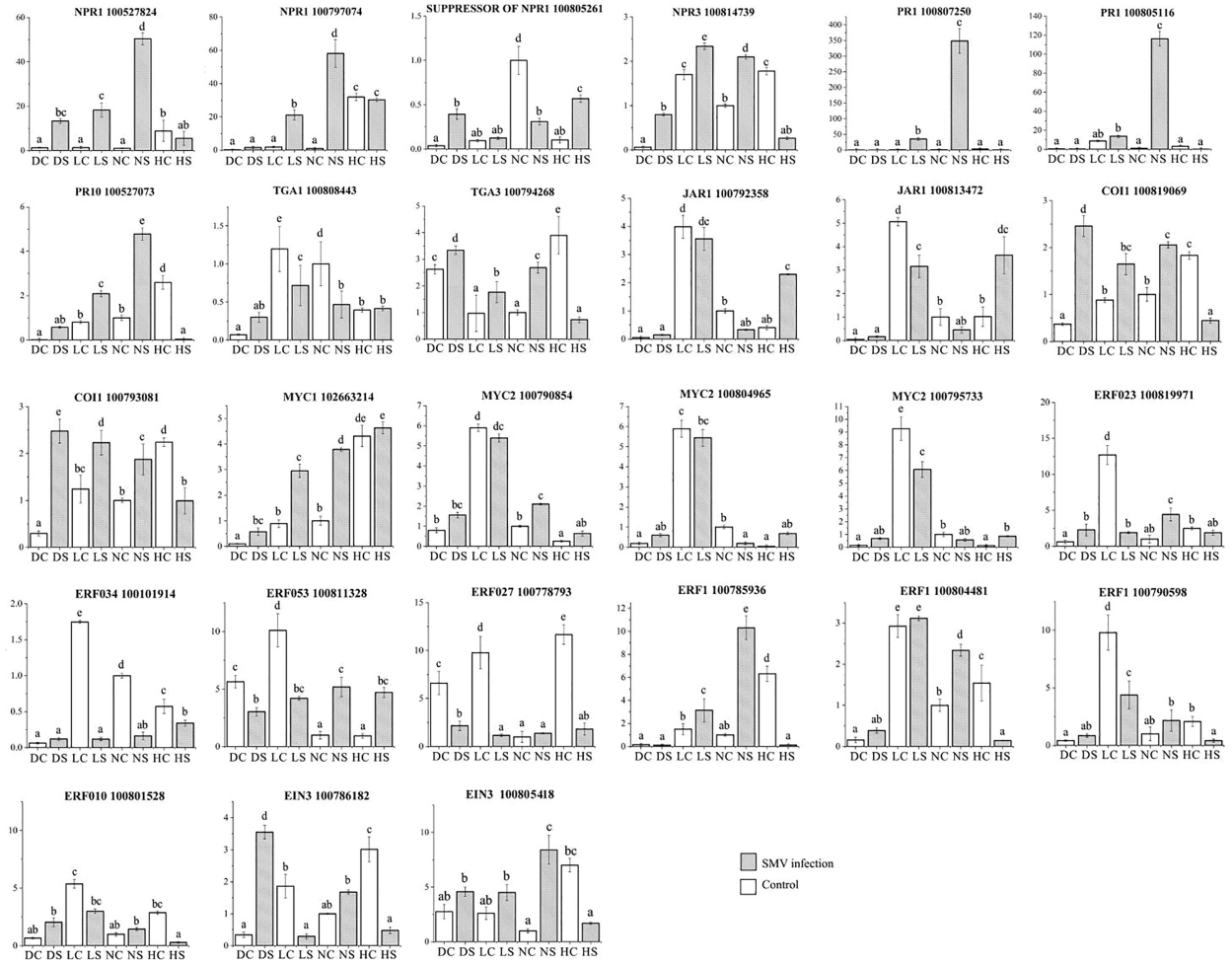

FIGURE 10
Quantitative analysis of differentially expressed genes related to hormone pathways by qPCR. DC: dark+control; DS: dark+SMV; LC: low light+control; LS: low light+SMV; NC: normal light+control; NS: normal light+SMV; HC: hard light+control; HS: hard light+SMV. Data are expressed as mean ± standard deviation. Values with different letters in a column differ significantly ($p < 0.05$).

The change of defense-related gene expression was confirmed by real-time quantitative PCR. In order to adapt to the change of light intensity, soybean balanced allocation of resources between growth and defense through a series of gene expression regulation. The results of this study will provide a theoretical basis for the research of SMV resistance in intercropping soybean. In the future, we aim to analyze the response of key resistance genes to light changes and their role in the antiviral process of soybean.

Data availability statement

The original contributions presented in the study are included in the article/Supplementary Material. Further inquiries can be directed to the corresponding author.

Author contributions

JS designed the study. JS, L-PZ, and C-SH collected the data. JS, X-MY, X-LQ, and J-FY analyzed the data and prepared the first draft. JS reviewed and edited the final draft. J-BD, KL, W-MW, and W-YY revised the manuscript. All authors contributed to the article and approved the submitted version.

Funding

This research was funded by Key Research and Development Plan of Sichuan Province (No. 23ZDYF3037); the project of the Sichuan innovation team of national modern agricultural industry technology system (No. Sccxtd-2023-20); Sichuan Province crop breeding project (No.2021YFYZ0021); the project of the 67th Batch of China Postdoctoral Science Foundation (No. 2020M673571XB).

Conflict of interest

The authors declare that the research was conducted in the absence of any commercial or financial relationships that could be construed as a potential conflict of interest.

Publisher's note

All claims expressed in this article are solely those of the authors and do not necessarily represent those of their affiliated organizations, or those of the publisher, the editors and the reviewers. Any product that may be evaluated in this article, or claim that may be made by its manufacturer, is not guaranteed or endorsed by the publisher.

Supplementary material

The Supplementary Material for this article can be found online at: https://www.frontiersin.org/articles/10.3389/fpls.2023.1150870/full#supplementary-material

References

Agrawal, G. K., Rakwal, R., and Jwa, N. S. (2000). Rice (*Oryza sativa* L.) OsPR1b gene is phytohormonally regulated in close interaction with light signals. *Biochem. Biophys. Res. Commun.* 278 (2), 290–298. doi: 10.1006/bbrc.2000.3781

Backer, R., Mahomed, W., Reeksting, B. J., Engelbrecht, J., Ibarra-Laclette, E., and van den Berg, N. (2015). Phylogenetic and expression analysis of the NPR1-like gene family from *Persea americana* (Mill). *Front. Plant Sci.* 6. doi: 10.3389/fpls.2015.00300

Caarls, L., Pieterse, C., and Wees, S. V. (2015). How salicylic acid takes transcriptional control over jasmonic acid signaling. *Front. Plant Sci.* 6. doi: 10.3389/fpls.2015.00170

Campos, M. L., Yoshida, Y., Major, I. T., Ferreira, D., Weraduwage, S. M., Froehlich, J. E., et al. (2016). Article rewiring of jasmonate and phytochrome b signalling uncouples plant growth-defense tradeoffs. *Nat. Commun.* 7, 12570. doi: 10.1038/ncomms12570

Cao, H., Li, X., and Dong, X. (1998). Generation of broad-spectrum disease resistance by overexpression of an essential regulatory gene in systemic acquired resistance. *Proc. Natl. Acad. Sci.* 95 (11), 6531–6536. doi: 10.1073/pnas.95.11.6531

Chang, H. L., Tseng, Y. L., Ho, K. L., Shie, S. C., Wu, P. S., Hsu, Y. T., et al. (2013). Reactive oxygen species modulate the differential expression of methionine sulfoxide reductase genes in *Chlamydomonas reinhardtii* under high light illumination. *Physiol. Plant* 150 (4), 550–564. doi: 10.1111/ppl.12102

Courbier, S., Grevink, S., Sluijs, E., Bonhomme, P., Van Wees, S., and Pierik, R. (2020). Far-red light promotes *Botrytis cinerea* disease development in tomato leaves via jasmonate dependent modulation of soluble sugars. *Plant Cell Environ.* 43 (11), 2587–2825. doi: 10.1111/pce.13870

Dodds, P. N., and Rathjen, J. P. (2010). Plant immunity: Towards an integrated view of plant-pathogen interactions. *Nat. Rev. Genet.* 11, 539–548. doi: 10.1038/nrg2812

Du, J., Han, T., Gai, J., Yong, T., Sun, X., Wang, X., et al. (2018). Maize–soybean strip intercropping: Achieved a balance between high productivity and sustainability. *J. Integr. Agric.* 17 (4), 747–754. doi: 10.1016/S2095-3119(17)61789-1

Genoud, T., Buchala, A. J., Chua, N. H., and Métraux, J. P. (2010). Phytochrome signalling modulates the SA–perceptive pathway in arabidopsis. *Plant J.* 31 (1), 87–95. doi: 10.1046/j.1365-313X.2002.01338.x

Griebel, T., and Zeier, J. (2008). Light regulation and daytime dependency of inducible plant defenses in arabidopsis: Phytochrome signaling controls systemic acquired resistance rather than local defense. *Plant Physiol.* 147 (2), 790–801. doi: 10.1104/pp.108.119503

Jeong, R. D., Kachroo, A., and Kachroo, P. (2010). Blue light photoreceptors are required for the stability and function of a resistance protein mediating viral defense in arabidopsis. *Plant Signaling Behav.* 5 (11), 1504–1509. doi: 10.4161/psb.5.11.13705

Li, X., Yang, C. Q., Chen, J., He, Y., Deng, J., Xie, C., et al. (2021). Changing light promotes isoflavone biosynthesis in soybean pods and enhances their resistance to mildew infection. *Plant Cell Environ.* 44 (8), 2536–2550. doi: 10.1111/pce.14128

Li, W., Zhu, Z., Chern, M., Yin, J., Yang, C., Ran, L., et al. (2017). A natural allele of a transcription factor in rice confers broad–spectrum blast resistance. *Cell* 170 (1), 114–126. doi: 10.1016/j.cell.2017.06.008

Manfre, A., Glenn, M., NuEz, A., Moreau, R. A., and Dardick, C. (2011). Light quantity and photosystem function mediate host susceptibility to *Turnip mosaic virus* via a salicylic acid–independent mechanism. *Mol. Plant Microbe Interact.* 24 (3), 315–327. doi: 10.1094/MPMI-08-10-0191

Pierik, R., and Ballare, C. L. (2021). Control of plant growth and defense by photoreceptors: from mechanisms to opportunities in agriculture. *Mol. Plant* 04, 14. doi: 10.1016/j.molp.2020.11.021

Shang, J., Xi, D. H., Wang, S. D., Cao, S., Xu, M. Y., Zhao, P. P., et al. (2011). A broad-spectrum, efficient and nontransgenic approach to control plant viruses by application of salicylic acid and jasmonic acid. *Planta* 233, 299–308. doi: 10.1007/s00425-010-1308-5

Shang, J., Xi, D. H., Yuan, S., Xu, F., Xu, M. Y., Qi, H. L., et al. (2010). Difference of physiological characters in dark green islands and yellow leaf tissue of CMV–infected nicotiana tabacum leaves. *Z. Naturforsch.* 65c, 73–78. doi: 10.1515/znc-2010-1-213

Shang, J., Zhang, L., Jia, Q., Tang, Z. Q., Yuan, S., Yang, H., et al. (2019). Early ROS accumulation in chloroplasts of nicotiana glutinosa infected by cucumber mosaic virus. *Int. J. Agric. Biol.* 6, 149–154. doi: 10.17957/IJAB/15.0875

Shang, J., Xi, D. H., Huang, Q. R., Xu, M. Y., Yuan, S., Wang, S. D., et al. (2009). Effect of two satellite RNAs on *Nicotiana glutinosa* infected with *Cucumber mosaic virus* (CMV). *Physiol. Mol. Plant Pathol.* 74, 184–190. doi: 10.1016/j.pmpp.2009.11.005

Shi, H., Shen, X., Liu, R., Xue, C., Wei, N., Deng, X., et al. (2016). The red light receptor phytochrome b directly enhances substrate–E3 ligase interactions to attenuate ethylene responses. *Dev. Cell* 39 (5), 597–610. doi: 10.1016/j.devcel.2016.10.020

Tang, Y., Kuang, J. F., Wang, F. Y., Chen, L., Hong, K. Q., Xiao, Y. Y., et al. (2013). Molecular characterization of *PR* and *WRKY* genes during SA- and MeJA-induced resistance against *Colletotrichum musae* in banana fruit. *Postharvest Biol. Technol.* 79, 62–68. doi: 10.1016/j.postharvbio.2013.01.004

Tang, Z. Q., Shang, J., Zhang, L., Du, J. B., Yang, H., Zeng, S. H., et al. (2019). Characterization of synergy between *Cucumber mosaic virus* and *Alternaria alternata* in *Nicotiana tabacum*. *Physiol. Mol. Plant Pathol.* 108, 101404–101404. doi: 10.1016/j.pmpp.2019.03.001

Telli, O., Jimenez-Quiros, C., Mcdowell, J. M., and Tr, M. (2020). Effect of light and dark on the growth and development of downy mildew pathogen *Hyaloperonospora arabidopsidis*. *Plant Pathol.* 69 (7), 1291–1300. doi: 10.1111/ppa.13207

Vuleta, A., and Manita, B. (2016). Adaptive flexibility of enzymatic antioxidants SOD, APX and CAT to high light stress: The clonal perennial monocot *Iris pumila* as a study case. *Plant Physiol. Biochem.* 100, 166–173. doi: 10.1016/j.plaphy.2016.01.011

Wu, N., Mao, H. T., Chen, M. Y., Dong, J., Yuan, M., Zhang, Z. W., et al. (2020). Different responses of photosystem and antioxidant defense system to three environmental stresses in wheat seedlings. *Photosynthetica* 58 (1), 87–99. doi: 10.32615/ps.2019.156

Xie, X. Z., Xue, Y. J., Zhoua, J. J., Zhang, B., Chang, H., and Takano, M. (2011). Phytochromes regulate SA and JA signaling pathways in rice and are required for developmentally controlled resistance to *Magnaporthe grisea*. *Mol. Plant* 4 (004), 688–696. doi: 10.1093/mp/ssr005

Zhang, L., Shang, J., Wang, W., Du, J., Li, K., Wu, X., et al. (2019). Comparison of transcriptome differences in soybean response to *Soybean mosaic virus* under normal light and in the shade. *Viruses* 11 (9), 793. doi: 10.3390/v11090793

frontiers | Frontiers in Plant Science

TYPE Review
PUBLISHED 10 May 2023
DOI 10.3389/fpls.2023.1147328

OPEN ACCESS

EDITED BY
Xiaofeng Zhang,
Fujian Agriculture and Forestry University, China

REVIEWED BY
Cecilia Karstin Blomstedt,
Monash University, Australia
Xin Wei,
Shanghai Normal University, China

*CORRESPONDENCE
Guangyuan He
hegy@hust.edu.cn
Zhiyong Xiong
xiongzy2003@aliyun.com
Yin Li
yinli2021@hust.edu.cn

†These authors have contributed equally to this work

RECEIVED 18 January 2023
ACCEPTED 21 April 2023
PUBLISHED 10 May 2023

CITATION
Tu M, Du C, Yu B, Wang G, Deng Y, Wang Y, Chen M, Chang J, Yang G, He G, Xiong Z and Li Y (2023) Current advances in the molecular regulation of abiotic stress tolerance in sorghum *via* transcriptomic, proteomic, and metabolomic approaches. *Front. Plant Sci.* 14:1147328. doi: 10.3389/fpls.2023.1147328

Current advances in the molecular regulation of abiotic stress tolerance in sorghum *via* transcriptomic, proteomic, and metabolomic approaches

Min Tu[1†], Canghao Du[2†], Boju Yu[2], Guoli Wang[2], Yanbin Deng[2], Yuesheng Wang[2], Mingjie Chen[2], Junli Chang[2], Guangxiao Yang[2], Guangyuan He[2*], Zhiyong Xiong[3*] and Yin Li[2*]

[1]School of Chemical and Environmental Engineering, Wuhan Polytechnic University, Wuhan, China, [2]The Genetic Engineering International Cooperation Base of Chinese Ministry of Science and Technology, The Key Laboratory of Molecular Biophysics of Chinese Ministry of Education, College of Life Science and Technology, Huazhong University of Science and Technology, Wuhan, China, [3]Laboratory of Forage and Endemic Crop Biology (Inner Mongolia University), Ministry of Education, School of Life Sciences, Hohhot, China

Sorghum (*Sorghum bicolor* L. Moench), a monocot C4 crop, is an important staple crop for many countries in arid and semi-arid regions worldwide. Because sorghum has outstanding tolerance and adaptability to a variety of abiotic stresses, including drought, salt, and alkaline, and heavy metal stressors, it is valuable research material for better understanding the molecular mechanisms of stress tolerance in crops and for mining new genes for their genetic improvement of abiotic stress tolerance. Here, we compile recent progress achieved using physiological, transcriptome, proteome, and metabolome approaches; discuss the similarities and differences in how sorghum responds to differing stresses; and summarize the candidate genes involved in the process of responding to and regulating abiotic stresses. More importantly, we exemplify the differences between combined stresses and a single stress, emphasizing the necessity to strengthen future studies regarding the molecular responses and mechanisms of combined abiotic stresses, which has greater practical significance for food security. Our review lays a foundation for future functional studies of stress-tolerance-related genes and provides new insights into the molecular breeding of stress-tolerant sorghum genotypes, as well as listing a catalog of candidate genes for improving the stress tolerance for other key monocot crops, such as maize, rice, and sugarcane.

KEYWORDS

sorghum, drought stress, salt and alkaline stress, temperature stress, omics analyses, gene expression regulation

Introduction

Globally, sorghum (*Sorghum bicolor* L.) ranks fifth in cereal crop production, serving as a staple for many countries in arid and semi-arid regions, being widely planted in tropical, subtropical to temperate regions as an important source of food, fiber, and fuel (Xie and Xu, 2019; Ngara et al., 2021). As one of the oldest cultivated cereal crops, the origin and domestication process of sorghum is very complex. To our best knowledge, the earliest evidence of human use of sorghum comes from Salt Lake Nabuta on the border between Egypt and Sudan, where carbonized sorghum grains were found and carbon-14 dated to 8000–8100 years old (Dahlberg et al., 1995). Sorghum cultivars may have originated from wild sorghum (*Sorghum verticilliflorum*) plants native to northeast Africa. The cultivation of sorghum ancestors may be traced back to 6 kyr before the present (kyr BP), and the domesticated bicolor race already existed ca. 5000 years ago in central eastern Sudan (Winchell et al., 2017; Smith et al., 2019).

As a C4 plant, sorghum features a combination of key traits: high photosynthetic efficiency, high nitrogen-use efficiency, outstanding tolerance to several abiotic stresses, and high biomass. These traits allow sorghum to be used not only as a food crop but also, more importantly, as a reliable feed resource and bioenergy crop (Hao et al., 2021). Sorghum cultivars can be grouped into grain sorghum, sweet sorghum, forage sorghum, and energy sorghum depending on their intended usage. Grain sorghum can serve as a staple or be used by breweries or as ingredient of pig feed, while forage sorghum cultivars attain high biomass and are used as dry forage. Interestingly, in sweet sorghum cultivars, the stem becomes a sink organ that accumulates a large amount of soluble sugars (*i.e.*, sucrose, fructose, and glucose), making it suitable for the production of silage or bioethanol (Yu et al., 2008; Laopaiboon et al., 2009). For example, compare with the commonly used silage maize, some sweet sorghum varieties produce two to three times more biomass, which is ideal for silage use and holds promising potential for sustainable agriculture (Xie and Xu, 2019). Further, sorghum biomass may be used for the conversion of various industrial chemicals (Mathur et al., 2017).

Unlike the major C4 feed crop maize and the sugar crop sugarcane, sorghum can be planted on marginal lands due to its outstanding tolerance of a variety of abiotic stresses, including drought, high salinity, and low nutrition (Shan and Xu, 2009). Some sorghum accessions are distinguished by their strong absorption capacity for heavy metals and show potential in phytoremediation of soils contaminated by heavy metals (Feng et al., 2018). Accordingly, sweet sorghum has been proposed as way forward to simultaneously restore soil health and produce plant biomass, while the latter and its subsequently generated bioenergy are useful for our society but do not enter the food chain (Li, 2013; Jia et al., 2016). These prominent advantages of sorghum allow it to be considered as an environmentally- friendly green energy plant to utilize on marginal lands with low agricultural input, to diversify energy sources and relieve pressure on limited land resources for growing staple crops (Liu et al., 2007; Sticklen, 2007; Cai et al., 2011).

Contemporary advances in both energy sorghum and grain sorghum have been reviewed (Mullet et al., 2014; Boyles et al., 2019), and, more recently, the overall advantages and prospective applications of sorghum have been well discussed (Hao et al., 2021). Meanwhile, our understanding of the responses and adaptation of sorghum to various abiotic stresses has been substantially improved by the wide application of omic technologies. Due to the sessile growth, plants have evolved complex molecular networks to respond and survive in fluctuating environments; in turn, a variety of environmental factors negatively affect aspects of plants' growth and development, leading to their yield declines and even death. These environmental stresses are generally divided into biotic versus abiotic, with the latter encompassing a wide range of factors, such as drought, salinity, alkalinity, high or low temperatures, and heavy metal toxicity. Among these abiotic stresses, drought, high salinity, and extreme temperatures are considered the most significant because they now severely threaten global food security and sustainable agriculture (Bailey-Serres et al., 2019). Extreme climatic events have adversely exacerbated global agricultural production in modern times (Fedoroff et al., 2010). It was recently estimated that, worldwide, drought conditions have caused about 30 billion dollars of losses in crop production (United Nations, 2011). Moreover, freshwater availability is predicted to drop by half due to climate change, far below than the expected global demand for agricultural water by 2050 (Gupta et al., 2020). Exacerbating matters, statistics have shown that about 6% of the global land area is damaged by salinization, yet effective measures are still lacking to control the spread of land salinization (Li et al., 2014). Collectively, this information highlights why and how abiotic stresses pose serious threats to agricultural production and food security, and that basic and applied research to mitigate the impacts of abiotic stresses deserves prioritization in most countries and global collaboration is imperative.

When facing abiotic stresses, plants utilize a combination of complicated biological and molecular processes, including morphological and physiological responses, tolerance, resistance, adaptations, and escapes. Usually, however, drought and salinity conditions induce multilevel stress signals (e.g., primary stress signals and secondary signals). Compared with primary signals, the secondary effects of drought and salt stresses are far more complex, including the induction of reactive oxygen species (ROS) stress, damage to biomolecules (such as membrane lipids, proteins, nucleic acids), and metabolic dysfunction (Zhu, 2016). The ability of plants to cope with and adapt to one or more given stresses after receiving corresponding stress signals is also generally referred to as stress tolerance (Zhang et al., 2022).

In the recent decade, numerous advances have been made in key genes regulating the response and adaptation to abiotic stresses in major crops (e.g., rice, maize, and wheat). It is known that crops can improve drought tolerance mainly by regulating root architecture and leaf transpiration efficiency, for instance, the *DEEPER ROOTING 1* gene (*DRO1*; Uga et al., 2013); Another example is that the receptor-like kinase *ERECTA* (*ER*) is major target to improve thermotolerance in rice (Shen et al., 2015). In addition, a cohort of drought-regulating transcription factors (TFs) including the members in the DREB, ERF, WRKY, ZFP, and MYB families have been functionally characterized in rice, wheat, and

maize. For saline response and tolerance, the factors affecting salt tolerance mainly include the rate of water loss in leaves, water uptake capacity in roots, the ability to scavenge ROS and to maintain cell wall signaling perception and metabolism (Landi et al., 2017). Research on the mechanism of crop response to high temperature stress is mainly focused on the regulation of protein homeostasis and reactive oxygen species homeostasis. The response to low temperature stress mainly revolves around the CBF signaling pathway, whose components mainly including membrane localization proteins, protein kinases, calcium channels and E3 ubiquitin ligases play important roles in plant cold tolerance response (Wang L. et al., 2021).

It is generally accepted that field crops are often exposed to several stresses at the same time, yet most lab-based studies of the physiology and molecular mechanisms of stress responses and tolerance have focused upon a single stress condition or signal. For instance, drought conditions are often accompanied by raised temperature and/or high salinity, but combined stress conditions often cause more severe damage to the crop than does a single stress, in either an additive or synergistic way (Mittler, 2006; Barnabas et al., 2008). Therefore, the responses of plants to combined stresses and corresponding growth outcomes are usually difficult to predict from simply using data obtained from studies of a single stress factor, especially when stress conditions act antagonistically or lead to conflicting responses (Prasch and Sonnewald, 2015). One such example is drought and heat conditions in tandem. The heat stress incurred usually induces the stomata to open, to cool the leaves *via* transpiration; by contrast, stomata tend to close under drought conditions, to limit water loss. Work using Arabidopsis and tobacco has revealed that plants are unable to open their stomata under the combined stress of drought and heat, resulting in a higher leaf temperature (Rizhsky et al., 2002; Rizhsky et al., 2004). Generally, our understanding of plant stress biology is limited in two major ways: (1) effective responses and coordination vis-à-vis the combination of multiple abiotic stresses; and (2) transcriptional and metabolic responses and re-programming in a systems biology context.

In most plant stress-biology studies, the identification of key genes/alleles involved in stress tolerance and regulation from the species or genotypes exhibiting strong stress tolerance or adaptability is considered an efficient and effective approach. Hence, sorghum has been recognized as a target species for such gene identification purposes, given its higher tolerance to abiotic stresses compared to other major crops (e.g., rice, maize, and sugarcane). On one hand, gene functional studies of sorghum have lagged those of model crops (rice and maize), largely due to the difficulty in tissue culture, genetic transformation, and limited mutant resources (Grootboom et al., 2010). *Agrobacterium*-mediated transformation can be achieved in sorghum, but only in a few genotypes and with low efficiency (Hiei et al., 2014). On the other hand, there has been much effort directed to utilizing multi-omics technologies to decipher the systematic responses of sorghum to abiotic stresses and to identify key genes and signaling pathways involved in stress regulation and tolerance. Here, we aim to summarize recent achievements of sorghum stress tolerance based on multi-omic approaches (e.g., transcriptomics, proteomics and metabolomics), and to highlight the key genes in need of functional validation and of potential use in molecular breeding. Given the relatively abundant studies available in the literature, our review focuses on drought, salinity, and extreme temperature treatments, while studies on other abiotic stress conditions, for instance, nutrient deficiency (Gelli et al., 2017; Zhang et al., 2019b) and heavy metal toxicity (Feng et al., 2018; Jia et al., 2021), are out of the scope of the present review. Comparative genomics and population genomic approaches (e.g., quantitative trait loci mapping, and genome-wide association study, GWAS) have been powerful for unlocking the genetic architecture of complex traits in sorghum (reviewed in Hao et al., 2021). While there are some GWAS studies regarding abiotic stress tolerance, our present manuscript focuses on sorghum transcriptomics, proteomics and metabolomics (Chen et al., 2017; Chopra et al., 2017).

Multi-omic research advances in drought and osmotic stresses

A sufficient water supply is one of the essential requirements for plant growth. Plants respond to water scarcity by altering their morphology, physiology, and biochemistry to mitigate the direct and indirect damage and to survive and/or to maintain their growth (Bray, 1993; Bray, 1997; Xiong and Zhu, 2002; Ngara et al., 2021). Plants' responses to drought fall into three categories: drought escape, avoidance, and tolerance, which have been well defined in previous reviews (Farooq et al., 2009; Basu et al., 2016; Rodrigues et al., 2019).

Sorghum is generally recognized as a drought-tolerant crop. For example, the water consumption of sorghum in its full growth-period is 1.53 kg per plant whereas maize consumes 2.32 kg of water per plant (Su, 1995). The evapotranspiration of sorghum is 300~600 mm under field conditions, lower than that of maize (400~750 mm), rice (500~950 mm) or cotton (550~950 mm) (FAO, 1981). It is thought that sorghum plants are well tolerant to drought conditions not only because of the special cuticular wax metabolism but, more importantly, because of the coordination between root-to-shoot water use efficiency and a number of dynamic physiological adjustments to cope with drought conditions.

Dehydrins (DHN), a group of the late embryogenesis abundant (LEA) D-11 family proteins, accumulate in dehydrated plant tissues and may act as stabilizers of cell components (Close, 1996; Campbell and Close, 1997). Dehydrins could protect plants directly by scavenging ROS or providing an overall protective effect to those enzymes responsible for the dismutation of free radicals. For instance, *SbDhn1*- and *SbDhn2*-overexpressing transgenic tobacco plants are able to protect against oxidative damage (Halder et al., 2018). In addition, overexpressing *OsDhn1* in transgenic rice was shown to enhance their tolerance to drought and salt *via* ROS scavenging (Kumar et al., 2016). Wood and Goldsbrough (1997) found that the abundance of *SbDHN1* increased significantly in both seedlings and mature plants under a water deficit condition but were barely detectable in the well-watered and drought-recovered plants. A number of studies concluded that *DHN1* is drought inducible and may play an essential role in the plant response to drought stress

(Close, 1996; Campbell and Close, 1997). The early and late responses of gene expression to the polyethylene glycol (PEG)-induced osmotic stress has been identified with microarray in the sorghum cultivar (cv.) BTx623, revealing ~2200 differentially expressed genes (DEGs) enriched in functions such as signaling transduction, gene expression regulation, dehydration protection, ROS scavenging, and defense (Buchanan et al., 2005). The PEG-upregulated genes include many encoding, for example, drought-responsive transcription factors and signaling proteins, LEA proteins, dehydrins, heat shock proteins (HSPs), ROS detoxification enzymes, biosynthesis of abscisic acid (ABA), and the metabolic enzymes of proline and raffinose family of oligosaccharides (RFOs). LEA proteins can enhance drought tolerance in many plants such as Arabidopsis, rice, wheat, and cabbage (Park et al., 2005; Xiao et al., 2007; Olvera-Carrillo et al., 2010; Chauhan and Khurana, 2011). Moreover, the proline and raffinose family of oligosaccharides (RFOs) plays a crucial role in how plants respond to drought stress. Overexpressing the galactose synthase gene *CsGolS4* in cucumbers led to significantly increased RFO content and drought resistance (Ma et al., 2021). Later, with the help of RNA-seq and a high-quality sorghum reference genome (Paterson et al., 2009), Dugas et al. (2011) uncovered changes in gene expression in response to the PEG or ABA treatment, finding that ABA could induce more genes than PEG, with the responsive genes (12% and 30% in the shoots and roots, respectively) differentially expressed in both treatments, suggesting ABA's vital role in the osmotic response.

To further mine important genes associated with strong drought tolerance in sorghum, the up-and downregulated genes associated with drought stress were profiled in the drought-tolerant sorghum cv. XGL-1 with RNA-seq (Zhang et al., 2019a), uncovering that many differentially expressed genes in the roots were enriched in the functions such as sucrose metabolism and raffinose family oligosaccharide biosynthetic process. These results emphasized the importance to adjust carbohydrate metabolism during the response of roots to osmotic stress. Besides, Johnson et al. (2014) compared the gene expression disparities between the drought, heat, and drought and heat treatments, finding that only ~3.5% of the genes were drought-responsive and a small proportion (~20%) overlapped with previously detected osmotic responsive genes, underscoring the difference between drought and osmotic stresses (Johnson et al., 2014). Notably, the drought-upregulated genes include the proline biosynthetic gene (delta 1-pyrroline-5-carboxylate synthase 2, P5CS2-a; ID), the gene encoding sodium transporter (high-affinity K+ transporter 1, HKT1-a, Sb06g027900), LEA genes (Sb01g046490, Sb09g027110, Sb07g015410, Sb03g032380) and those related to lipid transport. Proline accumulation is a drought response conserved between plant species (Su et al., 2011). Arabidopsis pyrroline-5-carboxylate synthase 1 (AtP5CS1) catalyzes the first step in proline biosynthesis and is critical for proline accumulation under osmotic stress (Szekely et al., 2008). In addition, functional studies in sorghum revealed that SbHKT1;4 gene has selective uptake of sodium and potassium ions and is involved in regulating cellular ion homeostasis and improving tolerance to drought and salt stress (Wang et al., 2014).

More recently, several studies used the comparative approach to identify DEGs between stress-tolerant and stress-sensitive sorghum genotypes. A transcriptomic comparison of drought-sensitive and drought-tolerant genotypes (i.e., IS20351 and IS22330) indicated the former responded to the stress by hydrolyzing carbohydrates in roots, while the latter genotype gained tolerance by promoting the synthesis of anti-osmotic agents and antioxidants (e.g., proline, betaine, and glutathione; Fracasso et al., 2016). Also, the upregulation of lipid metabolic genes is associated with high drought tolerance in sorghum; for example, the phosphatidylinositol biosynthetic genes (Sb08g016610, Sb08g022520, and Sb05g026855) were upregulated in sorghum cv. IS20351. Some studies found that two sorghum genes (Sb06g014320 and Sb07g027910) encoding a glycerol phosphodiester phosphodiesterase and a monogalactosyl-diacylglycerol (MGDG) synthase, respectively, tend to be upregulated during drought stress but downregulated in drought-sensitive genotypes (Pasini et al., 2014; Fracasso et al., 2016). Similarly, transcriptomic comparison between two genotypes with contrasting drought tolerance during a post-anthesis drought treatment identified upregulation of genes related to antioxidant capacity and transmembrane transporters (Azzouz-Olden et al., 2020). Another comparative transcriptomic study discovered that drought induced more dramatic transcriptomic changes in roots than in leaves in terms of the number of DEGs and the extent of expression levels (Varoquaux et al., 2019). More importantly, a number of genes potentially conferring drought tolerance have been highlighted: (1) downregulation of several *WRKY* genes and jasmonic acid- and salicylic acid-responsive genes in roots indicates the possible balance between drought tolerance and inhibition of plant defense to microbes and pathogens (Pandey and Somssich, 2009); (2) downregulation of the key photosynthetic genes (e.g., the light-harvesting complex subunit B encoding gene, *LHCB*: Sobic.003G209800 and Sobic.003G209900) and their subsequent upregulation during drought recovery suggests photosynthesis could be the target for drought recovery; (3) upregulation of the proline biosynthetic gene P5CS2 (Sobic. 003G356000) points to proline accumulation as a common way to tolerate drought-induced damage (Funck et al., 2020); (4) the ROS-scavenging genes encoding glutathione S-transferase (*GST29*, Sobic.003G264400) was upregulated in both pre- and post-anthesis drought treatments and localized within a stay-green quantitative trait locus (the *Stg2* loci) (Thangaraj et al., 2022), suggesting a possible association between the drought-involved leaf stay-green trait and ROS scavenging ability (Harris et al., 2007).

Membranes are sensitive to drought stress and easily degraded and modified. Lipidomics and transcriptomics have been applied to profile membrane lipid dynamics in sorghum drought-sensitive cv. Hongyingzi and drought-tolerant cv. Kangsi (Xu et al., 2022). The unsaturation indices (UI) of dilauryl-diacylglycerol (DGDG), MGDG, phosphatidylglycerol (PG), and phosphatidylcholine (PC) all decreased in both cultivars under drought stress. By integrating transcriptomic and lipidomic data, some candidate genes regulating membrane lipids under drought stress were detected, namely CCT2(Sobic.001G282900), CER1 (Sobic.001G2222700), DGK1 (Sobic.001G333900), DGK5(Sobic.003G318700), EMB3174(Sobic.

001G403400), KCS4(Sobic.002G268500), LCB2(Sobic.003G412700), PAH1(Sobic.009G165400), PLDP1(Sobic.009G109900), PKP-β1(Sobic.003G244700), and KCS11(Sobic.010G181500).

Besides those genes identified, the changes in miRNA and proteome during drought stress have also been profiled in sorghum plants. Analysis of eight representative miRNAs among 11 sorghum genotypes phenotypically varied in drought tolerance revealed the drought-associated miRNAs, namely miR396, miR393, miR397-5p, miR166, miR167, and miR168 (Hamza et al., 2016). In particular, miR160, miR166, and miR396 targeted 28 transcription factors (TFs)- encoding genes including auxin response factor (ARF), homeobox-leucine zipper family protein (HD-ZIP), and growth regulating factors (GRF). Among these miRNAs, miR166, upregulated in sorghum, has been known to be related to drought tolerance in soybean (Kulcheski et al., 2011). In addition, members of the soybean HD-ZIPIII family, targeted by miR166, play a role in stress response to drought and salt stress conditions (Chen et al., 2014a). It has been recently found that a HD-ZIP TF *MdHB-7* enhanced the drought tolerance in apple by regulating ABA accumulation, stomatal closure, and ROS detoxification (Zhao et al., 2020). Collectively, these results indicate that the miR166-HD-ZIP module may also play an important role in drought stress regulation in sorghum. Nevertheless, it is worth noting that these miRNAs' expression pattern during drought varies among sorghum genotypes, implying the complex involvement of miRNAs in drought-stress regulation and why further study to validate their functions in sorghum's drought tolerance is needed.

Proteomics has also been employed to profile the protein dynamics of sorghum roots in response to PEG-induced osmotic stress (Li et al., 2020). During drought stress, the contents of MDA and proline, and the activities of superoxide dismutase (SOD), peroxidase (POD), and polyphenol oxidase (PPO), were gradually increased. Consistently, several antioxidant proteins (e.g., SOD, Sb07g023950, POD, Sb06g033850 and catalase, CAT, Sb10g030840), were upregulated as well, supporting the importance of ROS scavenger upregulation to cope with the stress. Another comparative proteomic study in sorghum focused on drought stress and recovery showed that: (1) the protein level of methionine synthase remained upregulated in the drought-tolerant sorghum lines but dropped in the drought-sensitive line; (2) the drought-sensitive and -tolerance sorghum lines exhibited contrasting changes in the cytosolic isoform of fructose-1,6-bisphosphate aldolase (FBA; Jedmowski et al., 2014). Similarly, the increase or maintenance of high levels of methionine synthase may be an osmoregulant metabolic approach to tolerate stress conditions (Merewitz et al., 2011). For the FBA-mediated carbohydrate metabolism, plastidic FBA indicates a disturbance of carbon fixation while cytosolic FBA may be active in the aldehyde detoxification process during stress. Moreover, Goche et al. (2020) employed the gel-free isobaric tags for relative and absolute quantitation (iTRAQ) proteomic technology to compare the root proteomes between a drought-sensitive and a drought-tolerant cultivar (ICSB338 and SA1441, respectively), thereby detecting drought-induced upregulation of proteins related to protein synthesis, proteasome inhibition, signaling transduction, and defense. Similarly, proteomic characterization of the osmotic-induced proteins in the BTx623 roots identified proteins related to protein synthesis, degradation, and defense (Li et al., 2020). Collectively, these proteomic studies in sorghum tend to emphasize that drought-tolerant cultivars tend to upregulate their stress-related signaling, protein synthesis and antioxidant activity to acquire better tolerance to drought conditions.

Multi-omic research advances in salinity and alkaline stresses

Soil salinization is another major abiotic stress that severely limits crop production. About 6% of the global land area (~12 billion acres) is affected by salinization (Ismail and Horie, 2017), while the coverage of saline-alkali land has reached 100 million hectares in China. Moreover, secondary salinization of agricultural lands is becoming increasingly severe in China, posing a serious threat to the sustainable production of staple crops there (Fang et al., 2021; Wang L. et al., 2021). Generally, soil salinization refers to high salinity and alkaline stresses, which can distinctly influence plant growth. Salt stress is caused primarily by neutral salts (e.g., NaCl and Na_2SO_4). On one hand, high concentrations of sodium ions enter plant cells *via* ion channels and carrier proteins, resulting in ion toxicity. On the other hand, high concentrations of extracellular ions lead to greater extracellular osmotic potential, posing osmotic stresses and other secondary damage such as oxidative stress. By contrast, alkali stress is mainly caused by $NaHCO_3$ and Na_2CO_3, either of which can raise the soil pH, which destabilizes the integrity of cell membranes and reduces root vigor in addition to ionic toxicity and osmotic damage (Zhang et al., 2017).

Many sorghum cultivars are capable of growing on salinized soils and even on marginal lands (Xie and Xu, 2019). To understand the molecular mechanisms of high salinity tolerance in sorghum, the cultivar M-81E was used as a representative salt-tolerant genotype for a series of transcriptome studies (Sui et al., 2015; Yang et al., 2017; Yang et al., 2018). In comparison to the salt-sensitive genotype Roma, M-81E harbors distinct groups of DEGs induced by salt. For example, genes related to photosynthesis are less influenced in M-81E: (1) *Lhca2-4* and *Lhcb6* encoding subunits in the light-harvesting complex are not inhibited in M-81E; (2) the genes encoding phosphoenolpyruvate carboxylase and pyruvate orthophosphate dikinase, respectively, remain unchanged in M-81E (Sui et al., 2015). Besides, sucrose synthase genes are upregulated in M-81E while the genes encoding sucrose catabolic enzymes are downregulated, and vice versa in Roma, patterns which suggest that maintaining photosynthesis and sucrose metabolism underpins the salt-tolerant sorghum. A more recent study revealed the roles of phytohormones in salt tolerance in sorghum: ABA and its signaling genes were increased in the leaves of the salt-tolerant cv. M-81E, while JA and its functionally related genes were upregulated in roots of the salt-sensitive cv. Roma (Yang et al., 2017). In addition, 2085 and 3172 DEGs were identified by RNA-seq in the roots of M-81E and Roma, respectively (Yang et al., 2018). In particular, many genes known to be involved in salt exclusion were found: (1) *SbHKT1;5* encoding a high-affinity potassium (K+) transporter (HAK) is dramatically upregulated in M-81E but only moderately increased in Roma; wheat *TaHAK1;5-D*, a homolog of

SbHKT1;5, can enhance salt tolerance by expelling Na^+ outside the cells (Byrt et al., 2014); and (2) the genes functioning in the exoplasmic barrier exhibit significant upregulation in M-81E. Altogether, these analyses suggest that enhanced potassium transportation and salt exclusion may explain the salt tolerance of M-81E. Another study just revealed the physiological and transcriptomic differences induced by drought and salt, respectively, highlighting that salt conditions significantly inhibit antioxidant enzymes and the auxin and cytokinin contents, while drought stress mainly impairs sugar metabolism in leaves (Wang et al., 2022).

Other omics analyses have further revealed additional layers of complexity in the salt responses of sorghum. Long non-coding RNAs (lncRNAs) regulate gene expression to modulate plant development and stress responses (Chen et al., 2020). Full-length transcriptomic comparison between the cultivars M-81E and Roma identified three upregulated lncRNAs (*lncRNA13472*, *lncRNA11310*, and *lncRNA2846*) in M-81E and two downregulated lncRNAs (*lncRNA26929* and *lncRNA14798*) in Roma (Sun et al., 2020). Functional predictions indicate that these salt-responsive lncRNAs might serve as endogenous RNAs (ceRNAs) acting to regulate the target genes related to ion transport, protein modification, transcriptional regulation, and synthetic transport of substances. A recent lipidomics analysis profiled changes to leaf membrane lipids during salt stress, finding a salt-induced decrease in both MGDG and PG (Ge et al., 2022). This result provides new insight into salt-induced membrane lipid remodeling in sorghum leaves and how that impacts the fluidity, stability, and integrity of their photosynthetic membrane system.

A proteomic study using the two-dimensional gel electrophoresis and mass spectrometry technique profiled differential proteins in sorghum leaves responsive to salt stress (Swami et al., 2011) and identified upregulated protein, including the universal stress protein (XP 002443333), glutathione S-transferase (XP 002458541, XP 002465442), peroxidase (XP 002463451, XP 002463451, XP 002463451) that are involved in the detoxification of reactive electrophilic compounds. Despite efforts made to understand the physiological and molecular aspects of sorghum's response to and regulation of salt stress, such studies addressing the combination of salt and alkaline stresses remain quite limited. By using two-dimensional electrophoresis and proteomics, Dai et al. (2017) distinguished 30 upregulated proteins and 14 downregulated proteins under soda saline-alkali stress conditions ($NaHCO_3$ and Na_2CO_3), functionally enriched in carbon fixation, carbon metabolism and glycolysis.

Metabolomics has also been employed to gain insights into the distinct salt tolerant phenotypes of sorghum genotypes (de Oliveira et al., 2020). (1) Significant changes of osmolytes (e.g., proline and soluble sugars) were detected in sorghum under salt conditions. Salinity triggered a pronounced increase in proline by 35% and 126% in CSF18 (salt-sensitive genotype) and CSF20 (salt-tolerant genotype), respectively. (2) Salinity induced an increase in putrescine in the salt-sensitive genotype but spermidine, spermidine and cadaverine were increased in the salt-tolerant genotype, suggesting that osmolytes and polyamines may play a role in conferring salt tolerance to sorghum. More recently, another metabolomics study in sorghum indicated that salt stress affects photosynthesis by repressing both chlorophyll and carotenoid metabolism, while sorghum mitigates salinity damage by inhibiting oxidative stress and increasing antioxidant content/enzyme activities (Punia et al., 2020). Further, the involvement of ion transport/signaling-related genes (SOS1 [XM_015763865.2], SOS2 [KP330207.1], NHX-2 [EU482408.2], V-PPase-11 [GQ469975.1], CIPK24 [XM_002438609.2], PP2A [XM_002448914.2]) in salt stress regulation was verified in sorghum by qPCR-based expression analysis (Ma et al., 2020). A recent study integrated transcriptome and metabolome analyses discovered the dynamic changes in flavonoid metabolic pathways from moderate and severe saline –alkali stress. That is, (1) flavonoid synthesis—particularly of naringenin, chalcone, prunin, naringin, and some kaempferol derivatives—is significantly upregulated under the moderate saline –alkali stress but repressed under the severe saline-alkali stress; and (2) cyanidin is specifically accumulated under the severe saline–alkali stress, which might protect cells from severe oxidative damage. Coupling the transcriptomic and metabolomic data identified several stress-induced flavonoid metabolic genes, including the naringenin-correlated flavonoid 3'-hydroxylase (*F3H*) genes (Sobic.004G201100, Sobic.004G328700, and Sobic.006G254000), a shikimate O-hydroxycinnamoyl transferase (*HCT*) gene (Sobic.006G136900), and a chalcone-flavanone isomerase (*CHI*) gene (Sobic.001G035600). Evidently, the application of metabolomics is providing novel insight into the role of flavonoid metabolism in sorghum's salt tolerance.

Multi-omic research advances in high- and low-temperature stresses

In recent years, the climate is fluctuating more widely, and extreme weather disasters are now occurring more frequently. Thus, extreme temperature stresses have emerged as a major threat adversely affecting plant growth and crop production (Farooq et al., 2011).

Raised temperature (also known as heat stress) is particularly harmful when it happens during the reproductive stage of plants, because heat stress inhibits metabolism, causes chloroplast oxidative damage, affects reproductive organ development and suppresses vital nutrient accumulation in seeds. During heat stress, stress-induced accumulation of misfolded proteins can be sensed by heat shock proteins (HSPs) and further activate heat stress transcription factors (HSFs) and their downstream heat stress-responsive target genes (Scharf et al., 2012; Zhang et al., 2022).

A recent quantitative proteomic study investigated the heat-responsive proteins that were secreted into the extracellular matrix (Ngcala et al., 2020), revealing 31 secreted, heat-responsive proteins that falls into the classical secretory pathways including metabolism, detoxification, and protein modification. This proteomic study provides a useful, timely resource of extracellular proteins that could serve as targets for developing heat-tolerant crops. Moreover, some genes such as the *leucine-rich repeat* (Sobic.005G126200), *cysteine proteinase inhibitors* (Sobic.003G126800 and

Sobic.001G324800), and a *glycosyl hydrolase* (Sobic.002G055700) were validated by qPCR as heat-induced proteins.

By contrast, cold stress negatively impacts plant growth through distinct physiological mechanisms. First, cold stress decreases stomatal conductance and mainly affects photosystem II to reduce the net photosynthetic rate (Guo et al., 2021). Second, cold stress leads cell membranes to change from a liquid crystal phase to a gel phase, thereby impairing membrane permeability, and can even fully disrupt it (Chen et al., 2014b). Third, cold stress causes ROS bursts in cells. Plants respond to cold stress *via* C-repeat binding factors (CBFs)/dehydration-responsive-element binding factors (DREBs) for reprograming the metabolism (e.g., sugar and amino acid metabolism) to temporally adjust to the stress (Zhao et al., 2015; Ding et al., 2019; Guo et al., 2021).

Since sorghum originated in tropical and subtropical regions, most of its varieties are sensitive to low temperatures, especially during their germination and seedlings stages (Fiedler et al., 2016). So, to better understand the response to cold stress and to identify genes for improving cold tolerance in sorghum, several studies employing omics approaches have since been carried out. Transcriptomic comparison of seedlings of the cold-sensitive cv. BTx623 vis-à-vis those of the cold-tolerant cv. Hongkezi (HKZ) found several TF-encoding genes—i.e., *DREBs, CBFs*, and *ethylene responsive factors* (*ERFs*)—were drastically induced by the cold stress (Chopra et al., 2015). Additionally, several members from the plant cytochrome, glutathione s-transferase, and heat shock protein families were differentially regulated by cold treatment between those two cultivars. Nuclear factors Y (NF-Ys), these consisting of three subfamilies (i.e., NF-YA, NF-YB, and NF-YC), are involved in how plants respond to various stresses through complex interactions to form different hetero-trimmers (Petroni et al., 2012). Genome-wide characterization of the sorghum NF-Y family and expression analysis has revealed many members responsive to cold or heat stresses: For example, (1) *NF-YA2/4/6/7/8*, *NF-YB2/7/10/11/12/14/16/17*, and *NF-YC4/6/12/13* are induced by heat stress (40°C), and some of these genes are also regulated by cold stress (4°C); (2) *NF-YA8* is induced by both cold and heat stresses; (3) stress-related cis-elements, ABA-responsive element (ABRE), and heat shock-responsive element (HSE), are found in the promoter regions, but not the drought-responsive elements DRE and MYB (Maheshwari et al., 2019). Comparing the cold-induced DEGs between the cold-tolerant cv. Hongke4 and the cold-sensitive cv. SC407 uncovered not only classic cold-inducible genes—e.g., *CBL-interacting serine/threonine-protein kinase* (*CIPK16*; Sb02g024770) and *stress-activated protein kinase-3* (*SAPK3*; Sb01g028760)—but also important TFs warranting further functional studies (*MYB62*; Sb04g026210, *NAC1*; Sb01g003710, *WRKY55*; Sb02g011050, *WRKY51*; Sb03g003360 and *WRKY33*; Sb03g038510) (Jin et al., 2021; Zhou et al., 2022b). These cold-induced genes enriched metabolic functions, namely phenylpropanoid synthesis, carbon metabolism, amino acid biosynthesis, and starch and sucrose metabolism, thus indicating extensive metabolic reprogramming occurs under cold stress. Another transcriptomic comparison between the cold-tolerant cv. P61 and the cold-sensitive cv. H21 emphasized the differences in photosynthesis inhibition and oxidative damage (Shao et al., 2021). For example, the cold-tolerant cultivar showed significant upregulation for eight *SbSODs* genes, seven *SbPODs* genes, 11 sorghum lipoxygenase genes *SbLOXs*, and two *SbP5CS* genes, consistent with the physiological measurement of corresponding oxidative damage indicators: e.g., the enzyme activity of superoxide dismutase (SOD) and peroxidase (POD), and the content of malondialdehyde (MDA) and proline (Pro)).

Unlike the cold-stress response, sorghum exhibits substantially differing transcriptomic patterns in response to heat stress. According to one transcriptome study, the genes associated with high-temperature stress, intense light stress, and protein folding are differentially expressed during heat stress, with several genes encoding heat shock proteins or universal stress proteins—*HSP22.0* (Sb06g017850), *HSP101* (Sb03g034390), *HSP18.2* (Sb01g039990), and *SbUSP* (Sb04g034630)—being significantly upregulated (Johnson et al., 2014).

Omics-enabled insights into plant responses to combinatory stresses

In the past decade, our understanding of the molecular responses to various stresses in sorghum has improved greatly, largely driven by advances and applications of the omics technologies. The major biological processes, metabolites (including phytohormones and osmolytes), and key genes that have been identified to respond to or cope with the abiotic stresses are summarized in Figure 1. Compiling and synthesizing these pieces of knowledge leads us to conclude that, in sorghum plants, different physiological and/or metabolic processes are affected by distinct stresses and are utilized to ensure survival and maintain growth when the stress occurs. For example, sorghum cultivar XGL-1 could induce the expression of proline biosynthetic and carbohydrate metabolic genes to cope with osmotic stress (Zhang et al., 2019), whereas the cultivar M-81E tends to amplify their gene expression of antioxidant enzymes and ion transporters when salt stress occurs (Yang et al., 2018). Moreover, imposed drought stress (withhold watering) and osmotic stress (with a PEG treatment) induce distinctive transcriptomic responses, with only ~20%-overlap of DEGs between the two treatments (Dugas et al., 2011; Johnson et al., 2014). Such pronounced differences in the stress-induced expression profiles have also been detected for heat and drought stresses. The drought treatment led to ~4% of those sorghum's genes being differentially expressed, including those encoding the LEA proteins and proline synthetic enzyme P5CS2, while ~18% of them could be regulated in response to heat stress, including those encoding HSPs. By contrast, ~20% of the sorghum genes were DEGs under combined heat and drought stress, with around 1/3 of these DEGs being exclusively differentially expressed after applying the combined stresses (Johnson et al., 2014). These differences in stress-specific inducible genes in sorghum justify why it is imperative to compare the combination of stresses with each single stress at transcriptomic or other omic levels, given that such combinations typically arise in real field conditions. Therefore, the results may provide more practically meaningful insights into sorghum's molecular breeding and stress tolerance improvement.

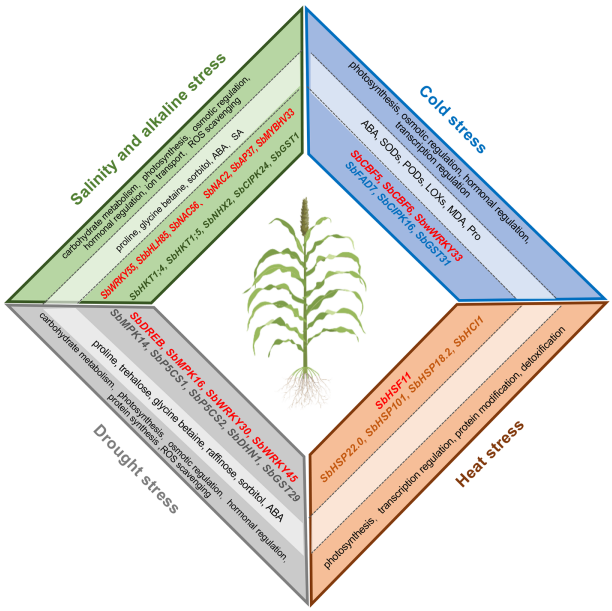

FIGURE 1
The diagram summarizing the molecular regulations involved in the response to and tolerance of abiotic stresses in sorghum. For each of the four abiotic stresses (drought, heat, cold, and salinity and alkaline) discussed herein, the candidate genes (transcription factors in red), metabolites, and physiological processes are depicted in three layers (from the innermost to outermost layer, respectively).

The plant response at the physiological, gene expression, or protein level cannot be simply predicted by pooling existing knowledge acquired from single-stress treatment experiments. Such differences between the single stress and combined stress impacts and responses have been detected from the expression patterns of stress-responsive or ROS-scavenging genes in sorghum. A few studies on the changed patterns of gene expression under drought, heat/cold and salt stresses in sorghum are selected to visualize the distinct responses at the expression level (Dugas et al., 2011; Johnson et al., 2014; Chopra et al., 2015; Yang et al., 2018; Azzouz-Olden et al., 2020; Ma et al., 2020)—as the full list of DEGs are readily available from these papers or the Supplemental Files—to unbiasedly profile the ROS-scavenging genes. Aquaporin (*AQP*) genes were investigated as well because this gene family encodes the AQP membrane proteins which regulate membrane permeability to water and other molecules (Hu et al., 2012; Huang et al., 2014). The antioxidant system in plants includes several major enzymes (i.e., catalase, CAT, superoxide dismutase, SOD, class III peroxidase, CIII Prx, ascorbate peroxidase, APX, glutathione transferase, GST), which are encoded by corresponding gene families (Rajput et al., 2021). In Figure 2, certain genes are preferentially responsive to certain stress or respond in specific tissues. For example, most of the ROS-scavenging genes tend respond to the stresses in the root but not in the leaf. The *SbSODs* are only differentially expressed in the heat or salt stress samples. By contrast, tonoplast membrane intrinsic proteins (TIPs) from the *AQP* family are apt to be upregulated during drought stress conditions, while the plasma membrane intrinsic protein (PIP) subfamily responds to multiple stresses. Further, *APX* and *CAT* genes are differentially expressed under drought or salt stress. For the large antioxidant gene families, such as *GST* and *Prx*, their genes are responsive to the stress treatment in a member-specific pattern rather than a subfamily-specific pattern. The Class III Prxs catalyze H_2O_2, produce ROS (OH^- or O^{2-}), and participate in diverse physiological processes, including seed germination, lignin metabolism, phytohormone catabolism, and pathogen resistance. Among the eight phylogenetic groups of Prxs (Liu et al., 2021), Prx groups 1, 5, and 6 tend to be responsive to drought stress, whereas Prx groups 2, 3, 7 and 8 tend to be responsive to salinity stress. The stark differences among the responsive patterns of antioxidant-related genes reflect well the different molecular regulations and specific ROS-scavenging capacity underlying the stresses.

On the other hand, different stresses could have the similar or distinct impacts on different physiological or biochemical pathways. For instance, in Arabidopsis, heat stress leads to elongated and thin leaves with increased leaf area and reduced root growth, while drought stress reduces leaf area and increases root growth to enhance water-use efficiency (Vile et al., 2012). However, both drought and heat stresses result in similar growth outcomes, including early flowering, higher rate of seed sterility, and yield losses (Zhang and Sonnewald, 2017). The counteracting effects of drought and heat stresses also depend on the stomata phenotype: heat stress leads to stomata opening to increase transpiration and to cool the leaf surface, while drought stress results in stomata closing to prevent water loss (Rizhsky et al., 2002; Rizhsky et al., 2004; Prasch and Sonnewald, 2015). By contrast, several stress treatments (i.e., drought, high salinity, or low temperature) all cause osmotic stress and oxidative damage (Mittler and Blumwald, 2010); to counteract the osmosis, sorghum plants generally secrete small molecules (such as soluble sugar, alginate, sorbitol, and proline) (Fang et al., 2021). These similarities and differences in physiological responses to various single stresses complicate our understanding of the molecular response to combined stresses.

Shaar-Moshe et al. (2017) investigated the transcriptional patterns and morpho-physiological acclimations of *Brachypodium distachyon* to single salinity, drought, and heat stresses, as well as their double- and triple-stress combinations. The combined stresses intensified the physiological effects when compared to single stresses, with some morphological traits more sensitive to salt stress while some physiological traits being more sensitive to heat stress. Transcriptome analysis revealed that the response patterns of the triple and the three double-stress combinations showed that only 37% of the common stress DEGs (574 genes out of 1550) maintained the same response mode, indicating limited consistency of expression for combined stresses. The response to heat stress at the transcriptional level contributed most to the major differential expression, with single and combined stresses with heat stress involvement showing stronger correlations. Conversely, single drought stress showed weaker correlations with both double- and triple-stress combinations with its involvement. Therefore, it is speculated that the contribution of drought in the combined stress treatments may lie with enhancing or attenuating the intensity of other stresses. In another example of the combination of drought and cold stresses that frequently occur in the northwestern and eastern China, Guo et al. (2021) investigated

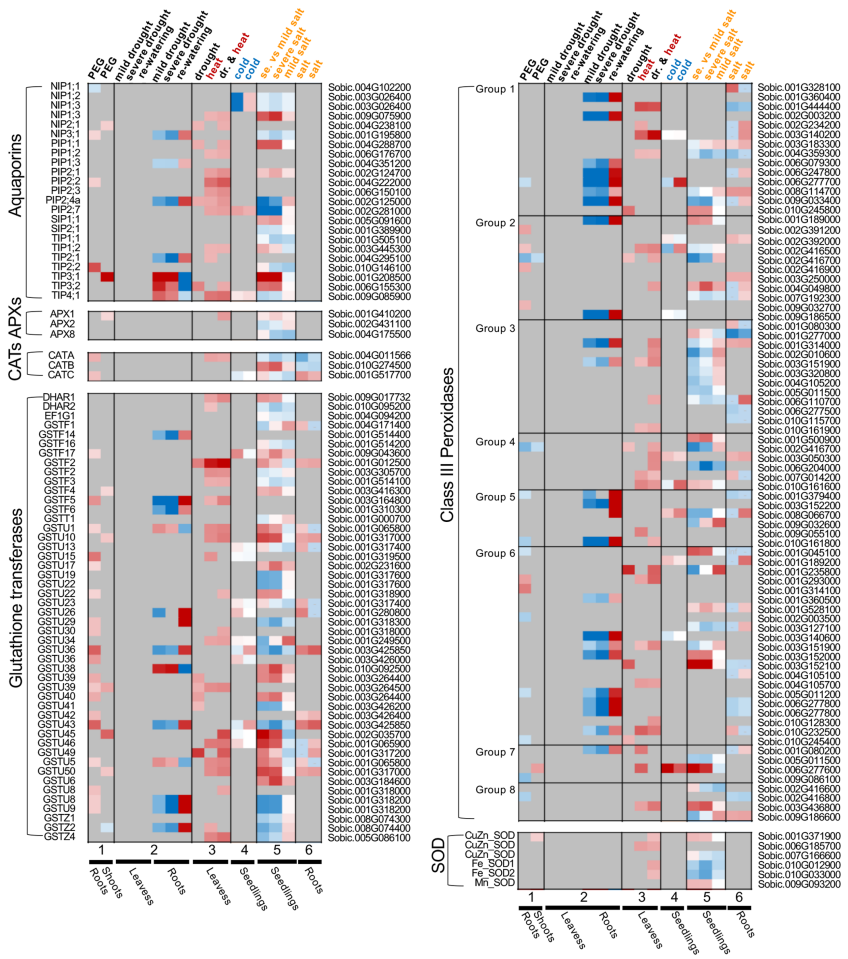

FIGURE 2
Comparison of the differences in gene expression in response to different abiotic stresses and their combination, exemplified using the stress-responsive gene families encoding aquaporins (AQPs) and the major antioxidant enzymes (i.e., APXs, CATs, GSTs, Prxs, and SODs). To avoid direct comparison of the expression levels between the studies, and to not include any batch effects between the studies, the log2(fold-change) of the expression data from each study were visualized by the heat map. These expression patterns are sorted by the studies (labeled as 1, 2, 3, 4, 5, 6 respectively for Dugas et al., 2011; Johnson et al., 2014; Chopra et al., 2015; Zhang et al., 2019; Azzouz-Olden et al., 2020; Ma et al., 2020, and Yang et al., 2018) and by the type of abiotic stress, with drought, heat, cold and salt stresses color-coded in black, red, blue and orange, respectively. Dr, drought. PEG, poly-ethylene glycol. For the study 2 (Dugas et al., 2011), fold changes of gene expression were compared between the leaf and root tissues; For the remaining studies, fold changes of gene expression were calculated in the way that the expression level in the non-stressed control as one. When a gene exhibited an increased or decreased expression (log2(fold-change)>1 or log2(fold-change)<-1), the color was indicated as red or blue, respectively, with the color shadiness indicating the extent of fold change.

molecular responses of maize to the drought and cold combined stress. They showed that both single and combined stresses significantly reduced leaf photosynthesis. Nevertheless, the photosynthetic indicators were similar to the control plants in drought-treated and drought-and-cold-treated plants, whereas cold-treated plants were unable to recover during the recovery stage. Transcriptomic and metabolomic analysis further revealed that drought and cold interacted to mitigate this irreversible damage. This multi-omics study on combined stress in maize also provides the take home message that the outcome of combinatorial stress depends not only upon the nature of the involved stressors but is also related to developmental stages of the plant, the timing of stress applications, and the severity of individual stresses incurred. These factors contribute to the complexity and unpredictability of combinatorial stresses. Overall, these omics studies of single and combined stresses in Brachypodium and maize have provided direct evidence supporting that the molecular responses (at least at the gene expression level) to a combined stress could not be simply predicted in sorghum by the existing multi-omic-based knowledge obtained in single-stress conditions, justifying the importance to study crops' response to combined stresses in agriculturally relevant circumstances.

Concluding remarks and future perspective

Understanding the responses to abiotic stresses and the molecular regulation enacted to cope with stressful conditions faced by sorghum are of great importance. This is because not only does sorghum have strong tolerance to several major abiotic stresses, but it also is closely related to other agriculturally and

economically important major crops (i.e., maize, sugarcane, and rice) with clear gene orthology/synteny between the species. Thus, our review does not only summarize a catalog of sorghum genes for molecular improvement but may also provide useful resource for stress-tolerance improvement in these related crops (Table S1).

The past decade has witnessed vast and rapid advances in our knowledge regarding the molecular responses of sorghum plants to drought, salinity-alkaline, and low/high temperature stresses. This burgeoning body of research has already pinpointed numerous pathways and genes that are associated with the tolerance of certain stress types and those should be prioritized for functional studies. Still, several challenges need to be addressed in future studies. (1) Arguably, systemic molecular insights into sorghum stress-tolerance can be obtained by integrating multi-omic technologies. Previous studies were dominated by transcriptomics with a few that used outdated proteomic technologies. Currently, proteomic technologies with higher throughput and sensitivity are available (Mergner et al., 2020), while metabolomics (such as widely-targeted metabolome) has become the mainstream tool to decipher the metabolite dynamics and genetic basis of plant stress response and regulation (Chen et al., 2013; Yuan et al., 2022). Single-cell omic and spatio-omic technologies have also been successfully applied in major crops (Do et al., 2016; Gutzat et al., 2020; Xu et al., 2020; Chen et al., 2021; Kajala et al., 2021; Li et al., 2021; Shaw et al., 2021; Wang Y. et al., 2021). The integration of multiple omics data and the application of cutting-edge technologies will broaden our understanding of the mechanisms related to stress response and regulation. (2) Large-scale comparisons between phenotypically diverse accessions would shed light on the genetic diversity and plasticity of stress tolerance in sorghum. Many previous studies relied on one or two cultivars at limited time points, thus we still lack large-scale comparisons across accessions and/or time series. (3) Combined stresses often happen in field conditions yet are heavily understudied in basic research. Clearly, our knowledge regarding the molecular response and resistance to combined stresses needs to be enhanced, but this usually cannot be simply inferred from existing knowledge obtained from single stress experiments. (4) The many candidate genes in sorghum revealed by omics are functionally known in other model species but they still lack functional validation in sorghum. Recently, sorghum's transformation *via* particle bombardment and *Agrobacterium* has markedly improved with the greater use of morphogenesis genes and optimization of transformation details (Mookkan et al., 2017; Wu and Zhao, 2017; Kuriyama et al., 2019; Liu et al., 2019). These advances now pave the way for gene functional studies in sorghum and will surely provide direct support for molecular breeding efforts aimed at stress-tolerance improvement. In addition, with the rapidly accumulated omics data of sorghum's abiotic stresses, the establishment of multi-omic platforms for sorghum and unified standards for its data aggregation and collation will greatly enhance both the mining and re-use of data for multi-omic research.

Author contributions

Conceptualization, MT, CD, ZX and YL. Literature review, MT, CD, BY, GW, YD, YW, MC and YL. Drafting the original version of the manuscript, MT, CD and YL. Writing—review and editing, YW, MC, JC, GY, GH, ZX and YL. Supervision, GY, GH, ZX and YL. Funding acquisition, GY, GH, ZX and YL. All authors contributed to the article and approved the submitted version.

Funding

This work was supported by the Opening Fund of Key Laboratory of Forage and Endemic Crop Biology, Ministry of Education (FECBOF2021002); the Opening Fund of Hubei Key Laboratory of Bioinorganic Chemistry and Materia Medica (BCMM202205); the Start-Up Research Funding of Wuhan Polytechnic University (2021RZ100, 53210052172); National Natural Science Foundation of China (32272126); the Fundamental Research Funds for Central Universities, HUST (2021XXJS070, 3004170157); and, the Wuhan Knowledge Innovation Project (2022020801010073).

Acknowledgments

We would like to express our appreciation to the editor and reviewers for their time and efforts to improve the quality of our manuscript.

Conflict of interest

The authors declare that the research was conducted in the absence of any commercial or financial relationships that could be construed as a potential conflict of interest.

Publisher's note

Supplementary material

The Supplementary Material for this article can be found online at: https://www.frontiersin.org/articles/10.3389/fpls.2023.1147328/full#supplementary-material

References

Azzouz-Olden, F., Hunt, A. G., and Dinkins, R. (2020). Transcriptome analysis of drought-tolerant sorghum genotype SC56 in response to water stress reveals an oxidative stress defense strategy. *Mol. Biol. Rep.* 47, 3291–3303. doi: 10.1007/s11033-020-05396-5

Bailey-Serres, J., Parker, J. E., Ainsworth, E. A., Oldroyd, G. E. D., and Schroeder, J. I. (2019). Genetic strategies or improving crop yields. *Nature* 575, 109–118. doi: 10.1038/s41586-019-1679-0

Barnabas, B., Jager, K., and Feher, A. (2008). The effect of drought and heat stress on reproductive processes in cereals. *Plant Cell Environ.* 31, 11–38. doi: 10.1111/j.1365-3040.2007.01727.x

Basu, S., Ramegowda, V., Kumar, A., and Pereira, A. (2016). Plant adaptation to drought stress. *F1000 Res.* 5, 1554. doi: 10.12688/f1000research.7678.1

Boyles, R. E., Brenton, Z. W., and Kresovich, S. (2019). Genetic and genomic resources of sorghum to connect genotype with phenotype in contrasting environments. *Plant J.* 97, 19–39. doi: 10.1111/tpj.14113

Bray, E. A. (1993). Molecular responses to water deficit. *Plant Physiol.* 103, 1035–1040. doi: 10.1104/pp.103.4.1035

Bray, E. A. (1997). Plant responses to water deficit. *Trends Plant Sci.* 2, 48–54. doi: 10.1016/S1360-1385(97)82562-9

Buchanan, C. D., Lim, S., Salzman, R. A., Kagiampakis, I., Morishige, D. T., Weers, B. D., et al. (2005). *Sorghum bicolor*'s transcriptome response to dehydration, high salinity and ABA. *Plant Mol. Biol.* 58, 699–720. doi: 10.1007/s11103-005-7876-2

Byrt, C. S., Xu, B., Krishnan, M., Lightfoot, D. J., Athman, A., Jacobs, A. K., et al. (2014). The na^+ transporter, TaHKT1,5-d, limits shoot na^+ accumulation in bread wheat. *Plant J.* 80, 516–526. doi: 10.1111/tpj.12651

Cai, X., Zhang, X., and Wang, D. (2011). Land availability for biofuel production. environ. *Sci. Technol.* 45, 334–339. doi: 10.1021/es103338e

Campbell, S. A., and Close, T. J. (1997). Dehydrins: genes, proteins, and associations with phenotypic traits. *New Phytol.* 137, 61–74. doi: 10.1046/j.1469-8137.1997.00831.x

Chauhan, H., and Khurana, P. (2011). Use of doubled haploid technology for development of stable drought tolerant bread wheat (*Triticum aestivum* l.) transgenics. *Plant Biotechnol. J.* 9, 408–417. doi: 10.1111/j.1467-7652.2010.00561.x

Chen, X., Chen, Z., Zhao, H., Zhao, Y., Cheng, B., and Xiang, Y. (2014a). Genome-wide analysis of soybean HD-zip gene family and expression profiling under salinity and drought treatments. *PloS One* 9, e87156. doi: 10.1371/journal.pone.0087156

Chen, J., Chopra, R., Hayes, C., Morris, G., Marla, S., Burke, J., et al. (2017). Genome-wide association study of developing leaves' heat tolerance during vegetative growth stages in a sorghum association panel. *Plant Genome* 10, 1–15. doi: 10.3835/plantgenome2016.09.0091

Chen, W., Gong, L., Guo, Z., Wang, W., Zhang, H., Liu, X., et al. (2013). A novel integrated method for large-scale detection, identification, and quantification of widely targeted metabolites: application in the study of rice metabolomics. *Mol. Plant* 6, 1769–1780. doi: 10.1093/mp/sst080

Chen, X., Song, F., Liu, F., Tian, C., Liu, S., Xu, H., et al. (2014b). Effect of different arbuscular mycorrhizal fungi on growth and physiology of maize at ambient and low temperature regimes. *Sci. World J.* 14, 1–7. doi: 10.1155/2014/956141

Chen, H., Yin, X., Guo, L., Yao, J., Ding, Y., Xu, X., et al. (2021). PlantscRNAdb: a database for plant single-cell RNA analysis. *Mol. Plant* 14, 855–857. doi: 10.1016/j.molp.2021.05.002

Chen, L., Zhu, Q., and Kaufmann, K. (2020). Long non-coding RNAs in plants: emerging modulators of gene activity in development and stress responses. *Planta* 252, 92. doi: 10.1007/s00425-020-03480-5

Chopra, R., Burow, G., Burke, J. J., Gladman, N., and Xin, Z. (2017). Genome-wide association analysis of seedling traits in diverse sorghum germplasm under thermal stress. *BMC Plant Biol.* 17, 12–26. doi: 10.1186/s12870-016-0966-2

Chopra, R., Burow, G., Hayes, C., Emendack, Y., Xin, Z., and Burke, J. (2015). Transcriptome profiling and validation of gene based single nucleotide polymorphisms (SNPs) in sorghum genotypes with contrasting responses to cold stress. *BMC Genomics* 16, 1040. doi: 10.1186/s12864-015-2268-8

Close, T. J. (1996). Dehydrins: emergence of a biochemical role of a family of plant dehydration proteins. *Physiol. Plant* 97, 795–803. doi: 10.1111/j.1399-3054.1996.tb00546.x

Dahlberg, J. A., Evans, J., Johnson, E., Hyman, M., Biehl, E., and Wendorf, F. (1995). Attempts to identify 8000-bp sorghum using image-analysis, infrared spectroscopy, and biotechnological procedures. *Acta Palaeobotanica.* 35, 167–173. https://www.webofscience.com/wos/alldb/full-record/BCI:BCI199598508756.

Dai, L., Du, J., Zhang, Y., Zhu, H., and Yin, K. (2017). Proteomics analysis of sweet sorghum in response to soda saline-alkali stress. *Chin. J. Ecol.* 36, 1597–1605. doi: 10.13292/j.1000-4890.201706.028

de Oliveira, D. F., Lopes, L. D., and Gomes, E. (2020). Metabolic changes associated with differential salt tolerance in sorghum genotypes. *Planta* 252, 34. doi: 10.1007/s00425-020-03437-8

Ding, Y., Shi, Y., and Yang, S. (2019). Advances and challenges in uncovering cold tolerance regulatory mechanisms in plants. *New Phytol.* 222, 1690–1704. doi: 10.1111/nph.15696

Do, T. P., Lee, H., Mookkan, M., Folk, W. R., and Zhang, Z. J. (2016). Rapid and efficient agrobacterium-mediated transformation of sorghum (*Sorghum bicolor*) employing standard binary vectors and bar gene as a selectable marker. *Plant Cell Rep.* 35, 2065–2076. doi: 10.1007/s00299-016-2019-6

Dugas, D. V., Monaco, M. K., Olson, A., Klein, R. R., Kumari, S., Ware, D., et al. (2011). Functional annotation of the transcriptome of sorghum bicolor in response to osmotic stress and abscisic acid. *BMC Genomics* 12, 514. doi: 10.1186/1471-2164-12-514

Fang, S., Hou, X., and Liang, X. (2021). Response mechanisms of plants under saline-alkali stress. *Front. Plant Sci.* 12. doi: 10.3389/fpls.2021.667458

Farooq, M., Bramley, H., Palta, J., and Siddique, K. (2011). Heat stress in wheat during reproductive and grain-filling phases. *Crit. Rev. Plant Sci.* 30. doi: 10.3389/fpls.2022.1005773

Farooq, M., Wahid, A., Kobayashi, N., Fujita, D., and Basra, S. M. A. (2009). Plant drought stress: effects, mechanisms and management. *Agron. Sustain. Dev.* 29, 185–212. doi: 10.1051/agro:2008021

Fedoroff, N. V., Battisti, D. S., Beachy, R. N., Cooper, P. J. M., Fischhoff, D. A., Hodges, C. N., et al. (2010). Radically rethinking agriculture for the 21st century. *Science* 327, 833–834. doi: 10.1126/science.1186834

Feng, J., Jia, W., Lv, S., Bao, H., Miao, F., Zhang, X., et al. (2018). Comparative transcriptome combined with morpho-physiological analyses revealed key factors for differential cadmium accumulation in two contrasting sweet sorghum genotypes. *Plant Biotechnol. J.* 16, 558–571. doi: 10.1111/pbi.12795

Fiedler, K., Bekele, W. A., Matschegewski, C., Snowdon, R., Wieckhorst, S., Zacharias, A., et al. (2016). Cold tolerance during juvenile development in sorghum: a comparative analysis by genome-wide association and linkage mapping. *Plant Breed.* 135, 598–606. doi: 10.1111/pbr.12394

Food and Agriculture Organization of the United Nations (1981). *Crop water requirement* (Rome: FAO), 40–41.

Fracasso, A., Trindade, L. M., and Amaducci, S. (2016). Drought stress tolerance strategies revealed by RNA-seq in two sorghum genotypes with contrasting WUE. *BMC Plant Biol.* 16, 115. doi: 10.1186/s12870-016-0800-x

Funck, D., Baumgarten, L., Stifit, M., Wiren, N. V., and Schonemann, L. (2020). Different contribution of P5CS isoforms to stress tolerance in arabidopsis. *Front. Plant Sci.* 11. doi: 10.3389/fpls.2020.565134

Ge, S., Liu, D., Chu, M., Liu, X., Wei, Y., Che, X., et al. (2022). Dynamic and adaptive membrane lipid remodeling in leaves of sorghum under salt stress. *Crop J.* 10, 1557–1569. doi: 10.1016/j.cj.2022.03.006

Gelli, M., Konda, A. R., Liu, K., Zhang, C., Clemente, T. E., Holding, D. R., et al. (2017). Validation of QTL mapping and transcriptome profiling for identification of candidate genes associated with nitrogen stress tolerance in sorghum. *BMC Plant Biol.* 17, 123. doi: 10.1186/s12870-017-1064-9

Goche, T., Shargie, N. G., Cummins, I., Brown, A. P., Chivasa, S., and Ngara, R. (2020). Comparative physiological and root proteome analyses of two sorghum varieties responding to water limitation. *Sci. Rep.* 10, 11835. doi: 10.1038/s41598-020-68735-3

Grootboom, A. W., Mkhonza, N. L., O`Kennedy, M. M., Chakauya, E., Kunert, K., and Chikwamba, R. K. (2010). Biolistic mediated sorghum (*Sorghum bicolor* l. moench) transformation *via* mannose and bialaphos based selection systems. *Int. J. Bot.* 6, 89–94. doi: 10.3923/ijb.2010.89.94

Guo, Q., Li, X., Niu, L., Jameson, P. E., and Zhou, W. (2021). Transcription-associated metabolomic adjustments in maize occur during combined drought and cold stress. *Plant Physiol.* 186, 677–695. doi: 10.1093/plphys/kiab050

Gupta, A., Rico-Medina, A., and Cano-Delagdo, A. I. (2020). The physiology of plant responses to drought. *Science* 368, 266–269. doi: 10.1126/science.aaz7614

Gutzat, R., Rembart, K., Nussbaumer, T., Hofmann, F., Pisuparti, R., Bradamante, G., et al. (2020). Arabidopsis shoot stem cells display dynamic transcription and DNA methylation patterns. *EMBO J.* 39, e103667. doi: 10.15252/embj.2019103667

Halder, T., Upadhyaya, G., Basak, H., Das, A., Chakraborty, C., and Ray, S. (2018). Dehydrins impart protection against oxidative stress in transgenic tobacco plants. *Front. Plant Sci.* 9, 136. doi: 10.3389/fpls.2018.00136

Hamza, N. B., Sharma, N., Tripathi, A., and Sanan-Mishra, N. (2016). MicroRNA expression profiles in response to drought stress in *Sorghum bicolor*. *Gene Expr. Patterns.* 20, 88–98. doi: 10.1016/j.gep.2016.01.001

Hao, H., Li, Z., Leng, C., Lu, C., Luo, H., Liu, Y., et al. (2021). Sorghum breeding in the genomic era: opportunities and challenges. *Theor. Appl. Genet.* 134, 1899–1924. doi: 10.1007/s00122-021-03789-z

Harris, K., Subudhi, P. K., Borrell, A., Jordan, D., Rosenow, D., Nguyen, H., et al. (2007). Sorghum stay-green QTL individually reduce post-flowering drought-induced leaf senescence. *J. Exp. Bot.* 58, 327–338. doi: 10.1093/jxb/erl225

Hiei, Y., Ishida, Y., and Komari, T. (2014). Progress of cereal transformation technology mediated by *Agrobacterium tumefaciens*. *Front. Plant Sci.* 5. doi: 10.3389/fpls.2014.00628

Hu, W., Yuan, Q., Wang, Y., Cai, R., Deng, X., Wang, J., et al. (2012). Overexpression of a wheat aquaporin gene, *TaAQP8*, enhances salt stress tolerance in transgenic tobacco. *Plant Cell Physiol.* 53, 2127–2141. doi: 10.1093/pcp/pcs154

Huang, C., Zhou, S., Hu, W., Deng, X., Wei, S., Yang, G., et al. (2014). The wheat aquaporin gene *TaAQP7* confers tolerance to cold stress in transgenic tobacco. *Z. Naturforsch.* 69c, 142–148. doi: 10.5560/znc.2013-0079

Ismail, A. M., and Horie, T. (2017). Genomics, physiology, and molecular breeding approaches for improving salt tolerance. *Annu. Rev. Plant Biol.* 68, 405–434. doi: 10.1146/annurev-arplant-042916-040936

Jedmowski, M., Ashoub, A., Beckhaus, T., Berberich, T., Karas, M., and Brüggemann, W. (2014). Comparative analysis of sorghum bicolor proteome in response to drought stress and following recovery. *Int. J. Proteomics.* 2014, 395905. doi: 10.1155/2014/395905

Jia, W., Lin, K., Lou, T., Feng, J., Lv, S., Jiang, P., et al. (2021). Comparative analysis of sRNAs, degradome and transcriptomics in sweet sorghum reveals the regulatory roles of miRNAs in cdaccumulation and tolerance. *Planta* 254, 16. doi: 10.1007/s00425-021-03669-2

Jia, W., Lv, S., Feng, J., Li, J., Li, Y., and Li, S. (2016). Morphophysiological characteristic analysis demonstrated the potential of sweet sorghum (*Sorghum bicolor* (L.) moench) in the phytoremediation of cadmium-contaminated soils. environ. *Sci. pollut. Res. Int.* 23, 18823–18831. doi: 10.1007/s11356-016-7083-5

Jin, X., Long, Y., Xiong, S., Yang, Z., Chen, W., Hawar, A., et al. (2021). SbNAC2 enhances abiotic stress tolerance by upregulating ROS scavenging activities and inducing stress-response genes in sorghum. *Environ. Exp. Bot.* 192, 104664. doi: 10.1016/j.envexpbot.2021.104664

Johnson, S. M., Lim, F. L., Finkler, A., Fromm, H., Slabas, A. R., and Knight, M. R. (2014). Transcriptomic analysis of *Sorghum bicolor* responding to combined heat and drought stress. *BMC Genomics* 15, 456. doi: 10.1186/1471-2164-15-456

Kajala, K., Gouran, M., Shaar-Moshe, L., Mason, G. A., Rodriguez-Medina, J., Kawa, D., et al. (2021). Innovation, conservation, and repurposing of gene function in root cell type development. *Cell* 184, 3333–3348. doi: 10.1016/j.cell.2021.04.024

Kulcheski, F. R., de Oliveira, L. F., Molina, L. G., Almerao, M. P., Rodrigues, F. A., Marcolino, J., et al. (2011). Identification of novel soybean microRNAs involved in abiotic and biotic stresses. *BMC Genomics* 12, 307. doi: 10.1186/1471-2164-12-307

Kumar, M., Lee, S. C., Kim, J. Y., Kim, S. J., Aye, S. S., and Kim, S. R. (2016). Over-expression of dehydrin gene, *OsDhn1*, improves drought and salt stress tolerance through scavenging of reactive oxygen species in rice (*Oryza sativa* l.). *J. Plant Biol.* 57, 383–393. doi: 10.1007/s12374-014-0487-1

Kuriyama, T., Shimada, S., and Matsui, M. (2019). Improvement of *Agrobacterium*-mediated transformation for tannin-producing sorghum. *Plant Biotechnol.* 36, 43–48. doi: 10.5511/plantbiotechnology.19.0131a

Landi, S., Hausman, J. F., Guerriero, G., and Esposito, S. (2017). Poaceae vs. abiotic stress: focus on drought and salt stress, recent insights and perspectives. *Front. Plant Sci.* 8, 1214. doi: 10.3389/fpls.2017.01214

Laopaiboon, L., Nuanpeng, S., Srinophakun, P., and Klanrit, P. (2009). Ethanol production from sweet sorghum juice using very high gravity technology: effects of carbon and nitrogen supplementations. *Bioresour. Technol.* 100, 4176–4182. doi: 10.1016/j.biortech.2009.03.046

Li, S. (2013). The roadmap of the development of biofuel industry. *China Brew* 32, 77–81. Available at: https://kns.cnki.net/kcms2/article/abstract?v=3uoqIhG8C44YLTlOAiTRKjw8pKedNdX5_mkCYmAjR9x9doD_VINuSTqu8KVijINbXiIblbfA74cFdSXfOJSwRGHNX25KW51x&uniplatform=NZKPT.

Li, H., Dai, X., Huang, X., Xu, M., Wang, Q., Yan, X., et al. (2021). Single-cell RNA sequencing reveals a high-resolution cell atlas of xylem in populus. *J. Inte. Plant Biol.* 63, 1906–1921. doi: 10.1111/jipb.13159

Li, H., Li, Y., Ke, Q., Kwak, S. S., Zhang, S., and Deng, X. (2020). Physiological and differential proteomic analyses of imitation drought stress response in *Sorghum bicolor* root at the seedling stage. *Int. J. Mol. Sci.* 21, 9174. doi: 10.3390/ijms21239174

Li, J., Pu, L., Han, M., Zhu, M., Zhang, R., and Xiang, Y. (2014). Soil salinization research in China: advances and prospects. *J. Geogr. Sci.* 24, 943–960. doi: 10.1007/s11442-014-1130-2

Liu, H., Dong, S., Li, M., Gu, F., Yang, G., Guo, T., et al. (2021). The class III peroxidase gene *OsPrx30*, transcriptionally modulated by the AT-hook protein OsATH1, mediates rice bacterial blight-induced ROS accumulation. *J. Integr. Plant Biol.* 63, 393–408. doi: 10.1111/jipb.13040

Liu, G., Li, J., and Godwin, I. D. (2019). Genome editing by CRISPR/Cas9 in sorghum through biolistic bombardment. *Methods Mol. Biol.* 1931, 169–183. doi: 10.1007/978-1-4939-9039-9_12

Liu, C., Zhang, Y., Zhang, F., Zhang, S., Yin., M., Ye, H., et al. (2007). Assessing pollutions of soil and plant by municipal waste dump. *Environ. Geol.* 52, 641–651. doi: 10.1007/s00254-006-0493-9

Ma, S., Lv, J., Li, X., Ji, T., Zhang, Z., and Gao, L. (2021). Galactinol synthase gene 4 (*CsGolS4*) increases cold and drought tolerance in *Cucumis sativus* l. by inducing RFO accumulation and ROS scavenging. *Environ. Exp. Bot.* 185, 104406. doi: 10.1021/acs.jafc.0c06249

Ma, S., Lv, L., Meng, C., Zhang, C., and Li, Y. (2020). Integrative analysis of the metabolome and transcriptome of sorghum bicolor reveals dynamic changes in flavonoids accumulation under saline–alkali stress. *J. Agric. Food Chem.* 68, 14781–14789. doi: 10.1021/acs.jafc.0c06249

Maheshwari, M., Kummari, D., Palakolanu, S. R., Tejaswi, U. N., Nagaraju, M., Rajasheker, G., et al. (2019). Genome-wide identification and expression profile analysis of nuclear factor y family genes in *Sorghum bicolor* l. (Moench). *PloS One* 14, e0222203. doi: 10.1371/journal.pone.0222203

Mathur, S., Umakanth, A. V., Tonapi, V. A., Sharma, R., and Sharma, M. K. (2017). Sweet sorghum as biofuel feedstock: recent advances and available resources. *Biotechnol. Biofuels* 10, 146. doi: 10.1186/s13068-017-0834-9

Merewitz, E. B., Gianfagna, T., and Huang, B. (2011). Protein accumulation in leaves and roots associated with improved drought tolerance in creeping bentgrass expressing an ipt gene for cytokinin synthesis. *J. Exp. Bot.* 62, 5311–5333. doi: 10.1093/jxb/err166

Mergner, J., Frejno, M., List, M., Papacek, M., Chen, X., Chaudhary, A., et al. (2020). Mass-spectrometry-based draft of the arabidopsis proteome. *Nature* 579, 409–414. doi: 10.1038/s41586-020-2094-2

Mittler, R. (2006). Abiotic stress, the field environment and stress combination. *Trends Plant Sci.* 11, 15–19. doi: 10.1016/j.tplants.2005.11.002

Mittler, R., and Blumwald, E. (2010). Genetic engineering for modern agriculture: challenges and perspectives. *Annu. Rev. Plant Biol.* 61, 443–462. doi: 10.1146/annurev-arplant-042809-112116

Mookkan, M., Nelson-Vasilchik, K., Hague, J., Zhang, Z. J., and Kausch, A. P. (2017). Selectable marker independent transformation of recalcitrant maize inbred B73 and sorghum P898012 mediated by morphogenic regulators BABY BOOM and WUSCHEL2. *Plant Cell Rep.* 36, 1477–1491. doi: 10.1007/s00299-017-2169-1

Mullet, J., Morishige, D., McCormick, R., Truong, S., Hilley, J., McKinley, B., et al. (2014). Energy sorghum–a genetic model for the design of c 4 grass bioenergy crops. *J. Exp. Bot.* 65, 3479–3489. doi: 10.1093/jxb/eru229

Ngara, R., Goche, T., Swanevelder, D. Z. H., and Chivasa, S. (2021). Sorghum's whole-plant transcriptome and proteome responses to drought stress: a review. *Life* 11, 704. doi: 10.3390/life11070704

Ngcala, M. G., Goche, T., Brown, A. P., Chivasa, S., and Ngara, R. (2020). Heat stress triggers differential protein accumulation n the extracellular matrix of sorghum cell suspension cultures. *Proteomes* 8, 29. doi: 10.3390/proteomes8040029

Olvera-Carrillo, Y., Campos, F., Reyes, J. L., Garciarrubio, A., and Covarrubias, A. A. (2010). Functional analysis of the group 4 late embryogenesis abundant proteins reveals their relevance in the adaptive response during water deficit in arabidopsis. *Plant Physiol.* 154, 373–390. doi: 10.1104/pp.110.158964

Pandey, S. P., and Somssich, I. E. (2009). The role of WRKY transcription factors in plant immunity. *Plant Physiol.* 150, 1648–1655. doi: 10.1104/pp.109.138990

Park, B. J., Liu, Z., Kanno, A., and Kameya, T. (2005). Genetic improvement of Chinese cabbage for salt and drought tolerance by constitutive expression of *B. napus LEA* gene. *Plant Sci.* 169, 553–558. doi: 10.1016/j.plantsci.2005.05.008

Pasini, L., Bergonti, M., Fracasso, A., Marocco, A., and Amaducci, S. (2014). Microarray analysis of differentially expressed mRNAs and miRNAs in young leaves of sorghum under dry-down conditions. *J. Plant Physiol.* 171, 537–548. doi: 10.1016/j.jplph.2013.12.014

Paterson, A. H., Bowers, J. E., Bruggmann, R., Dubchak, I., Grimwood, J., Gundlach, H., et al. (2009). The *Sorghum bicolor* genome and the diversification of grasses. *Nature* 457, 551–556. doi: 10.1038/nature07723

Petroni, K., Kumimoto, R. W., Gnesutta, N., Calvenzani, V., Fornari, M., Tonelli, C., et al. (2012). The promiscuous life of plant NUCLEAR FACTOR y transcription factors. *Plant Cell* 24, 4777–4792. doi: 10.1105/tpc.112.105734

Prasch, C. M., and Sonnewald, U. (2015). Signaling events in plants: stress factors in combination change the picture. *Environ. Exp. Bot.* 114, 4–14. doi: 10.1016/j.envexpbot.2014.06.020

Rajput, V. D., Singh, R. K., Verma, K. K., Sharma, L., Quiroz-Figueroa, F. R., Meena, M., et al. (2021). Recent developments in enzymatic antioxidant defence mechanism in plants with special reference to abiotic stress. *Biology* 10, 267. doi: 10.3390/biology10040267

Rizhsky, L., Liang, H., and Mittler, R. (2002). The combined effect of drought stress and heat shock on gene expression in tobacco. *Plant Physiol.* 130, 1143–1151. doi: 10.1104/pp.006858

Rizhsky, L., Liang, H., Shuman, J., Shulaev, V., Davletova, S., and Mittler, R. (2004). When defense pathways collide. the response of arabidopsis to a combination of drought and heat stress. *Plant Physiol.* 134, 1683–1696. doi: 10.1104/pp.103.033431

Punia, H., Tokas, J., Malik, A., Bajguz, A., El-Sheikh, M. A., and Ahmad, ,. P. (2021). Ascorbate–glutathione oxidant scavengers, metabolome analysis and adaptation mechanisms of ion exclusion in sorghum under salt stress. *Int. J. Mol. Sci.* 22, 13249. doi: 10.3390/ijms222413249

Rodrigues, J., Inze, D., Nelissen, H., and Saibo, N. J. M. (2019). Source-sink regulation in crops under water deficit. *Trends Plant Sci.* 24, 652–663. doi: 10.1016/j.tplants.2019.04.005

Scharf, K. D., Berberich, T., Ebersberger, I., and Nover, L. (2012). The plant heat stress transcription factor (Hsf) family: structure, function and evolution. *Biochim. Biophys. Acta* 1819, 104–119. doi: 10.1016/j.bbagrm.2011.10.002

Shaar-Moshe, L., Blumwald, E., and Peleg, Z. (2017). Unique physiological and transcriptional shifts under combinations of salinity, drought, and heat. *Plant Physiol.* 174, 421–434. doi: 10.1104/pp.17.00030

Shan, L., and Xu, B. (2009). Discussion on drought resistance of sorghum and its status in agriculture in arid and semiarid regions. *Scientia Agricultura Sin.* 42, 2342–2348. doi: 10.3864/j.issn.0578-1752.2009.07.011

Shao, W., Zhang, J., Ge, S., Wei, Y., Li, J., Wu, G., et al. (2021). Physiological changes and related genes expression analysis of sorghum (*Sorghum bicolor*) seedlings under low temperature stress. *J. Agric. Biotechnol.* 29, 857–870. doi: 10.3969/j.issn.1674-7968.2021.05.004

Shaw, R., Tian, X., and Xu, J. (2021). Single-cell transcriptome analysis in plants: advances and challenges. *Mol. Plant* 14, 115–126. doi: 10.1016/j.molp.2020.10.012

Shen, H., Zhong, X., Zhao, F., Wang, Y., Yam, B., Li, Q., et al. (2015). Overexpression of receptor-like kinase ERECTA improves thermotolerance in rice and tomato. *Nat. Biotechnol.* 33, 996–1003. doi: 10.1038/nbt.3321

Smith, O., Nicholson, W. V., Kistler, L., Mace, E., Clapham, A., Rose, P., et al. (2019). A domestication history of dynamic adaptation and genomic deterioration in sorghum. *Nat. Plants* 5, 369–379. doi: 10.1038/s41477-019-0397-9

Song, Y., and Sui, N. (2019). Functional analysis of *FAD7* gene in sweet sorghum. *Biotechnol. Bulletin.* 35, 35–41. doi: 10.13560/j.cnki.biotech.bull.1985.2018-1102

Sticklen, M. B. (2007). Feedstock crop genetic engineering for alcohol fuels. *Crop Sci.* 47, 2238–2248. doi: 10.2135/cropsci2007.04.0212

Su, P. (1995). *Physio-ecological adaptation of crops to the low and variable water conditions* (Yang ling: Institute of soil and water conservation, Chinese academy of sciences and water resources).

Su, M., Li, X., Ma, X., Peng, X., Zhao, A., Cheng, L., et al. (2011). Cloning two P5CS genes from bioenergy sorghum and their expression profiles under abiotic stresses and MeJA treatment. *Plant Sci.* 181, 652–659. doi: 10.1016/j.plantsci.2011.03.002

Sui, N., Yang, Z., Liu, M., and Wang, B. (2015). Identification and transcriptomic profiling of genes involved in increasing sugar content during salt stress in sweet sorghum leaves. *BMC Genomics* 16, 534. doi: 10.1186/s12864-015-1760-5

Sun, X., Zheng, H., Li, J., Liu, L., Zhang, X., and Sui, N. (2020). Comparative transcriptome analysis reveals new lncRNAs responding to salt stress in sweet sorghum. *Front. Bioeng Biotechnol.* 8. doi: 10.3389/fbioe.2020.00331

Swami, A. K., Alam, S. I., Sengupta, N., and Sarin, R. (2011). Differential proteomic analysis of salt stress response in sorghum bicolor leaves. *Environ. Exp. Bot.* 71, 321–328. doi: 10.1016/j.envexpbot.2010.12.017

Szekely, G., Abraham, E., Cesplo, A., Rigo, G., Zsigmond, L., Csiszar, J., et al. (2008). Duplicated *P5CS* genes of *Arabidopsis* play distinct roles in stress regulation and developmental control of proline biosynthesis. *Plant J.* 53, 11–28. doi: 10.1111/j.1365-313X.2007.03318.x

Thangaraj, K., Li, J., Mei, H., Hu, S., Han, R., Zhao, Z., et al. (2022). Mycorrhizal colonization enhanced *Sorghum bicolor* tolerance under soil water deficit conditions by coordination of proline and reduced glutathione (GSH). *J. Agric. Food Chem.* 70, 4243–4255. doi: 10.1021/acs.jafc.1c07184

Uga, Y., Sugimoto, K., Ogawa, S., Rane, J., Ishitani, M., Hara, M., et al. (2013). Control of root system architecture by DEEPER ROOTING 1 increases rice yield under drought conditions. *Nat. Genet.* 45, 1097–1102. doi: 10.1038/ng.2725

United Nations (2011) *Department of economic and social affairs, population division, world population prospects: the 2010 revision*. Available at: www.un.org/en/development/desa/population/publications/pdf/trends/WPP2010/WPP2010_Volume-I_Comprehensive-Tables.pdf.

Varoquaux, N., Cole, B., Gao, C., Pierroz, G., Baker, C. R., Patel, D., et al. (2019). Transcriptomic analysis of field-droughted sorghum from seedling to maturity reveals biotic and metabolic responses. *Proc. Natl. Acad. Sci. U.S.A.* 116, 27124–27132. doi: 10.1073/pnas.1907500116

Vile, D., Pervent, M., Belluau, M., Vasseur, F., Bresson, J., Muller, B., et al. (2012). Arabidopsis growth under prolonged high temperature and water deficit: independent or interactive effects? *Plant Cell Environ.* 35, 702–718. doi: 10.1111/j.1365-3040.2011.02445.x

Wang, L., Guo, Y., and Yang, S. (2021). Designed breeding for adaptation of crops to environmental abiotic stresses. *Sci. Sin. Vitae.* 51, 1424–1434. doi: 10.1360/SSV-2021-0162

Wang, Y., Huan, Q., Li, K., and Qian, W. (2021). Single-cell transcriptome atlas of the leaf and root of rice seedlings. *J. Genet. Genomics* 48, 881–898. doi: 10.1016/j.jgg.2021.06.001

Wang, T., Ren, Z., Liu, Z., Feng, X., Guo, R., Li, B., et al. (2014). *SbHKT1;4*, a member of the high-affinity potassium transporter gene family from sorghum bicolor, functions to maintain optimal Na + /K + balance under Na + stress. *J. Integr. Plant Biol.* 56, 315–332. doi: 10.1111/jipb.12144

Wang, Z., Wei, Y., Zhao, Y., and Wang, Y. (2022). A transcriptomic study of physiological responses to drought and salt stress in sweet sorghum seedlings. *Acta Prataculturae. Sinica.* 31, 71–84. doi: 10.11686/cyxb2020557

Winchell, F., Stevens, C. J., Murphy, C., Champion, L., and Fuller, D. Q. (2017). Evidence for sorghum domestication in fourth millennium BC eastern Sudan: spikelet morphology from ceramic impressions of the butana group. *Curr. Anthropol.* 58, 673–683. doi: 10.1086/693898

Wood, A. J., and Goldsbrough, P. B. (1997). Characterization and expression of dehydrins in water-stressed *Sorghum bicolor*. *Physiol. Plant* 99, 144–152. doi: 10.1111/j.1399-3054.1997.tb03442.x

Wu, E., and Zhao, Z. (2017). *Agrobacterium*-mediated sorghum transformation. *Methods Mol. Biol.* 1669, 355–364. doi: 10.1007/978-1-4939-7286-9_26

Xiao, B., Huang, Y., Tang, N., and Xiong, L. (2007). Over-expression of a LEA gene in rice improves drought resistance under the field conditions. *Theor. Appl. Genet.* 115, 35–46. doi: 10.1007/s00122-007-0538-9

Xie, Q., and Xu, Z. (2019). Sustainable agriculture: from sweet sorghum planting and ensiling to ruminant feeding. *Mol. Plant* 12, 603–606. doi: 10.1016/j.molp.2019.04.001

Xiong, L., and Zhu, J. (2002). Molecular and genetic aspects of plant responses to osmotic stress. *Plant Cell Environ.* 25, 131–139. doi: 10.1046/j.1365-3040.2002.00782.x

Xu, X., Crow, M., Rice, B. R., Li, F., Harris, B., Liu, L., et al. (2020). Single-cell RNA sequencing of developing maize ears facilitates functional analysis and trait candidate gene discovery. *Dev. Cell.* 56, 1–12. doi: 10.1016/j.devcel.2020.12.015

Xu, D., Ni, Y., Zhang, X., and Guo, Y. (2022). Multiomic analyses of two sorghum cultivars reveals the change of membrane lipids in their responses to water deficit. *Plant Physiol. Biochem.* 176, 44–56. doi: 10.1016/j.plaphy.2022.02.015

Yang, Z., Wang, Y., Wei, X., Zhao, X., Wang, B., and Sui, N. (2017). Transcription profiles of genes related to hormonal regulations under salt stress in sweet sorghum. *Plant Mol. Biol. Rep.* 35, 586–599. doi: 10.1007/s11105-017-1047-x

Yang, Z., Zheng, H., Wei, X., Song, J., Wang, B., and Sui, N. (2018). Transcriptome analysis of sweet sorghum inbred lines differing in salt tolerance provides novel insights into salt exclusion by roots. *Plant Soil* 430, 423–439. doi: 10.1007/s11104-018-3736-0

Yu, J., Zhang, X., and Tan, T. (2008). Ethanol production by solid state fermentation of sweet sorghum using thermotolerant yeast strain. *Fuel. Process. Technol.* 89, 1056–1059. doi: 10.1016/j.fuproc.2008.04.008

Yuan, H., Cao, G., Hou, X., Huang, M., Du, P., Tan, T., et al. (2022). Development of a widely targeted volatilomics method for profiling volatilomes in plants. *Mol. Plant* 15, 189–202. doi: 10.1016/j.molp.2021.09.003

Zhang, J., Jiang, F., Shen, Y., Zhan, Q., Bai, B., Chen, W., et al. (2019a). Transcriptome analysis reveals candidate genes related to phosphorus starvation tolerance in sorghum. *BMC Plant Biol.* 19, 306. doi: 10.1186/s12870-019-1914-8

Zhang, H., Liu, X., Zhang, R., Yuan, H., Wang, M., Yang, H., et al. (2017). Root damage under alkaline stress is associated with reactive oxygen species accumulation in rice (*Oryza sativa* l). *Front. Plant Sci.* 8. doi: 10.3389/fpls.2017.01580

Zhang, H., and Sonnewald, U. (2017). Differences and commonalities of plant responses to single and combined stresses. *Plant J.* 90, 839–855. doi: 10.1111/tpj.13557

Zhang, D., Zeng, T., Liu, X., Gao, C., Li, Y., Li, C., et al. (2019b). Transcriptomic profiling of sorghum leaves and roots responsive to drought stress at the seedling stage. *J. Integr. Agric.* 18, 1980–1995. doi: 10.1016/S2095-3119(18)62119-7

Zhang, H., Zhu, J., Gong, Z., and Zhu, J. (2022). Abiotic stress responses in plants. *Nat. Rev. Genet.* 23, 104–119. doi: 10.1016/j.cell.2016.08.029

Zhao, S., Gao, H., Jia, X., Wang, H., Mao, K., and Ma, F. (2020). The HD-zip I transcription factor *MdHB-7* regulates drought tolerance in transgenic apple (*Malus domestica*). *Environ. Exp. Bot.* 180, 104246. doi: 10.1016/j.envexpbot.2020.104246

Zhao, C., Lang, Z., and Zhu, J. (2015). Cold responsive gene transcription becomes more complex. *Trends Plant Sci.* 20, 466–468. doi: 10.1016/j.tplants.2015.06.001

Zheng, H., Gao, Y., Sui, Y., Dang, Y., Wu, F., Wang, X., et al. (2023). R2R3 MYB transcription factor SbMYBHv33 negatively regulates sorghum biomass accumulation and salt tolerance. *Theor. Appl. Genet.* 136, 5. doi: 10.1007/s00122-023-04292-3

Zhu, J. (2016). Abiotic stress signaling and responses in plants. *Cell* 167, 313–324. doi: 10.1016/j.cell.2016.08.029

frontiers | Frontiers in Plant Science

TYPE Original Research
PUBLISHED 02 June 2023
DOI 10.3389/fpls.2023.1092998

OPEN ACCESS

EDITED BY
Laura Medina-Puche,
University of Tübingen, Germany

REVIEWED BY
Rafael F. Rivera-Bustamante,
Center for Research and Advanced Studies - Irapuato Unit, Mexico
Huang Tan,
University of Tübingen, Germany

*CORRESPONDENCE
Fuh-Jyh Jan
fjjan@nchu.edu.tw

†These authors have contributed equally to this work

RECEIVED 08 November 2022
ACCEPTED 05 May 2023
PUBLISHED 02 June 2023

CITATION
Chang H-H, Gustian D, Chang C-J and Jan F-J (2023) Virus-virus interactions alter the mechanical transmissibility and host range of begomoviruses.
Front. Plant Sci. 14:1092998.
doi: 10.3389/fpls.2023.1092998

Virus-virus interactions alter the mechanical transmissibility and host range of begomoviruses

Ho-Hsiung Chang[1†], Deri Gustian[1†], Chung-Jan Chang[2] and Fuh-Jyh Jan[1,3*]

[1]Department of Plant Pathology, National Chung Hsing University, Taichung, Taiwan, [2]Department of Plant Pathology, University of Georgia, Griffin, GA, United States, [3]Advanced Plant and Food Crop Biotechnology Center, National Chung Hsing University, Taichung, Taiwan

Introduction: Begomoviruses are mainly transmitted by whiteflies. However, a few begomoviruses can be transmitted mechanically. Mechanical transmissibility affects begomoviral distribution in the field.

Materials and methods: In this study, two mechanically transmissible begomoviruses, tomato leaf curl New Delhi virus-oriental melon isolate (ToLCNDV-OM) and tomato yellow leaf curl Thailand virus (TYLCTHV), and two nonmechanically transmissible begomoviruses, ToLCNDV-cucumber isolate (ToLCNDV-CB) and tomato leaf curl Taiwan virus (ToLCTV), were used to study the effects of virus-virus interactions on mechanical transmissibility.

Results: *Nicotiana benthamiana* and host plants were coinoculated through mechanical transmission with inoculants derived from plants that were mix-infected or inoculants derived from individually infected plants, and the inoculants were mixed immediately before inoculation. Our results showed that ToLCNDV-CB was mechanically transmitted with ToLCNDV-OM to *N. benthamiana*, cucumber, and oriental melon, whereas ToLCTV was mechanically transmitted with TYLCTHV to *N. benthamiana* and tomato. For crossing host range inoculation, ToLCNDV-CB was mechanically transmitted with TYLCTHV to *N. benthamiana* and its nonhost tomato, while ToLCTV with ToLCNDV-OM was transmitted to *N. benthamiana* and its nonhost oriental melon. For sequential inoculation, ToLCNDV-CB and ToLCTV were mechanically transmitted to *N. benthamiana* plants that were either preinfected with ToLCNDV-OM or TYLCTHV. The results of fluorescence resonance energy transfer analyses showed that the nuclear shuttle protein of ToLCNDV-CB (CBNSP) and the coat protein of ToLCTV (TWCP) localized alone to the nucleus. When coexpressed with movement proteins of ToLCNDV-OM or TYLCTHV, CBNSP and TWCP relocalized to both the nucleus and the cellular periphery and interacted with movement proteins.

Discussion: Our findings indicated that virus-virus interactions in mixed infection circumstances could complement the mechanical transmissibility of nonmechanically transmissible begomoviruses and alter their host range. These findings provide new insight into complex virus-virus interactions and will help us to understand the begomoviral distribution and to reevaluate disease management strategies in the field.

KEYWORDS

begomovirus, virus-virus interaction, movement protein, mechanical transmissibility, host range

Introduction

To study virus-host interactions, viral infections are usually conducted with the use of a single infection in the laboratory. Viral infections in nature can occur as part of mixed infections involving more than one type of virus. The results of a field survey between 2008 and 2009 in Taiwan indicated that more than 41% of virus-infected tomato were coinfected by more than two different viruses (Tsai et al., 2011). A number of important plant viral diseases are the result of the interactions of causal agents (Xu et al., 2022b). For instance, a large outbreak of maize lethal necrosis in sub-Saharan East Africa, Southeast Asia, and Southern America (Redinbaugh and Stewart, 2018) was the outcome of the coinfection between maize chlorotic mottle virus (MCMV) and one of several viruses from the *Potyviridae* family. The coinfection of viruses results in frequent maize death and negligible yields. Although important advances have been made toward understanding the biology of individual viruses, little attention has been given to the investigation of intrahost interactions during viral coinfections.

Multiple infections cause a variety of intrahost virus-virus interactions. These interactions can result in the development of novel phenomena and alter the genetic structure of viruses (Syller, 2012). A study of virus-virus interactions may be important for the understanding of viral pathogenesis and evolution and for the development of control strategies. DaPalma et al. (2010) classified potential virus-virus interactions into three categories: (1) direct interactions that occur in nucleic acids or proteins of one virus physically interacting with those of another virus, (2) environmental interactions that result from the alterations of the host environment created by coinfection, and (3) immunological interactions that are unique in organisms equipped with an adaptive immune system. Since plants do not have an immune system like that of animals, virus-virus interactions of the first two categories mentioned above can therefore be investigated in plants.

Takács et al. (2014) identified five *in planta* virus-virus interactions based on various plant responses, including cross-protection, synergistic and antagonistic interactions, recombination, heteroencapsidation, and gene silencing (Takács et al., 2014). Cross-protection, first described by McKinney (Mckinney, 1929), has been successfully applied for controlling critical viral diseases in the field (Oberemok et al., 2021; Tran et al., 2022; Xu et al., 2022a). The mechanism of cross-protection involves several phases. One mechanism of cross-protection is protein-mediated resistance through interference with the uncoating of the second challenging virus (Lu et al., 1998; Lin et al., 2007). Another mechanism involved in cross-protection is posttranscriptional gene silencing in a sequence homology-dependent manner against the second related viral strain (Ziebell and Carr, 2010; Pechinger et al., 2019). Both mechanisms illustrate direct virus-virus interactions, viral protein to viral genome interactions and viral RNA to viral RNA interactions. Environmentally indirect virus-virus interactions through the sequestration of essential host factors responsible for the propagation and movement of the challenging virus have been proposed as a possible mechanism for cross-protection (Folimonova, 2012).

Synergism is a phenomenon in which a mixed infection of two or more viruses leads to an increased accumulation of at least one virus that induces symptoms with increased severity. Mechanisms of this synergism have been proposed: viral proteins of one invading virus facilitate the movement of another coinfecting virus (Karyeija et al., 2000) or suppress plant defense against viruses (Fukuzawa et al., 2010; Redinbaugh and Stewart, 2018) through indirect virus-virus interactions. Synergistic interactions have been reported in unrelated viruses, such as those of different begomovirus species (Chakraborty et al., 2008; Alves-Júnior et al., 2009; Rentería-Canett et al., 2011; Sufrin-Ringwald and Lapidot, 2011) and of two viruses belonging to different genera of the family *Potyviridae* (Tatineni et al., 2010). Syller classified the phenomenon of antagonistic interactions into two types: superinfection exclusion (also known as cross-protection) and mutual exclusion (Syller, 2012). In the situation of mutual exclusion, two different subgroups of CMV colonized different cells in coinfected cowpea plants. The spatial separation of mutual exclusion reduces the opportunities for competition between each variant and the recombination that may generate genetic variation (Elena et al., 2011). There are two other types of direct virus-virus interactions that may change the characteristics of viruses in the field. Genetic recombination, observed in both plant RNA and DNA viruses, allows coinfecting viruses to propagate in a parasexual reproductive manner and

promotes the evolution of viruses (Sztuba-Solińska et al., 2011; Lefeuvre and Moriones, 2015). Heteroencapsidation is the encapsidation of the genome of one virus by the coat protein (CP) of another virus. The viral CP is usually involved in long-distance viral movement around infected plants and in insect vector transmission. Heteroencapsidation often occurs under mixed-infection conditions to enhance systemic movement and provide insect transmissibility to a coinfecting virus (Bourdin and Lecoq, 1991; Takács et al., 2014).

The genus *Begomovirus*, belonging to the family *Geminiviridae*, is the largest genus in the entire virosphere and contains more than 440 species (Fiallo-Olivé et al., 2021). The genome of begomoviruses is composed of one (monopartite) or two (bipartite) circular single-stranded DNA genomes: DNA-A and DNA-B. Plants can be infected with multiple begomoviruses (Nawaz-Ul-Rehman and Fauquet, 2009; Kanakala et al., 2013). A high level of mixed infection increases opportunities for *in vivo* virus-virus interactions. The commonly observed virus-virus interactions of begomoviruses are genome reassortment and recombination; as such, begomoviruses represent the largest virus group (Hanley-Bowdoin et al., 2013; García-Arenal and Zerbini, 2019). Begomoviruses are mainly transmitted in the field. Heteroencapsidation between begomoviruses was shown to influence the efficiency of whitefly transmission (Kanakala et al., 2013). However, reports about virus-virus interactions of begomoviruses, especially at the viral protein level, are limited. Therefore, interactions associated with viral protein levels warrant further investigation.

Understanding the mechanical transmissibility of a virus is crucial for the study of the spread and control of that virus. In our previous study, we reported that the determinant of mechanical transmissibility is the begomoviral movement protein (MP) (Lee et al., 2020). In this study, we tried to understand whether virus-virus interactions affect begomoviral mechanical transmissibility. Four begomoviruses, namely, two nonmechanically transmissible begomoviruses, tomato leaf curl New Delhi virus-cucumber isolate (ToLCNDV-CB) and tomato leaf curl Taiwan virus (ToLCTV), and two mechanically transmissible begomoviruses, ToLCNDV-oriental melon isolate (ToLCNDV-OM) and tomato yellow leaf curl Thailand virus (TYLCTHV), were selected for analyses. Our results showed that virus-virus interactions during viral coinfection complemented mechanical transmissibility and altered the host range of nonmechanically transmissible begomoviruses.

Materials and methods

Plant materials

The plants used in this study included *N. benthamiana*, cucumber (*Cucumis sativus* cv. MY02363), oriental melon (*Cucumis melo* var. *makuwa* cv. Silver Light), and tomato (*Solanum lycopersicum* cv. ANT22). Cucumber and oriental melon seeds were purchased from Known-You Seed Company (Kaohsiung, Taiwan). Tomato seeds were kindly provided by Dr. Wen-Shi Tsai (National Chiayi University, Chiayi, Taiwan). The resulting seedlings were transplanted into pots one week after germination. Plants that had been transplanted for one to five weeks were subjected to virus inoculation (one week for cucumber, oriental melon and tomato and five weeks for tobacco plants). The inoculated plants were maintained in a greenhouse located at the National Chung Hsing University (Taichung, Taiwan).

Agroinfiltration and virus inoculum preparation

The preparations of the infectious clones of ToLCNDV-CB, ToLCNDV-OM, ToLCTV, and TYLCTHV were carried out as described in our previous studies (Chang et al., 2010; Tsai et al., 2011; Lee et al., 2020). Agroinfiltration was conducted with a previously described method (Chang et al., 2022), with some modifications. A single colony was picked and cultured overnight at 28°C in 4 ml of lysogeny broth (LB) media supplemented with appropriate antibiotics (50 mg/ml kanamycin for infectious clones of ToLCNDV-CB DNA-A and DNA-B, TYLCTHV DNA-A and DNA-B, ToLCTV and ToLCNDV-OM DNA-B and 50 mg/ml gentamycin for ToLCNDV-OM DNA-B). One milliliter of the overnight culture was transferred into 10 ml of LB media supplemented with appropriate antibiotics plus 100 μM acetosyringone (AS) and incubated further at 28°C until the bacterial density reached an OD600 of 1.0 (Multiskan FC, Thermo Fisher Scientific, Inc., Massachusetts). The culture was centrifuged at 5,000 × *g* (Rotor JA25.5, Beckman Coulter, Inc., California) for 10 min, after which the *Agrobacterium* cells were resuspended in 20 ml of infiltration media (10 mM 2-N morpholino-ethanesulfonic acid, 10 mM MgCl2, and 100 μM AS) and then incubated at room temperature for 2 h before infiltration. Agrobacteria carrying the infectious DNA-A or DNA-B constructs were coinjected in equal amounts into leaves of *N. benthamiana*.

Viral inocula were prepared in single and mixed-infection types. Infectious clones for one virus were agroinfiltrated into *N. benthamiana* for the single virus-infecting inoculum. Infectious clones for two viruses (one of which was a mechanically transmissible virus, such as ToLCNDV-OM and TYLCTHV, and the other was a nonmechanically transmissible virus, such as ToLCNDV-CB and ToLCTV) were mixed in equal amounts for agroinfiltration as mixed-infection inocula, namely, "virus A/virus B".

Mechanical inoculation

Symptomatic leaves of agroinfiltrated *N. benthamiana* plants were collected as inocula for mechanical inoculation. The leaf samples were ground in 10 mM potassium phosphate buffer (pH 7.0) at a 1:20 ratio (weight/volume). The resultant sap was inoculated onto *N. benthamiana*, cucumber, oriental melon, and tomato plants by rubbing with carborundum powder (400-500 mesh). Afterward, the inoculated leaves were washed with

distilled water to remove the inoculation buffer and carborundum powder from the leaf surface. The inoculated plants were subsequently grown in an insect-free greenhouse. Two to four weeks after inoculation, systemic leaf samples of the mechanically inoculated plants (two weeks for tobacco, cucumber and oriental melon and four weeks for tomato) were collected for virus detection.

Mechanical inoculation involved three inoculation types. The first one was a single-virus inoculation type with inocula derived from the diseased plants infected by only one virus isolate; the plants were labeled "virus A" or "virus B". The second one was a mixed-infection inoculation type with inocula derived from the diseased plants infected by two different viruses; the plants were labeled "virus A/virus B". The third type involved two viruses coinoculated (coinoculation type) with an inoculum mixture derived from two individual diseased plants infected by different viruses; the plants inoculated in this manner were labeled "virus A +virus B".

DNA extraction

Plant total DNA was extracted following the methods of Lin et al. (2012) *via* microprep buffer containing a mixture of three kinds of buffer, namely, DNA extraction buffer [0.35 M sorbitol, 1.1 M Tris and 5 mM EDTA (pH adjusted to 7.5)], nuclei lysis buffer (1.2 M Tris, 0.05 M EDTA, 2 M NaCl and 2% CTAB), and 5% sarkosyl, at a 5:5:2 volumetric ratio. The collected leaf samples (50-100 mg per sample) were ground in 750 µl of microprep buffer. The ground sample solution was incubated at 65 °C for 30-120 min. Five hundred microliters of chloroform/isoamyl (24:1) mixture was then added to the sample solution, which was then vortexed for 0.5-1 min. The homogenized samples were then centrifuged at 12000 × *g* (Rotor F45-24-11, Centrifuge 5415D, Eppendorf, Hamburg, Germany) for 5 min. The top layer of the centrifuged suspension was pipetted (500 µl) into a new 1.5 ml Eppendorf tube. Afterward, 500 µl of isopropanol was added to the tube, after which the contents were mixed gently. The samples were pelleted by centrifugation at 12,000 × *g* (Rotor F45-24-11, Centrifuge 5415D, Eppendorf) for 5 min. The DNA pellet was subsequently washed with 70% ethanol and then dried in an oven for 1-2 min to remove ethanol. The DNA pellet was subsequently resuspended in 50 µl of sterilized distilled water and kept at -20 °C for further analysis.

PCR detection

The detection process was carried out using specific primers (Supplementary Table S1). PCR was performed in a 40 µl reaction solution consisting of 100 ng of DNA, 40 ng of each forward and reverse primer, 0.05 mM dNTP, 0.25 U of *ProTaq* Plus DNA polymerase (Protech, Taipei, Taiwan) and reaction buffer. The conditions used for amplification were as follows: one cycle at 95°C for 5 min followed by 35 cycles of 95°C for 1 min, 50°C for 1 min and 72°C for 1 min. The PCR products were analyzed *via* electrophoresis involving a 0.8% agarose gel for 30 minutes with a voltage of 120 V.

Construction of plasmid vectors, bimolecular fluorescence complementation and fluorescence resonance energy transfer analysis

Full-length begomoviral genes [the MP genes of ToLCNDV-OM and TYLCTHV, nuclear shuttle protein (NSP) gene of ToLCNDV-OM and ToLCNDV-CB, and CP gene of ToLCTV] were amplified with specific primers (Supplementary Table S1) by PCR with infectious DNA clones serving as templates. The PCR-amplified gene fragments were cloned and ligated into the Gateway entry vector pENTR/D-TOPO (Invitrogen, Thermo Fisher Scientific, Inc.) to generate pEN-OMMP, pEN-THMP, pEN-OMNSP, pEN-CBNSP, and pEN-TWCP vectors. The movement protein-coding genes of ToLCNDV-OM and TYLCTHV were then inserted into pK7WG2.0-N-YFP and pUBC-nYFP-Dest (Karimi et al., 2003) to generate pK2-YFPOMMP, pK2-YFPTHMP, pUBOMMPnYFP and pUBTHMPnYFP vectors. The NSP gene of ToLCNDV and the CP gene of ToLCTV were inserted into pK7WG2.0-N-CFP and pUBC-cYFP-Dest to generate pK2-CFPOMNSP, pK2-CFPCBNSP, pK2-CFPTWCP, pUBOMNSPcYFP, pUBCBNSPcYFP and pUBTWCPcYFP vectors. These constructs were individually transformed into the *Agrobacterium tumefaciens* strain C58 and coinfiltrated into *N. benthamiana* leaves for transient overexpression. Visualization of fluorophores and BiFC and FRET analysis were performed using an Olympus FV3000 confocal microscope (Tokyo, Japan) with different wavelength channels, namely, CFP (excitation 405 nm/emission 460-500 nm), YFP (excitation 488 nm/emission 530-630 nm), and FRET (excitation 405 nm/emission 530-630 nm), and analyzed using FV31S-SW software (Olympus).

Results

ToLCNDV-OM complemented the mechanical transmissibility of ToLCNDV-CB in *Nicotiana benthamiana*, cucumber, and oriental melon plants

ToLCNDV-OM and ToLCNDV-CB, which have different mechanical transmissibilities, are two different isolates of the same virus species. In our previous study, we documented that the mechanical transmissibility of ToLCNDV-OM and ToLCNDV-CB could be changed by the introduction of a specific amino acid mutation (Lee et al., 2020). Here, we tried to illustrate whether the mechanical transmissibility of ToLCNDV-CB can be complemented *via* coinfection with ToLCNDV-OM. Symptomatic leaves of agroinfiltrated plants were collected as inocula for mechanical inoculation of *N. benthamiana*. Severe leaf curl symptoms were observed for *N. benthamiana* mechanically inoculated with ToLCNDV-OM, ToLCNDV-OM/ToLCNDV-CB, and ToLCNDV-OM+ToLCNDV-CB at 14 dpi, while no symptoms were observed in *N. benthamiana* inoculated with ToLCNDV-CB alone (Figure 1A). The results of PCR detection with virus-specific primers showed that ToLCNDV-CB could be detected only in

10.3389/fpls.2023.1092998

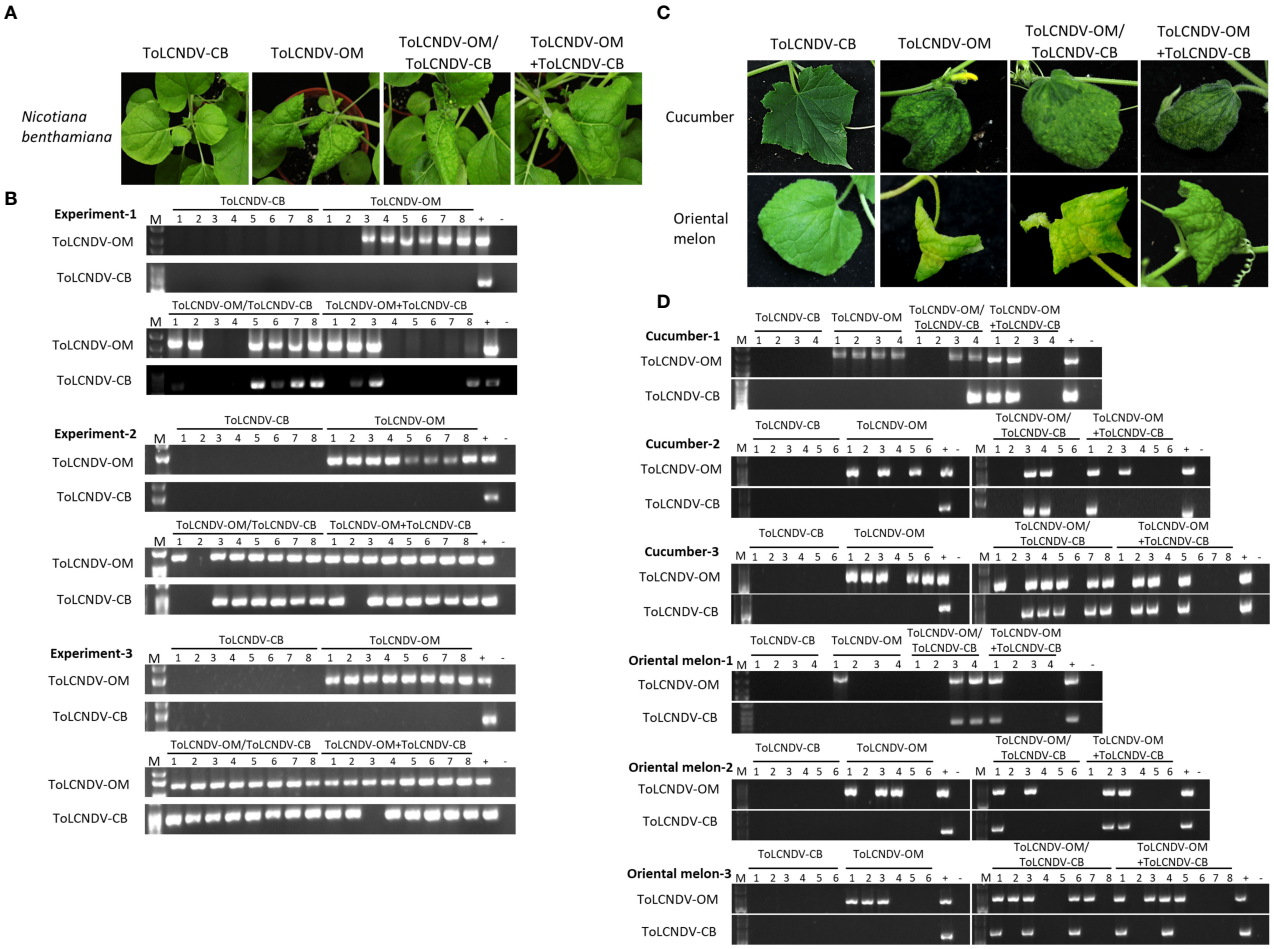

FIGURE 1
Symptom development and detection of tomato leaf curl New Delhi virus-oriental melon isolate (ToLCNDV-OM) and cucumber isolate (ToLCNDV-CB) in mechanically inoculated *Nicotiana benthamiana*, cucumber (*Cucumis sativus*) and oriental melon (*C. melo* var. *makuwa* cv. Silver Light). **(A)** Viruses in various combinations were mechanically inoculated into *N. benthamiana* plants. Severe leaf-curling symptoms were observed in the plants infected with ToLCNDV-OM, ToLCNDV-OM/ToLCNDV-CB, and ToLCNDV-OM+ToLCNDV-CB at 14 dpi. **(B)** Viruses in inoculated plants were detected *via* PCR with specific primers against DNA-B of ToLCNDV-OM and ToLCNDV-CB (Supplementary Table S1). Three biological replicates of *N. benthamiana* are individually presented. **(C)** Viruses in various combinations were mechanically inoculated into cucumber and oriental melon plants. Severe mosaic, yellowing, and leaf-curling symptoms were observed in plants infected with ToLCNDV-OM, ToLCNDV-OM/ToLCNDV-CB, and ToLCNDV-OM+ToLCNDV-CB at 14 dpi. **(D)** Viruses in inoculated plants were detected *via* PCR with specific primers against DNA-B of ToLCNDV-OM and ToLCNDV-CB (Supplementary Table S1). Three biological replicates of cucumber and oriental melon are individually presented. The positive control (+) for PCR detection is derived from plants infected with virus *via* agroinfiltration, and the negative control **(-)** is from uninoculated plants. The number indicates the number of plants used for inoculation.

plants in the presence of ToLCNDV-OM (Figure 1B). Similar results were observed across three biological replicates. In the ToLCNDV-OM/ToLCNDV-CB and ToLCNDV-OM+ToLCNDV-CB experimental sets, the prevalence of ToLCNDV-CB was as high as 85% (17/20) in plants coinfected with ToLCNDV-OM (Table 1).

To understand whether this phenomenon can also occur in cucurbit crop species, similar inoculations were performed on cucumber and oriental melon plants. Severe mosaic, yellowing, and leaf curl symptoms were observed in cucumber and oriental melon mechanically inoculated with ToLCNDV-OM, ToLCNDV-OM/ToLCNDV-CB, and ToLCNDV-OM+ToLCNDV-CB at 14 dpi, while no symptoms were observed in plants inoculated with ToLCNDV-CB alone (Figure 1C). Similar PCR results were observed, which showed that ToLCNDV-CB could be detected only in plants coinfected with ToLCNDV-OM (Figure 1B). Based on the results of the combined three replicates, infectivity of ToLCNDV-CB was as high as 80% (8/10) in cucumber and 66.7% (6/9) in oriental melon when both hosts were coinfected with ToLCNDV-OM (Table 1).

TYLCTHV complemented the mechanical transmissibility of ToLCTV in *N benthamiana* and tomato plants

To understand whether this complementation can occur between different viral species, TYLCTHV (a bipartite mechanically transmissible begomovirus) and ToLCTV (a monopartite nonmechanically transmissible begomovirus) were used for mechanical transmission analyses. Severe mosaic and leaf

10.3389/fpls.2023.1092998

TABLE 1 Mechanical inoculation of tomato leaf curl New Delhi virus-oriental melon isolate (ToLCNDV-OM) and ToLCNDV-cucumber isolate (ToLCNDV-CB) on *Nicotiana benthamiana*, cucumber (*Cucumis sativus*) and oriental melon (*C. melo* var. *makuwa* cv. Silver Light).

Detection\Inoculation†	OM	CB	OM/CB	OM+CB
N. benthamiana*				
ToLCNDV-OM	22/24 (92%)‡	0/24 (0%)	21/24 (87.5%)	20/24 (83%)
ToLCNDV-CB	0/24 (0%) [0/22]#	0/24 (0%) [0/0]	19/24 (79.2%) [19/21]	17/24 (70.8) [17/20]
Cucumber*				
ToLCNDV-OM	12/16 (75%)	0/16 (0%)	10/18 (55.6%)	7/18 (38.9%)
ToLCNDV-CB	0/16 (0%) [0/12]	0/16 (0%) [0/0]	8/18 (44.4%) [8/10]	6/18 (33.3%) [6/7]
Oriental melon*				
ToLCNDV-OM	7/16 (43.8%)	0/16 (0%)	9/18 (50%)	7/18 (38.9%)
ToLCNDV-CB	0/16 (0%) [0/7]	0/16 (0%) [0/0]	6/18 (33.3%) [6/9]	5/18 (27.8%) [5/7]

†: Mechanical inoculation was conducted using inoculum derived from N. benthamiana that was either agroinfiltrated with ToLCNDV-OM (OM), or agroinfiltrated with ToLCNDV-CB (CB), or coagroinfiltrated with ToLCNDV-OM and ToLCNDV-CB (OM/CB) or inoculum with mixed saps from individually agroinfiltrated plants (OM+CB).
‡: Results of specific PCR detection were illustrated as positive plants/total inoculated plants (% infection rate).
#: Detection results were illustrated as coinfection ratio (CB positive plants/OM infected plants).
*: The results represent the combined data of three independent experiments.

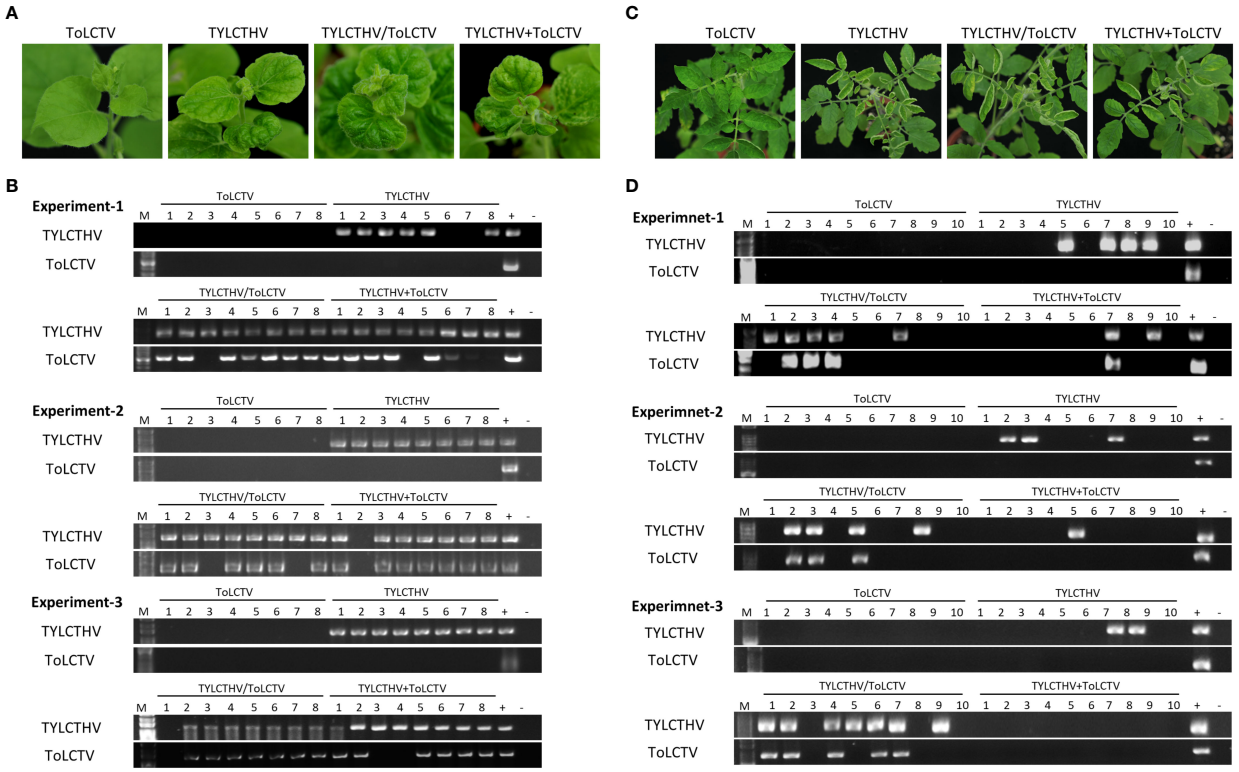

FIGURE 2
Symptom development and detection of tomato yellow leaf curl Thailand virus (TYLCTHV) and tomato leaf curl Taiwan virus (ToLCTV) in mechanically inoculated *Nicotiana benthamiana* and tomato (*Solanum lycopersicum* cv. ANT22). **(A)** Viruses in various combinations were mechanically inoculated in *N. benthamiana* plants. Severe mosaic and leaf curl symptoms were observed in plants infected with TYLCTHV, TYLCTHV/ToLCTV, and TYLCTHV+ToLCTV at 14 dpi. **(B)** Viruses in inoculated plants were detected *via* PCR with specific primers against DNA-B of TYLCTHV and DNA-A of ToLCTV (Supplementary Table S1). Three biological replicates of *N. benthamiana* are individually presented. **(C)** Viruses in various combinations were mechanically inoculated into cucumber and oriental melon plants. Severe mosaic and leaf curl symptoms were observed in plants infected with TYLCTHV, TYLCTHV/ToLCTV, and TYLCTHV+ToLCTV at 28 dpi. **(D)** Viruses in inoculated plants were detected *via* PCR with specific primers against DNA-B of TYLCTHV and DNA-A of ToLCTV (Supplementary Table S1). Three biological replicates of tomato are individually presented. The positive control (+) for PCR detection was derived from plants infected with virus *via* agroinfiltration, whereas the negative control **(-)** is from uninoculated plants. The number represents the number of plants used for inoculation.

TABLE 2 Mechanical inoculation of tomato yellow leaf curl Thailand virus (TYLCTHV) and tomato leaf curl Taiwan virus (ToLCTV) on *Nicotiana benthamiana* and tomato (*Solanum lycopersicum* cv. ANT22).

Detection\Inoculation†	TH	TW	TH/TW	TH+TW
N. benthamiana*				
TYLCTHV	22/24 (91.7%)‡	0/24 (0%)	23/24 (95.8%)	23/24 (95.8%)
ToLCTV	0/24 (0%) [0/22]#	0/24 (0%) [0/0]	20/24 (83.3%) [20/23]	20/24 (83.3%) [20/23]
Tomato*				
TYLCTHV	9/30 (30%)	0/30 (0%)	16/30 (53.3%)	3/30 (10%)
ToLCTV	0/30 (0%) [0/9]	0/30 (0%) [0/0]	11/30 (36.7%) [11/16]	1/30 (3.3%) [1/3]

†: Mechanical inoculation on N. benthamiana and tomato was conducted using inoculum derived from plants either agroinfiltrated with TYLCTHV (TH), or agroinfiltrated with ToLCTV (TW), or coagroinfiltrated with TYLCTHV and ToLCTV (TH/TW), or inoculum with mixed saps from individually agroinfiltrated plants (TH+TW).
‡: Results of specific PCR detection were illustrated as positive plants/total inoculated plants (% infection rate).
#: Detection results were illustrated as coinfection ratio (TW positive plants/TH infected plants).
*: The results represented combined data of three independent experiments.

curl symptoms were observed in *N. benthamiana* mechanically inoculated with TYLCTHV, TYLCTHV/ToLCTV, and TYLCTHV +ToLCTV at 14 dpi, whereas no symptoms developed in *N. benthamiana* inoculated with ToLCTV alone (Figure 2A). The results of PCR detection showed that ToLCTV was detected only in plants coinfected with TYLCTHV (Figure 2B). For both the TYLCTHV/ToLCTV and TYLCTHV+ToLCTV inoculation methods, the prevalence of ToLCTV was as high as 86.9% (20/23) when the plants were coinfected with TYLCTHV (Table 2). The complementation analyses were also applied to tomato plants. Severe mosaic and leaf curl symptoms were observed at 28 dpi in tomato that were mechanically inoculated with TYLCTHV, TYLCTHV/ToLCTV, and TYLCTHV+ToLCTV but not with ToLCTV alone (Figure 2C). The PCR results also corroborated that, when coinfected with TYLCTHV, ToLCTV was mechanically transmitted only at 33.3% (1/3) (Table 2).

Mechanically transmissible viruses altered the mechanical transmissibility and host range of other coinfecting viruses

ToLCNDV-OM and ToLCNDV-CB were isolated from cucurbit plants, while TYLCTHV and ToLCTV were isolated from tomato plants. The results of agroinfiltration of ToLCTV alone showed that oriental melon was not a host of ToLCTV (Figure 3A). However, when coagroinfiltrated with ToLCNDV-OM, ToLCTV could be infectious (Figures 3A, B). Based on host adaptation, a virus might alter the cellular environment by creating an optimal habitat to enable a second virus to infect a non-host plant. To understand whether an adapted virus can facilitate the infection of a nonhost virus when both are coinoculated, mixed-infection experiments were conducted.

To understand whether this type of complementation can occur between viruses adapted to different hosts, tests were conducted involving the inoculation of ToLCNDV-OM with ToLCTV or TYLCTHV with ToLCNDV-CB. ToLCNDV-OM and ToLCTV were mechanically inoculated onto *N. benthamiana* and oriental melon plants in the abovementioned combinations. The *N. benthamiana* plants inoculated with ToLCNDV-OM/ToLCTV and ToLCNDV-OM+ToLCTV presented severe leaf curling, and the oriental melon plants presented severe mosaic signs, yellowing, and leaf curling at 14 dpi, the effects of which were similar to those induced by ToLCNDV-OM alone (Figure 3C). When coinoculated with ToLCNDV-OM+ToLCTV, ToLCTV could be detected in plants coinfected with ToLCNDV-OM (Figure 3D) at 40% (2/5) in oriental melon (Table 3). These results showed that ToLCTV was mechanically transmitted with ToLCNDV-OM to a nonhost oriental melon without affecting the symptoms induced by ToLCNDV-OM alone.

N. benthamiana plants and tomato plants inoculated with TYLCTHV/ToLCNDV-CB and TYLCTHV+ToLCNDV-CB developed severe mosaic signs and leaf curling at 14 dpi and 28 dpi, respectively, the effects of which were similar to those induced by TYLCTHV alone (Figure 4A). ToLCNDV-CB could be detected in TYLCTHV/ToLCNDV-CB-inoculated *N. benthamiana* plants coinfected with TYLCTHV (Figure 4B) at 61.1% (11/18) (Table 4). This same test was also conducted by the inoculation of ToLCNDV-CB DNA-A with TYLCTHV on *N. benthamiana* and tomato. The infected plants developed symptoms similar to those of plants infected by TYLCTHV alone (Figure 4A). The PCR results showed that DNA-A of ToLCNDV-CB can be mechanically transmitted with TYLCTHV. These results showed that either DNA-A of ToLCNDV-CB alone or a complete ToLCNDV-CB could be mechanically transmitted with TYLCTHV to a nonhost tomato plants without altering symptoms induced by TYLCTHV alone.

Existing mechanically transmissible viruses allowed the mechanical infection of secondary nonmechanically transmissible viruses

Viral infection in the field does not always occur in accordance with a coinfection manner simultaneously. In the present study,

10.3389/fpls.2023.1092998

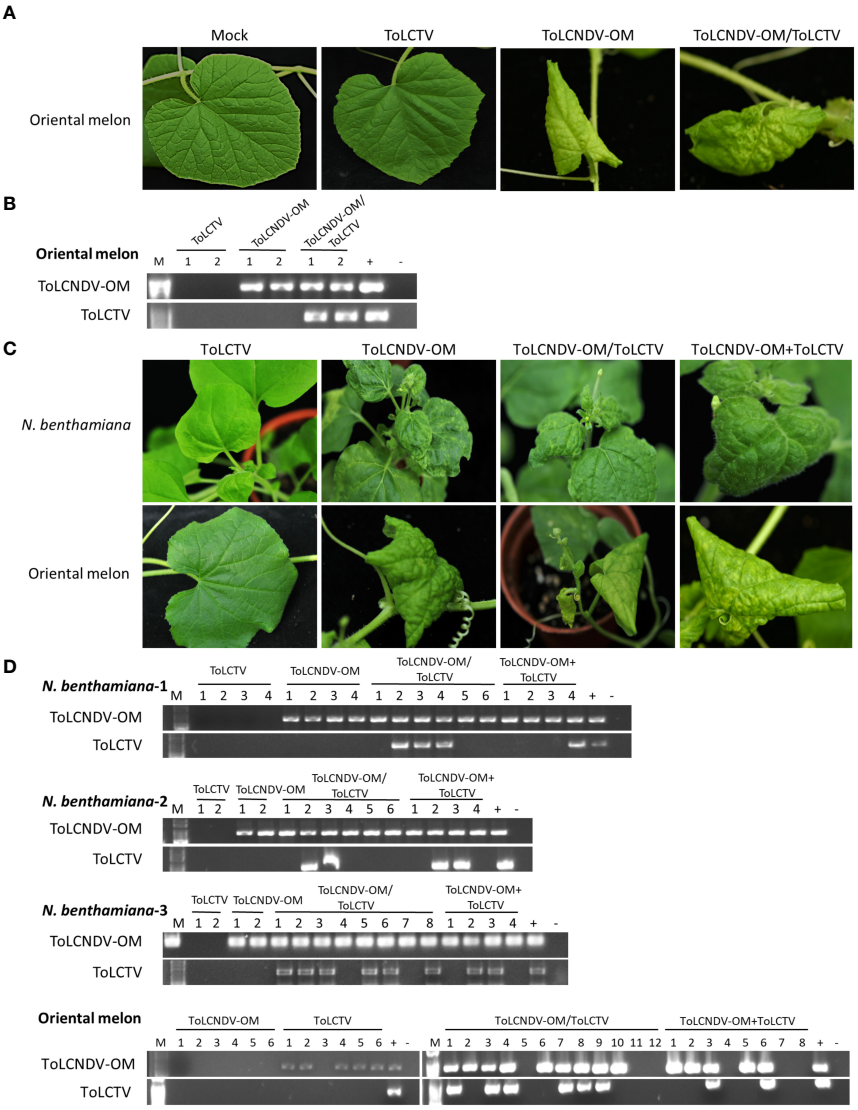

FIGURE 3
Symptom development and detection of tomato leaf curl New Delhi virus-oriental melon isolate (ToLCNDV-OM) and tomato leaf curl Taiwan virus (ToLCTV) in inoculated *Nicotiana benthamiana* and oriental melon (*C. melo* var. *makuwa* cv. Silver Light). **(A)** Viruses in various combinations were inoculated in oriental melon *via* agroinfiltration. Buffer infiltration was used as a mock control. **(B)** Viruses in agro-inoculated plants were detected *via* PCR with specific primers against DNA-B of ToLCNDV-OM and DNA-A of ToLCTV (Supplementary Table S1). **(C)** Viruses in various combinations were mechanically inoculated into *N. benthamiana* and oriental melon plants. Severe leaf curl symptoms were observed in *N. benthamiana* inoculated with ToLCNDV-OM, ToLCNDV-OM/ToLCTV and ToLCNDV-OM+ToLCTV, and severe mosaic patterns, yellowing, and leaf curling of oriental melon were observed at 14 dpi. **(D)** Viruses on inoculated plants were detected *via* PCR with specific primers against DNA-B of ToLCNDV-OM and DNA-A of ToLCTV (Supplementary Table S1). Three biological replicates of *N. benthamiana* are indicated, represented as *N. benthamiana*-1, 2, and 3. The results of the detection of all three biological replicates of oriental melon are presented together.

sequential inoculation was conducted with a mechanically transmissible virus for the first inoculation followed by another virus for the second inoculation. ToLCNDV-OM and TYLCTHV were first agroinfiltrated individually into *N. benthamiana* plants, which developed severe leaf curl symptoms two weeks later. The systemically symptomatic leaves infected with ToLCNDV-OM were then mechanically inoculated with ToLCNDV-CB, ToLCTV or TYLCTHV, while the plants infected with TYLCTHV were subsequently mechanically-inoculated with ToLCNDV-CB, ToLCTV, or ToLCNDV-OM. Two weeks later, the newest leaves from plants that received the 2nd inoculation were collected for PCR-based detection. The results of PCR detection showed that TYLCTHV could be mechanically transmitted to plants infected with ToLCNDV-OM, with a 26.9% infection rate. However, ToLCNDV-OM could not be inoculated into plants infected with TYLCTHV. ToLCNDV-CB was detected in plants infected with ToLCNDV-OM and TYLCTHV and presented 53.8% and 69.2% infection rates, respectively. ToLCTV was detected in plants infected with TYLCTHV, with a 73.1% infection rate, and in plants infected with ToLCNDV-OM, with a 15.4% infection rate (Table 5). At sampling time, the plants exhibited severe mosaic and leaf curl symptoms; however, no obvious differences in symptoms were observed after secondary inoculations of various viruses were performed.

10.3389/fpls.2023.1092998

TABLE 3 Mechanical inoculation of tomato leaf curl New Delhi virus-oriental melon isolate (ToLCNDV-OM) and tomato leaf curl Taiwan virus (ToLCTV) on *Nicotiana benthamiana* and oriental melon (*C. melo* var. *makuwa* cv. Silver Light) plants.

Detection\Inoculation[†]	OM	TW	OM/TW	OM+TW
N. benthamiana*				
ToLCNDV-OM	8/8 (100%)[‡]	0/8 (0%)	20/20 (100%)	12/12 (100%)
ToLCTV	0/8 (0%) [0/8][#]	0/8 (0%) [0/0]	11/20 (55%) [11/20]	5/12 (41.7%) [5/12]
Oriental melon*				
ToLCNDV-OM	5/6 (83.3%)	0/6 (0%)	9/12 (75%)	5/8 (62.5%)
ToLCTV	0/6 (0%) [0/5]	0/6 (0%) [0/0]	6/12 (50%) [6/9]	2/8 (25%) [2/5]

[†]: Mechanical inoculation on N. benthamiana and oriental melon was conducted using inoculum derived either from agroinfiltrated with ToLCNDV-OM (OM), or agroinfiltrated with ToLCTV (TW), or coagroinfiltrated with ToLCNDV-OM and ToLCTV (OM/TW), or inoculum with mixed saps from individually agroinfiltrated plants (OM+TW).
[‡]: Results of specific PCR detection were illustrated as positive plants/total inoculated plants (% infection rate).
[#]: Detection results were illustrated as coinfection ratio (TW positive plants/OM infected plants).
*: The results represented combined data of three independent experiments.

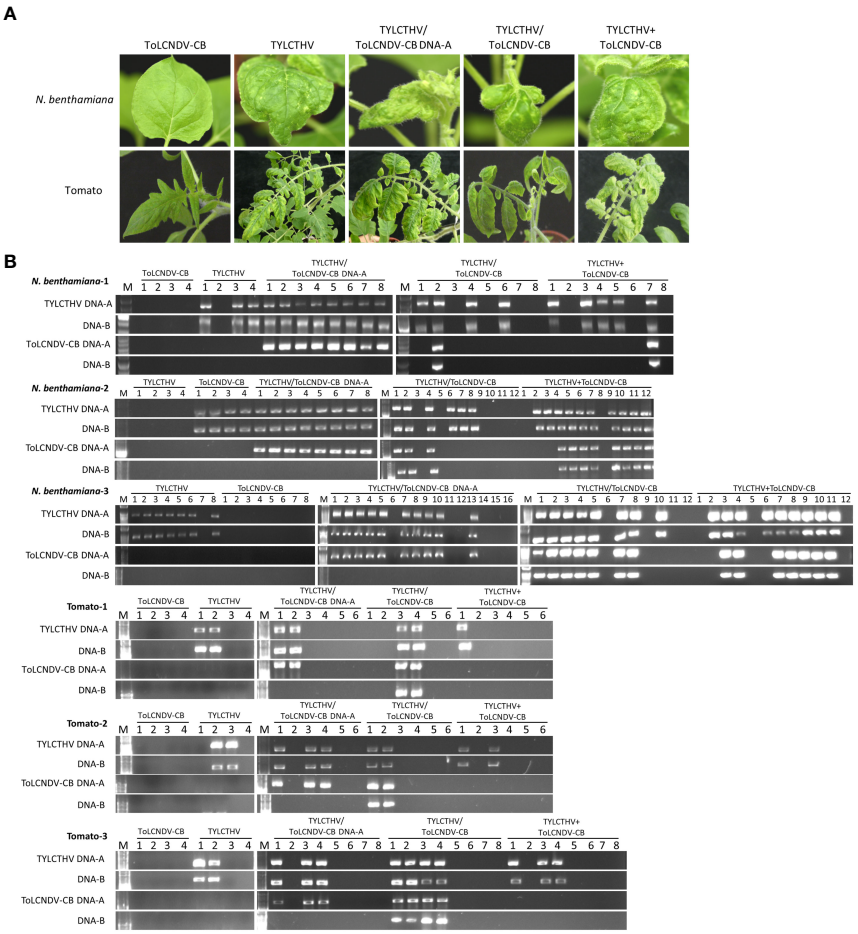

FIGURE 4
Symptom development and detection of tomato yellow leaf curl Thailand virus (TYLCTHV) and tomato leaf curl New Delhi virus-cucumber isolate (ToLCNDV-CB) on mechanically inoculated *Nicotiana benthamiana* and tomato (*Solanum lycopersicum* cv. ANT22). **(A)** Viruses in various combinations were mechanically inoculated into *N. benthamiana* and tomato plants. Severe mosaic and leaf curl symptoms were observed in *N. benthamiana* inoculated with TYLCTHV, TYLCTHV/ToLCNDV-CB, and TYLCTHV+ToLCNDV-CB at 14 dpi and in tomato at 28 dpi. **(B)** Viruses in inoculated plants were detected *via* PCR with specific primers against DNA-A and DNA-B of TYLCTHV and those of ToLCNDV-CB (Supplementary Table S1). Three biological replicates of *N. benthamiana* and tomato are individually presented.

TABLE 4 Mechanical inoculation of tomato yellow leaf curl Thailand virus (TYLCTHV) and tomato leaf curl New Delhi virus-cucumber isolate (ToLCNDV-CB) on *Nicotiana benthamiana* and tomato (*Solanum lycopersicum* cv. ANT22) plants.

Detection\Inoculation†	TH	CB	TH/CB-A	TH/CB	TH+CB
N. benthamiana*					
TYLCTHV	14/16 (87.5%)‡	0/16 (0%)	26/32 (81.25%)	18/32 (56.25%)	24/32 (75%)
ToLCNDV-CB	0/16 (0%) [0/14]#	0/16 (0%) [0/0]	26/32 (81.25%) [26/26]	11/32 (34.37%) [11/18]	16/32 (50%) [16/24]
Tomato*					
TYLCTHV	6/12 (50%)	0/12 (0%)	8/20 (40%)	8/20 (40%)	6/20 (30%)
ToLCNDV-CB	0/12 (0%) [0/6]	0/12 (0%) [0/0]	8/20 (40%) [8/8]	8/20 (40%) [8/8]	0/20 (0%) [0/6]

†: Mechanical inoculation on N. benthamiana and tomato was conducted using inoculum derived either from agroinfiltrated with TYLCTHV (TH), or agroinfiltrated with ToLCNDV-CB (CB), or coagroinfiltrated with TYLCTHV and ToLCNDV-CB DNA-A (TH/CB-A), or coagroinfiltrated with TYLCTHV and ToLCNDV-CB (TH/CB), or inoculum with mixed saps from individually agroinfiltrated plants (TH+CB).
‡: Results of specific PCR detection were illustrated as positive plants/total inoculated plants (% infection rate).
#: Detection results were illustrated as coinfection ratio (CB positive plants/TH infected plants).
*: The results represented combined data of three independent experiments.

Begomoviral MPs interacted with other viral proteins derived from different viruses

To further verify interactions between viral proteins derived from different begomoviruses, fluorescence resonance energy transfer (FRET) analyses were conducted with fusion proteins expressed in *N. benthamiana*. The yellow fluorescent protein (YFP) sequence was fused to the N-terminus of the MPs of ToLCNDV-OM (YFP-OMMP) and TYLCTHV (YFP-THMP). Yellow fluorescence (excitation 488 nm/emission 530-630 nm) emitted from the YFP-OMMP fusion protein was observed in the cells, and the fluorescence signal was evenly distributed along the periphery of the cells (Figure 5). A fluorescence signal of YFP-THMP was also observed, and the fluorescence formed spots along the periphery of the cells (Figure 5). The cyan fluorescent protein (CFP) sequence was fused to the N-terminus of the NSP-coding gene of ToLCNDV-OM (CFP-OMNSP) and ToLCNDV-CB (CFP-CBNSP) and the CP gene of ToLCTV (CFP-TWCP). Cyan fluorescence (excitation 405 nm/emission 460-500 nm) emitted from the CFP-OMNSP, CFP-CBNSP and CFP-TWCP fusion proteins was observed only in the nucleus (Figure 5). Interactions between YFP-OMMP and CFP-OMNSP were used as positive controls, while YFP-OMMP and CFP were used as negative controls. When YFP-OMMP was coexpressed with CFP-OMNSP, CFP-CBNSP or CFP-TWCP, the CFP signals were observed mainly in the nucleus, and some fluorescent signals formed continuous spots evenly displayed along the periphery of the cells (Figure 5). The FRET signals of YFP-OMMP/CFP-CBNSP and YFP-OMMP/CFP-TWCP were similar to those of the CFP signals (Figure 5). When YFP-THMP was coexpressed with CFP-CBNSP or CFP-

TABLE 5 Sequential mechanical inoculation of tomato yellow leaf curl Thailand virus (TYLCTHV), tomato leaf curl Taiwan virus (ToLCTV), tomato leaf curl New Delhi virus-cucumber isolate (ToLCNDV-CB), and oriental melon isolate (ToLCNDV-OM) on *Nicotiana benthamiana*.

1st Inoculation†	TH			OM		
2nd Inoculation‡ Detection\	OM	TW	CB	TH	TW	CB
TYLCTHV	26/26*	26/26	26/26	7/26	0/26	0/26
	(100%)	(100%)	(100%)	(26.9%)	(0%)	(0%)
ToLCNDV-OM	0/26	0/26	0/26	26/26	26/26	26/26
	(0%)	(0%)	(0%)	(100%)	(100%)	(100%)
ToLCNDV-CB	0/26	0/26	18/26	0/26	0/26	14/26
	(0%)	(0%)	(69.2%)	(0%)	(0%)	(53.8%)
ToLCTV	0/26	19/26	0/26	0/26	4/26	0/26
	(0%)	(73.1%)	(0%)	(0%)	(15.4%)	(0%)

The results are the combined data of three independent experiments.
†: 1st inoculation was conducted by agroinfiltration of TYLCTHV (TH) and ToLCNDV-OM (OM)
‡: 2nd inoculation was conducted mechanically. Mechanical inoculation on N. benthamiana was conducted using inoculum derived from either agroinfiltrated with TYLCTHV (TH), or agroinfiltrated with ToLCNDV-OM (OM), or agroinfiltrated with ToLCNDV-CB (CB), or agroinfiltrated with ToLCTV (TW). The second inoculation was conducted after plants exhibited symptoms from 1st inoculation.
*: Results of specific PCR detection were illustrated as positive plants/total inoculated plants (% infection rate).

10.3389/fpls.2023.1092998

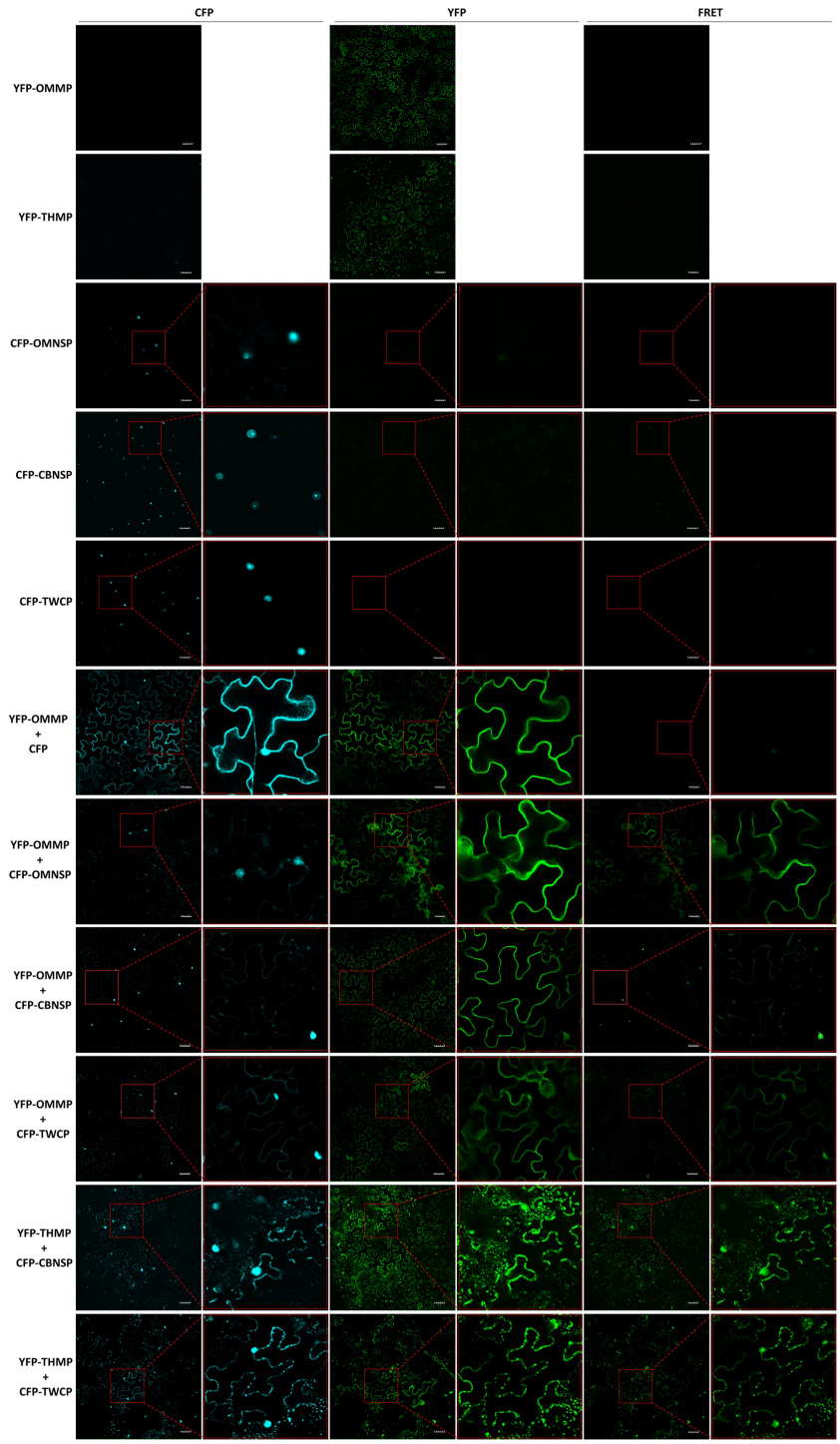

FIGURE 5
Fluorescence resonance energy transfer (FRET) analyses of *in planta* interactions between viral proteins derived from different begomoviruses. Movement protein-coding genes of tomato leaf curl New Delhi virus-oriental melon isolate (OMMP) and tomato yellow leaf curl Thailand virus (THMP) were fused to a yellow fluorescent protein (YFP) gene sequence, yielding pK2-YFPOMMP (YFP-OMMP) and pK2-YFPTHMP (YFP-THMP), respectively, and the nuclear shuttle protein-coding gene of ToLCNDV-oriental melon isolate (OMNSP) and ToLCNDV-cucumber isolate (CBNSP) and the coat protein gene of tomato leaf curl Taiwan virus (TWCP) were fused to a cyan fluorescent protein (CFP)-coding gene sequence, yielding pK2-CFPOMNSP (CFP-OMNSP), pK2-CFPCBNSP (CFP-CBNSP) and pK2-CFPTWCP (CFP-TWCP), respectively. These constructs were then expressed in leaf cells of *Nicotiana benthamiana via Agrobacterium*-mediated transformation. Agrobacteria carrying YFP-OMMP, YFP-THMP, CFP-OMNSP, CFP-CBNSP, and CFP-TWCP were infiltrated alone or coinfiltrated into *N. benthamiana* leaves. At two days post-infiltration, the leaves were collected and analyzed using an Olympus FV3000 confocal microscope at different wavelengths for detection of CFP (excitation 405 nm/emission 460-500 nm), YFP (excitation 488 nm/emission 530-630 nm), and FRET (excitation 405 nm/emission 530-630 nm). The resulting images were processed using FV31S-SW software. Scale bar = 50 μm. YFP-OMMP and CFP-OMNSP interactions (YFP-OMMP + CFP-OMNSP) were used as positive controls, and YFP-OMMP and CFP interactions (YFP-OMMP + CFP) were used as negative controls.

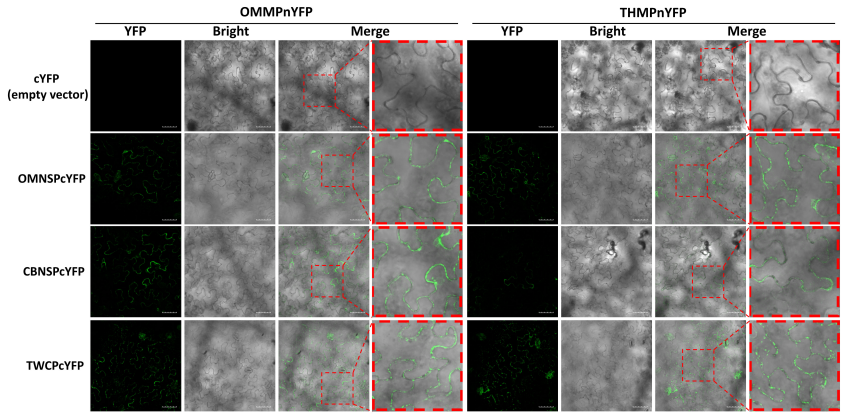

FIGURE 6
Bimolecular fluorescence complementation (BiFC) analyses of *in planta* interactions between viral proteins derived from different begomoviruses. Movement protein-coding genes of tomato leaf curl New Delhi virus-oriental melon isolate (OMMP) and tomato yellow leaf curl Thailand virus (THMP) were fused to the N half of the yellow fluorescent protein (YFP) gene sequence, yielding pUBOMMPnYFP (OMMPnYFP) and pUBTHMPnYFP (THMPnYFP), respectively. The nuclear shuttle protein-coding gene of ToLCNDV-oriental melon isolate (OMNSP) and ToLCNDV-cucumber isolate (CBNSP) and the coat protein gene of tomato leaf curl Taiwan virus (TWCP) were fused to C half of the YFP-coding gene sequence, yielding pUBOMNSPcYFP (OMNSPcYFP), pUBCBNSPcYFP (CBNSPcYFP) and pUBTWCPcYFP (TWCPcYFP), respectively. Agrobacteria carrying OMMPnYFP, THMPnYFP, OMNSPcYFP, CBNSPcYFP, and TWCPcYFP were infiltrated into *N. benthamiana* leaves. At two days post-infiltration, the leaves were collected and analyzed using an Olympus FV3000 confocal microscope for detection of YFP (excitation 488 nm/emission 530-630 nm) signal. Scale bar = 50 μm.

TWCP, the CFP signals were observed mainly in the nucleus, and some formed spots along the periphery of the cells, similar to what YFP-THMP alone did (Figure 5). The FRET signals of YFP-OMMP/CFP-CBNSP and YFP-OMMP/CFP-TWCP were similar to those of the CFP signals (Figure 5). These results showed that the locations of CBNSP and TWCP were changed by OMMP or THMP and that OMMP/THMP interacted with CBNSP and TWCP along the periphery of the cells.

The protein-protein interactions were also analyzed with BiFC. The N half of YFP sequence was fused to the C-terminus of the MPs of ToLCNDV-OM and TYLCTHV to yield OMMPnYFP and OMMPnYFP, respectively. The C half of YFP sequence was fused to the C-terminus of the NSP-coding gene of ToLCNDV-OM (OMNSPcYFP) and ToLCNDV-CB (CBNSPcYFP) and the CP gene of ToLCTV (TWCPcYFP). Interactions between OMMPnYFP and OMNSPcYFP were used as positive controls, and OMMPnYFP and cYFP empty vector (cYFP) were used as negative controls. The YFP fluorescence was observed in different combinations, OMMPnYFP/CBNSPcYFP, OMMPnYFP/TWCPcYFP, THMPnYFP/CBNSPcYFP, and THMPnYFP/TWCPcYFP, mainly along the periphery of the cells, but not in nucleus (Figure 6). Taken together, these results indicated that MPs of bipartite begomoviruses, the determinants of mechanical transmissibility, interacted with movement-related proteins of other begomoviruses.

Discussion

Infections involving a mixture of viruses can potentially trigger complex virus-virus interactions. Except for recombination, virus-virus interactions modify the characteristics of the infecting viruses, such as tissue tropism, infection and movement facilitation and insect transmissibility (Bourdin and Lecoq, 1991; Wege et al., 2001; Takács et al., 2014; Mascia and Gallitelli, 2016). Mechanical transmissibility is a critical factor for the spread of viruses in the field, which in turn makes disease management more complicated and difficult than simply controlling insect vectors alone. The mechanical transmissibility of begomoviruses is mainly determined by viral MPs (Lee et al., 2020), which always interact with viral DNA for intra- and intercellular trafficking. In this study, we found that nonmechanically transmissible begomoviruses can be complemented by a mechanically transmissible virus in a coinfection manner.

ToLCNDV-CB was mechanically transmitted to *N. benthamiana* and other crop species together with ToLCNDV-OM or TYLCTHV through coinoculation, as was ToLCTV. Based on our results, this complementation was observed in experiments involving coinoculation with both “virus A/virus B” and “virus A +virus B”. PCR detection and sequence analysis were used to confirm the presence of the infection viruses and rule out the possibility of contamination. These results corroborated that this complementation of mechanical transmissibility was not due to gene mutation or genomic recombination between the coinoculated viruses. In this study, the symptoms of the coinfected plants were not more severe than those of the single virus-infected plants (Figures 1-4). The accumulation of each virus detected by real-time PCR did not show consistent and significant changes (data not shown). These results revealed that the phenomena observed in this study were kinds of direct/indirect virus-virus interactions and not synergistic effects. Wege and Pohl (2007) reported that the DNA-B component supports the mechanical transmissibility of Abutilon mosaic virus (AbMV). Furthermore, our previous study indicated that the MP encoded in DNA-B is the key viral protein for mechanical transmissibility (Lee et al., 2020). ToLCNDV-OM and ToLCNDV-CB belong to the same virus species and have high nucleotide similarity (more than 92%) in terms of their genomic DNAs. The viral MP can recognize the genomic DNAs of both

ToLCNDV-OM and ToLCNDV-CB. ToLCTV, a monopartite begomovirus, lacks DNA-B encoding an MP and an NSP. The mechanism of mechanical transmission and the role of MPs in mechanical transmission are still unclear. However, MPs of begomoviruses were reportedly able to bind nonspecifically to both ss- and dsDNA (Rojas et al., 1998; Hehnle et al., 2004; Radhakrishnan et al., 2008). This may partly explain why ToLCTV can be mechanically transmitted with ToLCNDV-OM and TYLCTHV. Similarly, ToLCNDV-CB DNA-A alone can be complemented through mixed infection with TYLCTHV for systemic movement and mechanical transmission in *N. benthamiana* (Table 4 and Figure 4). In other words, the DNA-B of a mechanically transmissible begomovirus encodes an MP for systemic infection and mechanical transmission. This MP may also help a coinfected nonmechanically transmissible begomovirus to be mechanically transmitted through an unclear virus-virus interaction, such as MP-viral protein, MP-viral DNA or MP-host-virus interaction.

The results of sequential inoculation showed that nonmechanically transmissible ToLCNDV-CB and ToLCTV could be inoculated *via* sap into plants infected with ToLCNDV-OM or TYLCTHV. Complementation of mechanical transmissibility occurred not only in coinoculation but also in a sequential inoculation manner. It is assumed that the mechanical transmissibility of begomoviruses is not only determined by viral movement but also affected by host status. The preexisting mechanically transmissible begomovirus may switch host resistance against or a pathway allowing mechanical inoculation of other infecting begomoviruses. Further analysis is needed to accurately understand this regulation. Interestingly, TYLCTHV and ToLCNDV-OM were used as positive controls of mechanical transmission for inoculation into plants preinfected with ToLCNDV-OM and TYLCTHV. However, the results showed that ToLCNDV-OM cannot be mechanically inoculated into plants infected with TYLCTHV, whereas TYLCTHV can infect plants preinfected with ToLCNDV-OM (Table 5). Nonetheless, the competition or antagonism induced by TYLCTHV against ToLCNDV-OM warrants further study.

Based on our inoculation analyses, the "virus A+virus B" experimental set in most combinations showed lower transmission rates than did the "virus A/virus B" set. At least two likely possibilities can explain why this occurred. First, to minimize the inhibitors derived from host tissues, the inoculum was prepared such that there was an equal ratio of tissue weight/buffer volume. The "virus A+virus B" set containing tissues from two plants resulted in a lower viral titer in the inoculum solution than that in the "virus A/virus B" set. Second, the lower transmission rates may be associated with the timing of virus-virus interactions. Klinkenberg et al. (1989) reported that the time of interaction between viral DNA and protein could affect complex formation. Inoculants originating from the "virus A/virus B" plants may have already engaged in earlier interactions between viral DNAs and viral proteins, whereas those interactions may not yet definitively occur for the inoculants originating from the "virus A+virus B" set.

Nonspecific binding of CP and viral RNA resulted in heteroencapsidation that altered a nonaphid-transmissible potyvirus to become aphid transmissible, as reported by Bourdin and Lecoq (1991). In this study, we discovered the complementation of mechanical transmissibility in coinfected begomoviruses, and we also tried to determine possible mechanisms involved in this complementation. Based on the functions of begomoviral MPs, which participate in virus movement and mechanical transmissibility, we hypothesized that complementation occurred through interactions between MPs and viral DNA or viral proteins. MPs and NSPs of several begomoviruses were reportedly bound to DNA in a nonspecific manner (Pascal et al., 1994; Rojas et al., 1998; Hehnle et al., 2004). The coat protein of monopartite geminiviruses plays roles similar to those played by NSPs of bipartite begomoviruses—shuttling viral DNAs between the nucleus and cytoplasm and being involved in spreading in hosts (Rigden et al., 1993; Sanderfoot et al., 1996; Liu et al., 2001; Rojas et al., 2001). The NSP of AbMV expressed alone localizes to the nucleus, while, expressed with MP, it localizes to both the nucleus and cellular periphery (Happle et al., 2021). When the CP of tomato yellow leaf curl virus (TYLCV) is expressed alone or is coexpressed with replication-associated proteins of TYLCV in host cells, it localizes mainly to the nucleus (Kunik et al., 1998; Wang et al., 2017). Although the subcellular localization of many geminiviral proteins has been analyzed, the colocalization and interaction of viral proteins derived from different geminiviruses is still unclear. In this study, the results of FRET analyses showed that the NSP of ToLCNDV-CB and the CP of ToLCTV localized to the nucleus when expressed alone (Figure 5). Although dynamic translocation needs further analysis, these two proteins coexpressed with MPs of ToLCNDV-OM or TYLCTHV relocalized to both the nucleus and cellular periphery and interacted with MPs (Figure 5). Taken together, these results show that begomoviral proteins involved in intra- and intercellular movement can nonspecifically interact with DNAs and movement proteins of another coinfecting begomovirus, and this interaction may lead to the comovement and cotransmission of mix-infecting begomoviruses.

Méndez-Lozano et al. (2003) reported the following two phenomena observed in coinfected pepper huasteco virus and pepper golden mosaic virus: functional complementation of comovement and heterologous transactivation of CP promoters. These findings indicated that a begomovirus can complement both the gene expression and protein function of another coinfecting begomovirus. The host range of ToLCTV is reportedly limited to tomato (*Solanum* spp.), *S. melongena*, *N. benthamiana*, *Datura stramonium*, *Lonicera japonica*, *Petunia hybrida*, and *Physalis floridana* (Green et al., 1987). In our host range test involving agroinfiltration, ToLCTV did not infect oriental melon (Figures 3A, B), and ToLCNDV-CB did not infect tomato (data not shown). In this study, the results showed that, as part of a mixed infection with ToLCNDV-OM, ToLCTV infected nonhost oriental melon through agroinfiltration and mechanical inoculation (Figures 3A, C). ToLCNDV-CB was also mechanically transmitted to nonhost tomato plants with TYLCTHV (Figure 4A). The mechanically transmissible virus complemented the mechanical transmissibility and altered the host range of another coinfection virus. Alteration of the host range not only demonstrated the scenario of MP-mediated transmissibility but also illustrated how a virus replicates, expresses,

and moves in a nonhost plant. The first expressed replication-associated protein (Rep) of begomoviruses recognizes the replication origin in a virus-specific manner, and recruits the host DNA replication machinery to viral genome (Fontes et al., 1994; Fondong, 2013; Hanley-Bowdoin et al., 2013; Rizvi et al., 2015). The replication enhancer protein (REN) interacts with DNA polymerase subunits and plays an ancillary role in replication (Wu et al., 2021). An adapted begomovirus may turn on the host machinery for viral replication and benefit another coinfecting nonhost begomovirus. Transcription of begomoviral proteins relies nearly on the host machinery with a conserved RNA polymerase II system (Jeske, 2009; Hanley-Bowdoin et al., 2013). Early expressed transcriptional activator protein (TrAP) activates the transcription of CP and MP in a nonvirus-specific manner (Saunders and Stanley, 1995; Hanley-Bowdoin et al, 1999). Taking this information and the abovementioned nonspecific interactions of MP and CP for begomoviral movement and transmission together, mixed infections of begomoviruses can help each other in terms of propagation, movement, and transmission. This may explain why ToLCTV and ToLCNDV-CB infect nonhost plants in mixed-infection manners with ToLCNDV-OM and TYLCTHV. In addition, more physical interactions may also produce more virus recombinants, and more complicated virus interactions lead to more complicated epidemiology.

Based on a previous report by Tsai et al. (Tsai et al., 2011), throughout Taiwan in 2008-2009, TYLCTHV dominated the tomato planting area, with an incidence of 51%, while ToLCTV accounted for only 8%. This study demonstrated that the incidence caused by ToLCTV increased by 41% if this virus were mixed with TYLCTHV in the field (Tsai et al., 2011). Because of the use of greenhouses and insecticides in Taiwan, whitefly transmission has been reduced. Cutting, grafting, and thinning are common practices applied in the field that make mechanical transmission an even more efficient way for virus spreading. Overall, the single infection of ToLCTV that resulted in the lower distribution of the virus could well be attributed to its nonmechanical transmissibility. Once coinfection occurs, ToLCTV can be spread with TYLCTHV through mechanical transmission in the field. Indeed, most ToLCTVs were detected in coinfection samples.

In this study, we tried to analyze the complementation of mechanical transmissibility between begomovirus infection mixtures. Our results indicated that complex virus-virus interactions occurred during mixed infection and that these interactions complemented the mechanical transmissibility and altered the host range of the begomoviruses. This complementation can occur between unrelated and different species of either monopartite or bipartite begomoviruses. These findings indicated that the spread of begomoviruses *via* mechanical transmission is more likely than expected and consequently makes disease management more difficult. Complementation of mechanical transmissibility in sequential infection increased the rate of mixed infection in the field, and those complex interactions led to trait changes such as altered host range. Although our FRET and BiFC analyses revealed protein-protein interactions between different viral proteins, the virus-virus interaction leading to the alterations of mechanical transmission and host range may happen in other ways through an indirect or non-physical contact between begomoviruses. Further studies to elucidate virus-virus interactions will provide critical insights to aid in strategizing the control of viral spreading and reducing disease severity in the field.

Data availability statement

The original contributions presented in the study are included in the article/Supplementary Material. Further inquiries can be directed to the corresponding author.

Author contributions

H-HC designed the methods, performed the experiments, interpreted the data, and wrote the original draft. DG designed and performed the experiments, interpreted the data, and revised the manuscript. C-JC interpreted the data and revised the manuscript. F-JJ administered the research project, planned and designed the research, interpreted the data, and revised the manuscript. H-HC and DG contributed equally to this work. All authors contributed to the article and approved the submitted version.

Funding

This work was supported by grants from the Ministry of Science and Technology (MOST 108-2313-B-005-034-MY3 and 110-2313-B-005-012-MY3), Executive Yuan, Taiwan.

Acknowledgments

We are grateful to Dr. Kuang-Ren Chung for his critical review of this manuscript.

Conflict of interest

The authors declare that the research was conducted in the absence of any commercial or financial relationships that could be construed as a potential conflict of interest.

Publisher's note

Supplementary material

The Supplementary Material for this article can be found online at: https://www.frontiersin.org/articles/10.3389/fpls.2023.1092998/full#supplementary-material

References

Alves-Júnior, M., Alfenas-Zerbini, P., Andrade, E. C., Esposito, D. A., Silva, F. N., da Cruz, A. C. F., et al. (2009). Synergism and negative interference during co-infection of tomato and nicotiana benthamiana with two bipartite begomoviruses. *Virology* 387, 257–266. doi: 10.1016/j.virol.2009.01.046

Bourdin, D., and Lecoq, H. (1991). Evidence that heteroencapsidation between two potyviruses is involved in aphid transmission of a non-aphid-transmissible isolate from mixed infections. *Phytopathology* 81, 1459–1464. doi: 10.1094/Phyto-81-1459

Chakraborty, S., Vanitharani, R., Chattopadhyay, B., and Fauquet, C. M. (2008). Supervirulent pseudorecombination and asymmetric synergism between genomic components of two distinct species of begomovirus associated with severe tomato leaf curl disease in India. *J. Gen. Virol.* 89, 818–828. doi: 10.1099/vir.0.82873-0

Chang, H.-H., Ku, H.-M., Tsai, W.-S., Chien, R.-C., and Jan, F.-J. (2010). Identification and characterization of a mechanical transmissible begomovirus causing leaf curl on oriental melon. *Eur. J. Plant Pathol.* 127, 219–228. doi: 10.1007/s10658-010-9586-0

Chang, H.-H., Lee, C.-H., Chang, C.-J., and Jan, F.-J. (2022). FKBP-type peptidyl-propyl cis-trans isomerase interacts with the movement protein of tomato leaf curl new Delhi virus and impacts viral replication in *Nicotiana benthamiana*. *Mol. Plant Pathol.* 23, 561–575. doi: 10.1111/mpp.13181

DaPalma, T., Doonan, B. P., Trager, N. M., and Kasman, L. M. (2010). A systematic approach to virus-virus interactions. *Virus Res.* 149, 1–9. doi: 10.1016/j.virusres.2010.01.002

Elena, S. F., Bedhomme, S., Carrasco, P., Cuevas, J. M., de la Iglesia, F., Lafforgue, G., et al. (2011). The evolutionary genetics of emerging plant RNA viruses. *Mol. Plant-Microbe Interact.* 24, 287–293. doi: 10.1094/MPMI-09-10-0214

Fiallo-Olivé, E., Lett, J.-M., Martin, D. P., Roumagnac, P., Varsani, A., Zerbini, F. M., et al. (2021). ICTV virus taxonomy profile: geminiviridae 2021. *J. Gen. Virol.* 102, 001696. doi: 10.1099/jgv.0.001696

Folimonova, S. Y. (2012). Superinfection exclusion is an active virus-controlled function that requires a specific viral protein. *J. Virol.* 86, 5554–5561. doi: 10.1128/JVI.00310-12

Fondong, V. N. (2013). Geminivirus protein structure and function. *Mol. Plant Pathol.* 14, 635–649. doi: 10.1111/mpp.12032

Fontes, E. P. B., Eagle, P. A., Sipe, P. S., Luckow, V. A., and Hanley-Bowdoin, L. (1994). Interaction between a geminivirus replication protein and origin DNA is essential for viral replication. *J. Biol. Chem.* 269, 8459–8465. doi: 10.1016/S0021-9258(17)37216-2

Fukuzawa, N., Itchoda, N., Ishihara, T., Goto, K., Masuta, C., and Matsumura, T. (2010). HC-pro, a potyvirus RNA silencing suppressor, cancels cycling of cucumber mosaic virus in *Nicotiana benthamiana* plants. *Virus Genes* 40, 440–446. doi: 10.1007/s11262-010-0460-0

García-Arenal, F., and Zerbini, F. M. (2019). Life on the edge: geminiviruses at the interface between crops and wild plant hosts. *Annu. Rev. Virol.* 6, 411–433. doi: 10.1146/annurev-virology-092818-015536

Green, S. K., Sulyo, Y., and Lesemann, D. E. (1987). Outbreak and new records: leaf curl virus on tomato in Taiwan province. *FAO Plant Prot Bull.* 35, 62.

Hanley-Bowdoin, L., Bejarano, E. R., Robertson, D., and Mansoor, S. (2013). Geminiviruses: masters at redirecting and reprogramming plant processes. *Nat. Rev. Microbiol.* 11, 777–788. doi: 10.1038/nrmicro3117

Hanley-Bowdoin, L., Settlage, S. B., Orozco, B. M., Nagar, S., and Robertson, D. (1999). Geminiviruses: models for plant DNA replication, transcription, and cell cycle regulation. *Crit. Rev. Plant Sci.* 18, 71–106. doi: 10.1080/07352689991309162

Happle, A., Jeske, H., and Kleinow, T. (2021). Dynamic subcellular distribution of begomoviral nuclear shuttle and movement proteins. *Virology* 562, 158–175. doi: 10.1016/j.virol.2021.07.014

Hehnle, S., Wege, C., and Jeske, H. (2004). The interaction of DNA with the movement proteins of geminiviruses revisited. *Virology* 78, 7698–7706. doi: 10.1128/JVI.78.14.7698-7706.2004

Jeske, H. (2009). Geminiviruses. *Curr. Top. Microbiol. Immunol.* 331, 185–226. doi: 10.1007/978-3-540-70972-5_11

Kanakala, S., Jyothsna, P., Shukla, R., Tiwari, N., Veer, B. S., Swarnalatha, P., et al. (2013). Asymmetric synergism and heteroencapsidation between two bipartite begomoviruses, tomato leaf curl new Delhi virus and tomato leaf curl palampur virus. *Virus Res.* 174, 126–136. doi: 10.1016/j.virusres.2013.03.011

Karimi, M., Inzé, D., and Depicker, A. (2003). GATEWAYTM vectors for agrobacterium-mediated plant transformation. *Trends Plant Sci.* 7, 193–195. doi: 10.1016/S1360-1385(02)02251-3

Karyeija, R. F., Kreuze, J. F., Gibson, R. W., and Valkonen, J. P. T. (2000). Synergistic interactions of a potyvirus and a phloem-limited crinivirus in sweet potato plants. *Virology* 269, 26–36. doi: 10.1006/viro.1999.0169

Klinkenberg, F. A., Ellwood, S., and Stanley, J. (1989). Fate of African cassava mosaic virus coat protein deletion mutants after agroinoculation. *J. Gen. Virol.* 70, 1837–1844. doi: 10.1099/0022-1317-70-7-1837

Kunik, T., Palanichelvam, K., Czosnek, H., Citovsky, V., and Gafni, Y. (1998). Nuclear import of the capsid protein of tomato yellow leaf curl virus (TYLCV) in plant and insect cells. *Plant J.* 13, 393–399. doi: 10.1046/j.1365-313X.1998.00037.x

Lee, C.-H., Zheng, Y.-X., Chan, C.-H., Ku, H.-M., Chang, C.-J., and Jan, F.-J. (2020). A single amino acid substitution in the movement protein enables the mechanical transmission of a geminivirus. *Mol. Plant Pathol.* 21, 571–588. doi: 10.1111/mpp.12917

Lefeuvre, P., and Moriones, E. (2015). Recombination as a motor of host switches and virus emergence: geminiviruses as case studies. *Curr. Opin. Virol.* 10, 14–19. doi: 10.1016/j.coviro.2014.12.005

Lin, C.-Y., Tsai, W.-S., Ku, H.-M., and Jan, F.-J. (2012). Evaluation of DNA fragments covering the entire genome of a monopartite begomovirus for induction of viral resistance in transgenic plants *via* gene silencing. *Transgenic Res.* 21, 231–241. doi: 10.1007/s11248-011-9523-9

Lin, S.-S., Wu, H.-W., Jan, F.-J., Hou, R. F., and Yeh, S.-D. (2007). Modifications of the helper component-protease of zucchini yellow mosaic virus for generation of attenuated mutants for cross protection against severe infection. *Phytopathology* 97, 287–296. doi: 10.1094/PHYTO-97-3-0287

Liu, H., Lucy, A. P., Davies, J., and Boulton, M. I. (2001). A single amino acid change in the coat protein of maize streak virus abolishes systemic infection, but not interaction with viral DNA of movement protein. *Mol. Plant Pathol.* 2, 223–228. doi: 10.1046/j.1464-6722.2001.00068.x

Lu, B., Stubbs, G., and Culver, J. N. (1998). Coat protein interactions involved in tobacco mosaic tobamovirus cross-protection. *Virology* 248, 188–198. doi: 10.1006/viro.1998.9280

Mascia, T., and Gallitelli, D. (2016). Synergies and antagonisms in virus interactions. *Plant Sci.* 252, 176–192. doi: 10.1016/j.plantsci.2016.07.015

Mckinney, H. H. (1929). Mosaic diseases in the canary islands, West Africa and Gibraltar. *J. Agric. Res.* 39, 577–578. Available at: https://handle.nal.usda.gov/10113/IND43967734.

Méndez-Lozano, J., Torres-Pacheco, I., Fauquet, C. M., and Rivera-Bustamante, R. F. (2003). Interactions between geminiviruses in a naturally occurring mixture: pepper huasteco virus and pepper golden mosaic virus. *Phytopathology* 93, 270–277. doi: 10.1094/PHYTO.2003.93.3.270

Nawaz-Ul-Rehman, M. S., and Fauquet, C. M. (2009). Evolution of geminiviruses and their satellite. *FEBS Lett.* 583, 1825–1832. doi: 10.1016/j.febslet.2009.05.045

Oberemok, V., Laikova, K., Golovkin, I., Kryukov, L., and Kamenetsky-Goldstein, R. (2021). Biotechnology of virus eradication and plant vaccination in phytobiome context. *Plant Biol.* 24, 3–8. doi: 10.1111/plb.13338

Pascal, E., Sanderfoot, A. A., Ward, B. M., Medville, R., Turgeon, R., and Lazarowitz, S. G. (1994). The geminivirus BR1 movement protein binds single-stranded DNA and localizes to the cell nucleus. *Plant Cell* 6, 995–1006. doi: 10.1105/tpc.6.7.995

Pechinger, K., Chooi, K. M., Macdiarmid, R. M., Harper, S. J., and Ziebell, H. (2019). A new era for mild strain cross-protection. *Viruses* 11, 670. doi: 10.3390/v11070670

Radhakrishnan, G. K., Splitter, G. A., and Usha, R. (2008). DNA Recognition properties of the cell-to-cell movement protein (MP) of soybean isolate of mungbean yellow mosaic India virus (MYMIV-Sb). *Virus Res.* 131, 152–159. doi: 10.1016/j.virusres.2007.09.002

Redinbaugh, M. G., and Stewart, L. R. (2018). Maize lethal necrosis: an emerging, synergistic viral disease. *Annu. Rev. Virol.* 5, 301–322. doi: 10.1146/annurev-virology-092917-043413

Rentería-Canett, I., Xoconostle-Cázares, B., Ruiz-Medrano, R., and Rivera-Bustamante, R. F. (2011). Geminivirus mixed infection on pepper plants: synergistic interaction between PHYVV and PepGMV. *Virol. J.* 8, 104. doi: 10.1186/1743-422X-8-104

Rigden, J. E., Kdry, I. B., Mullineaux, P. M., and Rezaian, M. A. (1993). Mutagenesis of the virion-sense open reading frames of tomato leaf curl virus. *Virology* 193, 1001–1005. doi: 10.1006/viro.1993.1215

Rizvi, I., Choudhury, N. R., and Tuteja, N. (2015). Insights into the functional characteristics of geminivirus rolling-circle replication initiator protein and its interaction with host factors affecting viral DNA replication. *Arch. Virol.* 160, 375–387. doi: 10.1007/s00705-014-2297-7

Rojas, M. R., Jiang, H., Salati, R., Xoconostle-Cazares, B., Sudarshana, M. R., Lucas, W. J., et al. (2001). Functional analysis of proteins involved in movement of the monopartite begomovirus, tomato yellow leaf curl virus. *Virology* 291, 110–125. doi: 10.1006/viro.2001.1194

Rojas, M. R., Noueiry, A. O., Lucas, W. J., and Gilbertson, R. L. (1998). Bean dwarf mosaic geminivirus movement proteins recognize DNA in a form- and size-specific manner. *Cell* 95, 105–113. doi: 10.1016/S0092-8674(00)81786-9

Sanderfoot, A. A., Ingham, D. J., and Lazarowitz, S. G. (1996). A viral movement protein as a nuclear shuttle. the geminivirus BR1 movement protein contains domains essential for interaction with BL1 and nuclear localization. *Plant Physiol.* 110, 23–33. doi: 10.1104/pp.110.1.23

Saunders, K., and Stanley, J. (1995). Complementation of African cassava mosaic virus AC2 gene function in a mixed bipartite geminivirus infection. *J. Gen. Virol.* 76, 2287–2292. doi: 10.1099/0022-1317-76-9-2287

Sufrin-Ringwald, T., and Lapidot, M. (2011). Characterization of a synergistic interaction between two cucurbit-infecting begomoviruses: squash leaf curl virus and watermelon chlorotic stunt virus. *Phytopathology* 101, 281–289. doi: 10.1094/PHYTO-06-10-0159

Syller, J. (2012). Facilitative and antagonistic interactions between plant viruses in mixed infections. *Mol. Plant Pathol.* 13, 204–216. doi: 10.1111/j.1364-3703.2011.00734.x

Sztuba-Solińska, J., Urbanowicz, A., Figlerowicz, M., and Bujarski, J. J. (2011). RNA-RNA Recombination in plant virus replication and evolution. *Annu. Rev. Phytopathol.* 49, 415–443. doi: 10.1146/annurev-phyto-072910-095351

Takács, A., Gáborjányi, R., Horváth, J., and Kazinczi, G. (2014). "Virus-virus interaction," in *Plant virus-host interaction: Molecular approaches and viral evolution* eds. R. K. Gaur, T. Hohn and P. Sharma. (MA, USA: Academic Press), 385–394. doi: 10.1016/B978-0-12-411584-2.00021-4

Tatineni, S., Graybosch, R. A., Hein, G. L., Wegulo, S. N., and French, R. (2010). Wheat cultivar-specific disease synergism and alteration of virus accumulation during co-infection with wheat streak mosaic virus and triticum mosaic virus. *Phytopathology* 100, 230–238. doi: 10.1094/PHYTO-100-3-0230

Tran, T.-T.-Y., Lin, T.-T., Chang, C.-P., Chen, C.-H., Nguyen, V.-H., and Yeh, S.-D. (2022). Generation of mild recombinants of papaya ring spot virus to minimize the problem of strain-specific cross-protection. *Phytopathology* 112, 708–719. doi: 10.1094/PHYTO-06-21-0272-R

Tsai, W.-S., Shih, S.-L., Kenyon, L., Green, S. K., and Jan, F.-J. (2011). Temporal distribution and pathogenicity of the predominant tomato-infecting begomoviruses in Taiwan. *Plant Pathol.* 60, 787–799. doi: 10.1111/j.1365-3059.2011.02424.x

Wang, L., Tan, H., Wu, M., Jimenez-Gongora, T., Tan, L., and Lozano-Duran, R. (2017). Dynamic virus-dependent subnuclear localization of the capsid protein form a geminivirus. *Front. Plant Sci.* 8. doi: 10.3389/fpls.2017.02165

Wege, C., and Pohl, D. (2007). Abutilon mosaic virus DNA b component supports mechanical virus transmission, but does not counteract begomoviral phloem limitation in transgenic plants. *Virology* 36, 173–186. doi: 10.1016/j.virol.2007.03.041

Wege, C., Saunders, K., Stanley, J., and Jeske, H. (2001). Comparative analysis of tissue tropism of bipartite geminiviruses. *J. Phytopathol.* 149, 359–368. doi: 10.1046/j.1439-0434.2001.00640.x

Wu, M., Wei, H., Tan, H., Pan, S., Liu, Q., Bejarano, E. R., et al. (2021). Plant DNA polymerases α and δ mediate replication of geminiviruses. *Nat. Commun.* 12, 2780. doi: 10.1038/s41467-021-23013-2

Xu, Y., Ghanim, M., and Liu, Y. (2022b). Mixed infections of plant viruses in nature and the impact on agriculture. *Front. Microbiol.* 13, 922607. doi: 10.3389/fmicb.2022.922607

Xu, L., Zhang, W., Gao, Y., Meng, F., Nie, X., and Bai, Y. (2022a). Potato virus y strain n-wi offers cross-protection in potato against strain NTN-NW by superior competition. *Plant Dis.* 106, 1566–1572. doi: 10.1094/PDIS-11-21-2539-SC

Ziebell, H., and Carr, J. P. (2010). Cross-protection: acentury of mystery. *Adv. Virus Res.* 76, 211–264. doi: 10.1016/S0065-3527(10)76006-1

frontiers | Frontiers in Plant Science

TYPE Original Research
PUBLISHED 14 June 2023
DOI 10.3389/fpls.2023.1191029

OPEN ACCESS

EDITED BY
Zhenggang Li,
Guangdong Academy of Agricultural Sciences, China

REVIEWED BY
Muntazir Mushtaq,
Shoolini University, India
Zhiqian Pang,
University of Florida, United States

*CORRESPONDENCE
Zheng Zheng
zzheng@scau.edu.cn
Xiaoling Deng
xldeng@scau.edu.cn

†These authors have contributed equally to this work and share first authorship

RECEIVED 21 March 2023
ACCEPTED 29 May 2023
PUBLISHED 14 June 2023

CITATION
Gao C, Li C, Li Z, Liu Y, Li J, Guo J, Mao J, Fang F, Wang C, Deng X and Zheng Z (2023) Comparative transcriptome profiling of susceptible and tolerant citrus species at early and late stage of infection by "*Candidatus* Liberibacter asiaticus". *Front. Plant Sci.* 14:1191029. doi: 10.3389/fpls.2023.1191029

Comparative transcriptome profiling of susceptible and tolerant citrus species at early and late stage of infection by "*Candidatus* Liberibacter asiaticus"

Chenying Gao[1,2†], Cuixiao Li[1,2†], Ziyi Li[1,2], Yaoxin Liu[1,2,3], Jiaming Li[1,2], Jun Guo[1,2,4], Jiana Mao[1,2], Fang Fang[1,2], Cheng Wang[1,2], Xiaoling Deng[1,2*] and Zheng Zheng[1,2*]

[1]National Key Laboratory of Green Pesticide, South China Agricultural University, Guangzhou, Guangdong, China, [2]Guangdong Province Key Laboratory of Microbial Signals and Disease Control, South China Agricultural University, Guangzhou, China, [3]Horticulture Research Institute, Guangxi Academy of Agricultural Sciences, Nanning, Guangxi, China, [4]Institute of Tropical and Subtropical Cash Crops, Yunnan Academy of Agricultural Sciences, Baoshan, Yunnan, China

Citrus Huanglongbing (HLB), caused by "*Candidatus* Liberibacter asiaticus" (CLas), is the most destructive disease threatening global citrus industry. Most commercial cultivars were susceptible to HLB, although some showed tolerant to HLB phenotypically. Identifying tolerant citrus genotypes and understanding the mechanism correlated with tolerance to HLB is essential for breeding citrus variety tolerance/resistance to HLB. In this study, the graft assay with CLas-infected bud were performed in four citrus genotypes, including *Citrus reticulata* Blanco, *C. sinensis*, *C. limon*, and *C. maxima*. HLB tolerance was observed in *C. limon* and *C. maxima*, while *C. Blanco* and *C. sinensis* were susceptible to HLB. The time-course transcriptomic analysis revealed a significant variation in differentially expressed genes (DEGs) related to HLB between susceptible and tolerant cultivar group at early and late infection stage. Functional analysis of DEGs indicated that the activation of genes involved in SA-mediated defense response, PTI, cell wall associated immunity, endochitinase, phenylpropanoid and alpha-linolenic/linoleic lipid metabolism played an important in the tolerance of *C. limon* and *C. maxima* to HLB at early infection stage. In addition, the overactive plant defense combined with the stronger antibacterial activity (antibacterial secondary and lipid metabolism) and the suppression of pectinesterase were contributed to the long-term tolerance to HLB in *C. limon* and *C. maxima* at late infection stage. Particularly, the activation of ROS scavenging genes (catalases and ascorbate peroxidases) could help to reduce HLB symptoms in tolerant cultivars. In contrast, the overexpression of genes involved in oxidative burst and ethylene metabolism, as well as the late inducing of defense related genes could lead to the early HLB symptom development in susceptible cultivars at early infection stage. The weak defense response and antibacterial secondary metabolism, and the induce of pectinesterase were

responsible for sensitivity to HLB in *C. reticulata* Blanco and *C. sinensis* at late infection stage. This study provided new insights into the tolerance/sensitivity mechanism against HLB and valuable guidance for breeding of HLB-tolerant/resistant cultivars.

KEYWORDS

Huanglongbing, *Candidatus Liberibacter asiaticus*, tolerance, transcriptomics, host response

Introduction

Citrus Huanglongbing (HLB, also called citrus greening) is the most devastating disease for global citrus industry (Bové, 2006; Zheng et al., 2018). In China, HLB is caused by a phloem-limited unculturable Gram-negative alpha-proteobacteria, "*Candidatus* Liberibacter asiaticus" (CLas) (Bové, 2006). Citrus trees affected by HLB usually exhibited yellow shoots, mottling/yellowing of leaves, deformed fruit with color inversion, premature fruit abscission, aborted seeds, and ultimately the death of trees (Bové, 2006; Zheng et al., 2018). Management of HLB is difficult and expensive, particularly no cure is currently available for HLB. The recommended management practices for HLB in disease endemic regions in China mainly included the use of CLas-free nursery stocks, control of insect vectors and removal of infected trees (Zheng et al., 2018). Due to the lack of effective treatment for HLB-affected trees, the use of HLB resistant/tolerant varieties become one of the most effective approaches for the ultimate long-term HLB solution. Although most commercial citrus cultivars were susceptible to HLB (Bové, 2006), some were found to have potential tolerance to HLB (Folimonova et al., 2009). However, for breeding HLB-tolerant citrus varieties, it is essential to understand the differences in response of tolerant and susceptible citrus varieties to HLB.

To better understand the HLB tolerance mechanism in citrus, comparative transcriptomic profiling of susceptible and tolerant citrus varieties in response to CLas infection have been performed through microarray and high-through sequencing technologies (Albrecht and Bowman, 2008; Fan et al., 2012; Hu et al., 2017; Yu et al., 2017; Zou et al., 2019; Arce-Leal et al., 2020; Curtolo et al., 2020; Wei et al., 2021). Transcriptomic analysis revealed a stronger immune response in tolerant rough lemon (*Citrus jambhiri*) than in susceptible sweet orange (*Citrus sinensis*) during CLas infection (Yu et al., 2017). Genes involved in cell wall metabolism, secondary metabolism, signaling, transcription factors and redox reactions were contributed to the tolerance of Kaffir lime (*Citrus hystrix*) and Mexican lime (*Citrus aurantifolia*) to HLB (Hu et al., 2017; Arce-Leal et al., 2020). In addition, the Methyl salicylate signaling and its mediated systemic acquired resistance (SAR) response were also correlated with tolerance to HLB in sour pomelo (*Citrus grandis* Osbeck) (Zou et al., 2019). A wide-ranging transcriptomic analysis of *Poncirus trifoliata*, *Citrus sunki*, *Citrus sinensis* and three contrasting hybrids identified a specific genetic mechanism of HLB tolerance, including the downregulation of gibberellin (GA) synthesis and the induction of cell wall strengthening (Curtolo et al., 2020). A recent transcriptomic analysis showed that the HLB-tolerant Australian finger lime (*Citrus australasica*) had evolved specific redox control systems to mitigate the reactive oxygen species and modulate the plant defense response, and activated genes responsible for the production of Cys-rich secretory proteins and Pathogenesis-related 1 (PR1-like) proteins against CLas infection (Weber et al., 2022). Most recently, the anatomical study and the seasonal transcriptome profiling analysis of HLB-tolerant 'LB8-9' Sugar Belle® mandarin ("Clementine" mandarin × "Minneola" tangelo) showed that the phloem regeneration contributed to the tolerance to HLB (Deng et al., 2019; Ribeiro et al., 2023). The substantial transcriptomic studies in response to CLas infection in tolerant citrus varieties suggested that despite some cellular and defense response being common among tolerant cultivars against CLas, others responses were cultivars/genotypes-specific.

With no effective cure currently available for HLB-affected citrus trees, breeding of HLB-tolerant citrus varieties become one of promising strategies to control HLB in an effective long-term solution. Therefore, studies are still necessary to better understand the differences of host response between susceptible and tolerant citrus cultivars, which can provide useful guidance for developing HLB-resistant/-tolerant varieties in the future. In this study, we performed a greenhouse rigorous assay in four different citrus genotypes (*Citrus reticulata* Blanco, *C. Sinensis*, *C. limon*, *C. maxima*) by grafting with CLas-infected buds and comparing the disease development in four cultivars, aiming to evaluate their tolerance to HLB among four cultivars. HLB tolerance was observed in *C. limon*, and *C. maxima*, while *C. reticulata* Blanco and *C. sinensis* showed sensitive to HLB. A time-course comparative transcriptomic study was further performed in four cultivars at early and late CLas infection stage to provide a comprehensive overview of host response against CLas infection and to reveal the molecular mechanisms of tolerance/susceptibility of different citrus genotypes in response to CLas/HLB.

Materials and methods

Plant material and experimental design

Two-year-old CLas-free seedlings of four citrus cultivars, including 'Shatangju' mandarin (*Citrus reticulata* Blanco cv.

Shatangju, grafted on *Poncirus trifoliata*), 'Hongjiang' orange (*C. sinensis* cv. Hongjiang Cheng, grafted on *C. reticulata* Blanco cv. Hongju), 'Eureka' lemon (*C. limon* cv. Eureka, grafted on *Citrus jambhiri*), and 'Shatian' pomelo (*C. maxima* cv. Shatian Yu, grafted on *C. grandis*), were used as host sources for grafting with CLas-infected budwoods. All CLas-infected budwoods were collected from HLB-affected lemon trees (*Citrus limon*) located in Ruili city of Yunnan province and confirmed by CLas-specific Real-time PCR with primer set CLas4G/HLBr before using for grafting (Bao et al., 2020). For each cultivar, a total of 15 CLas-free two-year-old seedlings were grafted with CLas-infected budwoods and five others seedlings were grafted with budwood from healthy lemon plants as control (mock-grafted). After grafting, all plants were maintained in insect-proof greenhouse and fertilized as needed. The HLB symptom was recorded every four wpg. For each grafted plant, leaf samples (closed to grafting budwoods and from the new flush) were collected from each plant every 4 wpg. DNA was extracted from the leaf midribs and used for CLas quantification. For RNA-Seq analyses, six complete leaves, including three closed to grafting budwoods and three from new flush, were collected at 12 wpg and 48 wpg, respectively. Leave samples used for RNA-Seq analysis were immediately frozen with liquid nitrogen when sampling. Three biological replicates of CLas-infected citrus plants and two biological replicates of mock-grafted citrus plants were collected for RNA-Seq.

DNA and RNA extraction

For DNA extraction, 100 mg of fresh leaf midrib tissue was cut into small section and grinded with MP FastPrep®-24 Grinder (MP Biomedicals LLC, Santa Ana, CA, U.S.A.) using speed of 4 M/S for 1 min. Total DNA was extracted by using the E. Z. N. A. HP Plant DNA Kit (OMEGA Bio-Tek Co., Guangdong, China) according to the manufacturer's manual. For RNA extraction, the midribs (~250 mg) of six leaves from individual plant were dissected and mixed as one sample. Total RNA extraction was performed using E. Z. N. A. Total RNA Kit I (OMEGA Bio-Tek Co., Guangdong, China) following the manufacturer's manual. The concentration of all extracted DNA and RNA samples were tested by Qubit 2.0 (Thermo Fisher Scientific Inc., Waltham, MA, U.S.A.). The quality of RNA samples was examined by Agilent 2100 (Agilent Technologies Inc., Santa Clara, CA, U.S.A.) before sequencing.

Quantification of CLas

CLas quantification was performed by Real-time PCR with CLas-specific primer set (CLas4G: AGTCGAGCGC GTATGCGAAT/HLBr: GCGTTATCCCGTAGAAAAAGGTAG) and probe (HLBp: FAM-AGACGGGTGAGTAACGCG-BHQ) according to our previous study (Bao et al., 2020). TaqMan® quantitative Real-time PCR were performed in CFX Connect Real-Time System (Bio-Rad, Hercules, CA). PCR mixture (20 µL) contained 10 µL of PerfectStart® II Probe qPCR SuperMix (TransGen Biotech, Beijing), 1 µL of DNA template (~25 ng), 0.4 µL of each forward and reverse primer (10 µM), 0.2 µL of PCR Probe (10 µM) and 8 µL of ddH2O. The procedure of PCR included incubation at 95°C for 2 min followed by 40 cycles of amplification (95°C for 10 s and 58°C for 30 s, with fluorescence signal capture at the end of each 58°C step). PCR result (Ct value) was obtained by using Bio-Rad CFX Manager 2.1 software with automated baseline settings and threshold. DNA Sample with Ct value less than 34 was considered as CLas positive.

RNA sequencing and transcriptomic analysis

The library preparation for RNA-Seq was constructed with a NEBNext® Ultra™ RNA Library Prep Kit for Illumina (New England Biolabs, Ipswich, MA, USA). The high-throughput sequencing was performed on an Illumina HiSeq 3000 system with output of 150-bp paired-end reads by the Novogene Company (Beijing, China). All clean HiSeq data from each sample were mapped to *Citrus sinensis* reference genome (GCA_022201045.1) (Wang et al., 2021) by using Tophat2 with the mismatch penalty of no more than two nucleotides (Kim et al., 2013). Reads number mapped to each gene was counted by using HTSeq v0.61 (Anders et al., 2015) and RPKM (Reads Per Kilobase of exon model per Million mapped reads) was calculated based on the length of the gene and reads count mapped to this gene. Differentially expressed genes (DEGs) between CLas-infected sample and mock-grafted control sample were identified by DEGseq (Wang et al., 2010) with the cut-off values setting as Log2 Fold change $\geq |1|$ and q-value < 0.005. Gene Ontology (GO) enrichment analysis of all satisfied DEGs was implemented by the GOseq R package (Young et al., 2010). GO terms with corrected P-value less than 0.05 were considered significantly enriched by differential expressed genes. The statistical enrichment of differential expression genes in KEGG pathways was performed by using KOBAS 2.0 (Xie et al., 2011).

Gene expression validation

To validate result of DEGs identified from RNA-Seq analyses, a total of 15 DEGs involved in cell wall metabolism, secondary metabolism, hormone-related pathways, lipid metabolism, plant-pathogen interaction and antioxidant activity were selected for reverse transcription (RT) qPCR analysis. All primer sets were listed in Supplementary Table S12. The same set of RNA samples used for RNA-Seq analyses were used for RT-qPCR. The first strand cDNA was synthesized using TransScript® One-Step gDNA Removal and cDNA Synthesis SuperMix (TransGen Biotech, Beijing) according to the manufacture's protocol. The RT-qPCR was performed in CFX Connect Real-Time System (Bio-Rad, Hercules, CA). PCR mixture (20 µL) contained 10 µL of TransStart® Green qPCR SuperMix (TransGen Biotech, Beijing), 1 µL of cDNA template, 0.4 µL of each forward and reverse primer (10 µM) and 8 µL of ddH_2O. The procedure of PCR included incubation at 95°C for 30 s followed by 40 cycles of amplification

(95°C for 10 s and 60°C for 30 s, with fluorescence signal capture at the end of each 60°C step). The *Glyceraldehyde-3-phosphate dehydrogenase* (*GAPDH*) gene was selected as the internal reference control. The relative expression levels of selected genes were calculated by $2^{-\Delta\Delta Ct}$ method (Livak and Schmittgen, 2001). For each sample, the Log_2 fold change was obtained from the ratio of the relative expression value of CLas-infected plant vs. mock-grafted control. For each gene, the Log_2 fold change of RT-PCR was compared with the RNA-Seq analyses from the same sample (Supplementary Figure S1).

Results

Symptom development and bacterial quantification analysis of citrus plants after inoculation with CLas

qPCR result showed that CLas was first detected in four cultivars at 12 weeks post-grafting (wpg) (Figure 1), including six 'Shatangju' mandarin (40%), seven 'Hongjiang' orange (46.7%), four 'Eureka' lemon (26.7%) and eight 'Shatian' pomelo (53.3%). However, except one 'Shatangju' mandarin plant and one 'Hongjiang' orange plant showed early HLB symptoms (i.e. slight leaf yellowing) in new flush, others CLas-infected citrus plants were asymptomatic and phenotypically similar to the mock-grafted citrus plants at 12 wpg (Figure 1). All plants of four cultivars grafted with CLas-infected buds were confirmed to be CLas-positive at 20 wpg (Table 1). The typical HLB symptoms (i.e. blotchy mottling and yellowing of leaves) gradually exhibited in CLas-infected 'Shatangju' mandarin and 'Hongjiang' orange plants after 20 wpg. All infected 'Shatangju' mandarin plants and 'Hongjiang' orange plants showed HLB symptoms (yellowing/mottling leaf) at 32 and 36 wpg, respectively (Table 1). However, only four CLas-infected 'Shatian' pomelo plants and three 'Eureka' lemon plants showed leaf yellowing or zinc deficiency-like symptoms by the end of the study (48 wpg), although all 'Eureka' lemon and 'Shatian' pomelo plants had been identified as CLas-positive at 20 wpg (Table 1).

Quantification result showed a similar proliferation pattern of CLas among four cultivars, i.e. the CLas concentration initially increased, then slightly decreased and maintained at a certain level in grafted citrus plants (Table 1). However, the concentration of CLas in infected 'Shatangju' mandarin and 'Hongjiang' orange was higher (with lower Ct value) than those observed in 'Eureka' lemon and 'Shatian' pomelo at same infection stage after 20 wpg until to 48 wpg (Table 1). Considering the symptom development and CLas concentration in four cultivars, the 'Shatangju' mandarin and 'Hongjiang' orange were relatively sensitive to HLB, while the 'Eureka' lemon and 'Shatian' pomelo were more tolerance to HLB. To further analyze the host response of CLas infection between sensitive and tolerant citrus cultivars at different disease development stage, the CLas-infected leaf samples of four cultivars were collected at 12 wpg (early infection stage, mostly asymptomatic) and 48 wpg (late infection stage, mostly symptomatic) and used for RNA-Seq analyses (Figure 1). As control, the leaf samples from mock-grafted citrus plants at 12 wpg and 48 wpg were also selected (Supplementary Figure S2).

Identification of differentially expressed genes

A total of 40 libraries were constructed and sequenced. The Illumina HiSeq platform generated a sequencing depth of 40~55 million 150 paired-end reads per library (Q30 > 93) (Supplementary Table S1). The biological replicates were highly correlated, with

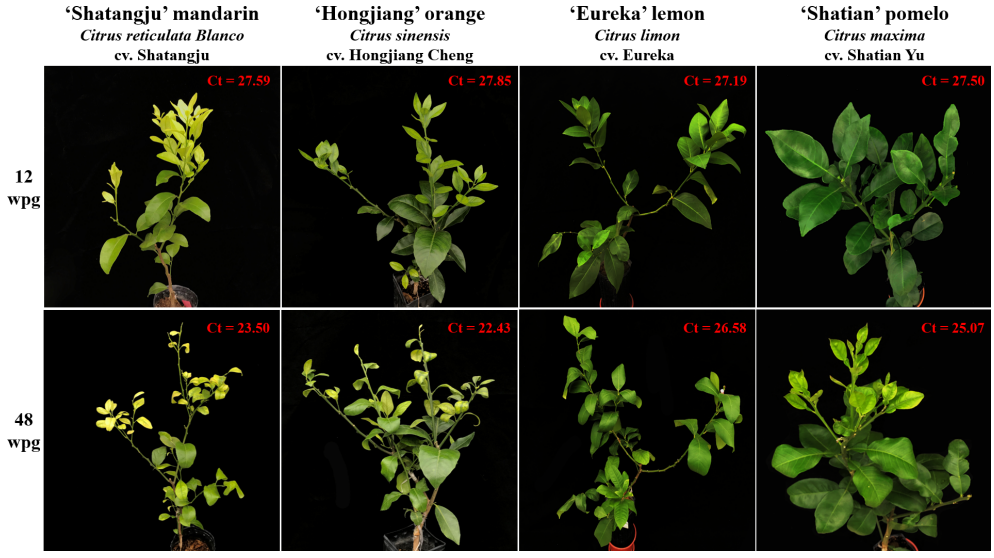

FIGURE 1
The representative infected plants of four citrus cultivars selected for RNA-Seq analysis after 12 and 48 weeks post-grafting (wpg). The Ct value was obtained with primer-probe set CLas4G/HLBp/HLBr.

10.3389/fpls.2023.1191029

TABLE 1 *"Candidatus* Liberibacter asiaticus" detection result and Huanglongbing symptoms record of grafted citrus plants.

Cultivars	Detection result and symptoms record*	4 wpg	8 wpg	12 wpg	16 wpg	20 wpg	24 wpg	28 wpg	32 wpg	36 wpg	40 wpg	44 wpg	48 wpg
Citrus reticulata Blanco cv. Shatangju	Positive plants/Total plants	0/15	0/15	6/15	15/15	15/15	15/15	15/15	15/15	15/15	15/15	15/15	15/15
	Ct value	NA	NA	28.09	25.33	23.23	23.38	24.77	25.04	26.45	25.7	26.01	24.53
	Symptomic plants/Total plants	AS	AS	S (1/15)	S (3/15)	S (6/15)	S (9/15)	S (11/15)	S (14/15)	S (15/15)	S (15/15)	S (15/15)	S (15/15)
Citrus sinensis cv. Hongjiang Cheng	Positive plants/Total plants	0/15	0/15	7/15	14/15	15/15	15/15	15/15	15/15	15/15	15/15	15/15	15/15
	Ct value	NA	NA	27.53	25.35	21.37	20.56	24.2	25.71	26.31	25.92	24.55	24.76
	Symptomic plants/Total plants	AS	AS	S (1/15)	S (2/15)	S (5/15)	S (9/15)	S (12/15)	S (15/15)	S (15/15)	S (15/15)	S (15/15)	S (15/15)
Citrus limon cv. Eureka	Positive plants/Total plants	0/15	0/15	4/15	11/15	15/15	15/15	15/15	15/15	15/15	15/15	15/15	15/15
	Ct value	NA	NA	26.34	25.2	25.59	25.16	25.6	28.03	28.13	29.12	27.93	28.45
	Symptomic plants/Total plants	AS	AS	AS	AS	S (2/15)	S (2/15)	S (3/15)	S (3/15)	S (3/15)	S (3/15)	S (4/15)	S (4/15)
Citrus maxima cv. Shatian Yu	Positive plants/Total plants	0/15	0/15	8/15	10/15	15/15	15/15	15/15	15/15	15/15	15/15	15/15	15/15
	Ct value	NA	NA	28.12	28.07	25.22	28.79	26.64	27.37	27.4	26.47	27.27	26.43
	Symptomic plants/Total plants	AS	AS	AS	AS	AS	AS	AS	S (1/15)	S (1/15)	S (1/15)	S (2/15)	S (3/15)

*Ct values = the average Ct value of all CLas-positive plant. NA, No amplification; AS, Asymptomatic; S, Symptomatic. The number of HLB symptomatic plants are listed in the bracket. Leaf midribs sample collected at 12 wpg and 48 wpg were used for RNA-Seq.

thePearson's correlation coefficient over 0.985 (Supplementary Table S2). Reference-based mapping to *Citrus sinensis* genome (GCA_022201045.1) showed that the ratio of mapped reads ranged from 88.17% to 93.47% for each HiSeq data (Supplementary Table S2). Overall, differential expression analysis identified a higher number of DEGs in late infection stage (48wpg) than those identified at early infection stage (12 wpg) in four cultivars when compared to the mock-grafted control (Figure 2). Notably, the DEGs number of 'Shatian' pomelo identified at 48 wpg was higher than those observed in other cultivars at 48 wpg (Figure 2). It was also found that two tolerant cultivars had more common DEGs than those identified in two susceptible cultivars at two infection stages (Figure 3). At 12 wpg, a total of 148 DEGs were commonly identified in susceptible 'Shatangju' mandarin and 'Hongjiang' orange and 212 DEGs were shared between tolerant 'Eureka' lemon and 'Shatian' pomelo (Figure 3A). A total of 145 common DEGs were identified between susceptible 'Shatangju' mandarin and 'Hongjiang' orange at late infection stage in compared to that of 393 common DEGs identified between tolerant 'Eureka' lemon and 'Shatian' pomelo (Figure 3B).

Gene ontology and KEGG enrichment analysis of DEGs

GO assignments of DEGs identified a total of 19 and 29 significant enriched GO terms in susceptible 'Shatangju' mandarin and 'Hongjiang' orange at 12 wpg, respectively, while an increased number of significant enriched GO terms in tolerant 'Eureka' lemon and 'Shatian' pomelo was found to be 75 and 79 at

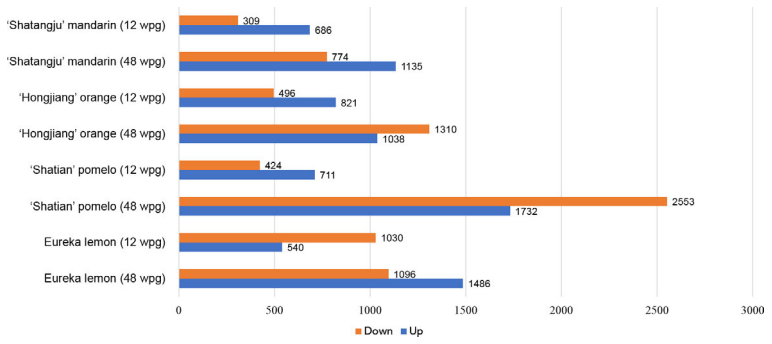

FIGURE 2
Statistic chart of differentially expressed genes (DEGs) of four citrus cultivars in response to "*Candidatus* Liberibacter asiaticus" infection at early (12 wpg) and late infection stage (48 wpg).

10.3389/fpls.2023.1191029

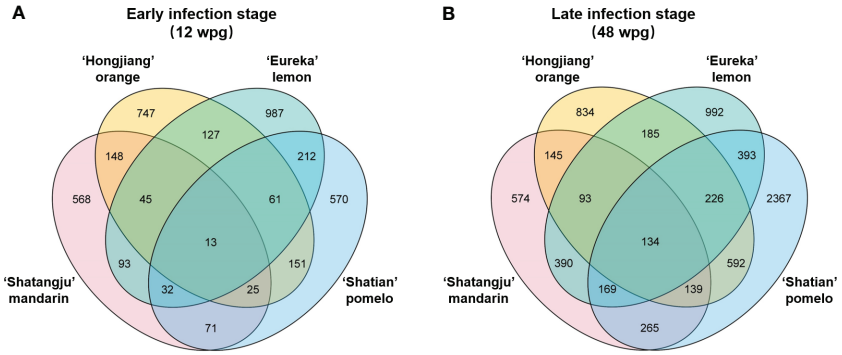

FIGURE 3
Venn diagram of differentially expressed genes (DEGs) among four cultivars in response to "*Candidatus* Liberibacter asiaticus" infection at early **(A)** and late infection stage **(B)**.

12 wpg, respectively (Supplementary Table S3). Thirty-eight significant enriched GO terms were commonly identified in 'Eureka' lemon and 'Shatian' pomelo at 12 wpg, mainly including hydrolase activity, response to stress, pyrophosphatase activity, nucleoside-triphosphatase activity, molecular function regulator, cell wall organization or biogenesis (Supplementary Figure S3, Supplementary TableS4). At 48 wpg, a total of 23, 64, 30, 47 significant enriched GO terms were identified in 'Shatangju' mandarin, 'Hongjiang' orange, 'Eureka' lemon and 'Shatian' pomelo, respectively (Supplementary Table S3). Five common significant enriched GO terms, including O-methyltransferase activity, cellular carbohydrate metabolic process, apoplast, extracellular region, and xyloglucan:xyloglucosyl transferase activity, were found in 'Shatangju' mandarin and 'Hongjiang' orange, while three significant enriched GO terms (transferring acyl groups, transferring acyl groups other than amino-acyl groups, terpene synthase activity) were commonly identified in 'Eureka' lemon and 'Shatian' pomelo at 48 wpg (Supplementary Figure S3, Supplementary Table S3).

KEGG pathways enrichment of DEGs showed that the MAPK signaling pathway, phenylpropanoid biosynthesis, plant hormone signal transduction, starch and sucrose metabolism, plant-pathogen interaction, amino sugar and nucleotide sugar metabolism, cysteine and methionine metabolism were mainly altered in four cultivars at two infection stages (Supplementary Table S5). More significant pathways were identified in four cultivars at 48 wpg than those observed at 12 wpg (Supplementary Table S5). The plant-pathogen interaction pathway and sesquiterpenoid and triterpenoid biosynthesis pathway were only significantly enriched in tolerant 'Eureka' lemon and 'Shatian' pomelo at 48 wpg (Supplementary Table S5). Especially, more DEGs were upregulated on the plant-pathogen interaction pathway in 'Eureka' lemon and 'Shatian' pomelo at 48 wpg (Supplementary TableS5). To further identify the DEGs that related to susceptibility and tolerance of citrus in response to HLB, the categories of DEGs related to disease response in susceptible cultivars group ('Shatangju' mandarin and 'Hongjiang' orange) and tolerant cultivars group ('Eureka' lemon and 'Shatian' pomelo) at early (12 wpg) and late (48 wpg) CLas infection stage were described in detail in the following section.

Cell wall metabolism

A total of 55 DEGs involved in cell wall metabolism were identified in four cultivars at two disease development stages (Figure 4, Supplementary Table S6). Overall, more upregulated genes involved in cell wall biogenesis, cell wall modification and organization were identified at 12 wpg than that those observed at 48 wpg in four cultivars (Figure 4). Particularly, 19 out of 23 DEGs were significantly upregulated in 'Shatian' pomelo at 12 wpg (Supplementary Table S6). At 12 wpg, five DEGs encoding endochitinase (102627878, 107175343, 102629565, 102628172, 112495475) were significantly upregulated in 'Eureka' lemon and 'Shatian' pomelo, while most of these genes were not significantly expressed in susceptible 'Shatangju' mandarin and 'Hongjiang' orange (Figure 4, Supplementary Table S6). In contrast, three DEGs encoding pectinesterase (102626812, 102626135, 102611144), two DEGs encoding COBRA-like protein (102628939, 102630593), and two DEGs encoding xyloglucan endotransglucosylase/hydrolase (XTH) (102609979, 102627641) were significantly downregulated in either 'Eureka' lemon or 'Shatian' pomelo, or both at 48 wpg (Figure 4, Supplementary Table S6). It was also found that genes encoded chitinase/endochitinase (102626061, 102606732, 107174675, 102629565, 107175343), pectinesterase (102610266, 102577945), XTH (102627064), COBRA-like protein (102610075) were either upregulated in 'Shatangju' mandarin or 'Hongjiang' orange at 48 wpg, whereas no significant difference of these genes was observed in tolerant 'Eureka' lemon and 'Shatian' pomelo (Figure 4, Supplementary Table S6).

Secondary metabolism

267 DEGs involved in several biological processes of secondary metabolism were identified in four cultivars at two CLas infection stages, mainly including the phenylpropanoid biosynthesis, flavonoids biosynthesis and sesquiterpenoid and triterpenoid biosynthesis. Among these processes, the phenylpropanoid biosynthesis were most enriched in four cultivars at both 12 wpg

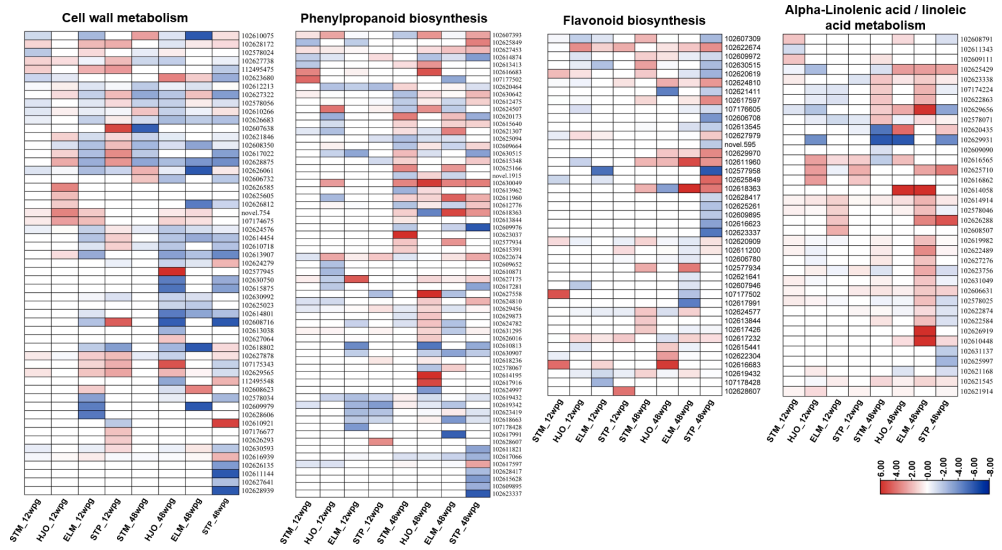

FIGURE 4
Heatmaps of differentially expressed genes (DEGs) involved in cell wall metabolism, phenylpropanoid biosynthesis, flavonoid biosynthesis and alpha-Linolenic acid/linoleic acid metabolism. STM, 'Shatangju' mandarin; HJO, 'Hongjiang' orange; ELM, 'Eureka' lemon; STP, 'Shatian' pomelo.

and 48 wpg (Supplementary Table S5), while the flavonoids biosynthesis and sesquiterpenoid and triterpenoid biosynthesis were only enriched in 'Eureka' lemon and 'Shatian' pomelo at 48 wpg (Supplementary Table S5). A higher number of upregulated DEGs involved in the phenylpropanoid biosynthesis and flavonoids biosynthesis were observed at 48 wpg compared to those identified in four cultivars at 12 wpg (Figure 4, Supplementary Table S5). Especially, a burst of upregulated DEGs involved in phenylpropanoid biosynthesis was identified in 'Eureka' lemon at 48 wpg compared to 12 wpg (Figure 4, Supplementary Table S5). Several key genes involved in biosynthesis of phenylpropanoid and flavonoids were only highly induced in either 'Eureka' lemon or 'Shatian' pomelo, or both at 48 wpg, whereas the expression of these genes was not in high level or downregulated in susceptible 'Shatangju' mandarin and 'Hongjiang' orange (Figure 4, Supplementary Table S7). These DEGs included three *shikimate O-hydroxycinnamoyl transferase* (102618363, 102624810, 102617597), two *caffeoyl-CoA O-methyltransferase* (102622674, 102627979), four *caffeic acid 3-O-methyltransferase* (102630642, 102621307, 102625166, 102612776), two *vinorine synthase-like* (102625849, 102611960) and one *flavonol synthase* (102629970) (Figure 4, Supplementary Table S7).

Lipid metabolism

Several pathways involved in lipid metabolism, mainly including alpha-linolenic acid metabolism, linoleic acid metabolism, and cutin, suberine and wax biosynthesis, were significantly enriched in four cultivars at two stages (Supplementary TableS5). Most of DEGs involved in alpha-linolenic acid metabolism and linoleic acid metabolism were upregulated in 'Eureka' lemon and 'Shatian' pomelo at both 12 wpg and 48 wpg (Figure 4). Particularly, all DEGs involved in alpha-linolenic acid and linoleic acid metabolism were upregulated in 'Eureka' lemon at 48 wpg (Figure 4, Supplementary Table S8), indicating a strong activation of alpha-linolenic and linoleic acid metabolism in 'Eureka' lemon in response to CLas infection at 48 wpg. It was found that four DEGs involved in alpha-linolenic and linoleic acid metabolism, including two *linoleate 13S-lipoxygenase* (102625710 and 102626288), one *4-coumarate-CoA ligase* (102606631) and one *alpha-dioxygenase* (102610448) were only significantly upregulated in both 'Eureka' lemon and 'Shatian' pomelo at 48 wpg (Figure 4, Supplementary Table S8).

Hormone-related pathways

A total of 80 DEGs were enriched in several hormone-related pathways, including ethylene (ET), abscisic acid (ABA), auxin (AUX) and gibberellin (GA), jasmonic acid (JA) and salicylic acid (SA) (Supplementary Table S9). Overall, more DEGs related to hormone pathways were identified in four cultivars at 48 wpg than those observed at 12 wpg (Figure 5). The ethylene metabolism was induced in 'Shatangju' mandarin at 12 wpg (Figure 5, Supplementary Table S9). Particularly, five DEGs involved in ethylene metabolism was only induced in 'Shatangju' mandarin at 12 wpg, including two ethylene-responsive transcription factor 1B (102611538, 102618338), one EIN3-binding F-box (102607641), one ethylene response 2 (102578028) and one ethylene response sensor (102577971) (Figure 5, Supplementary Table S9). In addition, three salicylic acid-binding protein 2 (SABP2) (102613996, 102612910, 102613503) were highly upregulated in 'Shatian' pomelo at 12 wpg (Figure 5, Supplementary Table S9), indicating SA pathway was strongly induced in 'Shatian' pomelo in response to CLas at early infection stage. In contrast, the auxin metabolism pathway was repressed at 48 wpg in four cultivars with most of DEGs related to auxin metabolism were downregulated

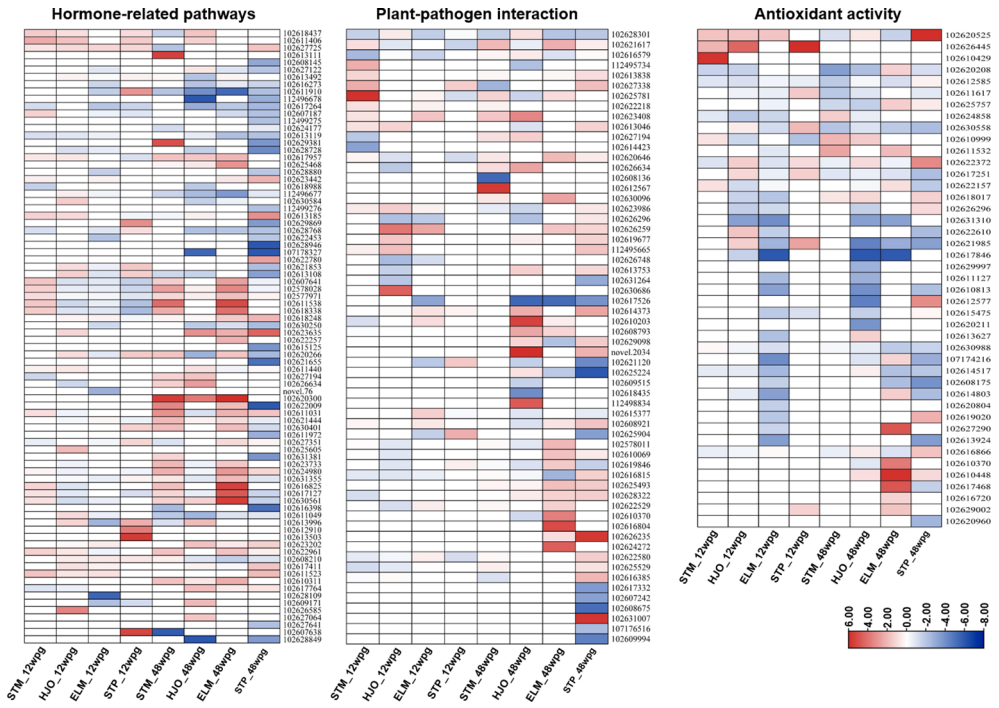

FIGURE 5
Heatmaps of differentially expressed genes (DEGs) involved in hormone-related pathways, plant-pathogen interaction and antioxidant activity. STM, 'Shatangju' mandarin; HJO, 'Hongjiang' orange; ELM, 'Eureka' lemon; STP, 'Shatian' pomelo.

(Supplementary Table S9). Particularly, for a total of 26 genes involved in auxin metabolism, 22 were repressed in 'Shatian' pomelo at 48 wpg (Figure 5, Supplementary Table S9). One auxin-induced protein AUX22-like (102607187) and one auxin-responsive protein IAA14 (102613119) were only downregulated in 'Eureka' lemon and 'Shatian' pomelo at 48 wpg (Supplementary Table S9). In addition, a gibberellin receptor GID1B, an important nuclear receptor for gibberellin signal transduction, was only upregulated in 'Eureka' lemon and 'Shatian' pomelo at 48 wpg (Supplementary Table S9).

Plant-pathogen interaction

A total of 63 DEGs involved in the plant-pathogen interaction were identified in response to CLas infection in four cultivars at 12 wpg and 48 wpg (Figure 5, Supplementary Table S10). Overall, most of DEGs related to plant-pathogen interaction in four cultivars were upregulated at both 12 wpg and 48 wpg (Figure 5, Supplementary Table S10). At 12 wpg, a slightly increased number of upregulated genes related to plant-pathogen interaction were identified in susceptible 'Shatangju' mandarin and 'Hongjiang' orange compared to tolerant 'Eureka' lemon and 'Shatian' pomelo (Figure 5, Supplementary Table S10). These upregulated DEGs in 'Shatangju' mandarin or 'Hongjiang' orange at 12 wpg mainly involved in cyclic nucleotide-gated ion channels (CNGCs) and cytosolic Ca^{2+} elevation, including six *cyclic nucleotide-gated ion channels* (CNGCs) (102625781, 102627338, 102626259, 112495665, 102619677, 102623986) and one *calcium-binding protein CML39-like* (102613838) (Figure 5, Supplementary Table S10). It was also found that three genes involved in CNGCs (102627338, 102626259, 102621120) were upregulated in either 'Shatian' pomelo or 'Eureka' lemon (Figure 5, Supplementary Table S10). In contrast, several genes involved in plant pathogen associated molecular pattern (PAMP)-triggered immunity (PTI) were only induced in 'Shatian' pomelo or 'Eureka' lemon at 12 wpg, including a *mitogen-activated protein kinase (MAPK) 6* (102625904), two *LRR receptor-like serine/threonine-protein kinase* (102614373, 102610203) and one *PTI1-like tyrosine-protein kinase 3* (102615377) (Figure 5, Supplementary Table S10).

A burst of upregulated DEGs involved in plant-pathogen interaction observed in infected 'Eureka' lemon and 'Shatian' pomelo at 48 wpg (Figure 5, Supplementary Table S10). The number of upregulated DEGs identified in 'Eureka' lemon (17 genes) and 'Shatian' pomelo (21 genes) at 48 wpg was higher than those identified in 'Shatangju' mandarin (8 genes) and 'Hongjiang' orange (12 genes) (Figure 5, Supplementary Table S10). DEGs involved in cyclic nucleotide-gated ion channel, calcium cell signaling pathways, leucine-rich repeat (LRR) receptor-like serine/threonine-protein kinase, WRKY transcription factor and pathogenesis-related genes transcriptional activator were strongly induced in 'Eureka' lemon or/and 'Shatian' pomelo at 48 wpg, while most of these genes were not significantly changed in 'Shatangju' mandarin and 'Hongjiang' orange at 48 wpg (Figure 5, Supplementary Table S10). Particularly, five DEGs involved in plant defense response were only upregulated in both 'Eureka' lemon and 'Shatian' pomelo at 48 wpg, including a *cyclic nucleotide-gated ion channel 1-like* (102626259), a *calcium-binding*

protein CML44 (102628322), a *pathogenesis-related genes transcriptional activator* (*PTI5*, 102625493), a *LRR receptor-like serine/threonine-protein kinase* (*At3g47570*, 102626235) and a *WRKY transcription factor 33* (102608921) (Figure 5, Supplementary Table S10).

Antioxidant activity

A total of 43 DEGs involved in antioxidant activity were identified in four cultivars at two stages, including various types of peroxidase, superoxide dismutase, catalase isozyme, alpha-dioxygenase and respiratory burst oxidase (Figure 5, Supplementary Table S11). Several types of *peroxidase* were significantly induced in 'Shatangju' mandarin, 'Hongjiang' orange and 'Shatian' pomelo at 12 wpg (Figure 5, Supplementary Table S11). Notably, a *peroxidase 51-like* (102610429) was significantly upregulated (Log_2FC = 5.85) in 'Shatangju' mandarin and a *peroxidase P7-like* (102626445) was significantly activated in 'Hongjiang' orange (Log_2FC = 4.36) and 'Shatian' pomelo (Log_2FC = 7.39) (Figure 5, Supplementary Table S11). In contrast, 22 out of 23 DEGs identified in 'Eureka' lemon at 12 wpg were downregulated and most of these DEGs were belonging to *peroxidase* (Figure 5, Supplementary TableS11).

At 48 wpg, most DEGs with antioxidant activity identified in 'Shatangju' mandarin and 'Hongjiang' orange were downregulated (Figure 5, Supplementary Table S11). However, compared to 'Shatangju' mandarin and 'Hongjiang' orange, an increased number of upregulated DEGs involved in antioxidant activity were identified in 'Eureka' lemon and 'Shatian' pomelo at 48 wpg (Figure 5, Supplementary Table S11). Three types of *respiratory burst oxidases homolog proteins* (*RBOHs*, including *protein E*, RBOHE: 102626296, *protein B*, RBOHB: 102610370 and *protein D*, RBOHD: 102616720), six *peroxidases* (102625757, 102612577, 102619020, 102627290, 102617468, 102629002, 102618017), one *L-ascorbate peroxidase* (102622372), one *catalase isozyme 1* (102616866) and one *alpha-dioxygenase 1-like* genes (102610448) were significantly upregulated in either 'Eureka' lemon or 'Shatian' pomelo, or both (Figure 5, Supplementary Table S11).

Discussion

Plant cell wall was not only known as a passive barrier upon pathogen attack, but also played an important role in plant immunity by undergoing dynamic remodeling in adaption to the pathogenic infection (Wan et al., 2021). In this study, a burst of genes involved in cell wall metabolism were observed in 'Shatian' pomelo at early infection stage (Figure 4, Supplementary Table S6), indicating a possible rapid cell wall associated immunity in 'Shatian' pomelo in response to CLas infection at early stage. Among enzymes involved in cell wall metabolism, plant endochitinase were generally upregulated by both biotic and abiotic stress and played an important role in plant resistance against distinct pathogens, including fungi and bacteria (Kasprzewska, 2003). Particularly, plant chitinases with lysozyme or lysozyme-like activity were able to cleave the peptidoglycan of bacteria (Collinge et al., 1993). Among five upregulated genes encoded endochitinase in 'Eureka' lemon and 'Shatian' pomelo, one (107175343) contained the lysozyme_like domain (cl00222) was onl y upregulated in 'Eureka' lemon and 'Shatian' pomelo at 12 wpg (Figure 4, Supplementary TableS6), suggested its possible role in resistance to CLas during infection at 12 wpg. However, the induce of chitinase/endochitinase in 'Shatangju' mandarin and 'Hongjiang' orange at 48 wpg indicated the antibacterial response could be delayed in susceptible cultivars. In addition to chitinase/endochitinase, the pectinesterase may increase the sensitivity of citrus plant during CLas infection. Plant pectinesterase catalyzed the de-esterification of pectin into pectate/methanol and its activity was critical for the outcome of plant-pathogen interactions by making the pectin more susceptibility to microbial pectic enzymes (Lionetti et al., 2012). Thus, the repression of pectinesterase in 'Eureka' lemon and 'Shatian' pomelo at 48 wpg may hinder the success of a subsequent CLas infection in 'Eureka' lemon and 'Shatian' pomelo at late infection stage, while the overexpression of pectinesterase genes in susceptible 'Shatangju' mandarin and 'Hongjiang' orange could increase the sensitivity to HLB and promote the disease development within plant at late infection stage (Figure 6).

The enhance of secondary metabolism promoted the tolerance of 'Eureka' lemon and 'Shatian' pomelo to HLB. Compared to HLB-susceptible cultivars, a burst of upregulated DEGs involved in secondary metabolism (phenylpropanoid, flavonoids, sesquiterpenoid and triterpenoid) were observed in HLB-tolerant cultivars (Figure 4, Supplementary Table S7). Particularly, several key genes (*shikimate O-hydroxycinnamoyl transferase*, *caffeoyl-CoA O-methyltransferase*, *caffeic acid 3-O-methyltransferase*, *flavonol synthase*) involved in biosynthesis of phenylpropanoid and flavonoids were only induced in 'Eureka' lemon and 'Shatian' pomelo (Figure 4, Supplementary Table S7). Plant secondary metabolites played an important role in plant defense response to pathogens infection with its antimicrobial activity (Zaynab et al., 2018). Among secondary metabolites, phenylpropanoids were widely distributed in the plant and played critical roles in plant development by serving as essential components of cell walls, or in response to abiotic or biotic stress, such as wounding, high light/UV radiation and pathogen infection (Korkina, 2007). Flavonoids were a family of plant-derived compounds with well-known antibacterial activity (Cushnie and Lamb, 2011). Previous study found that the *shikimate O-hydroxycinnamoyl transferase* was actively expressed in vascular tissues and played a key role in phenylpropanoids and lignin biosynthesis (Hoffmann et al., 2004). Both *caffeoyl-CoA O-methyltransferase* and *caffeic acid 3-O-methyltransferase* were involved in disease resistance to multiple pathogens by controlling the level of lignin and other metabolites of phenylpropanoid pathway and suppressing the programed cell death (Guo et al., 2001; Yang et al., 2017). In addition, the *flavonol synthase* catalyzed the conversion of dihydroflavonols to flavonols and played a central role in flavonoid biosynthesis (Liu et al., 2021). Therefore, the upregulation of genes involved in phenylpropanoid biosynthesis and flavonoids biosynthesis in 'Eureka' lemon and 'Shatian' pomelo at late CLas infection stage could contribute to their long-term tolerance to CLas (Figure 6).

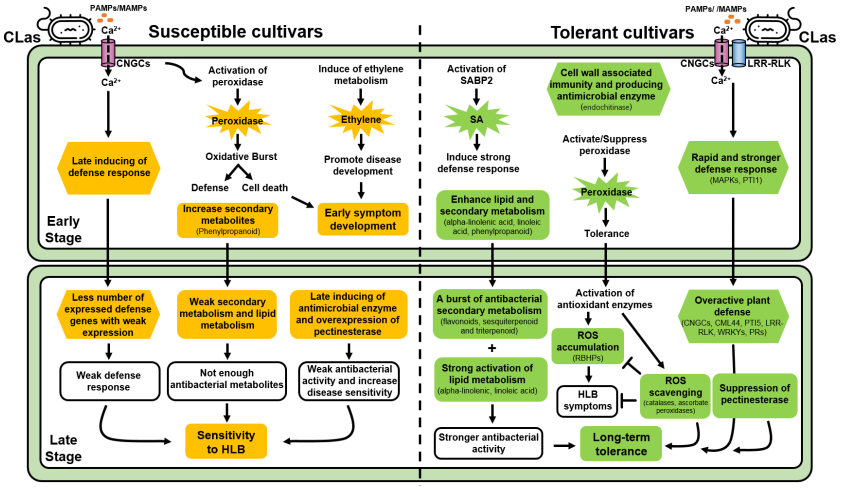

FIGURE 6
Schematic overview of important pathways of HLB-tolerant cultivars (*Citrus limon* cv. Eureka and *C. maxima* cv. Shatian Yu) and HLB-susceptible cultivars (*C. reticulata* Blanco cv. Shatangju and *C. sinensis* cv. Hongjiang Cheng) in response to "*Candidatus* Liberibacter asiaticus".

Plant antimicrobial lipids, mainly including fatty acids and monoglycerides, had been recognized as broad-spectrum antibacterial agents by lysing bacterial cell membrane and inhibiting bacterial growth through a range of mechanisms (Alves et al., 2020). In this study, the strong activation of alpha-linolenic acid and linoleic acid metabolism was observed in two HLB-tolerant cultivars, particularly the 'Eureka' lemon, at both early and late infection stage compared to 'Shatangju' mandarin and 'Hongjiang' orange (Figure 4, Supplementary Table S8). Both alpha-linolenic and linoleic acid were unsaturated fatty acid and had been found to exhibit antimicrobial activity against bacteria and fungi (Lee et al., 2002; Kusumah et al., 2020), which indicated they could be involved in plant defense during pathogen infection. A recent study showed that the alpha-linolenic acid metabolism was the only pathway enriched in citrus transgenic trees expressing *Arabidopsis thaliana NPR1* (AtNPR1), which showed potential resistance to HLB in field (Qiu et al., 2020). Overexpression of alpha-linolenic acid and linoleic acid metabolism suggested they should play an important role in the tolerance of 'Eureka' lemon and 'Shatian' pomelo during CLas infection (Figure 6).

Hormone was the central regulators of plant development and found to be involved in the plant defense against various pathogens infection (Verma et al., 2016). Most genes involved in ethylene metabolism was uniquely upregulated in susceptible 'Shatangju' mandarin at early infection stage (Figure 5, Supplementary Table S8). Ethylene can be induced by the pathogen invasion and showed the discrepancy of the double signaling function in disease resistance in studies of various plant-pathogen interactions (Lund et al., 1998; van Loon et al., 2006). Normally, the accumulation of ethylene in plant promoted the disease development simply through its acceleration of ripening or senescence (Panter and Jones, 2002). Previous study found that genes involved in the ethylene pathway were also upregulated in CLas-infected susceptible sweet orange (Fan et al., 2012). The activation of ethylene metabolism in 'Shatangju' mandarin at early infection stage may promote the HLB symptoms development, which contributed to the earlier presence of symptoms in 'Shatangju' mandarin compared to tolerant cultivars (Figure 1, Table 1). In addition, three *salicylic acid-binding proteins* were strongly induced in tolerant cultivar 'Shatian' pomelo at 12 wpg (Figure 5, Supplementary Table S8). SA was an essential plant defense hormone that promoted immunity in response to both biotic and abiotic stresses (Koo et al., 2020; Peng et al., 2021). The *SABP2* was a well-characterized protein essential for establishment of methyl salicylate (MeSA)-mediated systemic acquired resistance (SAR), which provided the enhanced immunity to a secondary pathogen infection in tissues distal to the site of primary infection (Liu et al., 2011; Soares et al., 2022). A recent study showed that the overexpression of *SABP2* was able to enhance tolerance to HLB in transgenic citrus by reducing HLB symptoms and repressing CLas titer in a low level (Soares et al., 2022). Therefore, the activated expression of *SABP2* genes could contribute to suppression of HLB symptoms development and CLas propagation in 'Shatian' pomelo at early infection stage (Figure 6). In addition, previous studies also found that SA was able to inhibit the auxin signaling pathways as part of the plant defense mechanism (Wang et al., 2007; Kazan and Manners, 2009). The global suppression of auxin signaling pathway in tolerant 'Shatian' pomelo at 48 wpg could be also caused by the significant upregulation of SA pathway, indicated that the SA-mediated plant defense may play important role in tolerance of 'Shatian' pomelo during CLas infection (Figure 6).

The different defense response pattern to CLas infection played an important role in susceptibility and tolerance to HLB at early infection. At 12 wpg, genes involved in CNGCs and cytosolic Ca^{2+} elevation were upregulated in susceptible cultivars group, while genes involved in PTI were only upregulated in tolerant cultivars group (Figure 5, Supplementary Table S10). Plant CNGCs played important roles in the pathogen signaling cascade and facilitated cytosolic Ca^{2+} elevation in response to pathogen and PAMP signals (Ma and Berkowitz, 2011; Moeder et al., 2011). The transient

cytosolic Ca^{2+} influx had been demonstrated to be a core event for triggering PTI (Boudsocq et al., 2010; Dodd et al., 2010), the first layer of plant immunity for microbial perception and restricting pathogen proliferation (Chisholm et al., 2006; Jones and Dangl, 2006). Based on different defense response pattern to CLas infection at early infection stage, the tolerant cultivars exhibited a rapid and stronger defense response to limit the CLas growth after infection, while the susceptible cultivars could be delayed in defense response at early infection stage. In addition, a burst of upregulated DEGs involved in plant defense pathways was identified in tolerance of 'Eureka' lemon and 'Shatian' pomelo compared to 'Shatangju' mandarin and 'Hongjiang' orange at 48 wpg (Figure 5, Supplementary Table S10). Taken together with the moderate symptoms and lower CLas concentration observed in 'Eureka' lemon and 'Shatian' pomelo during the whole infection stage, the rapid and stronger defense response at early CLas infection stage and overactive of plant defense reaction at late CLas infection stage could provide the long-term tolerance to HLB by suppressing the disease symptom development and CLas propagation in tolerant cultivars during CLas infection (Figure 6).

Plant peroxidases participated in various physiological process, such as lignification, wound healing, auxin catabolism and defense mechanisms against pathogen infection (Hiraga et al., 2001; Cosio and Dunand, 2009). In this study, several types of peroxidase were induced in 'Shatangju' mandarin, 'Hongjiang' orange and 'Shatian' pomelo at 12 wpg, while most *peroxidases* were suppressed 'Eureka' lemon at 12 wpg (Figure 5, Supplementary Table S11). Previous study found that the induce at transcript and protein level of multiple peroxidases in citrus during CLas infection was related to the activation of plant defense responses (Franco et al., 2020). In addition, peroxidase was also able to generate high reactive oxygen species (ROS), which induced the programmed cell death of plant (Cosio and Dunand, 2009). HLB was thought as a pathogen-triggered immune disease due to the accumulation of CLas-triggered ROS in phloem-enriched bark tissue, which following caused the systemic cell death of companion and sieve element cells (Ma et al., 2022). The diverse function of *peroxidase* indicated that the upregulation of *peroxidase* in susceptible 'Shatangju' mandarin and 'Hongjiang' orange at early stage could be mainly involved in defense during CLas infection by inducing oxidative burst, which further caused systemic cell death in infected citrus plant. However, the heterogeneous expression of *peroxidase* between 'Eureka' lemon and 'Shatian' pomelo at early infection stage suggested that the function of *peroxidase* may not be the major characteristics of HLB tolerance at early stage (Figure 6). Additionally, DEGs involved in antioxidant activity were mainly suppressed in 'Shatangju' mandarin and 'Hongjiang' orange at late infection stage (Figure 5, Supplementary Table S11), which indicated a weak antioxidant defense response at late infection stage. In contrast, an increased number of antioxidant-related genes and ROS related genes (*RBOHs*, *peroxidases*, *L-ascorbate peroxidase*, *catalase*) were upregulated in 'Eureka' lemon and 'Shatian' pomelo at late infection stage (Figure 5, Supplementary Table S11). Among RBOHs, the RBOHD was known as a central driving force of ROS signaling in plant cells in reaction to pathogen associated molecular patterns during plant-pathogen interaction (Torres et al., 2002). The RBOHD-dependent ROS accumulation triggered by CLas infection was able to cause the cell death of phloem tissue of citrus plant (Ma et al., 2022). However, the suppressing of ROS-mediated cell death caused by CLas infection was able to mitigate HLB symptoms in infection plants (Ma et al., 2022). Both catalases and ascorbate peroxidases were two main H_2O_2 scavenging enzymes in plants (Sofo et al., 2015). In this study, the activation of catalases and ascorbate peroxidases in tolerant cultivars could help to alleviate the oxidative stress caused by ROS, which in turn to reduce HLB symptoms at late infection stage. Therefore, the induce of genes involved in ROS signaling and scavenging process suggested they could not only enhance the tolerance to CLas infection but also limited the HLB symptom in 'Eureka' lemon and 'Shatian' pomelo at late infection stage (Figure 6).

Conclusion

Grafting-based CLas infection assay showed *C. limon* and *C. maxima* were tolerance to HLB, while *C. reticulata* Blanco and *C. sinensis* showed sensitive to HLB. Comparative transcriptomic analysis indicated that the stronger responses in SA-mediated immune, PTI, cell wall associated immunity, endochitinase, phenylpropanoid and alpha-linolenic/linoleic lipid metabolism, occurred in HLB-tolerant *C. limon* and *C. maxima* may play important roles against CLas infection at early infection stage. In contrast, the induce of oxidative burst and ethylene metabolism, as well as the delayed defense response may lead to the early HLB symptom development in susceptible *C. reticulata* Blanco and *C. sinensis* at early infection stage. In addition, the overactive plant defense, stronger antibacterial activity and the activation of ROS scavenging genes could contribute to the long-term tolerance to HLB in *C. limon* and *C. maxima* at late infection stage. However, the weak defense response and antibacterial secondary metabolism, as well as the induce of pectinesterase could be main reason of for HLB sensitivity in *C. reticulata* Blanco and *C. sinensis* at late infection stage.

Data availability statement

The original contributions presented in the study are publicly available. This data can be found here: https://www.ncbi.nlm.nih.gov/bioproject/PRJNA941950.

Author contributions

CG, CL, XD and ZZ conceived and designed the experiments. CG, CL, ZL, YL, JL, JG, JM, FF, CW and ZZ performed the experiments. CG, CL, JM and ZZ contributed to the bioinformatic and statistical analyses. CG and CL prepared the figures/tables and drafted the manuscript. CG, CL, XD and ZZ revised the manuscript. All authors contributed to the article and approved the submitted version.

Funding

This research was supported by National Key Research and Development Program of China (2021YFD1400800), National Natural Science Foundation of China (31901844), China Agriculture Research System of MOF and MARA and Guangzhou Basic and Applied Basic Research Foundation (SL2022A04J00758).

Conflict of interest

The authors declare that the research was conducted in the absence of any commercial or financial relationships that could be construed as a potential conflict of interest.

Publisher's note

Supplementary material

The Supplementary Material for this article can be found online at: https://www.frontiersin.org/articles/10.3389/fpls.2023.1191029/full#supplementary-material

References

Albrecht, U., and Bowman, K. D. (2008). Gene expression in *Citrus sinensis* (L.) osbeck following infection with the bacterial pathogen candidatus liberibacter asiaticus causing huanglongbing in Florida. *Plant Sci.* 175 (3), 291–306. doi: 10.1016/j.plantsci.2008.05.001

Alves, E., Dias, M., Lopes, D., Almeida, A., Domingues, M. D. R., and Rey, F. (2020). Antimicrobial lipids from plants and marine organisms: an overview of the current state-of-the-art and future prospects. *Antibiotics* 9 (8), 441. doi: 10.3390/antibiotics9080441

Anders, S., Pyl, P. T., and Huber, W. (2015). HTSeq–a Python framework to work with high-throughput sequencing data. *Bioinformatics* 31 (2), 166–169. doi: 10.1093/bioinformatics/btu638

Arce-Leal, Á.P., Bautista, R., Rodríguez-Negrete, E. A., Manzanilla-Ramírez, M.Á., Velázquez-Monreal, J. J., Santos-Cervantes, M. E., et al. (2020). Gene expression profile of Mexican lime (*Citrus aurantifolia*) trees in response to huanglongbing disease caused by *Candidatus* liberibacter asiaticus. *Microorganisms* 8 (4), 528. doi: 10.3390/microorganisms8040528

Bao, M., Zheng, Z., Sun, X., Chen, J., and Deng, X. (2020). Enhancing PCR capacity to detect '*Candidatus* liberibacter asiaticus' utilizing whole genome sequence information. *Plant Dis.* 104 (2), 527–532. doi: 10.1094/PDIS-05-19-0931-RE

Boudsocq, M., Willmann, M. R., McCormack, M., Lee, H., Shan, L., He, P., et al. (2010). Differential innate immune signalling via Ca2+ sensor protein kinases. *Nature* 464 (7287), 418–422. doi: 10.1038/nature08794

Bové, J. M. (2006). Huanglongbing: a destructive, newly-emerging, century-old disease of citrus. *J. Plant Pathol.* 88 (1), 7–37. doi: 10.4454/jpp.v88i1.828

Chisholm, S. T., Coaker, G., Day, B., and Staskawicz, B. J. (2006). Host-microbe interactions: shaping the evolution of the plant immune response. *Cell* 124 (4), 803–814. doi: 10.1016/j.cell.2006.02.008

Collinge, D. B., Kragh, K. M., Mikkelsen, J. D., Nielsen, K. K., Rasmussen, U., and Vad1, K. (1993). Plant chitinases. *Plant J.* 3 (1), 31–40. doi: 10.1046/j.1365-313X.1993.t01-1-00999.x

Cosio, C., and Dunand, C. (2009). Specific functions of individual class III peroxidase genes. *J. Exp. Bot.* 60 (2), 391–408. doi: 10.1093/jxb/ern318

Curtolo, M., de Souza Pacheco, I., Boava, L. P., Takita, M. A., Granato, L. M., and Galdeano, D. M. (2020). Wide-ranging transcriptomic analysis of *Poncirus trifoliata*, *Citrus sunki*, *Citrus sinensis* and contrasting hybrids reveals HLB tolerance mechanisms. *Sci. Rep.* 10 (1), 1–14. doi: 10.1038/s41598-020-77840-2

Cushnie, T. T., and Lamb, A. J. (2011). Recent advances in understanding the antibacterial properties of flavonoids. *Int. J. Antimicrob. Agents* 38 (2), 99–107. doi: 10.1016/j.ijantimicag.2011.02.014

Deng, H., Achor, D., Exteberria, E., Yu, Q., Du, D., and Stanton, D. (2019). Phloem regeneration is a mechanism for huanglongbing-tolerance of "Bearss" lemon and "LB8-9" sugar belle® mandarin. *Front. Plant Sci.* 10. doi: 10.3389/fpls.2019.00277

Dodd, A. N., Kudla, J., and Sanders, D. (2010). The language of calcium signaling. *Annu. Rev. Plant Biol.* 61, 593–620. doi: 10.1146/annurev-arplant-070109-104628

Fan, J., Chen, C., Yu, Q., Khalaf, A., Achor, D. S., Brlansky, R. H., et al. (2012). Comparative transcriptional and anatomical analyses of tolerant rough lemon and susceptible sweet orange in response to '*Candidatus* liberibacter asiaticus' infection. *Mol. Plant Microbe Interact.* 25 (11), 1396–1407. doi: 10.1094/MPMI-06-12-0150-R

Folimonova, S. Y., Robertson, C. J., Garnsey, S. M., Gowda, S., and Dawson, W. O. (2009). Examination of the responses of different genotypes of citrus to huanglongbing (citrus greening) under different conditions. *Phytopathology* 99 (12), 1346–1354. doi: 10.1094/PHYTO-99-12-1346

Franco, J. Y., Thapa, S. P., Pang, Z., Gurung, F. B., Liebrand, T. W., Stevens, D. M., et al. (2020). Citrus vascular proteomics highlights the role of peroxidases and serine proteases during huanglongbing disease progression. *Mol. Cell Proteomics* 19 (12), 1936–1952. doi: 10.1074/mcp.RA120.002075

Guo, D., Chen, F., Inoue, K., Blount, J. W., and Dixon, R. A. (2001). Downregulation of caffeic acid 3-o-methyltransferase and caffeoyl CoA 3-o-methyltransferase in transgenic alfalfa: impacts on lignin structure and implications for the biosynthesis of G and s lignin. *Plant Cell* 13 (1), 73–88. doi: 10.1105/tpc.13.1.73

Hiraga, S., Sasaki, K., Ito, H., Ohashi, Y., and Matsui, H. (2001). A large family of class III plant peroxidases. *Plant Cell Physiol.* 42 (5), 462–468. doi: 10.1093/pcp/pce061

Hoffmann, L., Besseau, S., Geoffroy, P., Ritzenthaler, C., Meyer, D., Lapierre, C., et al. (2004). Silencing of hydroxycinnamoyl-coenzyme a shikimate/quinate hydroxycinnamoyltransferase affects phenylpropanoid biosynthesis. *Plant Cell* 16 (6), 1446–1465. doi: 10.1105/tpc.020297

Hu, Y., Zhong, X., Liu, X., Lou, B., Zhou, C., and Wang, X. (2017). Comparative transcriptome analysis unveils the tolerance mechanisms of *Citrus hystrix* in response to '*Candidatus* liberibacter asiaticus' infection. *PloS One* 12 (12), e0189229. doi: 10.1371/journal.pone.0189229

Jones, J. D., and Dangl, J. L. (2006). The plant immune system. *Nature* 444 (7117), 323–329. doi: 10.1038/nature05286

Kasprzewska, A. N. N. A. (2003). Plant chitinases-regulation and function. *Cell Mol. Biol. Lett.* 8 (3), 809–824.

Kazan, K., and Manners, J. M. (2009). Linking development to defense: auxin in plant–pathogen interactions. *Trends Plant Sci.* 14 (7), 373–382. doi: 10.1016/j.tplants.2009.04.005

Kim, D., Pertea, G., Trapnell, C., Pimentel, H., Kelley, R., and Salzberg, S. L. (2013). TopHat2: accurate alignment of transcriptomes in the presence of insertions, deletions and gene fusions. *Genome Biol.* 14 (4), 1–13. doi: 10.1186/gb-2013-14-4-r36

Koo, Y. M., Heo, A. Y., and Choi, H. W. (2020). Salicylic acid as a safe plant protector and growth regulator. *Plant Pathol. J.* 36 (1), 1. doi: 10.5423/PPJ.RW.12.2019.0295

Korkina, L. G. (2007). Phenylpropanoids as naturally occurring antioxidants: from plant defense to human health. *Cell Mol. Bio.* 53 (1), 15–25. doi: 10.1170/T772

Kusumah, D., Wakui, M., Murakami, M., Xie, X., Yukihito, K., and Maeda, I. (2020). Linoleic acid, α-linolenic acid, and monolinolenins as antibacterial substances in the heat-processed soybean fermented with *Rhizopus oligosporus*. *Biosci. Biotechnol. Biochem.* 84 (6), 1285–1290. doi: 10.1080/09168451.2020.1731299

Lee, J. Y., Kim, Y. S., and Shin, D. H. (2002). Antimicrobial synergistic effect of linolenic acid and monoglyceride against *Bacillus cereus* and *Staphylococcus aureus*. *J. Agric. Food. Chem.* 50 (7), 2193–2199. doi: 10.1021/jf011175a

Lionetti, V., Cervone, F., and Bellincampi, D. (2012). Methyl esterification of pectin plays a role during plant–pathogen interactions and affects plant resistance to diseases. *J. Plant Physiol.* 169 (16), 1623–1630. doi: 10.1016/j.jplph.2012.05.006

Liu, W., Feng, Y., Yu, S., Fan, Z., Li, X., Li, J., et al. (2021). The flavonoid biosynthesis network in plants. *Int. J. Mol. Sci.* 22 (23), 12824. doi: 10.3390/ijms222312824

Liu, P. P., von Dahl, C. C., and Klessig, D. F. (2011). The extent to which methyl salicylate is required for signaling systemic acquired resistance is dependent on exposure to light after infection. *Plant Physiol.* 157 (4), 2216–2226. doi: 10.1104/pp.111.187773

Livak, K. J., and Schmittgen, T. D. (2001). Analysis of relative gene expression data using real-time quantitative PCR and the $2^{-\Delta\Delta CT}$ method. *Methods* 25 (4), 402–408. doi: 10.1006/meth.2001.1262

Lund, S. T., Stall, R. E., and Klee, H. J. (1998). Ethylene regulates the susceptible response to pathogen infection in tomato. *Plant Cell* 10 (3), 371–382. doi: 10.1105/tpc.10.3.371

Ma, W., and Berkowitz, G. A. (2011). Ca^{2+} conduction by plant cyclic nucleotide gated channels and associated signaling components in pathogen defense signal transduction cascades. *New Phytol.* 190 (3), 566–572. doi: 10.1111/j.1469-8137.2010.03577.x

Ma, W., Pang, Z., Huang, X., Xu, J., Pandey, S. S., Li, J., et al. (2022). Citrus huanglongbing is a pathogen-triggered immune disease that can be mitigated with antioxidants and gibberellin. *Nat. Commun.* 13 (1), 529. doi: 10.1038/s41467-022-28189-9

Moeder, W., Urquhart, W., Ung, H., and Yoshioka, K. (2011). The role of cyclic nucleotide-gated ion channels in plant immunity. *Mol. Plant* 4 (3), 442–452. doi: 10.1016/S0065-2296(02)38032-7

Panter, S. N., and Jones, D. A. (2002). Age-related resistance to plant pathogens. *Adv. Bot. Res.* 38, 251–280. doi: 10.1016/S0065-2296(02)38032-7

Peng, Y., Yang, J., Li, X., and Zhang, Y. (2021). Salicylic acid: biosynthesis and signaling. *Annu. Rev. Plant Biol.* 72, 761–791. doi: 10.1146/annurev-arplant-081320-092855

Qiu, W., Soares, J., Pang, Z., Huang, Y., Sun, Z., Wang, N., et al. (2020). Potential mechanisms of AtNPR1 mediated resistance against huanglongbing (HLB) in citrus. *Int. J. Mol. Sci.* 21 (6), 2009. doi: 10.3390/ijms21062009

Ribeiro, C., Xu, J., Hendrich, C., Pandey, S. S., Yu, Q., Gmitter, F. G.Jr., et al. (2023). Seasonal transcriptome profiling of susceptible and tolerant citrus cultivars to citrus huanglongbing. *Phytopathology* 113 (2), 286–298. doi: 10.1094/PHYTO-05-22-0179-R

Soares, J. M., Weber, K. C., Qiu, W., Mahmoud, L. M., Grosser, J. W., and Dutt, M. (2022). Overexpression of the salicylic acid binding protein 2 (SABP2) from tobacco enhances tolerance against huanglongbing in transgenic citrus. *Plant Cell Rep.* 41 (12), 2305–2320. doi: 10.1007/s00299-022-02922-6

Sofo, A., Scopa, A., Nuzzaci, M., and Vitti, A. (2015). Ascorbate peroxidase and catalase activities and their genetic regulation in plants subjected to drought and salinity stresses. *Int. J. Mol. Sci.* 16 (6), 13561–13578. doi: 10.3390/ijms160613561

Torres, M. A., Dangl, J. L., and Jones, J. D. (2002). *Arabidopsis* gp91phox homologues AtrbohD and AtrbohF are required for accumulation of reactive oxygen intermediates in the plant defense response. *PNAS* 99 (1), 517–522. doi: 10.1073/pnas.01245249

van Loon, L. C., Geraats, B. P., and Linthorst, H. J. (2006). Ethylene as a modulator of disease resistance in plants. *Trends Plant Sci.* 11 (4), 184–191. doi: 10.1016/j.tplants.2006.02.005

Verma, V., Ravindran, P., and Kumar, P. P. (2016). Plant hormone-mediated regulation of stress responses. *BMC Plant Biol.* 16, 1–10. doi: 10.1186/s12870-016-0771-y

Wan, J., He, M., Hou, Q., Zou, L., Yang, Y., Wei, Y., et al. (2021). Cell wall associated immunity in plants. *Stress Biol.* 1 (1), 3. doi: 10.1007/s44154-021-00003-4

Wang, L., Feng, Z., Wang, X., Wang, X., and Zhang, X. (2010). DEGseq: an r package for identifying differentially expressed genes from RNA-seq data. *Bioinformatics* 26 (1), 136–138. doi: 10.1093/bioinformatics/btp612

Wang, L., Huang, Y., Liu, Z., He, J., Jiang, X., He, F., et al. (2021). Somatic variations led to the selection of acidic and acidless orange cultivars. *Nat. Plants* 7 (7), 954–965. doi: 10.1038/s41477-021-00941-x

Wang, D., Pajerowska-Mukhtar, K., Culler, A. H., and Dong, X. (2007). Salicylic acid inhibits pathogen growth in plants through repression of the auxin signaling pathway. *Curr. Biol.* 17 (20), 1784–1790. doi: 10.1016/j.cub.2007.09.025

Weber, K. C., Mahmoud, L. M., Stanton, D., Welker, S., Qiu, W., Grosser, J. W., et al. (2022). Insights into the mechanism of huanglongbing tolerance in the Australian finger lime (*Citrus australasica*). *Front. Plant Sci.* 13. doi: 10.3389/fpls.2022.1019295

Wei, X., Mira, A., Yu, Q., and Gmitter, F. G.Jr. (2021). The mechanism of citrus host defense response repression at early stages of infection by feeding of diaphorina citri transmitting *Candidatus* liberibacter asiaticus. *Front. Plant Sci.* 12. doi: 10.3389/fpls.2021.635153

Xie, C., Mao, X., Huang, J., Ding, Y., Wu, J., Dong, S., et al. (2011). KOBAS 2.0: a web server for annotation and identification of enriched pathways and diseases. *Nucleic Acids Res.* 39 (suppl_2), W316–W322. doi: 10.1093/nar/gkr483

Yang, Q., He, Y., Kabahuma, M., Chaya, T., Kelly, A., Borrego, E., et al. (2017). A gene encoding maize caffeoyl-CoA O-methyltransferase confers quantitative resistance to multiple pathogens. *Nat. Genet.* 49 (9), 1364–1372. doi: 10.1038/ng.3919

Young, M. D., Wakefield, M. J., Smyth, G. K., and Oshlack, A. (2010). Gene ontology analysis for RNA-seq: accounting for selection bias. *Genome Biol.* 11 (2), 1–12. doi: 10.1186/gb-2010-11-2-r14

Yu, Q., Chen, C., Du, D., Huang, M., Yao, J., Yu, F., et al. (2017). Reprogramming of a defense signaling pathway in rough lemon and sweet orange is a critical element of the early response to '*Candidatus* liberibacter asiaticus'. *Hortic. Res. Horticulture Res.* 4, 17063. doi: 10.1038/hortres.2017.63

Zaynab, M., Fatima, M., Abbas, S., Sharif, Y., Umair, M., Zafar, M. H., et al. (2018). Role of secondary metabolites in plant defense against pathogens. *Microb. Pathog.* 124, 198–202. doi: 10.1016/j.micpath.2018.08.034

Zheng, Z., Chen, J., and Deng, X. (2018). Historical perspectives, management, and current research of citrus HLB in guangdong province of China, where the disease has been endemic for over a hundred years. *Phytopathology* 108 (11), 1224–1236. doi: 10.1094/PHYTO-07-18-0255-IA

Zou, X., Bai, X., Wen, Q., Xie, Z., Wu, L., Peng, A., et al. (2019). Comparative analysis of tolerant and susceptible citrus reveals the role of methyl salicylate signaling in the response to huanglongbing. *J. Plant Growth. Regul.* 38, 1516–1528. doi: 10.1007/s00344-019-09953-6

frontiers | Frontiers in Plant Science

TYPE Original Research
PUBLISHED 04 August 2023
DOI 10.3389/fpls.2023.1200674

OPEN ACCESS

EDITED BY
Kun Zhang,
Yangzhou University, China

REVIEWED BY
Yiyong Zhu,
Nanjing Agricultural University, China
Lang Qin,
Yangzhou University, China

*CORRESPONDENCE
Annette Niehl
Annette.niehl@julius-kuehn.de

RECEIVED 05 April 2023
ACCEPTED 14 July 2023
PUBLISHED 04 August 2023

CITATION
Gauthier K, Pankovic D, Nikolic M, Hobert M, Germeier CU, Ordon F, Perovic D and Niehl A (2023) Nutrients and soil structure influence furovirus infection of wheat. *Front. Plant Sci.* 14:1200674. doi: 10.3389/fpls.2023.1200674

Nutrients and soil structure influence furovirus infection of wheat

Kevin Gauthier[1], Dejana Pankovic[2], Miroslav Nikolic[3], Mirko Hobert[4], Christoph U. Germeier[5], Frank Ordon[2], Dragan Perovic[2] and Annette Niehl[1]*

[1]Julius Kühn Institute (JKI) – Federal Research Centre for Cultivated Plants, Institute for Epidemiology and Pathogen Diagnostics, Brunswick, Germany, [2]Julius Kühn Institute (JKI) – Federal Research Centre for Cultivated Plants, Institute for Resistance Research and Stress Tolerance, Quedlinburg, Germany, [3]Institute for Multidisciplinary Research, University of Belgrade, Belgrade, Serbia, [4]State Institute for Agriculture and Horticulture Saxony-Anhalt, Centre for Agricultural Investigations, Bernburg, Germany, [5]Julius Kühn Institute (JKI) – Federal Research Centre for Cultivated Plants, Institute for Breeding Research on Agricultural Crops, Quedlinburg, Germany

Soil-borne wheat mosaic virus (SBWMV) and *Soil-borne cereal mosaic virus* (SBCMV), genus *Furovirus*, family *Virgaviridae*, cause significant crop losses in cereals. The viruses are transmitted by the soil-borne plasmodiophorid *Polymyxa graminis*. Inside *P. graminis* resting spores, the viruses persist in the soil for long time, which makes the disease difficult to combat. To open up novel possibilities for virus control, we explored the influence of physical and chemical soil properties on infection of wheat with SBWMV and SBCMV. Moreover, we investigated, whether infection rates are influenced by the nutritional state of the plants. Infection rates of susceptible wheat lines were correlated to soil structure parameters and nutrient contents in soil and plants. Our results show that SBWMV and SBCMV infection rates decrease the more water-impermeable the soil is and that virus transmission depends on pH. Moreover, we found that contents of several nutrients in the soil (e.g. phosphorous, magnesium, zinc) and *in planta* (e.g. nitrogen, carbon, boron, sulfur, calcium) affect SBWMV and SBCMV infection rates. The knowledge generated may help paving the way towards development of a microenvironment-adapted agriculture.

KEYWORDS

furovirus, nutrients, *Polymyxa graminis*, wheat, modeling, prediction of infection rates, soil physical parameters, soil chemical parameters

Introduction

The availability of nutrients in the environment influences crop growth and thus impacts biomass, vitality, and grain quality or quantity of cereal crops (Chapin, 1980; Miao et al., 2006; Lee et al., 2017). It has been shown that the use of fertilizers allowed a yield increase of 50% during the 20th century, or a yearly increase in crop milling quality of around 2% during 50 years (Fageria and Baligar, 2005; Gu et al., 2015). In addition to these

direct effects on crops, nutrient availability acts as a major driver of interactions between organisms, shaping microorganism community composition and driving their interactions at both, the macroscopic (Borer et al., 2014) and microscopic scale, e.g. by regulating the abundance of bacteria (Francioli et al., 2016; Wang et al., 2018), fungi (Muneer et al., 2021) or viruses (Finke et al., 2017), as well as by modifying plant metabolism (Calabrese et al., 2017; Calabrese et al., 2019; Heyneke and Hoefgen, 2021). Carbon (C), nitrogen (N) and phosphorous (P) are believed to have a high impact on community composition according to the resource-ratio theory (Miller et al., 2005). Furthermore, the difference observed in C:N:P stoichiometry among virus, bacteria and fungi suggests that the different microorganisms have different needs for the different nutrients (Griffiths et al., 2012; Finke et al., 2017; Zhang and Elser, 2017). Reciprocally, living organisms directly influence the dynamics and availability of nutrients in their environment (Middelboe et al., 1996; Jones and Smith, 2004), especially in soils, in which they directly compete for nutrients. Beside its role as source of nutrients, soil has a physical role, serving as a support for plant roots, shaping their growth, driving water uptake (Jakobsen and Dexter, 1987) and influencing microbial activity (Jat et al., 2018). In return, roots and microorganisms influence the texture of soils, e.g. by storing organic matter or by colonizing the pores of the soil (Six et al., 2004). As pathogenic microorganisms cause substantial crop damage, studying the interactions between plants and pathogens is specifically important. However, it remains unclear how the availability of nutrients influences the plant- pathogen interaction. Besides their importance for plant growth by providing essential elements for the biosynthesis and function of proteins, nucleic acids, and sugars, macro- and micronutrients are involved in defense mechanisms against pathogens (Dordas, 2008). In the case of macronutrients, potassium (K) and nitrogen (N) were reported to promote a hypersensitivity response to infection as they are present in signaling molecules (Orober et al., 2002; Mur et al., 2017). Moreover, it has been shown that potassium increases the integrity of the cell wall and the speed of cell turgor recovery (Niehl et al., 2006; Wang et al., 2013). Concerning micronutrients, it has been reported that boron (B) favors cell wall integrity and improves the resistance to some pathogens (Dong et al., 2016), manganese (Mn) and copper (Cu) promote lignification (Eskandari et al., 2020), and zinc (Zn) is needed to form the zinc-finger domain in resistance proteins (Gupta et al., 2012). However, as nutrients play a role in pathogen growth and spread too, their role cannot be reduced to plant defense promoters, as their action seems to be very specific to each plant-pathogen-nutrient system. While some studies suggest that high nutrient availability increases the ability of plants to combat pathogens (Verly et al., 2020) or reduce the symptoms of infection (e.g. Chrpová et al., 2020; Chien and Huang, 2021), other studies report that it favors infection or leads to stronger disease symptoms (Snoeijers et al., 2000; Ballini et al., 2013).

Soil-borne pathogens may interact with soil nutrients directly or indirectly after infecting the host plant (DiTommaso and Aarssen, 1989). Soil-borne wheat mosaic virus (SBWMV) and Soil-borne cereal mosaic virus (SBCMV), genus *Furovirus*, family *Virgaviridae*, are among the most devastating cereal viruses worldwide, leading on average to yield losses of 30-40% (Adams, 1990; Lapierre and Hariri, 2008; Kroese et al., 2020). SBWMV and SBCMV are positive sense single stranded bi-partite RNA viruses (King et al., 2011; Niehl and Koenig, 2021). RNA1 encodes a replication protein, an RNA-dependent RNA polymerase and a movement protein while RNA2 encodes a major coat protein (CP) and a minor CP, initiated by an upstream start codon, a CP-RT protein produced from translational readthrough of the stop codon and a cysteine rich silencing suppressor protein (Te et al., 2005; Andika et al., 2016). Infections with SBWMV or SBCMV cause mosaic symptoms and light stunting, easily recognizable at field scale as chlorotic patches (Niehl and Koenig, 2021). The host range of SBWMV and SBCMV is relatively narrow, restricted to *Poaceae*, mostly cultivated, although infections of wild grasses of the genera *Bromus* were reported (McKinney, 1944; Lapierre and Signoret, 2004). The viruses are transmitted to the roots of cereals by the soil-borne plasmodiophorid *P. graminis*. Most of the infections of winter cereals are thought to occur in fall. The soil-borne motile spores of *P. graminis* reach the roots of the host plants by swimming in the free water of soils (Barr and Allan, 1982; Adams, 1990; Kanyuka et al., 2003). After reaching the roots, viruliferous *P. graminis* spores inject their cell content and along with it viruses into their host root cell. SBWMV and SBCMV replicate and move systemically in the host, while *P.graminis* replicates and locates only in the roots (Verchot et al., 2001). Viruliferous *P. graminis* spores are released from the roots into the soil where they can survive for decades (Rao and Brakke, 1969; Campbell, 1988), keeping contaminated soils infectious for a very long time.

P. graminis is currently divided into several formae speciales with different climatic preferences (Legrève et al., 2002). Currently, the only efficient disease control method involves breeding of resistant cultivars, relying on two known resistance genes in wheat: *Sbm1 and Sbm2* (Kanyuka et al., 2004; Bass et al., 2006; Perovic et al., 2009; Maccaferri et al., 2011). *Sbm1* and *Sbm2* are located on the 5DL and 2BS chromosomes, respectively (Bass et al., 2006; Liu et al., 2020). *Sbm1* and *Sbm2* were described as translocation resistances (Hunger and Sherwood, 1984; Driskel et al., 2002; Bass et al., 2006), not preventing the infection of roots, but limiting viral loads in the upper part of the plants to low amounts. The resistance mechanism underlying *Sbm3*, a recently identified additional resistance gene located on the A genome is still unknown (Schlegel et al., 2022). As the resources to combat SBWMV/SBCMV infection are very limited, optimizing the deployment of resistant plants and understanding additional factors influencing the infection is important.

In the SBWMV/SBCMV-*P. graminis*- host pathosystem it is well possible that the availability of nutrients in the soil and soil structure play a key role in determining the outcome of infection. *P. graminis* and the roots potentially compete for and modulate the uptake of micro- and macronutrients within the infected host. Nutrient availability within the host may determine the efficiency of virus replication and thus susceptibility of plants towards viruses. Soil structure and soil chemical composition likely influences the uptake of nutrients by the roots as well as the germination rate and movement of *P.graminis* spores. Here, we examined the influence of

soil nutrient availability and uptake by plants, as well as soil structure on SBWMV and SBCMV infection rates of susceptible wheat lines in greenhouse conditions using infected soil collected from several naturally infested fields in France, Germany, Italy, and the England between 2017 and 2020. Both, single and interacting effects of the soil properties (pH, percentage of fine particles) nutrient contents in the soil and in plant roots and leaves on infection rates were analyzed using generalized linear models. Our results give new insight into the influence of soil condition and fertilization on SBWMV/SBCMV infection rates in wheat. This knowledge may help to develop a microenvironment-adapted agriculture.

Materials and methods

Soil collection

100-200 l of soil infected with SBCMV or SBWMV were collected from fields in France, Italy, England and Germany, respectively in the period from 2017 to 2020 (Table S1). Except for samples from Heddesheim (Ger) and England, soil samples from all other locations were collected in at least two subsequent years. For samples from England, soil from each field was collected twice. Before use the soil was kept at at 1°C to 6°C in the dark.

Plant material

Three susceptible wheat lines, Avalon, Prevert and the durum wheat Pescadou were used. Seeds pre-germinated on filter paper at room temperature in the dark for three to five days were transplanted to pots (V= 520ml) filled with the infested field soils. Field soil were crushed to break up the larger clumps and were mixed before being filled into pots. Twenty plants were planted into each pot. Plants were grown in climate chambers at 14°C, 60% humidity, and a 16 h photoperiod with 10 klux. During the first 4 weeks plants were watered from the bottom and after that daily watering was applied. After 12 weeks in infected soil, the youngest leaves of each plant were harvested for the detection of SBCMV and SBWMV by ELISA. Subsequently, the foliage and roots of the plants were harvested for virus and *P. graminis* detection by RT-qPCR and for the analysis of nutrients. Roots were washed to remove soil particles and dried with filter paper to remove excess water. Leaf and root samples of six plants were pooled per wheat line, immediately snap frozen in liquid nitrogen and kept at -80°C.

Element analysis

Determination of the grain size composition of soil

10g air-dried soil were suspended in 15% w/vol H_2O_2 for 15 h and then heated in a water bath at 90°C until organic matter was completely destroyed. 25 ml 0,4 N $Na_4P_2O_7$ was added to the sample and incubated over night. The next day the sample volume was adjusted to 250 ml with distilled H_2O and shaken for 6 h. Subsequently, the suspension was sieved through a 0.2 mm mesh into a 1000 ml glass cylinder and purged with distilled H_2O to nearly 1000 ml. The grain size was determined by sieving through mesh sieves with 0,2 mm, 0,63 and 2,0 mm pore size. Resulting fractions for grain sizes were >0.2 mm, <0,2 to 0,63 mm <0,63 to 2,0 mm. The grain size fractions were dried at 105°C to constant weight. For the grain fraction <0.2 mm the glass cylinder was shaken six times overhead for 10 sec and then placed thermo-constant and vibration-free for sedimentation. For the individual fall-times of the fractions the pipette depth varied between 10 and 30 cm according to *DIN ISO 11277:2002-08* (Din, 2002). For every suspected fraction 10 ml suspension was pipetted to a scale dish and dried at 105°C to constant weight. The grain fractions were estimated in % weight in relation to dry matter.

Determination of pH, plant available phosphorous-, potassium- magnesium- and zinc contents and determination of nutrients in soil extracts

pH, plant available phosphorous-, potassium- and magnesium-contents were determined in soil extracts with the calcium-acetate-lactate (CAL) extraction method (Schüller, 1969). All other plant nutrients were determined in soil extracts according to VDLUFA Methodbook I (VDLUFA, 1991).

For determination of pH, plant available phosphorous and potassium, 5 g air-dried and to <2 mm sieved soil were suspended in 100 ml CAL-solution [0,05 M $C_6H_{10}CaO_6$; 0,05 M $(CH_3COO)_2Ca$; 0,3 M acetic acid], agitated overhead for 90 min and then filtered through a MN 616 md ¼ filter (Macherey-Nagel, Düren, Germany). The first 20 ml of the filtrate was discarded. The following filtrates were analyzed with calibration standards for each parameter in bubble gating with a continuous-flow-analyzer (Skalar Analytical, The Netherlands) according to the manufacturer's instructions. The pH sample was dialyzed against the indicator methyl red and photometric analysis performed at 540 nm. For plant-available phosphorous, extinction was measured photometrically at 880 nm and potassium was identified with a flame-photometer at 776 nm. Results were recorded in pH-Scale and mg per 100 g air-dried soil, respectively.

For identification of plant available magnesium, 5 g air-dried and to <2 mm sieved soil was suspended in 50 ml calcium chloride solution (0,01 M $CaCl_2$), shaken for 120 min and then filtered through a MN 280 1/4 (Macherey-Nagel) filter. The first 15 ml of the filtrate were discarded. The remaining filtrate was analyzed with a continuous-flow-analyzer (Skalar Analytical) in a complex with xylidil blue according to the manufacturer's instructions. The complex was measured photometrically in bubble gating at 470 nm with a calibration standard. Results were recorded in mg per 100 g air-dried soil.

For determination of plant available zinc 20 g air-dried and to <2 mm sieved soil was suspended in 100 ml EDTA-disodium salt-solution [0,05 M $C_{10}H_{14}N_2Na_2O_8$], agitated overhead for 120 min and subsequently filtrated through a MN 616 md 1/4 (Macherey-Nagel) filter. The first 10 ml of the filtrate were discarded. The filtrate was analyzed with calibration standards with a ICP-OES 5100 VDV

from Agilent (Agilent Technologies, Santa Clara, United States) according to manufacturer's instructions. Results were recorded in mg per kg air-dried soil.

For analytical determination of total nitrogen 2 g air-dried and to <2 mm sieved soil was pulverized in a Pulverisette 5 (Fritsch, Idar-Oberstein, Germany) and analyzed with a Dumas-Analyzer (VarioMax, Elementar Analysesysteme, Langenselbold, Germany) with a calibration standard according to the manufacturer's instructions. Results were recorded as % air-dried soil.

For all determined elements, the variation between two replicates of each analyzed soil sample was below 10%.

Determination of element content in plant tissue

Element contents of carbon (C) and nitrogen (N) were determined in root and shoot material with a Thermo EA1112 HT elemental analyzer according the Dumas combustion method. Samples were freeze dried at -20 °C, 1 mbar for 48 h in a CHRIST ALPHA 1-4 LD plus freeze-drier (Martin Christ GmbH, Germany). Freeze dried samples were ground to a fine powder using a ball mill and 2.200 µg weighed into tin capsules (3.3 x 5 mm, IVASA76980502). They were burned in a reactor with copper (IVASA99060102, IVA Analysentechnik, Meerbusch, Germany) as reductant, silvered cobaltous/IC oxide and chromium oxide (33824500 and 33822900, Thermo Fisher Scientific, Dreieich, Germany) as catalysts at 1020°C and resulting nitrogen (as N_2) and carbon (as CO_2) was determined by gas chromatography. Ratios of stable isotopes N^{14}/N^{15}, C^{12}/C^{13} in these gases were determined in a Thermo Delta V Advantage isotope ratio mass spectrometer (IRMS). A certified wheat flour standard (IVA33802157: 1.36% N, 39.38% C, $\delta^{15}N_{air}$ 2.85 ‰, $\delta^{13}C_{V\text{-}PDB}$ -27.21 ‰) in amounts of 600, 1200, 1800 and 2400 µg was used for calibration, besides isotope calibration of reference gas N_2 with standard materials from the International Atomic Energy Agency (IAEA N1, IAEA N2, USGS25). Each sample was measured in two runs.

For the analysis of phosphorous (P), potassium (K), magnesium (Mg), calcium (Ca), sulfur (S), manganese (Mn), copper (Cu), zinc (Zn), boron (B), and molybdenum (Mo), freeze dried plant material (0.2 g) was digested in 3 ml concentrated HNO_3 + 2 ml H_2O_2 for 1 h in a microwave oven (Speedwave MWS-3+; Berghof Products + Instruments GmbH, Eningen, Germany). The samples were diluted with deionised H_2O (1:5) and subjected to multi-elemental analyses by ICP-OES (Spectro-Genesis EOP II, Spectro Analytical Instruments GmbH, Kleve, Germany). The certified reference material (GBW10015 Spinach; Institute for Geophysical and Geochemical Exploration, Langfang, China) was used to assess the accuracy and precision of the analyses.

Characterization of infection rates

After 12 weeks in infected soil, the youngest leaves of each plant were harvested for the detection of SBCMV and SBWMV by Double Antibody Sandwich Enzyme-Linked Immunosorbent Assay (DAS-ELISA) according Clark and Adams (1977), as explained in Schlegel et al. (2022). 96-well plates were coated with IgG 1:100 (JKI-AS92 for SBCMV and JKI-AS69 for SBWMV, respectively) in coating buffer (0.05M sodium carbonate, pH 9,6; 0.02% NaN_3) for 4 h, washed four times with PBS pH 7,4 containing 0,05% Tween 20 using a Tecan ELISA washer (Tecan, Switzerland) and kept at -20°C until use. 50 mg fresh leaf or root material was homogenized (5000 rpm; 25 sec for leaf material and 50 sec for root at material) using metal beads in 500 µl of extraction buffer (PBS pH 7.4 containing 0.05% Tween 20, 2% polyvinylpyrrolidone MW 44,000, and 0.2% non-fat dry milk) using a Precellys homogenizer (Bertin Technologies, France). The extracts were incubated in coated ELISA plates overnight at 40 °C. The washing step consisted of four manual and four machine washing cycles (Tecan, Switzerland). The incubation step with the alkaline-phosphatase-labelled antibody (1:2000) was performed in a humid chamber at 37 °C for 4 h in conjugate buffer (PBS pH 7.4 containing 0.05% Tween 20, 2% polyvinylpyrrolidone MW 44,000, and 0.2% non-fat dry milk). After four washing cycles with a Tecan ELISA washer and incubation with 1 mg para-nitrophenylphosphate per ml substrate buffer (10% diethanolamine pH 9,8, 0.02% NaN_3) for 1 h, the OD of 405 nm was measured (Sunrise, Tecan, Switzerland). Samples were considered positive when their measured OD exceeded two times the negative control with a minimum threshold of 0.1 after blank reduction. The infection rate was calculated as ratio of infected over total number of plants (%).

Determination of virus and *P. graminis* subspecies

RNA extraction

Snap frozen root samples were finely ground using a ball mill (Retch mill, MM301, Germany), precooled in liquid nitrogen and kept at -80 °C. RNA extraction was performed with the ground root samples using NucleoZol (Macherey-Nagel, Düren, Germany) reagent according to the manufacturer's instructions. Briefly, 0.05 g of ground material were suspended in the same volume of reagent. After vortexing and centrifugation, RNA was precipitated using isopropanol and washed twice with ethanol before solubilization.

RT real-time PCR

Virus species and vector sub-species, respectively were identified with reverse transcription real time PCR (RT-qPCR) and reverse transcription real time nested PCR (RT-nested qPCR). Reverse transcription was performed on the extracted RNA after 10-fold dilution. 1 µL of the diluted RNA, 10 µmol of random primers, 2µL DTT and 20U ProtoScript®II Reverse Transcriptase (New England Biolabs, Ipswich, United States), 125 µmol of each dNTP and 4µL provided buffer were used for the synthesis according to manufacturer's instruction with minor modifications in a 20 µL reaction. Samples were placed in a FlexCycler PCR System (Analytik Jena, Jena, Germany) with the following cycle parameters: 25 °C for 5 min, reverse transcription at 42 °C for 1 hour followed by a step of 20 min at 65 °C for inactivation. For *Polymyxa* identification, the produced cDNA (of ITS-derived sequences specific for *P. graminis ssp. tepida* and *ssp. temperata*, respectively) were amplified using 2 µL cDNA, 500 nmol of each primer (PGG_166_FW and PGG_631_RV, Table S2), 125 µmol of each dNTP and 4 µL of buffer provided with 5 U One *Taq* polymerase (New England Biolabs) according to manufacturer's

instructions with minor modifications in a 20 µL reaction. Samples were placed in a FlexCycler with the following cycle parameters: 5 min at 94 °C followed by 15 cycles of 30 seconds at 94 °C, 1min at 50 °C and 2 min at 68 °C concluded with 10 min at 72 °C for final extension. The amplified PCR products were 10-fold diluted to serve as template for real-time PCR. Real-time PCR for the detection of *P. graminis* subspecies after PCR or for detection of SBWMV or SBCMV after cDNA synthesis was performed using a qTower 2.2 (Analytik Jena) with 1 µL template, 500 nmol of each primer (1-BWF-6541T and 1-BWR-6683 for SBWMV, PTP-409-FW and PTP-512-RV for *P.graminis ssp. tepida*, PTM-403-FW and PTM-481-RV for *Polymyxa graminis ssp. temperata*, Table S2), and Luna® Universal qPCR Master Mix (New England Biolabs) in a 10 µL reaction volume. The obtained Ct-values and melting temperatures were compared to standard curves and considered as positive when the measured melting temperature of the amplified product was less different than 1 °C when compared with the melting temperature of the highest concentration present in the melting curve and the average number of cycles needed for detection was lower than 35.

Preparation of the standard curves

After RNA extraction (as described above) a step of reverse transcription was performed (as described above). The cDNAs were amplified as described above but with the primers 1-BWF-6237 and 1-BWR-7018 for SBWMV, PGG-51-FW and PGG-882-RV for *P. graminis*. After a 10-fold dilution of the amplified DNA for *P. graminis*, another amplification was performed in the same conditions with the primers PGG_166_FW and PGG_631_RV. Amplified DNA was visualized and cut from Midori green stained gels and purified using a Nucleo Spin® PCR and Gel kit (Macherey-Nagel). Purified products were inserted into pDrive Cloning vector using a PCR Cloning Kit (QIAGEN, Venlo, Netherlands). Next, electro competent *Escherichia coli* of the DH5α strain were transformed using an Electroporator ® (Eppendorf, Hamburg, Germany). Concisely, bacteria were shortly incubated on ice before electroporation at 2500 V. After 1 h regeneration time in LB at 37 °C, 700 rpm in a Thermomixer (Eppendorf), cells were plated on agar plates containing 50 ng carbenicillin before being cultivated overnight at 37 °C. The presence of the insert in colonies was analyzed using the same primers as used for the cloning. Colonies containing the inserts of interest were cultivated in liquid agar at 37 °C over night. Plasmids were finally extracted using a Nucleo Spin® Plasmid kit (Macherey-Nagel) and sequenced (Eurofins MWG, Ebersberg, Germany) to confirm the identity of the insert.

Statistical analysis

All statistical analyses were performed using R version 3.6.3 (R Development Core Team, 2019). All the variables were analyzed using principal component analysis (PCA) from the package FactoMineR (Lê et al., 2008). All data were normalized before analysis by normalizing each value to the mean of all samples for the respective measured parameter divided by SD. Three modeling approaches were used to determine the influence of the studied parameters for the SBWMV/SBCMV infection rates. In the first approach, parameters influencing the infection rates in the soils were selected after a stepwise backward modelization (STBM) (Whittingham et al., 2006) in binomial or quasi-binomial generalized linear models, based on all studied parameters for soil parameters and plant nutrients. Every parameter was analyzed for its significance in the model and the parameter with the highest non-significant p-value was removed from the model. The model was re-evaluated until every remaining parameter was significant or no parameter remained in the model.

This modelization procedure was repeated for the element analysis performed with plant samples. A final Holm correction was performed on the obtained p-values (Holm, 1979). After identification of the parameters influencing the infection rates, predictive generalized linear models were used to determinate their exact influence on the SBWMV and SBCMV infection rates. In the second approach, inspired from Lacroix and collaborators (2017), the function dredge from the R package MuMin was used to fit all the possible models. A prior step of stepwise backward selection was eventually performed in case that the number of factors and interactions exceeded the number of analyzed samples. Parameter values, errors and AIC [Akaike information criterion, or QAIC (quasi Akaike information criterion)], respectively were estimated using the function model.avg using all the models with a delta value smaller than 4 (MAVG). The third approach used was a mixed approach between the first and the second method, in which the selected parameters after model averaging were checked (ST-MA) for their significance before being kept in the model. The significance of the tested factors was assessed using Fisher tests for STBM methods and Walt tests for the two other approaches. In the case of ST-MA, the weight of each parameter was determined between zero (irrelevant parameter) and one (parameter present in every model). Infection rates were predicted according to the identified factors using the function predict.glm. The predicting performance of STBM and ST-MA were then compared. For representation, in case the model contained more than four significant factors, only the four first are presented. Finally, a hierarchical classification of the soils relying on the tested parameters was performed by using the package dendextend (Galili, 2015). The number of groups was chosen according to the highest drop of inertia. All the graphics were drawn with the ggplot (Hadley, 2016), sjPlot and stats packages. Original data for all physical and chemical soil and plant parameters measured are presented in Supplemental Table S3.

Results

Soil classification and element analysis

To gain a first overview about the differences between the soils used in our study, we conduced principal component analysis (PCA) on the measured soil parameters (Figure 1A and

Supplemental text, Figure S1). All the studied soil parameters (percentage of fine particles, pH, available phosphorus (PCAL extractable) and potassium (KCAL extractable) quantities of plant available magnesium (Mg), nitrogen and zinc (Zn) had a similar contribution to the PCA and allowed a clear separation of the tested soils according to their geographical location (Figure 1A). Component 1 (PC1), explaining 39.8% of the variance of soil properties (Figure S1), was mostly associated with magnesium content, plant-available phosphorus (PCAL), plant-available potassium (KCAL) and pH. Samples with high Eigenvector values in PC1 were associated with high PCAL and alkaline pH but with low magnesium content and low KCAL. The percentage of fine particles accounts for almost 50% of the observed variance in the component 2 (PC2), which explains 24.4% of the variation in the dataset. Component 3 (PC3) displays the difference in nitrogen and, to a lesser extent, zinc content. Soils with high Eigenvector values in PC3 have high nitrogen and zinc contents (Figures S2, S3). We also classified the data by hierarchical ascendance using the studied parameters (Figures 1B, S4). With the exception of two samples gathered in Elxleben in 2018, all samples derived from the same location clustered in the same group (Figures 1B, S4).

When PCA was performed with nutrition-associated parameters measured in leaf and root samples grown in the different soils, the highest variance was between the leaves and the roots (Figures S5, S6). The segregation of the dataset into leaves and roots was mainly described by $\delta^{13}C$, nitrogen and potassium contents, as these parameters have the highest influence on PC1 (Figures S7, S8). Interestingly, when PC2 was plotted against PC4, the dataset was separated into the different locations from which the samples were derived (Figure 1C). PC2 explains 15.44% of the

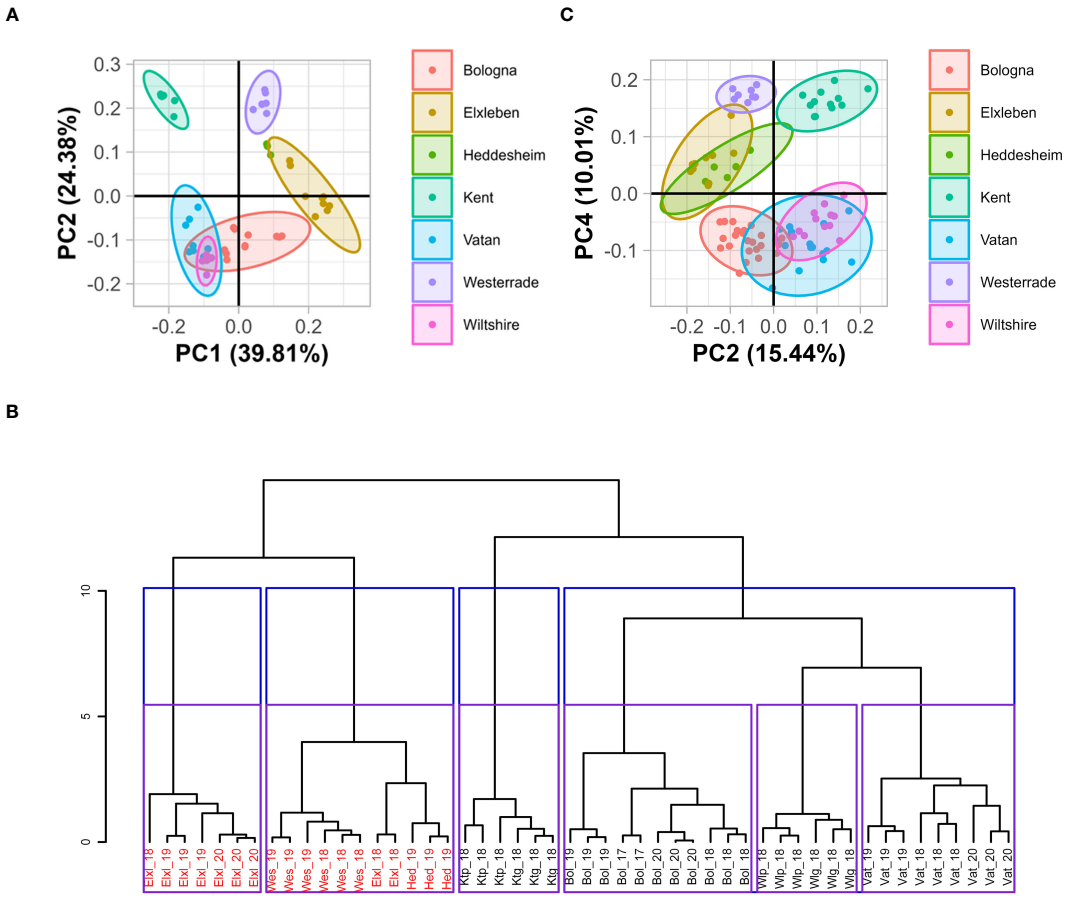

FIGURE 1
Presentation of the dataset obtained for soil data using PCA and hierarchical clustering **(A, B)** and of the dataset obtained for plant data using PCA **(C)**. **(A)** PCA on soil properties of the seven locations with seven parameters analyzed after normalization. Data were normalized to the mean of all samples for the respective measured parameter and divided by SD. 95% confidence intervals are represented by ellipses. No ellipse was drawn for Heddesheim data, as only three samples were available for this location. **(B)** Hierarchical classification by ascendance of the studied soils based on their physio-chemical properties. Bol: Bologna, Elxl: Elxleben, Hed: Heddesheim, Ktg: used Kent, Ktp: new Kent, Vat: Vatan, Wes: Westerrade, Wlg: used Wiltshire, Wltp: new Wiltshire. The number indicates the year of soil sampling. The ordinate shows the inertia of the analysis. Soils containing SBWMV are displayed in red, soils containing SBCMV are displayed in black. Blue and purple squares display the clustering in four or six groups, respectively as suggested by the analysis of the inertia drop (Figure S4). Three replicates of each soil per year were analyzed with the exception of Bol_17, where two replicates were analyzed. **(C)** Principal component analysis on element composition of leaf and root samples of plants grown in viruliferous *P. graminis*-containing soil using the second and fourth principal component. Samples were taken from plants grown in soils from the different fileds, respectively for 12 weeks. Thirteen parameters were analyzed after normalization (Figure S6). 95% confidence intervals are represented by ellipses.

variance, and the coordinates in PC2 represented high calcium, sulfur and zinc contents and low $\delta^{15}N$. Low molybdenum quantities and high $\delta^{13}C$ as well as carbon content values constituted high Eigenvector values in PC4 (Figures S7, S8).

Identification of vectors and viruses in relation to the soils and their physico-chemical properties

Presence of SBCMV and SBWMV in plants grown in different soils was analyzed by RT-qPCR. Consistent with previous findings (Kastirr and Ziegler, 2018), we found SBCMV in plants grown in soil from Bologna, Kent, Vatan and Wiltshire and SBWMV in plants grown in the soil from Elxleben, Heddesheim and Westerrade (Tables S4A, B). No co-infection with the respective other virus was observed. *P. graminis ssp. tepida* was identified in the roots of plants grown in soil form each location. By contrast, *P. graminis ssp. temperata* was only identified in the roots of plants grown in Elxleben, Kent and Vatan (Table S4B). Co-infections *with P. graminis ssp. tepida* and *temperata* occurred in Vatan (*Avalon*, 2020) and in Kent (*Prevert* and *durum Pescadou*, 2018). Interestingly, hierarchical ascendance clustering revealed a clear separation of soils in which SBWMV and soils in which SBCMV was present (Figure 2, red and black writing), demonstrating that SBWMV and SBCMV require different soil parameters. The classification by hierarchical ascendance did not highlight any relation between soil properties and *P. graminis* subspecies. No relation between virus species and vector subspecies was established either.

Analysis of infection rates

SBCMV infection rates ranged from 0% to 88.2% (Figure 2A), and SBWMV infection rates ranged from 10.2% to 92.6% (Figure 2B). Thus, we concluded that the data set contained enough variability to investigate the influence of soil- and nutrition parameters on infection efficiency. The factors field ($p=2.75E^{-4}$) and year ($p=2.90E^{-5}$) significantly affected SBCMV infection rates, while the cultivar did not (p=0.45). SBWMV infection rates were influenced by the interactions between year and field factors ($p=9.60E^{-3}$) and between cultivar and field (p=0.014).

To investigate the influence of soil properties on SBCMV and SBWMV infection rates and predict the influence of specific parameters on virus infection rates, different modeling approaches were applied and compared. We used STBM as a simple means to identify the most significant parameters and compared it with the results obtained by using MAVG. MAVG reveals all possible relevant contributions and finds the best model to describe the data, according to AIC or QAIC. However, MAVG is prone to generate underdispersed models by maintaining non-significant parameters, especially when the number of tested parameters is high. Thus, we combined STBM and MAVG approaches and applied a stepwise model averaging (ST-MA) approach.

Concerning the influence of soil proprieties on SBCMV infection rates, STBM identified only the interaction between soil pH and the percentage of fine particles as relevant factors to explain the observed differences in SBCMV infection rates (p=0.023, Table 1). By contrast, MAVG did not identify any significant parameter. The ST-MA analysis identified the amount of fine particles ($p=1.94E^{-7}$), magnesium ($p=1.61E^{-11}$), PCAL (p=0.021) and pH ($p=1.19E^{-11}$) as parameters to explain the observed differences in SBCMV infection rates (Table 1). PCAL, however, weighed less in the ST-MA model compared to the other factors (relative importance of 0.15 against 1 for all other factors).

SBWMV infection rates turned out to be influenced by the interaction between the amount of zinc and the percentage of fine particles (p=0.01), as well as by PCAL ($p=5.6E^{-3}$), when the STBM procedure was used (Table 2). MAVG identified the interaction between the quantity of fine particles in the soil and PCAL (p=0.024) and the interaction between zinc content and PCAL ($p=1.3E^{-4}$) as factors influencing SBWMV infection rates and ST-MA resulted in the same predictions for SBWMV infection rates compared to the MAVG procedure.

We also applied the modeling approaches to the plant samples to investigate if the concentration of specific nutrients inside plant roots and leaves may influence infection. For SBCMV, STBM identified $\delta^{15}N$ as factor to explain the observed differences in SBCMV infection rates in leaves ($p=1.87E^{-4}$) and roots ($p=3.04E^{-5}$) (Tables 3, 4). MAVG identified the interaction between $\delta^{15}N$ and calcium content (p=0.011), as well as the interaction between calcium and sulfur contents (p=0.009) and between boron and potassium (p=0.027) to influence SBCMV infection rates in leaves. For roots, MAVG predicted an influence of copper (p=0.038) and the interaction between boron and calcium (p=0.049) contents on SBCMV infection rates. ST-MA predicted the interaction between calcium and the sulfur quantities ($p=1.78E^{-4}$), boron ($p=5.29E^{-8}$) and copper (p=0,011) content, as well as $\delta^{15}N$ ($p=6.70E^{-6}$) to influence SBCMV infection rates in leaves (Table 3). For roots, ST-MA identified the interaction of calcium with boron ($p=3.58E^{-4}$) and sulfur with boron (p=0.011), interaction between calcium and sulfur ($p=2.0E^{-3}$), interaction between calcium and $\delta^{15}N$ ($p=1.00E^{-3}$), and interaction between copper and potassium ($p=3.00E^{-3}$) influencing SBCMV infection rates (Table 4).

For leaves, concerning SBWMV, STBM identified the interaction between carbon and manganese content ($p=5.2E^{-4}$) along with $\delta^{13}C$ (p=0.033) as the only significant factors explaining SBWMV infection rates variation (Table 5). MAVG further identified interactions between $\delta^{13}C$ and carbon content ($p=1.45E^{-4}$) between $\delta^{13}C$ and manganese content (p=0.014) to influence SBWMV infection rates. Interaction between carbon and nitrogen content was also shown to have an influence ($p=5.75E^{-4}$). ST-MA identified the interaction between the carbon and manganese content ($p=3.00E^{-3}$) as influencing the SBWMV infection rates while the $\delta^{13}C$ lost its significance upon averaging (p=0.065). $\delta^{13}C$ was however represented in 85% of the tested models. For roots, all three modeling approaches (STBM, MAVG and ST-MA) failed to identify any relevant effect linked to SBWMV infection rates.

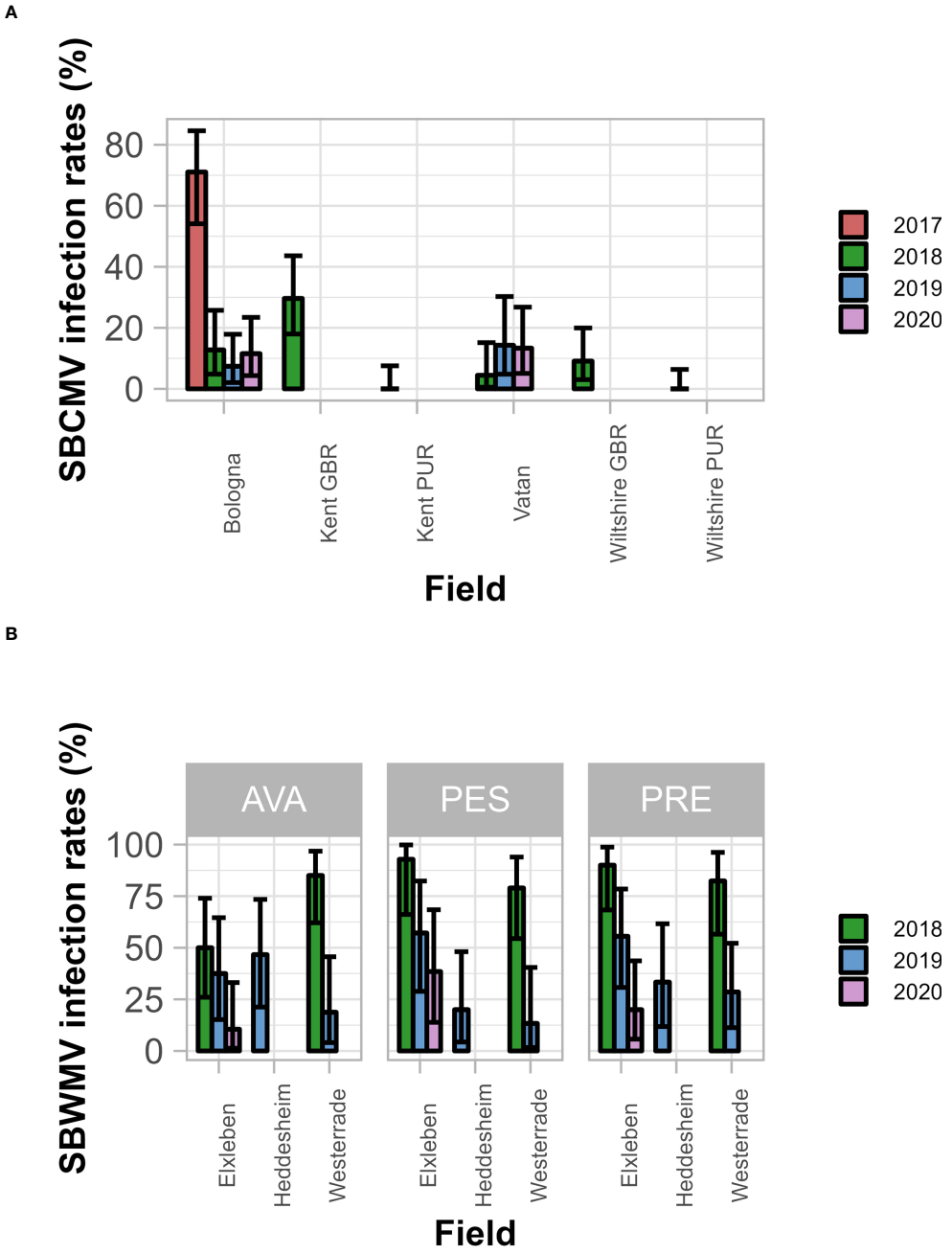

FIGURE 2
SBCMV **(A)** and SBWMV **(B)** infection rates of the different cultivars. Only the significant parameters for each virus are presented. Error bars represent 95% confidence intervals. A generalized linear mixed effects model was applied and significance determined *via* ANOVA. **(A)**, infection rates differ between soils (p=2.75E-4) and years (p=2.90E-5); not between the cultivars (p=0.45); **(B)**, infection rates differ between soil – year interaction (p=0.0096) and between soil - cultivar interaction (p=0.014). AVA, Avalon; PES, Pescadou; PRE, Prevert. Error bars represent 95% confidence intervals.

Prediction of SBCMV and SBWMV infection rates based on the factors identified by the different algorithms

For the prediction analysis, we chose STBM and ST-MA procedures, as these procedures led to the identification of the most crucial soil and nutrient parameters influencing infection rates without the risk of keeping non-significant factors. Using the factors identified by the element analysis of soil, STBM predicted SBCMV infection rates to increase from 5% to 87% for a percentage of fine particles in the soil of 32.03% when pH increased from slightly acidic to slightly alkaline (6.45 to 7.5). For the same pH values, infection rates were predicted to increase from 5% to 25% for 37.26% of fine particles. In contrast, for 42.48% fine particles, the percentage of infection was predicted to decrease from 5% to 0% when pH Increased from 6.5 to 7.5 (Figure 3A) Thus, according to the STBM model, an decreasing amount of fine particles, coupled with an increasing pH from slightly acidic to slightly alkaline

TABLE 1 Summary of the effects of soil parameters on SBCMV infection rates according to the three tested models.

Model	STBM			MAVG			ST-MA			
Factor	Value	Error	sg	Value	Error	sg	Value	Error	sg	Weight
Intercept	-138.8	57.16	0.02*	-4675.4	2663983.1	0.999	-26.981	5.265	2.98E-07***	NT
pH	21.13	8.56	0.325	449.0	360259.0	0.999	4.146	0.611	1.19E-11***	1
FP	3.45	1.58	0.0625	191.4	16458.8	0.991	-0.240	0.046	1.94E-07***	1
pH x FP	-0.53	0.24	0.023*	-20.1	2453.1	0.993	NT	NT	NT	NT
Mg	NT	NT	NT	36.5	69084.1	1.000	0.363	0.054	1.61E-11***	1
PCAL	NT	NT	NT	-226.4	122025.1	0.999	0.140	0.061	0.021*	0.15
FP x Mg	NT	NT	NT	-1.1	226.2	0.996	NT	NT	NT	NT
FP x PCAL	NT	NT	NT	-5.5	595.7	0.993	NT	NT	NT	NT
Mg x pH	NT	NT	NT	-8.0	7096.3	0.999	NT	NT	NT	NT
PCAL x pH	NT	NT	NT	60.5	18706.7	0.997	NT	NT	NT	NT
Mg x PCAL	NT	NT	NT	6.7	845.2	0.994	NT	NT	NT	NT

sg, significance; NT, not tested (the parameter was not included in the respective model); intercept, intercept of the model; FP, Amount of fine particles (%); PCAL, Calcium acetate lactate extractable phosphate (mg*100g^{-1} dry soil); Mg, plant-available magnesium (mg*100g^{-1} dry soil). Significance of effects is indicated by a 0.05 (*) and 0.001 (***) threshold.

increases SBCMV infection rates. Consistent with our results from STBM, ST-MA predicted an increase of SBCMV infection rates when pH increased from 6.45 to 7.5. This increase in SBCMV infection rates was higher, when more magnesium was present in the soil. In addition, increasing PCAL increased infection rates (Figure 3B). Moreover, a lower fine particle content was predicted to increase SBCMV infection compared to higher content of fine particles (Figure 3B).

For leaves and roots we predicted that δ15N decreased SBCMV infection rates about 90% in the leaves and 60% in the roots according to STBM (Figures 4A, 5A). When ST-MA was used to model the effect of elements in leaves, decreasing δ^{15}N levels also led to increasing SBCMV infection rates (Figure 4B). Moreover, a boron content augmentation from 4.7 to 15.1 ppm is predicted to increase SBCMV infection rates by 30%. Calcium and sulfur in leaves were predicted to synergistically affect SBCMV infection rates in leaves. SBCMV infection rates were high when calcium and sulfur were low or when both were high. When one of the two parameters was high and the other low, infection rates dropped (Figure 4B). ST-MA further predicted a 10% increase of SBCMV infection rates when copper content of leaves decreased from 12.67 to 4.70 ppm (result not displayed).

Among the factors predicted by ST-MA to influence infection rates in roots, was an increase of the SBCMV infection rates when δ^{15}N decreased and calcium content increased (Figure 5B). ST-MA further predicted an up to 60% increase in SBCMV infection rates when boron quantity increased (from 1.7 ppm to 6.7 ppm). This effect was most prominent when sulfur quantities were low. By contrast, SBCMV infection rates were predicted to increase up to 75% when sulfur quantity decreased (from 0.23% to 0.10%); this effect was more pronounced when boron quantities were low and calcium quantities high. However, ST-MA also predicted that the effects of δ^{15}N, boron and sulfur are reversed, when calcium quantity drops under 0.74% (Figure 5, limit not shown).

With respect to SBWMV infection rates, STBM predicted increased infection rates for soils with fine particle content of 29.3

TABLE 2 Summary of the effects of soil parameters on SBWMV infection rates according to the three tested models.

Model	STBM			MAVG			ST-MA			
Factor	Value	Error	sg	Value	Error	sg	Value	Error	sg	Weight
Intercept	71.34	20.57	0.004**	-123.46	68.03	0.070	-123.46	68.03	0.070	NT
Zn	-13.88	4.94	0.167	-2.31	14.93	0.877	-2.31	14.93	0.877	1
FP	-2.25	0.72	0.298	4.37	2.63	0.097	4.37	2.63	0.097	1
PCAL	-0.96	0.33	5.6E-3**	29.43	4.90	1.93E-09***	29.43	4.90	1.93E-09***	1
Zn x FP	0.47	0.17	0.01**	NT	NT	NT	NT	NT	NT	1
PCAL x FP	NT	NT	NT	-0.99	0.44	0.024*	-0.99	0.44	0.024*	0.83
Zn x PCAL	NT	NT	NT	-1.70	0.45	0.00013***	-1.70	0.45	0.00013***	1

sg, significance; NT, not tested (the parameter was not included in the respective model); intercept, intercept of the model; FP, Amount of fine particles (%); PCAL, Calcium acetate lactate extractable phosphate (mg*100g^{-1} dry soil); Zn, plant-available zinc content (mg*kg^{1} dry soil). Significance of effects is indicated by a 0.05 (*), 0.01 (**), and 0.001 (***) threshold.

TABLE 3 Summary of the effects of nutrients measured in leaves on SBCMV infection rates according to the three tested models.

Model	STBM			MAVG			ST-MA			
Factor	Value	Error	sg	Value	Error	sg	Value	Error	sg	Weight
Intercept	2.08	0.88	0.02*	*3.42*	21.4	0.872	6.232	1.758	3.94E-04***	1
$\delta^{15}N$	-0.51	0.12	1.87E-04***	1.33	1.72	0.439	-0.513	0.114	6.70E-06***	1
B	NT	NT	NT	3.86	2.05	0.060	0.208	0.038	5.29E-08***	1
Cu	NT	NT	NT	-1.76	2.48	0.476	-0.168	0.066	0.011*	1
S	NT	NT	NT	-8.49	30.11	0.778	-25.884	7.059	2.45E-04***	1
Ca	NT	NT	NT	-64.95	27.62	0.019*	-4.705	1.447	1.14E-03***	1
K	NT	NT	NT	8.56	9.84	0.384	NT	NT	NT	NT
B x Cu	NT	NT	NT	-0.02	0.04	0.502	NT	NT	NT	NT
Cu x S	NT	NT	NT	-6.71	4.09	0.101	NT	NT	NT	NT
B x S	NT	NT	NT	0.06	1.69	0.974	NT	NT	NT	NT
Cu x $\delta^{15}N$	NT	NT	NT	-0.16	0.38	0.672	NT	NT	NT	NT
B x $\delta^{15}N$	NT	NT	NT	-0.31	0.16	0.056	NT	NT	NT	NT
$\delta^{15}N$ x Ca	NT	NT	NT	5.29	2.1	0.011*	NT	NT	NT	NT
Cu x Ca	NT	NT	NT	6.44	4.59	0.161	NT	NT	NT	NT
$\delta^{15}N$ x K	NT	NT	NT	-1.31	0.84	0.119	NT	NT	NT	NT
B x Ca	NT	NT	NT	-3.22	2.02	0.110	NT	NT	NT	NT
S x Ca	NT	NT	NT	60.71	23.53	0.009**	24.327	6.487	1.78E-04***	1
B x K	NT	NT	NT	0.83	0.38	0.027*	NT	NT	NT	NT
Cu x K	NT	NT	NT	-0.70	1.03	0.497	NT	NT	NT	NT
S x K	NT	NT	NT	-0.98	16.20	0.952	NT	NT	NT	NT

sg, significance; NT, not tested (the parameter was not included in the respective model); intercept, intercept of the model. $\delta^{15}N$, $^{15}N/^{14}N$ isotopic ratio in the leaves; B, boron content in the leaves (ppm); Cu, copper content in the leaves (ppm); S, sulfur content in the leaves (%); Ca, calcium content in the leaves (%); K, potassium content in the leaves (%). Significance of the effects is indicated by a 0.05 (*), 0.01 (**), and 0.001 (***) threshold.

mg*100g^{-1} dry soil and 40.3 mg*100g^{-1} dry soil (Figure 6A). For these high soil fine particle contents, a higher zinc content was predicted to further increase infection rates. For soils with a fine particle content of 18.4% mg*100g^{-1} dry soil and 19% mg*100g^{-1} dry soil, infection rates were predicted to decrease at a zinc content above 4.2 mg*kg dry soil^{-1} when the PCAL values were 4.43 mg*100g^{-1} dry soil or lower. At higher PCAL levels, the decrease in infection rates was more prominent and occurred already at lower since content.

According to ST-MA, drastically reduced (100%) SBWMV infection rates were predicted at high PCAL values for soils with a high fine particle content (Figure 6B). By contrast, soils with low percentage of fine particles, infection rates were predicted to be high at high PCAL and high zinc concentrations. When the STBM and ST-MA algorithms were applied to model the effect of elements measured in leaves on SBWMV infection rates, both predicted very similar effects for the same set of parameters. The two models predicted increased infection rates at carbon contents above 38% and between 20ppm and 40 ppm manganese, and reduced infection rates at higher manganese concentrations (Figure 7). At low levels of carbon (38%), SBWMV infection rates were not influenced by manganese content. Furthermore, SBWMV infection rates increased at lower $\delta^{13}C$ levels (Figure 7). None of the models achieved to predict SBWMV infection rates using the samples derived from roots.

Analysis of the adequacy of the predictive model with respect to the observed data

Most of the models fitted the data with an R^2 ranging from 0.47 to 0.89 for STBM and from 0.60 to 0.91 for ST-MA when plotting their respective predicted infection rates against the observations (Figure 8 and Table S5). ST-MA performed better than STBM to predict infection rates of both SBCMV and SBWMV using soil parameters. ST-MA was better compared to STBM to predict SBCMV infection rates in root samples and SBWMV infection rates in leaf samples. ST-MA was calculated to have 3% (SBWMV, leaves) and 17% (SBWMV, roots) probability to lose information compared to 0.1% (SBCMV, leaves) and 27% (SBCMV, roots) respectively. By contrast, STBM performed better to predict SBCMV infection rates in leaf samples based on the measured

10.3389/fpls.2023.1200674

TABLE 4 Summary of the effects of nutrients measured in roots on SBCMV infection rates according to the three tested models.

Model	STBM			MAVG			ST-MA			
Factor	Value	Error	sg	Value	Error	sg	Value	Error	sg	Weight
Intercept	2.57	0.85	0.005**	-66.63	32.06	0.038*	-39.219	9.983	8.55E-05***	1
$\delta^{15}N$	-0.63	0.13	3.04E-05***	2.740	2.376	0.249	1.731	0.522	9.09E-04***	1
B	NT	NT	NT	0.785	2.181	0.718	0.394	0.427	0.355	1
Cu	NT	NT	NT	0.825	0.398	0.038*	0.600	0.187	1.37E-03**	1
S	NT	NT	NT	192.0	110.5	0.082	104.977	29.773	4.22E-04***	1
Ca	NT	NT	NT	66.97	50.86	0.188	15.571	6.661	0.019*	1
K	NT	NT	NT	2.635	3.323	0.937	12.414	4.541	0.006**	1
B x Cu	NT	NT	NT	-0.012	0.027	0.641	NT	NT	NT	NT
Cu x S	NT	NT	NT	-1.570	0,983	0.873	NT	NT	NT	NT
B x S	NT	NT	NT	-21.74	13.39	0.105	-9.929	3.882	0.011*	1
Cu x $\delta^{15}N$	NT	NT	NT	8.3 E-04	0.016	0.958	NT	NT	NT	NT
B x $\delta^{15}N$	NT	NT	NT	0.219	0.215	0.308	NT	NT	NT	NT
$\delta^{15}N$ x Ca	NT	NT	NT	-8.58	5.874	0.144	-2.674	0.813	0.001**	1
Cu x Ca	NT	NT	NT	-0.314	0.237	0.184	NT	NT	NT	NT
$\delta^{15}N$ x K	NT	NT	NT	1.610	3.532	0.649	NT	NT	NT	NT
B x Ca	NT	NT	NT	5.276	2.683	0.049*	2.287	0.641	3.58E-04***	1
S x Ca	NT	NT	NT	-140.4	104.7	0.180	-57.224	18.36	0.002**	1
B x K	NT	NT	NT	-1.495	1.119	0.181	NT	NT	NT	NT
Cu x K	NT	NT	NT	-0.481	0.254	0.058	-0520	0.175	0.0030**	1
S x K	NT	NT	NT	30.26	94.48	0.749	NT	NT	NT	NT

sg, significance; NT, not tested (the parameter was not included in the respective model); intercept, intercept of the model $\delta^{15}N$, $^{15}N/^{14}N$ isotopic ratio in the roots; B, boron content in the roots (ppm); Cu, copper content in the roots (ppm); S, sulfur content in the roots (%); Ca, calcium content in the roots (%); K, potassium content in the roots (%). Significance of the effects is indicated by a 0.05 (*), 0.01 (**), and 0.001 (***) threshold.

TABLE 5 Summary of the effects of nutrients measured in leaves on SBWMV infection rates according to the three tested models.

Model	STBM			MAVG			ST-MA			
Factor	Value	Error	sg	Value	Error	sg	Value	Error	sg	Weight
Intercept	-31.5	8.470	2E-04**	-925.2	267.1	5.32E-04***	-29.57	9.015	0.036*	1
C% dm	0.59	0.183	1.2E-03**	25.39	6.843	2.07E-04**	0.594	0.183	0.005**	1
Mn	0.50	0.150	8,1 E-04***	-0.692	0.510	0.175	0.492	0.150	0.004**	1
$\delta^{13}C$	-0.30	0.142	0.033*	-35.87	9.544	1.71E-04***	-0.302	0.142	0.065	0.79
C% dm x Mn	-0.01	0.004	5,2 E-04***	-0.008	0.009	0.354	-0.013	0.004	0.003**	1
N%	NT	NT	NT	-202.7	92.93	0.029*	NT	NT	NT	NT
C% dm x N% dm	NT	NT	NT	2.784	0.808	5.75E-04***	NT	NT	NT	NT
C% dm x $\delta^{13}C$	NT	NT	NT	0.959	0.252	1.45E-04***	NT	NT	NT	NT
$\delta^{13}C$ x Mn	NT	NT	NT	0.038	0.015	0.014*	NT	NT	NT	NT
N% dm x $\delta^{13}C$	NT	NT	NT	-2.724	2.253	0.226	NT	NT	NT	NT
N% dm x Mn	NT	NT	NT	0.234	1.861	0.208	NT	NT	NT	NT

sg, significance; NT, not tested (the parameter was not included in the respective model); intercept, intercept of the model. C% dm, carbon content in the leaves (% dry matter (dm)); Mn, manganese content in the leaves (ppm); δ13C, $^{13}C/^{12}C$ isotope ratio in the leaves; N% dm, nitrogen content in the leaves (% dry matter (dm)). Significance of the effects is indicated by a 0.05 (*), 0.01 (**), and 0.001 (***) threshold.

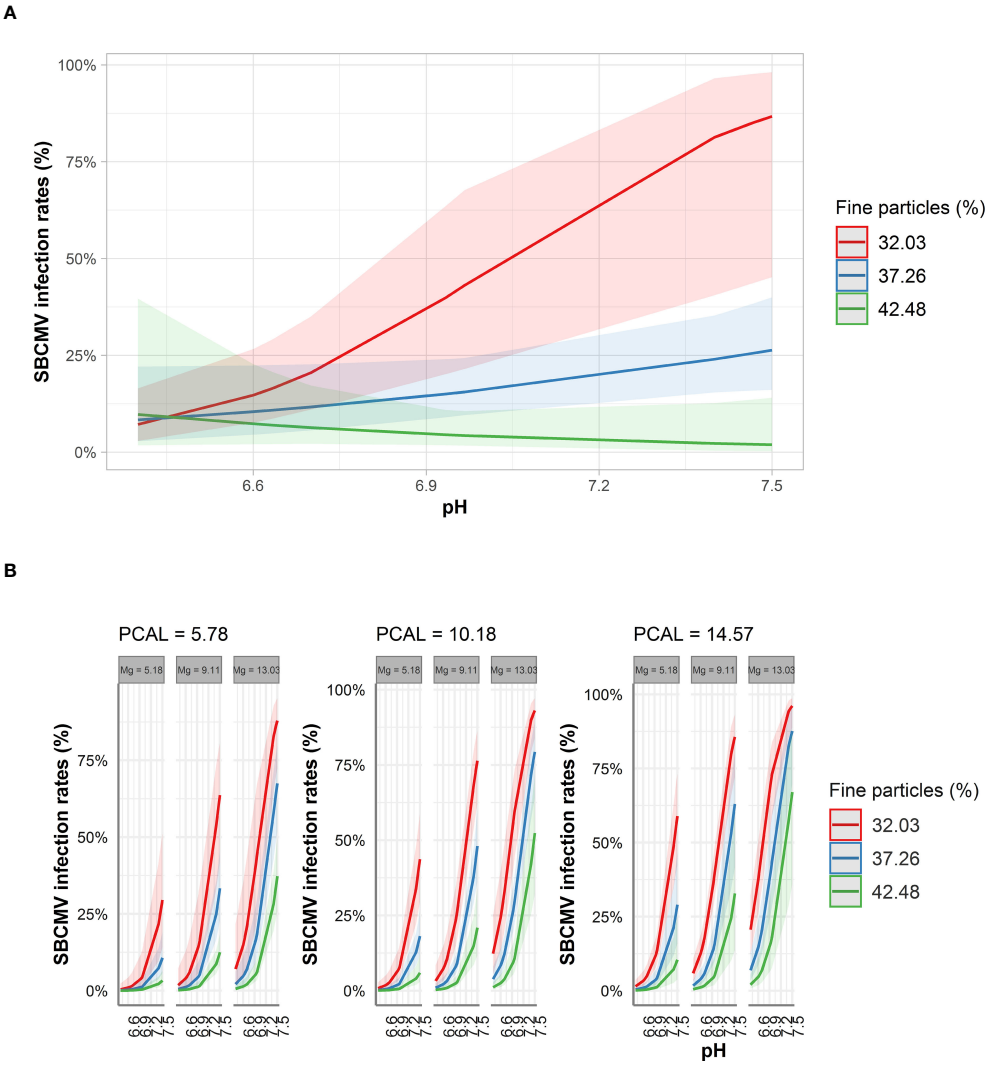

FIGURE 3
Predicted SBCMV infection rates based on soil parameters identified by STBM **(A)** and ST-MA **(B)**. Only the significant parameters for each model are presented. The colored zones depict 95% confidence intervals. Mg: plant-available magnesium (mg*100g^{-1} dry soil), PCAL: Calcium acetate lactate extractable phosphate (mg*100g^{-1} dry soil).

parameters (with less than 0.1% probability to lose information by choosing ST-MA instead of STBM).

Discussion

Intrinsic soil parameters differentiate between the different origins of the soil and virus species present

In our study, we unraveled soil-related environmental factors influencing furovirus infection. We reasoned that soil, as it represents the support for *P. graminis* survival and mobility as well as the source for plant nutrition (Rao and Brakke, 1969; Kanyuka et al., 2003) may represent a key factor to influence furovirus epidemiology. We found that the interplay between soil nutrients, pH and soil structure resulted in a clear differentiation between the different soils as shown by PCA. Surprisingly, hierarchical ascendance clustering revealed a clear separation between SBWMV- and SBCMV infested soils, suggesting that each virus requires specific and distinct soil conditions for efficient infection, and that the measured parameters reflect these conditions. However, it is likely that the measured parameters are coupled to additional parameters not measured in this study, such as soil organic matter (Dequiedt et al., 2011), microbiome (Coller et al., 2019) or micronutrient composition (Hengl et al., 2017). As the availability of nutrients determines the nutritional status of plants (Holford and Mattingly, 1976; Sparks, 1980; Calabrese et al., 2017; Weih et al., 2018; Calabrese et al., 2019) it is important to also examine the differences in nutrients absorbed by plants grown in the different locations.

The specific soil parameters that are predicted to influence furovirus infection rates in wheat presumably modulate *P. graminis* infection

Our study led to the identification of several soil factors influencing furovirus infection rates. Viruses, as obligate intracellular pathogens are unlikely to be directly affected by modulated soil parameters, in contrast to *P. graminis*, which lives in the soil. Therefore, furovirus infection rates probably represent a readout for *P. graminis* infection efficiency. However, a direct influence of the identified parameters on virus infection cannot be excluded.

The content of fine particles and plant available phosphorus (PCAL) was identified as parameters influencing infection rates of both virus species studied. In particular, ST-MA established that a decrease in soil fine particle quantity, leading to an increase of soil permeability (Alyamani and Şen, 1993) and an increase in plant available phosphorous increased SBWMV and SBCMV infection rates. These observations suggest that infection is promoted by permeable soils, facilitating the swimming of *P. graminis* zoospores to reach target root cells. Our results are consistent with previous studies, which used sand to multiply *P. graminis* (Adams and Swaby, 1988) or identified furovirus infection mostly in sandy soils (Kastirr et al., 2018). With respect to PCAL, which represents only the plant available part of the total phosphorous present in soils, a positive correlation was established between this parameter and furovirus infection rates. Interestingly, also amoeba abundance has been shown to increase in soils with increasing amounts of available phosphorous (Olatunji et al., 2018), supporting the idea that the germination of *P. graminis* zoospores from resting spores may be induced by the amount of available phosphorous. Consistently, it has been shown that root exudates as well as nutrient solution stimulate *Spongosphora subterranea* zoospore germination (Balendres et al., 2016; Balendres et al., 2018; Amponsah et al., 2021). Hence,

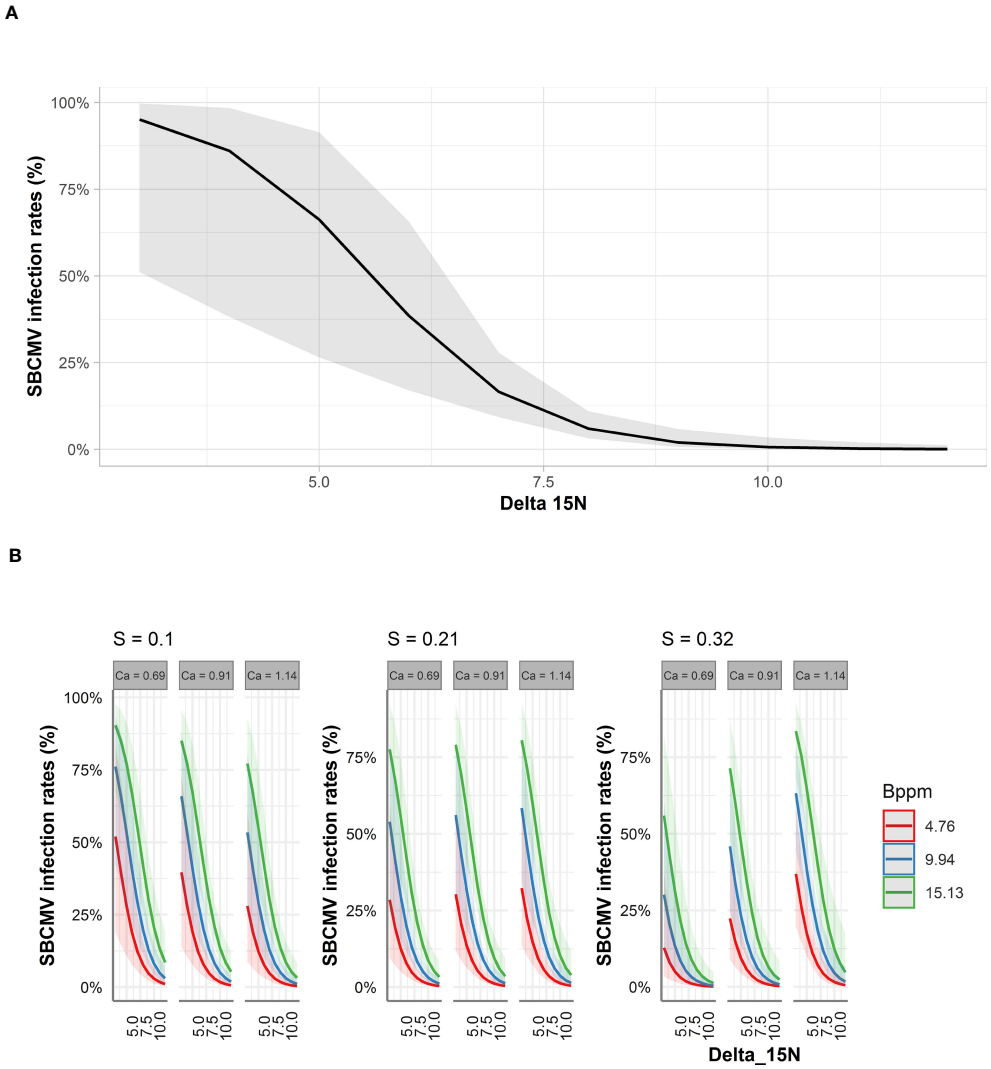

FIGURE 4
Predicted SBCMV infection rates based on STBM **(A)** and ST-MA **(B)** modeling of element data measured in leaves. Only the significant parameters for each model are presented. The colored zones depict 95% confidence intervals. Delta_15N: $^{15}N/^{14}N$ isotope ratio in the leaves, S: % sulfur content in the leaves, Ca: % calcium content in the leaves, Bppm: boron (ppm) content in the leaves.

increased plant-available P or increased soil fertility may lead to increased root exudation and consequently increased zoospore germination. Whether this would be for the benefit of infection or to its disadvantage may depend on other parameters like soil permeability and pH, which we indeed identified as parameters influencing infection rates in our models. With respect to pH, it is known that an increase in soil pH inhibits spore germination, a fact used in liming practices for agricultural management (Hwang et al., 2014; Amponsah et al., 2021). However, we only found an influence of pH on SBCMV infection rates in our experiments and our natural soil conditions only ranged from slightly acid to slightly alkaline. A slightly alkaline pH increased infection rates according to our models. Thus, factors coming along with a more alkaline pH, such as increased nitrification, may explain the increased infection rates at increased pH. Along with the before mentioned factors, an influence of Zn for SBWMV infection rates and Mg for SBCMV infection rates was detected. The influence of Zn on infection rates depended on the other parameters, i.e. fine particles and PCAL. Zn ions were shown to rapidly immobilize *P. graminis* zoospores in solution or at concentrations above 10 µg ml^{-1} (Adams and Swaby, 1988). For SBCMV, ST-MA predicted higher infection rates at higher Mg concentrations in the soil. A study on clubroot disease also identified magnesium as a factor influencing infection and clubbing (Myers and Campbell, 1985).

Plant nutrient composition allows differentiation between SBCMV and SBWMV-infected soils and the prediction of parameters influencing infection rates

When PCA was performed with the measured plant parameters, the separation of the dataset into SBWMV and SBCMV-infected soils still occurred when PC2 was plotted vs. PC4 (Figure 1C). The highest variation in the dataset was explained by PC1 and related to the separation of the samples

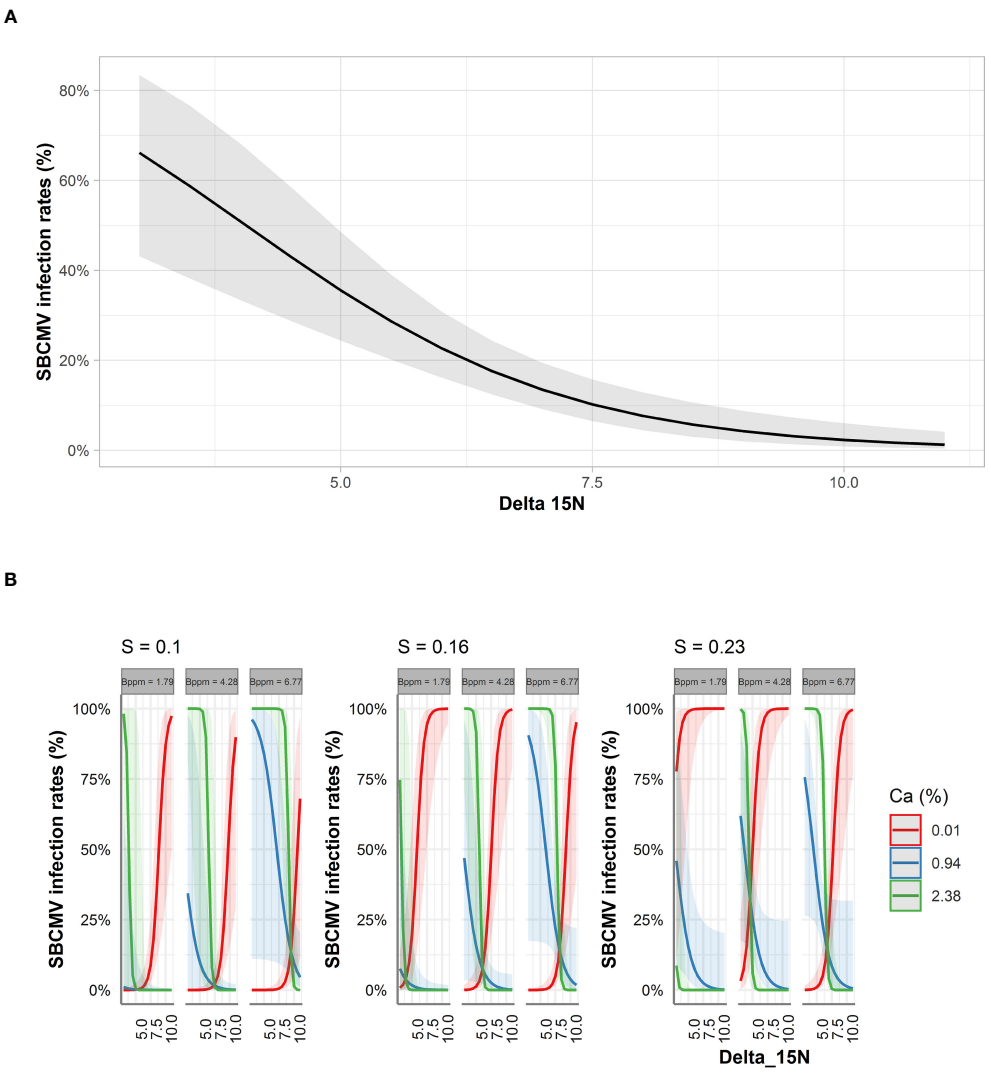

FIGURE 5
Predicted SBCMV infection rates based on STBM **(A)** and ST-MA **(B)** modeling of element data measured in roots. Only the significant parameters for each model are presented and only the four most represented parameters are shown in the figure. The colored zones depict 95% confidence intervals. Delta_15N: $^{15}N/^{14}N$ isotope ratio in the roots, S: % sulfur content in the roots, Bppm: boron (ppm) content in the roots, Ca: % calcium content in the roots.

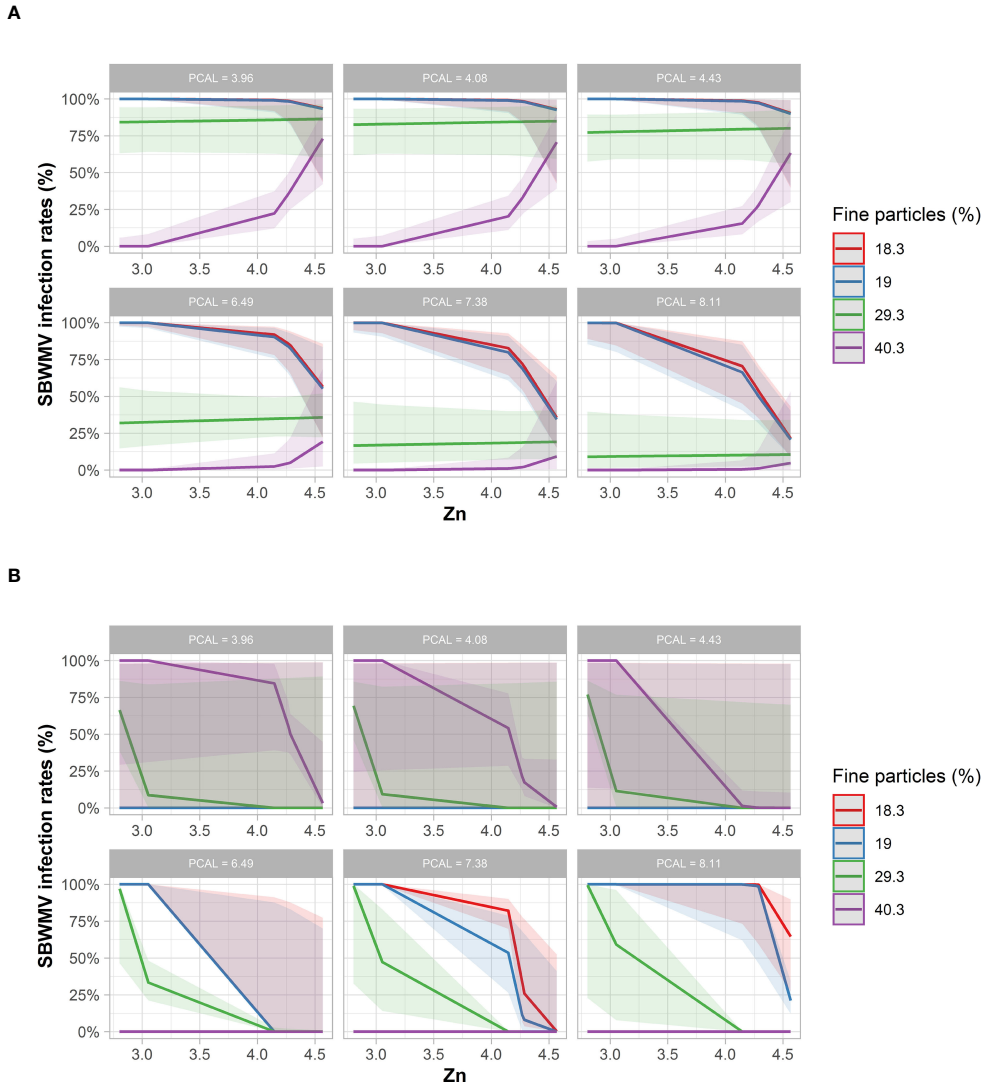

FIGURE 6
Predicted SBWMV infection rates based on soil parameters identified through STBM **(A)** and ST-MA **(B)**. Only the significant parameters for each model are presented. The colored zones depict 95% confidence intervals. PCAL: Calcium acetate lactate extractable phosphate (mg*100g^{-1} dry soil), Zn: plant-available zinc (mg*kg^{1} dry soil).

taken from leaves and roots, respectively. SBWMV and SBCMV are closely related viruses, sharing between 75% and 80% of homology on both RNAs (King et al., 2011) and are transmitted by same vector species. The fact that plant parameters can lead to the discrimination of SBWMV and SBCMV-infected soils suggests that either the difference in soil parameters selecting for SBWMV or SBCMV is reflected at the plant level or that the plant nutritional status, which is dependent on the soil parameters, supports infection by one or the other virus, respectively. We did not find significant differences in *P. graminis* species present in the roots of plants grown in SBWMV and SBCMV infected soils. This further confirms that the identified effects *in planta* are unlikely triggered or favored by *P. graminis* which is the common vector of both viruses.

Our models revealed common factors, which significantly influenced SBCMV infection rates in leaves and roots. It is important to stress, that we used natural field soils, thus the parameters we identify are parameters influencing infection under natural conditions. In contrast, many studies focusing on the influence of minerals on pathogen infection were conducted either with cultivated pathogens or by supplementing the tested nutrients, possibly in concentrations differing from *in vivo* situations (e.g. Holford and Mattingly, 1976; Aulakh and Dev, 1978; Adams and Swaby, 1988; Shevchenko et al., 2004; Soliman et al., 2020). In our study, one of the parameters identified to negatively influence infection rates was the increase of δ^{15}N. Moreover, ST-MA predicted similar effects of the interaction between sulfur and calcium contents and of boron content in roots and leaves. The similarity of the observations obtained with two paired datasets (leaves and roots) confirms the robustness of the analysis.

Ratios of stable N-isotopes in plants reflect δ^{15}N values in acquired N-sources (from soil and fertilizers) and the isotope

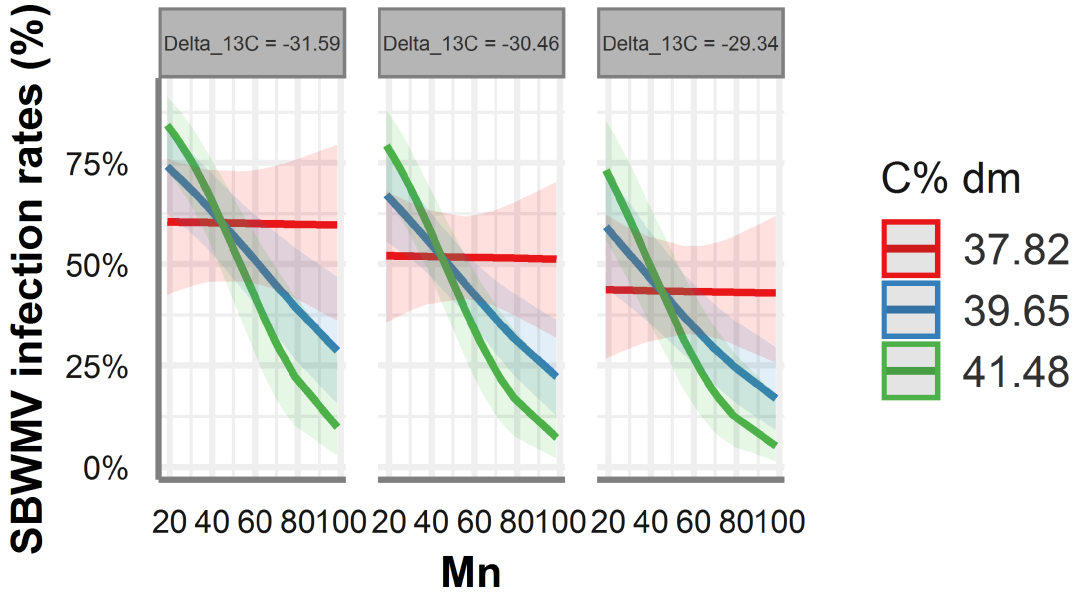

FIGURE 7
Predicted SBWMV infection rates based on modeling of element data measured in leaves. Only the significant parameters for the model are presented and only the four most represented parameters are shown in the figure. The colored zones depict 95% confidence intervals. Delta_13C: $^{13}C/^{12}C$ isotope ratio in the leaves, C% dm: % carbon content in the leaves, Mn: manganese (ppm) content in the leaves.

discrimination in various metabolic processes (Craine et al., 2015). Losses of ^{15}N depleted NH_3, N_2, N_2O and nitrate by volatilization, nitrification and denitrification in soils with high N-availability enrich the remaining soil pool by ^{15}N (Szpak, 2014). Plants from soils fertilized with animal manures have higher $\delta^{15}N$ (Choi et al., 2003; Szpak, 2014). Soil microbial biomass is ^{15}N enriched and interaction with mycorrhiza accounts for variation in the isotope ratio (Hobbie and Högberg, 2012; Craine et al., 2015). Soil organic matter gets ^{15}N enriched with age and extent of decomposition (Szpak, 2014). Soil microbial biomass and organic matter are again related to soil texture and pH (Dequiedt et al., 2011).

A higher $\delta^{15}N$ value indicates conditions rich in organic nitrogen (Ariz et al., 2011; Craine et al., 2015), thus favorable for plant development. Nitrogen is also important for the biosynthesis of active plant defense compounds (Calabrese et al., 2017; Mur et al., 2017; Verly et al., 2020; Ding et al., 2021). Therefore, the predicted drop of SBCMV infection rates at high $\delta^{15}N$ values could result, e.g. from interactions with soil microbiota or soil organic matter detrimental to the vector *Polymyxa graminis* or from increased plant fitness and capacity for active defense. A depletion of shoot and root $\delta^{15}N$ related to pathogens has been described for viruses and nematodes in *Petunia* by Neilson et al. (1999). They consider natural abundances of stable isotopes as subtle integrators of whole-plant physiology and attribute changes in $\delta^{15}N$ to metabolic reactions to the pathogens.

The increase of SBCMV infection rates with increasing boron quantities in leaves is consistent with studies showing increased boron quantities in virus infected plants (Overholt et al., 2009; Adkins et al., 2013), which may suggest that increased boron levels upon virus infection are a consequence of viral infection rather than a causality. However, boron is toxic at high concentrations, (e.g.(Camacho-Cristóbal et al., 2008; Hua et al., 2021). Boron toxicity could stress the plants and consequently weaken immunity to SBCMV infection. However, boron has also been described to limit virus symptoms in grapevine plants (Buoso et al., 2020). In the roots, the effect of boron differed dependent on calcium and sulfur levels. Sulfur is known to play an important role in plant defense as element in signaling- or defense molecules (Künstler et al., 2020; Zenda et al., 2021). Consistent with our data predicting an interaction of sulfur and calcium levels on SBCMV infection in leaves and roots, a recent study investigating the role of sulfur and calcium in plant fitness describes a role of both nutrients on photosynthetic performance and nitrogen metabolism in Indian mustard (Singh et al., 2018). Our study predicts a reduction of SBCMV infection rates in roots at increasing sulfur and calcium levels, but an opposite effect when only one reaches a high concentration. Further studies will be needed to understand the link between both of these elements and SBCMV infections.

The decrease of SBCMV infection rates at increasing copper concentrations observed in root samples may be explained by the anti-microbial and anti-viral properties of this element (Shevchenko et al., 2004; Soliman et al., 2020). We were not able to model the influence of nutrients and plant nutritional state on SBWMV infection rates in roots, due to small root sample numbers. For leaf samples, STBM and ST-MA identified the interaction between $\delta^{13}C$ and manganese content to influence SBWMV infection rates.

Photosynthetic processes in C3 plants like wheat discriminate strongly against ^{13}C (Farquhar et al., 1989). Stomatal closure, which occurs as a consequence e.g. of drought stress, by reducing CO_2 availability (partial pressure within the leaf), reduces this discrimination and leads to increased (less negative) $\delta^{13}C$ values. Nitrogen availability has the opposite effect and increases

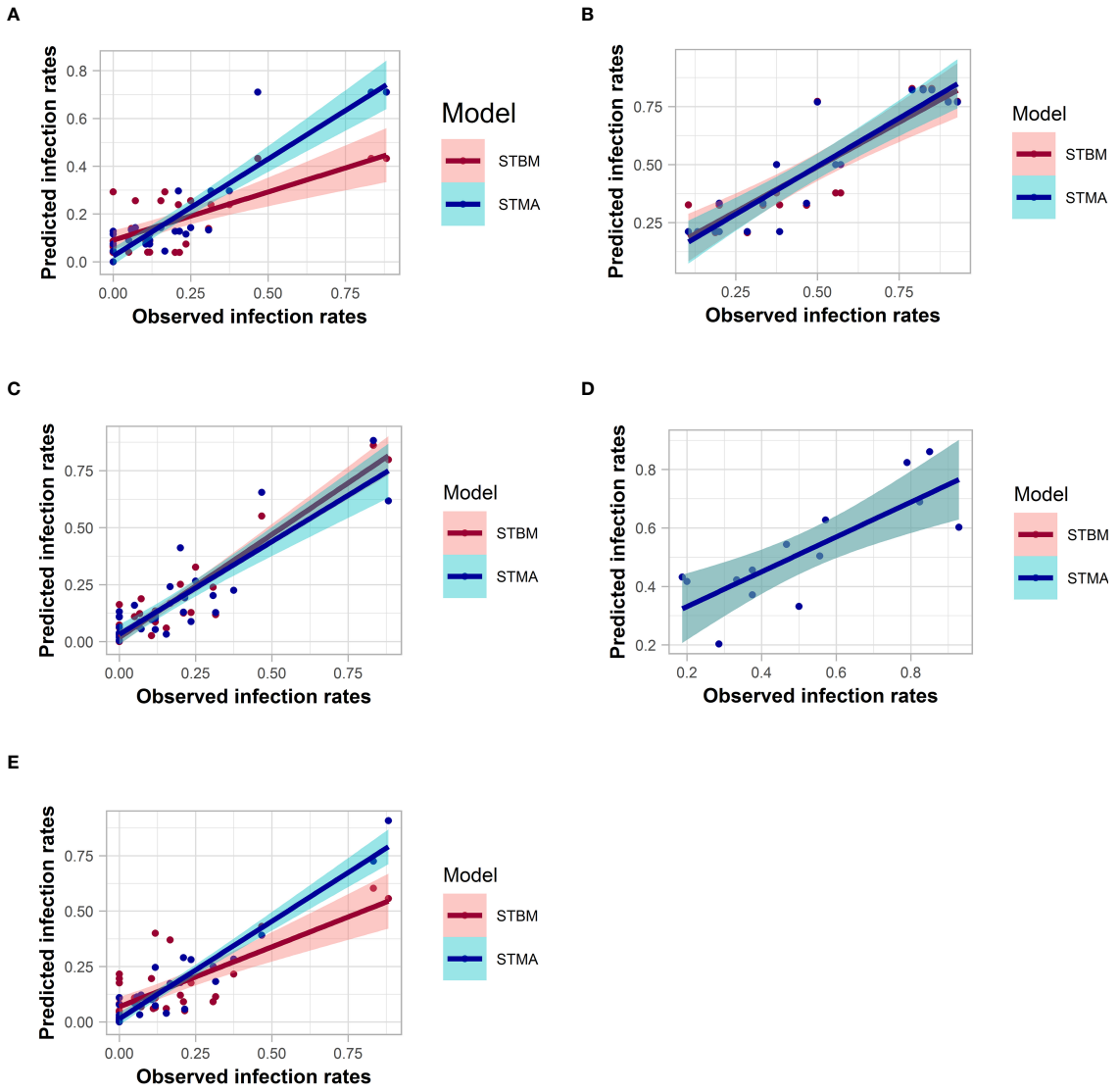

FIGURE 8
Correlation between the observed and predicted infection rates for SBMCV using soil **(A)**, leaf **(C)** or root **(E)** parameters, and for SBWMV using soil **(B)** and leaf **(D)** parameters. The colored zones depict 95% confidence intervals.

discrimination against ^{13}C (Shangguan et al., 2000). Neilson et al. (1999) reported minor effects of nematodes and viruses on $\delta^{13}C$ and limited to roots.

A decrease in $\delta^{13}C$ may also be linked to a decrease in chlorophyll content (Soundararajan, 2012) or to an increase of secondary metabolites, such as defense compounds (Gleixner et al., 1993).

This may reflect a plant response to furovirus infection, especially as infected, symptomatic leaves display chlorotic stripes. The increase of the manganese content led to a drop of SBWMV infection rates. Previous studies indicated a similar effect of manganese, leading to an increase of resistance to plant disease (Huber and Haneklaus, 2007; Luo et al., 2020).

Comparison of the model performance

Most of the models generated using the MAVG approach were very under dispersed, illustrating the importance of removing the non-significant factors from the model. Although ST-MA performed statistically better than STBM (except for the prediction of SBCMV infection rates using the data obtained from analysis of nutrients in leaves), it increases the complexity of the predictive model for a small gain of precision, only. This raises the question of the weight to give to the precision of the analysis in relation to the time and the cost of the extra analysis to reach it. However, during the analysis process, ST-MA is much faster compared to STBM, which requires to test every single possibility and factor one by one.

Conclusion

Our study used soils obtained from different geographic locations to identify soil parameters and plant nutrients impacting SBCMV and/or SBWMV infection rates. The soil parameters probably influence *P. graminis* movement or generation of zoospores. Future experiments will test if the identified parameters can confirm the predictions of our model. Interestingly, our study suggests that SBCMV and SBWMV require specific soil conditions for infection, as our analysis of the soil parameters clearly separated soils containing SBCMV from soils containing SBWMV. This is specifically interesting with respect to the absence of fields reported to contain both furovirus species, despite they are both transmitted by *P. graminis* and, at least in Germany, co-occur in the same regions. The dataset containing plant samples grown in the different soils, was also separable into soils containing SBWMV and SBCMV, suggesting that the specific conditions required by SBWMV and SBCMV are transduced to the plant level. Finally, our study identified several plant parameters influencing virus infection. Future studies will test the effect of the identified factors on virus infection and may reveal, whether they represent the cause or rather the consequence of successful infection. This study contributes new insight into conditions determining furovirus infection in wheat and may help to develop strategies for nutrient-based pathogen management.

Data availability statement

The original contributions presented in the study are included in the article/Supplementary Material. Further inquiries can be directed to the corresponding author.

Author contributions

Conceptualization: AN and DPe; data curation and formal analysis: KG; funding acquisition: AN, DPe and FO; investigation: KG, DPa, MN, MH, CG; Methodology: KG, AN, DPa, MN, MH, CG, DPe, FO; Project administration: KG, DPa; DPe, AN; Supervision: AN, DPe; visualization: KG and AN; writing - original draft preparation: KG and AN; writing - review and editing: KG, DPa, MN, MH, CG, DPe, AN and FO. All authors contributed to the article and approved the submitted version.

Funding

The project was supported by funds of the Federal Ministry of Food and Agriculture (BMEL) based on a decision of the Parliament of the Federal Republic of Germany *via* the Federal Office for Agriculture and Food (BLE) under the innovation support program, grant number 2818410B18 and the Fonds de Soutien à l'Obtention Végétale (FSOV), grant number JKI-RS-08-3393.

Acknowledgments

We thank Sabine Bonse, Nina Gräbitz, Franziska Koch, Kathy Niedung, Cordula Paris, Paula Weber, and Marlis Weilepp for help in the laboratory. We are grateful to Ellen Goudemand Dugué (Florimond Desprez), Michael Koch (DSV) Marco Maccaferri (University of Bologna), Matteo Bozzoli (University of Bologna), and Kostya Kanyuka (NIAB) for provision of soils from France, Italy and England, respectively.

Conflict of interest

The authors declare that the research was conducted in the absence of any commercial or financial relationships that could be construed as a potential conflict of interest.

Publisher's note

Supplementary material

The Supplementary Material for this article can be found online at: https://www.frontiersin.org/articles/10.3389/fpls.2023.1200674/full#supplementary-material

References

Adams, M. J. (1990). Epidemiology of fungally-transmitted viruses. *Soil Use Manage.* 6, 184–188. doi: 10.1111/j.1475-2743.1990.tb00833.x

Adams, M. J., and Swaby, A. G. (1988). Factors affecting the production and motility of zoospores of Polymyxa graminis and their transmission of barley yellow mosaic virus (BaYMV). *Ann. Appl. Biol.* 112, 69–78. doi: 10.1111/j.1744-7348.1988.tb02042.x

Adkins, S., McCollum, T. G., Albano, J. P., Kousik, C. S., Baker, C. A., Webster, C. G., et al. (2013). Physiological effects of squash vein yellowing virus infection on watermelon. *Plant Dis.* 97, 1137–1148. doi: 10.1094/PDIS-01-13-0075-RE

Alyamani, M. S., and Şen, Z. (1993). Determination of hydraulic conductivity from complete grain-size distribution curves. *Groundwater* 31, 551–555. doi: 10.1111/j.1745-6584.1993.tb00587.x

Amponsah, J., Tegg, R. S., Thangavel, T., and Wilson, C. R. (2021). Moments of weaknesses – exploiting vulnerabilities between germination and encystment in the *Phytomyxea*. *Biol. Rev.* 96, 1603–1615. doi: 10.1111/brv.12717

Andika, I. B., Kondo, H., and Sun, L. (2016). Interplays between soil-borne plant viruses and RNA silencing-mediated antiviral defense in roots. *Front. Microbiol.* 7. doi: 10.3389/fmicb.2016.01458

Ariz, I., Cruz, C., Moran, J., González-Moro, M., García-Olaverri, C., Gonzalez-Murua, C., et al. (2011). Depletion of the heaviest Stable N isotope is associated with NH4+/NH3 toxicity in NH4+-fed plants. *BMC Plant Biol.* 11, 83. doi: 10.1186/1471-2229-11-83

Aulakh, M. S., and Dev, G. (1978). Interaction effect of calcium and sulphur on the growth and nutrient composition of alfalfa (*Medicago sativa L. pers.*), using 35S. *Plant Soil* 50, 125–134. doi: 10.1007/BF02107162

Balendres, M. A., Tegg, R. S., Amponsah, J., and Wilson, C. R. (2018). Zoosporangial root infection of tomato by *Spongospora subterranea* in hydroponic and glasshouse culture results in diminished plant growth. *J. Phytopathol.* 166, 412–419. doi: 10.1111/jph.12701

Balendres, M. A., Tegg, R. S., and Wilson, C. R. (2016). Key events in pathogenesis of spongospora diseases in potato: a review. *Australas. Plant Pathol.* 45, 229–240. doi: 10.1007/s13313-016-0398-3

Ballini, E., Nguyen, T. T., and Morel, J.-B. (2013). Diversity and genetics of nitrogen-induced susceptibility to the blast fungus in rice and wheat. *Rice* 6, 32. doi: 10.1186/1939-8433-6-32

Barr, D. J. S., and Allan, P. M. E. (1982). Zoospore ultrastructure of *Polymyxa graminis (Plasmodiophoromycetes). Can. J. Bot.* 60, 2496–2504. doi: 10.1139/b82-302

Bass, C., Hendley, R., Adams, M., Hammond-Kosack, K., and Kanyuka, K. (2006). The *Sbm1* locus conferring resistance to soil-borne cereal mosaic virus maps to a gene-rich region on 5DL in wheat. *Genome* 49, 1140. doi: 10.1139/g06-064

Borer, E., Seabloom, E., Mitchell, C., and Cronin, J. P. (2014). Multiple nutrients and herbivores interact to govern diversity, productivity, composition, and infection in a successional grassland. *Oikos* 123, 214–224. doi: 10.1111/j.1600-0706.2013.00680.x

Buoso, S., Pagliari, L., Musetti, R., Fornasier, F., Martini, M., Loschi, A., et al. (2020). With or without you: altered plant response to boron-deficiency in hydroponically grown grapevines infected by grapevine pinot gris virus suggests a relation between grapevine leaf mottling and deformation symptom occurrence and boron plant availability. *Front. Plant Sci.* 11. doi: 10.3389/fpls.2020.00226

Calabrese, S., Cusant, L., Sarazin, A., Niehl, A., Erban, A., Brulé, D., et al. (2019). Imbalanced regulation of fungal nutrient transports according to phosphate availability in a symbiocosm formed by poplar, sorghum, and *Rhizophagus irregularis. Front. Plant Sci.* 10. doi: 10.3389/fpls.2019.01617

Calabrese, S., Kohler, A., Niehl, A., Veneault-Fourrey, C., Boller, T., and Courty, P.-E. (2017). Transcriptome analysis of the *Populus trichocarpa–Rhizophagus irregularis* mycorrhizal symbiosis: regulation of plant and fungal transportomes under nitrogen starvation. *Plant Cell Physiol.* 58, 1003–1017. doi: 10.1093/pcp/pcx044

Camacho-Cristóbal, J. J., Rexach, J., and González-Fontes, A. (2008). Boron in plants: deficiency and toxicity. *J. Integr. Plant Biol.* 50, 1247–1255. doi: 10.1111/j.1744-7909.2008.00742.x

Campbell, R. N. (1988). "Cultural characteristics and manipulative methods," in *Developments in applied biology. II. Viruses with fungal vectors*. Eds. J. I. Cooper and M. J. C. Asher (Wellesbourne: Association of Applied Biologists), 153–165.

Chapin, F. S. (1980). The mineral nutrition of wild plants. *Annu. Rev. Ecol. System.* 11, 233–260. doi: 10.1146/annurev.es.11.110180.001313

Chien, Y.-C., and Huang, C.-H. (2021). Effects of pH values and application methods of potassium silicate on nutrient uptake and bacterial spot of tomato. *Eur. J. Plant Pathol.* 162, 119–130. doi: 10.1007/s10658-021-02390-w

Choi, W.-J., Ro, H.-M., and Hobbie, E. A. (2003). Patterns of natural 15N in soils and plants from chemically and organically fertilized uplands. *Soil Biol. Biochem.* 35, 1493–1500. doi: 10.1016/S0038-0717(03)00246-3

Chrpová, J., Veškrna, O., Palicová, J., and Kundu, J. K. (2020). The evaluation of wheat cultivar resistance and yield loss thresholds in response to barley yellow dwarf virus-PAV infection. *Agriculture* 10, 20. doi: 10.3390/agriculture10010020

Clark, M. F., and Adams, A. N. (1977). Characteristics of the microplate method of enzyme linked immunosorbent assay for the detection of plant viruses. *J. Gen. Virol.* 34, 475–483.

Coller, E., Cestaro, A., Zanzotti, R., Bertoldi, D., Pindo, M., Larger, S., et al. (2019). Microbiome of vineyard soils is shaped by geography and management. *Microbiome* 7, 140. doi: 10.1186/s40168-019-0758-7

Craine, J. M., Brookshire, E. N. J., Cramer, M. D., Hasselquist, N. J., Koba, K., Marin-Spiotta, E., et al. (2015). Ecological interpretations of nitrogen isotope ratios of terrestrial plants and soils. *Plant Soil* 396, 1–26. doi: 10.1007/s11104-015-2542-1

Dequiedt, S., Saby, N. P. A., Lelievre, M., Jolivet, C., Thioulouse, J., Toutain, B., et al. (2011). Biogeographical patterns of soil molecular microbial biomass as influenced by soil characteristics and management. *Global Ecol. Biogeogr.* 20, 641–652. doi: 10.1111/j.1466-8238.2010.00628.x

Din, E. V. (Hrsg.). (2002). *DIN ISO 11277:2002-08, Bodenbeschaffenheit_- Bestimmung der Partikelgrößenverteilung in Mineralböden_- Verfahren mittels Siebung und Sedimentation (ISO_11277:1998_+ ISO_11277:1998 Corrigendum_1:2002)* (Germany: Beuth Verlag GmbH).

Ding, S., Shao, X., Li, J., Ahammed, G. J., Yao, Y., Ding, J., et al. (2021). Nitrogen forms and metabolism affect plant defence to foliar and root pathogens in tomato. *Plant Cell Environ.* 44, 1596–1610. doi: 10.1111/pce.14019

DiTommaso, A., and Aarssen, L. W. (1989). Resource manipulations in natural vegetation: a review. *Vegetatio* 84, 9–29. doi: 10.1007/BF00054662

Dong, X., Wang, M., Ling, N., Shen, Q., and Guo, S. (2016). Effects of iron and boron combinations on the suppression of Fusarium wilt in banana. *Sci. Rep.* 6, 38944. doi: 10.1038/srep38944

Dordas, C. (2008). Role of nutrients in controlling plant diseases in sustainable agriculture. *A Rev. Agron. Sustain. Dev.* 28, 33–46. doi: 10.1051/agro:2007051

Driskel, B. A., Hunger, R. M., Payton, M. E., and Verchot-Lubicz, J. (2002). Response of hard red winter wheat to soilborne wheat mosaic virus using novel inoculation methods. *Phytopathology* 92, 347–354. doi: 10.1094/PHYTO.2002.92.4.347

Eskandari, S., Höfte, H., and Zhang, T. (2020). Foliar manganese spray induces the resistance of cucumber to *Colletotrichum lagenarium. J. Plant Physiol.* 246–247, 153129. doi: 10.1016/j.jplph.2020.153129

Fageria, N. K., and Baligar, V. C. (2005). "Nutrient availability," in *Encyclopedia of Soils in the Environment*. Ed. D. Hillel (Oxford: Elsevier), 63–71.

Farquhar, G. D., Ehleringer, J. R., and Hubick, K. T. (1989). Carbon Isotope discrimination and photosynthesis. *Annu. Rev. Plant Physiol. Plant Mol. Biol.* 40, 503–537. doi: 10.1146/annurev.pp.40.060189.002443

Finke, J. F., Hunt, B. P. V., Winter, C., Carmack, E. C., and Suttle, C. A. (2017). Nutrients and other environmental factors influence virus abundances across oxic and hypoxic marine environments. *Viruses* 9, 152. doi: 10.3390/v9060152

Francioli, D., Schulz, E., Lentendu, G., Wubet, T., Buscot, F., and Reitz, T. (2016). Mineral vs. organic amendments: microbial community structure, activity and abundance of agriculturally relevant microbes are driven by long-term fertilization strategies. *Front. Microbiol.* 7. doi: 10.3389/fmicb.2016.01446

Galili, T. (2015). dendextend: an R package for visualizing, adjusting and comparing trees of hierarchical clustering. *Bioinformatics* 31, 3718–3720. doi: 10.1093/bioinformatics/btv428

Gleixner, G., Danier, H. J., Werner, R. A., and Schmidt, H. L. (1993). Correlations between the ^{13}C content of primary and secondary plant products in different cell compartments and that in decomposing *Basidiomycetes. Plant Physiol.* 102, 1287–1290. doi: 10.1104/pp.102.4.1287

Griffiths, B. S., Spilles, A., and Bonkowski, M. (2012). C:N:P stoichiometry and nutrient limitation of the soil microbial biomass in a grazed grassland site under experimental P limitation or excess. *Ecol. Processes* 1, 6. doi: 10.1186/2192-1709-1-6

Gu, J., Chen, J., Chen, L., Wang, Z., Zhang, H., and Yang, J. (2015). Grain quality changes and responses to nitrogen fertilizer of japonica rice cultivars released in the Yangtze River Basin from the 1950s to 2000s. *Crop J.* 3, 285–297. doi: 10.1016/j.cj.2015.03.007

Gupta, S. K., Rai, A. K., Kanwar, S. S., and Sharma, T. R. (2012). Comparative analysis of zinc finger proteins involved in plant disease resistance. *PloS One* 7, e42578. doi: 10.1371/journal.pone.0042578

Hadley, W. (2016). *ggplot2: elegant graphics for data analysis* (New York: Springer-Verlag).

Hengl, T., Leenaars, J. G. B., Shepherd, K. D., Walsh, M. G., Heuvelink, G. B. M., Mamo, T., et al. (2017). Soil nutrient maps of Sub-Saharan Africa: assessment of soil nutrient content at 250 m spatial resolution using machine learning. *Nutr. Cycl. Agroecosystems* 109, 77–102. doi: 10.1007/s10705-017-9870-x

Heyneke, E., and Hoefgen, R. (2021). Meeting the complexity of plant nutrient metabolism with multi-omics approaches. *J. Exp. Bot.* 72, 2261–2265. doi: 10.1093/jxb/eraa600

Hobbie, E. A., and Högberg, P. (2012). Nitrogen isotopes link mycorrhizal fungi and plants to nitrogen dynamics. *New Phytol.* 196, 367–382. doi: 10.1111/j.1469-8137.2012.04300.x

Holford, I. C. R., and Mattingly, G. E. G. (1976). Phosphate adsorption and availability plant of phosphate. *Plant Soil* 44, 377–389. doi: 10.1007/BF00015889

Holm, S. (1979). A simple sequentially rejective multiple test procedure. *Scand. J. Stat.* 6, 65–70.

Hua, T., Zhang, R., Sun, H., and Liu, C. (2021). Alleviation of boron toxicity in plants: mechanisms and approaches. *Crit. Rev. Environ. Sci. Technol.* 51, 2975–3015. doi: 10.1080/10643389.2020.1807451

Huber, D. M., and Haneklaus, S. (2007). Managing nutrition to control plant disease. *Haneklaus/Landbauforschung Völkenrode* 4, 313–322.

Hunger, R. M., and Sherwood, J. L. (1984). Inheritance of Septoria leaf blotch (*S. tritici*) and Pyrenophora Tan Spot (*P. tritici-repentis*) resistance in *Triticum aestivum* cv. Carifen 12. *Plant Dis.* 68, 848.

Hwang, S.-F., Howard, R. J., Strelkov, S. E., Gossen, B. D., and Peng, G. (2014). Management of clubroot (*Plasmodiophora brassicae*) on canola (*Brassica napus*) in western Canada. *Can. J. Plant Pathol.* 36, 49–65. doi: 10.1080/07060661.2013.863806

Jakobsen, B. F., and Dexter, A. R. (1987). Effect of soil structure on wheat root growth, water uptake and grain yield. A computer simulation model. *Soil Tillage Res.* 10, 331–345. doi: 10.1016/0167-1987(87)90022-5

Jat, M. L., Bijay-Singh, Stirling, C. M., Jat, H. S., Tetarwal, J. P., Jat, R. K., Singh, R., et al. (2018). "Chapter four - soil processes and wheat cropping under emerging climate change scenarios in south Asia," in *Advances in Agronomy*. Ed. D. L. Sparks (Newark, DE, United States: Academic Press), 111–171.

Jones, M., and Smith, S. (2004). Exploring functional definitions of mycorrhizas: Are mycorrhizas always mutualisms? *Can. J. Bot.* 82, 1089–1109. doi: 10.1139/b04-110

Kanyuka, K., Lovell, D. J., Mitrofanova, O. P., Hammond-Kosack, K., and Adams, M. J. (2004). A controlled environment test for resistance to soil-borne cereal mosaic virus (SBCMV) and its use to determine the mode of inheritance of resistance in wheat cv. Cadenza and for screening *Triticum monococcum* genotypes for sources of SBCMV resistance. *Plant Pathol.* 53, 154–160. doi: 10.1111/j.0032-0862.2004.01000.x

Kanyuka, K., Ward, E., and Adams, M. J. (2003). *Polymyxa graminis* and the cereal viruses it transmits: a research challenge. *Mol. Plant Pathol.* 4, 393–406. doi: 10.1046/j.1364-3703.2003.00177.x

Kastirr, U., and Ziegler, A. (2018). *Schlussbericht zum Vorhaben Vorkommen und Schadwirkung des Soil-borne wheat mosaic virus (SBWMV) in Winterweizen* (Quedlinburg: Julius-Kühn Institut).

Kastirr, U., Ziegler, A., and Niehl, A. (2018). *Schlussbericht zum Vorhaben Monitoring zum Vorkommen bodenbürtiger Viren in Weizen, Triticale und Roggen in den wichtigsten Getreideanbaugebieten Deutschlands* (Quedlinburg: Julius-Kühn Institut).

King, A. M., Lefkowitz, E., Adams, M. J., and Carstens, E. B. (2011). *Virus Taxonomy: Ninth Report of the International Committee on Taxonomy of Viruses* (USA: Elsevier).

Kroese, D. R., Schonneker, L., Bag, S., Frost, K., Cating, R., and Hagerty, C. H. (2020). Wheat soil-borne mosaic: yield loss and distribution in the US pacific northwest. *Crop Prot.* 132, 105102. doi: 10.1016/j.cropro.2020.105102

Künstler, A., Gullner, G., Ádám, A. L., Kolozsváriné Nagy, J., and Király, L. (2020). The versatile roles of sulfur-containing biomolecules in plant defense-a road to disease resistance. *Plants* 9, E1705. doi: 10.3390/plants9121705

Lacroix, C., Seabloom, E. W., and Borer, E. T. (2017). Environmental nutrient supply directly alters plant traits but indirectly determines virus growth rate. *Front. Microbiol.* 8. doi: 10.3389/fmicb.2017.02116

Lapierre, H. D., and Hariri, D. (2008). "Cereal viruses: wheat and barley," in *Encyclopedia of Virology (Third Edition)*. Eds. B. W. J. Mahy and M. H. V. Van Regenmortel (Oxford: Academic Press), 490–497.

Lapierre, H., and Signoret, P.-A. (2004). *Viruses and virus diseases of Poaceae (Gramineae)* (France: Editions Quae).

Lê, S., Josse, J., and Husson, F. (2008). FactoMineR: an R package for multivariate analysis. *J. Stat. Softw.* 25, 1–18.

Lee, M.-S., Wycislo, A., Guo, J., Lee, D. K., and Voigt, T. (2017). Nitrogen fertilization effects on biomass production and yield components of *Miscanthus ×giganteus*. *Front. Plant Sci.* 8. doi: 10.3389/fpls.2017.00544

Legrève, A., Delfosse, P., and Maraite, H. (2002). Phylogenetic analysis of *Polymyxa* species based on nuclear 5.8S and internal transcribed spacers ribosomal DNA sequences. *Mycol. Res.* 106, 138–147. doi: 10.1017/S0953756201005391

Liu, S., Bai, G., Lin, M., Luo, M., Zhang, D., Jin, F., et al. (2020). Identification of candidate chromosome region of *Sbwm1* for soil-borne wheat mosaic virus resistance in wheat. *Sci. Rep.* 10, 8119. doi: 10.1038/s41598-020-64993-3

Luo, Y., Yao, A., Tan, M., Li, Z., Qing, L., and Yang, S. (2020). Effects of manganese and zinc on the growth process of *Phytophthora nicotianae* and the possible inhibitory mechanisms. *PeerJ* 8, e8613. doi: 10.7717/peerj.8613

Maccaferri, M., Ratti, C., Rubies-Autonell, C., Vallega, V., Demontis, A., Stefanelli, S., et al. (2011). Resistance to soil-borne cereal mosaic virus in durum wheat is controlled by a major QTL on chromosome arm 2BS and minor loci. *Theor. Appl. Genet.* 123, 527–544. doi: 10.1007/s00122-011-1605-9

McKinney, H. H. (1944). Descriptions and revisions of several species of viruses in the genera *Marmor, Fractilinea*, and *Galla*. *J. Washington Acad. Sci.* 34, 322–329.

Miao, Y., Mulla, D., Robert, P., and Hernandez, J. (2006). Within-field variation in corn yield and grain quality responses to nitrogen fertilization and hybrid selection. *Agron. J.* 98, 129–140. doi: 10.2134/agronj2005.0120

Middelboe, M., Jorgensen, N., and Kroer, N. (1996). Effects of viruses on nutrient turnover and growth efficiency of noninfected marine bacterioplankton. *Appl. Environ. Microbiol.* 62, 1991–1997. doi: 10.1128/aem.62.6.1991-1997.1996

Miller, T. E., Burns, J. H., Munguia, P., Walters, E. L., Kneitel, J. M., Richards, P. M., et al. (2005). A critical review of twenty years' use of the resource-ratio theory. *Am. Nat.* 165, 439–448. doi: 10.1086/428681

Muneer, M. A., Huang, X., Hou, W., Zhang, Y., Cai, Y., Munir, M. Z., et al. (2021). Response of fungal diversity, community composition, and functions to nutrients management in red soil. *J. Fungi* 7, 554. doi: 10.3390/jof7070554

Mur, L. A. J., Simpson, C., Kumari, A., Gupta, A. K., and Gupta, K. J. (2017). Moving nitrogen to the centre of plant defence against pathogens. *Ann. Bot.* 119, 703–709.

Myers, D. F., and Campbell, R. N. (1985). Lime and the control of clubroot of crucifers: effects of pH, calcium, magnesium, and their interactions. *Phytopathology* 75, 670–673. doi: 10.1094/Phyto-75-670

Neilson, R., Handley, L. L., Robinson, D., Scrimgeour, C. M., and Brown, D. J. F. (1999). Natural abundances of ^{15}N and ^{13}C indicating physiological responses in *Petunia hybrida* to infection by longidorid nematodes and nepoviruses. *Nematology* 1, 315–320. doi: 10.1163/156854199508180

Niehl, A., and Koenig, R. (2021). Furoviruses (Virgaviridae). *Encyclopedia Virol.* 3, 405–410. doi: 10.1016/B978-0-12-809633-8.21312-5

Niehl, A., Lacomme, C., Erban, A., Kopka, J., Krämer, U., and Fisahn, J. (2006). Systemic Potato virus X infection induces defence gene expression and accumulation of β-phenylethylamine-alkaloids in potato. *Funct. Plant Biol.* 33, 593–604. doi: 10.1071/FP06049

Olatunji, O. A., Luo, H., Pan, K., Tariq, A., Sun, X., Chen, W., et al. (2018). Influence of phosphorus application and water deficit on the soil microbiota of N_2-fixing and non-N-fixing tree. *Ecosphere* 9, e02276. doi: 10.1002/ecs2.2276

Orober, M., Siegrist, J., and Buchenauer, H. (2002). Mechanisms of phosphate-induced disease resistance in cucumber. *Eur. J. Plant Pathol.* 108, 345–353. doi: 10.1023/A:1015696408402

Overholt, W. A., Markle, L., Rosskopf, E., Manrique, V., Albano, J., Cave, E., et al. (2009). The interactions of tropical soda apple mosaic tobamovirus and *Gratiana boliviana (Coleoptera: Chrysomelidae)*, an introduced biological control agent of tropical soda apple (*Solanum viarum*). *Biol. Control* 48, 294–300. doi: 10.1016/j.biocontrol.2008.10.018

Perovic, D., Förster, J., Devaux, P., Hariri, D., Guilleroux, M., Kanyuka, K., et al. (2009). Mapping and diagnostic marker development for soil-borne cereal mosaic virus resistance in bread wheat. *Mol. Breed.* 23, 641–653. doi: 10.1007/s11032-009-9262-2

Rao, A. S., and Brakke, M. K. (1969). Relation of soil-borne wheat mosaic virus and its fungal vector, *Polymyxa graminis*. *Phytopathology* 59, 581–587.

R Development Core Team. (2019). *R: a language and environment for statistical computing*. (Vienna, Austria: R Foundation for Statistical Computing).

Schlegel, R., Pankovic, D., Koch, F., Ordon, F., Kastirr, U., and Perovic, D. (2022). Transfer of resistance against soil-borne wheat mosaic virus from *Triticum monococcum* to hexaploid wheat (*T. aestivum*). *Cereal Res. Commun.* 50, 321–328. doi: 10.1007/s42976-021-00176-8

Schüller, H. (1969). Die CAL-Methode, eine neue Methode zur Bestimmung des pflanzenverfügbaren Phosphates in Böden. *Z. für Pflanzenernährung und Bodenkunde* 123, 48–63. doi: 10.1002/jpln.19691230106

Shangguan, Z. P., Shao, M. A., and Dyckmans, J. (2000). Nitrogen nutrition and water stress effects on leaf photosynthetic gas exchange and water use efficiency in winter wheat. *Environ. Exp. Bot.* 44, 141–149. doi: 10.1016/S0098-8472(00)00064-2

Shevchenko, O., Budzanivska, I., Shevchenko, T., Polischuk, V., and Spaar, D. (2004). Plant virus infection development as affected by heavy metal stress. *Arch. Phytopathol. Plant Prot.* 37, 139–146. doi: 10.1080/0323540042000203967

Singh, R., Parihar, P., and Prasad, S. M. (2018). Sulfur and calcium simultaneously regulate photosynthetic performance and nitrogen metabolism status in As-challenged *Brassica juncea* L. seedlings. *Front. Plant Sci.* 9. doi: 10.3389/fpls.2018.00772

Six, J., Bossuyt, H., Degryze, S., and Denef, K. (2004). A history of research on the link between (micro)aggregates, soil biota, and soil organic matter dynamics. *Soil Tillage Res.* 79, 7–31. doi: 10.1016/j.still.2004.03.008

Snoeijers, S. S., Pérez-García, A., Joosten, M. H. A. J., and De Wit, P. J. G. M. (2000). The effect of nitrogen on disease development and gene expression in bacterial and fungal plant pathogens. *Eur. J. Plant Pathol.* 106, 493–506. doi: 10.1023/A:1008720704105

Soliman, M. Y. M., Medema, G., Bonilla, B. E., Brouns, S. J. J., and van Halem, D. (2020). Inactivation of RNA and DNA viruses in water by copper and silver ions and their synergistic effect. *Water Res. X* 9, 100077. doi: 10.1016/j.wroa.2020.100077

Soundararajan, M. (2012). Leaf chlorophyll levels influence carbon isotope discrimination in soybean and maize. *Int. J. Biosci. Biochem. Bioinf.* 2, 207–211. doi: 10.7763/IJBBB.2012.V2.102

Sparks, D. L. (1980). Chemistry of soil potassium in Atlantic coastal plain soils: a review. *Commun. Soil Sci. Plant Anal.* 11, 435–449. doi: 10.1080/00103628009367051

Szpak, P. (2014). Complexities of nitrogen isotope biogeochemistry in plant-soil systems: implications for the study of ancient agricultural and animal management practices. *Front. Plant Sci.* 5. doi: 10.3389/fpls.2014.00288

Te, J., Melcher, U., Howard, A., and Verchot-Lubicz, J. (2005). Soilborne wheat mosaic virus (SBWMV) 19K protein belongs to a class of cysteine rich proteins that suppress RNA silencing. *Virol. J.* 2, 18. doi: 10.1186/1743-422X-2-18

VDLUFA (Hrsg.) (1991). *Die Untersuchung von Boden. Methodenbuch (Vierte Auflage)* (Darmstadt: VDLUFA), 1.

Verchot, J., Driskel, B. A., Zhu, Y., Hunger, R. M., and Littlefield, L. J. (2001). Evidence that soilborne wheat mosaic virus moves long distance through the xylem in wheat. *Protoplasma* 218, 57–66. doi: 10.1007/BF01288361

Verly, C., Djoman, A. C. R., Rigault, M., Giraud, F., Rajjou, L., Saint-Macary, M.-E., et al. (2020). Plant defense stimulator mediated defense activation is affected by nitrate fertilization and developmental stage in *Arabidopsis thaliana*. *Front. Plant Sci.* 11. doi: 10.3389/fpls.2020.00583

Wang, Q., Wang, C., Yu, W., Turak, A., Chen, D., Huang, Y., et al. (2018). Effects of nitrogen and phosphorus inputs on soil bacterial abundance, diversity, and community composition in *Chinese Fir Plantations*. *Front. Microbiol.* 9. doi: 10.3389/fmicb.2018.01543

Wang, M., Zheng, Q., Shen, Q., and Guo, S. (2013). The critical role of potassium in plant stress response. *Int. J. Mol. Sci.* 14, 7370–7390. doi: 10.3390/ijms14047370

Weih, M., Hamnér, K., and Pourazari, F. (2018). Analyzing plant nutrient uptake and utilization efficiencies: comparison between crops and approaches. *Plant Soil* 430, 7–21. doi: 10.1007/s11104-018-3738-y

Whittingham, M. J., Steohens, P. A., Bradbury, R. B., and Freckleton, R. P. (2006). Why do we still use stepwise modelling in ecology and behaviour? *J. Anim. Ecol.* 75, 1182–1189. doi: 10.1111/j.1365-2656.2006.01141.x

Zenda, T., Liu, S., Dong, A., and Duan, H. (2021). Revisiting sulphur—the once neglected nutrient: it's roles in plant growth, metabolism, stress tolerance and crop production. *Agriculture* 11, 626. doi: 10.3390/agriculture11070626

Zhang, J., and Elser, J. J. (2017). Carbon:nitrogen:phosphorus stoichiometry in fungi: a meta-analysis. *Front. Microbiol.* 8. doi: 10.3389/fmicb.2017.01281

frontiers | Frontiers in Plant Science

TYPE Original Research
PUBLISHED 06 October 2023
DOI 10.3389/fpls.2023.1272951

OPEN ACCESS

EDITED BY
Kun Zhang,
Yangzhou University, China

REVIEWED BY
Houxiang Kang,
Chinese Academy of Agricultural Sciences (CAAS), China
Qin Yang,
Northwest A&F University, China

*CORRESPONDENCE
Tiffany Jamann
tjamann@illinois.edu

RECEIVED 04 August 2023
ACCEPTED 19 September 2023
PUBLISHED 06 October 2023

CITATION
Lipps S, Lipka AE, Mideros S and Jamann T (2023) Inhibition of ethylene involved in resistance to *E. turcicum* in an exotic-derived double haploid maize population. *Front. Plant Sci.* 14:1272951. doi: 10.3389/fpls.2023.1272951

Inhibition of ethylene involved in resistance to *E. turcicum* in an exotic-derived double haploid maize population

Sarah Lipps, Alexander E. Lipka, Santiago Mideros and Tiffany Jamann*

Department of Crop Sciences, University of Illinois, Urbana, IL, United States

Northern corn leaf blight (NCLB) is an economically important disease of maize. While the genetic architecture of NCLB has been well characterized, the pathogen is known to overcome currently deployed resistance genes, and the role of hormones in resistance to NCLB is an area of active research. The objectives of the study were (i) to identify significant markers associated with resistance to NCLB, (ii) to identify metabolic pathways associated with NCLB resistance, and (iii) to examine role of ethylene in resistance to NCLB. We screened 252 lines from the exotic-derived double haploid BGEM maize population for resistance to NCLB in both field and greenhouse environments. We used a genome wide association study (GWAS) and stepwise regression to identify four markers associated with resistance, followed by a pathway association study tool (PAST) to identify important metabolic pathways associated with disease severity and incubation period. The ethylene synthesis pathway was significant for disease severity and incubation period. We conducted a greenhouse assay in which we inhibited ethylene to examine the role of ethylene in resistance to NCLB. We observed a significant increase in incubation period and a significant decrease in disease severity between plants treated with the ethylene inhibitor and mock-treated plants. Our study confirms the potential of the BGEM population as a source of novel alleles for resistance. We also confirm the role of ethylene in resistance to NCLB and contribute to the growing body of literature on ethylene and disease resistance in monocots.

KEYWORDS

***Exserohilum turcicum*, maize, BGEM, ethylene, disease resistance, quantitative disease resistance, GWAS**

1 Introduction

Northern corn leaf blight (NCLB), caused by the fungus *Exserohilum turcicum* (Pass.) K. J. Leonard and Suggs [syn. *Setosphaeria turcica* (Luttr.) K. J. Leonard and Suggs.], is one of the most important diseases of maize. *E. turcicum* is well-adapted to most maize growing regions in the world and causes yield losses globally (Savary et al., 2019). Over 7.62 million

metric tons (300 million bushels) have been lost due to NCLB between 2016 and 2019 in the United States and Ontario, Canada (Mueller et al., 2020). The cost of economic losses due to damage from NCLB was estimated in one study examining hybrids with a range of resistance levels to be from \$122.00 ha^{-1} to \$353.20 ha^{-1} in fields managed for optimized yield (De Rossi et al., 2022). Furthermore, *E. turcicum* has a high evolutionary potential, as the fungus has high genetic variability and undergoes sexual reproduction in the field. Thus, there is the potential for widespread loss of resistance to *E. turcicum* (McDonald and Linde, 2002; Galiano-Carneiro and Miedaner, 2017; Munoz-Zavala et al., 2023).

The disease cycle and pathogenesis process of *E. turcicum* have been well characterized (Kotze et al., 2019; Navarro et al., 2020). *E. turcicum* is a hemibiotroph with a biotrophic and a necrotrophic phase. The fungus overwinters as mycelia in crop residue. Conidia are spread to the host by wind and rain. In the biotrophic phase, an appressorium-like structure is formed, and the fungus penetrates the cuticle, grows through the mesophyll, then colonizes the xylem (Navarro et al., 2020). The necrotrophic phase of the disease cycle begins when the fungus exits the xylem and colonizes the mesophyll, resulting in cell death. Eventually, *E. turcicum* forms conidiophores resulting in polycyclic disease over the course of the growing season (Kotze et al., 2019; Navarro et al., 2020). The first symptoms of infection are tan flecks that develop into tan-grey ovular lesions. The most severe epiphytotics are observed when disease symptoms occur before flowering time and in warm, humid environments (Ullstrup and Miles, 1957; Raymundo and Hooker, 1981a; Perkins and Pedersen, 1987).

An integrated NCLB management program includes host resistance, fungicides, and cultural methods. Host resistance is an important management technique as it does not increase the cost of production and does not harm the environment (Galiano-Carneiro and Miedaner, 2017). Both qualitative resistance, conferred by a single gene, and quantitative resistance, conferred by multiple genes, have been characterized in maize. Qualitative resistance genes effective for managing *E. turcicum* include *Ht1, Ht2, Ht3*, and *HtN1* (Welz and Geiger, 2000; Hurni et al., 2015; Galiano-Carneiro and Miedaner, 2017). *Ht2, Ht3*, and *HtN1* are allelic and encode a wall-associated protein kinase (Hurni et al., 2015; Yang et al., 2021). *Ht1* encodes a nucleotide-binding leucine-rich repeat receptor, *PH4GP- Ht1* (Thatcher et al., 2022). In this pathosystem, the qualitative genes do not confer complete resistance, but instead delay the onset of symptoms after initial infection and or dramatically reduce the severity of symptoms.

Many quantitative trait loci (QTL) effective against NCLB have been identified in maize (Wisser et al., 2006). A recent meta-analysis evaluating 110 studies identified chromosomes 10, 6, 5, 1, and 2 as having the highest odds of contributing a major-effect QTL for resistance to fungal and viral diseases, with chromosome 10 have the highest likelihood and chromosome 2 having the lowest likelihood (Rossi et al., 2019). In addition to regions associated with resistance, progress has been made on identifying potential quantitative resistance mechanisms to *E. turcicum*. Receptor-like kinases (RLKs) have been implicated in resistance to NCLB and other diseases. Three FERONIA-like receptors (FLRs), a type of RLK, have been identified as conferring resistance to multiple fungal foliar diseases, including NCLB (Yu et al., 2022). Originally *pan1*, an RLK, was implicated in increasing susceptibility to *E. turcicum*, as well as *Pantoea stewartii*, in maize on bin 1.06 (Jamann et al., 2014). However, a recent study revealed that *pan1* is not responsible for the altered resistance but potentially an aldo-ketoreductase is responsible instead (Doblas-Ibáñez et al., 2019). Additionally, a remorin gene, *ZmREM6.3*, on bin 1.02 was implicated in resistance to *E. turcicum, P. stewartii* and *Puccinia sorghi* (Jamann et al., 2016). Recently, a transcription repressor, *ZmMM1*, was cloned in maize from teosinte, and found to confer a lesion mimic phenotype, as well as resistance to NCLB and other fungal diseases (Wang et al., 2021). Other biochemical processes, such as the production of phenylpropanoids, have also been implicated as mechanisms of resistance. In bin 9.02, a maize caffeoyl-CoA *O*-methyltransferase encoded by *ZmCCoAOMT2*, is involved in the production of phenylpropanoids and lignin and is associated with resistance to multiple diseases (Yang et al., 2017). The recent advances in understanding NCLB have elucidated both regions associated with and mechanism of resistance.

The role of hormones in pathogen defense has been reviewed (Glazebrook, 2005; Robert-Seilaniantz et al., 2011; Denance et al., 2013). Three hormone pathways have been well discussed regarding their overlapping roles in abiotic and biotic stress: salicylic acid (SA), jasmonates (JA), and ethylene (ET). In Arabidopsis, SA is typically associated with biotrophic pathogens, and JA and ET are associated with necrotrophic pathogens (Glazebrook, 2005). Resistance to biotrophic and necrotrophic pathogens has been thought of as antagonistic, meaning that heightened resistance to biotrophic pathogens is typically associated with increased susceptibility to necrotrophic pathogens (Robert-Seilaniantz et al., 2011). However, the relationship between phytohormones and pathogen resistance is complex. Some fungi are able to mimic phytohormones or produce effectors that interfere with *in planta* hormone signaling (Denance et al., 2013). Additionally, pathogens are able to disrupt the balance of active hormones by targeting the regulatory aspects of hormonal pathways or inducing *in planta* hormone production (Robert-Seilaniantz et al., 2011).

The role of ethylene in disease resistance is complex. Ethylene is produced *in planta* in response to abiotic or biotic stress, which can be sensed by receptors located in the endoplasmic reticulum (Muller and Munne-Bosch, 2015). The ethylene pathway was first characterized in horticultural crops. It is synthesized from methionine which is converted into S-adenosyl-L-methionine (SAM) by SAM synthase. SAM is converted to 1-aminocyclopropane-1-carboxylate (ACC) via ACC synthase (ACS), and ACC is finally converted to ethylene via ACC oxidase (ACO) (Yang, 1985; Xu and Zhang, 2015). When activated, ethylene response factors link ethylene sensing and the activation of pathogen related genes (Huang et al., 2016).

The role of ethylene in plant-pathogen interactions has been extensively studied in dicots. However, several recent studies have focused on the role of ethylene in resistance against necrotrophic pathogens in maize. In maize, there are five known ACS genes and 13 ACO gene family members (Park et al., 2021). In kernels treated

with *Fusarium verticillioides*, it was found that several ethylene production genes were induced upon infection, and ethylene production was associated with disease progression (Park et al., 2021). A similar trend was found in kernels inoculated with *Aspergillus flavus*, where ethylene production encouraged fungal conidiation and sporulation (Wang et al., 2017). Additionally, an ethylene signaling gene, *ZmEIN2*, regulated the abundance of metabolites associated with resistance to *Fusarium graminearum* in maize seedlings (Zhou et al., 2019). The bulk of research regarding ethylene in maize-pathogen interactions has focused on necrotrophic pathogens. Less is known about the role of hormone signaling and resistance to *E. turicucm*, a hemibiotrophic plant pathogen. Recently, an ethylene response factor, *ZmERF061*, was implicated in resistance against *E. turcicum* in maize (Zang et al., 2020; Zang et al., 2021). The plant's ability to sense and respond to ethylene is likely important in defense against hemibiotrophic pathogens like *E. turcicum*, but this hypothesis needs further investigation.

Recent research shows that pathogens are increasing in complexity. In the case of *E. turcicum*, this increased complexity enables certain strains to overcome multiple, and occasionally, all available qualitative disease resistance genes (Weems and Bradley, 2018; Jindal et al., 2019; Muñoz-Zavala et al., 2022). The emergence of novel physiological races of *E. turcicum* requires further development and utilization of host resistance to effectively manage NCLB (Muñoz-Zavala et al., 2022). The endemic region of *E. turcicum* has expanded due to global warming; thus, it is likely that NCLB prevalence and severity are increasing in regions where it was previously a less common disease (Miedaner and Juroszek, 2021). With the increased complexity and ability of *E. turicucm* to overcome resistance in maize, it is imperative to continue identifying novel sources of resistance in maize. One effective approach to discover novel resistance alleles is by screening exotic-derived materials to identify previously unknown sources of resistance.

The germplasm enhancement of maize (GEM) program was established in 1995 to increase allelic diversity in temperate maize through the release of exotic-derived germplasm (Pollak and Salhuana, 2001). The BGEM population is an exotic-derived double haploid (DH) population developed by Iowa State University in collaboration with the GEM program (Brenner et al., 2012). In total, the BGEM population is derived from 67 landraces originating from 13 different countries (Sanchez et al., 2018). The BGEM population has previously been evaluated for flowering traits, kernel quality, and root architecture (Sanchez et al., 2018; Vanous et al., 2018; Vanous et al., 2019). We selected the BGEM population for this study as it is adapted to temperate climates and is a source of novel alleles not currently present in midwestern United States commercial germplasm.

The goals of this study were to (i) identify markers associated with resistance to NCLB in the BGEM population, (ii) identify potential metabolic pathways associated with resistance, and (iii) confirm the role of *in planta* ethylene production in NCLB resistance. We hypothesized that allelic diversity in the BGEM population would confer a range of resistance responses sufficient for genetic mapping when challenged with *E. turcicum*. Subsequently, we used the pathway association study tool (Thrash et al., 2020) to identify metabolic pathways associated with resistance. We confirmed the role of ethylene in the *E. turcicum*-maize pathosystem in the greenhouse by evaluating resistance responses of plants after treatment with $AgNO_3$, a chemical which limits *in planta* ethylene action (Beyer, 1976; Kumar et al., 2009). Our results provide additional insight into the role of phytohormones and resistance to NCLB.

2 Materials and methods

2.1 Germplasm

The BGEM population is a BC_1F_1 exotic-derived DH population. The population was developed at Iowa State University in collaboration with the USDA-ARS Germplasm Enhancement of Maize project (Pollak and Salhuana, 2001). Briefly, BC_1F_1 lines were created by crossing exotic accessions to one of two expired Plant Variety Protection (PVP) lines, namely PHZ51 or PHB47, backcrossing the resulting F_1 accessions were backcrossed to their respective ex-PVP parent, and then DH lines were created and self-pollinated (Brenner et al., 2012). Any lines that were infertile, lacked uniformity, or with poor agronomic traits were discarded. Genetically, the BGEM population is comprised of roughly 25% donor parent and 75% recurrent parent (Sanchez et al., 2018). The BGEM population represents a broad diversity of exotic derived maize. In total 67 landraces from 13 different countries are represented (Sanchez et al., 2018).

2.2 Experimental design

The BGEM population was screened for resistance to *E. turcicum* in three environments from 2019 to 2021. In total, all lines were evaluated four times in the field between 2019 and 2021 and twice in the greenhouse in 2020. All experiments were designed as augmented randomized incomplete block designs using the *agricolae* package (de Mendiburu, 2021) in the statistical software R, version 3.6.0 (R Core Team, 2021). Lines from BGEM population were screened at the Crop Sciences Research and Education Centers in Urbana, IL in 2019 (n = 252) and 2021 (n = 240). Differences in the number of lines used in 2019 and the other years were due to seed availability. Field plots were planted in rows that were 3.65 m long with 0.91 m alleys. The 2019 field was irrigated to encourage disease development. Lines were replicated twice in 2019 and 2021. In 2019, incomplete blocks (n = 14) were augmented with Oh7B and NC344 as susceptible and resistant checks, respectively. In 2021, Oh7B, NC344, PHB47, and PHZ51 served as check lines in each incomplete block (n = 16). In 2021 the following NCLB differential lines were included in each replication: A619-*Ht1*, A619-*Ht2*, A619-*Ht3*, A619, B37-*HtN1*, and B37.

In 2020, BGEM lines (n=240) were screened at the Plant Care Facility in Urbana, IL. The 2020 greenhouse experiment was replicated twice with 13 incomplete blocks in each replication. Due to space constraints, replications had to be run separately.

One plant per line was grown in a one-gallon pot filled with 1:1:1 general purpose potting mix. Greenhouse conditions were set to 12/12 hr. light-dark cycle. Ambient temperatures were set to 24-28°C during the day and 20-22°C during the night. Lines were organized in an augmented randomized incomplete block design. Oh7B and NC344 were susceptible and resistant check lines in each block. PHB47 and PHZ51 were randomized once in each replication. The same qualitative check lines used in 2021 were also used in the greenhouse in each replication.

2.3 Inoculation and phenotyping

In 2019 natural inoculum was relied upon for infection, as the growing season was conducive for disease development and evaluation. For all other experiments, inoculum was prepared using five fungal isolates (19StM06, 19StM07, 19StM09, 19StM11, 19StM12) that were isolated from diseased maize tissue collected from the 2019 field experiment at Crop Science Research and Education Center in Urbana, IL. A mixture of isolates was used to best reproduce disease pressure observed in 2019. For the 2020 greenhouse experiment, plants were inoculated with a spore suspension at the V3 stage (Adhikari et al., 2021). Fungal isolates were grown on lactose-casein hydrolysate agar (LCA) media for 14 days under 12/12 hr light/dark photoperiod at room temperature. Spores were harvested from 14-day old plates and the concentration adjusted to 4×10^3 spores/mL in a 0.02% Tween 20 solution. For inoculations, 0.5 mL of the spore suspension was pipetted into the whorl of the plants. Following inoculation, plants were maintained in high humidity conditions for 24 hours to facilitate disease development. In 2021 plants were inoculated at the V4 to V5 stage using infested sorghum grains (Zhang et al., 2020). Fungal isolates were cultured on LCA for 14 days as described above. After 14 days of culturing, agar pieces cut directly from the plates were added to mushroom bags containing 1000 mL of soaked, autoclaved sorghum grains. The mushroom bags were cultured for two to three weeks at room temperature under 12/12 hr light/dark photoperiod. The infested grains were examined under a dissecting microscope to confirm the presence of conidia then dried and stored at room temperature. Each plant was inoculated with 1.3 g of the prepared inoculum in the whorl at the V3 growth stage.

Disease ratings for the 2019 and 2021 field experiments were taken on a whole plot basis using a 0-100% scale in 5% increments (Poland and Nelson, 2011) where no disease present was represented by 0%, and a rating of 100% indicated that the total leaf area of the plants was necrotic due to disease. In 2019 two field ratings were taken after lines had started flowering, and ratings were taken 7 days apart. In 2021 a total of four field ratings were taken. Ratings were conducted every 7-14 days starting two weeks before the onset of flowering in the earliest maturing plants.

Lines in the 2020 greenhouse experiment were evaluated for incubation period and disease severity. Incubation period is defined as the number of days after inoculation (DAI) that the first lesions were visible. Lines were evaluated for incubation period every 48 hours until all plants showed lesions. In the greenhouse experiment, a total of four diseased leaf area ratings were taken. Disease leaf area ratings were taken every 7-14 days starting the day when all plants had lesions present. Lines were rated on a single leaf per plant basis using the same 0-100% rating scale mentioned above.

2.4 Statistical analyses

Disease severity data was examined using the standardized area under the disease progress curve (sAUDPC). sAUDPC is used to compare disease progression between environments or experiments (Simko and Piepho, 2012). sAUDPC is calculated by first measuring the area under the disease progress curve (AUDPC), which is the area of a trapezoid between two or more time points on a progression curve and accounts for disease severity over time (Jeger and Viljanen-Rollinson, 2001; Madden et al., 2007). The sAUDPC value is then obtained by dividing AUDPC by the weighted total of the number of days of disease evaluation. sAUDPC was calculated using the R package *agricolae* (de Mendiburu, 2021). Both days to anthesis (DTA) and days to silking (DTS) were recorded for the 2019 field experiment. DTA is defined as the number of days after planting when 50% or more of the plot had visible anthers on the tassel. DTS is defined as the number of days after planting when 50% or more of the plot had visible silks emerging from the ears. Pearson correlation coefficients for sAUDPC across all environments were calculated using the *rcorr()* function in the R package *Hmisc* v4.5-0 (Harrell, 2021). Flowering data was only collected in 2019. Using AUDPC, DTS, and DTA data from 2019, Pearson correlation coefficients were calculated between each trait.

Both sAUDPC and incubation period values were used to fit mixed models and estimate least squared means (LS Means). The following model was fit to estimate LS Means for sAUDPC in the 2019 + 2021 dataset:

$$\boldsymbol{Y_{ijkl}} = \mu + \boldsymbol{G_i} + \boldsymbol{R_j} + \boldsymbol{B_{l(j(k))}} + \boldsymbol{E_l} + \boldsymbol{GE_{il}} + \boldsymbol{\varepsilon_{ijkl}}$$

The factors are defined as follows: Y_{ijkl} is the sAUDPC value from genotype i in replicate j in block k and environment l; G_i is the fixed effect of genotype I; R_j is the random effect of replicate j; $B_{k(j)}$ is the random effect of block k nested in replicate j nested in environment l; E_l the random effect of the environment l; GE_{il} the random effect of the interaction between genotype i and environment l; and ε_{ijkl} the error term. From this model, LS Means were calculated from the estimates of G_i from the fitted model. For the 2020 incubation period dataset the following mixed model was fit:

$$\boldsymbol{Y_{ij}} = \mu + \boldsymbol{G_i} + \boldsymbol{B_j} + \boldsymbol{\varepsilon_{ij}}$$

Terms in the model are described as follows Y_{ij} is the incubation period value in days of genotype i in block j; G_i is the fixed effect of genotype i; B_j is the random effect of block j; and ε_{ij} the error term associated with Y_{ij}. The fixed effects for genotype in each model were extracted and used for further analysis. As with the previous

model, LS Means were calculated from the estimates of G_i from the fitted model.

2.5 Genotyping

The BGEM population was previously genotyped (Sanchez et al., 2018). A dataset consisting of 62,077 single nucleotide polymorphisms (SNPs) was obtained from Sanchez, Liu (Sanchez et al., 2018). This dataset was generated for the DH BGEM lines via genotyping-by-sequencing (Elshire et al., 2011) by the Cornell University Genomic Diversity Facility with data analysis by the Buckler Lab for Maize Genetics and Diversity. The 62,077 SNP dataset was generated by filtering SNPs with a large amounts of missing data and low allele frequencies, followed by SNPs in the same genetic position (Sanchez et al., 2018). Within the BGEM population, the average number of recombination events was higher than expected. A Bayes theorem described by Sanchez, Liu (Sanchez et al., 2018) was implemented to correct for monomorphic markers that were flanked by markers with donor parent genotypes. After correction, the number of recombination events was reduced, and the donor genome composition was closer to 25%, as expected. All edits to the genotypic dataset were conducted prior to this study.

2.6 Identification of markers associated with disease resistance

To identify candidate regions associated with resistance to *E. turcicum* two mapping strategies were employed using TASSEL v5.2.81 (Bradbury et al., 2007). First, we used a generalized linear model (GLM) in TASSEL to identify significant markers, as well as a stepwise regression approach to identify markers that were associated with disease severity and incubation period. The Bayesian corrected genotypic dataset was filtered to remove markers with a minor allele frequency less than 0.05. Two principal components, calculated in TASSEL using the standard PCA plugin, were used to control for population structure. The phenotypic datasets used were the LS Means estimated using the 2019 + 2021 combined disease severity and the 2020 incubation period datasets (File S1). The same genotypic dataset was used for both phenotypes. The GLM model was ran for both phenotypes with 1000 permutations. A significance threshold of $\alpha = 0.10$ was applied using permutation corrected *p*-values. For the second approach, stepwise regression was implemented in TASSEL independently of the GLM association analysis. The two principal components calculated in TASSEL were included as numeric covariates along with the estimated LS Means value for each line. The stepwise regression analysis was implemented for both the 2019 + 2021 combined disease severity and the 2020 incubation period datasets. The *p*-value model was used with 1000 permutations with entry and exit limits of 1×10^{-5} and 2×10^{-5}, respectively. A significance threshold of $\alpha = 0.10$ was used to identify significant SNPs.

2.7 Pathways Association Study Tool

The Pathway Association Study Tool (PAST) approach (Thrash et al., 2020) was implemented via the MaizeGDB online platform (Woodhouse et al., 2021). PAST is designed to take outputs generated by TASSEL and provide biological insight into association study results. The software interprets the results from association analysis to identify metabolic pathways associated with genes that are strongly associated with the trait through significant markers or when genes are moderately associated with a trait, but the markers themselves may not have been significant in the original association study. PAST uses the output from association analysis, allelic effects files, and a linkage disequilibrium file to assign SNPs to genes based on LD and genomic distance between SNPs and genes before then identifying significant metabolic pathways. PAST analysis was conducted for the 2019 + 2021 combined disease severity dataset and the 2020 incubation period dataset. The association and effect files generated from the GLM were used as the input for the PAST analysis. A gene assignment window size of 1000 base pairs was used. Pathways with at least five genes were considered and significance was determined based on 1000 permutations. A Type I error rate of $\alpha = 0.05$ was used to determine statistical significance for each pathway.

2.8 Differentially expressed genes associated with ethylene

A recent study examined differences in gene expression in maize and sorghum plants inoculated with different strains of *E. turicum* (Adhikari et al., 2021) (File S2). Our hypothesis was that genes involved in the synthesis of ethylene were differentially expressed in mock-inoculated maize plants versus *E. turcicum* inoculated maize plants. A list of genes associated with ethylene biosynthesis was downloaded from CornCyc7.5 available through the MaizeGDB (corncyc-b73-v3.maizegdb.org) (File S3).

Transcriptome data were generated by Adhikari et al. (2021). Briefly the maize line B73 was grown in the greenhouse and either inoculated with *E. turcicum* or mock inoculated with sterile deionized H_2O (DI H_2O). RNA was extracted from plant tissue collected at 24 and 72 hours after inoculation (hai) and sequenced at the Roy J. Carver Biotechnology Center at the University of Illinois at Urbana-Champaign. Quality control, alignment, and normalization were conducted using standard procedures (Adhikari et al., 2021). We used the final dataset with annotated differentially expressed genes (DEGs) and calculated false discovery rates (FDR) (Adhikari et al., 2021). (File S2). Global FDR adjusted p-values were calculated based on the Benjamini & Hochberg procedure (Benjamini and Hochberg, 1995).

Our objective with the RNA data was to examine the expression of genes associated with ethylene biosynthesis in maize during the *E. turcicum* infection stage. Therefore, we are interested in three contrasts: DEG of maize 24 and 72 hai with *E. turcicum*, DEG of maize 24 hai with *E. turcicum* and DI H_2O, and DEG of maize 72

hai with *E. turcicum* and DI H_2O. Using a list of known genes involved in ethylene biosynthesis (File S3), we filtered the normalized list of DEGs for those only involved in ethylene biosynthesis. Then, for each contrast we only examined DEGs with an FDR value greater than or equal to 0.05. We hypothesized that ethylene biosynthesis could be involved in maize early defense against *E. turcicum*.

2.9 Greenhouse ethylene assay

A subset of DH lines was chosen to evaluate the role of ethylene in resistance against *E. turcicum*. In maize, ethylene is inhibited by the foliar application of $AgNO_3$ (Kumar et al., 2009). Using LS Means data from the 2021 field experiment, we examined disease phenotypes within exotic donor families. Only the ex-PVP recurrent parents have been genotyped, and there is no genotypic information for the landrace donor parents. We chose a resistant and susceptible line, as we wanted to see if inhibiting ethylene affected phenotypes of resistant or susceptible lines differently (Table 1). We selected pairs of lines categorized as resistant or susceptible within five exotic landrace groups. Both ex-PVP recurrent parents, PHB47 and PHZ51, were included in the assay. Our goal was to assess the role of ethylene between resistant and susceptible lines, within different exotic families, and within different recurrent parent backgrounds.

The experiment was arranged in a split-plot design. The whole-plot was a complete block of plants, and the subplot was each BGEM line randomly assigned to each treatment within each complete block. Lines were either treated with $AgNO_3$ followed by inoculation with *E. turcicum*, or treated with DI H_2O followed by inoculation with *E. turcicum*. There were three whole-plots (complete blocks) per treatment and each line occurred once in each whole-plot. Greenhouse growing conditions were the same as the conditions described previously. The *E. turcicum* spore suspension was prepared as explained above. At the V3 growth stage, plants were treated with either 20 mM $AgNO_3$ in 0.001% Tween 20 (Wang et al., 2017) or with sterile water in 0.001% Tween 20 at a rate of 187 L ha^{-1} at 207 kPa using a spray chamber (Technical Machinery Inc., Sacramento, CA). The chamber was equipped with an even flat-fan nozzle 8002E (TeeJet Technologies, Wheaton, IL) and plants were sprayed 45 cm above the tallest leaf. After treatment, plants were allowed to dry completely before inoculation with 4×10^3 spores/mL in a 0.02% Tween 20 solution prepared as mentioned previously. Plants were inoculated by pipetting 0.5 mL of spore suspension into the whorl. After inoculation, a high-humidity environment was maintained overnight to encourage disease development. All plants were evaluated for incubation period and disease severity on a per plant basis as described previously. AUDPC was calculated using the *agricolae* package (de Mendiburu, 2021) in the statistical software R, version 3.6.0 (R Core Team, 2021). We ran an ANOVA to appropriately account for the differences in the whole-plots and the subplot replicates.

3 Results

3.1 Characterization of the BGEM population

The BGEM population was evaluated for DTA and DTS in 2019 and for resistance to *E. turcicum* in 2019 and 2021 in the field at the Crop Sciences Research and Education Center in Urbana, IL. A field trial of the BGEM population was lost during the 2020 growing season due to poor emergence, followed by a hailstorm, which destroyed the field. Thus, the BGEM population was grown a second time and evaluated for resistance in the greenhouse in 2020 at the Plant Care Facility in Urbana, IL. All checklines performed as expected. In the 2019 and 2021 field environments, Oh7B was more susceptible than NC344. The BGEM recurrent parents, PHB47 and PHZ51, were moderately resistant in the 2021 field season with PHZ51 being the more resistant recurrent parent. The observed range of phenotypes suggest that there was sufficient disease pressure in each experiment to evaluate for disease severity and incubation period, even in the uninoculated field trial (Table 2).

Due to the high evolutionary potential of *E. turcicum*, we examined whether isolates collected from Champaign County could overcome major genes associated with resistance. In 2020 and 2021 A619-*Ht1*, A619-*Ht2*, A619-*Ht3*, A619, B37-*HtN1*, and B37 were included to evaluate whether the mixture of 19StM06, 19StM07, 19StM09, 19StM11, 19StM12 were able to overcome major genes associated with resistance. In the 2020 greenhouse experiment we did not observe a significant difference in AUDPC or incubation period among lines containing major genes and their respective background based on a Dunnett's test ($\alpha = 0.05$), but we observed typical resistant responses for *Ht2, Ht3*, and *HtN1*. In the 2021 field experiment the AUDPC for A619-*Ht2* and A619-*Ht3* were significantly different from A619 based on a Dunnett's test ($p < 0.001$), indicating that *Ht2* and *Ht3* conferred resistance. Additionally, B37-*HtN1* was significantly different from B37 ($\alpha = 0.01$), indicating that *HtN* conferred resistance. Discrepancies between genotype performance in the greenhouse and the field environment could be due to other *E. turcicum* genotypes present in the field environment. The effectiveness of qualitative and quantitative under greenhouse conditions differs from the field environment (Raymundo and Hooker, 1981b; Chung et al., 2010). Thus, it is possible that the observed discrepancy in phenotypes between the field and greenhouse environments could be attributed to environmental effects on the plants, as well as additional strains present in the field environments.

We observed a difference in resistance responses between the greenhouse and field environments. The 2019 and 2021 field environments were strongly and significantly correlated, ($r = 0.64$, $\alpha = 0.001$) while the 2020 greenhouse environment had a weaker correlation with the 2019 field environment ($r = -0.21$, $\alpha = 0.01$) and the 2021 field environment ($r = -0.29$, $\alpha = 0.01$, Table 3). The strong correlation between the 2019 and 2021 field data underscores that similar levels of resistance were observed even though one field was artificially inoculated while the other relied on natural inoculum. In

TABLE 1 Lines selected to evaluate the role of ethylene in resistance against *E. turcicum*.

Line	Landrace	RP*	Pedigree	R/S^
BGEM-0078-S	Cristalino Amarillo	PHB47	(CRISTALINO AMAR AR21004/PHB47 #001-(2n)-002	R
BGEM-0079-S	Cristalino Amarillo	PHB47	(CRISTALINO AMAR AR21004/PHB47 #005-(2n)-003	S
BGEM-0087-N	Dulcillo del Noroeste	PHZ51	(DULCILLO DE NO SON57/PHZ51)/PHZ51 #001-(2n)-001-001-B	R
BGEM-0088-N	Dulcillo del Noroeste	PHZ51	(DULCILLO DE NO SON57/PHZ51)/PHZ51 #002-(2n)-002	S
BGEM-0108-S	Elotes Occident	PHZ51	(ELOTES OCCIDENT NAY29/PHB47)/PHB47 #002-(2n)-001-001-B	R
BGEM-0109-N	Elotes Occident	PHZ51	(ELOTES OCCIDENT DGO236/PHZ51)/PHZ51 #004-(2n)-002-002-B	S
BGEM-0120-N	Jora	PHZ51	((Jora - ANC 1/PHZ61 B)/PHZ51)-(2n)-001-001-B	R
BGEM-0121-N	Jora	PHZ51	((Jora - ANC 1/PHZ61 B)/PHZ51)-(2n)-002-001-B	S
BGEM-0162-S	Morado	PHB47	(MORADO BOV567/PHB47)/PHB47 #002-(2n)-001	R
BGEM-0167-S	Morado	PHB47	(MORADO BOV567/PHB47)/PHB47 #005-(2n)-003	S
PHB47	-	-	-	R
PHZ51	-	-	-	R

*RP, recurrent parent.
^R/S, Resistant/Susceptible.
Lines were selected in pairs from five exotic landrace groups based on phenotype to see if exotic landrace background influenced ethylene production and if inhibiting ethylene influenced the phenotypes of resistant and susceptible lines differently. Both recurrent parents, PHZ51 and PHB47, were included in the experiment.

TABLE 2 Variation for standardized AUDPC (sAUDPC), incubation period (IP), days to anthesis (DTA) and days to silk (DTS) in each environment the BGEM population was screened in.

Environment	Trait	Minimum	Maximum	Mean
2019 Field	sAUDPC*	17.50	87.50	42.59
2021 Field	sAUDPC*	8.07	49.43	27.62
2020 GH	IP^	5	19	10
2019 Field	DTA#	61	84	69
2019 Field	DTS+	63	84	71

*sAUDPC, standardized area under the disease progress curve.
^IP, incubation period, the number of days from inoculation to the appearance of first lesions.
#DTA, days to anthesis, the number of days after planting until 50% of the plot has visible anthers.
+DTS, days to silking, the number of days after planting until 50% of the plot has visible silks.

TABLE 3 Pearson correlation coefficients between LS Means disease severity among environments.

	2021 Field	2020 GH DLA+	2020 GH IP^
2019 Field	0.64***	0.16**	-0.21**
2021 Field		0.34***	-0.29***
2020 GH DLA			-0.37***

Significance *** $p \leq 0.001$, ** $p \leq 0.01$.
+DLA, diseased leaf area.
^IP, incubation period.
Field environments were evaluated for diseased leaf area (DLA) while greenhouse experiments were evaluated for incubation period (IP) and diseased leaf area.

the mixed model for the 2019 + 2021 combined dataset, environment contributed the most variance, followed by the genotype × environment interaction (Table 4). The model used to estimate LS Means in the 2020 incubation period dataset only included block but not replication. Replication was not included as it had a covariance estimate of zero, indicating that block and replication were redundant. By including the blocking factor in the model, we are still able to account for variation in the greenhouse environment. The 2020 greenhouse diseased leaf area was analyzed in the same manner as the 2020 greenhouse incubation period. The estimated LS Means for the 2019 + 2021 combined dataset and the 2020 incubation period dataset showed a range of phenotypic responses suitable for association mapping (Figure 1, Table 1).

3.2 Identification of significant markers associated with resistance to NCLB

In order to identify candidate markers associated with resistance to NCLB, we employed genome-wide association analysis using TASSEL (Bradbury et al., 2007). To control for population structure, two principal components were included in the model, as most of the variation is explained by the first two components (Figure 2). We then employed a GLM model using TASSEL to examine the genetic architecture of resistance to NCLB. For both the 2019 + 2021 field dataset and the 2020 greenhouse incubation period dataset log quantile-quantile plots were constructed to assess the effectiveness of two principal components to control population structure (Figures 3B, D). Given the genetic design of the BGEM population, this approach is appropriate to control for population structure while controlling for any false positives. The same mapping approach was used for the 2019 + 2021 field dataset, the 2020

TABLE 4 Covariance estimates with standard deviation for all fixed factors included in each mixed model used to estimate LS Means for incubation period and the 2019 + 2021 combined disease severity datasets.

Factor	2019 + 2021 Fields	Incubation Period	2020 GH DLA
Environment	95.65(9.78)	–	–
Genotype × Environment	17.20(4.15)	–	–
Environment/Replication/Block	11.71(3.42)	–	–
Environment/Replication	3.62(1.90)	–	–
Block	–	0.17 (0.41)	5520 (74.29)
Residuals	31.75(5.6)	2.32 (1.52)	5499 (74.16)

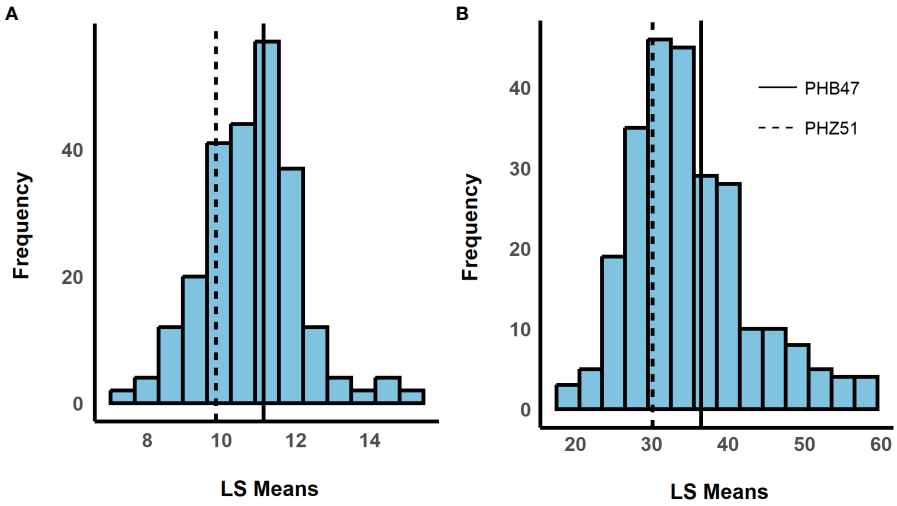

FIGURE 1
Histograms showing the distribution of least squared means (LS Means). The x-axis shows LS Means values, and the y-axis shows the frequency. LS Means were estimated for **(A)** incubation period and **(B)** standardized area under the disease progress curve (sAUDPC). Dashed and solid horizontal lines represent recurrent parents PHZ51 and PHB47, respectively. (180 x 100 mm, 300 dpi).

greenhouse incubation period dataset, and the 2020 greenhouse diseased leaf area dataset. We did not identify any significant markers using the 2020 greenhouse diseased leaf area dataset. In total, four significant markers were identified using the GLM model in TASSEL (Figure 3).

The BGEM-DH lines have a high percentage of recurrent parent genome, and as such, linkage disequilibrium (LD) decays at a much slower rate than expected. In some regions, the LD blocks are large and span 100,000,000 bp or beyond (Sanchez et al., 2018). Given the LD structure in this population, we considered genes within 1 Mbp of a significant marker when examining candidate genes. Three markers on chromosome 3 were associated with delayed incubation period (Table 5, Figure 3A). A stepwise regression approach using the same marker dataset identified a single significant marker for incubation period on chromosome three (S3_8266879; $p = 5 \times 10^{-5}$), which was also significant in the GLM model (p = 0.033, Table 5, Figure 3A). The marker S3_8266879 is within GRMZ2G108898, plant cysteine oxidase 1 (*PCO1*). *PCO1* spans from 8,263,929 bp to 8,269,675 bp on chromosome 3. The other two significant markers identified in the GLM model for incubation period, S3_15712704 (p = 0.53) and S3_18008517 (p = 0.55) were proximal to GRMZM2G445261 a probable carboxylesterase 15 and GRMZM2G380195 a pentatricopeptide repeat-containing protein chloroplastic, respectively. While these genes were the closest to the most significant marker, it is important to keep in mind the extensive LD structure in this population.

Resistance to diseased leaf area (DLA) is genetically distinct from incubation period; a single marker was significant on chromosome 2 (Figure 3C). The significant marker, S2_10777410 (p = 0.053), is proximal to GRMZM2G068982, a methionine aminopeptidase. Using the same marker dataset, a stepwise regression approach did not reveal any significant markers for the field DLA dataset (Table 5). Stepwise regression is more conservative than GLM, and our findings are consistent in that no significant markers were identified using stepwise regression.

There was no overlap in significant markers for incubation period and disease severity. We observed a weak negative

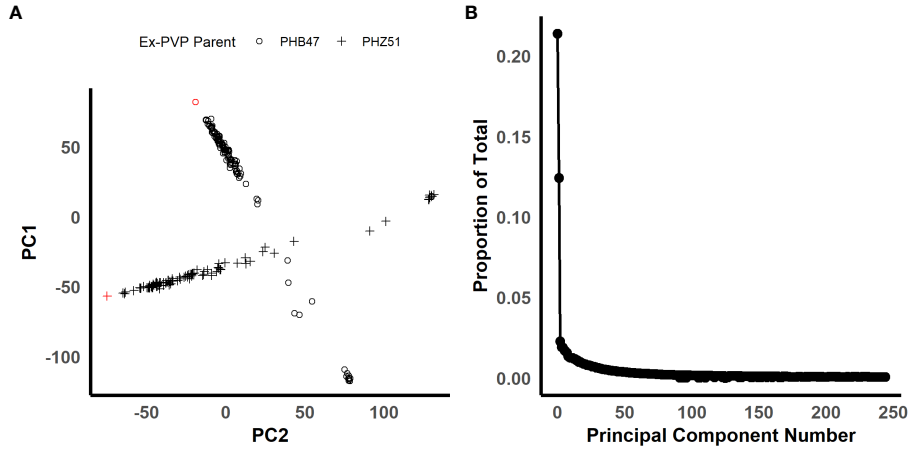

FIGURE 2
Figures illustrating the population structure of the BGEM population. **(A)** Is a scatter plot for principal components 1 and 2 plotted against each other. The shape of the points represents each ex-PVP background. The ex-PVP parents, PHB47 and PHZ51, are highlighted in red. **(B)** Is a scree plot of all principal components. The x-axis is the principal component number, and the y-axis is the proportion of total variation explained by each principal component. (200 x 100 mm, 300 dpi).

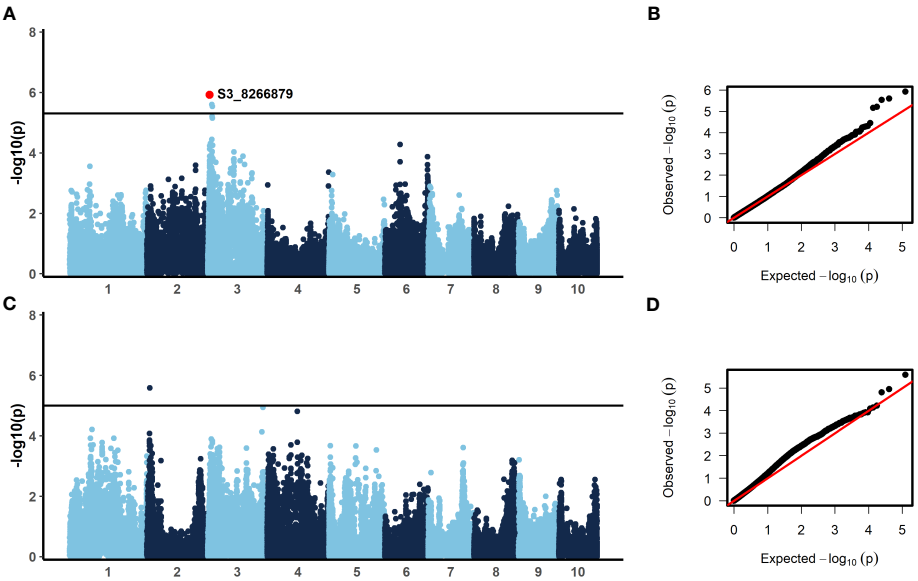

FIGURE 3
Results from the generalized linear model (GLM) with two principal components to control for population structure **(A, C)** and qq-plots showing observed versus expected -$\log_{10}(p)$ **(B, D)**. A significance threshold of α=0.1 was established based on 1000 permutations conducted in TASSEL. For incubation period, evaluated in the greenhouse in 2020, **(A, B)** three SNPs were significant. The annotated SNP, S3_8266879, was also significant with a stepwise regression model. For the 2019 + 2021 combined field sAUDPC data, **(C, D)** one SNP was significant. (300 x 180 mm, 300 dpi).

TABLE 5 SNPs associated with resistance to *E. turcicum* were identified in the BGEM populations using genome-wide association and stepwise regression models.

Dataset	Chr.*	SNP^	Perm. *p*-value (GWAS)	*p*-value (Step Reg.)	Nearest gene	Distance from marker (BP)
Incubation Period	3	S3_8266879	0.033	5×10^{-5}	GRMZM2G108898	Genic
Incubation Period	3	S3_15712704	0.053	–	GRMZM2G445261	10,690
Incubation Period	3	S3_18008517	0.055	–	GRMZM2G380195	1,896
2019 + 2021 LS Means	2	S2_10777410	0.053	–	GRMZM2G068982	5,033

* Chromosome.
^ Single Nucleotide Polymorphism.
The significant SNPs identified in the 2019 + 2021 combined dataset and for incubation period are shown.

correlation between disease severity and incubation period (Table 3). Although we observed some chlorotic resistant responses in our 2019 and 2021 field experiments and 2020 greenhouse experiment, we did not identify any significant markers near any of the major genes for NCLB resistance, *Ht1, Ht2, Ht3, HtN1* (Figure S1). If the qualitative resistance genes were present in the population, they may have been at too low of a frequency to detect any significant markers in these regions. It is also possible that these responses were due to novel resistance genes.

3.3 Metabolic pathways associated with disease resistance

To better understand the molecular mechanisms associated with resistance to NCLB we conducted a metabolic pathway analysis and examined a previously published RNA-seq dataset. We identified metabolic pathways associated with disease severity and incubation period using the results from the GLM model and the PAST software (Thrash et al., 2020). In total, 24 metabolic pathways ($\alpha = 0.05$) were associated with resistance to *E. turcicum* (Table 6), including nine associated with incubation period and 15 associated with disease severity. Several pathways associated with plant hormones were significant including jasmonic acid biosynthesis (PWY-735, $p = 0.02$) and cytokine-O-glucosides biosynthesis (PWY-2902, $p = 0.04$) in the combined disease severity dataset. Additionally, gibberellin inactivation I (PWY-102, $p = 0.01$) and brassinosteroids inactivation (PWY-6546, $p = 0.03$) were significant in the incubation period dataset. A pathway of particular interest is the ethylene biosynthesis pathway (ETHYL-PWY) which was significant for both incubation period ($p = 0.006$) and disease severity ($p = 0.01$). Ethylene synthesis has previously been associated with disease resistance in plants (Dong, 1987; van Loon et al., 2006). Additionally, S-adenosyl-L-methionine cycle II (PWY-5041) was significant for disease severity. S-adenosyl-L-methionine (SAM) is the starting substrate in ethylene synthesis. It is converted to 1-aminocyclopropane-1-carboxylic acid (ACC) by ACC synthase (ACS), which is subsequently converted into ethylene via oxidation by ACC oxidase (ACO) (Xu and Zhang, 2015).

Pathogens are known to mimic phytohormones and interfere with signaling (Denance et al., 2013), as well as to target regulatory components involved with *in planta* hormone production (Robert-Seilaniantz et al., 2011). Thus, we examined an RNA-seq dataset (Adhikari et al., 2021) for DEGs associated with ethylene biosynthesis during the early stages of infection. We examined three contrasts: inoculated versus uninoculated maize 24 hai, inoculated versus uninoculated maize 72 hai, and inoculated maize 24 versus 72 hai. Only one gene associated with ethylene biosynthesis, GRMZM2G07529 (FDR = 0.03), was upregulated, with a fold change of 16.87, in maize 24 hai with *E. turcicum* compared to maize 24 hai with DI H_2O. GRMZM2G07529 is annotated as ACC oxidase *ACO31*. ACO is the final oxidation step in the synthesis of ethylene (Xu and Zhang, 2015). Thus, during the initial phases of infection ethylene production may be increased, indicating that it may play a role in resistance to NCLB.

3.4 Investigation of ethylene and resistance to *E. turcicum*

We hypothesized that inhibiting ethylene would alter NCLB disease severity. We used a foliar treatment of $AgNO_3$ to examine the effect of ethylene on disease resistance. $AgNO_3$ inhibits ethylene action *in planta* by reducing the ability of ethylene receptors to bind to ethylene, which results in decreased ethylene sensitivity and the inhibition of continuous ethylene production (Kumar et al., 2009). We hypothesized that inhibition of ethylene by applying $AgNO_3$ would decrease disease severity and increase incubation period. Furthermore, we postulated that host resistant level and genetic background might alter the magnitude by which inhibiting ethylene improves resistance and increases incubation period.

To examine the role of ethylene in *E. turcicum* infection, a total of 10 DH lines and both recurrent parents were selected. We selected DH lines in pairs within each exotic family, where the pair had contrasting disease phenotypes. Plants were either treated with $AgNO_3$ or DI H_2O prior to a whorl inoculation with *E. turcicum*. From our ethylene inhibition assay, disease severity was significantly impacted by genotype (Table 7, $p = 0.012$) and by treatment with $AgNO_3$ or deionized H_2O (Table 7, $p = 1.756 \times 10^{-5}$). Similarly, incubation period was significantly impacted by genotype (Table 8, $p = 0.004$) and by treatment with $AgNO_3$ or deionized H_2O Table 8,

TABLE 6 Significant metabolic pathways associated with increasing or decreasing incubation period and the 2019 + 2021 combined disease severity datasets.

Pathway ID	Pathway Name	*p*-Value	Effect	Dataset
ETHYL-PWY	ethylene biosynthesis I (plants)	0.0062419	Decrease	IP*
PWY-5667	CDP-diacylglycerol biosynthesis I	0.0273528	Decrease	IP
PWY-5138	unsaturated, even numbered fatty acid-oxidation	0.0354694	Decrease	IP
PWY-3181	tryptophan degradation VI (via tryptamine)	0.0367993	Decrease	IP
PWY-581	indole-3-acetate biosynthesis II	0.0459157	Decrease	IP
PWY-5080	very long chain fatty acid biosynthesis I	0.0026768	Increase	IP
PWY-102	gibberellin inactivation I (2-hydroxylation)	0.0152976	Increase	IP
PWY-5097	lysine biosynthesis VI	0.0268191	Increase	IP
PWY-6546	brassinosteroids inactivation	0.0334693	Increase	IP
LIPASYN-PWY	phospholipases	0.007419	Decrease	DLA#
PWY-6441	spermine and spermidine degradation III	0.011873	Decrease	DLA
PWY-735	jasmonic acid biosynthesis	0.022039	Decrease	DLA
PWY-5097	lysine biosynthesis VI	0.032238	Decrease	DLA
PWY-6959	L-ascorbate degradation V	0.032430	Decrease	DLA
PWY-6803	phosphatidylcholine acyl editing	0.037275	Decrease	DLA
PWY-2902	cytokinin-O-glucosides biosynthesis	0.048633	Decrease	DLA
PWY-5041	S-adenosyl-L-methionine cycle II	0.007802	Increase	DLA
ETHYL-PWY	ethylene biosynthesis I (plants)	0.014177	Increase	DLA
PWY-5690	TCA cycle II (plants and fungi)	0.019701	Increase	DLA
PWY-6363	D-myo-inositol (1,4,5)-trisphosphate degradation	0.021242	Increase	DLA
PWY-702	methionine biosynthesis II	0.026966	Increase	DLA
PWY-6549	glutamine biosynthesis III	0.031528	Increase	DLA
UDPNACETYLGALSYN-PWY	UDP-N-acetyl-D-glucosamine biosynthesis II	0.047356	Increase	DLA
PWY-5138	unsaturated, even numbered fatty acid-oxidation	0.047695	Increase	DLA

*IP, incubation period.
#DLA, diseased leaf area.
Only pathways significant at $\alpha = 0.05$ are shown.

$p = 4.281 \times 10^{-5}$). In plants treated with $AgNO_3$, incubation period increased and AUDPC decreased (Figure 4). We did not observe a significant impact of the line's resistance level, exotic family, or recurrent parent on AUDPC or incubation period ($\alpha = 0.05$). In this experiment, application of $AgNO_3$ affected all genotypes similarly meaning that, of the lines screened, no line was more or less resistant relative to the other lines after $AgNO_3$ application; thus, inhibiting ethylene using $AgNO_3$ decreases disease severity similarly in the lines screened.

4 Discussion

We evaluated the exotic-derived BGEM population for resistance to NCLB and examined the role of metabolic pathways in resistance to NCLB, specifically ethylene. We identified several significant markers for diseased leaf area and incubation period. These markers can be used to enrich the repertoire of quantitative resistance genes effective against *E. turcicum*. Additionally, we report that the ethylene synthesis pathway modulates a defense response against *E. turcicum*. Finally, we report variation in the ethylene metabolic pathway as a whole that is associated with resistance to NCLB.

This is the first study to report on disease resistance in the BGEM population. While we did not map any previously identified qualitative genes, several interesting responses were observed during the early stages of infections in some lines (Figure S1). Of note, the lines BGEM-0081-S, BGEM-0027-S, BGEM-0087-S, BGEM-0116-S, and BGEM-0154-S showed defense responses that were the most unique, could be useful in breeding for resistance and are worth examining closer in future experiments (Figure S1). Allelic variation has been reported for the major genes *Ht2/3* (Hurni et al., 2015; Yang et al., 2021), and it would be reasonable to expect allelic variation for other qualitative resistance genes.

TABLE 7 Analysis of variance (ANOVA) output from the model used to evaluate the split-plot ethylene design to assess the effect of whole-plot and subplot on AUDPC.

Source	DF*	SS#	MS^	F-value	P-value
Whole Plot	2	5524	2762.1	1.6573	0.20764
Genotype	11	51549	4686.3	2.8117	0.01209
Whole Plot/Treatment	3	62622	20873.9	12.5241	1.756×10^{-5}
Whole Plot × Genotype	22	35546	1615.7	0.9694	0.52271
Error	30	50001	1666.7		

*DF, degrees of freedom.
#SS, sums of squares.
^MS, mean squares.

TABLE 8 Analysis of variance (ANOVA) output from the model used to evaluate the split-plot ethylene design to assess the effect of whole-plot and subplot on incubation period.

Source	DF*	SS#	MS^	F-value	P-value
Whole Plot	2	0.75	0.375	0.3123	0.7339
Genotype	11	43.042	3.9129	3.2587	0.00417
Whole Plot/Treatment	3	38.875	12.9583	10.7918	4.281×10^{-5}
Whole Plot × Genotype	22	30.583	1.3902	1.1577	0.34438
Error	33	39.625	1.2008		

*DF, degrees of freedom.
#SS, sums of squares.
^MS, mean squares.

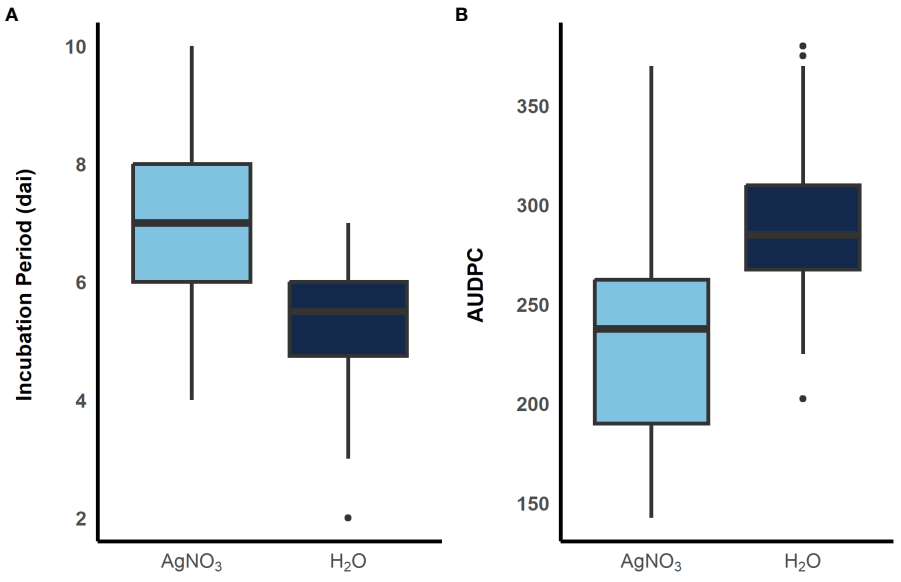

FIGURE 4
Boxplots showing distribution of incubation period **(A)** and AUDPC **(B)** when plants were sprayed with $AgNO_3$, light blue, and sterile water, dark blue, before inoculation with *E. turcicum*. A total of 12 plants were replicated three times in each treatment. (300 x 115 mm, 300 dpi).

We identified three markers associated with incubation period and one marker associated with DLA (Table 5). We observed no overlap between the significant markers associated with incubation period and the marker associated with diseased leaf area indicating that the genetic architecture underlying disease severity and incubation period are distinct. It was surprising to see no overlap in significant markers for disease severity and incubation period; however, this phenomenon has been reported previously (Balint-

Kurti et al., 2010). Incubation period and disease severity are important measures of resistance to *E. turccium*. Both traits are typically strongly correlated (Smith and Kinsey, 1993; Welz and Geiger, 2000). In this study we observed significant, weak negative correlations between disease severity and incubation period (Table 3), suggesting that the ability to delay the onset of lesions is a separate component of resistance than restricting the pathogen growth after initial lesion development. Both incubation period and disease severity are believed to be controlled by genetically similar mechanisms (Schechert et al., 1999; Welz et al., 1999).

Of the three significant markers associated with incubation period, one marker (S3_8266879) was significant after the stepwise regression approach in TASSEL and is within GRMZM2G108898, a plant cysteine oxidase 1 (PCO1). Plant cysteine oxidases are associated with oxygen sensing and stress response in plants (Weits et al., 2014). When under hypoxic conditions, such as flooding, PCOs initiate downstream ethylene production by stabilizing ethylene response factors (ERFs) such as ERF-VII (Hartman et al., 2021). In Arabidopsis, several PCOs were found to be sensitive to *in planta* oxygen levels and necessary for mediating the stability of ERF-VII transcription factors in low oxygen environments (White et al., 2018). Because ethylene is a stress hormone, it makes sense that ERFs would be important in plant hosts under abiotic and biotic stress factors. In maize two ERFs, *ZmERF061* and *ZmERF105*, have been implicated as important for NCLB resistance (Zang et al., 2020; Zang et al., 2021).

We identified a single marker associated with disease severity, S2_10777410. This marker is proximal to a methionine aminopeptidase, GRMZM2G068982. Methionine aminopeptidases function as catalysts in cleaving methionine from synthesized polypeptides. Methionine is involved in many metabolic pathways, including the production of ethylene. The ethylene biosynthesis pathway was significant (α = 0.05) in the post-GWAS PAST analysis. Interestingly, *ACO* was strongly upregulated in maize plants 24 hai with *E. turcicum* compared to mock inoculated control. It is known that ethylene production is upregulated in response to pathogen invasion (Li et al., 2012; Xu and Zhang, 2015). The final step in ethylene synthesis is the oxidation of ACC by ACO which yield ethylene. The upregulation of *ACO* during the initial stages of infection supports our hypothesis that ethylene is an important defense-related hormone for resistance against NCLB. In our ethylene experiment, we saw that the inhibition of ethylene significantly increased incubation period and significantly decreased disease severity. This same trend has been observed in other pathosystems, where inhibiting ethylene or decreasing ethylene production improves resistance (Dong, 1987; van Loon et al., 2006; Wang et al., 2017).

The role of ethylene in plant defense against biotic stress factors, such as pests and pathogens, is highly complex, as both the synthesis and response to ethylene can be modulated to confer resistance or susceptibility. In some pathosystems it has also been shown that plant sensitivity to ethylene production is important in mediating resistance. Ethylene insensitive mutants in Arabidopsis had higher disease severity to necrotrophic and hemibiotrophic pathogens, while disease severity was lower for biotrophic pathogens (van Loon et al., 2006). In rice, increased accumulation of ethylene increased host susceptibility to rice dwarf virus (Zhao et al., 2017), but decreased ethylene accumulation resulted in decreased resistance to the hemibiotrophic pathogen *Magnaporthe oryzae* (Zhai et al., 2022). In tomato, plants with antisense mutations for the ERF *LeETR4* were generally more resistant to the bacterial pathogen *Xanthomonas campestris* pv. *vesicatoria*, suggesting expression of ERFs may be important in rapid response to pathogen invasion (Ciardi et al., 2001). Two ERFs have been identified in maize. Transcription of these ERFs are upregulated during *E. turcicum* infection, suggesting that ethylene sensitivity may be as important as ethylene production in defense response (Zang et al., 2020; Zang et al., 2021). Given the complexity of the role of ethylene in stress response, it is likely that there are many pleiotropic effects associated with ethylene synthesis and sensing.

After ethylene is synthesized, there are several downstream effects, including interactions with JA, as well as potential pleiotropic roles. In Arabidopsis it was shown that ethylene biosynthesis is activated due to insect herbivory, with downstream effects, such as increased transcription of ethylene response factors and JA synthesis (Rehrig et al., 2014). Additionally, in Arabidopsis a calcium elongation factor and a glutathione S-transferase were upregulated when ethylene production was increased (Stotz et al., 2000). Other downstream effects of ethylene synthesis include increased callose accumulation and increased expression of *Tdy2*, enhancing overall resistance to aphids in maize (Varsani et al., 2019). In maize, ethylene production is shown to mediate the expression of *mir-1*, an insect defense related gene, and is believed to also interact with JA (Harfouche et al., 2006). Metabolite abundance has been implicated and ethylene synthesis have been shown to be interconnected in mediating resistance to the necrotrophic pathogen *Fusarium graminearum* (Zhou et al., 2019).

Most research has investigated the qualitative role of ethylene in plant-pathogen interactions. However, little is known about the effect of allelic variation in ethylene related genes on disease severity. Here we show that there is variation in the ethylene metabolic pathway as a whole that is signiciantly associated with NCLB resistance. Our study is limited in that we did not measure ethylene production or the expression of genes associated with the production or response to ethylene. However, the ethylene inhibition experiment suggests that ethylene is an important part of the maize-*E. turcicum* pathosystem. Other areas of exploration would be to measure quantitative differences in ethylene production in response to pathogen inoculation in lines with allelic diversity in the ethylene pathway, as well as to evaulate mutants and natural alleles of genes related to ethylene biosynthesis and sensing. Additionally, future studies could examine the effect of the exogenous application of ethylene on gene expression and disease resistance. While no individual genotypes were statistically different between treatment with $AgNO_3$ and sterile water, we observed a range in disease severity in each treatment. Based on our findings, it is plausible that allelic variation in genes associated with ethylene production and ethylene sensitivity could translate to altered defense responses.

5 Conclusion

Northern corn leaf blight is an economically important disease. We screened the BGEM population for resistance to NCLB, identified metabolic pathways associated with resistance to NCLB, and confirmed the role of ethylene in resistance to NCLB. In this study we demonstrate the utility of the BGEM population as a source of novel alleles for resistance, and contribute to the growing body of literature focused on the role of ethylene in plant-microbe interactions, specifically maize-*E. turcicum*. In this study, we contribute to the growing body of literature by examining the role of ethylene in NCLB resistance.

Data availability statement

The datasets presented in this study can be found in online repositories. The names of the repository/repositories and accession number(s) can be found in the article/Supplementary material.

Author contributions

SL: Conceptualization, Formal Analysis, Investigation, Methodology, Validation, Visualization, Writing – original draft. AL: Methodology, Validation, Writing – review and editing. SM: Conceptualization, Methodology, Resources, Writing – review and editing. TJ: Conceptualization, Data curation, Funding acquisition, Methodology, Project administration, Resources, Supervision, Writing – review and editing.

Funding

The authors declare financial support was received for the research, authorship, and/or publication of this article. This research was supported by the Department of Energy (DOE) Office of Science, Office of Biological and Environmental Research (BER), grant no. DE-SC0019189 to TJ and SM.

Acknowledgments

The authors would like to acknowledge Aislinn Geedey for critical feedback in the manuscript preparation.

Conflict of interest

The authors declare that the research was conducted in the absence of any commercial or financial relationships that could be construed as a potential conflict of interest.

Publisher's note

Supplementary material

The Supplementary Material for this article can be found online at: https://www.frontiersin.org/articles/10.3389/fpls.2023.1272951/full#supplementary-material

SUPPLEMENTARY FIGURE 1
Variation in chlorotic responses during the early stages of *E. turcicum* infection and colonization in multiple BGEM lines, **(A)** BGEM-0081-S, **(B)** BGEM-0027-S, **(C)** BGEM-0087-S, **(D)** BGEM-0016-S, **(E)** BGEM-0154-S.

References

Adhikari, P., Mideros, S. X., and Jamann, T. M. (2021). Differential regulation of maize and sorghum orthologs in response to the fungal pathogen exserohilum turcicum. *Front. Plant Sci.* 12, 675208. doi: 10.3389/fpls.2021.675208

Balint-Kurti, P. J., Yang, J., Van Esbroeck, G., Jung, J., and Smith, M. E. (2010). Use of a maize advanced intercross line for mapping of QTL for northern leaf blight resistance and multiple disease resistance. *Crop Sci.* 50 (2), 458–466. doi: 10.2135/cropsci2009.02.0066

Benjamini, Y., and Hochberg, Y. (1995). Controlling the false discovery rate: A practical and powerful approach to multiple testing. *J. R Stat. Soc. B.* 57 (1), 289–300. doi: 10.1111/j.2517-6161.1995.tb02031.x

Beyer, E. M. (1976). A potent inhibitor of ethylene action in plants. *Plant Physiol.* 58, 268–271. doi: 10.1104/pp.58.3.268

Bradbury, P. J., Zhang, Z., Kroon, D. E., Casstevens, T. M., Ramdoss, Y., and Buckler, E. S. (2007). TASSEL: Software for association mapping of complex traits in diverse samples. *Bioinformatics* 23 (19), 2633–2635. doi: 10.1093/bioinformatics/btm308

Brenner, E. A., Blanco, M., Gardner, C., and Lübberstedt, T. (2012). Genotypic and phenotypic characterization of isogenic doubled haploid exotic introgression lines in maize. *Mol. Breeding.* 30 (2), 1001–1016. doi: 10.1007/s11032-011-9684-5

Chung, C. L., Longfellow, J. M., Walsh, E. K., Kerdieh, Z., Van Esbroeck, G., Balint-Kurti, P., et al. (2010). Resistance loci affecting distinct stages of fungal pathogenesis: use of introgression lines for QTL mapping and characterization in the maize–*Setosphaeria turcica* pathosystem. *BMC Plant Biol.* 10, 103. doi: 10.1186/1471-2229-10-103

Ciardi, J. A., Tieman, D. M., Jones, J. B., and Klee, H. J. (2001). Reduced Expression of the Tomato Ethylene Receptor Gene LeETR4 Enhances the Hypersensitive Response to Xanthomonas campestris pv vesicatoria. *Mol. Plant-Microbe Interact* 14 (4), 9. doi: 10.1094/MPMI.2001.14.4.487

de Mendiburu, F., and Muhammad, Y. (2021). *agricolae: Statistical procedures for agricultural research*. Rpackage version 1.4.0, Available at: https://cran.r-project.org/package=agricolae.

Denance, N., Sanchez-Vallet, A., Goffner, D., and Molina, A. (2013). Disease resistance or growth: the role of plant hormones in balancing immune responses and fitness costs. *Front. Plant Sci.* 4, 155. doi: 10.3389/fpls.2013.00155

De Rossi, R. L., Guerra, F. A., Plazas, M. C., Vuletic, E. E., Brücher, E., Guerra, G. D., et al. (2022). Crop damage, economic losses, and the economic damage threshold for northern corn leaf blight. *Crop Prot.* 154 (2022), 105901. doi: 10.1016/j.cropro.2021.105901

Doblas-Ibáñez, P., Deng, K., Vasquez, M. F., Giese, L., Cobine, P. A., Kolkman, J. M., et al. (2019). Dominant, Heritable Resistance to Stewart's Wilt in Maize Is Associated with an Enhanced Vascular Defense Response to Infection withPantoea stewartii. *Mol. Plant-Microbe Interactions®* 32 (12), 1581–1597. doi: 10.1094/MPMI-05-19-0129-R

Dong, X. S. A. (1987). JA, ethylene, and disease resistance in plants. *Curr. Opin. Plant Biol.* 1, 8. doi: 10.1016/1369-5266(88)80053-0

Elshire, R. J., Glaubitz, J. C., Sun, Q., Poland, J. A., Kawamoto, K., Buckler, E. S., et al. (2011). A robust, simple genotyping-by-sequencing (GBS) approach for high diversity species. *PloS One* 6 (5), e19379. doi: 10.1371/journal.pone.0019379

Galiano-Carneiro, A. L., and Miedaner, T. (2017). Genetics of resistance and pathogenicity in the maize/*setosphaeria turcica* pathosystem and implications for breeding. *Front. Plant Sci.* 8, 1490. doi: 10.3389/fpls.2017.01490

Glazebrook, J. (2005). Contrasting mechanisms of defense against biotrophic and necrotrophic pathogens. *Annu. Rev. Phytopathol.* 43, 205–227. doi: 10.1146/annurev.phyto.43.040204.135923

Harfouche, A. L., Shivaji, R., Stocker, R., Williams, P. W., and Luthe, D. S. (2006). Ethylene signaling mediates a maize defense response to insect herbivory. *MPMI* 19 (2), 189–199. doi: 10.1094/MPMI-19-0189

Harrell, Jr. F. E. (2021). *Package 'Hmisc'*. Rpackage version 5.1-0. Available at: https://hbiostat.org/R/Hmisc/.

Hartman, S., Sasidharan, R., and Voesenek, L. A. C. J. (2021). The role of ethylene in metabolic acclimations to low oxygen. *New Phytol* 229 (1), 64–70. doi: 10.1111/nph.16378

Huang, P. Y., Catinot, J., and Zimmerli, L. (2016). Ethylene response factors in Arabidopsis immunity. *J. Exp. Bot.* 67 (5), 1231–1241. doi: 10.1093/jxb/erv518

Hurni, S., Scheuermann, D., Krattinger, S. G., Kessel, B., Wicker, T., Herren, G., et al. (2015). The maize disease resistance gene *Htn1* against northern corn leaf blight encodes a wall-associated receptor-like kinase. *Proc. Natl. Acad. Sci. U S A.* 112 (28), 8780–8785. doi: 10.1073/pnas.1502522112

Jamann, T. M., Luo, X., Morales, L., Kolkman, J. M., Chung, C. L., and Nelson, R. J. (2016). A remorin gene is implicated in quantitative disease resistance in maize. *Theor. Appl. Genet.* 129 (3), 591–602. doi: 10.1007/s00122-015-2650-6

Jamann, T. M., Poland, J. A., Kolkman, J. M., Smith, L. G., and Nelson, R. J. (2014). Unraveling genomic complexity at a quantitative disease resistance locus in maize. *Genetics* 198 (1), 333–344. doi: 10.1534/genetics.114.167486

Jeger, M. J., and Viljanen-Rollinson, S. L. H. (2001). The use of the area under the disease-progress curve (AUDPC) to assess quantitative disease resistance in crop cultivars. *Theor. Appl. Genet.* 102, 32–40. doi: 10.1007/s001220051615

Jindal, K. K., Tenuta, A. U., Woldemariam, T., Zhu, X., Hooker, D. C., and Reid, L. M. (2019). Occurrence and distribution of physiological races of exserohilum turcicum in ontario, Canada. *Plant Dis.* 103 (7), 1450–1457. doi: 10.1094/PDIS-06-18-0951-SR

Kotze, R. G., van der Merwe, C. F., Crampton, B. G., and Kritzinger, Q. (2019). A histological assessment of the infection strategy of Exserohilum turcicum in maize. *Plant Pathol.* 68 (3), 504–512. doi: 10.1111/ppa.12961

Kumar, V., Parvatam, G., and Ravishankar, G. A. (2009). AgNO3 - a potential regulator of ethylene activity and plant growth modulator. *Electronic J. Biotechnol.* 12 (2), 0–. doi: 10.2225/vol12-issue2-fulltext-1

Li, G., Meng, X., Wang, R., Mao, G., Han, L., Liu, Y., et al. (2012). Dual-level regulation of ACC synthase activity by MPK3/MPK6 cascade and its downstream WRKY transcription factor during ethylene induction in Arabidopsis. *PloS Genet.* 8 (6), e1002767. doi: 10.1371/journal.pgen.1002767

Madden, L. V., Hughes, G., and van den Bosch, F. (2007). *The study of plant disease epidemics* (St. Paul, Minnesota: APS Press).

McDonald, B. A., and Linde, C. (2002). Pathogen population genetics, evolutionary potential, and durable resistance. *Annu. Rev. Phytopathol.* 40, 349–379. doi: 10.1146/annurev.phyto.40.120501.101443

Miedaner, T., and Juroszek, P. (2021). Global warming and increasing maize cultivation demand comprehensive efforts in disease and insect resistance breeding in north-western Europe. *Plant Pathol.* 70 (5), 1032–1046. doi: 10.1111/ppa.13365

Mueller, D. S., Wise, K. A., Sisson, A. J., Allen, T. W., Bergstrom, G. C., Bissonnette, K. M., et al. (2020). Corn yield loss estimates due to diseases in the United States and ontario, Canada, from 2016 to 2019. *Plant Health Prog* 21 (4), 238–247. doi: 10.1094/PHP-05-20-0038-RS

Muller, M., and Munne-Bosch, S. (2015). Ethylene response factors: a key regulatory hub in hormone and stress signaling. *Plant Physiol.* 169 (1), 32–41. doi: 10.1104/pp.15.00677

Muñoz-Zavala, C., Loladze, A., Vargas-Hernández, M., García-León, E., Alakonya, A. E., Tovar-Pedraza, J. M., et al. (2022). Occurrence and distribution of physiological races of exserohilum turcicum in maize growing regions of Mexico. *Plant Dis.* 107, 1054-1059.

Munoz-Zavala, C., Loladze, A., Vargas-Hernandez, M., Garcia-Leon, E., Alakonya, A. E., Tovar-Pedraza, J. M., et al. (2023). Occurrence and distribution of physiological races of exserohilum turcicum in maize-growing regions of Mexico. *Plant Dis.* 107 (4), 1054–1059. doi: 10.1094/PDIS-03-22-0626-RE

Navarro, B. L., Hanekamp, H., Koopmann, B., and von Tiedemann, A. (2020). Diversity of expression types of ht genes conferring resistance in maize to exserohilum turcicum. *Front. Plant Sci.* 11, 607850. doi: 10.3389/fpls.2020.607850

Park, Y.-S., Borrego, E. J., Gao, X., Christensen, S. A., Schmelz, E., Lanubile, A., et al. (2021). *Fusarium verticillioides* induces maize-derived ethylene to promote virulence by engaging fungal G-protein signaling. *Mol. Plant-Microbe Interactions®*. 34 (10), 1157–1166. doi: 10.1094/MPMI-09-20-0250-R

Perkins, J. M., and Pedersen, W. L. (1987). Disease development and yield losses associated with northern leaf blight on corn. *Plant Dis* 71, 940–943. doi: 10.1094/PD-71-0940

Poland, J. A., and Nelson, R. J. (2011). In the eye of the beholder: the effect of rater variability and different rating scales on QTL mapping. *Phytopathology* 101 (2), 290–298. doi: 10.1094/PHYTO-03-10-0087

Pollak, L. M., and Salhuana, W. (2001). "*The Germplasm Enhancement of Maize (GEM) Project: Private and Public Sector Collaboration*. in H. D. Cooper, C. Spillane and T. Hodgkin (eds.), Broadening the Genetic Base of Crop Production (CABI Publishing).

R Core Team (2021). R: A language and environment for statistical computing. *R Foundation for Statistical Computing*, Vienna, Austria. Available at: https://www.R-project.org/.

Raymundo, A. D., and Hooker, A. L. (1981a). Measuring the relationship between northern corn leaf blight and yield losses. *Plant Dis* 65, 325–327. doi: 10.1094/PD-65-325

Raymundo, A. D., and Hooker, A. L. (1981b). Single and combined effects of monogenic and polygenic resistance on certain componenets of northern corn leaf blight development. *Am. Phytopathol Soc* 72, 99–103. doi: 10.1094/Phyto-72-99

Rehrig, E. M., Appel, H. M., Jones, A. D., and Schultz, J. C. (2014). Roles for jasmonate- and ethylene-induced transcription factors in the ability of Arabidopsis to respond differentially to damage caused by two insect herbivores. *Front. Plant Sci.* 5, 407. doi: 10.3389/fpls.2014.00407

Robert-Seilaniantz, A., Grant, M., and Jones, J. D. (2011). Hormone crosstalk in plant disease and defense: more than just jasmonate-salicylate antagonism. *Annu. Rev. Phytopathol.* 49, 317–343. doi: 10.1146/annurev-phyto-073009-114447

Rossi, E. A., Ruiz, M., Rueda Calderón, M. A., Bruno, C. I., Bonamico, N. C., and Balzarini, M. G. (2019). Meta-analysis of QTL studies for resistance to fungi and viruses in maize. *Crop Sci.* 59 (1), 125–139. doi: 10.2135/cropsci2018.05.0330

Sanchez, D. L., Liu, S., Ibrahim, R., Blanco, M., and Lubberstedt, T. (2018). Genome-wide association studies of doubled haploid exotic introgression lines for root system architecture traits in maize (Zea mays L.). *Plant Sci.* 268, 30–38. doi: 10.1016/j.plantsci.2017.12.004

Savary, S., Willocquet, L., Pethybridge, S. J., Esker, P., McRoberts, N., and Nelson, A. (2019). The global burden of pathogens and pests on major food crops. *Nat. Ecol. Evol.* 3 (3), 430–439. doi: 10.1038/s41559-018-0793-y

Schechert, A. W., Welz, H. G., and Geiger, H. H. (1999). QTL for resistance to setosphaeria turcica in tropical african maize. *Crop Sci* 39 (2), 514–523. doi: 10.2135/cropsci1999.0011183X003900020036x

Simko, I., and Piepho, H. P. (2012). The area under the disease progress stairs: calculation, advantage, and application. *Phytopathology* 102 (4), 381–389. doi: 10.1094/PHYTO-07-11-0216

Smith, D. R., and Kinsey, J. G. (1993). Latent Period - A Possible Selection Tool for *Exserohilum turcicum* Resistance in Corn (*Zea mays* L.). *Maydica* 38 (3), 205–208.

Stotz, H. U., Pittendrigh, B. R., Kroymann, J., Weniger, K., Fritsche, J., Bauke, A., et al. (2000). Induced Plant Defense Responses against Chewing insects. Ethylene Signaling Reduces Resistance of Arabidopsis against Egyptian Cotton Worm But Not Diamond Back Moth. *Plant Physiol.* 124, 1007–1017. doi: 10.1104/pp.124.3.1007

Thatcher, S., Leonard, A., Lauer, M., Panangipalli, G., Norman, B., Hou, Z., et al. (2022). The northern corn leaf blight resistance geneHt1 encodes an nucleotide-binding, leucine-rich repeat immune receptor. *Mol. Plant Pathol.* 24: 758-67. doi: 10.1111/mpp.13267

Thrash, A., Tang, J. D., DeOrnellis, M., Peterson, D. G., and Warburton, M. L. (2020). PAST: the pathway association studies tool to infer biological meaning from GWAS datasets. *Plants (Basel).* 9 (1). doi: 10.3390/plants9010058

Ullstrup, A. J., and Miles, S. R. (1957). The effects of some leaf blights of corn on grain yield. *Phytopathology* 47, 331–336.

van Loon, L. C., Geraats, B. P., and Linthorst, H. J. (2006). Ethylene as a modulator of disease resistance in plants. *Trends Plant Sci.* 11 (4), 184–191. doi: 10.1016/j.tplants.2006.02.005

Vanous, A., Gardner, C., Blanco, M., Martin-Schwarze, A., Lipka, A. E., Flint-Garcia, S., et al. (2018). Association mapping of flowering and height traits in germplasm enhancement of maize doubled haploid (GEM-DH) lines. *Plant Genome* 11 (2), 170083. doi: 10.3835/plantgenome2017.09.0083

Vanous, A., Gardner, C., Blanco, M., Martin-Schwarze, A., Wang, J., Li, X., et al. (2019). Stability analysis of kernel quality traits in exotic-derived doubled haploid maize lines. *Plant Genome* 12 (1), 170114. doi: 10.3835/plantgenome2017.12.0114

Varsani, S., Grover, S., Zhou, S., Koch, K. G., Huang, P. C., Kolomiets, M. V., et al. (2019). 12-oxo-phytodienoic acid acts as a regulator of maize defense against corn leaf aphid. *Plant Physiol.* 179 (4), 1402–1415. doi: 10.1104/pp.18.01472

Wang, H., Hou, J., Ye, P., Hu, L., Huang, J., Dai, Z., et al. (2021). A teosinte-derived allele of a MYB transcription repressor confers multiple disease resistance in maize. *Mol. Plant* 14 (11), 1846–1863. doi: 10.1016/j.molp.2021.07.008

Wang, S., Park, Y. S., Yang, Y., Borrego, E. J., Isakeit, T., Gao, X., et al. (2017). Seed-Derived Ethylene Facilitates Colonization but Not Aflatoxin Production by Aspergillus flavus in Maize. *Front. Plant Sci.* 8, 415. doi: 10.3389/fpls.2017.00415

Weems, J. D., and Bradley, C. A. (2018). *Exserohilum turcicum* race population distribution in the north central United States. *Plant Dis* 102 (2), 292–299. doi: 10.1094/PDIS-01-17-0128-RE

Weits, D. A., Giuntoli, B., Kosmacz, M., Parlanti, S., Hubberten, H.-M., Riegler, H., et al. (2014). Plant cysteine oxidases control the oxygen-dependent branch of the N-end-rule pathway. *Nat. Commun.* 5 (1), 3425. doi: 10.1038/ncomms4425

Welz, H. G., and Geiger, H. H. (2000). Genes for resistance to northern corn leaf blight in diverse maize populations. *Plant Breeding.* 119 (1), 1–14. doi: 10.1046/j.1439-0523.2000.00462.x

Welz, H. G., Schechert, A. W., and Geiger, H. H. (1999). Dynamic gene action at QTLs for resistance to Setosphaeria turcica in maize. *Theor. Appl. Genet.* 98 (6-7), 1036–1045. doi: 10.1007/s001220051165

White, M. D., Kamps, J. J. A. G., East, S., Taylor Kearney, L. J., and Flashman, E. (2018). The plant cysteine oxidases from Arabidopsis thaliana are kinetically tailored to act as oxygen sensors. *J. Biol. Chem.* 293 (30), 11786–11795. doi: 10.1074/jbc.RA118.003496

Wisser, R. J., Balint-Kurti, P. J., and Nelson, R. J. (2006). The genetic architecture of disease resistance in maize: A synthesis of published studies. *Phytopathology* 96 (2), 120–129. doi: 10.1094/PHYTO-96-0120

Woodhouse, M., Cannon, E., Portwood, J., Harper, L., Gardiner, J., Schaeffer, M., et al. (2021). A pan-genomic approach to genome databases using maize as a model system. *BMC Plant Biol.* 21 (285), 385. doi: 10.1186/s12870-021-03173-5

Xu, J., and Zhang, S. (2015). Ethylene biosynthesis and regulation in plants. *Ethylene Plants*, 1–25. doi: 10.1007/978-94-017-9484-8_1

Yang, S. F. (1985). Biosynthesis and action of ethylene. *HortScience* 20, 41–45. doi: 10.21273/HORTSCI.20.1.41

Yang, Q., He, Y., Kabahuma, M., Chaya, T., Kelly, A., Borrego, E., et al. (2017). A gene encoding maize caffeoyl-CoA O-methyltransferase confers quantitative resistance to multiple pathogens. *Nat. Genet.* 49 (9), 1364–1372. doi: 10.1038/ng.3919

Yang, P., Scheuermann, D., Kessel, B., Koller, T., Greenwood, J. R., Hurni, S., et al. (2021). Alleles of a wall-associated kinase gene account for three of the major northern corn leaf blight resistance loci in maize. *Plant J.* 106, 526–535. doi: 10.1111/tpj.15183

Yu, H., Ruan, H., Xia, X., Chicowski, A. S., Whitham, S. A., Li, Z., et al. (2022). Maize FERONIA-like receptor genes are involved in the response of multiple disease resistance in maize. *Mol. Plant Pathol* 23 (9), 1331–1345. doi: 10.1111/mpp.13232

Zang, Z., Lv, Y., Liu, S., Yang, W., Ci, J., Ren, X., et al. (2020). A novel ERF transcription factor, zmERF105, positively regulates maize resistance to exserohilum turcicum. *Front. Plant Sci.* 11, 850. doi: 10.3389/fpls.2020.00850

Zang, Z., Wang, Z., Zhao, F., Yang, W., Ci, J., Ren, X., et al. (2021). Maize ethylene response factor zmERF061 is required for resistance to exserohilum turcicum. *Front. Plant Sci.* 12, 630413. doi: 10.3389/fpls.2021.630413

Zhai, K., Liang, D., Li, H., Jiao, F., Yan, B., Liu, J., et al. (2022). NLRs guard metabolism to coordinate pattern- and effector-triggered immunity. *Nature* 601 (7892), 245–251. doi: 10.1038/s41586-021-04219-2

Zhang, X., Fernandes, S. B., Kaiser, C., Adhikari, P., Brown, P. J., Mideros, S. X., et al. (2020). Conserved defense responses between maize and sorghum to Exserohilum turcicum. *BMC Plant Biol.* 20 (1), 67. doi: 10.1186/s12870-020-2275-z

Zhao, S., Hong, W., Wu, J., Wang, Y., Ji, S., Zhu, S., et al. (2017). A viral protein promotes host SAMS1 activity and ethylene production for the benefit of virus infection. *eLife* 6, e27529. doi: 10.7554/eLife.27529.036

Zhou, S., Zhang, Y. K., Kremling, K. A., Ding, Y., Bennett, J. S., Bae, J. S., et al. (2019). Ethylene signaling regulates natural variation in the abundance of antifungal acetylated diferuloylsucroses andFusarium graminearum resistance in maize seedling roots. *New Phytol.* 221 (4), 2096–2111. doi: 10.1111/nph.15520

frontiers | Frontiers in Plant Science

TYPE Original Research
PUBLISHED 07 November 2023
DOI 10.3389/fpls.2023.1277585

OPEN ACCESS

EDITED BY
Laura Medina-Puche,
University of Tübingen, Germany

REVIEWED BY
Brett Hale,
Arkansas State University, United States
Jose Sebastian Rufian,
Universidad de Málaga, Spain

*CORRESPONDENCE
Leah K. McHale
mchale.21@osu.edu
Anne E. Dorrance
dorrance.1@osu.edu

†PRESENT ADDRESSES
Cassidy R. Million,
Ag Science, Heliae Agriculture, Gilbert, AZ, United States
Saranga Wijeratne,
Abigail Wexner Research Institute Nationwide Children's Hospital, Columbus, OH, United States
Stephanie Karhoff,
Department of Extension, The Ohio State University, Ottawa, OH, United States

‡These authors have contributed equally to this work and share senior authorship

RECEIVED 14 August 2023
ACCEPTED 16 October 2023
PUBLISHED 07 November 2023

CITATION
Million CR, Wijeratne S, Karhoff S, Cassone BJ, McHale LK and Dorrance AE (2023) Molecular mechanisms underpinning quantitative resistance to *Phytophthora sojae* in *Glycine max* using a systems genomics approach. *Front. Plant Sci.* 14:1277585. doi: 10.3389/fpls.2023.1277585

Molecular mechanisms underpinning quantitative resistance to *Phytophthora sojae* in *Glycine max* using a systems genomics approach

Cassidy R. Million[1,2†], Saranga Wijeratne[3†], Stephanie Karhoff[2,4†], Bryan J. Cassone[2,5], Leah K. McHale[2,6*‡] and Anne E. Dorrance[1,2*‡]

[1]Department of Plant Pathology, The Ohio State University, Wooster, OH, United States, [2]Center for Soybean Research and Center for Applied Plant Sciences, The Ohio State University, Columbus, OH, United States, [3]Molecular and Cellular Imaging Center, The Ohio State University, Wooster, OH, United States, [4]Translational Plant Sciences Graduate Program, The Ohio State University, Columbus, OH, United States, [5]Department of Biology, Brandon University, Brandon, Manitoba, MB, Canada, [6]Department of Horticulture and Crop Science, The Ohio State University, Columbus, OH, United States

Expression of quantitative disease resistance in many host–pathogen systems is controlled by genes at multiple loci, each contributing a small effect to the overall response. We used a systems genomics approach to study the molecular underpinnings of quantitative disease resistance in the soybean-*Phytophthora sojae* pathosystem, incorporating expression quantitative trait loci (eQTL) mapping and gene co-expression network analysis to identify the genes putatively regulating transcriptional changes in response to inoculation. These findings were compared to previously mapped phenotypic (phQTL) to identify the molecular mechanisms contributing to the expression of this resistance. A subset of 93 recombinant inbred lines (RILs) from a Conrad × Sloan population were inoculated with *P. sojae* isolate 1.S.1.1 using the tray-test method; RNA was extracted, sequenced, and the normalized read counts were genetically mapped from tissue collected at the inoculation site 24 h after inoculation from both mock and inoculated samples. In total, more than 100,000 eQTLs were mapped. There was a switch from predominantly *cis*-eQTLs in the mock treatment to an almost entirely nonoverlapping set of predominantly *trans*-eQTLs in the inoculated treatment, where greater than 100-fold more eQTLs were mapped relative to mock, indicating vast transcriptional reprogramming due to *P. sojae* infection occurred. The eQTLs were organized into 36 hotspots, with the four largest hotspots from the inoculated treatment corresponding to more than 70% of the eQTLs, each enriched for genes within plant–pathogen interaction pathways. Genetic regulation of *trans*-eQTLs in response to the pathogen was predicted to occur through transcription factors and signaling molecules involved in plant–pathogen interactions, plant hormone signal transduction, and MAPK pathways. Network analysis identified three co-expression modules that were correlated with susceptibility to *P. sojae* and associated with three

eQTL hotspots. Among the eQTLs co-localized with phQTLs, two *cis*-eQTLs with putative functions in the regulation of root architecture or jasmonic acid, as well as the putative master regulators of an eQTL hotspot nearby a phQTL, represent candidates potentially underpinning the molecular control of these phQTLs for resistance.

KEYWORDS

Glycine max, soybean, *Phytophthora sojae*, eQTL, systems genomics, master regulators, weighted gene co-expression network analysis

1 Introduction

Quantitative disease resistance (QDR) is a type of host resistance that generally involves multiple loci acting additively, each with a small to moderate overall effect on limiting disease development (Young, 1996; Poland et al., 2009; St. Clair, 2010; Roux et al., 2014; Niks et al., 2015; French et al., 2016; Corwin and Kliebenstein, 2017; Nelson et al., 2018). Numerous phenotypic quantitative trait loci (phQTL) (Jansen et al., 2009; Acharjee et al., 2018) for disease resistance have been mapped in soybean (Lin et al., 2022) to biotrophic pathogens, such as soybean cyst nematode (SCN: *Heterodera glycine*) (Wu et al., 2009) and powdery mildew (*Microsphaera diffusa*) (Jun et al., 2012); hemibiotrophic pathogens *Phytophthora sojae* (Burnham et al., 2003; Weng et al., 2007; Han et al., 2008; Li et al., 2010; Tucker et al., 2010; Wang et al., 2010; Wu et al., 2011; Nguyen et al., 2012; Wang et al., 2012b; Lee et al., 2013a; Lee et al., 2013b; Lee et al., 2014; Abeysekara et al., 2016; Stasko et al., 2016) and *Phialophora gregata* (Rincker et al., 2016); and necrotrophic pathogens *Sclerotinia sclerotiorum* (Kim and Diers, 2000; Arahana et al., 2001; Guo et al., 2008; Vuong et al., 2008; Zhao et al., 2015). However, the causal genes for QDR have only been identified and verified in the SCN soybean pathosystem through genetic mapping, gene silencing, and complementation experiments (Cook et al., 2012; Cook et al., 2014; Bayless et al., 2018). Impediments to the discovery of causal genes for QDR are often attributed to the intricate biology of plant-pathogen interactions (Zhou et al., 2009; Corwin et al., 2016; Corwin and Kliebenstein, 2017; Nelson et al., 2018). Additionally, the methods to functionally evaluate candidate genes underlying specific phQTLs are difficult, as each phQTL has a relatively small effect on the final phenotype, and modification of a single gene often yields inconclusive results (Salvi and Tuberosa, 2005; Poland et al., 2009; Corwin and Kliebenstein, 2017). Receptor-like kinases (RLKs) and nucleotide-binding leucine-rich repeat proteins (NLRs) are recognized as canonical resistance proteins (Niks et al., 2015; French et al., 2016; Pilet-Nayel et al., 2017); however, these proteins, which commonly function in qualitative or *R*-gene-mediated defense, only account for a small portion of genes involved in QDR to date (Poland et al., 2009; Corwin et al., 2016; Nelson et al., 2018). QDR has been hypothesized to be controlled by proteins with a wide range of functions, and that has, thus far, been born out through functional studies (Poland et al., 2009; St. Clair, 2010; Roux et al., 2014; Niks et al., 2015; French et al., 2016; Corwin and Kliebenstein, 2017). For example, genes with functions more commonly associated with plant development, cell wall reinforcement, RNA processing, and defense compounds were associated with QDR (Poland et al., 2009; Corwin et al., 2016; Corwin and Kliebenstein, 2017; Nelson et al., 2018). This functional diversity of genes involved in QDR makes it difficult to predict causal candidate genes based solely on homology-predicted functions and gene positions relative to phQTL.

Due to the adaptation of *P. sojae* populations to *R*-gene-mediated resistance in soybean, QDR is preferred in some growing regions to manage Phytophthora root and stem rot (PRR) (Grau et al., 2004; Dorrance et al., 2009; Schmitthenner 1985). In this plant-pathogen system, QDR is a partial resistance that allows for some pathogen growth and reproduction and generally consists of several loci, each contributing a minor effect or one major effect locus combined with several minor effect loci (Tooley and Grau, 1982; Mideros et al., 2007; Weng et al., 2007; Han et al., 2008; Li et al., 2010; Tucker et al., 2010; Wu et al., 2011; Nguyen et al., 2012; Wang et al., 2012a; Wang et al., 2012b; Lee et al., 2013a; Lee et al., 2013b; Lee et al., 2014; Abeysekara et al., 2016; Stasko et al., 2016; Scott et al., 2019; de Ronne et al., 2022). Nine different parental combinations have produced numerous phQTLs contributing towards *P. sojae* quantitative resistance in soybean (Burnham et al., 2003; Weng et al., 2007; Han et al., 2008; Li et al., 2010; Tucker et al., 2010; Wang et al., 2010; Wu et al., 2011; Nguyen et al., 2012; Wang et al., 2012a; Wang et al., 2012b; Lee et al., 2013a; Lee et al., 2013b; Lee et al., 2014; Abeysekara et al., 2016; Stasko et al., 2016). Of these, 60 phQTLs, most of small effect, were mapped in multiple generations of a 'Conrad' × 'Sloan' recombinant inbred line (RIL) population using different field, greenhouse, and lab screening methodologies to collect the phenotypic data (Burnham et al., 2003; Weng et al., 2007; Han et al., 2008; Li et al., 2010; Wang et al., 2010; Wu et al., 2011; Wang et al., 2012b; Stasko et al., 2016). Each of these phQTLs encompasses large regions of the chromosome, which contain many genes (Wang et al., 2012b; Stasko et al., 2016), making it difficult to identify the causal genes based on position alone.

Few studies have examined the physiological and molecular mechanisms of quantitative resistance in soybean to *P. sojae*; however, all have concluded that this is a complex trait. Although only a few mechanisms for QDR have been substantiated in plant

systems (Nelson et al., 2018), numerous hypotheses have been developed for resistance to *P. sojae* in soybeans from several previous studies. These hypotheses include plant hormone signal transduction, including auxin acting as a susceptibility factor (Wang et al., 2010; Wang et al., 2012b; Stasko et al., 2020); suberin playing a role in slowing *P. sojae* hyphal infection in epidermal walls and middle lamellae (Thomas et al., 2007; Ranathunge et al., 2008); and the phenylpropanoid pathway acting as a positive regulator of *P. sojae* infection by increased content of glyceollin, daidzein, genistein, and salicylic acid (SA) (Abbasi et al., 2001; Mohr and Cahill, 2001; Graham et al., 2003; Lygin et al., 2013; Zhang et al., 2017). Components of the isoflavonoid pathway have been implicated in acting as antioxidants to reduce reactive oxygen species (ROS) and enhance QDR to *P. sojae* (Xu et al., 2012; Wong et al., 2014; Cheng et al., 2015; Dastmalchi et al., 2017). QDR in *P. sojae* has also been associated with increased expression of genes coding for pathogenesis-related 1a protein (PR1a), matrix metalloproteinases, basic peroxidases, and β-1,3-endoglucanases (Vega-Sánchez et al., 2005), as well as ubiquitination, plant cell structural modifications, serine-threonine kinase, and basal resistance (Wang et al., 2012b; Karhoff et al., 2022). Recently, a gene annotated as a major latex protein expressed in the roots and associated with biotic stress was implicated in QDR (de Ronne et al., 2022). In addition to these pathways, there are other well-documented pathways involved in plant defense against pathogens, including mitogen-activated protein kinase (MAPK) cascades and plant-pathogen interaction pathways (e.g., pathogen-associated molecular patterns (PAMP) and effector-triggered immunity (ETI) pathways), which may also play a role in QDR (Ausubel, 2005; Glazebrook, 2005; Chisholm et al., 2006; Jones and Dangl, 2006; Boller and Felix, 2009; Dodds and Rathjen, 2010; Gassmann and Bhattacharjee, 2012; Spoel and Dong, 2012; Zipfel, 2014; Cui et al., 2015; Nelson et al., 2018). Taken together, these reports emphasize the complexity of QDR mechanisms and responses to infection. Zhou et al. (2009) showed that by 5 days postinoculation with *P. sojae*, from tissue collected in front of the advancing lesion, 97% of the genes in the soybean genome responded to infection or genetic variation based on microarray data. Amid this genome-wide transcriptional reprogramming, it is difficult to identify the specific causal mechanisms, pathways, and putative candidate genes. Thus, a more robust approach is needed to elucidate the molecular mechanisms underlying QDR.

Numerous studies in plant-pathogen interactions have utilized a systems genomics approach to identify the molecular mechanisms that are controlled by a complex of genes, pathways, and networks contributing to the overall expression of a phenotype (Jansen and Nap, 2001; Kliebenstein, 2009; Druka et al., 2010; Feltus, 2014). This approach maps both phQTLs and expression (eQTLs) and combines these data with a gene network analysis to identify the specific alleles that control or contribute to the overall expression of resistance during a plant–pathogen interaction (Kliebenstein, 2009; Druka et al., 2010; Feltus, 2014). Using this approach, advancements were made towards understanding the mechanisms of QDR resistance in barley (*Hordeum vulgare* L.) to *Puccinia hordei* (Druka et al., 2008; Chen et al., 2010) and in maize (*Zea mays* L.) to *Cercospora zeina* (Christie et al., 2017). In the barley-*Puccinia hordei* system, the total number of candidate genes underlying phQTLs was reduced at four different loci, with the identification of a histidine kinase as a novel resistance gene at one locus (Druka et al., 2008). In a later study, the total number of candidate genes for QDR to *Puccinia hordei* was reduced to six candidates for barley *Rphq11* (Chen et al., 2010). Co-expression of *coronatine-insensitive 1* (*COI1*) and jasmonate responses in maize were correlated with resistance to *C. zeina*, while pathogen manipulation of the host plant through the diterpenoid biosynthesis pathway was associated with susceptibility (Christie et al., 2017).

Due to the nature of the *P. sojae*-soybean pathosystem response, in which a small proportion of the total phenotype is contributed by each locus and a large number of loci encompassing numerous genes respond to *P. sojae* infection, we have taken a systems genomics approach to elucidate the molecular mechanisms of QDR in soybean toward *P. sojae*. In this study, we aimed to (1) understand the transcriptional reprogramming that occurs earlier in the infection process during the transition from biotrophic to necrotrophic between the well-studied soybean cultivars, Conrad, which has high levels of QDR, and Sloan, which is moderately susceptible; (2) map the genetic control of the differential transcriptional response to inoculation with *P. sojae*; (3) identify functional enrichment of genes within eQTL hotspots and co-expression modules associated with disease; and (4) identify candidate genes. The emphasis in this study is placed on identifying factors that elicit expression of quantitative resistance and not those expressed during the *R*-gene (*Rps* gene) response, which have also been recently studied using a transcriptomic approach (Lin et al., 2014; Hale et al., 2023a).

Three types of analyses were used, including phQTL mapping, eQTL mapping, and weighted gene co-expression analysis (WGCNA). The integration of the three analyses allowed for a greater understanding of the relationships between gene expression and the resulting disease phenotypes. Ultimately, using the expression data of 93 RILs during the early stages of the infection process [24 hours after inoculation (hai)] as the switch from biotrophy to necrotrophy is occurring (Moy et al., 2004), we were able to map more than 100,000 eQTLs, identifying co-regulated gene modules associated with disease and five putative candidate genes for three phQTLs. Putative master regulators were identified for 16 key eQTL hotspots. This study is the first to our knowledge to elucidate the specific candidate genes that may regulate the extensive changes that occur during transcriptional reprogramming due to pathogen infection by utilizing eQTL mapping in inoculated and non-inoculated tissues within the same population.

2 Materials and methods

2.1 Phenotyping and RNA extraction

A subset of 93 $F_{9:11}$ RILs from the full population of 316 RILs derived from a cross between the cultivars Conrad (resistant) and Sloan (susceptible) were selected randomly for the eQTL study. The parents and RILs were inoculated with *P. sojae* 1.S.1.1 as previously

described (Wang et al., 2012b). Briefly, the roots of 7-day-old plants that were grown for one week in 29.5-ml Styrofoam cups containing vermiculite (Perlite Vermiculite Packing Industries, Inc., North Bloomfield, OH, USA) were washed in tap water. Seedlings were placed on a plastic tray on top of a cotton wicking pad and a polyester cloth. A wound on the main tap root of each plant was made with a scalpel approximately 2.5 cm below the crown and covered with a mycelial slurry of seven-day-old 1.S.1.1 of *P. sojae* grown on lima bean (*Phaseolus lunatus* L.) agar. These trays were placed in buckets and kept in a growth chamber at 25°C, 20% relative humidity (RH), on a 14-h light:10-h dark cycle. The experimental design was a randomized incomplete block design with three replications with each block containing 50–100 RILs. There were three trays for each RIL in each block. The first two trays were for RNA isolation where each tray was either inoculated with 1.S.1.1 or mock inoculated with lima bean agar (without *P. sojae*). No RNA was isolated from the third tray which was inoculated with 1.S.1.1, and the lesion length was measured 7 days after inoculation (dai) from the top of the inoculation site to the leading edge of the lesion margin to ensure that inoculations had been successful. A schematic for the experimental design is shown in Supplementary Figure S1.

All agar was gently removed using a Kimwipe, and a 1-cm section of tissue from the inoculation site was collected 24 hai from the mock and inoculated trays. Tissue from eight to 10 plants from a single RIL was collected, and tissue from all three replicates of each RIL was pooled for RNA extraction for a total of ~24–30 plants per RIL. Tissue was ground in liquid nitrogen, and RNA was extracted using a Qiagen RNeasy Plant Mini Kit (Hilden, Germany) following the manufacturer's protocols.

RNA was quality and quantity checked using the TapeStation (Agilent Technologies, Santa Clara, CA, USA) and Qubit 2.0 Fluorometer (Invitrogen, Carlsbad, CA, USA), respectively. RNA quality and quantity standards were met for both the mock-inoculated and inoculated treatment for each of the 93 RILs. Sequence data from this study can be found in the NCBI BioProject: PRJNA478334.

2.2 Genotypic and phenotypic data

Phenotypic QTLs have been previously reported in the Conrad × Sloan recombinant inbred population of 316 individuals (Stasko et al., 2016), a subset of which was used for this study. The methods for inoculation, experimental design, and statistical analysis for mapping were described in greater detail (Wang et al., 2010; Wang et al., 2012b; Stasko et al., 2016). To construct a genetic map to carry out both eQTL and phQTL mapping, genotypic data was obtained from Stasko et al. (2016). While included in WGCNA, RIL 12280 was removed from the phQTL and eQTL analyses due to missing genotypic data. The normality of the data was evaluated using the Shapiro–Wilk test and visually assessed by histograms and QQ plots.

To account for environment variation, best linear unbiased predictor (BLUP) values for RILs were extracted from the model by adjusting mean lesion lengths of 92 RILs to the checks (cultivars OX20-8 (*Rps1a*, no partial resistance), Williams 82 (*Rps1k*, moderate partial resistance), Conrad (parent, high partial resistance), Sloan (parent, moderately susceptible)) and removing environmental variation in R version 3.5.1 (R Core Team, 2018) with the package -'lme4' using the lmer function in version 1.1-19 (Bates et al., 2014). The model applied was $Y_{ijk} = \mu + R_i + T_j + G(C)_{jk} + \epsilon_{ijk}$ where μ = overall mean, R_i = effect of the ith replication, T_j = effect of the jth type of entry, $G(C)_{jk}$ = effect of the kth genotype within the type for RIL only, and ϵ_{ijk} = experimental error. The RILs in this study represent a subset of all possible genetic combinations and were treated as random (Green and Tukey, 1960). The same principle was applied to the random effect of replication, while the assigned category of type of entry (a category for RILs as well as each of the checks) was treated as fixed. Variance components were estimated using the maximum likelihood method. Composite interval mapping (R/qtl; Broman et al., 2003) was utilized to confirm phQTL peaks that were associated with lesion length BLUP values in the 316 RIL population from Stasko et al. (2016).

2.3 RNA sequencing

For each of the 184 samples consisting of ~24–30 plants per RIL per treatment, 1 µg of total RNA was converted to complementary DNA libraries (Molecular and Cellular Imaging Center, Ohio Agricultural Research and Development Center) and sequenced using Illumina HiSeq paired-end (PE) 100 base-pair reads. The average reads per sample was 3,126,863, ranging from 2,484,193 to 5,087,094 reads per sample. While only a single sample was sequenced for each RIL:treatment combination, the use of a highly inbred RIL population makes it such that each allele is represented approximately 46 times per treatment (50% of 92) and therefore provides replication within the genome-wide analyses. In brief, all reads were quality checked, adapter removed, and quality trimmed using bioinformatics tools FastQC (Andrews, 2010) and BBTools (BBMap; Bushnell, 2014). All reads were mapped to the reference genome (*Glycine max* Wm82.a2.v1) retrieved from Phytozome[1], using CLCBio (CLC Genomics Workbench 9.5.3[2]. Reads mapped to the reference genome were counted using FeatureCounts (Liao et al., 2014). Data were normalized using edgeR (Robinson et al., 2010) using the trimmed mean of the M-values (TMM) normalization.

2.4 iBMQ eQTL mapping

The integrated hierarchical Bayesian model for multivariate eQTL mapping (iBMQ; Imholte et al., 2013) is a multivariate mapping method that implements a multi-loci approach to allow for the identification of complex traits that are being controlled by multiple genes. iBMQ parameters are estimated using a Markov Chain Monte Carlo (MCMC) algorithm that models concurrently all genes and SNPs. The current version of iBMQ executed is available online[3]. Normalized unfiltered expression data (RNA-seq data) and genotyping data, including SNPs that were identified in the newly conducted linkage map for all RILs, were

used as inputs into iBMQ. These data sets were formatted into an *ExpressionSet* and *Snpset* using Biobase in Bioconductor 3.7 (Huber et al., 2015). The eQTLs were mapped by using gene expression (e-trait) as a phenotypic trait identifying the SNP association for mock and inoculated treatments and mapped separately with 100,000 iterations with a burn-in of 50,000 to produce a posterior probability of association (PPA). A false discovery rate (FDR) of 10% was used to determine the PPA significance cutoff (Imholte et al., 2013).

Significantly mapped eQTLs were classified as either *cis*- or *trans*- using the eqtlClassifier in the iBMQ package. Classification of *cis*- or *trans*-eQTLs was determined by physical position; if a SNP was within 5 Mb of the gene it controlled, it was classified as *cis*-, and if a SNP was farther than 5Mb from the gene controlled, it was classified as *trans*-. The physical positions of genes and SNPs were determined using the reference genome annotation, Williams 82 v.a2.v1[4].

The function *hotspot finder* inside the iBMQ package was used to identify individual markers (SNPs) that are associated with the expression of several genes and indicate eQTL, hotspots as described by Imholte et al. (2013). A SNP was identified as a hotspot if it was associated with >20 genes.

2.5 Gene enrichment

Significant *cis*- and *trans*-eQTLs, gene suites at eQTL hotspots, and co-expression modules were subjected to GO enrichment. AgriGO (v2.0; Tian et al., 2017) was used for GO enrichment analysis. Targeted QDR pathway mechanisms were also explored by extracting genes via KEGG (Kanehisa and Goto, 2000[5]) from NCBI BioSystems[6]. Gene models from the reference soybean genome that met read-mapping thresholds for inclusion in eQTL mapping were used as the reference set for enrichment analyses (Schmutz et al., 2010). Fisher's exact test (Fisher, 1935) and multitest Hochberg FDR adjustment (Benjamini and Hochberg, 1995) were used to determine significance.

2.6 Weighted gene co-expression analysis

WGCNA was carried out according to Langfelder and Horvath (2008) using modified R-scripts (WGCNA Methods M1). Prior to WGCNA analysis, RNA-sequencing counts from 92 RILs plus the parents of the population were normalized using R Bioconductor package edgeR (Robinson et al., 2010). First trimmed means of *M*-values (TMM) were used to calculate normalization factors for all sample counts and were subjected to a log2 transformation. Genes were filtered by the threshold of greater than 2 counts per million (cpm) across 50 samples. Ultimately, 27,666 genes were used in the input matrix. Due to sample count bias, a consensus approach was taken. Based on the smallest standard deviation representing susceptible and resistant individuals separately, 30 resistant and 30 susceptible individuals were selected, and the minimum standard deviation was determined (10,000 iterations) and used as a cutoff to select the subsample of 30 resistant and 30 susceptible individuals. The process of subsampling individuals who met the standard deviation cutoff through generating modules was done in 20,000 iterations and generated for 20 network analyses.

To examine the physiological relevance of each module within the network analyses, phenotypic traits were correlated to the module genes' expression using log expression eigengene values for each module regressed against the lesion length values of the RILs. Consensus networks were constructed independently for the positively and negatively correlated modules and again related to phenotypic traits (WGCNA Methods M2).

To determine the driving factors of co-expression modules, modules that were significantly correlated to PRR disease (p-value ≤ 0.05) were also correlated to inoculated eQTL hotspots, adapting methods from Zhang and Horvath (2005) to integrate SNP-based significance (PPA of eQTL) with network properties (gene significance) of co-expression module (WGCNA Methods M3).

2.7 Co-localization of eQTLs with phQTLs

Co-localization of *cis*-eQTLs with phQTLs was based on the physical coordinates of the *cis*-eQTLs gene model being within the flanking marker positions for selected phQTLs reported from the present and previous studies (Table 1). All phQTLs that could not be positioned onto the genome based on marker positions were removed from the data set, for a total of six out of 28 phQTLs. Based on the physical coordinates of markers flanking phQTLs, overlapping phQTLs were consolidated. To determine if the number of co-localized *cis*-eQTLs and consolidated phQTLs was significantly greater than expected, *cis*-eQTLs were permuted across all gene models eligible for eQTL analysis. A threshold ($\alpha = 0.05$) was set based on 1,000 permutations.

Methods to determine the co-localization of *trans*-eQTLs with phQTLs were adapted from Christie et al. (2017). Base pair positions of consolidated phQTLs and a window using the average linkage disequilibrium (LD) block size (242 kb) around the marker to which *trans*-eQTLs mapped were used to determine phQTL/trans-eQTL co-localization. Linkage disequilibrium blocks were determined using the Haploview four-gamete method (Barrett et al., 2005). To determine if the number of co-localized *trans*-eQTLs and phQTLs was significantly greater than expected, *trans*-eQTLs were permuted across available markers on the genetic map. A threshold (alpha = 0.05) was set based on 1,000 permutations.

2.8 Identification of putative master regulators

Methods for identifying master regulators for eQTL hotspots were adapted from Wang et al. (2017). Genes within an up- and downstream 242-kb window (average LD block size for this population) of the hotspot SNP that also had *cis*-eQTLs mapping were identified as initial candidate master regulators. If no genes within the window were associated with *cis*-eQTLs, genes with no mapping e-traits were considered. From these *cis*-eQTLs or positional candidates, putative master regulators were selected according to predicted functions of transcription factor (TF) or signaling molecules (SM).

TABLE 1 Co-localization of *cis*- and *trans*-eQTL as well as hotpots with consolidated phenotypic quantitative trait loci (phQTLs) mapped in the sub-population and previous phQTL mapped in multiple generations of the Conrad × Sloan RIL population.

phQTL ID	Left marker-right marker	Physical position[a]	*Cis*-eQTL gene	*Trans*-eQTL gene or hotspot (marker)
phQTL_1[b,c]	ss715583994-ss715582762	1: 49814688-51043150	*Glyma.01G160600*	*Glyma.10G026500* (ss715579958)
			Glyma.01G162600	
			Glyma.01G170600	*Glyma.10G026500* (ss715579975)
			Glyma.01G171300	
phQTL_4[c]	ss715588277-ss715588347	4: 46096228-46536196	NA	NA
phQTL_9[c]	ss715603084	9: 15487393-19208849	NA	NA
phQTL_16[c]	ss715624395-ss715624634	16: 3124736-3362395	NA	NA
phQTL_18a[b,d]	ss715582789-BARCSOYSSR_18_1710	18: 53019336-53902882	NA	NA
phQTL_18b[b–e]	BARCSOYSSR_18_1777-BARCSOYSSR_18_1949	18: 54744147-57972957	*Glyma.18G270900*	*Glyma.08G249200* (ss715632217)
phQTL_19a[b]	ss715582079-BARCSOYSSR_19_1243	19:43023466-43533756	NA	NA
phQTL_19b[b–d]	BARCSOYSSR_19_1286-BARCSOYSSR_19_1532	19: 44370710-49060065	*Glyma.19G224300*	GM_19 (ss107929955)
				GM_19_A (BARCSOYSSR_19_1452)
				GM_19_B (OSU_SNP_Glyma19g41210)

[a]Chromosome and physical base pair (bp) position derived from version Wm82.a2.v1.
[b]phQTL reported in Wang et al. (2012b).
[c]phQTL reported in Stasko et al. (2016).
[d]phQTL reported in Wang et al. (2012a).
[e]phQTL reported in the present study.
NA, not applicable.

3 Results

3.1 Genetic map reconstruction and quantitative disease resistance to *Phytophthora sojae*

While phQTLs for QDR have been previously mapped in the $F_{9:11}$ RIL population derived from a cross between Conrad (resistant) and Sloan (susceptible) (Stasko et al., 2016), in order to ensure that the phQTLs were directly relevant to the expression data collected in this study (Supplementary Figure S2), we mapped phQTLs using data from only the subset of 92 RILs for which RNA-seq, phenotypic data, and previous genotypic data were available (Stasko et al., 2016). A genetic map was constructed consisting of 1,122 markers assembled in 28 linkage groups, with most of the 20 soybean chromosomes represented as a single linkage group and chromosomes 5, 6, 7, 11, 12, 13, 17, and 19 each represented by two linkage groups (Supplementary Table S1). A suggestive phQTL, significant at the chromosome but not genome-wide level, on chromosome 18 and nonsignificant associations with regional peaks but nonsignificant logarithm of the odds (LOD) scores on chromosomes 1, 16, and 19a correspond to phQTLs previously identified in the full RIL population (Supplementary Figure S2; Stasko et al., 2016). In comparison to previous studies, reduced significance is expected due to the smaller subset of RILs.

3.2 Genetic architecture of gene expression in mock and inoculated treatments

To identify the loci contributing to variation in gene expression, eQTLs were mapped under both mock and inoculated conditions. Gene expression levels were interpreted as quantitative traits (e-traits), and the locus or loci for each e-trait were mapped separately for inoculated and mock treatments. A total of 114,197 eQTLs were mapped from e-traits for the inoculated treatment from root samples collected 24 hai from the site of inoculation, representing transcripts from 35,781 unique genes associated with 74 unique loci (Supplementary Table S2). In contrast, the number of eQTLs mapped in the mock treatment was far lower but distributed across more loci, with 794 eQTLs representing 788 unique genes across 234 unique loci. The eQTLs identified in the inoculated treatment were distributed across most chromosomes, the exceptions being chromosomes 9 and 10 (Figure 1A), while eQTLs from the mock

10.3389/fpls.2023.1277585

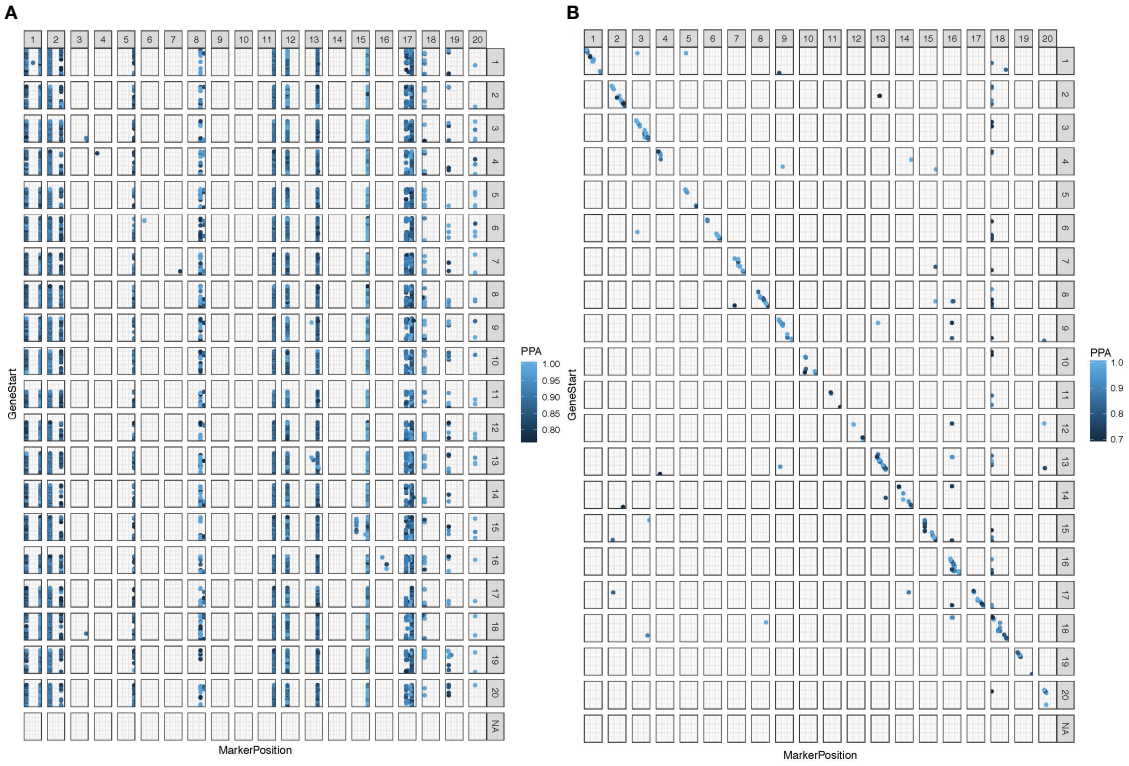

FIGURE 1
Expression quantitative trait loci (eQTL) were mapped in 92 Conrad × Sloan $F_{9:11}$ RIL population at false discovery rate (FDR) of 10% with 100,000 iterations. **(A)** Significantly mapped inoculated treatment eQTL at a significance posterior probabilities of association (PPA) cutoff of 0.786 for the inoculated treatment. **(B)** Significantly mapped mock treatment eQTL at a significance PPA cutoff of 0.688. Base-pair positions are shown with zero at the bottom of the *y*-axis and right of the *x*-axis. Markers in a vertical formation indicate *trans*-eQTL, and markers in a diagonal formation indicate *cis*-eQTL. Chromosomes with no data contain nonclassified eQTL due to missing physical location data.

treatments were relatively evenly distributed across all chromosomes in the genome (Figure 1B). Interestingly, only two eQTLs were in common between mock and inoculated treatments, including the SNP, ss715580997, associated with e-trait *Glyma.02G107800* (putatively coding an uncharacterized protein), and the SNP OSU_SNP_Glyma19g41210, associated with e-trait, *Glyma.19G224300* (putatively coding a protein involved in regulation of root development and cell wall).

The eQTLs associated with e-traits of nearby genes are considered *cis*-eQTLs, while eQTLs altering the expression of physically distant genes are classified as *trans*-eQTLs (Hubner et al., 2005; Kliebenstein, 2009). In the inoculated treatment, the vast majority (111,568; ~98%) of the eQTLs were in the *trans* configuration (Figure 1A; Supplementary Table S2). In contrast, in the mock treatment, 83% (657) of the eQTLs were in the *cis* configuration (Figure 1B; Supplementary Table S2).

Key regulatory genes are expected to influence the expression of many genes. Therefore, eQTL hotspots, genomic regions enriched for eQTLs, are likely localized to these key regulatory genes (Kliebenstein, 2009; Tian et al., 2016). Thirty-six hotspots distributed across 12 chromosomes were identified for the inoculated treatment, with seven located on chromosome 17. Of the 36 hotspots in the inoculated treatment, there were two very large hotspots, GM_1 and GM_15, associated with 23,919 and 25,727 e-traits, respectively. For the mock treatment, there were three hotspots located on chromosomes 13, 16, and 18. The mock and inoculated eQTL hotspots did not overlap with each other (Table 2).

3.3 Term enrichment and functional annotations of genes associated with each hotspot

Genes that are co-regulated may be associated with specific coordinated functions or resistance mechanisms. To identify a commonality of functions among e-traits mapping to each eQTL hotspot, GO term enrichment analysis was done. The e-traits associated with 10 of the 36 hotspots for the inoculated treatment were significantly enriched (p-value ≤ 0.05) for biological and/or cellular processes and molecular function terms. We were particularly interested in the enrichment of biological process GO terms, as enrichment of these terms may provide clues to the mechanisms of QDR. The biological process GO terms were significant for the e-traits associated with six of the 36 hotspots (Supplementary Table S3). A total of 16 and 31 biological processes were enriched among e-traits mapping to the large hotspots GM_1 (23,919 e-traits) and GM_15 (25,727 e-traits), respectively. Some of the most significantly enriched biological process terms were "intracellular

10.3389/fpls.2023.1277585

TABLE 2 Summary of inoculated and mock causal hotspots for number and regulation of expression quantitative trait loci (eQTLs) positively correlated to resistance towards *Phytophthora sojae*.

eQTL hotspot [associated co-expression module][a]	Physical location[b]	Hotspot SNP[c]	Number of eQTLs
GM_1	1: 3033126	ss715578942[d]	23,919
GM_1_A	1: 3237203	ss715579001	110
GM_1_B	1: 49435179	Satt198	2,136
GM_2	2: 113491276	ss715580997	578
GM_2_A	2: 47857148	ss715583466	34
GM_2_B	2: 48192942	ss715583515[d]	16,909
GM_5 [Grey]	5: 1960856	ss715590397	423
GM_5_A	5: 2357871	ss715592433	24
GM_8	8: 3373388	ss715601478	44
GM_8_A	8: 15062941	ss715599654	367
GM_8_B	8: 15084953	ss715599658	119
GM_11	11: 3866567	ss715610573[d]	14,081
GM_12	12: 37942902	ss715612810	108
GM_12_A	12: 38033264	ss715612824	233
GM_12_B	12: 38161783	ss715612847	13,736
GM_12_C	12: 38314956	ss715612859	84
GM_13	13: 16051820	ss715616825[d]	6,889
GM_13_A [Honeydew, Darkred]	13: 14567149	ss715617113	20
GM_15	15: 4283809	ss715621908[d]	25,727
GM_15_A	15: 4334070	ss715621926	164
GM_15_B	15: 4425676	ss715621953	186
GM_15_C	15: 4541338	ss715622010	82
GM_17	17: 13225475	ss715626059[d]	6,966
GM_17_A	17: 17603614	ss715626313	59
GM_17_B	17: 24925330	ss715626528	29
GM_17_C	17: 28203907	ss715626623	93
GM_17_D [Honeydew, Darkred]	17: 31742522	ss715626724[d]	303
GM_17_E	17: 32295875	ss715626744	95
GM_17_F	17: 33008592	ss715626767	120
GM_18	18: 49185950	ss715631455[d]	91
GM_18_A	18: 49536028	ss715631507[d]	88
GM_19	19: 47232949	ss107929955	30
GM_19_A	19: 47528159	BARCSOYSSR_19_1452	34
GM_19_B	19: 47633059	OSU_SNP_Glyma19g41210	67
GM_20	20: 36332679	ss715637679	41
GM_20_A	20: 36720824	ss715637735	40
Mock GM_13	13: 30875555	ss715615049[d]	31
Mock GM_16	16: 34372952	ss715624691[d]	22
Mock GM_18	18: 57425465	ss715632465[d]	55

[a]Module listed in brackets indicates a significant association between the posterior probability of association (PPA) value and the respective module eigengene expression value at p-value <0.001.
[b]Chromosome and physical base pair (bp) position derived from version Wm82.a2.v1.
[c]Hotspots identified based on the SNP regulating the expression of >20 genes.
[d]Genes controlled by this SNP have significant gene ontology (GO) enrichment at a false discovery rate (FDR) of 5%.

transport," "gene expression," and "cellular processes" (Supplementary Table S3). Similar terms were also found for GM_2_B, GM_11, and GM13 as well as "intracellular signal transduction". Four additional hotspots (GM_17_D, GM_17_F, GM_18, and GM_18_A) were not enriched for biological process GO terms but were enriched for cellular and molecular function GO terms. Overall, biological process GO term enrichment provided evidence of a functional relationship among e-traits within 10 hotspots and hinted at cell-to-cell signaling and protein modification roles but did not elucidate their involvement in a specific mechanism or pathway for QDR.

GO term enrichment for the e-traits associated with the three mock eQTL hotspots was also identified but revealed very general terms (Supplementary Table S4). While e-traits associated with each of the three mock eQTL hotspots were enriched for GO terms, only e-traits associated with GM_18_M were enriched for biological process terms. These included the terms "regulation of cellular process" and "biological regulation." Any significant enrichment of GO terms indicates functional relationships among the genes at a hotspot; however, these general terms do little to inform the specific role of the e-traits at these hotspots.

The e-traits associated with each eQTL hotspot were also examined for enrichment of genes predicted to be involved in specific mechanisms of QDR in soybeans by *P. sojae*. The e-traits for six of 36 hotspots from the inoculated treatment (GM_1, GM_1_B, GM_2_B, GM_11, GM_13, and GM_15) were significantly enriched for genes in the plant–pathogen interaction pathway, and one hotspot (GM_11) was additionally significantly enriched for genes in the isoflavonoid pathway (Table 3). These findings suggest that these six hotspots are most likely regulating genes involved in PAMP-triggered immunity, defense-related gene induction, and/or programmed cell death, implicating leucine-rich repeat (LRR) encoding and other PAMP-triggering genes as likely candidate genes.

We identified no enrichment for hypothesized resistance mechanisms for e-traits mapping to the three hotspots from the mock treatment nor for the remaining 30 of 36 hotspots from the inoculated treatment. While these findings may indicate a lack of concerted functional relationships among e-traits mapping to these hotspots, it may also be due to a lack of statistical power in the smaller hotspots or that the associated e-traits may be involved in unknown or untested mechanisms of QDR.

3.4 Weighted gene co-expression network analysis in the Conrad × Sloan RIL population

To confirm and further characterize the transcriptional reprogramming that occurs following infection with *P. sojae* of

TABLE 3 Pathway enrichment of expression quantitative trait loci hotspots.

Hotspot	KEGG pathway[a]			No. genes in hotspot
	Plant-pathogen interactions	Isoflavonoid	Phenylpropanoid	
GM_1	175***	3	1	23,919
GM_1_B	16*	1	0	2,136
GM_2	2	0	0	578
GM_2_B	115*	2	0	16,909
GM_5	5	0	0	423
GM_8	1	0	0	44
GM_8_A	2	0	0	367
GM_8_B	1	0	0	119
GM_11	115***	5**	0	14,081
GM_12_A	1	0	0	233
GM_12_B	79	1	0	13,736
GM_12_C	1	0	0	84
GM_13	51***	2	0	6,889
GM_15	174**	4	1	25,727
GM_15_A	2	0	0	164
GM_15_B	2	0	0	186
GM_17_D	1	0	0	303
GM_17	40	2	1	6,966
GM_18	1	0	0	91
GM_18_A	1	0	0	88
Mock GM_18	1	0	0	55
No. genes in pathway	314	17	297	

[a]Gene list derived from the KEGG pathway database (accessed, February 2018; http://www.genome.jp/kegg/pathway.html); of the six pathways assessed, only those with genes represented by e-traits within hotspots are shown.

*p-value < 0.05, **p-value < 0.001, ***p-value < 0.0001—levels of significance (Fisher's exact test with Benjamini–Hochberg correction; Fisher, 1935; Benjamini and Hochberg, 1995).

this RIL population, we constructed expression networks, or weighted gene co-expression networks, determined by pairwise correlation of gene expression profiles (Langfelder and Horvath, 2007). This network analysis resulted in a total of six robustly defined modules (Supplementary Figures S4–S6). Module eigengene expression values from three modules, honeydew1, dark red, and grey, comprised of 20,976, 2,785, and 385 genes, respectively, had significant positive correlations with both BLUP values and lesion length for the PRR disease phenotype (Figure 2), indicating that as the expression of genes within these modules increased, susceptibility to PRR increased.

3.5 Term enrichment and functional annotations of co-expression modules

Following similar methods as to how we assessed the putative functions of eQTL hotspots, to ascertain the potential roles of the

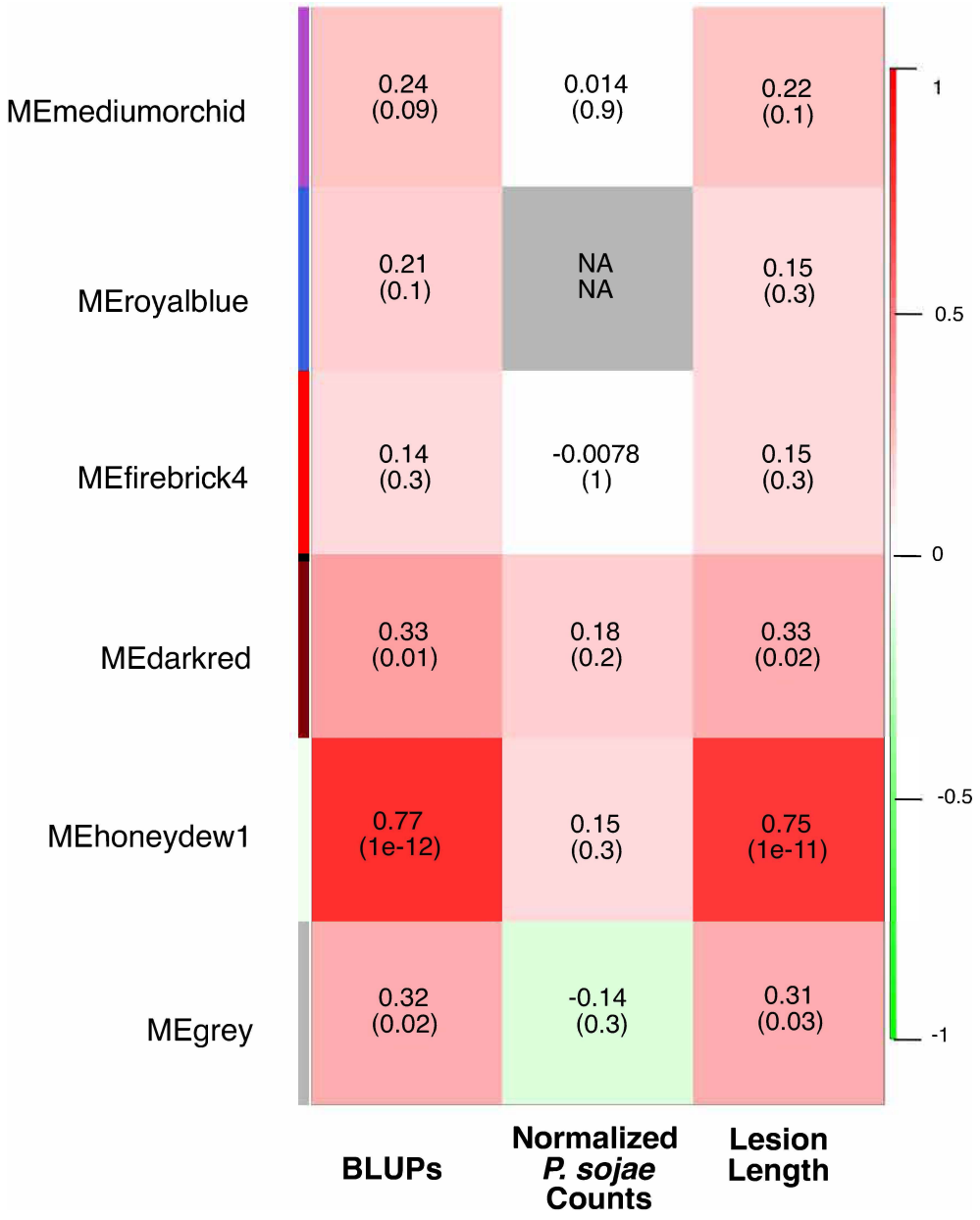

FIGURE 2
Consensus-weighted gene co-expression network analysis (WGCNA) for positively correlated modules. The best linear unbiased predictors (BLUPs) and lesion length values positively correlated to co-expression modules are in red, and those negatively correlated are in green. The first number represents the correlation coefficient, the number in parenthesis indicates the *p*-value. N/A indicates no consensus co-expression module was preserved.

modules in susceptibility to PRR, GO term enrichment and functional annotations were assessed for genes within the honeydew1, dark red, and grey modules. While no significant GO enrichment was observed for the smaller dark red and grey modules, for the honeydew1 module, the most significantly enriched GO terms for biological processes included "translation," "protein localization," and "macromolecule localization" (Supplementary Table S5).

Genes within the co-expression modules were also evaluated for gene enrichment within the six known QDR pathways, for which we had previously evaluated e-traits in each hotspot for enrichment. The honeydew1 module was enriched for five of the six evaluated pathways: plant hormone signal transduction, phenylpropanoid biosynthesis, isoflavonoid biosynthesis, MAPK signaling, and plant-pathogen interaction pathways (Table 4). The dark red module was also significantly enriched for plant hormone signal transduction, MAPK signaling, and plant–pathogen interaction pathways. None of the six pathways were significantly enriched in the grey module, possibly due to the relatively smaller size of this module or indicating that there may be other pathways associated with resistance.

3.6 Genetic architecture of co-expression modules

We integrated genetic markers associated with inoculated eQTL hotspots and co-expression modules (Zhang and Horvath, 2005) to further investigate the genetic loci influencing the three co-expression modules that were significantly correlated with PRR (honeydew1, dark red, and grey). The expression of each of the three module eigengenes was significantly correlated with the SNP (s) marking one or more of the eQTL hotspots. The correlation of an eQTL hotspot and a co-expression module to the same SNP suggests regulation of both by a common genetic mechanism (Table 2; Supplementary Figures S7A–C). The grey module was significantly correlated to the genetic marker for hotspot GM_5 (423 e-traits). The expression of both the honeydew1 and dark red module eigengenes was significantly correlated to SNPs from hotspots GM_13_A (20 e-traits) and GM_17_D (303 e-traits).

3.7 Co-localization of phQTLs and eQTLs

In order to understand the regulation of QDR by *P. sojae*, co-localizations of eQTLs or eQTL hotspots with phQTLs were identified. Among all of the 8 phQTLs mapped to unique locations in populations derived from Conrad × Sloan for *P. sojae* isolate 1.S.1.1 (Wang et al., 2010; Wang et al., 2012a; Stasko et al., 2016; Table 1), three phQTLs, which mapped to chromosomes 1, 18, and 19, co-localized with three hotspots and nine eQTLs (three inoculated *trans*- and six inoculated *cis*-eQTLs (Table 1). For both *cis*- and *trans*-eQTLs, this is significantly more co-localization than expected by random chance.

Co-localized with phQTL_1 were four *cis*-eQTLs for *Glyma.01G160600*, *Glyma.01G162600*, *Glyma.01G170600*, and *Glyma.01G171300* and two *trans*-eQTLs, both representing *Glyma.10G026500*, which had e-traits mapping independently to two markers within this phQTL region (Table 1). The e-traits of genes mapping in *cis* are towards genes annotated as a vacuolar iron transporter homolog, two-component response regulator ARR2, and an uncharacterized expressed sequence. The predicted protein of *Glyma.10G026500*, mapping to the two *trans*-eQTLs, was also uncharacterized. Interestingly, *just* outside (138 kb) of the average LD block size window (242 kb), which we used to consider co-localization between mapped *trans*-eQTL and phQTL, is the hotspot GM_1_B.

The e-traits for the paralogs *Glyma.18G270900* and *Glyma.08g249200* are both co-localized with phQTL_18b in *cis* and *trans*, respectively (Table 1). The gene sequences are present in syntenic blocks from the recent duplication within the soybean genome (Schmutz et al., 2010). Both genes are predicted to encode a malectin/receptor-like protein kinase.

Covering 4.7 Mb, phQTL_19b represented the largest genomic size of the phQTL we considered. As such, it co-localized with all three hotspots on chromosome 19 (GM_19, GM_19_A, and GM_19_B). However, these hotspots, all relatively small and possessing between 30 and 67 e-traits, were not enriched for any function or GO annotation, providing little evidence of a coordinated function. However, in addition to co-localization with the three hotspots, phQTL_19b also co-localized with both the mock and inoculated *cis*-eQTLs for the *Glyma.19G224300* e-traits.

TABLE 4 Enrichment of genes within KEGG pathways for each co-expression module related to susceptibility.

KEGG pathway[a]		Plant hormone signal transduction	Phenylpropanoid biosynthesis	Isoflavonoid biosynthesis	MAPK signaling pathway	Plant-pathogen interaction	Total no. of genes in module
Total No. of genes in the pathway		587	297	17	281	314	–
No. of pathway genes in the module	**Honeydew1**	244	1**	8***	135*	160***	20,976
	Darkred	41*	0	0	27**	26*	2,785
	Grey	3	0	0	2	1	385

[a]Gene list derived from the KEGG pathway database (accessed, February 2018; http://www.genome.jp/kegg/pathway.html) and extracted from NCBI BioSystems (accessed, February 2018; https://www.ncbi.nlm.nih.gov/biosystems).

*p-value < 0.05, **p-value < 0.001, ***p-value < 0.0001—levels of significance (Fisher's exact test with Benjamini–Hochberg correction; Fisher, 1935; Benjamini and Hochberg, 1995).

10.3389/fpls.2023.1277585

3.8 Identification of master regulators controlling the expression of downstream suites of genes

Master regulators control the expression of a suite of downstream genes. To identify master regulators in QDR for *P. sojae*, we examined the key eQTL hotspots, which we defined as those that were significantly enriched for e-traits, correlated with modules, or co-localized with phQTL. From the 36 total eQTL hotspots, our primary and meta-analyses identified 16 key eQTL hotspots through the significant pathway or GO term enrichment of e-traits within a hotspot (GM_1, GM_1_B, GM_2_B, GM_11, GM_13, GM_15, GM_17, GM_17_D, GM_17_F, GM_18, GM_18_A), by the significant correlation of co-expression modules (GM_5, GM_13_A, GM_17_D), and/or the co-localization with a phQTL for resistance to *P. sojae* (GM_19, GM_19_A, GM_19_B). To better understand the regulation of these key hotspots, we identified their putative master regulators by integrating genetic position and putative gene function (methods adapted from Wang et al., 2017). We identified genes within the hotspot regions predicted to encode transcription factors or signaling molecules as putative master regulators (Table 5).

For nine of the 16 hotspots evaluated for master regulators (GM_1, GM_1_B, GM_2_B, GM_5, GM_11, GM_13, GM_13_A, GM_15, GM_17), we identified co-localized *cis*-eQTLs putatively encoding signal molecules and/or transcription factors (Table 5). To note, numerous hotspots were associated with multiple putative master regulators with genes for *cis*-eQTLs encoding both signaling molecules and transcription factors. For the four remaining eQTL hotspots (GM_17_D, MD_17_F, GM_18, and GM_18_A), while no genes

TABLE 5 Candidate master regulators of key hotspots.

eQTL hotspot[a]	Candidate master regulators[b]	Description[c]	TF/ SM/ *cis*-eQTL[d]
GM_1[e,f] (23,919)	*Glyma.01G017000*	3-Phosphoinositide-dependent protein kinase-1, putative	SM/*cis*-eQTL
	Glyma.01G021000	Auxin response factor 19	SM/*cis*-eQTL
	Glyma.01G022000	Methyl-CPG-binding domain protein 02; IPR011124 (zinc finger, CW-type)	TF/*cis*-eQTL
	Glyma.01G002400	Phospholipase A2 family protein	SM/*cis*-eQTL
GM_1_B[f,i] (2,136)	*Glyma.01G156200*	Membrane transport protein, auxin efflux carrier	SM/*cis*-eQTL
	Glyma.01G156600	Thioredoxin reductase, pyridine nucleotide disulfide oxidoreductase	SM/*cis*-eQTL
	Glyma.01G156700	Hydroxymethylglutaryl-CoA reductase, mevalonate pathway 1	SM/*cis*-eQTL
GM_2_B[e,f,j] (16,909)	*Glyma.02G306300*	WRKY DNA-binding domain, zinc-dependent activator protein	TF/*cis*-eQTL
	Glyma.02G307300	Aldo/keto reductase family, flavonoid biosynthesis-	SM/*cis*-eQTL
	Glyma.02G307900[k]	FIMBRIN/PLASTIN, Ca^{2+}-binding actin-bundling protein, EF-Hand protein superfamily	TF/*cis*-eQTL
	Glyma.02G308800	5′-AMP-activated protein kinase beta subunit, interaction domain, involved assembly of snf1 protein complex	SM/*cis*-eQTL
	Glyma.02G309100	Zinc finger, C3HC4 type (RING finger), E3 Ubiquitin protein ligase	TF/*cis*-eQTL
	Glyma.02G310400	Leucine-rich repeat receptor-like protein kinase, BR-signaling kinase 1	SM/*cis*-eQTL
GM_5[h] (423)	*Glyma.05G021300*	Zinc-finger double-stranded RNA-binding, DNAJ homolog	TF/*cis*-eQTL
	Glyma.05G021800	Cytochrome P450, CYP2 subfamily, leucopelargonidin and leucocyanidin biosynthesis	SM/*cis*-eQTL
	Glyma.05G021900	Cytochrome P450, CYP2 subfamily, leucopelargonidin and leucocyanidin biosynthesis	SM/*cis*-eQTL
GM_11[e,f,g] (14,801)	*Glyma.11G051500*	Mn^{2+} and Fe^{2+} transporters of the NRAMP family, natural resistance-associated macrophage protein	SM/*cis*-eQTL
	Glyma.11G052100	Myb-like DNA-binding domain, TF, MYB superfamily	TF/*cis*-eQTL
	Glyma.11G053100	WRKY DNA-binding protein, transcription factor	TF/*cis*-eQTL
GM_13[e,f,j] (6,889)	*Glyma.13G062400*	Reticulon	SM/*cis*-eQTL
	Glyma.13G062700[k]	Glycosyl transferases group 1, glycogen biosynthesis (ADP-D-glucose)	SM/*cis*-eQTL
GM_13_A[h] (20)	*Glyma.13G049000*	GDSL/SGNH-like acyl-esterase family found in Pmr5 and Cas1p	SM/*cis*-eQTL
GM_15[e,f] (25,727)	*Glyma.15G053600*	IPT/TIG domain, calmodulin binding transcription activator	TF/*cis*-eQTL
	Glyma.15G053700		

(Continued)

TABLE 5 Continued

(Continued)

10.3389/fpls.2023.1277585

TABLE 5 Continued

eQTL hotspot[a]	Candidate master regulators[b]	Description[c]	TF/ SM/ *cis*-eQTL[d]
		Protein phosphatase 2C, serine/threonine protein phosphatase	SM/*cis*-eQTL
	Glyma.15G054100	Caspase domain, metacaspase is involved in the regulation of apoptosis	SM/*cis*-eQTL
	Glyma.15G054500	UDP-glucoronosyl and UDP-glucosyl transferase	SM/*cis*-eQTL
	Glyma.15G054600	Phosphate-induced protein 1 conserved region	SM/*cis*-eQTL
	Glyma.15G054800	RNA recognition motif (a.k.a. RRM, RBD, or RNP domain), splicing factor RNPS1, SR protein superfamily	SM/*cis*-eQTL
	Glyma.15G055100	EF-hand domain pair, calcium-binding protein	TF/*cis*-eQTL
	Glyma.15G055200	F-box domain	TF/*cis*-eQTL
	Glyma.15G055500	Amidohydrolase family, thymine degradation	SM/*cis*-eQTL
	Glyma.15G056000	Ring finger domain, anaphase-promoting complex	TF/*cis*-eQTL
GM_17[e] (6,966)	*Glyma.17G155500*	Kinesin motor domain	SM/*cis*-eQTL
GM_17_D[h] (303)	*Glyma.17G200200*	C2H2 type zinc-finger	TF
	Glyma.17G200500	Transcription factor PCC	TF
GM_17_F[e] (120)	*Glyma.17G204300*	PHD finger proteins	TF
	Glyma.17G204600	Leucine-rich repeat receptor-like protein kinase, cytoplasmic	SM
GM_18[e] (91)	*Glyma.18G206400*	Leucine-rich repeat receptor-like protein kinase (serine/threonine)	SM
	Glyma.18G207700	Dirigent-like protein, disease resistance responsive	SM
	Glym.18G208100	Protein phosphatase 2C, serine/threonine protein phosphatase	SM
	Glyma.18G208800	WRKY DNA-binding domain	TF
	Glyma.18G209400	SWIM zinc finger	SM
GM_18_A[e] (88)	*Glyma.18G209400*	SWIM zinc finger	TF
	Glyma.18G209500	Wound-induced protein WI12	TF
GM_19[i] (30)	*Glyma.19G217800*	WRKY DNA-binding	TF
	Glyma.19G218800	MYB-LIKE DNA-binding	TF
	Glyma.19G219000	MYB-LIKE DNA-binding	TF
	Glyma.19G220000	Zinc finger protein	SM
	Glyma.19G220300	Leucine-rich repeat receptor kinase (serine/threonine)	SM
GM_19_A[i] (34)	*Glyma.19G221700*	WRKY DNA-binding domain (overlap with GM_19)	TF
GM_19_B[i] (67)	*Glyma.19G222200*	MYB-LIKE DNA-binding (overlap with GM_19 and 19_A)	TF
	Glyma.19G244200	Two-component sensor histidine kinase—SNP in the gene (overlap with GM_19_A)	SM
	Glyma.19G224600	MYB-LIKE DNA binding (overlap with GM_19_A)	TF
	Glyma.19G224700	Basic helix-loop-helix/ leucine zipper transcription factor (overlap with GM_19_A)	TF
	Glyma.19G226000	Interleukin-1 receptor-associated kinase (serine/ threonine)	SM
	Glyma.19G226900	Zinc finger five domain-containing protein	SM

[a]Parenthetical number is the number of eQTL associated with each key hotspot. Key eQTL hotspots were those enriched QDR pathways based on the iBMQ analysis or overlap a phQTL of the Conrad × Sloan recombinant inbred population following inoculation with Phytophthora sojae.

[b]Candidate master regulators were identified as genes within a 242-kb (average linkage disequilibrium (LD) block size) upstream or downstream of the hotspot SNP, and genes with cis-eQTL mapping were identified as initial candidate master regulators. Genes were then selected as candidate master regulators if their putative function included transcription factors, signaling molecules, or known associations involved in the enriched quantitative disease resistance (QDR) pathways. Gene ID based on the Wms82.a2.v1 sequence (soybase.org).

[c]Description, PFAM, Panther, and pathway were retrieved from https://phytozome.jgi.doe.gov (accessed July 2023).

[d]Results from mapping genes to the KEGG Pathway database (accessed August 2023; http://www.genome.jp/kegg/pathway.html). Classification of the putative master regulator: putative signaling molecule (SM), putative transcription factor (TF), and cis-eQTL for this gene (cis-eQTL).

[e]Genes controlled by this SNP have significant gene ontology (GO) enrichment at a false discovery rate (FDR) of 5%.

[f]Significant pathway enrichment of the plant interaction pathway (adjusted p-value ≤ 0.05; Fisher's exact test with Benjamini–Hochberg correction). Gene lists derived from the KEGG pathway database (accessed, February 2018; http://www.genome.jp/kegg/pathway.html).

[g]Significant pathway enrichment of the isoflavonoid pathway (p-value ≤ 0.05; Fisher's exact test with Benjamini–Hochberg correction). Gene lists derived from the KEGG pathway database (accessed, February 2018; http://www.genome.jp/kegg/pathway.html).

[h]Significantly correlated with co-expression modules at a p-value <0.05 (Fisher's exact test).

[i]Co-localizes with phenotypic quantitative trait loci (phQTL).

[j]Intragenic hotspot SNP.

[k]The hotspot SNP is located within this putative master regulator.

within the LD window (242 kb) had *cis*-eQTLs, genes within the LD windows were putatively encoding transcription factors and/or signaling molecules and identified as candidate master regulators of these hotspots. In total, 15 genes putatively encoding transcription factors and 24 genes

putatively encoding signaling molecules were identified as candidate master regulators for the 16 key eQTL hotspots (Table 5).

4 Discussion

Many phQTLs have been mapped through several generations in this Conrad × Sloan population (Wang et al., 2010; Wang et al., 2012a; Wang et al., 2012b; Stasko et al., 2016); however, identifying the mechanisms underpinning these phQTLs has, thus far, been unsuccessful. Studies using the resistant parent 'Conrad' have identified many putative mechanisms of quantitative resistance, demonstrating the complex nature of QDR and the potential that these mechanisms could be interacting (Vega-Sánchez et al., 2005; Thomas et al., 2007; Ranathunge et al., 2008; Zhou et al., 2009; Wang et al., 2012b). The application of a systems genomics approach in this study has allowed us to disentangle the complex genetic architecture of gene expression related to QDR for *P. sojae* using multiple approaches, including eQTL mapping, co-expression network analysis, and the co-localizations of phQTLs, eQTLs, and co-expression modules. The approaches taken in this study confirmed hypothesized mechanisms as well as provided evidence to suggest potential novel mechanisms of QDR for this pathosystem.

4.1 Inoculation with *P. sojae* causes transcriptional reprogramming that occurs in a *trans*-regulatory manner

Expression QTLs were successfully mapped in both the inoculated and mock treatments; however, there were 144-fold more eQTLs mapped for the inoculated treatment compared to the mock treatment. An average of two eQTLs per gene were mapped in the inoculated treatment, which is consistent with previous eQTL mapping studies (Schadt et al., 2003; Swanson-Wagner et al., 2009; Christie et al., 2017). Yet, in this study, only 794 eQTLs were identified for the mock, the majority of which were *cis*-eQTL. In stark contrast to the mock-inoculated treatment, nearly all eQTLs identified from the inoculated treatment in this study were *trans*-eQTLs (98%).

Gene expression has been shown in previous eQTL studies to be controlled by *trans*- or a combination of both *trans*- and *cis*-elements (West et al., 2007; Christie et al., 2017; Sun et al., 2017; Li et al., 2018). However, the number of eQTLs mapped, as well as the proportion of *trans*- vs. *cis*-eQTLs, has not followed a specific trend between species and populations (Keurentjes et al., 2007; West et al., 2007; Potokina et al., 2008; Swanson-Wagner et al., 2009; Hammond et al., 2011; Christie et al., 2017). For example, the number of eQTLs varied approximately ninefold between RIL populations in *Arabidopsis* (Keurentjes et al., 2007; West et al., 2007). While some studies have reported nearly equal ratios of *trans*- and *cis*-eQTLs detected in both *Arabidopsis* and barley (Keurentjes et al., 2007; Potokina et al., 2008), other studies have revealed a predominance of *trans*-regulation of eQTLs in *Arabidopsis* (86% and greater *trans*-eQTLs) (West et al., 2007; Soltis et al., 2020), barley (70% *trans*-eQTLs) (Druka et al., 2008), *Brassica rapa* (77% *trans*-eQTLs) (Hammond et al., 2011), and maize (up to 80% *trans*-eQTLs) (Swanson-Wagner et al., 2009; Christie et al., 2017). These varying results have been attributed to statistical power to detect *trans*-eQTLs, the size of the mapping population, the high polymorphism rate among genotypes in the study, and true biological differences between systems and their overall genetic architecture (Kliebenstein, 2009; Soltis et al., 2020). To date, only a few studies have been completed to address these questions of differing detection of eQTL types across plant species and populations (Franceschini et al., 2012; Saha and Battle, 2018).

The majority of plant-based eQTL studies to date have focused on natural genetic variation within breeding populations, different stages of maturation, or specific production or accumulation of compounds, and few have focused on mechanisms of disease resistance. Specifically in soybean, previous eQTL analyses identified predominantly *trans*-eQTLs for the genetic architecture of immature soybean seed (86.6%, *trans*-eQTLs) (Bolon et al., 2014) and dissection of isoflavonoid accumulation in soybean seed (60.6%, *trans*-eQTLs) (Wang et al., 2014).

The large number of *trans*-eQTLs mapped in this study were primarily associated with only eight eQTL hotspots, indicating massive transcriptional reprogramming resulting from the inoculation of soybean with *P. sojae*. This confirms several previous studies for quantitative resistance (Zhou et al., 2009; Soltis et al., 2020) and *Rps*-gene-related responses (Lin et al., 2014; Hale et al., 2023b). The eQTL hotspots identified in this study at 24 hai may represent key regulatory hubs and the control of signaling networks specifically in response to infection by *P. sojae*. More importantly, none of the 36 hotspots identified from the inoculated treatment overlap with the three hotspots identified from the mock treatment. This suggests that these hotspots in the mock represent either constitutive differences in regulation between Conrad and Sloan or a response specific to the mock treatment at the 24-hai time point. Of the few eQTL studies that have mapped transcriptional responses to disease, only a fraction of these studies compared eQTLs mapped in disease versus non-disease conditions in plant systems. Moscou et al. (2011), using microarrays to assay transcripts in barley following both inoculations with *Puccinia graminis* and mock inoculation, had findings that differed from this study, with similar numbers of eQTLs mapped in both mock and inoculated samples and the majority classified as *cis*. Here, the differences in the number of eQTL mapped between treatments, the lack of concordance of the hotspots between the mock and inoculated treatments, the correspondence with phQTLs, and the functional enrichment of genes within hotspots together suggest that the changes in transcription are due to infection by *P. sojae* through a coordinated transcriptional response of multiple plant defense mechanisms.

4.2 Major eQTL hotspots and co-expression networks elucidated potential QDR mechanisms, including signal integration and defense action via cell wall strengthening

Expression QTL hotspots are a single polymorphism associated with the expression of numerous genes (Neto et al., 2012), and the

genetic regions may harbor important regulatory genes. In this study, the four largest hotspots, mapping to chromosomes 1, 2, 11, and 15, accounting for more than 80,000 eQTLs (>70%) from the inoculated treatment, were each enriched for genes within the plant–pathogen interaction (PPI) pathways. Specifically, PPI pathway genes found within the hotspots were predicted to function throughout the pattern-triggered immunity (PTI) pathway. The separation of the PTI and ETI pathways within the context of plant resistance to oomycetes has recently come into question in favor of a three-layer plant immune system (consisting of the recognition, signal integration, and defense-action layers) describing both PTI and ETI for plant-pathogenic oomycete infection (Wang et al., 2019; Naveed et al., 2020). The signal-integration layer represents a complex network of pathway cascades including phosphorylation, ubiquitination, relocation, degradation, stabilization of proteins, transcriptional regulation, and chemical signaling (Wang et al., 2019). The QDR pathway enrichment within these major hotspots, along with the significantly enriched GO terms related to cell-to-cell signaling and protein modification, support the involvement of these hotspots in the signal-integration layer of defense. This aligns with previously implicated defense mechanisms in plant–oomycete interactions and specifically within the *P. sojae*-soybean pathosystem (Wang et al., 2012b; Wang et al., 2019).

These four eQTL hotspots represent genetic variation for transcriptional reprogramming resulting from inoculation with *P. sojae*, a phenomenon that has been previously reported (Zhou et al., 2009; Wang et al., 2010). Yet, these hotspots do not localize to the regions of any phQTLs identified in this study or previous studies. Samad-Zamini et al. (2017) had similar findings, where none of the hotspots co-localized with phQTLs during a time-course assay of *Fusarium graminearum* (FHB) infection of wheat (*Triticum aestivum* L.). This lack of co-localization may be due to residual genetic variation of e-traits not significantly attributed to phQTL; this variation may involve complex genetic interactions, including epistasis (Li, 2019).

In this study, we also identified a total of 24,146 genes within three co-expression modules that were significantly correlated to the PRR disease resistance response. The SNPs corresponding to two hotspots, GM_13_A and GM_17_D, were also both significantly correlated to the co-expression modules dark red and honeydew1. GM_17_D was enriched for GO terms including "hydrolase activity" and "cell wall structure," functions that align with the third layer of resistance, defense-action (Wang et al., 2019). Genes involved in the modification of the cell wall and hydrolase activity have been shown to be involved in plant defense responses (Smith et al., 1988; Smith et al., 1990; Walton, 1994; Minic, 2008). Hydrolase expression has been previously associated with quantitative resistance to *P. sojae* with specific hydrolases suppressed at 48 hai in the resistant parent Conrad and suppressed at 72 hai in the susceptible parent Sloan (Wang et al., 2012b). The GM_17_D hotspot may be involved in the coordinated regulation of these two modules, and importantly, these co-expressed genes may play a role in limiting pathogen penetration into the cell wall in response to pathogen presence. The dark red and honeydew1 co-expression modules, along with the third co-expression module, grey, were also each enriched for genes involved in the plant hormone signal transduction, MAPK signaling pathway, and PPI pathways, providing evidence for coordinated regulation of expression among each of these defense mechanisms.

The honeydew1 module was further described by its additional enrichment of genes from the phenylpropanoid biosynthesis and isoflavonoid pathways. The role of phenylpropanoid and isoflavonoid in the *R*-gene-mediated response has been well studied (Graham et al., 2007), including the recent identification of a transcription factor that modulates this response (Jahan et al., 2020). However, the specific role of phenylpropanoid and isoflavonoid pathways in QDR has been more elusive. Gene expression in the honeydew1 module is correlated with increased susceptibility, supporting recent evidence in the cross-talk that occurs between the pathways for *R*-gene-mediated and QDR. Previous studies showed both SA and JA increasing at inoculated roots, with JA further increased in later time points after inoculation (Stasko et al., 2020; Karhoff et al., 2022). This 24-hai time point could be a critical time as the pathogen switches from hemibiotrophy to the necrotrophic phase (Moy et al., 2004). Several genes in the phenylpropanoid pathway have been identified as playing a role in resistance to *P. sojae* in soybeans. For example, soybean cinnamate 4-hydrolase (GmC4H1; first hydroxylation step of the phenylpropanoid pathway) was induced at 24 hai in the resistant parent Conrad, and greater colonization of *P. sojae* was measured in *GmC4H1*-silenced plants (Yan et al., 2019). Recently, in the wheat-*Fusarium graminearum* system, it was reported that wheat genotypes with greater levels of resistance had a constitutive expression of genes for plant cell wall biogenesis and terpene biosynthesis (Buerstmayr et al., 2021).

4.3 Genetic regulation of trans-eQTLs in response to the pathogen is predicted to occur through TF and signaling molecules involved in PPI, plant hormone signal transduction, and novel mechanisms of resistance

Numerous studies have proposed that *cis*-acting mechanisms (i.e., transcription factors) can affect the expression of e-traits at *trans*-eQTL hotspots (Albert and Kruglyak, 2015; Wang et al., 2017). Thus, *cis*-eQTLs located near regulatory genes have the potential to be master regulators for these e-traits in a given hotspot (Bryois et al., 2014; Albert and Kruglyak, 2015; Yao et al., 2015). We identified candidate master regulators for the key hotspots that had significant GO or pathway enrichment, were correlated to a co-expression module, and/or were co-localized with phQTL. Of these, four putative master regulators were predicted to function in the PPI pathway as LRR-RLKs, or EF-hand motif proteins.

LRR-RLKs were predicted to be encoded by candidate master regulators for GM_2_B, GM_17F, GM_18, and GM_19. These LRR-RLKs are crucial for plant function and adaptation in numerous processes such as growth and development, as well as responses to abiotic and biotic stresses (Chinchilla et al., 2009; De Smet et al., 2009). Among their numerous functions, LRR-RLKs are known to function in

all three layers of defense through the perception of microbe-associated molecular patterns resulting in a basal defense (e.g., *FLS2*), defense signaling (e.g., *SIF2*), and defense response (e.g., *PEPR2*) (Gómez-Gómez and Boller, 2000; Becraft, 2002; Shiu et al., 2004; Zipfel et al., 2006; Yamaguchi et al., 2010; Kemmerling et al., 2011; Soyars et al., 2016; Hohmann et al., 2017; Zipfel and Oldroyd, 2017; Yuan et al., 2018; Wang et al., 2019). LRR-RLKs have been identified as candidates for resistance to *Phytophthora* spp. in numerous studies including this *P. sojae*-soybean system (Schneider et al., 2016; Stasko et al., 2016; Rolling et al., 2020).

Two EF-hand motif proteins were each identified as candidate master regulators associated with the PPI pathway for hotspots GM_2_B and GM_15, respectively, with GM_2_B being a hotspot enriched for genes within the PPI pathway. Approximately 250 EF-hand motifs have been identified in plants and are involved with Ca^{2+}, which acts as a messenger that regulates responses to external stimuli, development, and hormones, including plant defense and stress response (Poovaiah and Reddy, 1993; Trewavas and Mahlo, 1998; Reddy and Reddy, 2001; Zielinski, 1998). The majority of Ca^{2+} sensors in soybeans possess the EF-hand motif and have at least one or more hormone- or stress-response-related *cis*-elements in their promoter region (Zeng et al., 2017). These hormone- or stress-response-related elements have been characterized by functioning in the regulation of abscisic acid (ABA) signaling, auxin response, ethylene response, and phosphate starvation response. Of these signaling and responses potentially regulated by EF-hand motif encoding genes, ABA has been shown to be a negative regulator of *R*-gene-mediated resistance (Ward et al., 1989; MacDonald and Cahill, 1999), and auxin has been reported to enhance plant susceptibility to *P. sojae* in soybean (Stasko et al., 2020) and other pathogens (Wang et al., 2007; Domingo et al., 2009; Kidd et al., 2011). Auxin transporters and auxin-induced proteins have been upregulated in susceptible parents in the *P. sojae*-soybean pathosystem (Wang et al., 2012b). Auxin transport transcripts of *GmPIN* were higher in expression in the resistant Conrad following inoculation with *P. sojae* compared to mock, whereas in the susceptible, fewer *GmPIN* changed in expression levels (Stasko et al., 2020). Additionally, ethylene-responsive genes have also been known to induce resistance in the *P. sojae*-soybean pathosystem (Sugano et al., 2013; Zhao et al., 2017), as well as play a role in the regulation of pathogenesis-related gene expression (Lorenzo et al., 2003; Pieterse et al., 2009; Rehman and Mahmood, 2015). Taken together, the EF-hand motif-encoding genes are excellent candidate master regulators for GM_2_B and GM_15.

In addition to these candidate master regulators within the PPI pathway and those that overlap phQTLs, several MYB-TFs were identified as candidate master regulators for GM_11 and GM_19, GM_19_A, and GM_19_B. MYB transcription factors are one of the six major TF families functioning in plant defense (Ng et al., 2018), responding to both abiotic and biotic stresses, and functioning in primary and secondary metabolism (Stracke, 2001; Ambawat et al., 2013), including the regulation of the phenylpropanoid pathway (Liu et al., 2015). Additionally, GmMYB29A2 is essential for the *R*-gene response to *P. sojae* in soybeans, regulating the accumulation of glyceollin in Williams 82 (Jahan et al., 2020), and *MYB* transcripts were also detected by capture-seq from a transcriptome data set of the *R*-gene response in Williams 82 (Hale et al., 2023b). They are known to act as a positive regulator of hypersensitive response in PCD in response to fungal and bacterial pathogens (Vailleau et al., 2002). Thus, these may be putative master regulators involved with the positive regulation of PCD in the soybean-*P. sojae* pathosystem.

GM_17_D did not have any *cis*-eQTLs mapping to this hotspot. However, significant differential expression is not a requirement for a master regulator. For example, *hunchback* (*hb*), encoding a ZN-finger TF in *Drosophila melanogaster*, was identified as a candidate master regulator for mitigation of lead exposure, located near a *trans*-eQTL hotspot, yet the candidate itself had no e-traits mapped (Qu et al., 2018). Here, we note that the zinc finger TF (*Glyma.17G200200*) is a candidate master regulator of GM_17_D because it is not only physically located near the hotspot but is also within the honeydew1 co-expression network that is correlated with PRR disease.

In addition to the candidate master regulators functioning in known or hypothesized pathways for QDR, we also identified candidate master regulators that putatively influence novel pathways for QDR. These novel pathways for QDR in *P. sojae* included secondary metabolite biosynthesis, RNA transport, thioredoxin metabolism (GM_1_B), lysine degradation (Glyma_2_B), reticulon (Lee et al., 2011), starch and sucrose metabolism (GM_13), thymine degradation (GM_15), and a number of serine/threonine protein kinases and phosphatases that impact other metabolic pathways. These candidate master regulators of novel QDR pathways include TFs and signaling molecules that potentially regulate the expression of downstream genes related to hotspots. Further studies will be needed to determine if and how these pathways are playing a role in the *P. sojae*-soybean pathosystem.

4.4 Co-localization of phQTLs with eQTL points to causal candidate genes for QDR

To identify gene expression variation that may be causal to PRR disease resistance, we focused on those eQTLs that co-localized with phQTLs, indicating a strong link between transcriptional phenotype and the genes underpinning the disease resistance phenotype. Specifically, co-localized *cis*-eQTLs, the genes regulating co-localized *trans*-eQTLs, or *trans*-eQTL hotspots may be causal for resistance to PRR.

While none of the four *cis*-eQTLs co-localized with phQTL_1 have obvious functions in quantitative disease resistance, the hotspot GM_1_B, which neighbors phQTL_1, is enriched for genes functioning in PPI pathways, making regulators of this hotspot viable causal genes for phQTL_1. Three *cis*-eQTLs were identified as candidate master regulators for this hotspot: *Glyma.01G156600*, *Glyma.01G156200*, and *Glyma.01G156700*. These genes are predicted to encode a thioredoxin reductase, a membrane transport protein, and a hydroxymethylglutaryl-CoA reductase, respectively. The predicted thioredoxin reductase (*Glyma.01G156600*) is of interest given the role of thioredoxin in disease resistance and potentially QDR to *P. sojae*, with thioredoxin-encoding genes identified as candidate genes for several quantitative disease resistance loci (QDRL) towards *P.*

sojae (Huang et al., 2016; Stasko et al., 2016). Additionally, a thioredoxin-encoding gene has been shown to be the causal gene for resistance at the *Scmv1* phQTL for sugarcane mosaic virus in maize (Liu et al., 2017). The predicted membrane transport protein encoded by *Glyma.01G156200* is an auxin efflux carrier. Auxin has been previously described in numerous studies as being involved in susceptibility to plant pathogens (Wang et al., 2007; Domingo et al., 2009; Kidd et al., 2011; Pieterse et al., 2012). Finally, hydroxymethylglutaryl-CoA reductase, predicted to be encoded by *Glyma.01G156700*, is involved in terpenoid and secondary metabolite biosynthesis (Antolin-Llovera et al., 2011). Thus, these potential master regulators for the Gm_1_B hotspot may represent the causal genetic variation for phQTL_1.

The phQTL_18b was co-localized with two eQTLs controlling the expression of *Glyma.18G270900* and *Glyma.08g249200* in *cis* and *trans*, respectively, each putatively encoding a malectin/receptor-like protein kinase. In *Arabidopsis*, the homolog of these genes, *FERONIA*, has been experimentally shown to have multiple functions, including as a modulator of ethylene response (Deslauriers and Larsen, 2010) and in reactive oxygen species (ROS)-mediated root hair development (Duan et al., 2010). ROS is a well-known mediator of stress-induced responses and functions in growth and development (Werner, 2004; Swanson and Gilroy, 2010; Torres, 2010). *FERONIA* also functions to inhibit jasmonic acid (JA) signaling through phosphorylation of the transcription factor MYC2 in Arabidopsis (Guo et al., 2018). In soybean, a role for JA was proposed in the later stages of infection by *P. sojae* (Stasko et al., 2020). The JA pathway was suppressed in incompatible *R*-gene reactions to *P. sojae* (Lin et al., 2014), and JA accumulation significantly increased in *P. sojae*-inoculated susceptible lines in contrast to the mock-inoculated and to lines with quantitative resistance alleles (Karhoff et al., 2022).

In addition to co-localization with the three hotspots (GM_19, GM_19_A, and GM_19_B), phQTL_19b co-localized with both the mock and inoculated *cis*-eQTLs for the *Glyma.19G224300* e-traits. This inoculated *cis*-eQTL is also part of the GM_19_B eQTL hotspot. The e-traits for *Glyma.19G224300* represented one of only two pairs of e-QTLs that were found under both mock and inoculated conditions, indicating possible constitutive control of both GM_19_B and of phQTL_19b. *Glyma.19G224300* is predicted to encode a germin-like protein (GLP). Among their functions, GLPs can be involved in response to abiotic stress (Barman and Banerjee, 2015). In *Arabidopsis*, upregulation of the *Glyma.19G224300* homolog *AT1G09560* results in reduced primary root and enhanced lateral root growth (Ham et al., 2012). *Glyma.19G224300* may function in root architecture, providing constitutive quantitative resistance to *P. sojae*, with the differences in disease resulting from expression changes mapping to GM_19_B.

5 Concluding remarks

This vast transcriptional reprogramming due to pathogen infection compared to the nondisease state had not been previously explored through eQTL methodology using RNA-sequencing data in this host–pathogen system. Ultimately, this study identified gene co-expression modules associated with resistance and susceptibility to *P. sojae* in this RIL population. Clearly, the transcriptional response to this pathogen is complex, as there were more than 100-fold greater number of eQTLs in the inoculated compared to the mock treatment, as well as a predominance of *trans*-eQTLs in the inoculated over the mock treatment. Further evidence supporting cell wall structure, auxin response, jasmonic acid signaling, and PPI receptor and signaling genes as mechanisms of resistance are provided, as well as several new potential mechanisms for regulating resistance as well as potential susceptibility factors. Further confirmation of the candidate genes regulating *trans*-eQTLs and/or acting as the causal variation of phQTLs will need to be explored through functional studies. The development of this large dataset and analyses through co-expression networks, eQTLs, and phQTLs have the potential to be expanded to elucidate more biologically relevant information on *P. sojae* infection as well as constitutive differences between two cultivars.

Data availability statement

The datasets presented in this study can be found in online repositories. The names of the repository/repositories and accession number(s) can be found below: https://www.ncbi.nlm.nih.gov/, PRJNA478334.

Author contributions

CM: Data curation, Formal analysis, Investigation, Methodology, Visualization, Writing – original draft, Writing – review & editing. SW: Formal analysis, Methodology, Supervision, Writing – review & editing. SK: Formal analysis, Investigation, Writing – original draft, Writing – review & editing. BC: Conceptualization, Funding acquisition, Investigation, Writing – review & editing. LM: Conceptualization, Methodology, Supervision, Writing – original draft, Writing – review & editing. AD: Methodology, Resources, Supervision, Writing – original draft, Writing – review & editing.

Funding

The author(s) declare financial support was received for the research, authorship, and/or publication of this article. Funding for this project was provided by the Ohio Soybean Council (projects Nos. 14-2-18, 17-2-03, 16-R-06, 17-R-03, and 18-R-05); the United Soybean Board (project No. 1720-172-0125); The Ohio State University Center for Applied Plant Sciences and Molecular and Cellular Imaging Center; State and Federal funds appropriated to The Ohio State University, College of Food, Agricultural, and Environmental Sciences; the National Institute of Food and Agriculture, U.S. Department of Agriculture Hatch projects for Development of Disease Management Strategies for Soybean Pathogens in Ohio OHO01303; and the Genetic Analysis of Soybean Added-Value Traits and Soybean Variety Development for Ohio OHO01279.

Acknowledgments

We wish to thank Kelsey Scott, Linda Webber, Krystel Navarro, Deloris Veney, and Gabrielle Hayward-Lara for assistance in inoculation, tissue collection, and RNA extraction of the recombinant inbred lines. We would also like to thank Drs. Anna Stasko and William Rolling for their communication of data derived from previous and ongoing studies and Layne Connolly for editing.

Conflict of interest

The authors declare that the research was conducted in the absence of any commercial or financial relationships that could be construed as a potential conflict of interest.

Publisher's note

All claims expressed in this article are solely those of the authors and do not necessarily represent those of their affiliated organizations, or those of the publisher, the editors and the reviewers. Any product that may be evaluated in this article, or claim that may be made by its manufacturer, is not guaranteed or endorsed by the publisher.

Supplementary material

The Supplementary Material for this article can be found online at: https://www.frontiersin.org/articles/10.3389/fpls.2023.1277585/full#supplementary-material

METHODS M1
Constructing 20 networks to use as reference networks for input into module consensus analysis R script.

METHODS M2
Creating consensus network from two selected reference modules R script.

METHODS M3
Correlation of hotspots to co-expression modules R script.

References

Abbasi, P. A., Graham, M. Y., and Graham, T. L. (2001). Effects of soybean genotype on the glyceollin elicitation competency of cotyledon tissues to *Phytophthora sojae* glucan elicitors. *Physiol. Mol. Plant Pathol.* 59, 95–105. doi: 10.1006/pmpp.2001.0342

Abeysekara, N. S., Matthiesen, R. L., Cianzio, S. R., Bhattacharyya, M. K., and Robertson, A. E. (2016). Novel sources of partial resistance against *Phytophthora sojae* in soybean PI 399036. *Crop Sci.* 56, 2322–2335. doi: 10.2135/cropsci2015.09.0578

Acharjee, A., Chibon, P., Kloosterman, B., America, T., Renaut, J., Maliepaard, C., et al. (2018). Genetical genomics of quality related traits in potato tubers using proteomics. *BMC Plant Biol.* 18, 20. doi: 10.1186/s12870-018-1229-1

Albert, F. W., and Kruglyak, L. (2015). The role of regulatory variation in complex traits and disease. *Nat. Rev. Genet.* 16, 197–212. doi: 10.1038/nrg3891

Ambawat, S., Sharma, P., Yadav, N. R., and Yadav, R. C. (2013). MYB transcription factor genes as regulators for plant responses: an overview. *Physiol. Mol. Biol. Plants* 19, 307–321. doi: 10.1007/s12298-013-0179-1

Andrews, S. (2010). *FastQC: A quality control tool for high throughput sequence data*. Available at: http://www.bioinformatics.babraham.ac.uk/projects/fastqc/.

Antolin-Llovera, M., Leivar, P., Arro, M., Ferrer, A., Boronat, A., and Campos, N. (2011). Modulation of plant HMG-CoA reductase by protein phosphates 2A positive and negative control at a key node of metabolism. *Plant Signal Behav.* 8, 1127–1131. doi: 10.4161/psb.6.8.16363

Arahana, V. S., Graef, G. L., Specht, J. E., Steadman., J. R., and Eskridge, K. M. (2001). Identification of QTLs for resistance to *Sclerotinia sclerotiorum* in soybean. *Crop. Sci.* 41, 180–188. doi: 10.2135/cropsci2001.411180x

Ausubel, F. M. (2005). Are innate immune signaling pathways in plants and animals conserved? *Nat. Immunol.* 6, 973–979. doi: 10.1038/ni1253

Barman, A. R., and Banerjee, J. (2015). Versatility of germin-like proteins in their sequences, expressions, and functions. *Funct. Integ. Genomics* 15, 533–548. doi: 10.1007/s10142-015-0454-z

Barrett, J. C., Fry, B., Maller, J., and Daly, M. J. (2005). Haploview: Analysis and visualization of LD and haplotype maps. *Bioinformatics* 21, 263–265. doi: 10.1093/bioinformatics/bth457

Bates, D., Maechler, M., Bolker, B., and Walker, S. (2014). Fitting linear mixed-effects models using lme4. *J. Stat. Software* 67, 1–48. doi: 10.48550/arXiv.1406.5823

Bayless, A. M., Zapotocony, R. W., Grunwald, D. J., Amundson, K. K., Diers, B. W., and Bent, A. F. (2018). An atypical N-ethylmaleimide sensitive factor enables the viability of nematode-resistant *Rhg1* soybeans. *Proc. Natl. Acad. Sci. U.S.A.* 115, E4512–E4521. doi: 10.1073/pnas.1717070115

Becraft, P. W. (2002). Receptor kinase signaling in plant development. *Annu. Rev. Cell Dev. Biol.* 18, 163–192. doi: 10.1146/annurev.cellbio.18.012502.083431

Benjamini, Y., and Hochberg, Y. (1995). Controlling the false discovery rate: A practical and powerful approach to multiple testing. *J. R. Stat. Soc.: Ser. B (Methodological)* 57, 289–300. doi: 10.1111/j.2517-6161.1995.tb02031.x

Boller, T., and Felix, G. (2009). A renaissance of elicitors: perception of microbe-associated molecular patterns and danger signals by pattern-recognition receptors. *Annu. Rev. Plant Biol.* 60, 379–406. doi: 10.1146/annurev.arplant.57.032905.105346

Bolon, Y. T., Hyten, D. L., Orf, J. H., Vance, C. P., and Muehlbauer, G. J. (2014). eQTL Networks reveal complex genetic architecture in the immature soybean seed. *Plant Genome* 7, 1–14. doi: 10.3835/plantgenome2013.08.0027

Broman, K. W., Wu, H., Sen, Ś., and Churchill, G. A. (2003). R/qtl: QTL mapping in experimental crosses. *Bioinformatics* 19, 889–890. doi: 10.1093/bioinformatics/btg112

Bryois, J., Buil, A., Evans, D. M., Kemp, J. P., Montgomery, S. B., Conrad, D. F., et al. (2014). Cis and trans effects of human genomic variants on gene expression. *PLoS Genet.* 10, e1004461. doi: 10.1371/journal.pgen.1004461

Buerstmayr, M., Wagner, C., Nosenko, T., Omony, J., Steiner, B., Nussbaumer, T., et al. (2021). Fusarium head blight resistance in European winter wheat: insights from genome-wide transcriptome analysis. *BMC Genomics* 22, 1–17. doi: 10.1186/s12864-021-07800-1

Burnham, K. D., Dorrance, A. E., VanToai, T. T., and St. Martin, S. K. (2003). Quantitative trait loci for partial resistance to *Phytophthora sojae* in soybean. *Crop Sci.* 43, 1610–1617. doi: 10.2135/cropsci2003.1610

Bushnell, B. (2014). *BBMap: A fast, accurate, splice-aware aligner* (Berkeley, CA: Ernest Orlando Lawrence Berkeley National Laboratory). Available at: https://www.osti.gov/servlets/purl/1241166.

Chen, X., Hackett, C. A., Niks, R. E., Gedley, P., Booth, C., Druka, A., et al. (2010). An eQTL analysis of partial resistance to *Puccinia hordei* in barley. *PLoS One* 5, e8598. doi: 10.1371/journal.pone.0008598

Cheng, Q., Li, N., Dong, L., Zhang, D., Fan, S., Jiang, L., et al. (2015). Overexpression of soybean isoflavone reductase (*GmIFR*) enhances resistance to *Phytophthora sojae* in soybean. *Front. Plant Sci.* 6. doi: 10.3389/fpls.2015.01024

Chinchilla, D., Shan, L., He, P., de Vries, S., and Kemmerling, B. (2009). One for all: The receptor-associated kinase BAK1. *Trends Plant Sci.* 14, 535–541. doi: 10.1016/j.tplants.2009.08.002

Chisholm, S. T., Coaker, G., Day, B., and Staskawicz, B. J. (2006). Host-microbe interactions: shaping the evolution of the plant immune response. *Cell* 124, 803–814. doi: 10.1016/j.cell.2006.02.008

Christie, N., Myburg, A. A., Joubert, F., Murrasy, S. L., Carstens, M., Lin, Y. C., et al. (2017). Systems genetics reveals a transcriptional network associated with susceptibility in the maize-grey leaf spot pathosystem. *Plant J.* 89, 746–763. doi: 10.1111/tpj.13419

Cook, D. E., Bayless, A. M., Wang, K., Guo, X., Song, Q., Jiang, J., et al. (2014). Distinct copy number, coding sequence, and locus methylation patterns underlie *Rhg1*-mediated soybean resistance to soybean cyst nematode. *Plant Physiol.* 165, 630–647. doi: 10.1104/pp.114.235952

Cook, D. E., Lee, T. G., Guo, X., Meltio, S., Wang, K., Bayless, A. M., et al. (2012). Copy number variation of multiple genes at *Rhg1* mediates nematode resistance in soybean. *Science* 338, 1206–1209. doi: 10.1126/science.1228746

Corwin, J. A., Copeland, D., Feusier, J., Subedy, A., Eshbaugh, R., Palmer, C., et al. (2016). The quantitative basis of the *Arabidopsis* innate immune system to endemic pathogens depends on pathogen genetics. *PLoS Genet.* 12, e1005789. doi: 10.1371/journal.pgen.1005789

Corwin, J. A., and Kliebenstein, D. J. (2017). Quantitative resistance: More than just perception of a pathogen. *Plant Cell* 29, 655–665. doi: 10.1105/tpc.16.00915

Cui, H., Tsuda, K., and Parker, J. E. (2015). Effector-triggered immunity: from pathogen perception to robust defense. *Annu. Rev. Plant Biol.* 66, 487–511. doi: 10.1146/annurev-arplant-050213-040012

Dastmalchi, M., Chapman, P., Yu, J., Austin, R. S., and Dhaubhadel, S. (2017). Transcriptomic evidence for the control of soybean root isoflavonoid content by regulation of overlapping phenylpropanoid pathways. *BMC Genomics* 18, 1–15. doi: 10.1186/s12864-016-3463-y

de Ronne, M., Santhanam, P., Cinget, B., Labbé, C., Lebreton, A., Ye, H., et al. (2022). Mapping of partial resistance to *Phytophthora sojae* in soybean PIs using whole-genome sequencing reveals a major QTL. *Plant Genome* 15, e20184. doi: 10.1002/tpg2.20184

Deslauriers, S. D., and Larsen, P. B. (2010). FERONIA is a key modulator of brassinosteroid and ethylene responsiveness in *Arabidopsis* hypocotyls. *Mol. Plant* 3, 626–640. doi: 10.1093/mp/ssq015

De Smet, I., Voss, U., Jürgens, G., and Beeckman, T. (2009). Receptor-like kinases shape the plant. *Nat. Cell Biol.* 11, 1166–1173. doi: 10.1038/ncb1009-1166

Dodds, P. N., and Rathjen, J. P. (2010). Plant immunity: towards an integrated view of plant-pathogen interactions. *Nat. Rev. Genet.* 11, 539–548. doi: 10.1038/nrg2812

Domingo, C., Andrés, F., Tharreau, D., Iglesias, D. J., and Talón, M. (2009). Constitutive expression of OsGH3.1 reduces auxin content and enhances defense response and resistance to a fungal pathogen in rice. *Mol. Plant Microbe Interact.* 22, 201–210. doi: 10.1094/MPMI-22-2-0201

Dorrance, A. E., Robertson, A. E., Cianzo, S., Giesler, L. J., Grau, C. R., Draper, M. A., et al. (2009). Integrated management strategies for *Phytophthora sojae* combining host resistance and seed treatments. *Plant Dis.* 93, 875–882. doi: 10.1094/PDIS-93-9-0875

Druka, A., Potokina, E., Luo, Z., Bonar, N., Druka, I., Zhang, L., et al. (2008). Exploiting regulatory variation to identify genes underlying quantitative resistance to the wheat stem rust pathogen *Puccinia graminis* f. sp. *tritici* in barley. *Theor. Appl. Genet.* 117, 261–272. doi: 10.1007/s00122-008-0771-x

Druka, A., Potokina, E., Luo, Z., Jiang, N., Chen, X., Kearsey, M., et al. (2010). Expression quantitative trait loci analysis in plants. *J. Plant Biotechnol.* 8, 10–27. doi: 10.1111/j.1467-7652.2009.00460.x

Duan, Q., Kita, D., Li, C., Cheung, A. Y., and Wu, H. M. (2010). FERONIA receptor-like kinase regulates RHO GTPase signaling of root hair development. *Proc. Natl. Acad. Sci.* 107, 17821–17826. doi: 10.1073/pnas.1005366107

Feltus, F. A. (2014). Systems genetics: A paradigm to improve discovery of candidate genes and mechanisms underlying complex traits. *Plant Sci.* 223, 45–48. doi: 10.1016/j.plantsci.2014.03.003

Fisher, R. A. (1935). The logic of inductive inference. *J. R. Stat. Soc.* 98, 39–82. doi: 10.2307/2342435

Franceschini, A., Szklarczyk, D., Frankild, S., Kuhn, M., Simonovic, M., Roth, A., et al. (2012). STRING V9.1: Protein-protein interaction networks, with increased coverage and integration. *Nucleic Acids Res.* 41, D808–D815. doi: 10.1093/nar/gks1094

French, E., Kim, B. S., and Iyer-Pascuzzi, A. S. (2016). Mechanisms of quantitative disease resistance in plants. *Semin. Cell Dev. Biol.* 56, 201–208. doi: 10.1016/j.semcdb.2016.05.015

Gassmann, W., and Bhattacharjee, S. (2012). Effector-triggered immunity signaling: from gene-for-gene pathways to protein-protein interaction networks. *Mol. Plant Microbe Interact.* 25, 862–868. doi: 10.1094/MPMI-01-12-0024-IA

Glazebrook, J. (2005). Contrasting mechanisms of defense against biotrophic and necrotrophic pathogens. *Annu. Rev. Phytopathol.* 43, 205–227. doi: 10.1146/annurev.phyto.43.040204.135923

Gómez-Gómez, L., and Boller, T. (2000). FLS2: An LRR receptor-like kinase involved in the perception of the bacterial elicitor flagellin in *Arabidopsis*. *Mol. Cell* 5, 1003–1011. doi: 10.1016/s1097-2765(00)80265-8

Graham, T. L., Graham, M. Y., Subramanian, S., and Yu, O. (2007). RNAi silencing of genes for elicitation or biosynthesis of 5-deoxyisoflavonoids suppresses race-specific resistance and hypersensitive cell death in Phytophthora sojae infected tissues. *Plant Physiol.* 144, 728–740. doi: 10.1104/pp.107.097865

Graham, M. Y., Weidner, J., Wheeler, K., Pelow, M. L., and Graham, T. L. (2003). Induced expression of pathogenesis-related protein genes in soybean by wounding and the *Phytophthora sojae* cell wall glucan elicitor. *Mol. Plant Pathol.* 63, 141–149. doi: 10.1016/j.pmpp.2003.11.002

Grau, C. R., Dorrance, A. E., Bond, J., and Russin, J. S. (2004). "Fungal diseases," in *Soybeans: Improvement, Production, and Uses*. Eds. R. M. Shibles, J. E. Harper, R. F. Wilson and R. C. Shoemaker (Madison, WI: American Society of Agronomy, Inc), 679–763. doi: 10.2134/agronmonogr16.3ed.c14

Green, B. F., and Tukey, J. W. (1960). Complex analyses of variance: general problems. *Psychometrika* 25, 127–152. doi: 10.1007/BF02288577

Guo, H., Nolan, T. M., Song, G., Liu, S., Xie, Z., Chen, J., et al. (2018). FERONIA receptor kinase contributes to plant immunity by suppressing jasmonic acid signaling in *Arabidopsis thaliana*. *Curr. Biol.* 28, 3316–3324. doi: 10.1016/j.cub.2018.07.078

Guo, X., Wang, D., Gordon, S. G., Helliwell, E., Smith, T., Berry, S. A., et al. (2008). Genetic mapping of QTLs underlying partial resistance to *Sclerotinia sclerotiorum* in soybean PI 391589A and PI 391589B. *Crop Sci.* 48, 1129–1139. doi: 10.2135/cropsci2007.04.0198

Hale, B., Brown, E., and Wijeratne, A. (2023a). An updated assessment of the soybean-*Phytophthora sojae* pathosystem. *Plant Pathology.* 72, 843–860. doi: 10.1111/ppa.13713

Hale, B., Ratnayake, S., Flory, A., Wijeratne, R., Schmidt, C., Robertson, A. E., et al. (2023b). Gene regulatory network inference in soybean upon infection by *Phytophthora sojae*. *PLoS One* 18, e0287590. doi: 10.1371/journal.pone.0287590

Ham, B. K., Li, G., Kang, B. H., Zeng, F., and Lucas, W. J. (2012). Overexpression of *Arabidopsis* plasmodesmata germin-like proteins disrupts root growth and development. *Plant Cell* 24, 3630–3648. doi: 10.1105/tpc.112.101063

Hammond, J. P., Mayes, S., Bowen, H. C., Chram, N. S., Hayden, R. M., Love, C. G., et al. (2011). Regulatory hotspots are associated with plant gene expression under varying soil phosphorus supply in *Brassica rapa*. *Plant Physiol.* 156, 1230–1241. doi: 10.1104/pp.111.175612

Han, Y., Teng, W., Yu, K., Poysa, V., Anderson, T., Qiu, L., et al. (2008). Mapping QTL tolerance to Phytophthora root rot in soybean using microsatellite and RAPD/SCAR derived markers. *Euphytica* 162, 231–239. doi: 10.1007/s10681-007-9558-4

Hohmann, U., Lau, K., and Hothorn, M. (2017). The structural basis of ligand perception and signal activation by receptor kinases. *Annu. Rev. Plant Biol.* 68, 109–137. doi: 10.1146/annurev-arplant-042916-040957

Huang, J., Guo, N., Li, Y., Sun, J., Hu, G., Zhang, H., et al. (2016). Phenotypic evaluation and genetic dissection of resistance to *Phytophthora sojae* in the Chinese soybean mini core collection. *BMC Genet.* 17, 85. doi: 10.1186/s12863-016-0383-4

Huber, W., Carey, V. J., Gentleman, R., Anders, S., Carlson, M., Carvalho, B. S., et al. (2015). Orchestrating high-throughput genomic analysis with Bioconductor. *Nat. Methods* 12, 115–121. doi: 10.1038/nmeth.3252

Hubner, N., Wallace, C. A., Zimdahl, H., Petretto, E., Schulz, H., Maciver, F., et al. (2005). Integrated transcriptional profiling and linkage analysis for identification of genes underlying disease. *Nat. Genet.* 37, 243–253. doi: 10.1038/ng1522

Imholte, G. C., Scott-Boyer, M. P., Labbe, A., Deschepper, C. F., and Gottardo, R. (2013). iBMQ: R/Bioconductor package for integrated Bayesian modeling of eQTL data. *Bioinformatics* 29, 2797–2798. doi: 10.1093/bioinformatics/btt485

Jahan, M. A., Harris, B., Lowery, M., Infante, A. M., Percifield, R. J., and Kovinich, N. (2020). Glyceollin transcription factor GmMYB29A2 regulates soybean resistance to *Phytophthora sojae*. *Plant Physiol.* 183, 530–546. doi: 10.1104/pp.19.01293

Jansen, R. C., and Nap, J. P. (2001). Genetical genomics: The added value from segregation. *Trends Genet.* 17, 388–391. doi: 10.1016/S0168-9525(01)02310-1

Jansen, R. C., Tesson, B. M., Fu, J., Yang, Y., and McIntyre, L. M. (2009). Defining gene and QTL networks. *Curr. Opin. Plant Biol.* 12, 241–246. doi: 10.1016/j.pbi.2009.01.003

Jones, J. D., and Dangl, J. L. (2006). The plant immune system. *Nature* 444, 323–329. doi: 10.1038/nature05286

Jun, T. H., Mian, M. A. R., Kang, S. T., and Michel, A. P. (2012). Genetic mapping of the powdery mildew resistance gene in soybean PI 567301B. *Theor. Appl. Genet.* 125, 1159–1168. doi: 10.1007/s00122-012-1902-y

Kanehisa, M., and Goto, S. (2000). KEGG: Kyoto encyclopedia of genes and genomes. *Nucleic Acids Res.* 28, 27–30. doi: 10.1093/nar/28.1.27

Karhoff, S., Vargas-Garcia, C., Lee, S., Mian, M. A. R., Graham, M. A., Dorrance, A. E., et al. (2022). Identification of candidate genes for a major quantitative disease resistance locus from soybean PI 427105B for resistance to *Phytophthora sojae*. *Front. Plant Sci.* 13. doi: 10.3389/fpls.2022.893652

Kemmerling, B., Halter, T., Mazzotta, S., Mosher, S., and Nürnberger, T. (2011). A genome-wide survey for *Arabidopsis* leucine-rich repeat receptor kinases implicated in plant immunity. *Front. Plant Sci.* 2. doi: 10.3389/fpls.2011.00088

Keurentjes, J. J. B., Fu, J., Terpstra, I. R., Garcia, J. M., van den Ackerveken, G., Snoek, L. B., et al. (2007). Regulatory network construction in *Arabidopsis* by using genome-wide gene expression quantitative trait loci. *Proc. Natl. Acad. Sci. U.S.A.* 104, 1708–1713. doi: 10.1073/pnas.0610429104

Kidd, B. N., Kadoo, N. Y., Dombrecht, B., Tekeoglu, M., Gardiner, D. M., Thatcher, L. F., et al. (2011). Auxin signaling and transport promote susceptibility to the root-infecting fungal pathogen *Fusarium oxysporum* in *Arabidopsis*. *Mol. Plant Microbe Interact.* 24, 733–748. doi: 10.1094/MPMI-08-10-0194

Kim, H., and Diers, B. (2000). Inheritance of partial resistance to Sclerotinia stem rot in soybean. *Crop Sci.* 40, 55–61. doi: 10.2135/cropsci2000.40155x

Kliebenstein, D. (2009). Quantitative genomics: Analyzing intraspecific variation using global gene expression polymorphisms or eQTLs. *Annu. Rev. Plant Biol.* 60, 93–114. doi: 10.1146/annurev.arplant.043008.092114

Langfelder, P., and Horvath, S. (2007). Eigengene networks for studying the relationships between co-expression modules. *BMC Syst. Biol.* 1, 1–17. doi: 10.1186/1752-0509-1-54

Langfelder, P., and Horvath, S. (2008). WGCNA: An R package for weighted correlation network analysis. *BMC Bioinf.* 9, 559. doi: 10.1186/1471-2105-9-559

Lee, H. Y., Bowen, C. H., Popescu, G. V., Kang, H.-G., Kato, N., Ma, S., et al. (2011). *Arabidopsis* RTNLB1 and RTNLB2 reticulon-like proteins regulate intracellular trafficking and activity of the FLS2 immune receptor. *Plant Cell.* 9, 3374–3391. doi: 10.1105/tpc.111.089656

Lee, S., Mian, M. A. R., McHale, L. K., Sneller, C. H., and Dorrance, A. E. (2013a). Identification of quantitative trait loci conditioning partial resistance to Phytophthora sojae in soybean PI 407861A. *Crop Sci.* 53, 1022–1031. doi: 10.2135/cropsci2012.10.0578

Lee, S., Mian, M. A. R., McHale, L. K., Wang, H., Wijeratne, A. J., Sneller,, et al. (2013b). Novel quantitative trait loci for partial resistance to *Phytophthora sojae* in soybean PI 398841. *Theor. Appl. Genet.* 126, 1121–1132. doi: 10.1007/s00122-013-2040-x

Lee, S., Mian, M. A. R., Sneller, C. H., Wang, H., Dorrance, A. E., and McHale, L. K. (2014). Joint linkage QTL analyses for partial resistance to *Phytophthora sojae* in soybean using six nested inbred populations with heterogeneous conditions. *Theor. Appl. Genet.* 127, 429–444. doi: 10.1007/s00122-013-2229-z

Li, Z. (2019). "Molecular analysis of epistasis affecting complex traits," in *Molecular Dissection of Complex Traits*. Ed. A. H. Patterson (Boca Raton, FL: CRC Press), 119–130. doi: 10.1201/9780429117770-8

Li, X., Han, Y., Teng, W., Zhang, A., Yu, K., Poysa, V., et al. (2010). Pyramided QTL underlying tolerance to Phytophthora root rot in mega-environments from soybean cultivars "Conrad" and "Hefeng 25". *Theor. Appl. Genet.* 121, 651–658. doi: 10.1007/s00122-010-1337-2

Li, R., Jeong, K., Davis, J. T., Kim, S., Lee, S., Michelmore, R. W., et al. (2018). Integrated QTL and eQTL mapping provides insights and candidate genes for fatty acid composition, flowering time, and growth traits in a F2 population of a novel synthetic allopolyploid *Brassica napus*. *Front. Plant Sci.* 9. doi: 10.3389/fpls.2018.01632

Liao, Y., Smyth, G. K., and Shi, W. (2014). featureCounts: An efficient general purpose program for assigning sequence reads to genomic features. *Bioinformatics* 30, 923–930. doi: 10.1093/bioinformatics/btt656

Lin, F., Chhapekar, S. S., Vieira, C. C., Da Silva, M. P., Rojas, A., Lee, D., et al. (2022). Breeding for disease resistance in soybean: a global perspective. *Theor. Appl. Gen.* 135 (11), 3773–3872. doi: 10.1007/s00122-022-04101-3

Lin, F., Zhao, M., Baumann, D. D., Ping, J., Sun, L., Liu, Y., et al. (2014). Molecular response to the pathogen *Phytophthora sojae* among ten soybean near isogenic lines revealed by comparative transcriptomics. *BMC Genomics* 15, 18. doi: 10.1186/1471-2164-15-18

Liu, Q., Liu, H., Gong, Y., Tao, Y., Jiang, L., Zuo, W., et al. (2017). An atypical thioredoxin imparts early resistance to *Sugarcane mosaic virus* in maize. *Mol. Plant* 10, 483–497. doi: 10.1016/j.molp.2017.02.002

Liu, J., Osbourn, A., and Ma, P. (2015). MYB transcription factors regulators of phenylpropanoid metabolism in plants. *Mol. Plant* 8, 689–708. doi: 10.1016/j.molp.2015.03.012

Lorenzo, O., Piqueras, R., Sanchez-Serrano, J. J., and Solano, R. (2003). Ethylene response factor 1 integrates signals from ethylene and jasmonate pathways in plant defense. *Plant Cell* 15, 165–178. doi: 10.1105/tpc.007468

Lygin, A. V., Zernova, O. V., Hill, C. B., Kholina, N. A., Widholm, J. M., Hartman, G. L., et al. (2013). Glyceollin is an important component of soybean plant defense against *Phytophthora sojae* and *Macrophomina phaseolina*. *Phytopathology* 103, 984–994. doi: 10.1094/PHYTO-12-12-0328-R

MacDonald, K. L., and Cahill, D. M. (1999). Influence of abscisic acid and the abscisic acid biosynthesis inhibitor, norflurazon, on interactions between *Phytophthora sojae* and soybean (*Glycine max*). *Eur. J. Plant Pathol.* 60, 185–195. doi: 10.1023/A:1008705321113

Mideros, S., Nita, M., and Dorrance, A. E. (2007). Characterization of components of partial resistance, *Rps2*, and root resistance to *Phytophthora sojae* in soybean. *Phytopathology* 97, 655–662. doi: 10.1094/PHYTO-97-5-0655

Minic, Z. (2008). Physiological roles of plant glycoside hydrolases. *Planta* 227, 723–740. doi: 10.1007/s00425-007-0668-y

Mohr, P. G., and Cahill, D. M. (2001). Relative roles of glyceollin, lignin and the hypersensitive response and the influence of ABA incompatible and incompatible interactions of soybeans with *Phytophthora sojae*. *Physiol. Mol. Plant Pathol.* 58, 31–41. doi: 10.1006/pmpp.2000.0306

Moscou, M. J., Lauter, N., Steffenson, B., and Wise, R. P. (2011). Quantitative and qualitative stem rust resistance factors in barley are associated with transcriptional suppression of defense regulons. *PLoS Genet.* 7, e1002208. doi: 10.1371/journal.pgen.1002208

Moy, P., Qutob, D., Chapman, B. P., Atkinson, I., and Gijzen, M. (2004). Patterns of gene expression upon infection of soybean plants by *Phytophthora sojae*. *Mol. Plant Microbe Interact.* 17, 1051–1062. doi: 10.1094/MPMI.2004.17.10.1051

Naveed, Z. A., Wei, X., Chen, J., Mubeen, H., and Ali, G. S. (2020). The PTI to ETI continuum in *Phytophthora*-plant interactions. *Front. Plant Sci.* 11. doi: 10.3389/fpls.2020.593905

Nelson, R., Wiesner-Hanks, T., Wisser, R., and Balint-Kurti, P. (2018). Navigating complexity to breed disease-resistant crops. *Nat. Rev. Genet.* 19, 21–33. doi: 10.1038/nrg.2017.82

Neto, E. C., Keller, M. P., Broman, A. F., Attie, A. D., Jansen, R. C., Broman, K. W., et al. (2012). Quantile-based permutation thresholds for quantitative trait loci hotspots. *Genetics* 191, 1355–1365. doi: 10.1534/genetics.112.139451

Ng, D. K., Abeysinghe, J. K., and Kamali, M. (2018). Regulating the regulators: The control of transcription factors in plant defense signaling. *Int. J. Mol. Sci.* 19, 3737. doi: 10.3390/ijms19123737

Nguyen, V. T., Vuong, T. D., VanToai, T., Lee, J. D., Wu, X., Rouf Mian, M. A., et al. (2012). Mapping of quantitative trait loci associated with resistance to *Phytophthora sojae* and flooding tolerance in soybean. *Crop Sci.* 52, 2481–2493. doi: 10.2135/cropsci2011.09.0466

Niks, R. E., Qi, X. Q., and Marcel, T. C. (2015). Quantitative resistance to biotrophic filamentous plant pathogens: concepts, misconceptions, and mechanisms. *Annu. Rev. Phytopathol.* 53, 445–470. doi: 10.1146/annurev-phyto-080614-115928

Pieterse, C., Leon-Reyes, A., van der Ent, S., and Van Wees, S. (2009). Networking by small-molecule hormones in plant immunity. *Nat. Chem. Biol.* 5, 308–316. doi: 10.1038/nchembio.164

Pieterse, C. M., van der Does, D., Zamioudis, C., Leon-Reyes, A., and Van Wees, S. C. (2012). Hormonal modulation of plant immunity. *Ann. Rev. Cell Dev. Biol.* 28, 489–521. doi: 10.1146/annurev-cellbio-092910-154055

Pilet-Nayel, M. L., Moury, B., Caffier, V., Montarry, J., Kerlan, M. C., Fournet, S., et al. (2017). Quantitative resistance to plant pathogens in pyramiding strategies for durable crop protection. *Front. Plant Sci.* 8. doi: 10.3389/fpls.2017.01838

Poland, J. A., Balint-Kurti, P. J., Wisser, R. J., Pratt, R. C., and Nelson, R. J. (2009). Shades of gray: The world of quantitative disease resistance. *Trends Plant Sci.* 14, 21–29. doi: 10.1016/j.tplants.2008.10.006

Poovaiah, B. W., and Reddy, A. S. (1993). Calcium and signal transduction in plants. *CRC Crit. Rev. Plant Sci.* 12, 185–211. doi: 10.1080/07352689309701901

Potokina, E., Druka, A., Luo, Z., Wise, R., Waugh, R., and Kearsey, M. (2008). Gene expression quantitative trait locus analysis of 16,000 barley genes reveals a complex pattern of genome-wide transcriptional regulation. *Plant J.* 53, 90–101. doi: 10.1111/j.1365-313X.2007.03315.x

Qu, W., Gurdziel, K., Pique-Regi, R., and Ruden, D. M. (2018). Lead modulated trans- and cis- expression quantitative trait loci (eQTLs) in *Drosophila melanogaster* heads. *Front. Genet.* 9. doi: 10.3389/fgene.2018.00395

Ranathunge, K., Thomas, R. H., Fang, X., Peterson, C. A., Gijzen, M., and Bernards, M. A. (2008). Soybean root suberin and partial resistance to root rot caused by *Phytophthora sojae*. *Phytopathology* 98, 1179–1189. doi: 10.1094/PHYTO-98-11-1179

R Core Team. (2018). *R: A language and environment for statistical computing* (Vienna, Austria: R Foundation for Statistical Computing). Available at: https://www.R-project.org/.

Reddy, A. S. N., and Reddy, V. (2001). "Calcium as a messenger in stress signal transduction," in *Handbook of Plant and Crop Physiology*. Ed. M. Pessarakali (Boca Raton, FL: CRC Press), 697–732. doi: 10.1201/9780203908426.ch35

Rehman, S., and Mahmood, T. (2015). Functional role of DREB and ERF transcription factors: regulating stress-responsive network in plants. *Acta Physiol. Plant* 37, 1–14. doi: 10.1007/s11738-015-1929-1

Rincker, K., Hartman, G. L., and Diers, B. W. (2016). Fine mapping of resistance genes from five brown stem rot resistance sources in soybean. *Plant Genome* 9. doi: 10.3835/plantgenome2015.08.0063

Robinson, M. D., McCarthy, D. J., and Smyth, G. K. (2010). edgeR: A Bioconductor package for differential expression analysis of digital gene expression data. *Bioinformatics* 26, 139–140. doi: 10.1093/bioinformatics/btp616

Rolling, W., Lake, R., Dorrance, A. E., and McHale, L. K. (2020). Genome-wide association analyses of quantitative disease resistance in diverse sets of soybean [*Glycine max* (L.) Merr.] plant introductions. *PLoS One* 15, e0227710. doi: 10.1371/journal.pone.0227710

Roux, F., Voisin, D., Badet, T., Balagué, C., Barlet, X., Huard-Chauveau, C., et al. (2014). Resistance to phytopathogens *e tutti quanti*: placing plant quantitative disease resistance on the map. *Mol. Plant Pathol.* 15, 427–432. doi: 10.1111/mpp.12138

Saha, A., and Battle, A. (2018). False positives in trans-eQTL and co-expression analyses arising from RNA-sequencing alignment errors. *F1000Research* 7, 1860. doi: 10.12688/f1000research.17145.2

Salvi, S., and Tuberosa, R. (2005). To clone or not to clone plant QTLs: Present and future challenges. *Trends Plant Sci.* 10, 297–304. doi: 10.1016/j.tplants.2005.04.008

Samad-Zamini, M., Schweiger, W., Nussbaumer, T., Mayer, K. F. X., and Buerstmayr, H. (2017). Time-course expression QTL atlas of the global transcriptional response of wheat to *Fusarium graminearum*. *Plant Biotechnol. J.* 15, 1453–1464. doi: 10.1111/pbi.12729

Schadt, E. E., Monks, S. A., Drake, T. A., Lusis, A. J., Che, N., Colinayo, V., et al. (2003). Genetics of gene expression surveyed in maize, mouse and man. *Nature* 422, 297–302. doi: 10.1038/nature01434

Schmitthenner, A. F. (1985). Problems and progress in control of Phytophthora root rot of soybean. *Plant Dis.* 69, 362–368. doi: 10.1094/PD-69-362

Schmutz, J., Cannon, S. B., Schlueter, J., Ma, J., Mitros, T., Nelson, W., et al. (2010). Genome sequence of the paleopolyploid soybean. *Nature* 463, 178–183. doi: 10.1038/nature08670

Schneider, R., Rolling, W., Song, Q., Cregan, P., Dorrance, A. E., and McHale, L. K. (2016). Genome-wide association mapping of partial resistance to *Phytophthora sojae* in soybean plant introductions from the Republic of Korea. *BMC Genomics* 17, 607. doi: 10.1186/s12864-016-2918-5

Scott, K., Balk, C., Veney, D., McHale, L. K., and Dorrance, A. E. (2019). Quantitative disease resistance loci towards *Phytophthora sojae* and three species of *Pythium* in six soybean nested association mapping populations. *Crop Sci.* 59, 605–623. doi: 10.2135/cropsci2018.09.0573

Shiu, S. H., Karlowski, W. M., Pan, R., Tzeng, Y. H., Mayer, K. F., and Li, W. H. (2004). Comparative analysis of the receptor-like kinase family in *Arabidopsis* and rice. *Plant Cell* 16, 1220–1234. doi: 10.1105/tpc.020834

Smith, C. J., Watson, C. F., Morris, P. C., Bird, C. R., Seymour, G. B., Gray, J. E., et al. (1990). Inheritance and effect on ripening of antisense polygalacturonase genes in transgenic tomatoes. *Plant Molec. Biol.* 14 (3), 369–379. doi: 10.1007/BF00028773

Smith, C. J. S., Watson, C. F., Ray, J., Bird, C. R., Morris, P. C., Schuch, W., et al. (1988). Antisense RNA inhibition of polygalacturonase gene expression in transgenic tomatoes. *Nature* 334, 724–726. doi: 10.1038/334724a0

Soltis, N. E., Caseys, C., Zhang, W., Corwin, J. A., Atwell, S., and Kliebenstein, D. J. (2020). Pathogen genetic control of transcriptome variation in the *Arabidopsis thaliana – Bortrytis cinerea* pathosystem. *Genetics* 215, 253–266. doi: 10.1534/genetics.120.303070

Soyars, C. L., James, S. R., and Nimchuk, Z. L. (2016). Ready, aim, shoot: Stem cell regulation of the shoot apical meristem. *Curr. Opin. Plant Biol.* 29, 163–168. doi: 10.1016/j.pbi.2015.12.002

Spoel, S. H., and Dong, X. (2012). How do plants achieve immunity? Defence without specialized immune cells. *Nat. Rev. Immunol.* 12, 89–100. doi: 10.1038/nri3141

Stasko, A. K., Batnini, A., Bolanos-Carriel, C., Lin, J. E., Lin, Y., Blakeslee, J., et al. (2020). Auxin profiling and *GmPIN* expression in *Phytophthora sojae*-soybean root interactions. *Phytopathology* 110, 1988–2002. doi: 10.1094/PHYTO-02-20-0046-R

Stasko, A. K., Wickramasinghe, D., Nauth, B. J., Acharya, B., Ellis, M. L., Taylor, C. G., et al. (2016). High-density mapping of resistance QTL toward *Phytophthora sojae*, *Pythium irregulare*, and *Fusarium graminearum* in the same soybean population. *Crop Sci.* 56, 2476–2492. doi: 10.2135/cropsci2015.12.0749

St. Clair, D. A. (2010). Quantitative disease resistance and quantitative resistance loci in breeding. *Annu. Rev. Phytopathol.* 48, 247–268. doi: 10.1146/annurev-phyto-080508-081904

Stracke, R. (2001). The R2R3-MYB gene family in *Arabidopsis thaliana*. Curr. *Opin. Plant Biol.* 4, 447–456. doi: 10.1016/S1369-5266(00)00199-0

Sugano, S., Sugimoto, T., Takatsuji, H., and Jiang, C. J. (2013). Induction of resistance to *Phytophthora sojae* in soyabean (*Glycine max*) by salicylic acid and ethylene. *Plant Pathol.* 62, 1048–1056. doi: 10.1111/ppa.12011

Sun, Y., Wu, Y., Yang, C., Sun, S., Lin, X., Liu, L., et al. (2017). Segmental allotetraploidy generates extensive homoeologous expression rewiring and phenotypic diversity at the population level in rice. *Mol. Ecol.* 26, 5451–5466. doi: 10.1111/mec.14297

Swanson, S., and Gilroy, S. (2010). ROS in plant development. *Physiol. Plant* 138 (4), 384–392. doi: 10.1111/j.1399-3054.2009.01313.x

Swanson-Wagner, R. A., DeCook, R., Jia, Y., Bancroft, T., Ji, T., Zhao, X., et al. (2009). Paternal dominance of trans-eQTL influences gene expression patterns in maize hybrids. *Science* 326, 1118–1120. doi: 10.1126/science.1178294

Thomas, R., Fang, X., Ranathunge, K., Anderson, T. R., Peterson, C. A., and Bernards, M. A. (2007). Soybean root suberin: Anatomical distribution, chemical composition, and relationship to partial resistance to *Phytophthora sojae*. *Plant Physiol.* 144, 299–311. doi: 10.1104/pp.106.091090

Tian, J., Keller, M. P., Broman, A. T., Kendziorski, C., Yandell, B. S., Attie, A. D., et al. (2016). The dissection of expression quantitative trait locus hotspots. *Genetics* 202, 1563–1574. doi: 10.1534/genetics.115.183624

Tian, T., Liu, Y., Yan, H., You, Q., Yi, X., Du, Z., et al. (2017). agriGO v2.0: A GO analysis toolkit for the agricultural community 2017 update. *Nucleic Acids Res.* 45, W122–W129. doi: 10.1093/nar/gkx382

Tooley, P. W., and Grau, C. (1982). Identification and quantitative characterization of rate-reducing resistance to *Phytophthora megasperma* f.sp. *glycinea* in soybean seedlings. *Phytopathology* 72, 727–733. doi: 10.1094/Phyto-72-727

Torres, M. A. (2010). ROS in biotic interactions. *Physiol. Plant* 138 (4), 414–429. doi: 10.1111/j.1399-3054.2009.01326.x

Trewavas, A. J., and Mahlo, R. (1998). Ca^{2+} signaling in plant cells: The big network! *Curr. Opin. Plant Biol.* 1, 428–433. doi: 10.1016/S1369-5266(98)80268-9

Tucker, D. M., Saghai Maroof, M. A., Mideros, S., Skoneczka, J. A., Nabati, D. A., Buss, G. R., et al. (2010). Mapping quantitative trait loci for partial resistance to *Phytophthora sojae* in a soybean interspecific cross. *Crop Sci.* 50, 628–635. doi: 10.2135/cropsci2009.03.0161

Vailleau, F., Daniel, X., Tronchet, M., Montillet, J. L., Triantaphylides, C., and Roby, D. (2002). A R2R3-MYB gene, AtMYB30, acts as a positive regulator of the hypersensitive cell death program in plants in response to pathogen attack. *Proc. Natl. Acad. Sci. U.S.A.* 99, 10179–10184. doi: 10.1073/pnas.152047199

Vega-Sánchez, M., Redinbaugh, M., Costanzo, S., and Dorrance, A. E. (2005). Spatial and temporal expression analysis of defense-related genes in soybean cultivars with different levels of partial resistance to *Phytophthora sojae*. *Physio. Mol. Plant Pathol.* 66, 175–182. doi: 10.1016/j.pmpp.2005.07.001

Vuong, T. D., Diers, B. W., and Hartman, G. L. (2008). Identification of QTL for resistance to Sclerotinia stem rot in soybean plant introduction 194639. *Crop Sci.* 48, 2209–2214. doi: 10.2135/cropsci2008.01.0019

Walton, J. D. (1994). Deconstructing the cell wall. *Plant Physiol.* 104, 1113–1118. doi: 10.1104/pp.104.4.1113

Wang, X., Chen, Q., Wu, Y., Lemmon, Z. H., Xu, G., Huang, C., et al. (2017). Genome-wide analysis of transcriptional variability in large maize-teosinte population. *Mol. Plant* 11, 443–459. doi: 10.1016/j.molp.2017.12.011

Wang, Y., Han, Y., Teng, W., Zhao, X., Li, Y., Wu, L., et al. (2014). Expression quantitative trait loci infer the regulation of isoflavone accumulation in soybean (*Glycine max* L. Merr.) seed. *BMC Genomics* 15, 1–11. doi: 10.1186/1471-2164-15-680

Wang, H., St. Martin, S. K., and Dorrance, A. E. (2012a). Comparison of phenotypic methods and yield contributions of quantitative trait loci for partial resistance to Phytophthora sojae in soybean. *Crop Sci.* 52, 1–14. doi: 10.2135/cropsci2011.06.0336

Wang, Y., Tyler, B. M., and Wang, Y. (2019). Defense and counter defense during plant-pathogenic oomycete infection. *Annu. Rev. Microbiol.* 73, 667–696. doi: 10.1146/annurev-micro-020518-120022

Wang, H., Waller, L., Tripathy, S., St. Martin, S. K., Zhou, L., Krampis, K., et al. (2010). Analysis of genes underlying soybean quantitative trait loci conferring partial resistance to *Phytophthora sojae*. *Plant Genome J.* 3, 23–40. doi: 10.3835/plantgenome2009.12.0029

Wang, H., Wijeratne, A., Wijeratne, S., Lee, S., Taylor, C. G., St. Martin, S. K., et al. (2012b). Dissection of two soybean QTL conferring partial resistance to *Phytophthora sojae* through sequence and gene expression analysis. *BMC Genomics* 13, 428. doi: 10.1186/1471-2164-13-428

Wang, S., Zheng, T., and Wang, Y. (2007). Transcription activity hot spot, is it real or an artifact? *BMC Proc.* 1, S94. doi: 10.1186/1753-6561-1-S1-S94

Ward, E. W. B., Cahill, D. N., and Bhattacharyya, M. (1989). Abscisic acid suppression of phenylalanine ammonia lyase activity and mRNA, and resistance of soybeans to *Phytophthora megasperma* f. sp. *glycinea*. *Plant Physiol.* 91, 23–27. doi: 10.1104/pp.91.1.23

Weng, C., Yu, K., Anderson, T. R., and Poysa, V. (2007). A quantitative trait locus influencing tolerance to Phytophthora root rot in the soybean cultivar "Conrad". *Euphytica* 158, 81–86. doi: 10.1007/s10681-007-9428-0

Werner, E. (2004). GTPases and reactive oxygen species: switches for killing and signaling. *J. Cell Sci.* 117 (2), 143–153. doi: 10.1242/jcs.00937

West, M. A. L., Kim, K., Kliebenstein, D. J., van Leeuwnen, H., Michelmore, R. W., Doerge, R. W., et al. (2007). Global eQTL mapping reveals the complex genetic architecture of transcript-level variation in *Arabidopsis*. *Genetics* 175, 1441–1450. doi: 10.1534/genetics.106.064972

Wong, J., Gao, L., Yang, Y., Zhai, J., Arikit, S., Yu, Y., et al. (2014). Roles of small RNAs in soybean defense against *Phytophthora sojae* infection. *Plant J.* 79, 928–940. doi: 10.1111/tpj.12590

Wu, X., Blake, S., Sleper, D. A., Shannon, J. G., Cregan, P., and Nguyen, H. T. (2009). QTL, additive and epistatic effects for SCN resistance in PI 437654. *Theor. Appl. Genet.* 118, 1093–1105. doi: 10.1007/s00122-009-0965-x

Wu, X., Zhou, B., Zhao, J., Guo, N., Zhang, B., Yang, F., et al. (2011). Identification of quantitative trait loci for partial resistance to *Phytophthora sojae* in soybean. *Plant Breed* 130, 144–149. doi: 10.1111/j.1439-0523.2010.01799.x

Xu, P., Wu, J., Xue, A., Li, W. B., Chen, W. Y., Wei, L., et al. (2012). Differentially expressed genes of soybean during infection by *Phytophthora sojae*. J. *Integr. Agric.* 11, 368–377. doi: 10.1016/S2095-3119(12)60021-5

Yamaguchi, Y., Huffaker, A., Bryan, A. C., Tax, F. E., and Ryan, C. A. (2010). PEPR2 is a second receptor for the Pep1 and Pep2 peptides and contributes to defense responses in *Arabidopsis*. *Plant Cell* 22, 508–522. doi: 10.1105/tpc.109.068874

Yan, Q., Si, J., Cui, X., Peng, H., Chen, X., Xing, H., et al. (2019). The soybean cinnamate 4-hydroxylase gene *GmC4H1* contributed positively to plant defense *via* increasing lignin content. *Plant Growth Regul.* 88, 139–149. doi: 10.1007/s10725-019-00494-2

Yao, L., Berman, B. P., and Farnham, P. J. (2015). Demystifying the secret mission of enhancers: Linking distal regulatory elements to target genes. *Crit. Rev. Biochem. Mol. Biol.* 50, 550–573. doi: 10.3109/10409238.2015.1087961

Young, N. D. (1996). QTL mapping and quantitative disease resistance in plants. *Annu. Rev. Phytopathol.* 34, 479–501. doi: 10.1146/annurev.phyto.34.1.479

Yuan, N., Yuan, S., Li, Z., Zhou, M., Wu, P., Hu, Q., et al. (2018). STRESS INDUCED FACTOR 2, a leucine-rich repeat kinase regulates basal plant pathogen defense. *Plant Physiol.* 176, 3062–3080. doi: 10.1104/pp.17.01266

Zeng, H., Zhang, Y., Zhang, X., Pi, E., and Zhu, Y. (2017). Analysis of EF-hand proteins in soybean genome suggests their potential roles in environmental and nutritional stress signaling. *Front. Plant Sci.* 8. doi: 10.3389/fpls.2017.00877

Zhang, B., and Horvath, S. (2005). A general framework for weighted gene co-expression network analysis. *Stat. Appl. Genet. Mol. Biol.* 4. doi: 10.2202/1544-6115.1128

Zhang, C., Wang, X., Zhang, F., Dong, L., Wu, J., Cheng, Q., et al. (2017). Phenylalanine ammonia-lyase2.1 contributes to the soybean response towards *Phytophthora sojae* infection. *Sci. Rep.* 7, 7242. doi: 10.1038/s41598-017-07832-2

Zhao, Y., Chang, X., Qi, D., Dong, L., Wang, G., Fan, S., et al. (2017). A novel soybean ERF transcription factor, GmERF113, increases resistance to *Phytophthora sojae* infection in soybean. *Front. Plant Sci.* 8. doi: 10.3389/fpls.2017.00299

Zhao, X., Han, Y., Li, Y., Lui, D., Sun, M., Zhao, Y., et al. (2015). Loci and candidate gene identification to *Sclerotinia sclerotiorum* in soybean (*Glycine max* L. Merr.) *via* association and linkage maps. *Plant J.* 82, 245–255. doi: 10.1111/tpj.12810

Zhou, L., Mideros, S. X., Bao, L., Hanlon, R., Arredondo, F. D., Tripathy, S., et al. (2009). Infection and genotype remodel the entire soybean transcriptome. *BMC Genomics* 10, 49. doi: 10.1186/1471-2164-10-49

Zielinski, R. E. (1998). Calmodulin and calmodulin-binding proteins in plants. *Ann. Rev. Physiol. Mol. Biol.* 49, 697–725. doi: 10.1146/annurev.arplant.49.1.697

Zipfel, C. (2014). Plant pattern-recognition receptors. *Trends Immunol.* 35, 345–251. doi: 10.1016/j.it.2014.05.004

Zipfel, C., Kunze, G., Chinchilla, D., Caniard, A., Jones, J. D., Boller, T., et al. (2006). Perception of the bacterial PAMP EF-Tu by the receptor EFR restricts Agrobacterium-mediated transformation. *Cell* 125, 749–760. doi: 10.1016/j.cell.2006.03.037

Zipfel, C., and Oldroyd, G. E. D. (2017). Plant signaling in symbiosis and immunity. *Nature* 543, 328–336. doi: 10.1038/nature22009

frontiers | Frontiers in Plant Science

TYPE Original Research
PUBLISHED 13 November 2023
DOI 10.3389/fpls.2023.1270531

OPEN ACCESS

EDITED BY
Kun Zhang,
Yangzhou University, China

REVIEWED BY
Charles Y. Chen,
Auburn University, United States
Imran Ul Haq,
Faisalabad, Pakistan

*CORRESPONDENCE
Rajagopalbabu Srinivasan
babusri@uga.edu

†These authors have contributed equally to this work

RECEIVED 31 July 2023
ACCEPTED 11 October 2023
PUBLISHED 13 November 2023

CITATION
Chen Y-J, Catto MA, Pandey S, Leal-Bertioli S, Abney M, Hunt BG, Bag S, Culbreath A and Srinivasan R (2023) Characterization of gene expression patterns in response to an orthotospovirus infection between two diploid peanut species and their hybrid.
Front. Plant Sci. 14:1270531.
doi: 10.3389/fpls.2023.1270531

Characterization of gene expression patterns in response to an orthotospovirus infection between two diploid peanut species and their hybrid

Yi-Ju Chen[1†], Michael A. Catto[1†], Sudeep Pandey[1], Soraya Leal-Bertioli[2,3], Mark Abney[4], Brendan G. Hunt[1], Sudeep Bag[5], Albert Culbreath[5] and Rajagopalbabu Srinivasan[1*]

[1]Entomology Department, University of Georgia, Griffin, GA, United States, [2]Plant Pathology Department, University of Georgia, Athens, GA, United States, [3]Institute of Plant Breeding, Genetics and Genomics, University of Georgia, Athens, GA, United States, [4]Entomology Department, University of Georgia, Tifton, GA, United States, [5]Plant Pathology Department, University of Georgia, Tifton, GA, United States

Tomato spotted wilt orthotospovirus (TSWV) transmitted by thrips causes significant yield loss in peanut (*Arachis hypogaea* L.) production. Use of peanut cultivars with moderate field resistance has been critical for TSWV management. However, current TSWV resistance is often not adequate, and the availability of sources of tetraploid resistance to TSWV is very limited. Allotetraploids derived by crossing wild diploid species could help introgress alleles that confer TSWV resistance into cultivated peanut. Thrips-mediated TSWV screening identified two diploids and their allotetraploid possessing the AA, BB, and AABB genomes *Arachis stenosperma* V10309, *Arachis valida* GK30011, and [*A. stenosperma* × *A.* valida]^{4x} (ValSten1), respectively. These genotypes had reduced TSWV infection and accumulation in comparison with peanut of pure cultivated pedigree. Transcriptomes from TSWV-infected and non-infected samples from *A. stenosperma*, *A. valida*, and ValSten1 were assembled, and differentially expressed genes (DEGs) following TSWV infection were assessed. There were 3,196, 8,380, and 1,312 significant DEGs in *A. stenosperma*, *A. valida*, and ValSten1, respectively. A higher proportion of genes decreased in expression following TSWV infection for *A. stenosperma* and ValSten1, whereas a higher proportion of genes increased in expression following infection in *A. valida*. The number of DEGs previously annotated as defense-related in relation to abiotic and biotic stress was highest in *A. valida* followed by ValSten1 and *A. stenosperma*. Plant phytohormone and photosynthesis genes also were differentially expressed in greater numbers in *A. valida* followed by ValSten1 and *A. stenosperma*, with over half of those exhibiting decreases in expression.

KEYWORDS

***Arachis*, tomato spotted wilt orthotospovirus, transcriptomics, differential expression, gene ontology**

1 Introduction

Tomato spotted wilt orthotospovirus (TSWV) is transmitted by thrips in a persistent propagative manner (Ullman, 1992). TSWV infection in peanut causes the spotted wilt disease (SWD). SWD has been the major concern in peanut production in the southeastern United States for the past three decades (Culbreath and Srinivasan, 2011; Srinivasan et al., 2017). Successful breeding efforts have led to the release of numerous peanut cultivars with moderate field resistance to TSWV (Culbreath and Srinivasan, 2011; Boukar et al., 2016). Peanut cultivars with moderate field resistance combined with other cultural practices have been instrumental in managing the SWD (Culbreath and Srinivasan, 2011; Srinivasan et al., 2017).

Field resistant peanut cultivars are not immune to the virus. They can be systemically infected with the virus and display TSWV characteristic symptoms upon infection (Srinivasan et al., 2017). The mechanism of field resistance to TSWV seems to be different in peanut than in other crops such as tomato and pepper, wherein resistance is governed by single dominant genes such as *Sw5, SlCHS3*, and *Tsw* (Stevens et al., 1991; Moury et al., 1997; Hoffmann et al., 2001; Lv et al., 2022; Lahre et al., 2023; Rodríguez-Negrete et al., 2023). In contrast, in peanut, five quantitative trait loci (QTLs) on chromosome A01 and one QTL on chromosome A09 have been found to be associated with TSWV resistance (Tseng et al., 2016; Zhao et al., 2018; Agarwal et al., 2019). The QTLs on A01 alone were responsible for 36% phenotypic variation associated with TSWV resistance, and A09 QTL contribution to TSWV resistance also was significant but not estimated (Tseng et al., 2016; Agarwal et al., 2019). Unlike tomato and pepper wherein the selection pressure induced by TSWV has led to resistance-breaking variants, no such resistance-breaking variants have been documented in peanut thus far (Sundaraj et al., 2014; Lai et al., 2021a). Therefore, it is likely that TSWV resistance in peanut is governed by multiple genes. Nevertheless, TSWV incidence in moderately field resistant cultivars is not robust and often dependent upon external factors such as vector and virus pressure. Peanut cultivars developed thus far with TSWV resistance are mostly from one peanut accession PI 203396 (Clevenger et al., 2018). The sources of TSWV resistance are extremely narrow, and reiterates the critical need to breed for robust TSWV resistance from other durable sources.

The *Arachis* genus is native to South America and contains 83 described species (Valls and Simpson, 2005; Valls et al., 2013; Santana and Valls, 2015; Valls and Simpson, 2017; Seijo et al., 2021). Many diploid accessions of *A. cardenasii* (Krapov. and W.C. Greg.), *A. correntina* ((Burkart) Krapov. and W.C. Greg.), *A. diogoi* (Hoehne), *A. villosa* (Bentham), and *A. stenosperma* (Krapov and W.C. Greg.) have exhibited resistance to TSWV (Lyerly et al., 2002). For instance, *A. diogoi* (GKP 10602) was identified as resistant to TSWV among 46 wild *Arachis* accessions (Milla et al., 2005; Lai, 2015; Stalker, 2017). Several QTLs linked to TSWV resistance have been mapped in wild diploid genotypes. Five markers for TSWV resistance were found from two AA genome wild species, *A. kuhlmannii* (Krapov. and W.C. Greg.) (VRGeSv 7639) and *A. diogoi* (GKP 10602) (Moretzsohn et al., 2013). In addition to TSWV, wild species also have been documented to confer resistance to its vector –thrips. Twelve diploid species were considered as potential sources for resistance to the thrips *Frankliniella fusca* (Hinds) (Stalker and Campbell, 1983; Lyerly et al., 2002), and antibiosis-based resistance to thrips was also found in *A. diogoi* and its hybrid (*A. hypogaea* × *A. diogoi*) (Lai, 2015; Srinivasan et al., 2018).

The cultivated allotetraploid peanut *Arachis hypogaea* (L.) (4n=40 chromosomes; AABB-type genome) was generated from the natural hybridization of two wild diploid species: *A. duranensis* (Krapov. and W.C. Greg.) (2n=20 chromosomes; AA-type genome) and *A. ipaensis* (Krapov. and W.C. Greg.) (2n=20 chromosomes; BB-type genome) (Husted, 1930). Additionally, genetic deletions and exchanges within and between the subgenomes of the progenitors have been found to be advantageous in domestication (Bertioli et al., 2016). Cultivated peanut is a self-pollinating crop with very low genetic variability (Moretzsohn et al., 2013). Consequently, resistance to TSWV and other pathogens is limited. On the contrary, several diploid wild species possess more resistance to TSWV and many other pathogens than cultivated peanut. However, transferring TSWV resistance across ploidy levels has been limiting due to hybrid incompatibility. Recent advancements have overcome such issues and have led to the development of allotetraploids from diploids via artificial hybridization (Simpson, 1991; Leal-Bertioli et al., 2015; Stalker, 2017). Such allotetraploids are increasingly being utilized in peanut breeding (Stalker, 2017; Chu et al., 2021).

In induced tetraploid genotypes, TSWV resistance conferring QTLs were located on chromosomes A03 and B08 in ValSten1, B05 and B10 in IpaCor, and A02, A05, and A06 in IpaCor (Levinson, 2021). More wild species related materials have been registered as TSWV resistant genotypes, such as ValSten1-GA-NC, IpaCor2-GA-NC, and IpaDur3-GA-NC (Chu et al., 2021). Next-generation sequencing (NGS) and transcriptome analysis have provided insights on virus-host interactions in TSWV susceptible and resistant peanut cultivars (Catto et al., 2021). Defense responses in general were overexpressed following TSWV infection, and more so in the case of TSWV-resistant cultivar than in the susceptible cultivar (Catto et al., 2021). The goal of this study was to develop transcriptomes and examine differential gene expression following TSWV inoculation in wild peanut. Candidate genotypes were selected based on phenotypic responses caused by thrips feeding and virus infection, whereby *A. stenosperma* and *A. valida*, and the resulting allotetraploid [*A. stenosperma* × *A. valida*]^{4x} (ValSten1) showed the lowest TSWV infection indices among the investigated genotypes in an associated study (Chen et al., 2023). Furthermore, the TSWV-induced gene expression changes in the selected wild species and their hybrid were compared with the expression changes of orthologs in the cultivated peanut genotypes.

2 Materials and methods

2.1 Maintenance of *Arachis* species plants

Two diploid species and their allotetraploid hybrid, namely *A. stenosperma* V10309 (PI666100) (Figure 1A), *A. valida* GK30011 (PI468154) (Figure 1B), and [*A. valida* GK30011 × *A. stenosperma*

V10309 (PI695393)]^{4x} (Figure 1C) were used in this study (Additional File 1: Figure S1) (Chu et al., 2021; Gao et al., 2021; Chen et al., 2023). *A. valida* is a diploid species with the BB genome; *A. stenosperma* is a diploid species with the AA genome; and induced allotetraploid ValSten1 has AABB genome. Seeds of these genotypes were treated with two to three ml of a 0.5% solution of Florel® Growth Regulator (Monterey Lawn and Garden, Fresno, California, USA) and incubated in a petri dish at 28°C for 18-24h to break seed dormancy. Seeds were sown in individual 4" pots with commercial potting mix Promix (Premier Horticulture Inc, Quakertown, PA, USA). The plants were kept in thrips-proof cages (47.5 cm^3) (Megaview Science, Taichung, Taiwan) at 25-30°C, 80-90% RH, and a photoperiod of L14: D10 in the greenhouse. Seeds of the allotetraploid cultivar Georgia Green were pre-geminated in moistened paper towel and incubated in a growth chamber kept at 28°C for two to three days and used for thrips maintenance. One-to-two-week-old seedlings with one-to-two nodes and up to 16 leaflets of each genotype were used for TSWV transmission.

2.2 Development of *Arachis* hybrid ValSten1

The hybrid ValSten1 plants were developed based on the protocol described in Gao et al. (2021). Briefly, in the greenhouse, *A. valida* plants were emasculated and pollinated with fresh pollen of *A. stenosperma*. Hybrid plants were identified by a series of pollen traits and tests as described in Gao et al. (2021). Once the hybrid plants were identified, whole genome duplication using small 20-cm lateral branch sections and colchicine was undertaken. Cuttings and resulting plants were then maintained in the greenhouse as stated in Gao et al. (2021). Pods harvested from these plants were assessed by cytological and phenotypic analysis. Three morphological variations viz., flower width, branch angle, and pod wieight variations further confirmed the induced allotetraploid status of ValSten1 plants.

2.3 Thrips maintenance

Non-viruliferous thrips and viruliferous *Frankliniella fusca* thrips were maintained in separate growth chambers. Non-viruliferous thrips were maintained on leaflets of non-infected plants (cv. Georgia Green) within Petri dishes stuffed with a wet cotton round. Colonies were maintained by successive releases of ten adult female thrips, allowed to oviposit for 48h on a peanut leaflet dusted with a trace of pine pollen, and placed in growth chambers at 28-30°C and a photoperiod of L14: D10. Fresh leaflets and water were added to the Petri plates three times a week until emergence of the F_1 generation. TSWV viruliferous thrips colony was maintained similarly on TSWV-infected leaflets collected from the field in a separate growth chamber as described previously (Shrestha et al., 2013). During the off-season, viruliferous thrips

FIGURE 1
TSWV- induced symptoms on diploid *Arachis* species and their hybrid: **(A)** *A. stenosperma* V10309 **(B)** *A. valida* GK30011, and **(C)** the allotetraploid hybrid ValSten1 Left photograph represents a non-infected leaf, middle photograph represents a TSWV- infected leaf, and right photograph represents the whole plant after two weeks of thrips- mediated inoculation including infected and non-infected plants.

were maintained on TSWV-infected leaflets generated by mechanical inoculation in the greenhouse (Marasigan et al., 2015; Shrestha et al., 2015).

TSWV viruliferous and non-viruliferous nature of thrips colonies was periodically tested by RT-qPCR using N-gene-specific primers as previously described with appropriate controls (Rotenberg et al., 2009; Shrestha et al., 2012; Shrestha et al., 2017). At each instance, a subset (~ten each) of viruliferous and non-viruliferous thrips were evaluated for TSWV infection status. All the viruliferous thrips evaluated tested positive and all the non-viruliferous thrips tested negative for TSWV. These indicated that the thrips colonies were true to their infection status or lack thereof.

2.4 Thrips-mediated inoculation of diploids and their hybrid

F. fusca-mediated inoculation was conducted as per the established protocol previously (Shrestha et al., 2015). The experiment included two treatments: mock inoculation via non-viruliferous *F. fusca* thrips (non-infected) and TSWV inoculation via viruliferous thrips (TSWV-infected). Inoculated plants were maintained in thrips-proof cages (47.5 cm^3) in the growth chamber at 27°C and ~80% humidity (Conviron, Pembina, ND, USA). After two weeks, the first fully expanded leaf of inoculated peanuts (ca 0.03 g) was tested by RT-qPCR following methods described previously (Shrestha et al., 2015; Chen et al., 2023) to assess TSWV-infection status.

2.5 Sample preparation, total RNA extraction, and quality control

Samples from plants two-to-three weeks post-inoculation were used. Five replications for each genotype were used. Leaflets were collected from the first fully expanded leaf below the terminal of each plant for RNA extraction. Total RNA was extracted by RNeasy plant mini kit following the manufacturer's protocol (Qiagen, Valencia, CA, UGA). For each replicate, a leaflet sample was obtained from an individual plant. Thus, a total of 30 RNA samples were prepared for sequencing (three genotypes × two infection status × five replicates) and were stored at -80°C before shipping. Prior to library preparation, each sample's integrity (RNA integrity number, RIN) was measured by using Aglient 2100 Bioanalyzer (Agilent Technologies, Santa Clara, CA, USA) for RNA quality control (QC). Two samples failed the QC test; therefore 28 samples were used for library preparation and sequencing.

2.6 Library preparation and sequencing

The complementary DNA (cDNA) synthesis, cDNA libraries (messenger RNA library), and sequencing were undertaken by Novogene Corporation Inc. (Sacramento, CA, USA), as described in Catto et al. (2021). Illumina sequencing libraries were constructed using TruSeq RNA sample preparation kits. Briefly, mRNA was selected, fragmented, and first-strand cDNA was synthesized using random primers and reverse transcriptase. Subsequently, Polymerase I and RNase H were used to make the second-strand cDNA. An Illumina TruSeqLT adapter was ligated to the DNA fragments, and PCR amplification was performed for a minimal number of cycles with standard Illumina primers to produce the final cDNA libraries. Twenty-eight libraries were constructed and sequences using two lanes in the Illumina NovaSeq 6000 platform (pair-end 150 cycle sequencing setting, > 6GB raw data per sample).

2.7 Raw read processing for transcript abundance

In advance of the *A. valida*, *A. stenosperma*, and ValSten1 transcriptome assemblies (Additional File 1: Figure S2), FastQC v0.11.9 and multiQC v1.11 were used to check the quality of raw reads before and after trimming (Andrews, 2010; Ewels et al., 2016). Trimmomatic v0.39 software was used with the default setting to remove adapters (Bolger et al., 2014). Also, Sortmerna v4.3.3 software was used with the SILVA database to remove rRNA contamination (Kopylova et al., 2012; Yilmaz et al., 2014; Glöckner et al., 2017). The rRNA decontaminated trimmed reads were converted from interleaved to paired files using BBMap v38.93 software for configuring files and for transcriptome assembly (Bushnell, 2014).

2.8 Transcriptome assembly pipeline and quality control

The rRNA decontaminated and trimmed reads from *A. valida*, *A. stenosperma*, and ValSten1 were used to generate respective *de novo* assemblies using Trinity v2.10.0 software with the default parameters (Grabherr et al., 2011). The sra2genes v4 software was used to clean up the assemblies using prior evidence from closely related species to address the possibility of over assembly of the transcriptome. Sra2genes is a complete pipeline to reconstruct genes from RNA data sources, and it includes several tools such as Cluster Database as High Identity of Tolerance (CD-HIT) v4.8.1, Exonerate v2.4.0, Blast+ 2.10.1, and A Genomic Mapping and Alignment Program for mRNA and expressed sequence tag (EST) Sequences – Genomic Short-read Nucleotide Alignment Program (GMAP-GSNAP) (Slater and Birney, 2005; Fu et al., 2012; Wu et al., 2016). CD-HIT v4.8.1 was used for the removal of potentially chimeric or misassembled transcripts from the input reads. Exonerate v2.4.0 was involved in the removal of all duplicated sequences. Blast+ 2.10.1 was used to separate the transcripts as various isoforms. GMAP-GSNAP was used to align the reads to the assemblies. Benchmarking Universal Single Copy Orthologs (BUSCO) v4.0.6 was used to determine assembly completeness before and after cleaning of the *de novo* assemblies against the Fabales odb10 lineage (n=5,366) (Simão et al., 2015; Seppey et al., 2019; Manni et al., 2021).

2.9 Mapping of reads and differential expression

Trimmed reads were mapped to the respective *de novo* assemblies (see Data Availability for NCBI assessions) using Bowtie2 v2.4.1 with default mapping parameters (Langmead et al., 2009; Langmead and Salzberg, 2012; Langmead et al., 2019). Gene count estimates were derived from the mapped reads using RNA-Seq by Expectation Maximization (RSEM) v1.3.3 for *A. stenosperma* (Additional File 2: Table S1), *A. valida* (Additional File 2: Table S2), and ValSten1 (Additional File 2: Table S3) (Li and Dewey, 2011). Custom R script was used to determine the fragments per kilobase million (FPKM) across all samples on R v4.1.0 using the following R libraries: dplyr, tidyverse, and stringr (Additional File 1: Figures S3–S5) (R Core Team, 2021). DESeq2 was used to measure differentially expressed genes by comparing the gene counts from non-infected samples with virus-infected samples, where genes that had a $|\log_2$ fold change (LFC)$| \geq 4$ and a false discovery rate (FDR) < 0.05 were classified as being significantly differentially expressed (Love et al., 2014).

2.10 Functional annotation

The *de novo* assemblies for *A. stenosperma* (Additional File 3: Table S4), *A. valida* (Additional File 3: Table S5), and ValSten1 (Additional File 3: Table S6) were compared against an *Arachis* filtered subset of the NCBI database for non-redundant proteins (NR) and RefSeq genes using OmicsBox (Götz et al., 2008; Camacho et al., 2009). The OmicsBox tool also performed Blast2GO and Gene Ontology (GO) mapping to assign functional annotations to genes within each assembly (Conesa et al., 2005; Götz et al., 2008; Mi et al., 2019). Additional annotations were performed using InterProScan and the Kyoto Encyclopaedia of Genes and Genomes (KEGG) (Kanehisa and Goto, 2000; Jones et al., 2014; Kanehisa et al., 2016). The GO terms were processed with topGO (https://www.bioconductor.org/packages/release/bioc/html/topGO.html) and visualized using rrvgo (https://bioconductor.org/packages/release/bioc/html/rrvgo.html) and the reduced + visualize Gene Ontology (REVIGO) web tool (Supek et al., 2011). GO terms down to level 3 were analysed.

2.11 Clustering of differentially expressed genes into orthogroups

DEGs from two wild peanut species: *A. stenosperma* and *A. valida*, their respective hybrid ValSten1, and previously published DEGs from two domestic peanut cultivars: *A. hypogaea* (SunOleic 97R) and *A. hypogaea* (Tifguard) (Catto et al., 2021) were used to determine DEG clusters using the online tool OrthoVenn2 (Xu et al., 2019). The parameters for DEG ortholog clustering in OrthoVenn2 were run with the cut-off value of $1e^{-5}$. Overlapping regions were tested for significance using GeneOverlap (https://bioconductor.org/packages/release/bioc/vignettes/GeneOverlap/inst/doc/GeneOverlap.pdf).

2.12 Validation of RNA sequence using RT-qPCR

Quantitative reverse transcription-polymerase chain reaction (RT-qPCR) was utilized to validate *Arachis* species transcripts following TSWV infection. Three sequences from each genotype with a |LFC| ≥4 and a false discovery rate (FDR) < 0.05 were randomly selected. The sequences were extracted with the tool seqtk. RT-qPCR was performed on plant samples obtained from four biological repeats from the remaining samples. Primers for targeted DEGs were designed by NCBI primer design (https://www.ncbi.nlm.nih.gov/tools/primer-blast/). Primer sequences are listed in Additional File 1: Table S7.

The cDNA was synthesized by a Go-Script reverse transcription system (Promega Corporation, Madison, WI) following the manufacturer's protocol and then diluted 20-fold for quantitative polymerase chain reaction (qPCR). The reaction mix for qPCR included 2x GoTaq qPCR Master Mix, 1 µl of sequence-specific primers (final concentration of 250 mM), 2 µl cDNA of sample, and nuclease-free water for a final reaction volume of 20 µl. The reaction was run at 95°C for 2 min, followed by 40 cycles at 95°C for 15s, 58°C for 20s, and 72°C for 30s. The reaction was extended with a melting curve in a QuantStudio 3 System (applied biosystems by Thermo Fisher Scientific, Waltham, MA) to rule out non-specific binding. Two technical replicates for targeted transcripts and the reference gene (alcohol dehydrogenase class III) (Lai et al., 2021b), and water control were included in each RT-qPCR run. The $\log_2$fold change of each target transcript in infected plants against mock-inoculated plants was calculated after normalization to the reference gene. The $\log_2$ transformed (ratio of infected samples/ratio of non-infected samples) expression of target genes (transcripts) were correlated with Pearson's correlation using the function "cor" in software R.

3 Results

3.1 Transcriptome assembly and sequencing statisitics

Total raw reads obtained from infected plants and non-infected plants of *A. valida* GK30011 (PI468154), *A. stenosperma* V10309 (PI666100), and ValSten1 were assembled *de novo* using Trinity platform. Total raw reads generated from the three genotypes were 222, 234, and 253 million pair reads, respectively, which after trimming amounted to 218, 231, and 250 million pair reads, respectively. The percentage of reads mapped to the *de novo* assembled transcriptome for *A. stenosperma*, *A. valida*, and ValSten1 genotypes were 86%, 87%, and 80%, respectively (Additional File 1: Table S8). These reads were assembled into 141,144 (*A. valida*), 106,374 (*A. stenosperma*), and 137,039 (ValSten1) contigs. The assembly of *A. stenosperma* contained 4,571 (85%) complete BUSCOs, which included 2,571 (48%) single-copy and 2,000 (37%) duplicated orthologs. Similarly, *A. valida* contained 4,724 (88%) complete BUSCOs, which included 2,545 (47%) single-copy and 2,179 (41%) duplicated orthologs. For

ValSten1, there were 4,670 (87%) complete BUSCOs, which included 2,209 (41%) single-copy and 2,461 (46%) duplicated orthologs. One infected sample of *A. stenosperma* showed low RIN (RNA integrity number) and one non-infected sample of *A. valida* that showed uneven baseline at QC were not processed from the initial 30 libraries.

3.2 Quantitation of differential expression analysis profile

The reads obtained from infected and non-infected samples from the three genotypes were normalized and clustered using FPKM and principal component analysis (PCA) for comparison. The PCA clustered TSWV infected samples of the three genotypes separately from the non-infected ones (Figure 2). However, one sample (asten_paired_V3B) in *A. stenosperma* was removed due to the unexpected clustering in PCA, although it did not have a reduced FPKM value (Additional File 1: Figure S6). Additional checks on infection status were performed by mapping reads, using RSEM and Bowtie2, from *A. stenosperma* and *A. valida* to the ValSten1 *de novo* assembly and clustering the samples via PCA (Additional File 1: Figure S7). Differentially expressed genes (DEGs) observed for *A. stenosperma*, *A. valida*, and ValSten1 in response to TSWV were 3,196 (596 overexpressed and 2,627 underexpressed; Figure 3A), 8,380 (6,332 overexpressed and 2,048 underexpressed; Figure 3B), and 1,312 (633 overexpressed and 679 underexpressed; Figure 3C), respectively. TSWV-infected samples of *A. valida* had more DEGs (8,380) compared with *A. stenosperma* (3,196) and ValSten1 (1,312). A higher percentage of DEGs for *A. stenosperma* were underexpressed, whereas more overexpressed genes were identified in *A. valida*. Similar numbers of underexpressed and overexpressed genes were found within ValSten1.

3.3 Functional annotation of genes

DEGs observed in the wild species in response to TSWV infection were functionally annotated. The *de novo* assemblies included 107,043 transcripts, 149,877 transcripts, and 138,389 transcripts (non-significant and significant genes) of *A. valida*, *A. stenosperma*, and ValSten1, respectively.

Gene ontology (GO) provided context for the functionality of genes and comprised three level 1 categories: biological process (BP), cellular component (CC), and molecular function (MF). GO terms within the BP category provided biological relevance by attributing biological objectives to gene products. Significantly enriched GO terms were determined by the Revigo tool (Supek et al., 2011) by comparing the GO terms distribution from DEGs to that of the entire transcriptome, also referred to as the background genes. DEG specific GO terms that were overrepresented were considered significantly enriched ($p < 0.05$) with respect to the background.

In *A. stenosperma*, 127 BP GO terms were significantly enriched among DEGs across all GO term levels (Additional File 1: Figures S8A, B; Additional File 4: Tables S9, S10), with 14 terms being classified as levels 2 & 3 (Figures 4A, B). In *A. valida*, 256 BP GO terms were significantly enriched among DEGs across all GO term levels (Additional File 1: Figures S8C, D; Additional File 4: Tables S11, S12), with 19 terms being classified as levels 2 & 3 (Figures 4C, D). In ValSten1, 135 BP GO terms were significantly enriched among DEGs across all GO term levels (Additional File 1: Figures

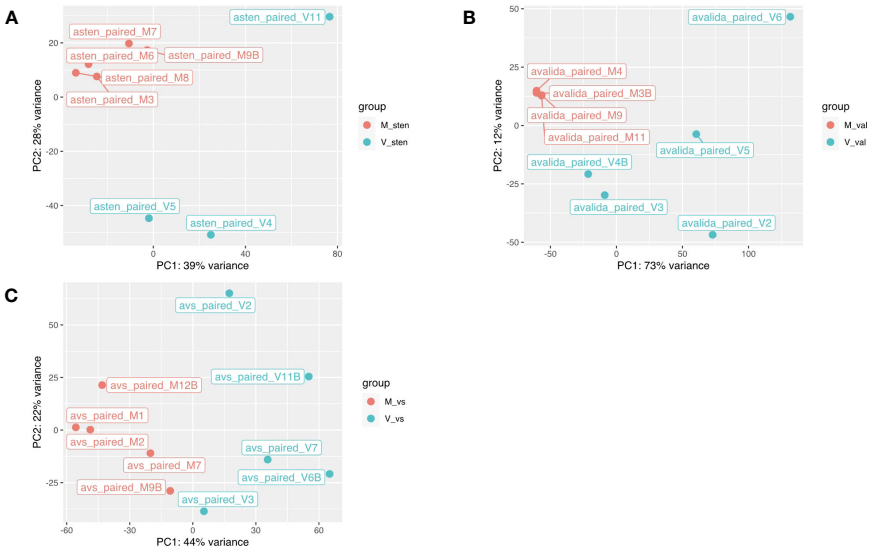

FIGURE 2
Principal component analysis based on the gene expression levels in two diploid Arachis species and their hybrid. **(A)** *A. stenosperma* V10309, **(B)** *A. valida* GK30011, and **(C)** ValSten1 clustered together according to being either non-inoculated (M, in red color) or TSWV-infected (V, in blue color). .

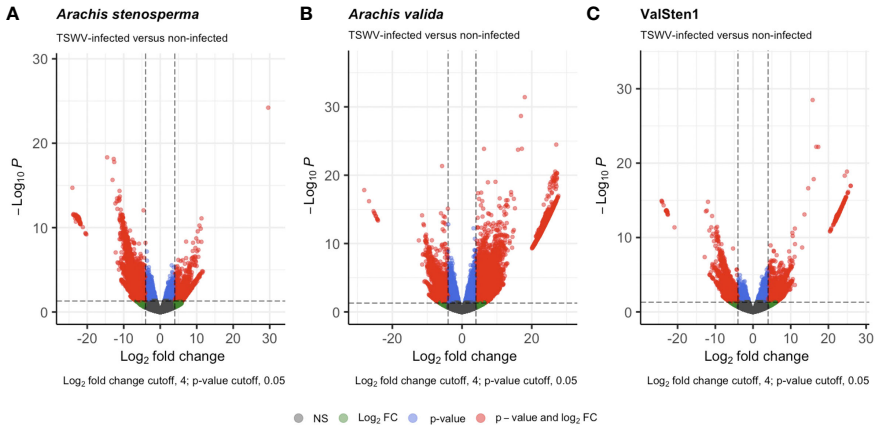

FIGURE 3
Volcano plots detailing the differential expression profiles of TSWV-infected versus non-infected samples of two diploid Arachis species and their hybrid. Genes with a |LFC| >4 and a false discovery rate (FDR) < 0.05 are highlighted in red were considered to be differentially expressed: **(A)** 3,196 DEGs from *A. stenosprema* V10309 (PI666100), **(B)** 8,380 DEGs from *A. valida* GK30011 (P1468154), and **(C)** 1,312 DEGs from ValSten1 (P1695393).

S8E, F; Additional File 4: Tables S13, S14), with 9 terms being classified as levels 2 & 3 (Figures 4E, F).

3.4 Comparison of DEGs between genotypes

To determine the transcriptional changes in each genotype related to TSWV infection, the number of orthologous clusters between *A. stenosperma*, *A. valida*, ValSten1, *A. hypogaea* (SunOleci 97R), and *A. hypogaea* (Tifguard) (Catto et al., 2021) were compared using the OrthoVenn2 web platform (Figure 5). Orthologous clustering analysis resulted in 3,965 clusters of DEGs that were commonly shared by at least two genotypes (Additional File 5: Table S15) and 15 single-copy DEG clusters from all five genotypes (Additional File 5: Table S16). In total, 71 DEG clusters were found to contain DEGs shared between all five genotypes, with cluster53, cluster179, and cluster185 relating to the putative disease resistance protein RGA3 (Song et al., 2003; Van Der Vossen et al., 2003) (UniProt ID: Q7XA40) and defense response (GO:0006952; Additional File 5: Table S15). There were 17 DEG clusters that comprised four of the genotypes, but not in the susceptible *A. hypogaea* (SunOleic 97R), with cluster674 relating to the TMV resistance protein N (UniProt ID: Q40392) (Whitham et al., 1994; Dinesh-Kumar and Baker, 2000; Dinesh-Kumar et al., 2000; Caplan et al., 2008) and signal transduction (GO:0007165; Additional File 5: Table S15). The highest overexpressed gene, with a LFC of 29.6, was found in *A. stenosperma* and was annotated as linoleate 9S-lipoxygenase (ArasteEVm001500t4). Manual assessment determined that such a large LFC was caused by lack of mapped reads (no detectable expression) in the mock inoculated/non-infected samples. This gene was found to be in cluster4, containing genes from all genotypes, and was functionally annotated as linoleate 9S-lipoxygenase (P38414) (Hilbers et al., 1994) and oxylipin biosynthetic process (GO:0031408; Additional File 5: Table S15).

With respect to *A. stenosperma*, *A. valida*, and ValSten1, orthologous DEG clustering analysis resulted in 1,507 DEG clusters that were commonly shared by at least two genotypes: *A. stenosperma* ⋂ *A. valida* (779), *A. stenosperma* ⋂ ValSten1 (79), *A. valida* ⋂ ValSten1 (412), or *A. stenosperma* ⋂ *A. valida* ⋂ ValSten1 (237) (Additional File 1: Figure S9). Additionally, 1,574 DEG clusters were found to be specific to *A. stenosperma* (269), *A. valida* (1,230), and ValSten1 (75) (Additional File 1: Figure S9). Sixty nine of the 237 orthologous clusters shared by the three wild peanut genotypes were reported as containing single-copy DEGs (Additional File 5: Table S17). All pairwise comparisons of DEG clusters from *A. stenosperma* ⋃ *A. valida* (2,404), *A. stenosperma* ⋃ ValSten1 (1,439), *A. valida* ⋃ ValSten1 (2,357) showed more overlap than expected by chance (Fisher's exact test) $p=1.1e^{-50}$, $p=3.5e^{-12}$, and $p=7.4e^{-47}$, respectively.

The phytovirus response DEGs from *A. stenosperma* (3,196), *A. valida* (8,380), and ValSten1 (1,312) were grouped into three major categories: defense, phytohormone, and photosynthesis related genes (Table 1). The categories were chosen based on the study with resistant and susceptible cultivated peanuts (Catto et al., 2021). Within the defense related DEGs, the percentage (No. of overexpressed DEGs out of total DEGs within category) in *A. stenosperma, A. valida*, and ValSten1 were 34% (25/73), 64% (490/763), and 55% (69/126), respectively (Table 1). A similar pattern was observed in the case of phytohormone related DEGs. Upregulation of phytohormone related DEGs of the eight examined categories was higher in *A. valida*. The percentages (No. of overexpressed DEGs out of total DEGs within category) in *A. stenosperma, A. valida*, and ValSten1 were 9% (1/11), 51% (100/198), and 36% (16/44), respectively (Table 1). Regarding photosynthesis related DEGs, the percentages (No. of overexpressed DEGs out of total DEGs within category) in *A. stenosperma, A. valida*, and ValSten1 were 10% (3/29), 46% (249/536), and 38% (28/73), respectively.

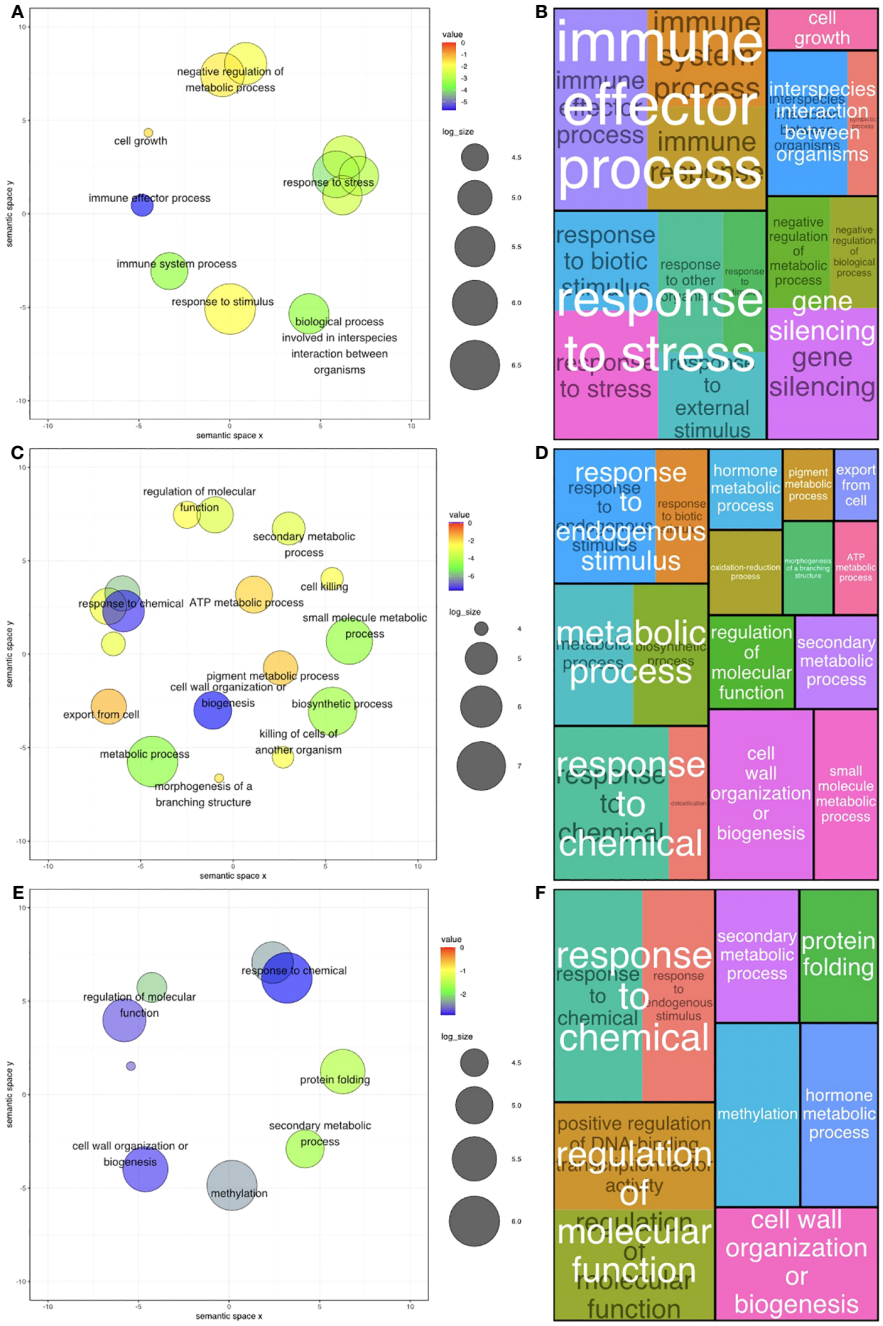

FIGURE 4
Gene Ontology (GO) level 2 & 3 terms ratios across two diploid *Arachis* species and their hybrid. **(A)** Ratio of all significant GO terms assigned to differentially expressed genes (DEGs) present in *A. stenosperma*. **(B)** Tree map of significant levels 2 & 3 GO terms of DEGs compared to the background in *A. stenosperma*. **(C)** Ratio of all significant GO terms assigned to differentially expressed genes (DEGs) present in *A. valida* **(D)** Tree map of significant levels 2 & 3 GO terms of DEGs compared to the background in *A. valida*. **(E)** Ratio of all significant GO terms assigned to differentially expressed genes (DEGs) present in ValSten1 **(F)** Tree map of significant levels 2 & 3 GO terms of DEGs compared to the background in ValSten1.

3.5 Validation of RNA-sequencing

Three DEGs from each genotype were randomly selected and their expression values were validated using RT-qPCR (Additional File 1: Table S7). A positive correlation was found between the expression from both RNASeq and RT-qPCR across all three genotypes (cor=0.87, t=4.6, df=7, p=0.002; Additional File 1: Figure S10).

4 Discussion

Peanut production could be severely impacted by orthotospoviruses such as TSWV (Culbreath et al., 2003; Culbreath and Srinivasan, 2011). Resistance against the pathogen and/or the vector is often the ideal management option. The cultivated peanut has a narrow genetic base due to relatively recent polyploidization and self-pollination (Pandey et al., 2012).

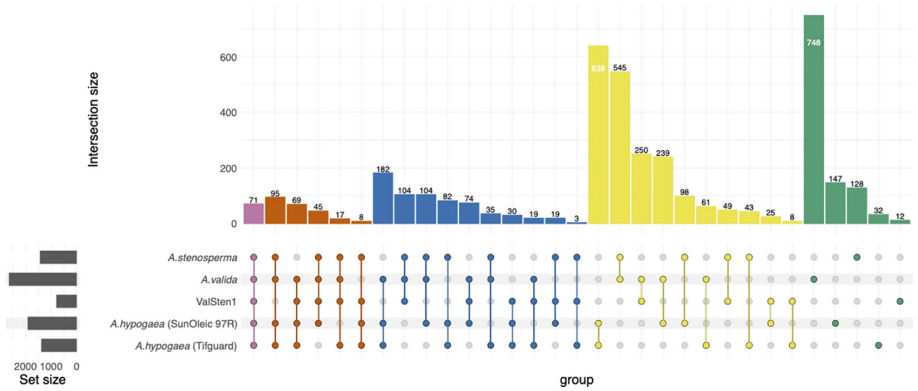

FIGURE 5
Distribution of shared peanut (*Arachis spp.*) gene families containing expressed genes in response to TSWV infection. Venn diagram represents the expressed common, unique, and core set of DEGs within gene families between *A. stenosperma*, *A. valida*, ValSten1 (*A. valida x A. stenosperma*), *A. hypogaea* (SunOleic 97R), and *A. hypogaea* (Tifguard).

Therefore, peanut genetics is prohibitive to crop improvement and/or enhancing pathogen resistance. While wild species can confer increased resistance against pathogens such as orthotospoviruses, introgressing that resistance into cultivated peanut is challenging mainly due to ploidy level differences (wild species are typically diploids) (Pandey et al., 2012; Bertioli et al., 2016). Several wild species have been recognized for innate resistance against orthotospoviruses, particularly TSWV (Moretzsohn et al., 2013; Lai, 2015; Stalker, 2017). Ability to induce allotetraploid hybrids from wild species with the same genetic makeup as the cultivated peanut, *A. hypogaea* (AABB genome), has allowed for transferring useful genes and increasing the genetic diversity of tetraploid peanut (Gao et al., 2021). As a part of continuing effort, numerous wild species and their hybrids were evaluated at the University of Georgia (Chen et al., 2023). The evaluations indicated that wild diploids such as *A. stenosperma* and *A. valida* and their allotetraploid hybrid, ValSten1, had reduced TSWV infection and accumulation than other diploids and the cultivated tetraploid evaluated following thrips-mediated inoculation (Chen et al., 2023). The severity of TSWV-induced symptoms also was reduced on *A. stenosperma* and *A. valida* and their allotetraploid hybrid than on the cultivated tetraploid (Chen et al., 2023).

To gain insights on interactions of *A. stenosperma* and *A. valida* and their allotetraploid hybrid with TSWV, gene expression patterns post thrips-mediated TSWV inoculation were examined in this study. Following thrips-mediated TSWV inoculation, based on *de novo* transcriptome assemblies, gene expression was substantially higher in *A. valida* than in *A. stenosperma* and ValSten1. Overall, in this study, expression of defense-related genes and genes associated with plant physiology such as phytohormones and photosynthesis were examined. Numerous genes pertaining to defense against biotic stress, including pathogens, were overexpressed in *A. valida* (BB genome) than in *A. stenosperma* (AA genome) following TSWV infection.

A greater proportion of contigs associated with pathogen defense such as heat shock proteins, lectins, and leucine zippers were overexpressed in *A. valida* followed and *A. stenosperma*. A heat shock protein was associated with virus infection in *Arabidopsis thaliana* (Roux and Bergelson, 2016). Lectins were known to upregulate plant defenses by facilitating recognition of phytoviruses (Fliegmann et al., 2004). Nucleotide binding-leucine rich repeats (NB-LRR) were known to provide defense against a range of pathogens including phytoviruses (Noman et al., 2017; Mishra et al., 2019; Zhang et al., 2023). A greater proportion of NB-LRR genes were overexpressed in *A. valida* than in *A. stenosperma* and in their hybrid in this study. Similarly, NB-LRR genes were overexpressed in a TSWV resistant tetraploid peanut cultivar than the susceptible tetraploid cultivar following TSWV infection (Catto et al., 2021). NB-LLR genes also were overexpressed in response to TSWV infection in TSWV-resistant tomato lines in another study (Lv et al., 2023). The overexpression of defense genes following thrips-mediated TSWV inoculation in this study provides mechanistic reasons for the observed response against TSWV in *A. valida*.

A suite of other defense genes such as calcium-modulated calmodulin, stilbene synthase, and serine carboxypeptidases also were overexpressed substantially in the case of *A. valida* followed by the hybrid, and *A. stenosperma*. These genes have been documented to mediate resistance against a wide array of pathogens including phytoviruses (Fraser et al., 2005; Yu et al., 2005; Takabatake et al., 2007; Hong et al., 2017; Catto et al., 2021). The differential gene expression pattern seems to be consistent, wherein defense genes' upregulation in *A. valida* was almost always higher than in the hybrid and least in the other diploid, *A. stenosperma*. In addition, induced defense response related genes such as those associated with RNA interference and salicylic acid were overexpressed in a similar pattern in *A. valida* followed by the hybrid and *A. stenosperma*.

Besides the above-stated categories of genes, dominant genes that confer hypersensitive response were overexpressed in *A. valida* than in the other two genotypes. Hypersensitive response inducing genes such as nucleocapsid (N) gene from tobacco (*Nicotiana glutinosa* L.), which imparts resistance to several tobamoviruses including the tobacco mosaic virus (TMV), and disease resistance (R) proteins, were underexpressed in three resistant wild genotypes in this study. However, the R proteins were overexpressed in two cultivated genotypes in a previous study (Catto et al., 2021). In pepper, *Tsw*

TABLE 1 Counts of defense-, phytohormone-, and photosynthesis-related significant differentially expressed genes with a |LFC| > 4 and a false discovery rate (FDR) < 0.05 cutoff in wild *Arachis* species in response to TSWV infection.

Gene description	*A. stenosperma* (Sten)		*A. valida* (Val)		ValSten1	
	Overexpressed	Underexpressed	Overexpressed	Underexpressed	Overexpressed	Underexpressed
Argonaute	0	0	1	6	0	0
MATH domain	0	0	1	1	0	0
Dicer	0	1	3	1	0	0
Heat shock protein	11	0	49	1	15	0
Lectin	1	2	47	12	12	2
Leucine zipper	1	0	10	4	3	1
Mitogen-activated protein kinase	0	1	13	4	0	0
MYB	1	2	23	13	2	2
P450	1	4	51	18	6	8
PAMP	0	0	1	0	0	0
Disease resistance (R) protein	1	12	11	49	4	13
WRKY transcription factor	0	1	22	3	2	0
LRR	1	4	24	25	1	2
Serine/threonine	7	11	129	89	14	23
Salicylic acid	0	0	3	1	0	0
Calmodulin	0	1	25	12	3	0
TMV resistance protein N	1	8	25	20	2	5
Stilbene synthase	0	0	33	0	0	0
Serine Carboxypeptidase	0	1	19	11	5	0
Alpha-Dioxygenase	0	0	0	3	0	1
(Total of genes related to defense)	(25)	(48)	(490)	(273)	(69)	(57)
Auxin	0	1	7	37	3	14
Gibberellin	0	0	5	8	1	3
Cytokinin	0	0	13	4	2	2
Abscisic acid	0	1	5	8	0	0
Ethylene	0	1	29	9	5	1

(Continued)

10.3389/fpls.2023.1270531

TABLE 1 Continued

Gene description	*A. stenosperma* (Sten)		*A. valida* (Val)		ValSten1	
	Overexpressed	Underexpressed	Overexpressed	Underexpressed	Overexpressed	Underexpressed
Brassinosteroid	0	0	0	0	1	0
Salicylic acid	0	0	0	0	1	0
ABC transporter	1	7	41	32	3	8
(Total of genes related to phytohormones)	(1)	(10)	(100)	(98)	(16)	(28)
Chloroplastic	3	23	243	256	26	44
Protochlorophyllide	0	0	1	3	0	0
Photosystem	0	1	0	26	0	1
NADP-dependent malic enzyme	0	2	5	2	2	0
(Total of genes related to phytosynthesis)	(3)	(26)	(249)	(287)	(28)	(45)

was the only identified R gene against TSWV (Wu et al., 2023), and Sw5 in tomato conferred hypersensitive response against TSWV (de Oliveira et al., 2018). Similarly, in tomato, the disease- resistant R gene *Mi* conferred resistance against nematodes and potato aphids (Rossi et al., 1998). However, HR can be uncoupled with resistance and may vary depending on species in some cases (Balint-Kurti, 2019). Perhaps this explains the absence of hypersensitive response in peanut following TSWV infection. Generally, R protein in plants recognizes the effectors in pathogens and are known to trigger a defense response. WRKY transcription factors also were involved in triggering immunity against a range of pathogens including viruses by recognizing pathogen associated molecular patterns (PAMPs) (Pandey and Somssich, 2009; Lee et al., 2023). WRKY was overexpressed in a tomato genotype with resistance to TSWV (Catoni et al., 2009; Lv et al., 2023). Similarly, WRKY contigs were substantially overexpressed in *A. valida* and slightly in the hybrid.

The results in the current study clearly illustrate that several classes of defense genes were overexpressed in *A. valida* (BB genome) and its hybrid ValSten1 (AABB genome). However, the obtained results were in contrast with previous studies, which showed wild species such as *A. stenosperma* and *A. cardenasii* with AA genomes harbored more defense genes' containining QTLs than the wild species with the BB genomes (Bertioli et al., 2016; Pandey et al., 2017). The results from the current study indicate that the resistance to TSWV in wild peanut may have interspecific differences and need to be further examined in depth. Also, the current study was conducted at one time point, *i.e.*, three weeks post inoculation. Time-series profiling of DEGs will be beneficial for better understanding the changing pattern of gene expression in relation to TSWV infection. Further, not many studies thus far have evaluated gene expression in wild peanut species following TSWV infection, especially following thrips-mediated inoculation. Perhaps, some of these differences could explain the observed expression profiles of defense genes associated with the BB genome in *A. valida* as opposed to the AA genome in *A. stenosperma*. Despite this reoccurring pattern of overexpression of defense related genes in *A. valida* and its hybrid ValSten1, overall comparison of functional annotation in defense-related DEGs between cultivated and wild peanut (AA, BB, and AABB) showed that genes in many categories were underexpressed in wild species than in the case of cultivated peanut (Table 1). The host phenotype alteration in the wild species and their hybrid in comparison with the tetraploid cultivars following TSWV infection was not as severe. This could have resulted in less physiological perturbances in the wild diploid species and their hybrid than in the cultivated tetraploids.

In addition to differential expression of defense related genes, other genes such as phytohormones and photosynthesis related genes also were differentially expressed. Altogether, more than half-a-dozen phytohormones were downregulated in *A. stenosperma* and the hybrid ValSten1. Phytohormones were slightly overexpressed in the case of *A. valida*. Phytohormones can induce systemic resistance and inhibit infection of viruses such as TSWV (Zhao et al., 2020). Similarly, the increased flavonoid content facilitated by the overexpression of *SlCHS3* played a significant role in TSWV resistance in tomato plants (Lv et al., 2022). In another study, resistance against the thrips-borne virus in pepper was associated

with auxin-related pathway (Zhao et al., 2022). Results in this study showed that genes related to abscisic acid (ABA) and auxin were underexpressed in wild peanut species. Likewise, the DEGs associated with auxin were underexpressed following TSWV infection in susceptible and resistant tomato lines, while DEGs related to ethylene were overexpressed (Lv et al., 2023). In contrast, the miRNA associated with auxin pathways were overexpressed in pepper plants following TSWV infection (Tao et al., 2022). Although ABA plays a role against bacteria and fungi (Alazem and Lin, 2017), virus infection did not result in overexpression of ABA in some incompatible interactions (Kovač et al., 2009; Baetz and Martinoia, 2014). For example, infection by potato virus Y (PVY) of the resistant potato cultivar did not induce ABA (Kazan and Manners, 2009). PVY, like TSWV, is non-tissue specific. Phytohormone gene expression results in this study are in contrast with the tetraploid cultivars examined in another study, wherein phytohormone related genes were overexpressed (Catto et al., 2021). The overexpression was more prominent in the TSWV-resistant cultivar, Tifguard, than in the susceptible cultivar (Catto et al., 2021).

Chloroplast and photosynthesis related genes also were underexpressed overall in both diploids and their hybrid, with the reduced expression being more prominent in *A. stenosperma* followed by the hybrid ValSten1 and *A. valida*. The results were congruent with the other study, in which photosynthesis related genes were underexpressed in both TSWV resistant and susceptible genotypes, with the underexpression being substantial in the case of the TSWV-susceptible cultivar, SunOleic 97R (Catto et al., 2021). Similarly, in the current study, the downregulation of photosynthesis related genes was less substantial in the case of the *A. valida* followed by the hybrid and *A. stenosperma*. These results reiterate that the *A. valida*, and by extension the BB genome, could be more tolerant to thrips-mediated TSWV inoculation.

TSWV resistance in wild diploid species and their hybrids could play a pivotal role in broadening the resistance base against TSWV and possibly other pathogens and pests. The wild diploid species and the hybrid transcriptomes developed in this study provide significant insights into virus-host interactions. Even though, the roles of the differentially expressed genes remain to be functionally validated, DEG analyses provide an overview of the mechanistic underpinning for the observed resistance/tolerance against TSWV. The differential gene expression analyses indicated that defense related genes were consistently overexpressed in the diploid species with the BB genome as opposed to the species with the AA genome. If the pattern remains consistent, then it would be beneficial to focus on wild species such as *A. valida* for enhancing TSWV resistance in cultivated peanut. Further exploration into other molecular factors, such as differential methylation and microRNA expression, in relation to virus resistance in peanut might also be critical (Bertioli et al., 2016; Arora et al., 2022; Tao et al., 2022; Huang et al., 2023).

Data availability statement

The data for this article can be found in the NCBI GenBank repository at https://www.ncbi.nlm.nih.gov/ under the BioProject PRJNA834809. Raw sequence data for the BioSamples: SAMN28103668-SAMN28103695 are deposited in the SRA accessions: SRR19119579-SRR19119606. The transcriptome shotgun assembly (TSA) submission accessions for *A. valida, A. stenosperma*, and ValSten1 are GJYP00000000, GJYQ00000000, and GJYX00000000 respectively.

Author contributions

RS: Conceptualization, Funding acquisition, Project administration, Resources, Supervision, Validation, Visualization, Writing – review & editing. YC: Conceptualization, Methodology, Formal Analysis, Software, Writing – review & editing. MC: Data curation, Formal Analysis, Methodology, Software, Writing – review & editing. SP: Data curation, Formal Analysis, Methodology, Software, Writing – review & editing. SL-B: Conceptualization, Funding acquisition, Project administration, Resources, Supervision, Visualization, Writing – review & editing. MA: Project administration, Resources, Supervision, Writing – review & editing. BH: Data curation, Formal Analysis, Writing – review & editing. SB: Supervision, Writing – review & editing. AC: Writing – review & editing.

Funding

The author(s) declare financial support was received for the research, authorship, and/or publication of this article. The authors acknowledge the funding support from the National Peanut Research Initiative -National Peanut Board and Georgia Peanut Commission awarded Srinivasan and Leal-Bertioli.

Conflict of interest

The authors declare that the research was conducted in the absence of any commercial or financial relationships that could be construed as a potential conflict of interest.

Publisher's note

Supplementary material

The Supplementary Material for this article can be found online at: https://www.frontiersin.org/articles/10.3389/fpls.2023.1270531/full#supplementary-material

Supplementary material data files 3 and 4 are available via Figshare: 10.6084/m9.figshare.23811546.

References

Agarwal, G., Clevenger, J., Kale, S. M., Wang, H., Pandey, M. K., Choudhary, D., et al. (2019). A recombination bin-map identified a major QTL for resistance to Tomato Spotted Wilt Virus in peanut (Arachis hypogaea). *Sci. Rep.* 9, 1–13. doi: 10.1038/s41598-019-54747-1

Alazem, M., and Lin, N. S. (20171760). Antiviral roles of abscisic acid in plants. *Front. Plant Sci.* 8. doi: 10.3389/fpls.2017.01760

Andrews, S., and FastQC, A. (2010). *A quality control tool for high throughput sequence data*. Available at: http://www.bioinformatics.bbsrc.ac.uk/projects/fastqc/.

Arora, H., Singh, R. K., Sharma, S., Sharma, N., Panchal, A., Das, T., et al. (2022). DNA methylation dynamics in response to abiotic and pathogen stress in plants. *Plant Cell Rep.* 41, 1931–1944. doi: 10.1007/s00299-022-02901-x

Baetz, U., and Martinoia, E. (2014). Root exudates: The hidden part of plant defense. *Trends Plant Sci.* 19, 90–98. doi: 10.1016/j.tplants.2013.11.006

Balint-Kurti, P. (2019). The plant hypersensitive response: concepts, control and consequences. *Mol. Plant Pathol.* 20, 1163–1178. doi: 10.1111/mpp.12821

Bertioli, D. J., Cannon, S. B., Froenicke, L., Huang, G., Farmer, A. D., Cannon, E. K. S., et al. (2016). The genome sequences of Arachis duranensis and Arachis ipaensis, the diploid ancestors of cultivated peanut. *Nat. Genet.* 484 48, 438–446. doi: 10.1038/ng.3517

Bolger, A. M., Lohse, M., and Usadel, B. (2014). Trimmomatic: A flexible trimmer for Illumina sequence data. *Bioinformatics* 30, 2114–2120. doi: 10.1093/bioinformatics/btu170

Boukar, O., Fatokun, C. A., Huynh, B. L., Roberts, P. A., and Close, T. J. (2016). Genomic tools in cowpea breeding programs: Status and perspectives. *Front. Plant Sci.* 7. doi: 10.3389/fpls.2016.00757

Bushnell, B. (2014). *BBMap: A fast, accurate, splice-aware aligner*. Available at: https://www.osti.gov/biblio/1241166 (Accessed September 26, 2023).

Camacho, C., Coulouris, G., Avagyan, V., Ma, N., Papadopoulos, J., Bealer, K., et al. (2009). BLAST+: architecture and applications. *BMC Bioinf.* 10, 1–9. doi: 10.1186/1471-2105-10-421

Caplan, J. L., Mamillapalli, P., Burch-Smith, T. M., Czymmek, K., and Dinesh-Kumar, S. P. (2008). Chloroplastic protein NRIP1 mediates innate immune receptor recognition of a viral effector. *Cell* 132, 449–462. doi: 10.1016/j.cell.2007.12.031

Catoni, M., Miozzi, L., Fiorilli, V., Lanfranco, L., and Accotto, G. P. (2009). Comparative analysis of expression profiles in shoots and roots of tomato systemically infected by tomato spotted wilt virus reveals organ-specific transcriptional responses. *Mol. Plant-Microbe Interact.* 22, 1504–1513. doi: 10.1094/MPMI-22-12-1504

Catto, M. A., Shrestha, A., Abney, M. R., Champagne, D. E., Culbreath, A. K., Leal-Bertioli, S. C. M., et al. (2021). Defense-related gene expression following an orthotospovirus infection is influenced by host resistance in arachis hypogaea. *Viruses* 13, 1303. doi: 10.3390/v13071303

Chen, Y.-J., Pandey, S., Catto, M., Leal-Bertioli, S., Abney, M. R., Bag, S., et al. (2023). Evaluation of wild peanut species and their allotetraploids for resistance against thrips and thrips-transmitted tomato spotted wilt orthotospovirus (TSWV). *Pathogens* 12, 1102. doi: 10.3390/pathogens12091102

Chu, Y., Stalker, H. T., Marasigan, K., Levinson, C. M., Gao, D., Bertioli, D. J., et al. (2021). Registration of three peanut allotetraploid interspecific hybrids resistant to late leaf spot disease and tomato spotted wilt. *J. Plant Regist.* 15, 562–572. doi: 10.1002/plr2.20146

Clevenger, J., Chu, Y., Chavarro, C., Botton, S., Culbreath, A., Isleib, T. G., et al. (2018). Mapping late leaf spot resistance in peanut (Arachis hypogaea) using QTL-seq reveals markers for marker-assisted selection. *Front. Plant Sci.* 9. doi: 10.3389/fpls.2018.00083

Conesa, A., Götz, S., García-Gómez, J. M., Terol, J., Talón, M., and Robles, M. (2005). Blast2GO: A universal tool for annotation, visualization and analysis in functional genomics research. *Bioinformatics* 21, 3674–3676. doi: 10.1093/bioinformatics/bti610

Core Team, R. (2021). *R: A language and environment for statistical computing. R foundation for statistical computing. R foundation for statistical computing* (Vienna, Austria: R Found. Stat. Comput). Available at: https://www.r-project.org/.

Culbreath, A. K., and Srinivasan, R. (2011). Epidemiology of spotted wilt disease of peanut caused by Tomato spotted wilt virus in the southeastern U.S. *Virus Res.* 159, 101–109. doi: 10.1016/j.virusres.2011.04.014

Culbreath, A. K., Todd, J. W., and Brown, S. L. (2003). Epidemiology and management of tomato spotted wilt in peanut. *Annu. Rev. Phytopathol.* 41, 53–75. doi: 10.1146/annurev.phyto.41.052002.095522

de Oliveira, A. S., Boiteux, L. S., Kormelink, R., and Resende, R. O. (2018). The Sw-5 gene cluster: Tomato breeding and research toward orthotospovirus disease control. *Front. Plant Sci.* 9. doi: 10.3389/fpls.2018.01055

Dinesh-Kumar, S. P., and Baker, B. J. (2000). Alternatively spliced N resistance gene transcripts: Their possible role in tobacco mosaic virus resistance. *Proc. Natl. Acad. Sci. U. S. A.* 97, 1908–1913. doi: 10.1073/pnas.020367497

Dinesh-Kumar, S. P., Tham, W. H., and Baker, B. J. (2000). Structure-function analysis of the tobacco mosaic virus resistance gene N. *Proc. Natl. Acad. Sci. U. S. A.* 97, 14789–14794. doi: 10.1073/pnas.97.26.14789

Ewels, P., Magnusson, M., Lundin, S., and Käller, M. (2016). MultiQC: Summarize analysis results for multiple tools and samples in a single report. *Bioinformatics* 32, 3047–3048. doi: 10.1093/bioinformatics/btw354

Fliegmann, J., Mithöfer, A., Wanner, G., and Ebel, J. (2004). An ancient enzyme domain hidden in the putative β-glucan elicitor receptor of soybean may play an active part in the perception of pathogen-associated molecular patterns during broad host resistance. *J. Biol. Chem.* 279, 1132–1140. doi: 10.1074/jbc.M308552200

Fraser, C. M., Rider, L. W., and Chapple, C. (2005). An expression and bioinformatics analysis of the Arabidopsis serine carboxypeptidase-like gene family. *Plant Physiol.* 138, 1136–1148. doi: 10.1104/pp.104.057950

Fu, L., Niu, B., Zhu, Z., Wu, S., and Li, W. (2012). CD-HIT: Accelerated for clustering the next-generation sequencing data. *Bioinformatics* 28, 3150–3152. doi: 10.1093/bioinformatics/bts565

Gao, D., Araujo, A. C. G., Nascimento, E. F. M. B., Chavarro, M. C., Xia, H., Jackson, S. A., et al. (2021). ValSten: a new wild species derived allotetraploid for increasing genetic diversity of the peanut crop (Arachis hypogaea L.). *Genet. Resour. Crop Evol.* 68, 1471–1485. doi: 10.1007/s10722-020-01076-2

Glöckner, F. O., Yilmaz, P., Quast, C., Gerken, J., Beccati, A., Ciuprina, A., et al. (2017). 25 years of serving the community with ribosomal RNA gene reference databases and tools. *J. Biotechnol.* 261, 169–176. doi: 10.1016/J.JBIOTEC.2017.06.1198

Götz, S., García-Gómez, J. M., Terol, J., Williams, T. D., Nagaraj, S. H., Nueda, M. J., et al. (2008). High-throughput functional annotation and data mining with the Blast2GO suite. *Nucleic Acids Res.* 36, 3420–3435. doi: 10.1093/nar/gkn176

Grabherr, M. G., Haas, B. J., Yassour, M., Levin, J. Z., Thompson, D. A., Amit, I., et al. (2011). Full-length transcriptome assembly from RNA-Seq data without a reference genome. *Nat. Biotechnol.* 297 29, 644–652. doi: 10.1038/nbt.1883

Hilbers, M. P., Rossi, A., Finazzi-agrò, A., Veldink, G. A., and Vliegenthart, J. F. G.. (1994). The primary structure of a lipoxygenase from the shoots of etiolated lentil seedlings derived from its cDNA. *Biochim. Biophys. Acta.* 1211, 239–242. doi: 10.1016/0005-2760(94)90275-5

Hoffmann, K., Qiu, W. P., and Moyer, J. W. (2001). Overcoming host- and pathogen-mediated resistance in tomato and tobacco maps to the M RNA of Tomato spotted wilt virus. *Mol. Plant-Microbe Interact.* 14, 242–249. doi: 10.1094/MPMI.2001.14.2.242

Hong, C. E., Ha, Y. I., Choi, H., Moon, J. Y., Lee, J., Shin, A. Y., et al. (2017). Silencing of an α-dioxygenase gene, Ca-DOX, retards growth and suppresses basal disease resistance responses in Capsicum annum. *Plant Mol. Biol.* 93, 497–509. doi: 10.1007/s11103-016-0575-3

Huang, R., Li, H., Gao, C., Yu, W., and Zhang, S. (2023). Advances in omics research on peanut response to biotic stresses. *Front. Plant Sci.* 14. doi: 10.3389/fpls.2023.1101994

Husted, L. (1930). Cytological studies on th Peanut, Arachis. II. Chromosom number, morphology and behaviour, and their application to the problem of the origin of the cultivated forms. *Cytologia (Tokyo).* 7, 396–423.

Jones, P., Binns, D., Chang, H. Y., Fraser, M., Li, W., McAnulla, C., et al. (2014). InterProScan 5: Genome-scale protein function classification. *Bioinformatics* 30, 1236–1240. doi: 10.1093/bioinformatics/btu031

Kanehisa, M., and Goto, S. (2000). KEGG: kyoto encyclopedia of genes and genomes. *Nucleic Acids Res.* 28, 27–30. doi: 10.1093/nar/28.1.27

Kanehisa, M., Sato, Y., Kawashima, M., Furumichi, M., and Tanabe, M. (2016). KEGG as a reference resource for gene and protein annotation. *Nucleic Acids Res.* 44, D457–D462. doi: 10.1093/nar/gkv1070

Kazan, K., and Manners, J. M. (2009). Linking development to defense: auxin in plant-pathogen interactions. *Trends Plant Sci.* 14, 373–382. doi: 10.1016/j.tplants.2009.04.005

Kopylova, E., Noé, L., and Touzet, H. (2012). SortMeRNA: Fast and accurate filtering of ribosomal RNAs in metatranscriptomic data. *Bioinformatics* 28, 3211–3217. doi: 10.1093/bioinformatics/bts611

Kovač, M., Müller, A., Milovanovič Jarh, D., Milavec, M., Düchting, P., and Ravnikar, M. (2009). Multiple hormone analysis indicates involvement of jasmonate signalling in the early defence of potato to potato virus YNTN. *Biol. Plant* 53, 195–199. doi: 10.1007/s10535-009-0034-y

Lahre, K., Shekasteband, R., Meadows, I., Whitfield, A. E., and Rotenberg, D. (2023). First report of resistance-breaking variants of tomato spotted wilt virus (TSWV) infecting tomatoes with the sw-5 resistance gene in north carolina. *Plant Dis.* 107, 2271. doi: 10.1094/PDIS-11-22-2637-PDN

Lai, P. C. (2015). Evaluation of cultural tactics, insecticides, and peanut genotypes for thrips and spotted wilt disease management in peanut. *MS Thesis, University of Georgia, USA*.

Lai, P. C., Abney, M. R., Bag, S., Culbreath, A. K., and Srinivasan, R. (2021a). Impact of host resistance to tomato spotted wilt orthotospovirus in peanut cultivars on virus population genetics and thrips fitness. *Pathogens* 10, 1418. doi: 10.3390/pathogens10111418

Lai, P. C., Abney, M. R., Chen, Y. J., Bag, S., and Srinivasan, R. (2021b). Discrepancies in serology-based and nucleic acid-based detection and quantitation of tomato spotted

wilt orthotospovirus in leaf and root tissues from symptomatic and asymptomatic peanut plants. *Pathogens* 10, 1476. doi: 10.3390/pathogens10111476

Langmead, B., and Salzberg, S. L. (2012). Fast gapped-read alignment with Bowtie 2. *Nat. Methods* 94 9, 357–359. doi: 10.1038/nmeth.1923

Langmead, B., Trapnell, C., Pop, M., and Salzberg, S. L. (2009). Ultrafast and memory-efficient alignment of short DNA sequences to the human genome. *Genome Biol.* 10, 1–10. doi: 10.1186/gb-2009-10-3-r25

Langmead, B., Wilks, C., Antonescu, V., and Charles, R. (2019). Scaling read aligners to hundreds of threads on general-purpose processors. *Bioinformatics* 35, 421–432. doi: 10.1093/bioinformatics/bty648

Leal-Bertioli, S. C. M., Cavalcante, U., Gouvea, E. G., Ballén-Taborda, C., Shirasawa, K., Guimarães, P. M., et al. (2015). Identification of QTLs for rust resistance in the peanut wild species Arachis magna and the development of KASP markers for marker-assisted selection. *G3 Genes Genomes Genet.* 5, 1403–1413. doi: 10.1534/g3.115.018796

Lee, K. P., Li, M., Li, M., Liu, K., Medina-Puch, L., Qi, S., et al. (2023). Hierarchical regulatory module GENOMES UNCOUPLED1-GOLDEN2-LIKE1/2-WRKY18/40 modulates salicylic acid signaling. *Plant Physiol.* 192, 3120–3133. doi: 10.1093/plphys/kiad251

Levinson, C. M. (2021). Morphological, reproductive, genetic, and disease and insect resistance characterization in nascent allotetraploids cross-compatible to cultivated peanut (Arachis hypogaea L.). *PhD Thesis, University of Georgia, USA*.

Li, B., and Dewey, C. N. (2011). RSEM: Accurate transcript quantification from RNA-Seq data with or without a reference genome. *BMC Bioinformatics* 12, 1–16. doi: 10.1186/1471-2105-12-323

Love, M. I., Huber, W., and Anders, S. (2014). Moderated estimation of fold change and dispersion for RNA-seq data with DESeq2. *Genome Biol.* 15, 1–21. doi: 10.1186/s13059-014-0550-8

Lv, J., Deng, M., Jiang, S., Zhu, H., Li, Z., Wang, Z., et al. (2022). Mapping and functional characterization of the tomato spotted wilt virus resistance gene SlCHS3 in Solanum lycopersicum. *Mol. Breed.* 42, 1–11. doi: 10.1007/s11032-022-01325-5

Lv, J., Deng, M., Li, Z., Zhu, H., Wang, Z., Yue, Y., et al. (2023). Integrative analysis of the transcriptome and metabolome reveals the response mechanism to tomato spotted wilt virus. *Hortic. Plant J* 9 (5), 958–970. doi: 10.1016/j.hpj.2022.12.008

Lyerly, J. H., Stalker, H. T., Moyer, J. W., and Hoffman, K. (2002). Evaluation of arachis species for resistance to tomato spotted wilt virus. *Peanut Sci.* 29, 79–84. doi: 10.3146/pnut.29.2.0001

Manni, M., Berkeley, M. R., Seppey, M., and Zdobnov, E. M. (2021). BUSCO: assessing genomic data quality and beyond. *Curr. Protoc.* 1, e323. doi: 10.1002/cpz1.323

Marasigan, K., Toews, M., Kemerait, R., Abney, M. R., Culbreath, A., and Srinivasan, R. (2015). Evaluation of alternatives to carbamate and organophosphate insecticides against thrips and tomato spotted wilt virus in peanut production. *J. Econ. Entomol.* 109, 544–557. doi: 10.1093/jee/tov336

Mi, H., Muruganujan, A., Ebert, D., Huang, X., and Thomas, P. D. (2019). PANTHER version 14: More genomes, a new PANTHER GO-slim and improvements in enrichment analysis tools. *Nucleic Acids Res.* 47, D419–D426. doi: 10.1093/nar/gky1038

Milla, S. R., Isleib, T. G., and Stalker, H. T. (2005). Taxonomic relationships among Arachis sect. Arachis species as revealed by AFLP markers. *Genome* 48, 1–11. doi: 10.1139/G04-089

Mishra, A., Behura, A., Mawatwal, S., Kumar, A., Naik, L., Mohanty, S. S., et al. (2019). Structure-function and application of plant lectins in disease biology and immunity. *Food Chem. Toxicol.* 134, 110827. doi: 10.1016/J.FCT.2019.110827

Moretzsohn, M. C., Gouvea, E. G., Inglis, P. W., Leal-Bertioli, S. C. M., Valls, J. F. M., and Bertioli, D. J. (2013). A study of the relationships of cultivated peanut (Arachis hypogaea) and its most closely related wild species using intron sequences and microsatellite markers. *Ann. Bot.* 111, 113–126. doi: 10.1093/AOB/MCS237

Moury, B., Palloix, A., Gebre Selassie, K., and Marchoux, G. (1997). Hypersensitive resistance to tomato spotted wilt virus in three capsicum chinense accessions is controlled by a single gene and is overcome by virulent strains. *Euphytica* 94, 45–52. doi: 10.1023/A:1002997522379

Noman, A., Liu, Z., Aqeel, M., Zainab, M., Khan, M. I., Hussain, A., et al. (2017). Basic leucine zipper domain transcription factors: the vanguards in plant immunity. *Biotechnol. Lett.* 3912 39, 1779–1791. doi: 10.1007/S10529-017-2431-1

Pandey, M. K., Monyo, E., Ozias-Akins, P., Liang, X., Guimarães, P., Nigam, S. N., et al. (2012). Advances in Arachis genomics for peanut improvement. *Biotechnol. Adv.* 30, 639–651. doi: 10.1016/J.BIOTECHADV.2011.11.001

Pandey, S. P., and Somssich, I. E. (2009). The role of WRKY transcription factors in plant immunity. *Plant Physiol.* 150, 1648–1655. doi: 10.1104/PP.109.138990

Pandey, M. K., Wang, H., Khera, P., Vishwakarma, M. K., Kale, S. M., Culbreath, A. K., et al. (2017). Genetic dissection of novel QTLs for resistance to leaf spots and tomato spotted wilt virus in peanut (Arachis hypogaea L.). *Front. Plant Sci.* 8. doi: 10.3389/FPLS.2017.00025/BIBTEX

Rodríguez-Negrete, E. A., Guevara-Rivera, E. A., Arce-Leal, Á.P., Leyva-López, N. E., and Méndez-Lozano, J. (2023). A novel tomato spotted wilt virus isolate encoding a noncanonical NSm C118F substitution associated with Sw-5 tomato gene resistance breaking. *Mol. Plant Pathol.* 24, 1300–1311. doi: 10.1111/MPP.13371

Rossi, M., Goggin, F. L., Milligan, S. B., Kaloshian, I., Ullman, D. E., and Williamson, V. M. (1998). The nematode resistance gene Mi of tomato confers resistance against the potato aphid. *Proc. Natl. Acad. Sci. U. S. A.* 95, 9750–9754. doi: 10.1073/pnas.95.17.9750

Rotenberg, D., Kumar, N. K. K., Ullman, D. E., Montero-Astúa, M., Willis, D. K., German, T. L., et al. (2009). Variation in Tomato spotted wilt virus titer in Frankliniella occidentalis and its association with frequency of transmission. *Phytopathology* 99, 404–410. doi: 10.1094/PHYTO-99-4-0404

Roux, F., and Bergelson, J. (2016). The genetics underlying natural variation in the biotic interactions of arabidopsis thaliana: the challenges of linking evolutionary genetics and community ecology. *Curr. Top. Dev. Biol.* 119, 111–156. doi: 10.1016/BS.CTDB.2016.03.001

Santana, S. H., and Valls, J. F. M. (2015). Arachis veigae. *Bonplandia* 24, 139–150. doi: 10.30972/bon.242238

Seijo, G. J., Atahuachi, M., Simpson, C. E., and Krapovickas, A. (2021). Arachis inflata: A New B Genome species of Arachis (Fabaceae). *Bonplandia* 30, 169–174. doi: 10.30972/BON.3024942

Seppey, M., Manni, M., and Zdobnov, E. M. (2019). BUSCO: Assessing genome assembly and annotation completeness. *Methods Mol. Biol.* 1962, 227–245. doi: 10.1007/978-1-4939-9173-0_14

Shrestha, A., Champagne, D. E., Culbreath, A. K., Rotenberg, D., Whitfield, A. E., and Srinivasan, R. (2017). Transcriptome changes associated with Tomato spotted wilt virus infection in various life stages of its thrips vector, Frankliniella fusca (Hinds). *J. Gen. Virol.* 98, 2156–2170. doi: 10.1099/jgv.0.000874

Shrestha, A., Srinivasan, R., Riley, D. G., and Culbreath, A. K. (2012). Direct and indirect effects of a thrips-transmitted Tospovirus on the preference and fitness of its vector, Frankliniella fusca. *Entomol. Exp. Appl.* 145, 260–271. doi: 10.1111/EEA.12011

Shrestha, A., Srinivasan, R., Sundaraj, S., Culbreath, A. K., and Riley, D. G. (2013). Second generation peanut genotypes resistant to thrips-transmitted tomato spotted wilt virus exhibit tolerance rather than true resistance and differentially affect thrips fitness. *J. Econ. Entomol.* 106, 587–596. doi: 10.1603/EC12430

Shrestha, A., Sundaraj, S., Culbreath, A. K., Riley, D. G., Abney, M. R., and Srinivasan, R. (2015). Effects of thrips density, mode of inoculation, and plant age on tomato spotted wilt virus transmission in peanut plants. *Environ. Entomol.* 44, 136–143. doi: 10.1093/EE/NVU013

Simão, F. A., Waterhouse, R. M., Ioannidis, P., Kriventseva, E. V., and Zdobnov, E. M. (2015). BUSCO: assessing genome assembly and annotation completeness with single-copy orthologs. *Bioinformatics* 31, 3210–3212. doi: 10.1093/BIOINFORMATICS/BTV351

Simpson, C. E. (1991). Pathways for Introgression of Pest Resistance into Arachis hypogaea L. *Peanut Sci.* 18, 22–26. doi: 10.3146/I0095-3679-18-1-8

Slater, G. S. C., and Birney, E. (2005). Automated generation of heuristics for biological sequence comparison. *BMC Bioinf.* 6, 1–11. doi: 10.1186/1471-2105-6-31

Song, J., Bradeen, J. M., Naess, S. K., Raasch, J. A., Wielgus, S. M., Haberlach, G. T., et al. (2003). Gene RB cloned from Solanum bulbocastanum confers broad spectrum resistance to potato late blight. *Proc. Natl. Acad. Sci. U. S. A.* 100, 9128–9133. doi: 10.1073/PNAS.1533501100

Srinivasan, R., Abney, M. R., Culbreath, A. K., Kemerait, R. C., Tubbs, R. S., Monfort, W. S., et al. (2017). Three decades of managing Tomato spotted wilt virus in peanut in southeastern United States. *Virus Res.* 241, 203–212. doi: 10.1016/J.VIRUSRES.2017.05.016

Srinivasan, R., Abney, M. R., Lai, P. C., Culbreath, A. K., Tallury, S., and Leal-Bertioli, S. C. M. (2018). Resistance to thrips in peanut and implications for management of thrips and thrips-transmitted orthotospoviruses in peanut. *Front. Plant Sci.* 871. doi: 10.3389/FPLS.2018.01604/BIBTEX

Stalker, H. T. (2017). Utilizing wild species for peanut improvement. *Crop Sci.* 57, 1102–1120. doi: 10.2135/CROPSCI2016.09.0824

Stalker, H. T., and Campbell, W. V. (1983). Resistance of wild species of peanut to an insect complex1. *Peanut Sci.* 10, 30–33. doi: 10.3146/i0095-3679-10-1-9

Stevens, M. R., Scott, S. J., and Gergerich, R. C. (1991). Inheritance of a gene for resistance to tomato spotted wilt virus (TSWV) from Lycopersicon Peruvianum Mill. *Euphytica* 59, 9–17. doi: 10.1007/BF00025356

Sundaraj, S., Srinivasan, R., Culbreath, A. K., Riley, D. G., and Pappu, H. R. (2014). Host Plant Resistance Against Tomato spotted wilt virus in Peanut (Arachis hypogaea) and Its Impact on Susceptibility to the Virus, Virus Population Genetics, and Vector Feeding Behavior and Survival. *Virology* 104, 202–210. doi: 10.1094/PHYTO-04-13-0107-R

Supek, F., Bošnjak, M., Škunca, N., and Šmuc, T. (2011). Revigo summarizes and visualizes long lists of gene ontology terms. *PloS One* 6, e21800. doi: 10.1371/journal.pone.0021800

Takabatake, R., Karita, E., Seo, S., Mitsuhara, I., Kuchitsu, K., and Ohashi, Y. (2007). Pathogen-induced calmodulin isoforms in basal resistance against bacterial and fungal pathogens in tobacco. *Plant Cell Physiol.* 48, 414–423. doi: 10.1093/pcp/pcm011

Tao, H., Jia, Z., Gao, X., Gui, M., Li, Y., and Liu, Y. (2022). Analysis of the miRNA expression profile involved in the tomato spotted wilt orthotospovirus–pepper interaction. *Virus Res.* 312, 198710. doi: 10.1016/j.virusres.2022.198710

Tseng, Y. C., Tillman, B. L., Peng, Z., and Wang, J. (2016). Identification of major QTLs underlying tomato spotted wilt virus resistance in peanut cultivar Florida-EPTM "113.". *BMC Genet.* 17, 1–14. doi: 10.1186/s12863-016-0435-9

Ullman, D. E. (1992). A midgut barrier to tomato spotted wilt virus acquisition by adult western flower thrips. *Phytopathology* 82, 1333. doi: 10.1094/phyto-82-1333

Valls, J. F. M., Da Costa, L. C., and Custódio, A. R. (2013). A novel trifoliolate species of Arachis (Fabaceae) and further comments on taxonomic section Trierectoides. *Bonplandia* 22, 91–97. doi: 10.30972/bon.2211257

Valls, J. F. M., and Simpson, C. E. (2005). New species of arachis (Leguminosae) from Brazil, Paraguay and Bolivia. *Bonplandia* 14, 35–63. doi: 10.30972/bon.141-21387

Valls, J. F. M., and Simpson, C. E. (2017). A new species of Arachis (Fabaceae) from Mato Grosso, Brazil, related to Arachis matiensis. *Bonplandia* 26, 143–149. doi: 10.30972/bon.2622575

Van Der Vossen, E., Sikkema, A., Te Lintel Hekkert, B., Gros, J., Stevens, P., Muskens, M., et al. (2003). An ancient R gene from the wild potato species Solanum bulbocastanum confers broad-spectrum resistance to Phytophthora infestans in cultivated potato and tomato. *Plant J.* 36, 867–882. doi: 10.1046/j.1365-313X.2003.01934.x

Whitham, S., Dinesh-Kumar, S. P., Choi, D., Hehl, R., Corr, C., and Baker, B. (1994). The product of the tobacco mosaic virus resistance gene N: Similarity to toll and the interleukin-1 receptor. *Cell* 78, 1101–1115. doi: 10.1016/0092-8674(94)90283-6

Wu, T. D., Reeder, J., Lawrence, M., Becker, G., and Brauer, M. J. (2016). GMAP and GSNAP for genomic sequence alignment: Enhancements to speed, accuracy, and functionality. *Methods Mol. Biol.* 1418, 283–334. doi: 10.1007/978-1-4939-3578-9_15

Wu, X., Zhang, X., Wang, H., Fang, R. X., and Ye, J. (2023). Structure–function analyses of coiled-coil immune receptors define a hydrophobic module for improving plant virus resistance. *J. Exp. Bot.* 74, 1372–1388. doi: 10.1093/jxb/erac477

Xu, L., Dong, Z., Fang, L., Luo, Y., Wei, Z., Guo, H., et al. (2019). OrthoVenn2: a web server for whole-genome comparison and annotation of orthologous clusters across multiple species. *Nucleic Acids Res.* 47, W52–W58. doi: 10.1093/NAR/GKZ333

Yilmaz, P., Parfrey, L. W., Yarza, P., Gerken, J., Pruesse, E., Quast, C., et al. (2014). The SILVA and "all-species Living Tree Project (LTP)" taxonomic frameworks. *Nucleic Acids Res.* 42, D643–D648. doi: 10.1093/nar/gkt1209

Yu, C. K. Y., Springob, K., Schmidt, J., Nicholson, R. L., Chu, I. K., Wing, K. Y., et al. (2005). A stilbene synthase gene (SbSTS1) is involved in host and nonhost defense responses in orghum. *Plant Physiol.* 138, 393–401. doi: 10.1104/PP.105.059337

Zhang, C., Xie, W., Fu, H., Chen, Y., Chen, H., Cai, T., et al. (2023). Whole genome resequencing identifies candidate genes and allelic diagnostic markers for resistance to Ralstonia solanacearum infection in cultivated peanut (Arachis hypogaea L.). *Front. Plant Sci.* 13. doi: 10.3389/fpls.2022.1048168

Zhao, L., Hu, Z., Li, S., Zhang, L., Yu, P., Zhang, J., et al. (2020). Tagitinin A from Tithonia diversifolia provides resistance to tomato spotted wilt orthotospovirus by inducing systemic resistance. *Pestic. Biochem. Physiol.* 169, 104654. doi: 10.1016/J.PESTBP.2020.104654

Zhao, Z., Tseng, Y. C., Peng, Z., Lopez, Y., Chen, C. Y., Tillman, B. L., et al. (2018). Refining a major QTL controlling spotted wilt disease resistance in cultivated peanut (Arachis hypogaea L.) and evaluating its contribution to the resistance variations in peanut germplasm. *BMC Genet.* 19. doi: 10.1186/S12863-018-0601-3

Zhao, L., Zhang, L., Hu, Z., Li, B., Zheng, X., Qiu, R., et al. (2022). Tomato zonate spot virus induced hypersensitive resistance *via* an auxin-related pathway in pepper. *Gene* 823. doi: 10.1016/j.gene.2022.146320

frontiers | Frontiers in Microbiology

TYPE Original Research
PUBLISHED 15 November 2023
DOI 10.3389/fmicb.2023.1285796

OPEN ACCESS

EDITED BY
Takashi Osanai,
Meiji University, Japan

REVIEWED BY
Pau Loke Show,
University of Nottingham Malaysia Campus, Malaysia
Jisheng Li,
Northwest A&F University, China

*CORRESPONDENCE
Shenkui Liu
✉ shenkuiliu@nefu.edu.cn
Xuejiao Jin
✉ jinxuejiao1991@cau.edu.cn

RECEIVED 04 September 2023
ACCEPTED 31 October 2023
PUBLISHED 15 November 2023

CITATION
Qiu J, Zhang J, Zhao H, Wu C, Jin C, Hu X, Li J, Cao X, Liu S and Jin X (2023) Cellulose and *JbKOBITO 1* mediate the resistance of $NaHCO_3$-tolerant chlorella to saline-alkali stress.
Front. Microbiol. 14:1285796.
doi: 10.3389/fmicb.2023.1285796

Cellulose and *JbKOBITO 1* mediate the resistance of $NaHCO_3$-tolerant chlorella to saline-alkali stress

Jiale Qiu, Jie Zhang, Huihui Zhao, Cuiping Wu, Caoliang Jin, Xiangdong Hu, Jian Li, Xiuling Cao, Shenkui Liu* and Xuejiao Jin*

State Key Laboratory of Subtropical Silviculture, School of Forestry and Biotechnology, Zhejiang A&F University, Hangzhou, China

Carbonate stress has profound impacts on both agricultural and industrial production. Although a number of salinity-tolerant genes have been reported and applied in plants, there is a lack of research on the role of cell wall-related genes in resistance to carbonate. Likewise, in industry, current strategies have not been able to more effectively address the conflict between stress-induced microalgal biofuel accumulation and microalgal growth inhibition. It is of great significance to study the adaptation mechanism of carbonate-tolerant organisms and to explore related genes for future genetic modification. In this study, the role of the cell wall in the $NaHCO_3$-tolerant chlorella JB17 was investigated. We found that JB17 possesses a relatively thick cell wall with a thickness of 300–600 nm, which is much higher than that of the control chlorella with a thickness of about 100 nm. Determination of the cell wall polysaccharide fractions showed that the cellulose content in the JB17 cell wall increased by 10.48% after $NaHCO_3$ treatment, and the decrease in cellulose levels by cellulase digestion inhibited its resistance to $NaHCO_3$. Moreover, the saccharide metabolome revealed that glucose, rhamnose, and trehalose levels were higher in JB17, especially rhamnose and trehalose, which were almost 40 times higher than in control chlorella. Gene expression detection identified an up-regulated expressed gene after $NaHCO_3$ treatment, *JbKOBITO1*, overexpression of which could improve the $NaHCO_3$ tolerance of *Chlamydomonas reinhardtii*. As it encodes a glycosyltransferase-like protein that is involved in cellulose synthesis, the strong tolerance of JB17 to $NaHCO_3$ may be partly due to the up-regulated expression of *JbKOBITO 1* and *JbKOBITO 1*-mediated cellulose accumulation. The above results revealed a critical role of cellulose in the $NaHCO_3$ resistance of JB17, and the identified $NaHCO_3$-tolerance gene will provide genetic resources for crop breeding in saline-alkali soils and for genetic modification of microalgae for biofuel production.

KEYWORDS

algae, cell wall, *Chlamydomonas reinhardtii*, JB17, saccharide metabolism

1. Introduction

Carbonate is an important limiting factor for biological growth and for the development of industry and agriculture. On the one hand, carbonate stress not only causes ionic toxicity and osmotic stress, but also further increase the pH of saline-alkaline soils, which seriously affects crop growth and yield (Wang Y. et al., 2020). On the other hand, microalgae, as a potential

feedstock for biofuel production (Khoo et al., 2020), has been limited in the commercialisation of microalgae biofuels due to the contradiction between microalgal growth under environmental stress (including carbonate stress) and biofuel accumulation (Ji et al., 2018). Therefore, it is of great significance to study the tolerance mechanism of organisms to carbonate stress and excavate carbonate-tolerant genes to improve the tolerance in plants and industrial microbial strains.

Current research on saline–alkali soils has screened a number of carbonate-tolerant plant resources, with the more familiar ones including *Suaeda corniculata*, *Puccinellia tenuiflora*, oats, etc. (Pang et al., 2016; Bai et al., 2018; Qin et al., 2018; Ye et al., 2019). A range of genes for carbonate tolerance have also been reported. For instance, *SlWRKY28*, a gene cloned from the WRKY family of *Salix linearistipular*, improves the saline-alkali tolerance of transgenic lines by inducing regulatory responses of enzyme genes in the reactive oxygen scavenging pathway (Wang X. et al., 2020). Zheng et al. (2021) reported that *CrPIP23*, a membrane Aquaporins (AQPs) protein gene from *Canavalia rosea*, enhanced alkaline tolerance of transgenic plants by promoting water transport. Liu et al. (2020) reported that a chitinase gene *LcCHI2* from *Leymus chinensis* helped reduce osmotic stress other than Na^+ ion toxicity or improved water-use-efficiency, improves salt-alkali tolerance in transgenic maize. However, the cell wall, as the first barrier against stress, and its regulatory gene, which has been extensively studied in plant resistance to salt and cadmium stress in recent years (Jia et al., 2021; Dabravolski and Isayenkov, 2023), has not been strongly implicated in resistance to carbonate stress.

Carbonate stress also limits the growth of certain engineered strains for biofuel production. In the industrial field, microalgae are regarded as an important resource for biofuel production. Previous study reported that many environmental stress conditions can promoted cell wall thinning and significantly increased lipid production in *Chlorella vulgaris* (Nadzir et al., 2023). For example, the study by Li et al. (2018) reported that treatment with high concentrations of $NaHCO_3$ (160 mM) stimulated the accumulation of *Chlorella vulgaris* lipids, but inhibited cell growth. Therefore, the conflict, between the use of stress to promote biofuel accumulation and stress-induced microbial growth inhibition, limits the industrial production of biofuels in large quantities. Although certain study has reported that product content can be effectively increased by two-stage cultivation of algae, it is simpler and more effective to search for carbonate-tolerant genes and apply them to improve stress resistance (Yun et al., 2019). A recent review summarised the use of genetic modification strategies to improve lipid production in microalgae but these studies have focused on genes that promote lipid synthesis in microalgae (Khoo et al., 2023). Since many genes in algae can be involved in stress response (Hong et al., 2023), the mining of carbonate-tolerant genes is important to optimise the balance between microalgal growth and lipid accumulation.

JB17, is a member of the *Nannochloris* species that we previously isolated from extremely saline-alkali soil in northeastern China. It showed higher tolerance to NaCl and $NaHCO_3$, surviving in $NaHCO_3$ medium at concentrations up to 1 M (Qiao et al., 2015). JB17, as a eukaryotic microalga, is a unicellular microorganism with both plant and microbial properties. Specifically, it has a structure similar to plant cells, such as a nucleus, chloroplasts and mitochondria, as well as other organelles surrounded by cell membranes, which enable it to photosynthesise to produce high-value bioactive substances (Khoo et al., 2023). In addition, its characteristic of rapid microbial growth enables the response to carbonate stress to be observed in a short period of time, and the unicellular structure makes it easier to study its physiological and molecular responses at the cellular level. Therefore, studying the mechanism of JB17 $NaHCO_3$ tolerance and identifying carbonate-tolerant genes will not only benefit agricultural development but also the commercialisation of microalgal biofuels.

In this study, we analyzed the changes in the composition of the cell wall of the saline-alkali tolerant JB17 before and after $NaHCO_3$ exposure, and identified a key cell wall gene involved in resistance to $NaHCO_3$ through transcriptome analysis and transgenic experiments. Our results not only revealed the mechanism of $NaHCO_3$ tolerance in JB17, but also the identified cell wall-related gene would provide valuable genetic resources for agricultural and industrial production.

2. Materials and methods

2.1. Microalgae strains and culture conditions

The control chlorella (*Chlorella variabilis*) and *Chlamydomonas reinhardtii* were obtained from the Freshwater Algae Culture Collection (Institute of Hydrobiology, Chinese Academy of Science, Wuhan, China). The saline-alkali-tolerant *Chlorella* JB17 was previously isolated from extremely alkaline-saline soil (pH > 10) from the Songnen Plain (46°27′N, 125°22′E, Heilongjiang Province, China) (Qiao et al., 2015). For algal growth, JB17 and *C. variabilis* were cultured using Blue-Green Medium (BG11) medium, while *C. reinhardtii* was cultured using Tris-Acetate-Phosphate (TAP) medium. The medium was prepared according to the information provided by the Freshwater Algae Culture Collection at the Institute of Hydrobiology (http://algae.ihb.ac.cn/, accessed on 5 March 2023). All algae were cultured at 23 ± 1°C, with illumination at 40 μM photons m^{-1} s^{-1} under 16 h light/8 h dark photoperiod (Wang M. et al., 2020).

2.2. Transmission electron microscopy

Transmission electron microscopy (TEM) was performed according to previously described methods (Jin et al., 2018). 15 mL algae culture in logarithmic growth phase (at approximately 0.5×10^8 cells/mL) were collected and centrifugated at 800 g for 10 min, and fixed overnight at 4°C in 1 mL fixation buffer (2.5% glutaraldehyde, 0.05 M phosphate, pH 7.2). The glutaraldehyde-fixed algae were washed three times with fixation buffer and then fixed in 2% osmium tetroxide (OsO_4) at 4°C for 2 h in the dark. Then the algae were dehydrated through a series of graded ethanol (70, 80, 90, 95, and 100%) for 10 min each time, and then embedded in Spurr's resin. Ultrathin sections (70 nm) were cut with an ultramicrotome (EM UC7; Leica, Germany) and sequentially stained with uranyl acetate for 20 min and Reynolds' lead citrate for 5 min. The specimens were observed using a Hitachi H-7650 (Hitachi, Japan) or a JEM-1230 (JEOL Co. Ltd., Japan) transmission electron microscope operated at 80 kV.

2.3. Plasmid construction

Firstly, total RNA was extracted from JB17, and mRNA was reverse transcribed into cDNA using M-MLV reverse transcription kit (Thermo Fisher, Shanghai, China). The full-length coding sequence (CDS) of *JbKOBITO 1* was amplified from cDNA and inserted into the *Hpa* I-linearized plasmid pLM006 by homologous recombination methods to generate a vector for electro-transformation of *C. reinhardtii*. The pLM006 plasmid was expressed under the control of the PASD promoter, and mCherry protein was expressed at the C-terminus of the target gene. The primers used for plasmid construction are listed in Supplementary Table S1. The correctness of the plasmid was verified by DNA sequencing.

2.4. Expression analysis of *JbKOBITO 1*

The expression changes of *JbKOBITO 1* before and after $NaHCO_3$ treatment were detected by RT–qPCR as described previously (Li et al., 2023). The primers used are listed in Supplementary Table S1.

2.5. Nuclear transformation of *Chlamydomonas reinhardtii* by electroporation

The generation of transgenic algae lines overexpressing *JbKOBITO 1* was performed as described previously (Li et al., 2023). After the colonies had grown, different primers were designed to identify the mcherry fusion fluorescent protein gene, the PASD promoter and the target gene by PCR, to obtain the positive strains into which the plasmid had been successfully transferred. Three overexpression lines were analyzed for their $NaHCO_3$ tolerance, and the results showed the same trends.

2.6. Cell wall component extraction and detection

Log-phase cells were aspirated and added to a modified TAP liquid medium containing 0 mM and 300 mM $NaHCO_3$ for 3 days. Then, the cells were cultured in the dark for 12 h to consume starch before being rapidly frozen in liquid nitrogen, after which the cells were disrupted to obtain the cell wall by milling using a steel bead and FastPrep-24™ 5G bead-beating grinder (MP Biomedicals, United States). All the cells were examined under a microscope for disruption to ensure that the cell wall preparation was as clean as possible. The cell samples were added to 80% (vol/vol) ethanol, extracted on ice and the supernatant was removed by centrifugation. This was repeated until a clean sample was obtained. Samples were then extracted with acetone for 10 min at room temperature, and the supernatant was removed by centrifugation. Methanol was extracted for 10 min, and the supernatant was removed by centrifugation to obtain the final white substance as a cell wall. The samples were dried in an oven, the weights were recorded, and the dried cell walls were sent to Wuhan ProNets Biotechnology Co., Ltd. (Wuhan, China, http://www.pronetsbio.com, accessed on 20 March 2023) for detection. The experiments were repeated three times.

2.7. Cell wall saccharide metabolome detection

Chlorella variabilis and JB17 were cultivated in BG11 for 7 days, and then diluted to the fresh BG11 medium with 0 mM or 300 mM $NaHCO_3$, respectively. After 3 days of treatment, the cells were treated in the dark for 12 h to consume starch before collection, and then sent to Wuhan Metwell Biotechnology Co., Ltd. (Wuhan, China, http://www.metware.cn, accessed on 25 March 2023) for monosaccharide or disaccharide detection.

2.8. Cellulase digestion assays

JB17 was cultured in BG11 liquid medium for 7 days and then were collected by centrifugation. Each gram of algae was treated with 0, 50 and 100 U cellulase (Solarbio, Beijing, China) for 3 days. The cultures with a cell density of approximately 1×10^8 cells/mL, were then gradient diluted in 96-well plates with sterile water and 4 μL of the dilutions were spotted in modified BG11 solid medium supplemented with 0, 50 and 100 mM $NaHCO_3$, respectively. After 16 days of culture, algal growth was observed.

2.9. Determination of $NaHCO_3$ tolerance of transgenic *Chlamydomonas reinhardtii*

Log-phase *C. reinhardtii* cells (at approximately 0.5×10^8 cells/mL) were collected, serially diluted and spotted onto the modified TAP solid medium containing 0 or 40 mM $NaHCO_3$, respectively. After growth for about 10 days, algal growth was observed. For the growth curve determination, the log-phase *C. reinhardtii* cells were diluted to an OD_{680} of 0.15 in TAP medium containing 0 mM, 35 mM, and 40 mM $NaHCO_3$, respectively, and the cell density of the cultures was determined using a spectrophotometer (Ultrospec 2,100 Pro, Biochrom, St. Albans, UK), at different time points from 0 to 120 h.

2.10. Accession numbers

Sequence data of glycosyltransferase-like KOBITO 1 from different organisms in this work can be found in NCBI under the following accession number: *Nannochloris* sp. JB17 (OR486971), *Arabidopsis thaliana* (NP187467.1), *Chlorella vulgaris* (KAI3434462.1), *Micractinium conductrix* (PSC67501.1), *Chlorella variabilis* (XP005843966.1), *Chlorella sorokiniana* (PRW20664.1), *Coccomyxa* sp. Obi (BDA46538.1), *Oryza sativa* Japonica Group (NP001393036), and *Capsicum annuum* (PHT71472.1).

3. Result

3.1. *Nannochloris* sp. JB17 has a more stable ultrastructure under $NaHCO_3$ stress compared to the control

In order to study the ultrastructural changes of JB17 before and after treatment with high concentrations of $NaHCO_3$, the morphology

was observed using TEM. It showed that under normal conditions, the control chlorella and JB17 had intact cellular structures (Figures 1A,B). Interestingly, the cell wall of JB17 was thicker, with a thickness of about 300–600 nm, while that of the control chlorella was only about 100 nm thick (Figures 1A,B). After 300 mM $NaHCO_3$ treatment, the cell wall morphology of JB17 was similar to that before stress, whereas the cell wall of the control chlorella was deformed and damaged, and the internal structure of the cell was affected to some extent (Figures 1C,D). These results suggest that the stable and thick cell walls of JB17 may be involved in its tolerance to high concentrations of $NaHCO_3$.

3.2. Changes in JB17 cell wall composition before and after $NaHCO_3$ treatment

The composition of cell wall polymers usually determines the cell wall structure. Plant cell walls are mainly composed of cellulose, hemicellulose, pectin, and lignin (Lampugnani et al., 2018). Many studies have reported that changes in these components are involved in plant resistance to salt stress (Dabravolski and Isayenkov, 2023), but the role of these components in resistance to carbonate stress is unclear. Therefore, in order to elucidate the changes in JB17 cell wall components in response to $NaHCO_3$ stress, the contents of major polysaccharide components including cellulose, hemicellulose, lignin, and pectin of JB17 cell walls before and after $NaHCO_3$ treatment were measured. When exposed to 300 mM $NaHCO_3$, the levels of all four components changed, with the exception of lignin, which did not change significantly (Table 1). Of these, cellulose content was the highest as a percentage of dry weight and showed the greatest percentage change in response to $NaHCO_3$ treatment. The cellulose content was significantly increased by 10.48% compared to that of 0 mM $NaHCO_3$ (Table 1). These results suggest that JB17 may adapt to $NaHCO_3$ stress by altering the polysaccharide composition of the cell wall.

3.3. Cellulose content affects JB17 tolerance to $NaHCO_3$

Previous study has found that the cell wall cellulose content of rice increased by 10.64% under drought stress, thereby enhancing the drought tolerance of rice (Sun et al., 2022). Therefore, we followed up with a cellulase digestion assay to test whether the accumulated cellulose in JB17 cell wall is critical for $NaHCO_3$ tolerance. Under the treatment of different concentrations of cellulase, there were no significant differences in the growth of JB17 on 0 and 50 mM $NaHCO_3$ plates, indicating that cellulase digestion did not affect the normal growth of algae (Figure 2). When JB17 was grown on 100 mM $NaHCO_3$ plates, the growth of 50 U/g cellulase-treated algae showed a

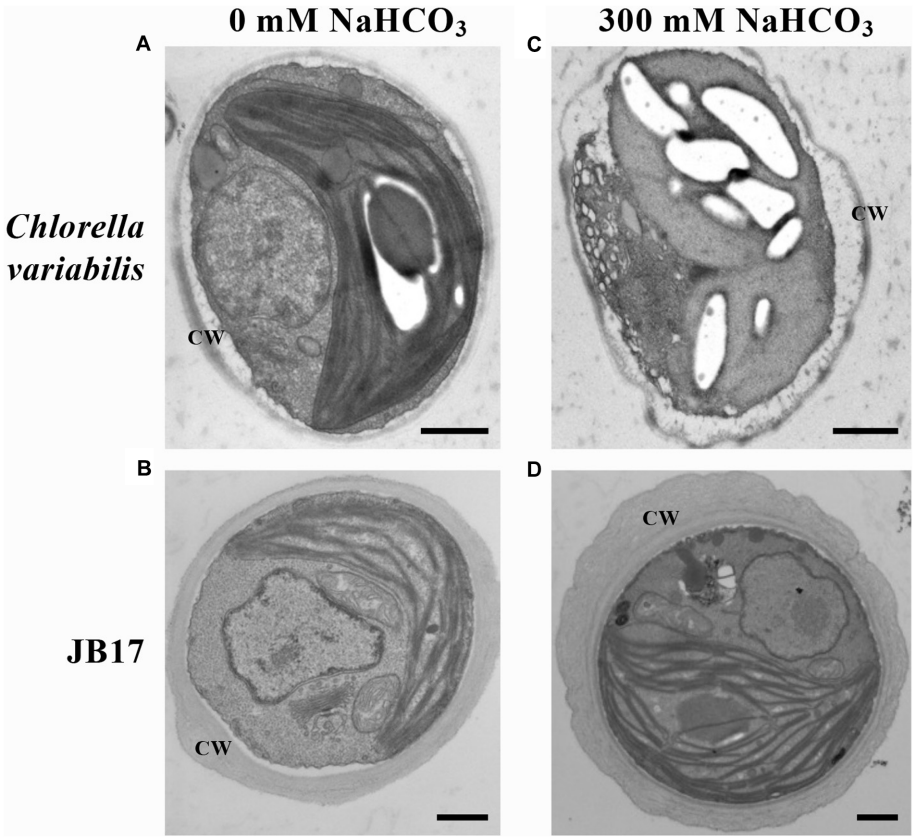

FIGURE 1
Electron microscopic visualization of *C. variabilis* and JB17 exposed to $NaHCO_3$ stress. **(A,B)** Untreated *C. variabilis* and JB17 were used as controls. **(C,D)** Representative images of the ultrastructure of *C. variabilis* and JB17 treated with $NaHCO_3$. CW, cell wall; scale bars, 500 nm.

10.3389/fmicb.2023.1285796

TABLE 1 Changes in polysaccharides in JB17 cell walls exposed to $NaHCO_3$ stress.

Constituent	Content (mg/g)				Ralative content
	0 mM $NaHCO_3$	Mean ± SD	300 mM $NaHCO_3$	Mean ± SD	
Cellulose	340.82	341.35 ± 4.37	371.32	377.14 ± 5.07	110.48%**
	337.27		379.55		
	345.96		380.56		
Hemicellulose	254.45	250.71 ± 5.09	229.79	233.49 ± 4.72	93.13%*
	244.91		231.87		
	252.78		238.80		
Lignin	78.33	76.68 ± 2.69	79.78	79.34 ± 0.95	103.47%$^{ns.}$
	73.57		78.25		
	78.13		79.98		
Protopectin	2.02	2.02 ± 0.03	1.84	1.85 ± 0.01	91.58%**
	1.99		1.86		
	2.04		1.86		
Soluble pectin	2.02	2.00 ± 0.02	1.79	1.81 ± 0.02	90.50%**
	1.99		1.83		
	1.98		1.82		

ns., no significant difference; **, $p < 0.01$, *, $0.01 < p < 0.05$, Student's *t*-test.

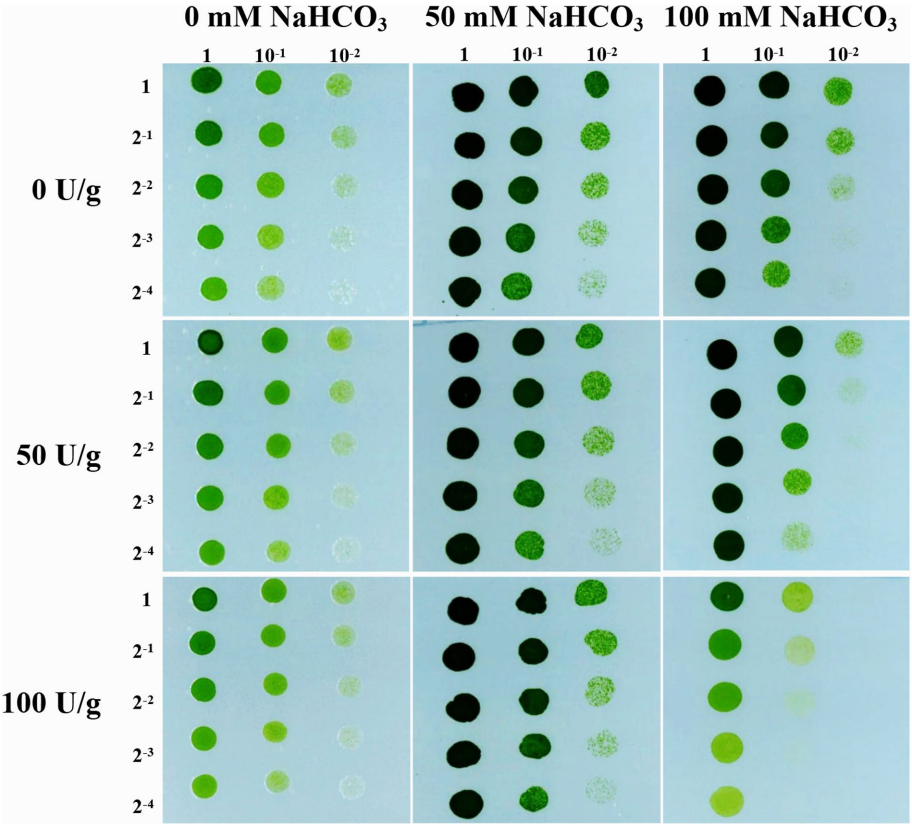

FIGURE 2
Cellulose content affects JB17 tolerance to $NaHCO_3$. The treatment without cellulase addition was used as control. Each treatment was carried out in three biological replicates. The numbers labelled in the figure are the dilution multiples for the gradient dilution assays.

slight degree of inhibition, and the growth defects were more pronounced when the concentration of cellulase reached 100 U/g (Figure 2). In addition, the results of cellulose content determination showed that the cellulose content of JB17 cell wall decreased significantly by 18.472% after 100 U/g cellulase treatment (Supplementary Figure S1). These results indicate that the decrease in cellulose content of JB17 affects its tolerance to high concentrations of $NaHCO_3$ stress, which confirms our hypothesis that $NaHCO_3$-induced cellulose accumulation in the cell wall contributes to the tolerance of JB17 to $NaHCO_3$.

3.4. Effect of $NaHCO_3$ on saccharide metabolism in JB17

Metabolites are downstream products of the genome and final products (Qiu et al., 2023). They reflect the final changes in biological systems when they are subjected to genetic and environmental alterations (Alawiye and Babalola, 2021). Changes in cell wall polysaccharides are closely related to saccharide metabolism. Therefore, we further studied the changes in saccharide metabolism in JB17 before and after $NaHCO_3$ treatment. We determined nine monosaccharide and disaccharide components in *C. variabilis* without $NaHCO_3$ treatment, and JB17 treated with 0 mM, 100 mM, and 300 mM $NaHCO_3$, including galactose, fucose, sucrose, glucose, inositol, xylitol, maltose, rhamnose, and trehalose. Under untreated $NaHCO_3$ conditions, sucrose was the major component of both JB17 and the control chlorella, and galactose, fucose, xylitol, and sucrose were lower in JB17 cell walls than the control chlorella. In contrast, glucose, rhamnose, and trehalose in JB17 were higher, especially rhamnose and trehalose, which were nearly 40-fold higher than the control chlorella (Figure 3). After $NaHCO_3$ treatment, the sucrose in JB17 did not change significantly, while other eight saccharide components, including galactose, fucose, glucose, inositol, xylitol, maltose, rhamnose, and trehalose, showed significant decreases, among which rhamnose and trehalose showed the most significant changes with a decrease of about 100-fold (Figure 3). These saccharide fractions were able to undergo significant changes in response to $NaHCO_3$, and their metabolic processes may be involved in the cell wall polysaccharide changes and $NaHCO_3$ adaptation in JB17.

3.5. $NaHCO_3$ stress induces up-regulation of *JbKOBITO 1* expression

To search for key genes that respond to $NaHCO_3$ stress and improve $NaHCO_3$ tolerance, we analyzed the transcriptome sequencing data of JB17 cells after 0 mM and 300 mM $NaHCO_3$ treatment (data not shown). Among the genes whose expressions were up-regulated by 300 mM $NaHCO_3$, a gene involved in saccharide metabolism and related to cell wall synthesis was identified. And a search for its homologous proteins with known functions in the Uniprot protein database (https://www.uniprot.org/, accessed on 15 July 2023) revealed that it shares 55% amino acid sequence identity with the *A. thaliana* glycosyltransferase-like protein KOBITO 1 (Gen Bank NP 187467.1). Therefore, it was tentatively named *JbKOBITO 1*.

The amino acid sequence of the glycosyltransferase-like KOBITO 1 from *Nannochloris* sp. JB17, *C. vulgaris*, *C. variabilis*, *C. sorokiniana*, and *A. thaliana* were analyzed using NCBI Batch CD-search (https://www.ncbi.nlm.nih.gov/Structure/bwrpsb/bwrpsb.cgi, accessed on 15 July 2023). MEME software (https://meme-suite.org/meme/tools/, accessed on 15 July 2023) was used to identify conserved motifs of glycosyltransferase-like KOBITO 1 from different organisms. All these proteins shared a conserved Glyco_tranf_GTA_type superfamily domain (Figure 4A), which is involved in synthesizing and modifying of saccharide molecules. Comparing with JbKOBITO 1 in JB17, the sequences of the homologous proteins in *C. variabilis* and *C. sorokiniana* were much shorter in size, and the homologous protein sequences in *A. thaliana* and *C. vulgaris* were similar in size, but lacked the motif 7, 8, 9, 10, 12 in *A. thaliana* (Figure 4B).

Evolutionary tree was constructed using MEGA 11 software. It was clear that the evolutionary relationship between JbKOBITO 1 and *C. vulgaris* hypothetical protein (D9Q98_002539) was close (Figure 4C). Sequence alignment was performed using the software Jalview (http://www.jalview.org/, accessed on 16 July 2023), and Muscle with Defaults was selected to align. Some highly conserved sites were found (Supplementary Figure S2). Therefore, JbKOBIOT 1 may have a similar function to the *Arabidopsis* glycosyltransferase-like protein KOBITO 1, which is involved in the coordination between cell elongation and cellulose synthesis by promoting the expression of related genes (Pagant et al., 2002). Moreover, to elucidate whether $NaHCO_3$ stress up-regulated the expression of *JbKOBITO 1*, the transcript levels of *JbKOBITO 1* were tested by RT-qPCR. And the results showed that *JbKOBITO 1* was significantly up-regulated in the context of 300 mM $NaHCO_3$ treatment, which was consistent with the results of the transcriptome (Figure 4D). It prompted us to speculate that the $NaHCO_3$-induced up-regulation of *JbKOBITO 1* may be involved in the synthesis of accumulated cellulose in the JB17 cell wall.

3.6. Overexpression of *JbKOBITO 1* improves $NaHCO_3$ tolerance of transgenic *Chlamydomonas reinhardtii*

In order to verify whether *JbKOBITO 1* is involved in $NaHCO_3$ tolerance, the recombinant plasmid expressing *JbKOBITO 1* was electroporated into *C. reinhardtii*. Then, the $NaHCO_3$ tolerance of the positively transformed strains was monitored. Gradient dilution assays showed no significant difference in the growth of *C. reinhardtii* overexpressing the empty vector and overexpressing the target gene on 0 mM $NaHCO_3$ plate, indicating that *JbKOBITO 1* overexpression did not affect the growth of algae (Figure 5A). With the increase of $NaHCO_3$ concentration, the growth of the control was significantly inhibited, whereas the growth of *C. reinhardtii* overexpressing *JbKOBITO 1* was significantly better than that of the control (Figure 5A). Similarly, the sensitivity of transgenic *C. reinhardtii* to different concentrations of $NaHCO_3$ in liquid medium was consistent with the results from gradient dilution assays. The cell density of *C. reinhardtii* expressing the empty vector was not significantly different from that of *C. reinhardtii* expressing *JbKOBITO 1* in the absence of $NaHCO_3$ (Figure 5B). However, at $NaHCO_3$ concentrations of 35 mM, the cell density of *C. reinhardtii* expressing *JbKOBITO 1* was significantly higher than that of the control group from 60 h, with final cell densities (120 h) of 0.903 and 0.740, respectively (Figure 5B). When the concentration of $NaHCO_3$ was 40 mM, the difference was

10.3389/fmicb.2023.1285796

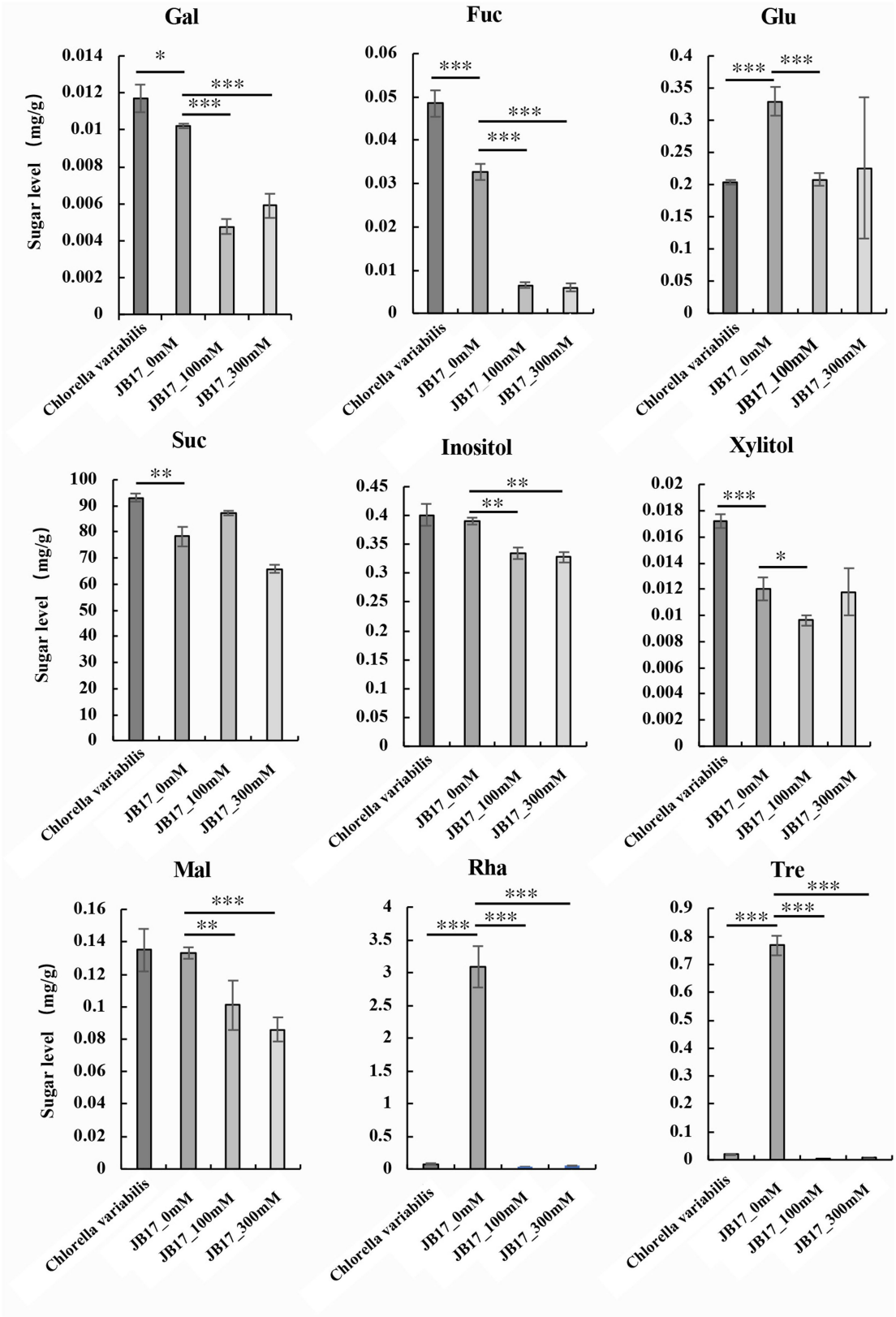

FIGURE 3
Changes in saccharide metabolism in JB17 before and after $NaHCO_3$ treatment. Gal, galactose; Fuc, fucose; Glu, glucose; Suc, sucrose; Mal, maltose; Rha, rhamnose; Tre, trehalose. Error indicates standard deviation (SD) from three independent experiments. ***$p < 0.001$, **$p < 0.01$, *$0.01 < p < 0.05$, Student's *t*-test.

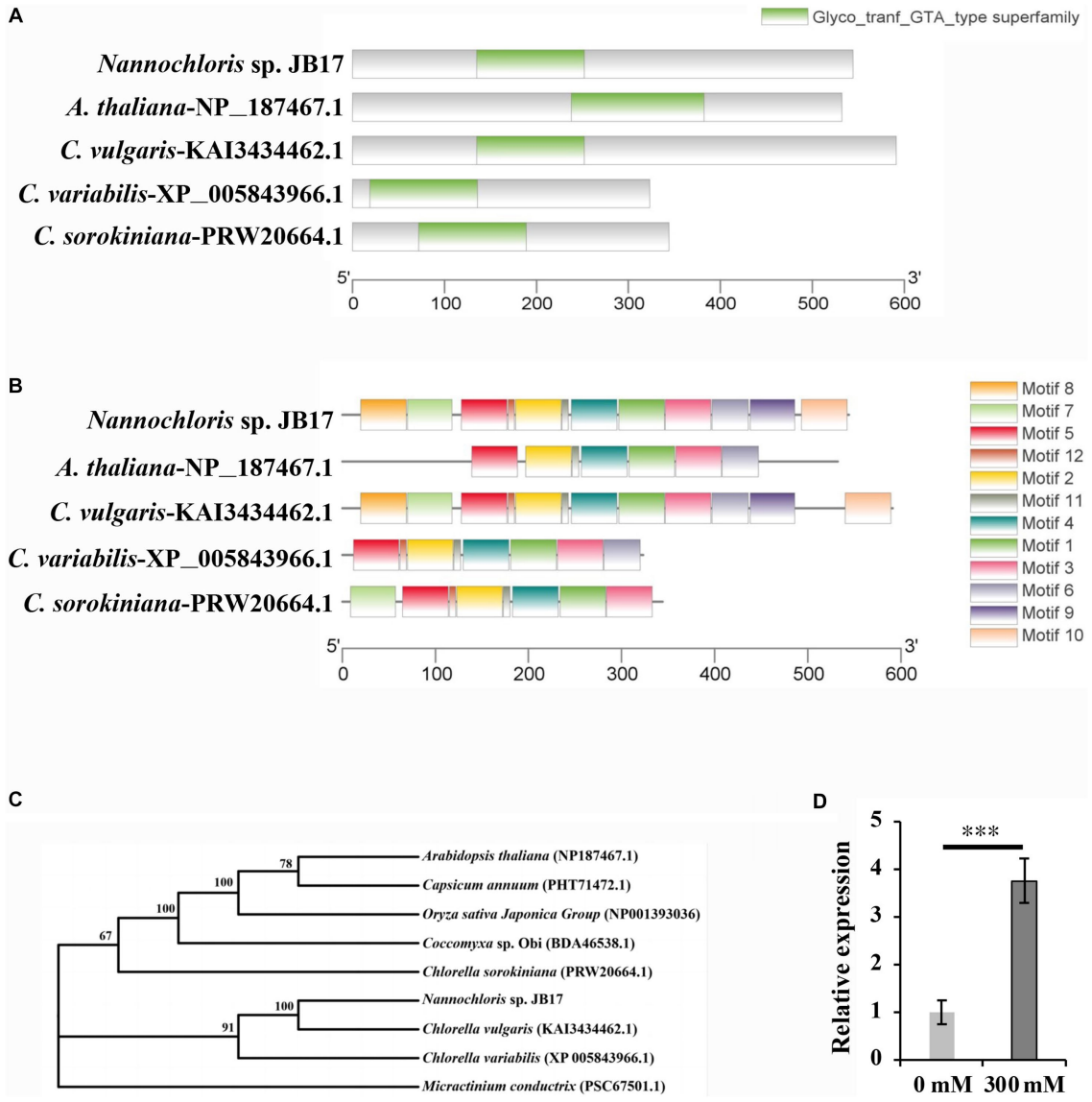

FIGURE 4
Sequence analysis and expression detection of JbKOBITO 1. **(A)** JbKOBITO 1 possesses a conserved Glyco_tranf_GTA_type superfamily domain. **(B)** Conserved motif analysis of glycosyltransferase-like protein KOBITO 1 from algae and *A. thaliana*. The different colored boxes represent different motifs and their position in each protein sequence. All motifs were identified by MEME. **(C)** Neighbor-joining (NJ) phylogenetic relationships of the KOBITO 1 protein from JB17 and predicted homologs from other species or organisms. Bootstrap values were calculated 1,000 times; values <50% are not shown. **(D)** The expression of *JbKOBITO 1* was induced by $NaHCO_3$ treatment. Error bars indicate standard deviation (SD). ***, $p < 0.001$.

more obvious, with final cell densities (120 h) of 0.802 and 0.594, respectively (Figure 5B). These results demonstrated that the introduction of *JbKOBITO 1* into algae could improve the ability of *C. reinhardtii* to resist $NaHCO_3$.

4. Discussion

Plant cell walls play an important role in sensing and responding to stress. Recent studies have suggested that the plant cell wall is highly dynamic, with changes in structure and composition occurring during plant growth and development or in response to abiotic stresses to maintain normal life activities (Le Gall et al., 2015; Jia et al., 2021). In order to investigate the role of the JB17 cell wall in carbonate tolerance, we first observed its ultrastructure by TEM, and found that it has a thicker cell wall than the control chlorella, and the morphology and structure of the cell are still stable under the high concentration of carbonate stress. Previous studies have found that salt-adapted cells of *A. thaliana* acquire a thicker cell wall structure than control cells, which physically strengthens the cells, provides better mechanical strength, reduces salt ion invasion and enhances tolerance to salt stress (Chun et al., 2019). Nadzir et al. (2023) also found that the cell wall thickness of *Chlorella vulgaris* increased from 175 nm to 321 nm at higher salt salinity. Therefore, the ability of JB17 to tolerate high concentrations of $NaHCO_3$ may be closely related to its cell wall.

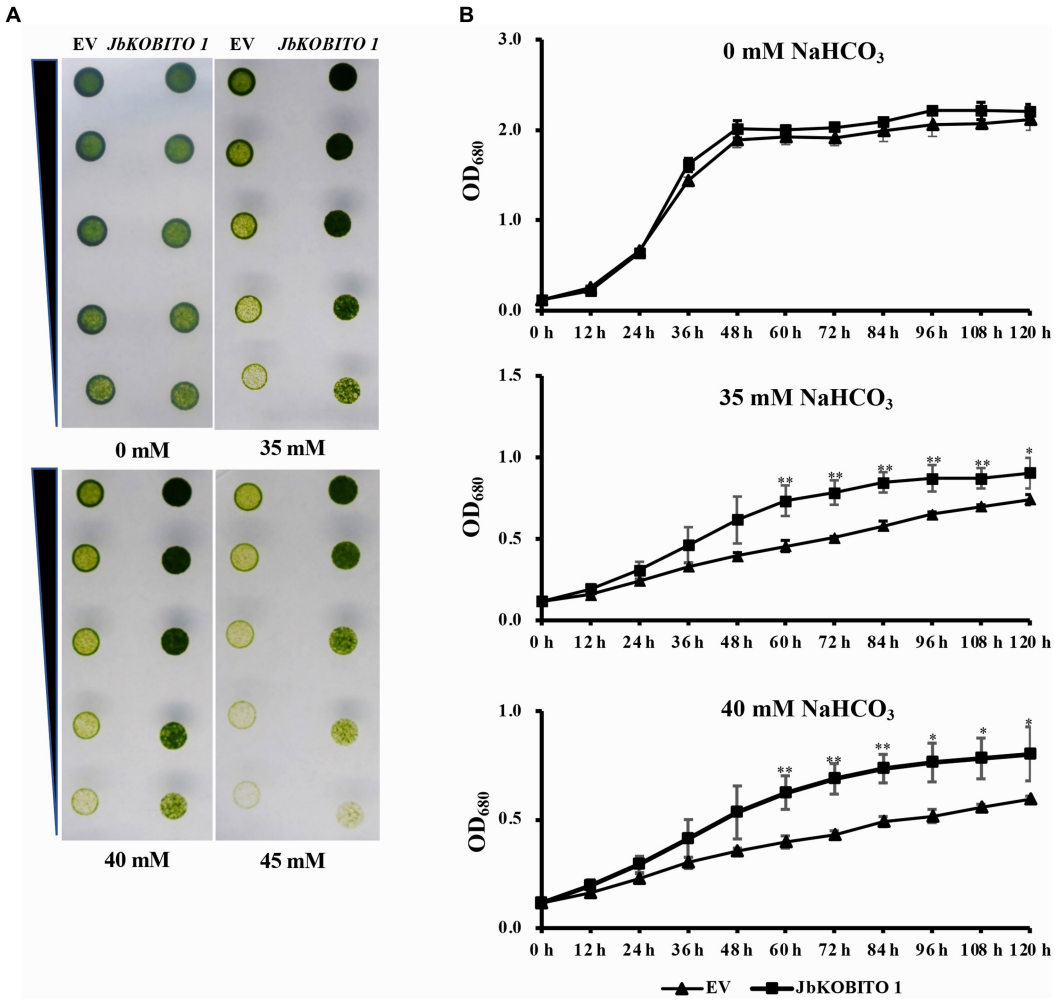

FIGURE 5
Overexpression of *JbKOBITO 1* enhanced *C. reinhardtii* $NaHCO_3$ tolerance. **(A)** Gradient dilution assays of transgenic *C. reinhardtii* on solid medium with different concentrations of $NaHCO_3$. **(B)** Growth curve of transgenic *C. reinhardtii* in liquid medium with different concentrations of $NaHCO_3$. $^{**}p < 0.01$, $^{*}0.01 < p < 0.05$, Student's *t*-test.

Subsequently, we examined the changes in the main components of the cell wall before and after treatment with $NaHCO_3$, which showed a significant increase in cellulose content, and a significant decrease in hemicellulose, soluble pectin and protopectin content. But of these, the change in cellulose content is the most pronounced, as cellulose content was the highest as a percentage of dry weight and showed the greatest percentage change in response to $NaHCO_3$ treatment. This suggests that carbonate stress induces complex cell wall polysaccharide modifications and that the ability of JB17 to tolerate carbonate stress may be closely related to changes in cellulose. It is consistent with recent research advances which have demonstrated the impact of cellulose synthesis on plant tolerance to abiotic stresses. For example, DROUGHT1 (DROT1) encodes a COBRA-like protein that confers drought resistance in rice. It has been shown that under drought stress, DROT1 enhances drought tolerance in rice by regulating cell structure through increasing cellulose content by 10.64% and maintaining cellulose crystallinity (Sun et al., 2022). Moreover, Liu et al. reported that the cellulose content in the cell wall of the halophyte *Suaeda salsa* was significantly higher than that of the glycophyte *Spinacia oleracea* in a high-salinity environment, giving the cell wall a relatively high hardness, which resisted the deformation of the cell wall under this pressure, and protected the stability of the cell wall structure under salinity stress (Liu et al., 2022). Our results of a cellulase digestion assay also indicated that the decrease in cellulose content of JB17 affects its tolerance to high concentrations of $NaHCO_3$.

Previous studies have also reported on the relationship between the content of pectin and the resistance to stress. An et al. (2014) observed that salt-tolerant soybean varieties contained higher pectin content than salt-sensitive varieties. Jin et al. (2020) reported that *OsEIL2* (ethylene insensitive 3-like2) regulates the β-subunit of the polygalacturonase (PG1β-like) subfamily of genes in rice *OsBURP16*. Overexpression of *OsEIL2* in rice resulted in lower pectin content and reduced salt stress tolerance. In these studies, higher pectin levels appeared to favor plant salt tolerance. In addition, pectin was also found to undergo structural changes under the action of modifying enzymes, affecting cell wall characteristics and further affecting its ability to cope with salt stress (Yan et al., 2018). However, in our study, protopectin and soluble pectin content decreased under $NaHCO_3$

stress. This may be due to the different stress response mechanisms of pectin in higher plants and microorganisms. Alternatively, changes in pectin content in JB17 did not play an important role in stress tolerance, as evidenced by the fact that the pectin content in higher plant cell walls is up to 40% (Dabravolski and Isayenkov, 2023), whereas the JB17 cell wall contained very little pectin.

In order to identify the key genes involved in $NaHCO_3$ tolerance, transcriptome data of JB17 before and after $NaHCO_3$ treatment were analyzed. *JbKOBITO 1*, whose expression was up-regulated in response to $NaHCO_3$, caught our attention. It is homologous to the *A. thaliana* glycosyltransferase-like protein KOBITO 1 and has a conserved Glyco_tranf_GTA_type superfamily domain. Previous studies have reported that the functions of this protein include coordinating cell elongation and cellulose synthesis by promoting the expression of genes involved in cell elongation and cellulose synthesis, acting as a regulator of intercellular junction filament permeability, and mediating the saccharide response essential for ABA and growth (Pagant et al., 2002; Dinneny et al., 2008; Kong et al., 2012; Wang et al., 2015). We found that both the expression of *JbKOBITO 1* and the cellulose content in JB17 cell wall were significantly up-regulated after $NaHCO_3$ treatment, and the overexpression of *JbKOBITO 1* in *C. reinhardtii* can enhance the tolerance of *C. reinhardtii* to $NaHCO_3$. Therefore, we speculated that the strong tolerance of JB17 to $NaHCO_3$ may be partially attributed to the *JbKOBITO 1*-mediated cellulose accumulation under $NaHCO_3$ stress. Of course, it cannot be excluded that other genes are also involved in this process. For example, Tang et al. (2022) reported a gene *OsUGE3* in rice, which exhibits UDP-galactose/glucose epimerase activity and provides substrate for cellulose synthesis, thereby promoting cellulose accumulation. *OsUGE3*-mediated increase in cellulose accumulation enhances rice tolerance to salt stress by means of cellular bulking that maintains the integrity of the cell wall. Therefore, there may be other genes involved in JB17 cellulose synthesis, although no other cellulose synthesis-related genes with significant up-regulation in expression were found in our transcriptome data, they may function through post-translational modification or changes in enzyme activity.

Changes in polysaccharides are closely related to saccharide metabolism, which prompted us to investigate JB17 saccharide metabolism. Our results showed higher levels of JB17 glucose, rhamnose and trehalose compared to the $NaHCO_3$ low-tolerance control chlorella, especially rhamnose and trehalose, which are nearly 40 times higher than the control chlorella. Since the discovery of the gene family encoding active trehalose phosphate synthase (TPS; EC 2.4.1.15) and trehalose phosphatases (TPP; EC 3.1.3.12) in *A. thaliana*, the metabolism of trehalose has been recognized as playing an essential and pervasive role in the life of plants (Lunn et al., 2014). Trehalose (Tre), a non-reducing disaccharide, is an excellent osmolyte for inducing salt tolerance (Ye et al., 2023). Joshi et al. (2020) reported that transgenic lines overexpressing trehalose biosynthetic fusion gene (TPSP) in rice had higher trehalose accumulation and enhanced tolerance to salt and alkali stress. Exogenously applied Tre increases endogenous Tre, another strategy to reduce the adverse effects of salt stress (Kosar et al., 2019). Several studies have reported that exogenous application of trehalose improves salt tolerance in plants (Yuan et al., 2022; Yang et al., 2022a,b). Siddiqui et al. (2020) reported that endogenous glucose content increases when plants are subjected to various abiotic stresses as well as exogenous supply of glucose. Ghorbani Javid et al. (2011) suggested that glucose has a direct role in osmoregulation and radical scavenging in rice grains under salt stress. All these studies suggest that the accumulation of trehalose and glucose may play an important role in plant salt tolerance. This is consistent with our study in which JB17 had a higher trehalose and glucose content. Although there is a lack of research on the role of rhamnose in plant resistance to saline and alkaline stress, it has been found in some studies that rhamnose is beneficial in maintaining osmoregulation and enhancing tolerance to osmotic stress in plants (Ghouili et al., 2021).

Taken together, our study provides an experimental basis for understanding the role of the cell wall polysaccharide, especially the role of cellulose in resistance to carbonate stress. The obtained $NaHCO_3$ tolerance gene *JbKOBITO 1* will provide genetic resources for crop breeding in saline-alkali soils and for genetic modification of strains for biofuel production. In the future, genetic modification strategies can be used to increase the cellulose content in the cell walls of crops to increase tolerance to saline-alkali stress for agricultural development, as well as to solve the problem of microalgae that accumulate more lipids under $NaHCO_3$ stress but whose growth is inhibited.

Data availability statement

The datasets presented in this study can be found in online repositories. The names of the repository/repositories and accession number(s) can be found in the article/Supplementary material.

Author contributions

JQ: Formal analysis, Investigation, Methodology, Writing – original draft. JZ: Formal analysis, Investigation, Methodology, Writing – review & editing. HZ: Formal analysis, Investigation, Methodology, Writing – review & editing. CW: Formal analysis, Investigation, Methodology, Writing – review & editing. CJ: Formal analysis, Investigation, Methodology, Writing – review & editing. XH: Formal analysis, Investigation, Methodology, Writing – review & editing. JL: Writing – review & editing, Data curation, Investigation. XC: Writing – review & editing, Funding acquisition. SL: Conceptualization, Writing – review & editing, Resources. XJ: Conceptualization, Formal analysis, Funding acquisition, Investigation, Methodology, Writing – review & editing.

Funding

The author(s) declare financial support was received for the research, authorship, and/or publication of this article. Zhejiang Provincial Natural Science Foundation of China (LY23C060001): experimental reagent purchase the Scientific Research Foundation of Zhejiang A&F University (2021LFR053): labour costs of researchers the National Natural Science Foundation of China (32000387): measurement of cell wall composition.

Conflict of interest

The authors declare that the research was conducted in the absence of any commercial or financial relationships that could be construed as a potential conflict of interest.

Publisher's note

All claims expressed in this article are solely those of the authors and do not necessarily represent those of their affiliated organizations, or those of the publisher, the editors and the reviewers. Any product that may be evaluated in this article, or claim that may be made by its manufacturer, is not guaranteed or endorsed by the publisher.

Supplementary material

The Supplementary material for this article can be found online at: https://www.frontiersin.org/articles/10.3389/fmicb.2023.1285796/full#supplementary-material

References

Alawiye, T. T., and Babalola, O. O. (2021). Metabolomics: current application and prospects in crop production. *Biologia* 76, 227–239. doi: 10.2478/s11756-020-00574-z

An, P., Li, X., Zheng, Y., Matsuura, A., Abe, J., Eneji, A. E., et al. (2014). Effects of NaCl on root growth and cell wall composition of two soya bean cultivars with contrasting salt tolerance. *J. Agron. Crop Sci.* 200, 212–218. doi: 10.1111/jac.12060

Bai, J. H., Yan, W. K., Wang, Y. Q., Yin, Q., Liu, J. H., Wight, C., et al. (2018). Screening oat genotypes for tolerance to salinity and alkalinity. *Front. Plant Sci.* 9:1302. doi: 10.3389/fpls.2018.01302

Chun, H. J., Baek, D., Cho, H. M., Jung, H. S., Jeong, M. S., Jung, W. H., et al. (2019). Metabolic adjustment of Arabidopsis root suspension cells during adaptation to salt stress and mitotic stress memory. *Plant Cell Physiol.* 60, 612–625. doi: 10.1093/pcp/pcy231

Dabravolski, S. A., and Isayenkov, S. V. (2023). The regulation of plant cell wall organisation under salt stress. *Front. Plant Sci.* 14:1118313. doi: 10.3389/fpls.2023.1118313

Dinneny, J. R., Long, T. A., Wang, J. Y., Jung, J. W., Mace, D., Pointer, S., et al. (2008). Cell identity mediates the response of Arabidopsis roots to abiotic stress. *Science* 320, 942–945. doi: 10.1126/science.1153795

Ghorbani Javid, M., Sorooshzadeh, A., Modarres Sanavy, S. A. M., Allahdadi, I., and Moradi, F. (2011). Effects of the exogenous application of auxin and cytokinin on carbohydrate accumulation in grains of rice under salt stress. *Plant Growth Regul.* 65, 305–313. doi: 10.1007/s10725-011-9602-1

Ghouili, E., Sassi, K., Jebara, M., Hidri, Y., Ouertani, R. N., Muhovski, Y., et al. (2021). Physiological responses and expression of sugar associated genes in faba bean (*Vicia faba* L.) exposed to osmotic stress. *Physiol. Mol. Biol. Plants* 27, 135–150. doi: 10.1007/s12298-021-00935-1

Hong, D. D., Hien, H. T. M., Thom, L. T., Ha, N. C., Huy, L. A., Thu, N. T. H., et al. (2023). Transcriptome analysis of Spirulina platensis sp. at different salinity and nutrient compositions for sustainable cultivation in Vietnam. *Sustainability* 15:11906. doi: 10.3390/su151511906

Ji, C. L., Mao, X., Hao, J. Y., Wang, X. D., Xue, J. N., Cui, H. L., et al. (2018). Analysis of bZIP transcription factor family and their expressions under salt stress in. *Int. J. Mol. Sci.* 19:2800. doi: 10.3390/ijms19092800

Jia, H. L., Wang, X. H., Wei, T., Wang, M., Liu, X., Hua, L., et al. (2021). Exogenous salicylic acid regulates cell wall polysaccharides synthesis and pectin methylation to reduce cd accumulation of tomato. *Ecotoxicol. Environ. Saf.* 207:111550. doi: 10.1016/j.ecoenv.2020.111550

Jin, J., Duan, J., Shan, C., Mei, Z., Chen, H., Feng, H., et al. (2020). Ethylene insensitive3-like2 (OsEIL2) confers stress sensitivity by regulating OsBURP16, the β subunit of polygalacturonase (PG1β-like) subfamily gene in rice. *Plant Sci.* 292:110353. doi: 10.1016/j.plantsci.2019.110353

Jin, X., Jiang, Z., Zhang, K., Wang, P., Cao, X., Yue, N., et al. (2018). Three-dimensional analysis of chloroplast structures associated with virus infection. *Plant Physiol.* 176, 282–294. doi: 10.1104/pp.17.00871

Joshi, R., Sahoo, K. K., Singh, A. K., Anwar, K., Pundir, P., Gautam, R. K., et al. (2020). Enhancing trehalose biosynthesis improves yield potential in marker-free transgenic rice under drought, saline, and sodic conditions. *J. Exp. Bot.* 71, 653–668. doi: 10.1093/jxb/erz462

Khoo, K. S., Ahmad, I., Chew, K. W., Iwamoto, K., Bhatnagar, A., and Show, P. L. (2023). Enhanced microalgal lipid production for biofuel using different strategies including genetic modification of microalgae: a review. *Prog. Energy Combust. Sci.* 96:101071. doi: 10.1016/j.pecs.2023.101071

Khoo, K. S., Chew, K. W., Yew, G. Y., Leong, W. H., Chai, Y. H., Show, P. L., et al. (2020). Recent advances in downstream processing of microalgae lipid recovery for biofuel production. *Bioresour. Technol.* 304:122996. doi: 10.1016/j.biortech.2020.122996

Kong, D., Karve, R., Willet, A., Chen, M. K., Oden, J., and Shpak, E. D. (2012). Regulation of plasmodesmatal permeability and stomatal patterning by the glycosyltransferase-like protein KOBITO1. *Plant Physiol.* 159, 156–168. doi: 10.1104/pp.112.194563

Kosar, F., Akram, N. A., Sadiq, M., Al-Qurainy, F., and Ashraf, M. (2019). Trehalose: a key organic osmolyte effectively involved in plant abiotic stress tolerance. *J. Plant Growth Regul.* 38, 606–618. doi: 10.1007/s00344-018-9876-x

Lampugnani, E. R., Khan, G. A., Somssich, M., and Persson, S. (2018). Building a plant cell wall at a glance. *J. Cell Sci.* 131:jcs207373. doi: 10.1242/jcs.207373

Le Gall, H., Philippe, F., Domon, J. M., Gillet, F., Pelloux, J., and Rayon, C. (2015). Cell wall metabolism in response to abiotic stress. *Plan. Theory* 4, 112–166. doi: 10.3390/plants4010112

Li, J. Y., Li, C. H., Lan, C. Q., and Liao, D. K. (2018). Effects of sodium bicarbonate on cell growth, lipid accumulation, and morphology of *Chlorella vulgaris*. *Microb. Cell Factories* 17:111. doi: 10.1186/s12934-018-0953-4

Li, W. J., Zhang, Y. T., Ren, H. M., Wang, Z., OuYang, Y. H., Wang, S., et al. (2023). Identification of potassium transport proteins in algae and determination of their role under salt and saline-alkaline stress. *Algal Res.* 69:102923. doi: 10.1016/j.algal.2022.102923

Liu, J., Shao, Y., Feng, X., Otie, V., Matsuura, A., Irshad, M., et al. (2022). Cell wall components and extensibility regulate root growth in Suaeda salsa and *Spinacia oleracea* under salinity. *Plan. Theory* 11:900. doi: 10.3390/plants11070900

Liu, X. G., Yu, Y., Liu, Q., Deng, S. R., Jin, X. B., Yin, Y. J., et al. (2020). A Na_2CO_3-responsive chitinase gene from leymus chinensis improve pathogen resistance and saline-alkali stress tolerance in transgenic tobacco and maize. *Front. Plant Sci.* 11:504. doi: 10.3389/fpls.2020.00504

Lunn, J. E., Delorge, I., Figueroa, C. M., Van Dijck, P., and Stitt, M. (2014). Trehalose metabolism in plants. *Plant J.* 79, 544–567. doi: 10.1111/tpj.12509

Nadzir, S. M., Yusof, N., Kamari, A., and Nordin, N. (2023). "Effect of environmental stress on biomolecules production and cell wall degradation in *Chlorella vulgaris*" in *Proceedings of the 8th international conference on the applications of science and mathematics. EduTA 2022, springer proceedings in physics*. eds. A. Mustapha, N. Ibrahim, H. Basri, M. S. Rusiman and S. Zuhaib Haider Rizvi, vol. *294* (Singapore: Springer)

Pagant, S., Bichet, A., Sugimoto, K., Lerouxel, O., Desprez, T., McCann, M., et al. (2002). KOBITO1 encodes a novel plasma membrane protein necessary for normal synthesis of cellulose during cell expansion in Arabidopsis. *Plant Cell* 14, 2001–2013. doi: 10.1105/tpc.002873

Pang, Q. Y., Zhang, A. Q., Zang, W., Wei, L., and Yan, X. F. (2016). Integrated proteomics and metabolomics for dissecting the mechanism of global responses to salt and alkali stress in Suaeda corniculata. *Plant Soil* 402, 379–394. doi: 10.1007/s11104-015-2774-0

Qiao, K., Takano, T., and Liu, S. (2015). Discovery of two novel highly tolerant $NaHCO_3$ Trebouxiophytes: identification and characterization of microalgae from extreme saline–alkali soil. *Algal Res.* 9, 245–253. doi: 10.1016/j.algal.2015.03.023

Qin, Y., Bai, J. H., Wang, Y. Q., Liu, J. H., Hu, Y., Dong, Z., et al. (2018). Comparative effects of salt and alkali stress on photosynthesis and root physiology of oat at anthesis. *Arch. Biol. Sci.* 70, 329–338. doi: 10.2298/Abs171124050q

Qiu, S., Guo, S. F., Yang, Q., Xie, Y. Q., Tang, S. Q., and Zhang, A. H. (2023). Innovation in identifying metabolites from complex metabolome-highlights of recent analytical platforms and protocols. *Front. Chem.* 11:1129717. doi: 10.3389/fchem.2023.1129717

Siddiqui, H., Sami, F., and Hayat, S. (2020). Glucose: sweet or bitter effects in plants-a review on current and future perspective. *Carbohydr. Res.* 487:107884. doi: 10.1016/j.carres.2019.107884

Sun, X., Xiong, H., Jiang, C., Zhang, D., Yang, Z., Huang, Y., et al. (2022). Natural variation of DROT1 confers drought adaptation in upland rice. *Nat. Commun.* 13:4265. doi: 10.1038/s41467-022-31844-w

Tang, Y., Wang, M., Cao, L., Dang, Z., Ruan, N., Wang, Y., et al. (2022). OsUGE3-mediated cell wall polysaccharides accumulation improves biomass production, mechanical strength, and salt tolerance. *Plant Cell Environ.* 45, 2492–2507. doi: 10.1111/pce.14359

Wang, X., Ajab, Z., Liu, C., Hu, S., Liu, J., and Guan, Q. (2020). Overexpression of transcription factor SlWRKY28 improved the tolerance of Populus davidiana × P. Bolleana to alkaline salt stress. *BMC Genet.* 21:103. doi: 10.1186/s12863-020-00904-9

Wang, X., Jing, Y. J., Zhang, B. C., Zhou, Y. H., and Lin, R. C. (2015). Glycosyltransferase-like protein ABI8/ELD1/KOB1 promotes Arabidopsis hypocotyl elongation through regulating cellulose biosynthesis. *Plant Cell Environ.* 38, 411–422. doi: 10.1111/pce.12395

Wang, M., Liu, H., Qiao, K., Ye, X., Takano, T., Liu, S., et al. (2020). Exogenous $NaHCO_3$ enhances growth and lipid accumulation of the highly $NaHCO_3$-tolerant Nannochloris sp. JB17. *J. Appl. Phycol.* 33, 241–253. doi: 10.1007/s10811-020-02293-z

Wang, Y., Wang, M., Ye, X. X., Liu, H., Takano, T., Tsugama, D., et al. (2020). Biotin plays an important role in *Arabidopsis thaliana* seedlings under carbonate stress. *Plant Sci.* 300:110639. doi: 10.1016/j.plantsci.2020.110639

Yan, J. W., He, H., Fang, L., and Zhang, A. (2018). Pectin methylesterase31 positively regulates salt stress tolerance in Arabidopsis. *Biochem. Biophys. Res. Commun.* 496, 497–501. doi: 10.1016/j.bbrc.2018.01.025

Yang, Y., Xie, J. M., Li, J., Zhang, J., Zhang, X. D., Yao, Y. D., et al. (2022a). Trehalose alleviates salt tolerance by improving photosynthetic performance and maintaining mineral ion homeostasis in tomato plants. *Front. Plant Sci.* 13:974507. doi: 10.3389/fpls.2022.974507

Yang, Y., Yao, Y. D., Li, J., Zhang, J., Zhang, X. D., Hu, L. X., et al. (2022b). Trehalose alleviated salt stress in tomato by regulating ROS metabolism, photosynthesis, osmolyte synthesis, and trehalose metabolic pathways. *Front. Plant Sci.* 13:772948. doi: 10.3389/fpls.2022.772948

Ye, X., Wang, H., Cao, X., Jin, X., Cui, F., Bu, Y., et al. (2019). Transcriptome profiling of *Puccinellia tenuiflora* during seed germination under a long-term saline-alkali stress. *BMC Genomics* 20:589. doi: 10.1186/s12864-019-5860-5

Ye, N. H., Wang, Y. X., Yu, H. H., Qin, Z. E., Zhang, J. H., Duan, M. J., et al. (2023). Abscisic acid enhances trehalose content via OsTPP3 to improve salt tolerance in rice seedlings. *Plan. Theory* 12:2665. doi: 10.3390/plants12142665

Yuan, G. P., Sun, D. X., An, G. L., Li, W. H., Si, W. J., Liu, J. P., et al. (2022). Transcriptomic and metabolomic analysis of the effects of exogenous trehalose on salt tolerance in watermelon (*Citrullus lanatus*). *Cells* 11:2338. doi: 10.3390/cells11152338

Yun, C. J., Hwang, K. O., Han, S. S., and Ri, H. G. (2019). The effect of salinity stress on the biofuel production potential of freshwater microalgae *Chlorella vulgaris* YH703. *Biomass Bioenergy* 127:105277. doi: 10.1016/j.biombioe.2019.105277

Zheng, J. X., Lin, R. Y., Pu, L., Wang, Z. F., Mei, Q. M., Zhang, M., et al. (2021). Ectopic expression of CrPIP2;3, a plasma membrane intrinsic protein gene from the halophyte *Canavalia rosea*, enhances dought and salt-alkali stress tolerance in Arabidopsis. *Int. J. Mol. Sci.* 22:565. doi: 10.3390/ijms22020565

frontiers | Frontiers in Plant Science

TYPE Original Research
PUBLISHED 20 November 2023
DOI 10.3389/fpls.2023.1281373

OPEN ACCESS

EDITED BY
Kun Zhang,
Yangzhou University, China

REVIEWED BY
Sumit Jangra,
University of Florida, United States
Du Seok Choi,
LG Chem, Republic of Korea

*CORRESPONDENCE
Kexuan Deng
wmjbrj@swu.edu.cn
Jiankui Zhang
jkzhang@swu.edu.cn

†These authors have contributed equally to this work and share first authorship

RECEIVED 22 August 2023
ACCEPTED 26 October 2023
PUBLISHED 20 November 2023

CITATION
Yang K, Huang Y, Li Z, Zeng Q, Dai X, Lv J, Zong X, Deng K and Zhang J (2023) Overexpression of Nta-miR6155 confers resistance to *Phytophthora nicotianae* and regulates growth in tobacco (*Nicotiana tabacum* L.). *Front. Plant Sci.* 14:1281373. doi: 10.3389/fpls.2023.1281373

Overexpression of Nta-miR6155 confers resistance to *Phytophthora nicotianae* and regulates growth in tobacco (*Nicotiana tabacum* L.)

Kaiyue Yang[1†], Yuanyuan Huang[1†], Zexuan Li[1], Qian Zeng[1], Xiumei Dai[1,2,3], Jun Lv[1,2], Xuefeng Zong[1,2], Kexuan Deng[1,2,3*] and Jiankui Zhang[1,2,3*]

[1]College of Agronomy and Biotechnology, Southwest University, Chongqing, China, [2]Engineering Research Center of South Upland Agriculture, Ministry of Education, Chongqing, China, [3]Chongqing Tobacco Science Research Institute, Chongqing, China

Tobacco black shank induced by *Phytophthora nicotianae* causes significant yield losses in tobacco plants. MicroRNAs (miRNAs) play a pivotal role in plant biotic stress responses and have great potential in tobacco breeding for disease resistance. However, the roles of miRNAs in tobacco plants in response to *P. nicotianae* infection has not been well characterized. In this study, we found that Nta-miR6155, a miRNA specific to *Solanaceae* crops, was significantly induced in *P. nicotianae* infected tobacco. Some of predicted target genes of Nta-miR6155 were also observed to be involved in disease resistance. To further investigate the function of miR6155 in tobacco during *P. nicotianae* infection, Nta-miR6155 overexpression plants (miR6155-OE) were generated in the Honghua Dajinyuan tobacco variety (HD, the main cultivated tobacco variety in China). We found that the Nta-miR6155 overexpression enhanced the resistance in tobacco towards *P. nicotianae* infections. The level of reactive oxygen species (ROS) was significantly lower and antioxidant enzyme activities were significantly higher in miR6155-OE plants than those in control HD plants during *P. nicotianae* infection. In addition, we found that the accumulation of salicylic acid and the expression of salicylic acid biosynthesis and signal transduction-related genes is significantly higher in miR6155-OE plants in comparison to the control HD plants. Furthermore, we found that Nta-miR6155 cleaved target genes *NtCIPK18* to modulate resistance towards *P. nicotianae* in tobacco plants. Additionally, phenotypic analysis of miR6155-OE plants showed that Nta-miR6155 could inhibit the growth of tobacco by suppressing nitrogen uptake and photosynthesis. In conclusion, our findings indicated that miR6155 plays a crucial role in the regulation of growth and resistance against *P. nicotianae* infections in tobacco plants.

KEYWORDS

***Nicotiana tabacum*, *Phytophthora nicotianae*, tobacco black shank, Nta-miR6155, NtCIPK18, nitrogen**

1 Introduction

Tobacco (*Nicotiana tabacum* L.) is a high value plant of the *Solanaceae* family (Meng et al., 2021). *Phytophthora nicotianae* induced tobacco black shank is one of the most destructive diseases that causes huge economic losses in tobacco production (Liu et al., 2022). *P. nicotianae*, belonging to the phylum Oomycota, is parasitic on plants or resides in the soil in the form of hyphae or chlamydospores (Jin and Shew, 2021). Under favorable growth conditions, the spores of *P. nicotianae* germinate and invade plants through stomata or wounds. After a period of growth, they release a large number of zoospores to infect other tobacco plants. *P. nicotianae* can infect tobacco at different stages of tobacco growth and development, and the most typical infectious symptom is a black stem in tobacco (Yang et al., 2017). The main control measures for tobacco black shank are planting disease-resistant varieties, optimizing cultivation and management measures, and chemical and biological control methods (Guo et al., 2020). Among them, planting disease-resistant varieties is one of the most economical and effective methods. Therefore, it is important to identify *P. nicotianae* resistance genes and breed highly resistant varieties of tobacco.

MicroRNAs (miRNAs) play important roles in regulating plant growth and development and stress response by shearing target messengerRNAs (mRNAs) genes or inhibiting the translation of target mRNAs (Zhu et al., 2020; Han and Wang, 2022). In recent years, many miRNAs have been discovered through miRNA sequencing (Evers et al., 2015), and the biosynthesis, mechanism of action, and functions of plant miRNAs have gradually been revealed (Song et al., 2019; Li and Yu, 2021). Since Lee et al. identified the first miRNA lin-4 in *Caenorhabditis elegans* (Lee et al., 1993), thousands of plant and animal miRNAs have been discovered (Llave et al., 2002; Mette et al., 2002; Reinhart et al., 2002). The process by which plant miRNAs modulate stability of their target mRNAs consists of three main steps: transcription of miRNAs, processing and maturation, and assembly of functional complexes to cleave the target mRNAs (Addo-Quaye et al., 2008; German et al., 2008; Kurihara and Watanabe, 2010; Achkar et al., 2016). However, when the degree of complementarity between the miRNA and target mRNA is low, the miRNA is unable to mediate cleavage and will then inhibit its translation by binding to the target mRNA (Zamore and Haley, 2005).

In recent decades, the function of plant miRNAs in regulating plant biotic stress has been revealed (Zheng et al., 2020; Song et al., 2021). Overexpression of miR394 downregulates the transcription level of its target gene, *LCR* (Leaf Curling Responsiveness), and ultimately decreases the resistance against *Phytophthora infestans* in tomato plants (Zhang et al., 2021). In potatoes, overexpression of miR482e was reported to increase sensitivity to *Verticillium dahliae* infection (Yang et al., 2015). Overexpression of Osa-miR162a enhances resistance towards *Magnaporthe oryzae* and fine-tunes the effect on yield in rice plant (Li et al., 2020). Recently, Yang et al. showed that the overexpression of miR395 could promote resistance to *Xanthomonas oryzae pv. oryzae* (*Xoo*) and *X. oryzae pv. oryzicola* (*Xoc*) by regulating sulfate accumulation and distribution in rice (Yang et al., 2022). MiRNAs have also been found to be involved in biotic stress tobacco response in tobacco plants. The expression profile of miRNA is significantly affected in tobacco following potato virus Y infection (Guo et al., 2017). Overexpression of miR396 has been reported with enhanced tobacco susceptibility to *P. nicotianae* (Chen et al., 2015). However, only a few studies have been conducted on the role of miRNAs in the response of tobacco to *P. nicotianae*.

In view of the above, the present study was designed to reveal the function of miRNA in tobacco in response to *P. nicotianae* infection and provide new genetic resources for breeding of *P. nicotianae* resistant tobacco varieties.

2 Methods

2.1 Plant materials, *P. nicotianae* strains, and culture conditions

Seeds of *N. benthamiana* and Honghua Dajinyuan (HD, a main cultivated *N. tabacum* (tobacco) variety in China) were sown in sterile soil and grown in a greenhouse at a temperature of 25°C, 16/8 hours dark and 10000 LX light intensity.

P. nicotianae strain WL1-7 was cultured on 10% V8 vegetable juice medium (100 mL/L vegetable juice, 0.2 g/L $CaCO_3$, 20 g/L agar) at 25°C in a growth chamber without light.

2.2 Construction of Nta-miR6155 and *NtCIPK18* overexpression vector

Primers for generation of Nta-miR6155 overexpression vector were designed based on the Nta-miR6155 genome sequence by using Primer Premier 5.0 software, and the adaptor for seamless cloning was added in primers (Table S1). Tobacco genomic DNA was extracted using the CTAB method and the precursor gene of Nta-miR6155 was cloned using tobacco genomic DNA as a template. The modified pCAMBIA2300 vector was digested by XbaI and AscI restriction enzymes, and the fragment of Nta-miR6155 was inserted into pCAMBIA2300 vector by using In-Fusion Snap Assembly Master Mix kit (Takara) to generate Nta-miR6155 overexpression vector.

Primers for generation of *NtCIPK18* overexpression vectors were designed based on the CDS of the *NtCIPK18* gene by using Primer Premier 5.0 software (Table S1). The coding sequences of *NtCIPK18* were amplified using the corresponding primers, and *NtCIPK18* fragments were fused with the *GUS* (*β-glucuronidase*) gene. The fragments with the fused GUS gene were introduced into the entry vector P35S-8GWN. Finally, the *NtCIPK18* genes with a GUS tag were recombined into the binary vector KANA303 by using Gateway LR Clonase (Thermo Fisher Scientific) to generate overexpression vector. The detail steps of plasmid construction were performed as described elsewhere (Li et al., 2015). The plasmid was transformed into *Agrobacterium tumefaciens* for further experiments.

2.3 *Agrobacterium*-mediated transient expression in *N. benthamiana* leaves

Agrobacterium containing Nta-miR6155 or *NtCIPK18-GUS* overexpression plasmid was resuspended in an infiltration medium (10 μM MES, 10 μM $MgCl_2$, 200 μM acetosyringone and 500 mg glucose), and an empty vector (EV, 2300YFP) was used as a control. After transient expression of Nta-miR6155 for 36h, the infiltrated leaves were inoculated with *P. nicotianae*. Injections were performed based on the methods of previous studies (Yu et al., 2020) and each infiltration experiment was repeated more than 3 times.

2.4 *P. nicotianae* inoculation experiments

N. tabacum seedlings at 5-6 true leaf stage and *N. benthamiana* seedlings at 7-8 true leaf stage were selected for *P. nicotianae* infection, respectively. *N.tabacum* or *N. benthamiana* leaves of similar size were inoculated with *P. nicotianae* and placed in a high temperature and humidity environment (30°C and 100% relative humidity) to promote *P. nicotianae* infection. For entire plants, the stem-base of tobacco seedling was inoculated with *P. nicotianae* and placed at 30°C and 100% relative humidity. After 48 hours post-inoculation (48 hpi), the lesion diameters were measured, and lesion size and disease index were calculated according to previous methods (Zhang et al., 2021). Three biological replicates were performed for each experiment.

2.5 RNA extraction, cDNA preparation, and RT-qPCR

The processing conditions for plant samples are described in the main text or figure legends in detail. After collecting plant samples, total RNA was extracted with the RNAprep Pure Plant Plus Kit (TIANGEN). RNA was reverse transcribed into cDNA by using PrimeScript™ RT reagent Kit with gDNA Eraser (TaKaRa). RT-qPCR was performed by TB Green Premix Ex Taq II (TaKaRa) and miRcute Plus miRNA qPCR Kit (TIANGEN). The following default program was used: 94°C for 5 min, followed by 40 cycles of 94°C for 15 s and 60°C for 30 s each, and a dissociation stage of 95°C for 15 s, 60°C for 30 s, and 95°C for 15 s. *GAPDH* was selected as internal reference genes to calculate the relative expression levels of mRNA. All reactions were conducted with 3 biological replicates, and the relative expression of genes was conducted using the $2^{-\Delta\Delta c(t)}$ method. Primers used for qRT-PCR assay are shown in Table S1.

To measure miRNA expression, RNA was reverse-transcribed into cDNA using miRcute Plus miRNA First-Strand cDNA Kit (TIANGEN), and RT-qPCR was performed using miRcute Plus miRNA qPCR Kit (TIANGEN). The following default program was used: 95°C for 15 min, followed by 40 cycles of 94°C for 20 s and 60°C for 30 s each, and a dissociation stage of 95°C for 10 s, 60°C for 5 s, and 95°C for 5 s. GAPDH and *U6* were selected as internal reference genes to calculate the relative expression levels of mRNA and miRNA, respectively. All reactions were conducted with 3 biological replicates, and the relative expression of genes was calculated using the $2^{-\Delta\Delta c(t)}$ method. Primers used for qRT-PCR assay are shown in Table S1.

To relatively quantify the biomass of *P. nicotianae* in control HD and miR6155-OE plants, 100mg stem tissue was collected at 48 hpi for genomic DNA extraction. The purified genomic DNA was used as templates for RT-qPCR to relatively quantify the biomass of *P. nicotianae*. The RT-qPCR program is consistent with the program used for detecting the expression of mRNA. All reactions were conducted with 3 biological replicates, and the relative expression of genes was conducted using the $2^{-\Delta\Delta c(t)}$ method. Primers used for qRT-PCR assay are shown in Table S1.

2.6 3,3′-diaminobenzidine, Nitro Blue Tetrazolium and β-glucuronidase staining and salicylic acid measurement in miR6155-OE and control HD plants post *P. nicotianae* infection

48 h post *P. nicotianae* infection, the leaves of control HD and miR6155-OE plants were collected for NBT and DAB staining, according to previously described methods (Chen et al., 2015). The GUS staining was performed to identify the expression of *NtCIPK18* according to methods described previously (An et al., 2022). Extraction of SA from tobacco and the quantification of the total SA content in plant were performed using Plant SA ELISA test kit (MEIMIAN) following the manufacturer's instructions.

2.7 Phenotypic observation and nitrogen quantification in miR6155-OE and control HD plants under normal conditions

Various phenotypic characteristics including plant height, internode length, and fresh weight were measured in miR6155-OE and control HD tobacco seedlings at 5-6 true leaf stage. Subsequently, photosynthetic rate was measured in leaves of similar size using a portable photosynthetic system LI-6400. Further the nitrogen content was quantified in the seedlings using the Kjeldahl method. To analyze antioxidant enzymes and phenylalanine ammonia lyase activities in miR6155-OE and HD tobacco seedlings, After miR6155-OE and HD tobacco seedlings reached 5-6 true leaves stages, the leaves of miR6155-OE plants and HD were inoculated with *P. nicotianae* for 48h, and enzymes activities were detected by using Peroxidase (POD) Assay Kit (Solarbio), Superoxide Dismutase(SOD) Assay Kit (Solarbio), Catalase (CAT) Assay Kit (Solarbio), Total Antioxidant Capacity (T-AOC) Assay Kit (Solarbio) and Phenylalnine Ammonialyase (PAL)Assay Kit (Solarbio) in accordance with the manufacturer's instructions.

2.8 Statistical analysis

Statistical analysis of data was performed with the software SPSS 22.0 (United States). Student's t test was used to determine the significance of differences (*P<0.05; **P<0.01).

3 Results

3.1 Nta-miR6155 modulates response towards *P. nicotianae* infections in tobacco plants

As a highly pathogenic oomycete, *P. nicotianae* can quickly infect tobacco plants within 48 hours under suitable conditions (Figure 1A). During this process, we found that the expression of Nta-miR6155, a miRNA specific to *Solanaceae* crops, is significantly induced by *P. nicotianae* infection in *N.tabacum* (Figure 1B; Figure S1) (Tang et al., 2012). Consistently, the ortholog of Nta-miR6155 in *N.benthamiana* is also induced by *P. nicotianae* infection (Figure S2).The tissue expression pattern of Nta-miR6155 showed that it was differentially expressed in root, stem, leaf, and shoot, suggesting that Nta-miR6155 may function in different tissues of tobacco (Figure 1C). To determine whether it has a crucial role in conferring resistance against *P. nicotianae* infections in *Nicotiana* species, an overexpression vector of Nta-miR6155 was constructed. Transient expression of Nta-miR6155 was performed in *N. benthamiana*, and then leaves expressing Nta-miR6155 or empty vector (control) were inoculated with *P. nicotianae* to observe its infection in *N.benthamiana* by *P. nicotianae*. The results showed that the lesion size of Nta-miR6155 overexpressed group was reduced to half that of the control group, suggesting that Nta-miRNA6155 could significantly help prevent against *P. nicotianae* infection in *N.benthamiana* (Figures 1D–F). Salicylic acid (SA) plays important roles in plant response to biotic and abiotic stresses (Ku et al., 2018). We found that the expression of Nta-miRNA6155 can be significantly induced by salicylic acid in a dose-dependent manner, suggesting that Nta-miR6155 may be involved in salicylic acid signaling mediated regulation of abiotic stress responses (Figures 1G, H). Based on the mature sequence of Nta-miRNA6155, we predicted target genes of Nta-miR6155, and a total of 106 potential target genes of Nta-miR6155 using TargetFinder software (Tables S2, S3) (Bo and Wang, 2005). GO and KEGG enrichment analysis showed that potential target genes of Nta-miRNA6155 are involved in multiple biological processes, metabolic pathways, and signaling transduction, such as autophagy, MAPK signaling, photosynthesis, and wax biosynthesis, etc., suggesting that Nta-miRNA6155 may affect tobacco disease resistance by regulating these corresponding target genes (Figures 1I, J and Table S3).

3.2 Overexpression of miR6155 enhanced resistance against *P. nicotianae* in tobacco

To further investigate the function of Nta-miRNA6155 in the tobacco plants in response to *P. nicotianae*, we generated Nta-miRNA6155 overexpression plants (miR6155-OE9 and miR6155-OE10), and RT-qPCR data showed that the expression level of Nta-miR6155 was four times higher in miR6155-OE9 and miR6155-OE10 than that of in the control HD plants (Figure 2A). Consistent with results in *N.benthamiana*, lesion size of detached miR6155-OE9 and miR6155-OE10 leaves were significantly smaller than those of the control HD plant leaves after inoculating with *P. nicotianae* (Figures 2B, C). In addition, the stem-base of miR6155-OE and HD plants were inoculated with *P. nicotianae* to observe the phenotype of miR6155-OE and HD plants after infection, and results showed that HD had been infected by *P. nicotianae* and displayed wilting and black shank phenotype. On the contrary, no obvious disease phenotype was observed in miR6155-OE9 and miR6155-OE10 under the same conditions, and the disease index and fungal biomass of miR6155-OE plants is significantly lower than that of HD (Figures 2D–F). These data suggest that Nta-miRNA6155 can enhance resistance to *P. nicotianae* in tobacco.

ROS as a signaling molecule plays an indispensable role in the process of disease resistance in plants. ROS accumulates rapidly when plants sense the presence of pathogens, and this process is an important signal for the activation of the plant immune system (Bi et al., 2022). We investigated whether Nta-miR6155 affected ROS accumulation in tobacco after inoculation with *P. nicotianae*. The accumulation of H_2O_2 and O^{2-} in tobacco leaves was examined using DAB and NBT staining methods, respectively. Under normal conditions, minimal H_2O_2 and O^{2-} were detected in control HD and miR6155-OE tobacco leaves. After inoculation with *P. nicotianae* for 48h, DAB and NBT staining results showed that there were higher levels of H_2O_2 and O^{2-} accumulation in HD compared to miR6155-OE plants (Figure 3A). We also tested the activity of different antioxidant enzymes in miR6155-OE plants and HD, including peroxidase (POD), surperoxide dismutase (SOD), catalase (CAT), and total antioxidant capacity (T-AOC). Consistently, we found that the activity of antioxidant enzymes is higher in miR6155-OE plants than that of in HD under normal conditions or after *P. nicotianae* inoculation (Figure 3B). In summary, miR6155-OE plants had stronger antioxidant activity than that of HD, and the level of ROS produced by miR6155-OE plants after *P. nicotianae* infection was significantly lower than that of HD. The higher accumulation of ROS in HD leaves after *P. nicotianae* inoculation implies that HD are subjected to more severe oxidative stress, thus resulting in reduced resistance to *P. nicotianae*.

As salicylic acid has been implicated in disease resistance in plants and the expression of Nta-miRNA6155 can be induced by SA, we also examined the concentration of SA in HD and miR6155-OE plants. The results indicated that overexpression of Nta-miR6155 induced more SA accumulation in the transgenic plants than that of HD under normal conditions or after *P. nicotianae* inoculation (Figure 3C). In addition, we detected the expression and enzyme activity of *NtPAL* (*Phenylalanine Ammonia Lyase*), a salicylic acid biosynthesis related gene, and data showed that the expression and enzyme activity of *PAL* is higher in miR6155-OE plants than that of in HD under normal condition or after *P. nicotianae* inoculation (Figures 3D, E). Furthermore, we also detected the expression of salicylic acid signal transduction

10.3389/fpls.2023.1281373

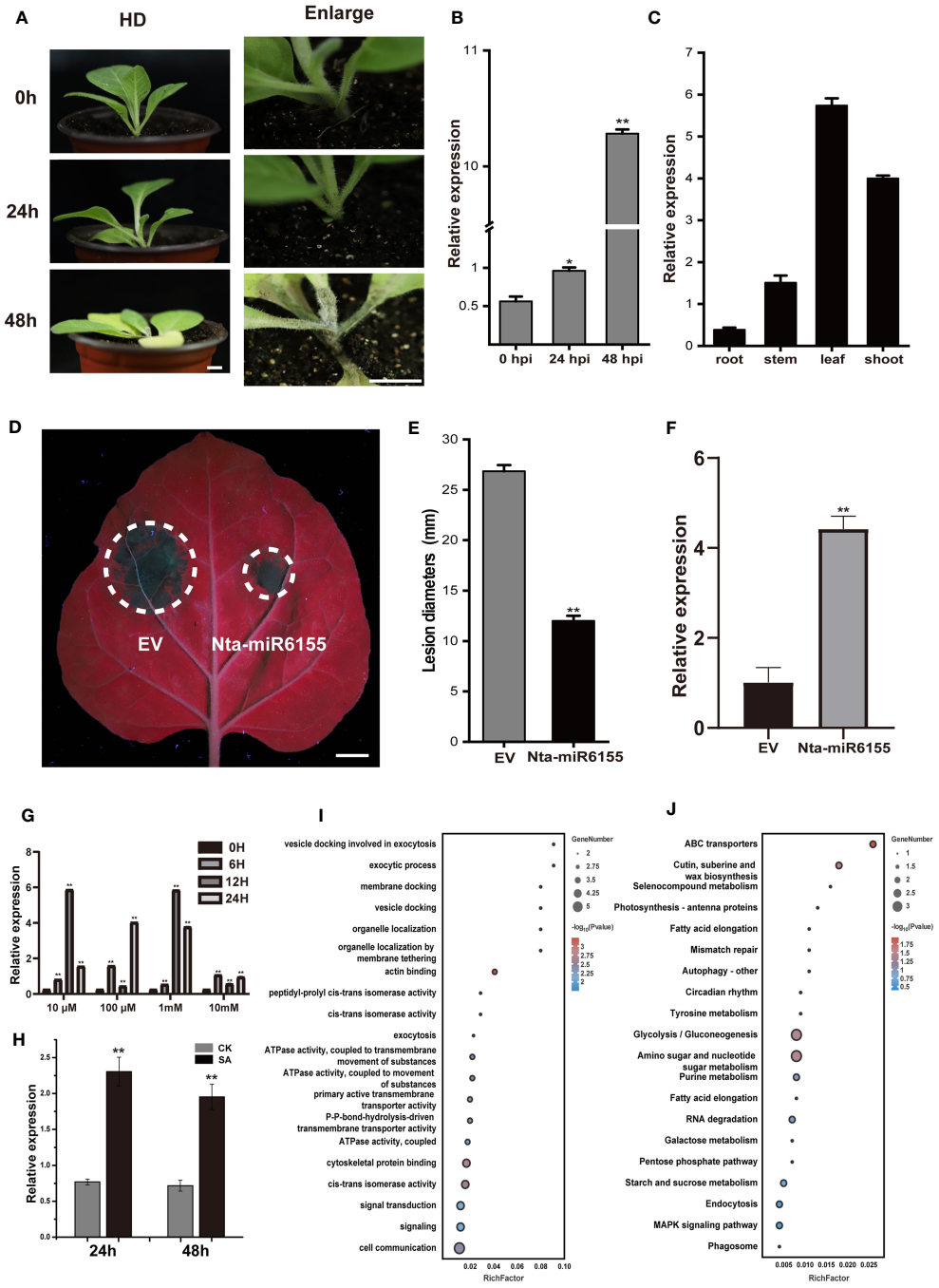

FIGURE 1
Transient expression of Nta-miR6155 in *N. benthamiana* enhanced resistance towards *P. nicotianae*. **(A)** The phenotype of tobacco after inoculation with *P. nicotianae*, bar=1cm. **(B)** The expression level of Nta-miR6155 in tobacco leaves on infected with *P. nicotianae* at 0, 24, and 48 hpi (hours post infection). **(C)** The expression level of Nta-miR6155 in different tobacco tissues, including root, stem, leaf, and shoot. **(D)** Representative photographs of *N. benthamiana* leaves after 48h infection. *Agrobacterium*-mediated transient expression of empty vector (EV, left) and Nta-miR6155 (right), bar=1cm. The infiltrated leaves (36 hours after infiltration) were inoculated with *P. nicotianae*, and photographed after 48 hpi. **(E)** Lesion diameters (mm) of *N. benthamiana* leaves. **(F)** The expression level of Nta-miR6155 in *N. benthamiana* leaves after transient expression of EV (left) and Nta-miR6155 (right). **(G, H)** The expression level of Nta-miR6155 in tobacco after treatment with salicylic acid (SA). HD seedlings at 5-6 true leaf stage were sprayed with SA at different concentrations (10 μM, 100 μM, 1mM, and 10mM), and double distilled water (ddH_2O) was used as control (CK). After 3h, 6h, 12h, and 24h, the seedlings were collected for RNA extraction **(G)**. HD seedlings at 5-6 true leaf stage were sprayed with SA at concentration 1mM, and ddH_2O was used as control (CK). After 24h and 48h, the seedlings were collected for RNA extraction **(H)**. **(I)** GO enrichment based on prediction of Nta-miR6155 target genes. **(J)** KEGG enrichment based on prediction of Nta-miR6155 target genes. The data was calculated from three independent experiments and statistically analyzed by Student's t test (*P<0.05, **P < 0.01).

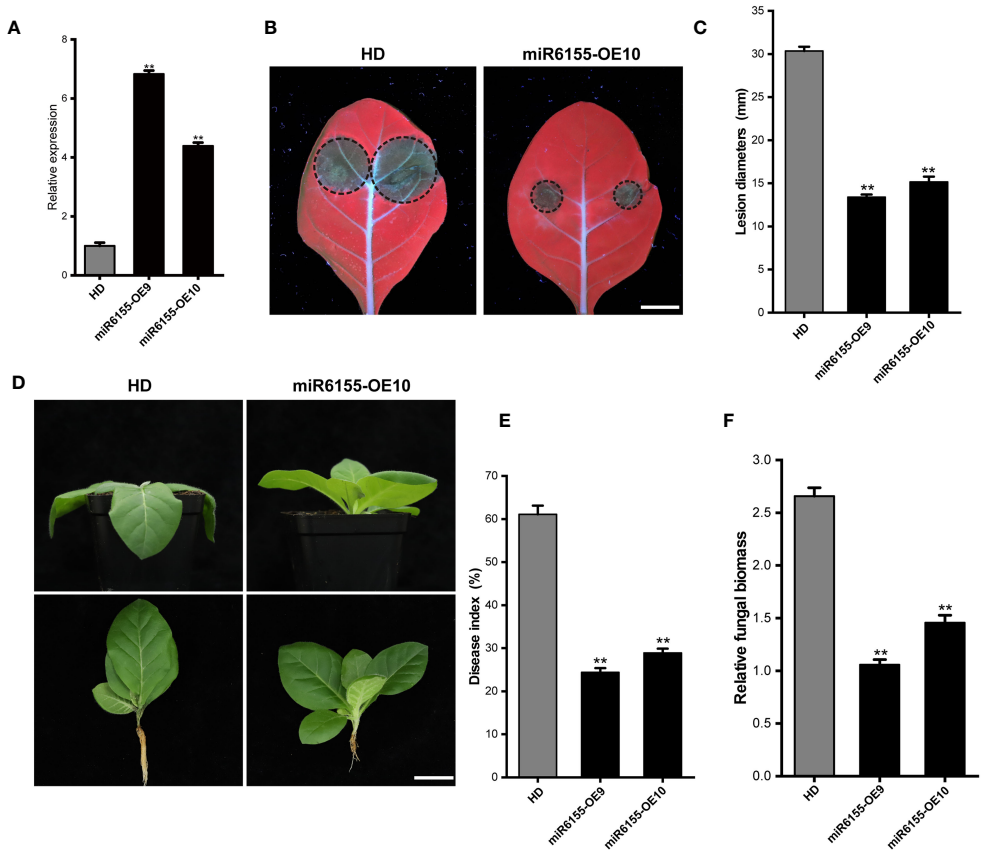

FIGURE 2
The miR6155-OE plants are resistant to *P. nicotianae*. **(A)** The expression level of Nta-miR6155 in miR6155-OE plants. At 5-6 true leaf stage, the leaves of Nta-miR6155 and control HD plants were collected to detect the expression level of Nta-miR6155 in miR6155-OE plants. **(B)** Disease symptoms in detached leaves from control HD and miR6155-OE plants at 48 hpi, bar=1.5cm. **(C)** Lesion diameters in the detached leaves from miR6155-OE plants at 48hpi with *P. nicotianae*. **(D)** Disease symptoms in control HD and miR6155-OE plants tobacco at 48hpi with *P. nicotianae*. Scale bars=3 cm. **(E, F)** Disease index and the fungal biomass in the control HD and miR6155-OE plants at 48h after inoculation. The data was calculated from three independent experiments and statistically analyzed by Student's t test (**P < 0.01).

related genes, including *NtNPR1* (*nonexpressor of pathogenesis-related genes 1*), *NtTGA2.1* (*TGACG sequence-specific binding protein*) and *NtPR1a/c* (*pathogenesis-related genes 1*) (Peng et al., 2021). Data showed that the expression of *NtNPR1, NtTGA2.1 and NtPR1a/c* is higher in miR6155-OE plants than that of HD under normal conditions or after *P. nicotianae* inoculation (Figure 3D). Consistently, we also found that the resistance of *N.benthamiana* to *P. nicotianae* was increased after spraying salicylic acid (Figure S3). These data indicate that Nta-miR6155 could enhance tobacco resistance to *P. nicotianae* by modulating the salicylic acid biosynthesis and signal transduction.

3.3 Nta-miR6155 - *NtCIPK18* modulate tobacco resistance to *P. nicotianae*

To shed light on the biological function of Nta-miR6155, it is of great importance to identify its direct target genes. Among the putative target genes, seven target genes were selected for RT-qPCR analysis. The results showed that most of these genes were significantly down-regulated in miR6155-OE plants compared with HD except *NtCIPK3* and *NtSVP15*, implying that Nta-miR6155 did not directly regulate *NtCIPK3* and *NtSVP15* (Figure 4A). In addition, the expression profile of these genes under the condition of *P. nicotianae* infection was examined. Data showed that they were significantly down-regulated after *P. nicotianae* infection (Figure 4B), suggesting that these genes may be involved in modulating the response to *P. nicotianae* infection in tobacco, and Nta-miR6155 may be able to regulate plant resistance through these potential target genes.

Furthermore, *NtCIPK18* was selected to further examine its role in *P. nicotianae* infections. Phylogenetic analysis showed that NtCIPK18 is closely related to SlCIPK18 and StCIPK18, and analysis of the protein domain of NtCIPK18 showed that NtCIPK18 had a conserved kinase domain and NAF domain unique to CIPK family (Figures 5A, B) (Tang et al., 2020). Gene expression analysis showed that the expression pattern of *NtCIPK18* was inconsistent with Nta-miR6155, and *NtCIPK18* has the highest expression in tobacco stem (Figure 5C). Nta-miR6155 was predicted to target *NtCIPK18* at its first exon region (Figure 5B), and GUS-staining and RT-qPCR analysis confirmed that *NtCIPK18* is a target of Nta-miR6155 in tobacco (Figures 5D, E). Finally, transient expression assay showed that overexpression of *NtCIPK18*

10.3389/fpls.2023.1281373

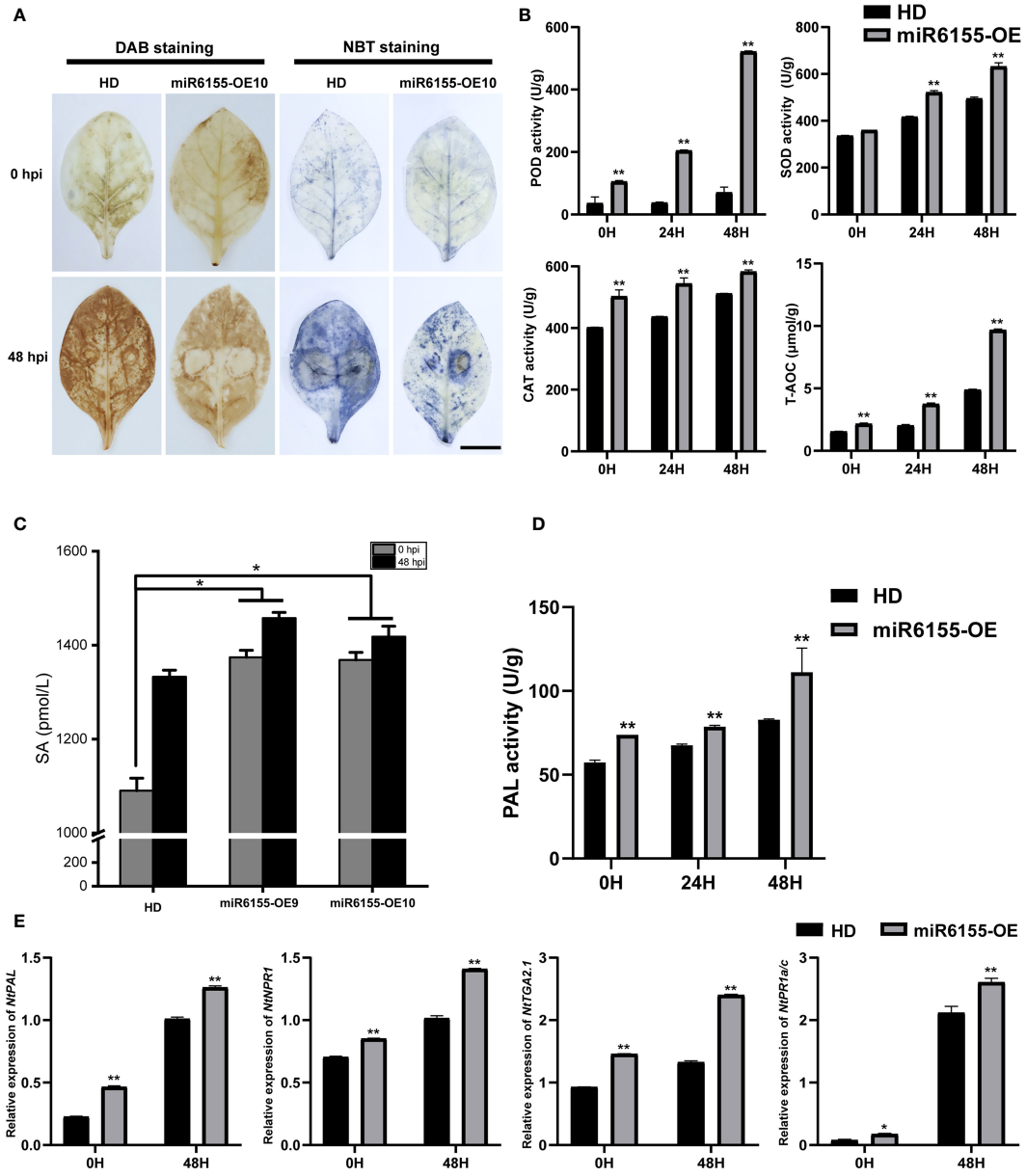

FIGURE 3
Nta-miR6155 enhances tobacco antioxidant capacities and biosynthesis and signal transduction of salicylic acid. **(A)** DAB and NBT staining of control HD and miR6155-OE tobacco leaves at 48h post *P. nicotianae* inoculation, bar =2.5cm. **(B)** Detection of antioxidant enzyme activities in control HD and miR6155-OE plants. **(C)** SA content determination. **(D)** The PAL activities in miR6155-OE and HD plants. **(E)** The expression level of salicylic acid biosynthesis and signal transduction-related genes in tobacco leaves at 0 hpi and 48 hpi with *P. nicotianae*. The data was calculated from three independent experiments and statistically analyzed by Student's t test (*P<0.05, **P < 0.01).

in *N. benthamiana* reduced its resistance to *P. nicotianae*, indicating that Nta-miR6155 could partially modulate resistance to *P. nicotianae* by suppressing the function of *NtCIPK18* in tobacco plants (Figures 5F, G).

3.4 Overexpression of Nta-miR6155 delayed the growth of tobacco

In addition to significant enhancement in disease resistance in miR6155-OE plants, we also found that overexpression of Nta-miR6155 suppressed growth and development of tobacco (Figure 6A). The plant height, internode length and fresh weight of miR6155-OE plants were significantly lower than that of the control HD plants (Figures 6B–D). Analyzing the target genes of Nta-miR6155, we found that *Ammonium Transport 2* (*NtAMT2*) is a potential target gene of Nta-miR6155, and *NtAMT2* encodes a high-affinity ammonium transporter. In addition, RT-qPCR data showed that the expression of *NtAMT2* was reduced fourfold in miR6155-OE plants compared with HD, and the tissue-level expression pattern analysis showed that *NtAMT2* was highly expressed in the roots (Figures 6E, F), implying that NtAMT2

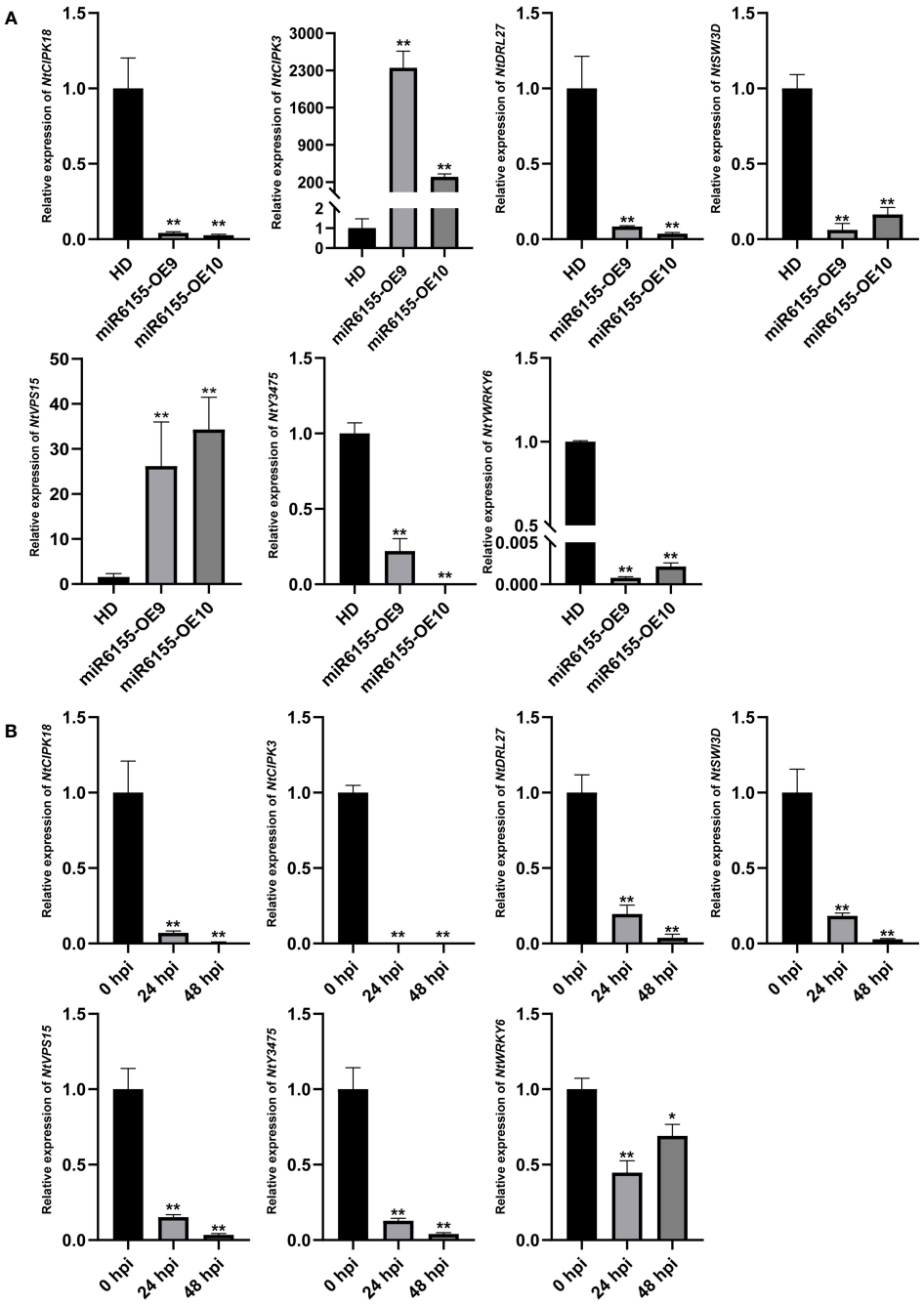

FIGURE 4
Validation of the target genes by RT-qPCR. **(A)** Expression level of target genes in miR6155-OE plants. **(B)** Expression level of target genes in tobacco leaves infected by *P. nicotianae* at 0 hpi, 24 hpi, and 48 hpi. The data was calculated from three independent experiments and statistically analyzed by Student's t test (*P<0.05, **P < 0.01).

may be involved in the absorption of nitrogen by roots. We speculate whether overexpression of Nta-miR6155 resulted in suppression of *AMT2* expression, thereby inhibiting the uptake of ammonium and growth of the miR6155-OE plants. Thus, the nitrogen content and photosynthetic rate of miR6155-OE plants and HD were measured. Consistent with our speculation, nitrogen content and photosynthetic value in miR6155-OE plants were significantly lower than that of HD (Figures 6G, H). These data indicate that Nta-miR6155 also plays an important role in regulating nitrogen uptake and growth and development in tobacco.

4 Discussion

Many studies have reported that miRNAs play essential role in plant response to biotic stresses (Robert-Seilaniantz et al., 2011; Šečić et al., 2021).For example, miR393 could regulate different

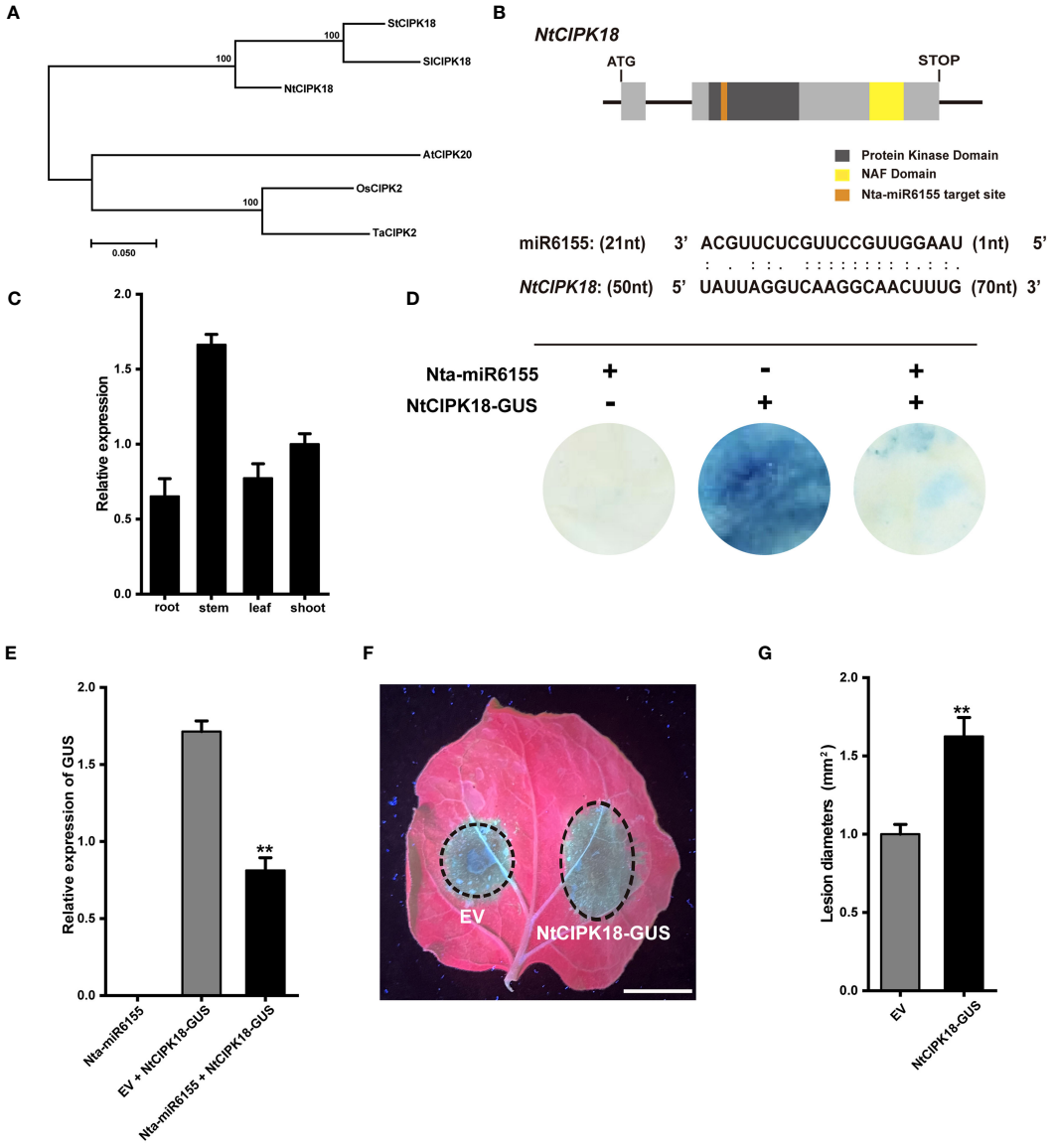

FIGURE 5
Nta-MiR6155 targets *NtCIPK18* to regulate resistance against *P. nicotianae* in *N. benthamiana*. **(A)** Phylogenetic analysis of NtCIPK18 by using MEGA 11 software shows that it is closely related to AtCIPK20 and OsCIPK2. **(B)** Diagram of *NtCIPK18* structure and the miR6155 target site (yellow box means kinase domain, brick red box means NAF domain, and green box means miR6155 target site.). **(C)** The expression pattern of *NtCIPK18* in tobacco seedling. **(D, E)** GUS staining and qRT-PCR analysis shows that miR6155 cleaves *NtCIPK18*. *P35S:: NtCIPK18-GUS* was co-expressed with P35S::*miR6155* or not, and GUS staining and qRT-PCR analysis was performed 48hpi. **(F)** Representative photographs of *N. benthamiana* leaves after 48h infection, bar=1cm. Agrobacterium-mediated transient expression of EV (left) and *P35S::CIPK18-GUS*. (right). The infiltrated leaves (after 36 h) were inoculated with *P. nicotianae*, and photographed at 48 hpi. **(G)** Lesion diameters (mm) of *N. benthamiana* leaves. The data was calculated from three independent biological replicates (**P < 0.01).

target genes to modulate biotic stress response in different plants. In *Arabidopsis*, pattern-triggered immunity could induce the expression of Ath-miR393, which further represses the expression of ARF1/9 to modulate *Arabidopsis* response to biotrophic and necrotrophic pathogens by increasing glucosinolate and decreasing camalexin levels (Robert-Seilaniantz et al., 2011). In soybean, miR393 is induced by PAMPs and act as a positive regulator in soybean response to *Phytophthora sojae* (Wong et al., 2014). Besides miR393, there are many other miRNAs involved in plant response to various biotic stress in plants, such as miR160, miR167, miR164, miRNA166 and miR398, are also known to be the regulators of plant biotic stress response (Šečić et al., 2021). The expression of miR160 could be affected by different pathogens, and like miR393, miR160 can target ARFs to modulate plant response to MAMP responses in plants (Rhoades et al., 2002; Li et al., 2010). MiR164 can target NAC transcription factors to regulate auxin homeostasis and plant cell death responses in plants (Guo et al., 2005; Lee et al., 2017). miR398 could negatively regulate callose deposition and PTI by targeting superoxide dismutases (*SODs*) in *Arabidopsis* (Li et al., 2010). Recent studies have shown that miRNAs play an important role in response to *P. nicotianae* infections in tobacco plants. The overexpression of tomato miR396a-5p in tobacco has been shown

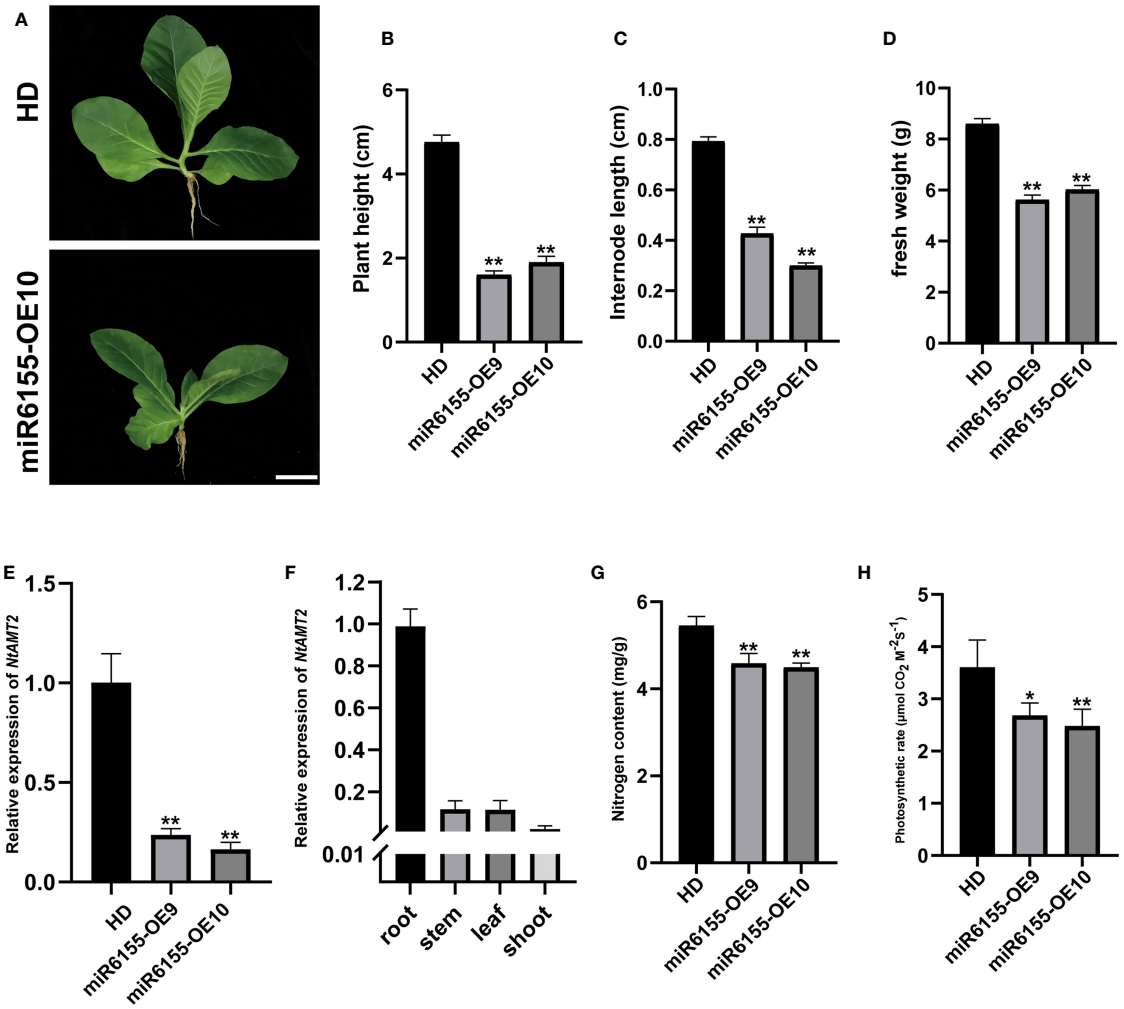

FIGURE 6
Phenotypic characterization of miR6155 transgenic plants. **(A)** The phenotype of miR6155-OE and control HD seedlings under normal conditions, bars=5 cm. **(B–D)** Plant height, internode length and fresh weight of miR6155-OE and control HD plants. **(E)** Expression level of *NtAMT2* in miR6155-OE and control HD seedlings. **(F)** The expression level of *NtAMT2* in different tobacco tissues, including root, stem, leaf and shoot. **(G, H)** Nitrogen content and photosynthetic rate in miR6155-OE and control HD plants. The data was calculated from three independent biological replicates (*P<0.05, **P < 0.01).

to increase its susceptibility to *P. nicotianae* (Chen et al., 2015), and silencing of miR159 could enhance tobacco resistance to *P. nicotianae* infections (Zheng et al., 2020). In *Arabidopsis*, miR398b could negatively regulate plant immunity to *P. parasitica* by suppressing the expression of the *core-2/I-branching beta-1,6-N-acetylglucosaminyltransferase* gene (*AtC2GnT*) (Gou et al., 2022). However, so far, only a few miRNAs have been found to be associated with *P. nicotianae*, and studies were focused on the conserved miRNA family in plants. Research on species-specific miRNAs is limited. In this study, we found that miRNA6155, a species-specific miRNA in the *Solanaceae* species, can significantly enhance resistance to *P. nicotianae* in tobacco. Recent miRNA omics also identified many species-specific miRNA in different species (Islam et al., 2015; Chhapekar et al., 2021; Lopez-Ortiz et al., 2021). The predicted target genes of miRNAs indicate that these miRNAs can target different functional genes, including protein kinases, resistance genes and transcription factors (Chhapekar et al., 2021). In previous studies, it has found that some *Solanaceae* specific miRNA could regulate innate immunity by targeting *R* genes and *NLR* (*nucleotide-binding leucine-rich repeat*) genes (Li et al., 2012; Deng et al., 2018). Further research will help reveal the role of species-specific miRNA in plant development and defense signaling pathways.

P. nicotianae causes significant economic losses in tobacco cultivation, and only a few genes that can participate in tobacco response to *P. nicotianae* have been identified in previous studies, such as *NpPP2-B10* and *EIN3* (Cho et al., 2013; Wen et al., 2023). MiRNA mainly regulates the function of target genes at the post transcriptional level by directly cleaving target genes or inhibiting their translation. In this study, we predicted target genes of Nta-miR6155, and RT-qPCR data showed some target genes were significantly down-regulated in Nta-miR6155 overexpression lines. Nta-miR6155 may affect the tobacco resistance to *P. nicotianae* by modulating the function of its target genes. CIPKs belong to a

subclass of serine/threonine (Ser/Thr) protein kinases, and play crucial roles in plants development and stress response (Yang et al., 2022). In previous studies, it has been found that CIPKs were involved in plant response to biotic stress by regulation of reactive oxygen species (ROS) production (Yang et al., 2022). For instance, CIPK26 and CIPK6 could promote ROS production through NADPH oxidases (de la Torre et al., 2013; Kimura et al., 2013). TaCIPK10 could interact and phosphorylate TaNH2, a homologous of AtNPR3/4, and phosphorylate it to enhance wheat resistance to wheat stripe rust (Liu et al., 2019). In this study, we showed that *NtCIPK18* was significantly suppressed under *P. nicotianae*, and transient expression of *NtCIPK18* resulted in significantly reducing *N. benthamiana* resistance to *P. nicotianae*, suggesting that *NtCIPK18* is a negative regulator of plant resistance to *P. nicotianae*.

Furthermore, our data showed that overexpression of miR6155 resulted in slow growth and smaller internode length in tobacco. In previous studies, miRNAs have been found to be involved in plant growth and development under nitrogen starvation conditions (Liang et al., 2012; Kant, 2018). He et al. showed that miR826 and miR5090 are involved in mediating nitrogen starvation adaptation by regulating *Alkenyl Hydroxalkyl Producing2* (*AOP2*) (He et al., 2014). Overexpression of miR169a resulted in significantly decreased nitrogen starvation tolerance in *Arabidopsis* (Zhao et al., 2011). Interestingly, we found that *AMT2*, encoding a high-affinity ammonium transporter, is a potential target gene of miR6155. In previous studies, it has been shown that AMT2 potentially regulates ammonium uptake in different plants (Zhang et al., 2022). Additionally, Giehl et al. has shown that *AMT2;1* was crucial for root-to-shoot translocation of ammonium in *Arabidopsis* (Giehl et al., 2017). Our RT-qPCR data showed that the expression level of *AMT2* was significantly down-regulated in miR6155-OE plants, and nitrogen content also significantly decreased in miR6155-OE plants, suggesting that miR6155 may participate in regulating ammonium uptake through *AMT2*. These results indicate that miRNA6155 plays an important role not only in regulating disease resistance but also in nutrient absorption.

Overall, we identified and investigated the function of miR6155 in tobacco in response to *P. nicotianae* infection. Meanwhile, our results indicate that species-specific miRNAs have important functions in regulating growth and development and stress response in plants, and future research on these species-specific miRNAs may provide more important genetic resources for stress-resistance targeted crop breeding.

Data availability statement

The original contributions presented in the study are included in the article/Supplementary Material. Further inquiries can be directed to the corresponding authors.

Author contributions

KY: Data curation, Formal Analysis, Writing – original draft. YH: Formal Analysis, Methodology, Writing – original draft. ZL: Data curation, Formal Analysis, Writing – review & editing. QZ: Data curation, Formal Analysis, Writing – original draft. XD: Formal Analysis, Writing – review & editing. JL: Formal Analysis, Writing – original draft. XZ: Formal Analysis, Writing – original draft. KD: Conceptualization, Methodology, Writing – original draft, Writing – review & editing. JZ: Conceptualization, Methodology, Writing – original draft, Writing – review & editing.

Funding

The author(s) declare financial support was received for the research, authorship, and/or publication of this article. This work was supported by the Science and Technology Project of Chongqing Tobacco Monopoly Bureau (B20211NY1314 and C20221NY3433) and the Fundamental Research Funds for the Central Universities (SWU120072). The funder was not involved with the study design, collection, analysis, interpretation of data, the writing of this article or the decision to submit it for publication.

Acknowledgments

The authors would like to thank Guoqing Niu and Fangjie Xiong for revising the manuscript.

Conflict of interest

The authors declare that the research was conducted in the absence of any commercial or financial relationships that could be construed as a potential conflict of interest.

Publisher's note

Supplementary material

The Supplementary Material for this article can be found online at: https://www.frontiersin.org/articles/10.3389/fpls.2023.1281373/full#supplementary-material

SUPPLEMENTARY FIGURE 1
The expression level of Nta-miR6155 at early time points after *P. nicotianae* inoculation.

SUPPLEMENTARY FIGURE 2
The ortholog of Nta-miR6155 in *N.benthamiana* is induced by *P. nicotianae*. **(A)** The phenotype of *N.benthamiana* after inoculation with *P. nicotianae*, bar=2 cm. **(B)** The expression level of miR6155 in *N.benthamiana* on infection with *P. nicotianae* at 48 hpi.

SUPPLEMENTARY FIGURE 3

Salicylic acid enhances resistance against *P. nicotianae* in *N.benthamiana*. bar=1 cm. **(A)** Representative photographs of *N. benthamiana* leaves after 48h infection. bar= 1 cm. *N. benthamiana* seedlings at 7-8 true leaf stage were sprayed with SA (1mM) and double distilled water (ddH2O) was used as control (CK). After 24h, the leaves of *N. benthamiana* seedlings were inoculated with *P. nicotianae*, and photographed at 48 hpi. **(B)** Lesion diameters (mm) of *N. benthamiana* leaves.

References

Achkar, N. P., Cambiagno, D. A., and Manavella, P. A. (2016). miRNA biogenesis: A dynamic pathway. *Trends Plant Sci.* 21 (12), 1034–1044. doi: 10.1016/j.tplants.2016.09.003

Addo-Quaye, C., Eshoo, T. W., Bartel, D. P., and Axtell, M. J. (2008). Endogenous siRNA and miRNA targets identified by sequencing of the Arabidopsis degradome. *Curr. Biol.* 18 (10), 758–762. doi: 10.1016/j.cub.2008.04.042

An, P., Qin, R., Zhao, Q., Li, X., Wang, C., and Zhang, L. (2022). Genetic transformation of LoHDZ2 and analysis of its function to enhance stress resistance in Larix olgensis. *Sci. Rep.* 12 (1), 12831. doi: 10.1038/s41598-022-17191-2

Bi, G., Hu, M., Fu, L., Zhang, X., and Zuo, J. (2022). The cytosolic thiol peroxidase PRXIIB is an intracellular sensor for H(2)O(2) that regulates plant immunity through a redox relay. *Nat Plants* 8, 1160–1175. doi: 10.1038/s41477-022-01252-5

Bo, X., and Wang, S. (2005). TargetFinder: a software for antisense oligonucleotide target site selection based on MAST and secondary structures of target mRNA. *Bioinformatics* 21 (8), 1401–1402. doi: 10.1093/bioinformatics/bti211

Chen, L., Luan, Y., and Zhai, J. (2015). Sp-miR396a-5p acts as a stress-responsive genes regulator by conferring tolerance to abiotic stresses and susceptibility to *Phytophthora nicotianae* infection in transgenic Tobacco. *Plant Cell Rep.* 34 (12), 2013–2025. doi: 10.1007/s00299-015-1847-0

Chhapekar, S. S., Kumar, N., Sarpras, M., Brahma, V., Rawoof, A., and Jaiswal, V. (2021). Profiling of miRNAs in Bhut Jolokia (Capsicum chinense) and Kon Jolokia (C. frutescens) of Northeast India. *Scientia Hortic.* 281, 109952. doi: 10.1016/j.scienta.2021.109952

Cho, K., Kim, Y., Wi, Sj, Seo, J. B., Kwon, J., Chung, J. H., et al. (2013). Metabolic survey of defense responses to a compatible hemibiotroph, *Phytophthora parasitica* var. *nicotianae*, in ethylene signaling-impaired tobacco. *J. Agric. Food Chem.* 61 (35), 8477–8489. doi: 10.1021/jf401785w

de la Torre, F., Gutiérrez-Beltrán, E., Pareja-Jaime, Y., Chakravarthy, S., Martin, G.B., Del Pozo, O., et al. (2013). The tomato calcium sensor Cbl10 and its interacting protein kinase Cipk6 define a signaling pathway in plant immunity. *Plant Cell* 25 (7), 2748–2764. doi: 10.1105/tpc.113.113530

Deng, Y., Wang, J., Tung, J., Liu, D., Zhou, Y., and He, S. (2018). A role for small RNA in regulating innate immunity during plant growth. *PLoS Pathog.* 14 (1), e1006756. doi: 10.1371/journal.ppat.1006756

Evers, M., Huttner, M., Dueck, A., Meister, G., and Engelmann, J. C. (2015). miRA: adaptable novel miRNA identification in plants using small RNA sequencing data. *BMC Bioinf.* 16, 370. doi: 10.1186/s12859-015-0798-3

German, M. A., Pillay, M., Jeong, D. H., Hetawal, A., Luo, S., and Janardhanan, P. (2008). Global identification of microRNA-target RNA pairs by parallel analysis of RNA ends. *Nat. Biotechnol.* 26 (8), 941–946. doi: 10.1038/nbt1417

Giehl, R. F. H., Laginha, A. M., Duan, F., Rentsch, D., Yuan, L., and Von Wirén, N. (2017). A critical role of AMT2;1 in root-to-shoot translocation of ammonium in arabidopsis. *Mol. Plant* 10 (11), 1449–1460. doi: 10.1016/j.molp.2017.10.001

Gou, X., Zhong, C., Zhang, P., Mi, L., Li, Y., and Lu, W. (2022). miR398b and AtC2GnT form a negative feedback loop to regulate Arabidopsis thaliana resistance against Phytophthora parasitica. *Plant J.* 111 (2), 360–373. doi: 10.1111/tpj.15792

Guo, Y., Jia, M. A., Yang, Y., Zhan, L., et al. (2017). Integrated analysis of tobacco miRNA and mRNA expression profiles under PVY infection provids insight into tobacco-PVY interactions. *Sci. Rep.* 7 (1), 4895. doi: 10.1038/s41598-017-05155-w

Guo, H. S., Xie, Q., Fei, J. F., and Chua, N. H. (2005). MicroRNA directs mRNA cleavage of the transcription factor NAC1 to downregulate auxin signals for arabidopsis lateral root development. *Plant Cell* 17 (5), 1376–1386. doi: 10.1105/tpc.105.030841

Guo, D., Yuan, C., Luo, Y., Chen, Y., Lu, M., and Chen, G. (2020). Biocontrol of tobacco black shank disease (*Phytophthora nicotianae*) by Bacillus velezensis Ba168. *Pestic Biochem. Physiol.* 165, 104523. doi: 10.1016/j.pestbp.2020.01.004

Han, W. H., Wang, J. X., Zhang, F. B., Liu, Y. X., Wu, H., and Wang, X. W. (2022). Small RNA and Degradome Sequencing Reveal Important MicroRNA Function in *Nicotiana tabacum* Response to *Bemisia tabaci*. *Genes (Basel)* 13 (2), 361. doi: 10.3390/genes13020361

He, H., Liang, G., Li, Y., Wang, F., and Yu, D. (2014). Two young MicroRNAs originating from target duplication mediate nitrogen starvation adaptation via regulation of glucosinolate synthesis in Arabidopsis thaliana. *Plant Physiol.* 164 (2), 853–865. doi: 10.1104/pp.113.228635

Islam, M. T., Ferdous, A. S., Najnin, R. A., Sarker, S. K., and Khan, H. (2015). High-throughput sequencing reveals diverse sets of conserved, nonconserved, and species-specific miRNAs in Jute. *Int. J. Genomics* 2015, 125048. doi: 10.1155/2015/125048

Jin, J., and Shew, H. D. (2021). Components of aggressiveness in *Phytophthora nicotianae* during adaptation to multiple sources of partial resistance in Tobacco. *Plant Dis* 105 (7), 1960–1966. doi: 10.1094/pdis-09-20-1929-re

Kant, S. (2018). Understanding nitrate uptake, signaling and remobilisation for improving plant nitrogen use efficiency. *Semin. Cell Dev. Biol.* 74, 89–96. doi: 10.1016/j.semcdb.2017.08.034

Kimura, S., Kawarazaki, T., Nibori, H., Michikawa, M., Imai, A., and Kaya, H. (2013). The CBL-interacting protein kinase CIPK26 is a novel interactor of Arabidopsis NADPH oxidase AtRbohF that negatively modulates its ROS-producing activity in a heterologous expression system. *J. Biochem.* 153 (2), 191–195. doi: 10.1093/jb/mvs132

Ku, Y. S., Sintaha, M., Cheung, M. Y., and Lam, H. M. (2018). Plant hormone signaling crosstalks between biotic and abiotic stress responses. *Int. J. Mol. Sci.* 19 (10), 3206. doi: 10.3390/ijms19103206

Kurihara, Y., and Watanabe, Y. (2010). Processing of miRNA precursors. *Methods Mol. Biol.* 592, 231–241. doi: 10.1007/978-1-60327-005-2_15

Lee, R. C., Feinbaum, R. L., and Ambros, V. (1993). The C. elegans heterochronic gene lin-4 encodes small RNAs with antisense complementarity to lin-14. *Cell* 75 (5), 843–854. doi: 10.1016/0092-8674(93)90529-y

Lee, M. H., Jeon, H. S., Kim, H. G., and Park, O. K. (2017). An Arabidopsis NAC transcription factor NAC4 promotes pathogen-induced cell death under negative regulation by microRNA164. *New Phytol.* 214 (1), 343–360. doi: 10.1111/nph.14371

Li, X. P., Ma, X. C., Wang, H., Zhu, Y., Liu, X. X., and Li, T. T. (2020). Osa-miR162a fine-tunes rice resistance to *Magnaporthe oryzae* and Yield. *Rice (N Y)* 13 (1), 38. doi: 10.1186/s12284-020-00396-2

Li, F., Pignatta, D., Bendix, C., Brunkard, J. O., Cohn, M. M., and Tung, J. (2012). MicroRNA regulation of plant innate immune receptors. *Proc. Natl. Acad. Sci. U.S.A.* 109 (5), 1790–1795. doi: 10.1073/pnas.1118282109

Li, L., Song, Y., Wang, K., Dong, P., Zhang, X., Li, F., et al. (2015). TOR-inhibitor insensitive-1 (TRIN1) regulates cotyledons greening in Arabidopsis. *Front. Plant Sci.* 6. doi: 10.3389/fpls.2015.00861

Li, M., and Yu, B. (2021). Recent advances in the regulation of plant miRNA biogenesis. *RNA Biol.* 18 (12), 2087–2096. doi: 10.1080/15476286.2021.1899491

Li, Y., Zhang, Q., Zhang, J., Wu, L., Qi, Y., and Zhou, J. M. (2010). Identification of microRNAs involved in pathogen-associated molecular pattern-triggered plant innate immunity. *Plant Physiol.* 152 (4), 2222–2231. doi: 10.1104/pp.109.151803

Liang, G., He, H., and Yu, D. (2012). Identification of nitrogen starvation-responsive microRNAs in Arabidopsis thaliana. *PloS One* 7 (11), e48951. doi: 10.1371/journal.pone.0048951

Liu, P., Guo, J., Zhang, R., Zhao, J., Liu, C., and Qi, T. (2019). TaCIPK10 interacts with and phosphorylates TaNH2 to activate wheat defense responses to stripe rust. *Plant Biotechnol. J.* 17 (5), 956–968. doi: 10.1111/pbi.13031

Liu, Y., Sun, M., Jiang, Z., Wang, X., Xiao, B., and Yang, A. (2022). Screening of Tobacco genotypes for *phytophthora nicotianae* resistance. *J. Vis. Exp.* 182. doi: 10.3791/63054

Llave, C., Kasschau, K. D., Rector, M. A., and Carrington, J. C. (2002). Endogenous and silencing-associated small RNAs in plants. *Plant Cell* 14 (7), 1605–1619. doi: 10.1105/tpc.003210

Lopez-Ortiz, C., Peña-Garcia, Y., Bhandari, M., Abburi, V. L., Natarajan, P., and Stommel, J. (2021). Identification of miRNAs and Their Targets Involved in Flower and Fruit Development across Domesticated and Wild Capsicum Species. *Int. J. Mol. Sci.* 22 (9), 4866. doi: 10.3390/ijms22094866

Meng, H., Sun, M., Jiang, Z., Liu, Y., Sun, Y., and Liu, D. (2021). Comparative transcriptome analysis reveals resistant and susceptible genes in tobacco cultivars in response to infection by *Phytophthora nicotianae*. *Sci. Rep.* 11 (1), 809. doi: 10.1038/s41598-020-80280-7

Mette, M. F., van der Winden, J., Matzke, M., and Matzke, A. J. (2002). Short RNAs can identify new candidate transposable element families in Arabidopsis. *Plant Physiol.* 130 (1), 6–9. doi: 10.1104/pp.007047

Peng, Y., Yang, J., Li, X., and Zhang, Y. (2021). Salicylic acid: biosynthesis and signaling. *Annu. Rev. Plant Biol.* 72, 761–791. doi: 10.1146/annurev-arplant-081320-092855

Reinhart, B. J., Weinstein, E. G., Rhoades, M. W., Bartel, B., and Bartel, D. P. (2002). MicroRNAs in plants. *Genes Dev.* 16 (13), 1616–1626. doi: 10.1101/gad.1004402

Rhoades, M. W., Reinhart, B. J., Lim, L. P., Burge, C. B., Bartel, B., and Bartel, D. P. (2002). Prediction of plant microRNA targets. *Cell* 110 (4), 513–520. doi: 10.1016/s0092-8674(02)00863-2

Robert-Seilaniantz, A., MacLean, D., Jikumaru, Y., Hill, L., Yamaguchi, S., and Kamiya, Y. (2011). The microRNA miR393 re-directs secondary metabolite biosynthesis away from camalexin and towards glucosinolates. *Plant J.* 67 (2), 218–231. doi: 10.1111/j.1365-313X.2011.04591.x

Šečić, E., Kogel, K. H., and Ladera-Carmona, M. J. (2021). Biotic stress-associated microRNA families in plants. *J. Plant Physiol.* 263, 153451. doi: 10.1016/j.jplph.2021.153451

Song, L., Fang, Y., Chen, L., Wang, J., and Chen, X. (2021). Role of non-coding RNAs in plant immunity. *Plant Commun.* 2 (3), 100180. doi: 10.1016/j.xplc.2021.100180

Song, X., Li, Y., Cao, X., and Qi, Y. (2019). MicroRNAs and their regulatory roles in plant-environment interactions. *Annu. Rev. Plant Biol.* 70, 489–525. doi: 10.1146/annurev-arplant-050718-100334

Tang, S., Wang, Y., Li, Z., Gui, Y., Xiao, B., Xie, J., et al. (2012). Identification of wounding and topping responsive small RNAs in tobacco (*Nicotiana tabacum*). *BMC Plant Biol.* 12, 28. doi: 10.1186/1471-2229-12-28

Tang, R. J., Wang, C., Li, K., and Luan, S. (2020). The CBL-CIPK calcium signaling network: unified paradigm from 20 years of discoveries. *Trends Plant Sci.* 25 (6), 604–617. doi: 10.1016/j.tplants.2020.01.009

Wen, G., Xie, Z., Yang, Y., Yang, Y., Guo, Q., and Liang, G. (2023). NpPP2-B10, an F-Box-Nictaba Gene, Promotes Plant Growth and Resistance to Black Shank Disease Incited by *Phytophthora nicotianae* in *Nicotiana tabacum*. *Int. J. Mol. Sci.* 24 (8), 7353. doi: 10.3390/ijms24087353

Wong, J., Gao, L., Yang, Y., Zhai, J., Arikit, S., and Yu, Y. (2014). Roles of small RNAs in soybean defense against Phytophthora sojae infection. *Plant J.* 79 (6), 928–940. doi: 10.1111/tpj.12590

Yang, Z., Hui, S., Lv, Y., Zhang, M., Chen, D., and Tian, J. (2022). miR395-regulated sulfate metabolism exploits pathogen sensitivity to sulfate to boost immunity in rice. *Mol. Plant* 15 (4), 671–688. doi: 10.1016/j.molp.2021.12.013

Yang, L., Mu, X., Liu, C., Cai, J., Shi, K., and Zhu, W. (2015). Overexpression of potato miR482e enhanced plant sensitivity to Verticillium dahliae infection. *J. Integr. Plant Biol.* 57 (12), 1078–1088. doi: 10.1111/jipb.12348

Yang, J. K., Tong, Z. J., Fang, D. H., Chen, X. J., Zhang, K. Q., and Xiao, B. G. (2017). Transcriptomic profile of tobacco in response to *Phytophthora nicotianae* infection. *Sci. Rep.* 7 (1), 401. doi: 10.1038/s41598-017-00481-5

Yang, C., Yi-Feng, J., Yushu, W., Yansong, G., Qi, W., and Xue, Y. (2022). Diverse roles of the CIPK gene family in transcription regulation and various biotic and abiotic stresses: A literature review and bibliometric study. *Front. Genet.* 13, 1041078. doi: 10.3389/fgene.2022.1041078

Yu, J., Chai, C., Ai, G., Jia, Y., Liu, W., and Zhang, X. (2020). A Nicotiana benthamiana AP2/ERF transcription factor confers resistance to Phytophthora parasitica. *Phytopathol. Res.* 2 (1), 4. doi: 10.1186/s42483-020-0045-3

Zamore, P. D., and Haley, B. (2005). Ribo-gnome: the big world of small RNAs. *Science* 309 (5740), 1519–1524. doi: 10.1126/science.1111444

Zhang, Y. Y., Hong, Y. H., Liu, Y. R., Cui, J., and Luan, Y. S. (2021). Function identification of miR394 in tomato resistance to *Phytophthora infestans*. *Plant Cell Rep* 40 (10), 1831–1844. doi: 10.1007/s00299-021-02746-w

Zhang, W., Lin, L., Wang, T., Chen, M., Song, B., and Sun, W. (2022). Genome-Wide Identification of AMT2-Type Ammonium Transporters Reveal That CsAMT2.2 and CsAMT2.3 Potentially Regulate NH(4)(+) Absorption among Three Different Cultivars of Camellia sinensis. *Int. J. Mol. Sci.* 23 (24), 15661. doi: 10.3390/ijms232415661

Zhao, M., Ding, H., Zhu, J. K., Zhang, F., and Li, W. X. (2011). Involvement of miR169 in the nitrogen-starvation responses in Arabidopsis. *New Phytol.* 190 (4), 906–915. doi: 10.1111/j.1469-8137.2011.03647.x

Zheng, Z., Wang, N., Jalajakumari, M., Blackman, L., Shen, E., and Verma, S. (2020). miR159 represses a constitutive pathogen defense response in Tobacco. *Plant Physiol.* 182 (4), 2182–2198. doi: 10.1104/pp.19.00786

Zhu, X., He, S., Fang, D., Guo, L., Zhou, X., and Guo, Y. (2020). High-Throughput Sequencing-Based Identification of Arabidopsis miRNAs Induced by Phytophthora capsici Infection. *Front. Microbiol.* 11, 1094. doi: 10.3389/fmicb.2020.01094

Frontiers in
Plant Science

Cultivates the science of plant biology and its applications

The most cited plant science journal, which advances our understanding of plant biology for sustainable food security, functional ecosystems and human health.

Discover the latest Research Topics

See more →

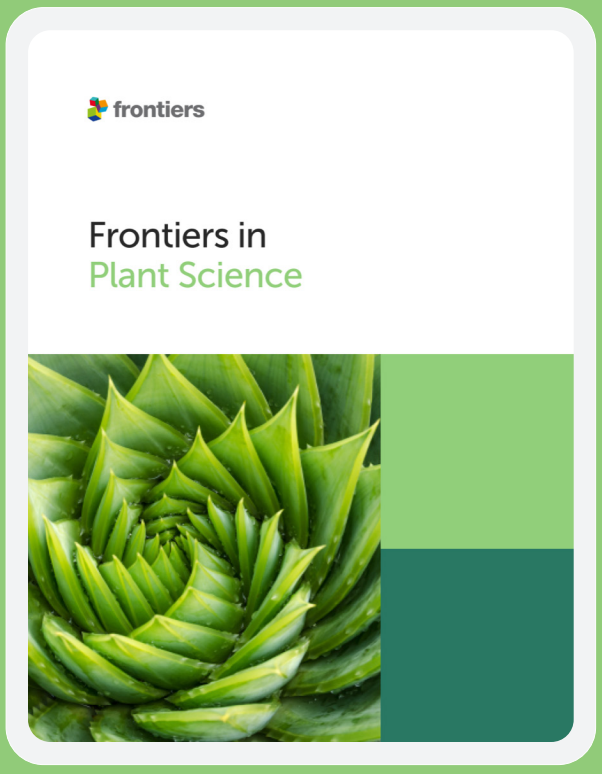

Frontiers

Avenue du Tribunal-Fédéral 34
1005 Lausanne, Switzerland
frontiersin.org

Contact us

+41 (0)21 510 17 00
frontiersin.org/about/contact